$31.85

CYPRUS CRUSTAL STUDY PROJECT: INITIAL REPORT, HOLES CY-1 and 1a

Editors:

I.L. GIBSON, J. MAPAS, P.T. ROBINSON, and C. XENOPHONTOS

Energy, Mines and Resources Canada
Énergie, Mines et Ressources Canada

Canada

GEOLOGICAL SURVEY OF CANADA
PAPER 90-20

CYPRUS CRUSTAL STUDY PROJECT: INITIAL REPORT, HOLES CY-1 and 1a

edited by
I.L. Gibson, J. Malpas, P.T. Robinson, and C. Xenophontos

1991

Available in Canada through

authorized bookstore agents and other bookstores

or by mail from

Canada Communication Group - Publishing
Ottawa, Canada K1A 0S9

and from

Geological Survey of Canada offices:

601 Booth Street
Ottawa, Canada K1A 0E8

3303-33rd Street N.W.,
Calgary, Alberta T2L 2A7

A deposit copy of this publication is also available for reference
in public libraries across Canada

Cat. No. M44-90/20E
ISBN 0-660-14395-X

Price subject to change without notice

This volume has been printed by the Geological Survey of Canada on behalf of the Cyprus Crustal Study project from camera-ready copy prepared, under the direction of the volume editors, by Wendy MacIntosh in the Department of Earth Sciences, University of Waterloo. The material is set in 10 pt and 8 pt Adobe Times Roman and was printed using the Varityper 600W Phototypesetter, and the LaTeX Document Preparation System, in the Department of Graphic Services, University of Waterloo.

Foreword

In 1978, an international consortium of scientists from Canada, Denmark, the United Kingdom, Iceland, the United States, and West Germany successfully completed a research deep drilling project in Iceland. These scientists subsequently formed the International Crustal Research Drilling Group (ICRDG), to organize further deep drilling investigations and to compare the results with those from the Deep Sea and Ocean Drilling Projects. It was hoped, in this way, to better understand the structure and composition of the ocean crust. The projects undertaken by the group were selected and organized by a Management Panel and each project was overseen by a Project Director. The members of the Management Panel during the period of 1980 to 1986 were: Dr. Abdul Razzak Bakor, King Abdul Aziz University, Saudi Arabia; Dr. Robert Baragar, Geological Survey of Canada, Canada; Dr. Tom Calon, Memorial University, Canada; Dr. George Constantinou, Geological Survey Department, Cyprus; Dr. Martin F.J. Flower, University of Illinois, U.S.A.; Dr. Ingvar Birgir Fridleifsson, Orkustofnun, Iceland; Dr. Ian G. Gass, The Open University, U.K.; Dr. Ian L. Gibson, University of Waterloo, Canada; Dr. James Hall, Dalhousie University, Canada; Dr. James Hawkins, Scripps Institution of Oceanography, U.S.A.; Dr. H.P. Johnson, University of Washington, U.S.A.; Dr. John Malpas, Memorial University, Canada; Dr. Eldridge Moores, University of California, U.S.A.; Dr. John Orcutt, Scripps Institution of Oceanography, U.S.A.; Dr. Andreas Panayiotou, Geological Survey Department, Cyprus; Dr. Paul T. Robinson, Chairman, Dalhousie University, Canada; Dr. Fritz Rummel, Ruhr-Universität Bochum, West Germany; Dr. Matthew Salisbury, Dalhousie University, Canada; Dr. Andrew Saunders, University of Leicester, U.K.; Dr. Hans-Ulrich Schmincke, Ruhr-Universität Bochum, West Germany; Dr. Gunther Schoenharting, University of Copenhagen, Denmark; Dr. M. Treuil, Université Pierre et Marie Curie, France; Dr. Fred Vine, University of East Anglia, U.K.

Ophiolites have long been recognized as portions of ancient oceanic lithosphere emplaced on to continental margins during periods of orogenesis. As such, complete ophiolites present a stratigraphy of the oceanic crust and the underlying upper mantle. P.T. Robinson proposed that ICRDG investigate the Troodos ophiolite in Cyprus. The Troodos ophiolite is one of the best studied and least deformed ophiolites available for investigation, and its unique domal structure permits sampling of the complete stratigraphy in a series of relatively shallow holes. An integrated petrological, structural, and geophysical study of the ophiolite, involving both field mapping and diamond drilling was therefore planned. The proposal was formally approved by the Management Panel in May, 1980. P.T. Robinson was appointed Project Director with overall responsibility for the drilling operations and organization of the scientific investigations.

Avant-propos

En 1978, un groupe international de scientifiques du Canada, du Danemark, du Royaume-Uni, de l'Islande, des États-Unis et de l'Allemagne de l'Ouest a complété avec succès, en Islande, un projet expérimental de forage à grande profondeur. Ces scientifiques ont notamment fondé le groupe international (International Crustal Research Drilling Group, ICRDG) afin d'organiser d'autres forages experimentaur de la croûte terrestre et de comparer les résultats de projets de forage profond aux résultats obtenus dans le cadre du Projet de forage des fonds marins. Il était espéré, de cette façon, à permettre une meilleure compréhension de la structure et de la composition de la croûte océanique. Les projets entrepris par le groupe étaient choisis et organisés par un comité de gestion, et chaque projet était supervisé par un directeur de projet. Les membres nommés au comité de gestion durant la période allant de 1980 à 1986 étaient: M. Abdul Razzak Bakor, université King Abdul Aziz, Arabie Saoudite; M. Robert Baragar, Commission géologique du Canada, Canada; M. Tom Calon, université Memorial, Canada; M. George Constantinou, Commission géologique de Chypre, Chypre; M. Martin F.J. Flower, université de l'Illinois, É.-U.; M. Ingvar Birgir Fridlefsson, Orkustofnun, Islande; M. Ian Gass, The Open University, R.-U.; M. Ian Gibson, université de Waterloo, Canada; M. James Hawkins, Scripps Institution of Oceanography, É.-U.; M.H.P. Johnson, université de Washington, É.-U.; M. John Malpas, université Memorial, Canada; M. Eldridge Moores, université de Californie, É.-U.; M. John Orcutt, Scripps Institution of Oceanography, É.-U.; M. Andreas Panayiotou, Commission géologique de Chypre, Chypre; M. Paul T. Robinson, Président, université Dalhousie, Canada; M. Fritz Rummel, Ruhr-Universität Bochum, Allemagne de l'Ouest; M. Matthew Salisbury, université Dalhousie, Canada; M. Andrew Saunders, université de Leicester, R.-U.; M. Hans-Ulrich Schmincke, Ruhr-Universität Bochum, Allemagne de l'Ouest, M. Gunther Schoenharting, université de Copenhague, Danemark; M. M. Treuil, université Pierre et Marie Curie, France; M. Fred Vine, université de East Anglia, R.-U.

On admet depuis longtemps que les ophiolites sont des portions de l'ancienne lithosphère océanique dont la mise en place a eu lieu sur les marges continentales durant des périodes d'orogénèse. De ce fait, les ophiolites complètes représentent une stratigraphie de la croûte océanique et du manteau supérieur. M. P.T. Robinson a suggéré que ICRDG assume l'investigation de l'ophiolite de Troodos à Chypre. L'ophiolite du Troodos est l'une des ophiolites a mieux étudiée et la moins déformée que l'on puisse examiner, et sa structure exceptionnelle en forme de dôme permet l'échantillon de la colonne stratigraphique toute entière au moyen d'une série de sondages relativement peu profonds.

During the period 1980 to 1982, the Cyprus Government approved the project, supporting funds were obtained from a variety of sources, and field studies were started. A drilling contract with Bradley Bros., Noranda, Quebec, Canada was approved by the Management Panel in October 1981, and drilling began in April, 1982. The drilling continued intermittently until March, 1985, by which time five holes had been drilled at three sites. Total penetration was approximately 4563 metres with an average core recovery of over 95%.

Funding for the project came from a number of agencies: The National Science and Engineering Research Council, the International Development Research Centre, Dalhousie University, Memorial University, and the University of Western Ontario (Canada); the Natural Science Research Council (Denmark); the Natural Environment Research Council and the Royal Society (United Kingdom); the National Science Foundation (United States); the Volkswagen Foundation (West Germany); King Abdul Aziz University (Saudi Arabia); and the Government of Cyprus. In all, a total of approximately Can. $1,575,000 was spent on drilling and related work and roughly equal amounts on field studies, geophysical logging, and laboratory studies.

The core recovered from the drillholes is stored in a facility provided by the Government of Cyprus in Nicosia and can be accessed with the permission of the Geological Survey Department of Cyprus. Lithological core logs were produced on site after recovery of the core and are available from ICRDG at the Centre for Marine Geology, Dalhousie University, Nova Scotia, Canada.

The ICRDG Management Panel acknowledges with thanks the support provided by the Geological Survey of Canada in publishing the Initial Report volumes as GSC Papers. Paper 85–29, Cyprus Crustal Study Project, Initial Report, Holes CY-2 and 2a, was published in 1987, and describes work on holes drilled to investigate the Agrokipia ore deposit. Paper 89–9, Cyprus Crustal Study Project, Initial Report, Hole CY-4, was published in 1989 and describes work on a deep hole drilled through the sheeted dykes and gabbros and into the ultramafic unit. This final volume on Holes CY-1 and 1A discusses holes drilled through the pillow lava succession. The volumes aim to present descriptions of the cores along with other geological, geophysical, and geochemical data. No attempt has been made to reconcile differences in interpretation between authors of papers in the volume. The papers were reviewed by the editors who are grateful to colleagues who provided external reviews. The editors gratefully acknowledge the assistance of Wendy MacIntosh in supervising the compilation of this volume.

Durant la période 1980 à 1982 les études de terrain ont débutées, les propositions concernant la recherche ont été rédigées et une approbation du projet par le gouvernement de Chypre a été obtenu. Un contrat de forage conclu avec la société Bradley Bros. à Noranda (Québec) au Canada, et les sondages ont commencé en avril 1982. Les forages ont continué de façon intermittente jusqu'en mars 1985, époque à laquelle cinq sondages avaient déja été effectués à trois endroits. La profondeur totale de pénétration était d'environ 4563 m, et le taux moyen de récupération des carottes dépassait 95%.

Le financement du projet a été assuré par un certain nombre d'organismes: le Conseil national de recherches scientifiques et technologiques, l'International Development Research Centre (Centre de recherches sur le développement international), l'université Dalhousie, l'université Memorial et l'université de Western Ontario (Canada); le Conseil de recherches des sciences naturelles (Danemark); le National Environmental Research Council et la Royal Society (R.-U.); la National Science Foundation (É.-U.); la fondation Volkswagen (Allemagne de l'Ouest); l'université King Abdul Aziz (Arabie Saoudite); et le gouvernement de Chypre. En tout, a été consacré un total d'environ 1 575 000 $ CAN aux forages et aux travaux connexes, et une quantité approximativement égale aux études de terrain, aux diagraphies géophysiques et aux études en laboratoire.

Les carottes extraites des trous de sondage sont entreposées dans une installation fournie par le gouvernement de Chypre à Nicosie, et il et possible d'avoir accès à ces échantillons avec la permission de la Commission géologique de Chypre. Des diagraphies litholoqiques des sondages one été produites à l'endroit du forage, après l'extraction des carottes, et peuvent être obtenues auprès de l'ICRDG au Centre de géologie marine (Centre for Marine Geology) de l'université Dalhousie (Nouvelle-Écosse) au Canada.

Le Comité de gestion de l'ICRDG remercie la Commission géologique du Canada qui l'a aidé à publier les volumes du Rapport initial en tant que documents GSC. Le document 85–29, l'etude de projet de la croûte de Chypre, rapport initial concernant les trous CY-2 et 2A, a été publié en 1987 et donne une description de travail sur le trou de forage profond dans les couches de dykes, gabbros et la section ultramafique. Ce dernier volume sur les trous CY-1 et 1A décrit l'ensemble des trous de forage dans les laves en coussins. Ces volumes donnent des descriptions des carottes de sondage, de même que d'autres données géologiques, géophysiques et géochimiques. On n'a pas cherché à accommoder toutes les différences d'interprétation que l'on peut noter entre articles rédigés par divers auteurs et regroupés dans ce volume. Les articles one été examinés par les rédacteurs, qui remercient leurs collègues d'avoir présenté leurs critiques. Les rédacteurs expriment leur reconnaissance à Madame Wendy MacIntosh pour l'aide qu'elle leur a prodiguée au compilation du présent volume.

ICRDG acknowledges with gratitude those agencies which have supported its research drilling programmes. Special thanks are due to Drs. G. Constantinou, A. Panayiotou, and C. Xenophontos of the Geological Survey Department, Cyprus. This project is an example of the successful cooperation between a number of national governments, the industrial sector, and the academic community.

ICRDG Management Panel
September, 1991

L'ICRDG exprime sa reconnaissance aux organismes qui ont appuyé ces programmes de forage expérimental. Les membres du comité de gestion remercient en particulier MM. G. Constantinou, A. Panayiotou et C. Xenophontos de la Commission géologique de Chypre. Ce projet est un exemple de succès de la coopération entre un certain nombre de gouvernements nationaux, le secteur industriel et la collectivité académique.

Comité de gestion de l'ICRDG
septembre 1991

Table of Contents

Holes CY-1 and 1A of the Cyprus Crustal Study Project: Background and Objectives

PAUL T. ROBINSON

Centre for Marine Geology, Dalhousie University, Halifax, Nova Scotia, Canada B3H 3J5

Robinson, P.T., 1991: Holes CY-1 and 1A of the Cyprus Crustal Study Project: background and objectives; in Cyprus Crustal Study Project: Initial Report, Holes CY-1 and 1A, eds. Gibson, I.L., Malpas, J., Robinson, P.T., and Xenophontos, C.; Geological Survey of Canada, Paper 90–20, p. 1–4, 1991.

Abstract

A 2 km-deep research borehole (CY-1) was planned as part of the Cyprus Crustal Study Project (CCSP) to sample the lavas and upper sheeted dykes of the Troodos ophiolite. This hole was spudded at the top of the lava pile in the Akaki Canyon, about 1 km north of the village of Malounda. Specific questions to be addressed included: (1) What is the structure of the extrusive section and how does it vary with depth? (2) What geochemical variations exist in the Troodos lavas? (3) How does alteration of the lavas and dykes vary with depth? (4) What is the nature of the lava-dyke transition? and (5) How do the physical and magnetic properties of the lavas and dykes vary with depth? Hole CY-1, drilled in the summer of 1982, penetrated 485 m into the lavas before being terminated due to poor hole conditions. Subsequently, an offset hole (CY-1A), was drilled in 1984 and 1985 to sample the lower part of the lavas and upper sheeted dykes. This hole penetrated 700 m before being terminated due to high water pressure. These two holes, coupled with associated field studies, provided a three-dimensional picture of the upper part of the ophiolite. Studies of the core material and field samples are detailed in the accompanying papers.

Résumé

Le trou de forage (CY-1) destinés à la recherche, a été planifié dans le cadre du projet d'étude de la croûte cypriote pour échantillonner les laves et le complexe de dykes supérieurs de l'ophiolite de Troodos. Le forage a été effectué au sommet de la pile de lave dans le canyon d'Akaki à environ 1 km au nord du village de Malounda. On s'est adressé aux questions spécifiques suivantes: (1) Quelle est la structure de la section extrusive et comment varie-t-elle avec la profondeur? (2) Quelles sont les variations géochimiques existantes dans les coulées de lave de Troodos? (3) Comment l'altération des dykes et des laves varient-elles avec la profondeur? (4) Quelle est la nature de la transition lave-dyke? (5) Comment les propriétés physiques et magnétiques des dykes et des laves varient-elles avec la profondeur? Le sondage s'est fait jusqu'à une profondeur de 485 m dans la lave pendant l'été de 1982 avant de mettre fin aux travaux CY-1 à cause des mauvaises conditions que présentaient le trou. Un trou de compensation CY-1A a donc été foré en 1984–1985 afin d'échantillonner la partie inférieure des laves et la partie supérieure du complexe de dykes. Le forage s'est fait jusqu'à une profondeur de 700 m lorsqu'on a arrêté les travaux à cause de la forte pression en eau. Ces deux trous de forage ainsi que les études sur le terrain s'y rapportant présentent un profil tri-dimensionnel de la partie supérieure de l'ophiolite. Les études du matériel brut ainsi que les échantillons prélevés sur le terrain sont présentés en détails dans les documents ci-inclus.

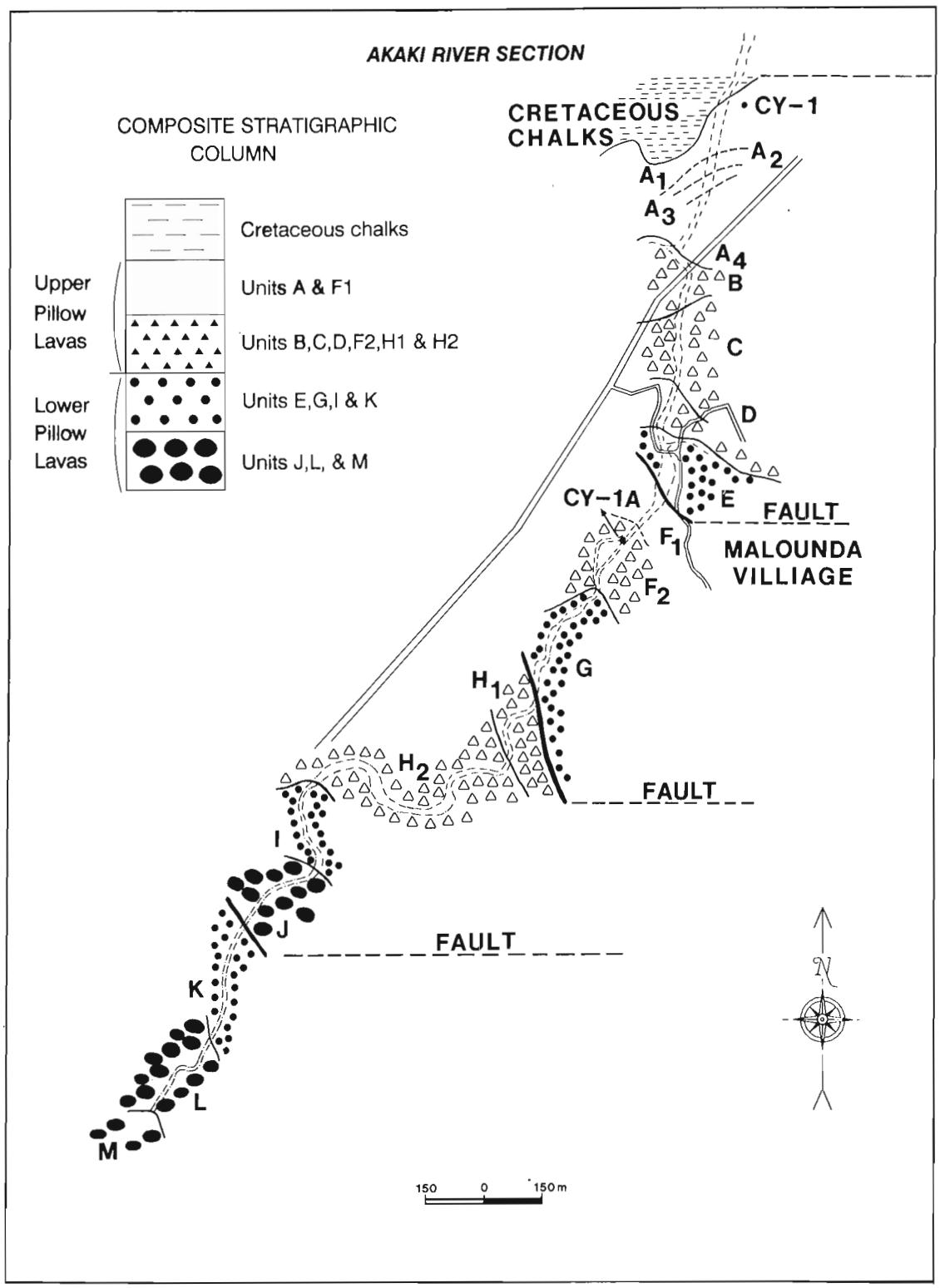

Figure 1: Generalized geologic map of the Akaki Canyon showing locations of CCSP Boreholes CY-1 and 1A (modified from Schmincke et al., 1983; Mehegan and Robinson, this volume).

INTRODUCTION

The Cyprus Crustal Study Project was a combined field and research drilling investigation of the Troodos massif of Cyprus, undertaken by the International Crustal Research Drilling Group (ICRDG). The main aims of the project were to determine the structure, petrology, tectonic environment and mode of emplacement of the ophiolite in order to evaluate the ophiolite model for oceanic crust. The research drilling was undertaken primarily as a means of recovering a complete section of the ophiolite from the top of the extrusive sequence to the underlying mantle. The domal structure of the Troodos massif suggested that the entire crustal section could be sampled in two offset holes, each about 2.5 km deep. One hole (CY-1) was planned to extend from the top of the lavas to the lower part of the sheeted dykes and the other (CY-4) was intended to sample the lower dykes and the plutonic section.

Hole CY-1, spudded at the lava-sediment contact in the Akaki Canyon north of the village of Malounda (Figure 1), penetrated 485 m into the lavas before it had to be abandoned because of hole instability. Hole CY-1A, located about 1 km south of CY-1, penetrated the lower lava section and the upper part of the sheeted dykes to a depth of 700 m before it was terminated due to high water pressure. The lower dykes and most of the plutonic section were sampled in Hole CY-4, located near the village of Palekhori (Gibson et al., 1989). Holes CY-2 and 2A sampled a stockwork zone beneath the Agrokipia ore deposit (Robinson et al., 1987). Hole CY-3 was not drilled.

Drilling in the lavas and sheeted dykes was intended to complement field studies in the area and to help answer a number of specific questions:

1. What is the structure of the lava pile and how does it vary with depth?,
2. What geochemical variations exist in the lavas and how can these be related to the lava stratigraphy?
3. Does alteration of the lavas increase systematically with depth or are there distinct alteration zones? Can the alteration be related to an axis and off-axis sequence? Holes CY-1 and 1A are located well away from any known sulphide ore deposit and were intended to sample a zone of downwelling, perhaps associated with upwelling beneath the Agrokipia ore deposit sampled in Holes CY-2 and 2A (Robinson et al., 1987).
4. What is the nature of the boundary between the lavas and the sheeted dykes? Early studies suggest that the boundary is transitional and that the dykes increase from about 50% to over 90% in a 100-m-thick interval (Gass, 1980).
5. What physical and magnetic variations can be detected in the lavas and dykes through sample measurements and downhole logging and how can these be correlated with lava stratigraphy and alteration patterns?

It was anticipated that the drilling results, combined with field studies of the volcanic rocks and sheeted dykes would provide a complete three-dimensional picture of the upper part of the ophiolite. In fact, Holes CY-1 and 1A were highly successful, with a combined penetration of nearly 1200 m and a core recovery of more than 90%. These two holes provide a nearly continuous sample of the extrusive section and of the dyke-lava boundary. Studies of the core material and adjacent field relationships, as outlined in this volume, provided answers to most of the questions posed and yielded a much better understanding of the origin and evolution of the lavas.

Site Selection

Holes CY-1 and 1A were selected on both geologic and operational criteria. Geologically, we hoped to complete all of the planned drilling in a single structural block on the northern flank of Troodos. Thus, the holes were planned to lie approximately along the trend of the sheeted dykes in an area of little structural complexity. Furthermore, Holes CY-1 and 1A were intended to lie within the downwelling zone surrounding the Agrokipia ore deposits, which were sampled in Holes CY-2 and 2A. Operational constraints included the need for a relatively flat area on which to place the drill rig, road access sufficient for heavy-duty trucks, and availability of water.

Based on the above criteria, a site for CY-1 was selected about 1 km north of the village of Malounda, just off the road linking Nicosia and Palekhori (Figure 1). The site is located in the Akaki Canyon at the boundary between the lavas and the overlying sediments. A flat area on which the rig could be placed already existed on the valley floor and water was available from the adjacent stream.

The geologic relationships at this site turned out to be roughly as expected from the study of adjacent outcrops, but drilling was more difficult than anticipated. The rubbly and unconsolidated nature of the rock led to frequent caving of the borehole walls and caused torquing and sticking of the pipe. When the pipe became irretrievably stuck at 485 m, the hole had to be abandoned.

In order to sample the remainder of the lava pile, Hole CY-1A was located about 1 km south and 400 m updip of Hole CY-1. The site was selected to provide about 50 m of stratigraphic overlap with the base of CY-1 and to sample the lower part of the extrusive section including the lava-dyke contact. This hole is also located in the Akaki Valley where water and a suitable drilling site were both available.

Operations

The drilling portion of the Cyprus Crustal Study Project began with Hole CY-1. The drill rig was shipped from Canada and arrived on site on April 22, 1982. Site preparation and assembly of the rig took a week to complete, and drilling commenced on April 29th.

Because the hole was planned to go to a depth of 2–3 km, the initial drilling was done with HQ rod, producing a hole

about 96 cm in diameter. Some torquing of the drill string was experienced but the early drilling proceeded smoothly. However, after about a week, hole conditions worsened significantly and the bit became stuck. Casing was reamed down around the drill rod and drilling continued. Drilling and coring continued until June 3rd, at which time unstable hole conditions and slippage of the casing forced termination of the hole at 474.88 m. The average rate of penetration was just under 15 m / operational day, including time spent in reaming casing. The rocks were highly brecciated and recovery was only 92%, the lowest of the five holes drilled in Troodos.

After termination of Hole CY-1, the ICRDG Steering Committee decided to proceed with the other drilling objectives, particularly sampling a stockwork zone beneath an ore deposit (Holes CY-2, 2A) and sampling the plutonic section of the ophiolite (Hole CY-4) before drilling deeper in the lavas. These objectives were achieved in 1983 and 1984.

Upon completion of Hole CY-4 in the summer of 1984, the drill rig was moved back to the Akaki Canyon to drill Hole CY-1A, an extension of Hole CY-1. Site preparation began on July 23, 1984 and was completed on July 30th, at which time drilling commenced. Again, the hole was started with HQ rod. Later, the HQ rod was cemented in place as casing and drilling continued with NQ rod. Drilling continued successfully at this site until September 6, 1984, at which time work was suspended for financial reasons. Drilling resumed on February 20, 1985 and continued for about a week. At a depth of 700.19 m, the bit encountered very high water pressures, forcing termination of the hole on February 28, 1985. After removal of the rod and casing, the hole was capped and abandoned. The rig was then dismantled, packed in containers and shipped back to Canada.

The average penetration rate in Hole CY-1A, including reaming of casing, was about 17 m / day with an average core recovery of 94.5%. Recovery was lowest in the upper parts of the hole and improved as more massive dyke rocks were encountered at depth.

Core Description

The core recovered from Holes CY-1 and 1A was washed, reassembled and marked with an orientation line indicating the 'up' direction. A continuous orientation line was used to indicate pieces that could be fitted together and aligned relative to one another. Where pieces could not be fitted together a terminating mark was used to indicate a gap in the core. After alignment, the depth was marked on the core in centimetres, extrapolated between drilling markers, which were usually placed in the core at 15-foot intervals.

A visual representation of each 1.5-m-long core section was drawn on a core sheet and cooling units were identified and described. Individual units were recognized on the basis of cooling breaks, marked changes in grain size, lithology or mineralogy or by changes in degree or type of alteration. During description of the core, units were number sequentially down the hole. The unit numbers designate the core box in which the unit first appears.

After checking and editing, the core descriptions were printed, bound and distributed to interested parties. Copies of these are available from the International Crustal Research Drilling Group, Centre for Marine Geology, Dalhousie University, Halifax, Nova Scotia, Canada. The individual cooling units recognized in the core were later grouped into larger scale lithologic units. These are presented in the papers on lithologic descriptions of Holes CY-1 and CY-1A (this volume).

REFERENCES

Gass, I.G.

1980: The Troodos massif: its role in the unravelling of the ophiolite problem and its significance in the understanding of constructive plate margin processes; *in* Panayiotou, A., Ophiolites: proceedings of the International Ophiolite Symposium, Cyprus, 1979, Cyprus Geological Survey Department, Nicosia, p. 23–35.

Gibson, I.L., Malpas, J., Robinson, P.T., and Xenophontos, C., eds.

1989: Cyprus Crustal Study Project: Initial Report, Hole CY-4, Geological Survey of Canada, Paper 88–9, 393 p.

Robinson, P.T., Gibson, I.L., and Panayiotou, A., eds.

1987: Cyprus Crustal Study Project: Initial Report, Holes CY-2 and CY-2A, Geological Survey of Canada, Paper 85–29, 381 p.

Schmincke, H.-U., Rautenschlein, M., Robinson, P.T., and Mehegan, J.M.

1983: Troodos extrusive series of Cyprus: a comparison with oceanic crust; Geology, v. 11, p. 405–409.

Cyprus Crustal Study Project Hole CY-1: Lithologic Unit Summaries

P.T. ROBINSON[1], I.L. GIBSON[2], AND L.V.-B. HORNE[1]

[1]Centre For Marine Geology, Dalhousie University, Halifax, Nova Scotia, Canada
[2]Department of Earth Sciences, University of Waterloo, Waterloo, Ontario, Canada

Robinson, P.T., Gibson, I.L., and Horne, L.V.-B., Cyprus Crustal Study Project Hole CY-1: lithologic unit summaries; in Cyprus Crustal Study Project: Initial Report, Holes CY-1 and 1A, eds. Gibson, I.L., Malpas, J., Robinson, P.T., and Xenophontos, C.; Geological Survey of Canada, Paper 90–20, p. 5–16, 1991.

Abstract

Hole CY-1 is located at Lat. 35°02′54″N; Long. 33°10′46″E in the Akaki Canyon, on the north side of the Troodos ophiolite, Cyprus. CY-1 was drilled to a depth of 474.88 m. Core recovery was 92%. Cooling units have been grouped into thirty major lithologic units, varying in thickness from 1.37 m (Unit XXIV) to 54.89 m (Unit VIII). For each of these major units, the following information is given: the position and nature of the upper and lower contact, the unit thickness, the dominant lithology, and the identification numbers of the cooling units grouped within the major lithologic unit. For each major lithologic unit, this heading is followed by a description detailing the lithology, texture, alteration mineralogy, and major megascopic features.

Résumé

Le trou de forage CY-1 est situé à une Lat. 35°02′54″N, et une Lon. 33°10′46″E dans le canyon d'Akaki sur le côté nord de l'ophiolite de Troodos, Chypre. Le forage a atteint une profondeur de 474,88 mètres. La récupération fut de 92%. Les unités de refroidissement ont été groupées en trente unités lithologiques principales, dont l'épaisseur varie entre 1,37 m (Unité XXIV) et 54,89 m (Unité VIII). Pour chacune de ces unités majeures, on donne les renseignements suivants : la position et la nature du contact supérieur et inférieur, l'épaisseur de l'unité, la lithologie dominante, et les numéros d'identification des unités de refroidissement groupées dans l'unité lithologique majeure, et ce renseignement est suivie d'une description détaillée de la lithologie, de la texture, de la minéralogie d'altération et des principaux aspects mégascopiques.

Site Data

Location:	Lat. 35°02′54″N, Long. 33°10′46″E
Date occupied:	22 April 1982
Drilling started:	29 April 1982
Drilling ended:	03 June 1982
Date departed:	14 June 1982
Depth drilled:	474.88 m
Recovery:	92%
Lithology:	Pillowed and massive lava flows

Unit I

Upper contact:	11.90 m, ambiguous
Lower contact:	23.80 m, depositional
Thickness:	11.90 m
Lithology:	Pillowed lava
Cooling units:	1.01 to 3.13

The top of the unit is taken arbitrarily at the first coherent material in the core; the base is marked by about 10 cm of light-greyish-red, fine-grained, thinly bedded sediment between 23.70 and 23.80 m. The unit is a light-grey or greyish-brown to greyish-red, fine-grained, aphyric to very sparsely phyric, pillowed basalt. Pillow margins are composed of fragmented glassy material which is completely replaced by green smectite and white carbonate. Some thin layers of sedimentary(?) carbonate occur at pillow margins. The basalts are non-vesicular to sparsely vesicular near pillow margins; vesicles are irregular, 1–3 mm across, and filled with smectite and carbonate. Olivine phenocrysts are mostly rare (<1%), but a few pillow centres (e.g. at 23.00 m) are picritic with 15–20% phenocrysts. The olivine crystals are 1–7 mm across, subhedral, and completely altered to red-brown smectite and iron oxides. Pillow centres are light grey to reddish grey with red staining permeating inward from pillow margins. The rock is abundantly veined in an irregular pattern; most veins are 1 mm to 1.5 cm wide and filled with white carbonate and zeolite. A few thicker veins, particularly at pillow margins, appear to be carbonate sediment.

Unit II

Upper contact:	23.80 m, depositional
Lower contact:	46.10 m, depositional
Thickness:	22.30 m
Lithology:	Pillowed lava and breccia
Cooling units:	3.14 to 8.03

Unit II consists of 4.05 m of volcanic breccia (Subunit IIa) overlying 18.25 m of fine-grained, sparsely phyric, pillowed basalt (Subunit IIb).

Subunit IIa (23.80–27.85 m) (cooling unit 3.14) is a reddish-brown to greenish-grey volcanic breccia. The breccia consists of angular fragments of fine-grained, aphyric basalt, 1–6 cm across, in a matrix of altered glass fragments and small pieces of crystalline material. The lithic fragments are light grey to reddish grey and mostly altered. Altered glassy fragments are green to brown, often with concentric structures. Fragments are non-vesicular to very sparsely vesicular. Veins are mostly narrow, 1–2 mm wide, rarely up to 5 mm. Most veins occur in altered glass zones and are filled with light-green clay minerals or carbonate.

Subunit IIb (27.85–46.10 m) (cooling units 4.01 to 8.03) is a light-grey, to greenish-grey, fine-grained, aphyric to sparsely olivine-phyric, pillowed basalt with minor breccia. Phenocrysts (1–2%) are irregularly distributed, 1–2 mm across, subhedral, and altered to clay minerals and carbonate. In the interval between 38.00 and 41.50 m, phenocrysts make up 3–5% and are up to 6 mm across. Vesicles are mostly sparse and small, and most abundant just inside pillow rinds. Here, irregular vesicles, mostly 1–2 mm in diameter, make up to 2% of the rock and are filled chiefly with carbonate. Pillow rinds consist of green fragments of altered glass in a carbonate and zeolite(?) matrix. Veins comprise 15–20% of the pillow rinds and are up to 1 cm across; elsewhere they are less abundant (1–2%), 1–3 mm wide, and filled mostly with carbonate. Some pillow margins have small slickensided surfaces. Groundmass alteration is moderate and consists mostly of brown staining just inside of the glassy rinds. Small altered olivine crystals often give the rock a somewhat mottled appearance. The basal 0.50 m of the subunit (cooling unit 8.03) consists of a red-brown breccia composed of angular fragments of sparsely olivine-phyric basalt, 2 mm to 5 cm across, in a matrix of comminuted basalt containing some small patches of green, altered glass.

Unit III

Upper contact:	46.10 m, depositional
Lower contact:	71.00 m, depositional
Thickness:	24.90 m
Lithology:	Pillowed lava
Cooling units:	8.04 to 13.14

This unit is a light-grey to reddish-grey, moderately to highly phyric, pillowed lava. About 50 cm of breccia at the top are composed of green fragments of altered glass in a matrix of carbonate. The remainder of the unit is pillowed basalt with an average pillow thickness of about 0.5 m. Pillow margins are marked by altered, often brecciated, glassy rinds, usually 2–3 cm thick, but up to 10 cm thick. Glassy rinds are completely altered to green clay minerals and minor white carbonate. Altered glass often has concentric structures preserved. Phenocrysts (5–25%) are chiefly olivine and clinopyroxene. Olivine grains, 2 mm to 2 cm in diameter, are subhedral, and are altered to iron oxides and clay minerals. Clinopyroxene phenocrysts, 1–3 mm in diameter, are anhedral, fresh, green, and glassy. Spinel occurs as minute inclusions in olivine and as rare, euhedral microphenocrysts. Phenocrysts are variably distributed and are most abundant in pillow centres, some of which are picritic. Vesicles vary from 1–5% and are usually most abundant in pillow centres. Here they are 1–2 mm across, round to irregular, and filled with carbonate or clay minerals. Veins are common, irregularly spaced, mostly 1–5 mm wide, and filled with white carbonate. Rare vugs up to 5 cm across are lined and filled with euhedral calcite crystals. Overall, the groundmass is only weakly altered and is less oxidized than in the overlying cooling units. The groundmass is medium-grained with some clinopyroxene and plagioclase needles visible under the hand lens.

Unit IV

Upper contact:	71.00 m, depositional
Lower contact:	88.35 m, depositional
Thickness:	17.35 m
Lithology:	Pillowed lavas and breccias
Cooling units:	14.01 to 18.02

Unit IV comprises a series of light-grey to reddish-grey, sparsely to moderately phyric, pillowed lavas and thin volcanic breccias, divided into three subunits.

Subunit IVa (71.00–77.62 m) (cooling units 14.01 to 15.07) is a light-grey to reddish-grey, moderately olivine-phyric, pillowed basalt with a thin (20 cm) zone of coarse-grained, poorly sorted breccia at the top. The average thickness of pillows is 0.5 m (range 10–80 cm). Glassy pillow margins are altered to a bright-green layer silicate with reddish-brown alteration halos grading inward. Pillow cores are light brownish grey. Thin zones of glassy fragments in a clay-carbonate matrix are common. Phenocrysts range from 5–15% of the rock and are concentrated in pillow centres. They are chiefly olivine crystals, 1–5 mm across, altered to reddish-brown clay minerals and iron oxides. The largest crystals show evidence of settling. The subunit is moderately vesicular, with vesicles concentrated at the tops of pillows. Vesicles, 1–6 mm in diameter, are filled with white carbonate and lined with black clay minerals. Some vesicles are open. Irregular fractures are filled with calcite. The groundmass is aphanitic to fine grained, and relatively fresh.

Subunit IVb (77.62–80.17 m) (cooling units 15.08 to 16.04) is a volcanic breccia grading downward into a pillow lobe breccia. The fragments are aphyric to sparsely olivine-phyric, and are set in a carbonate-clay matrix. They are petrographically the same as the pillows of subunit IVa. Cooling unit 16.02 (78.91 to 78.95 m) is a thin, aphyric dyke with green altered glassy margins and a fresh interior.

Subunit IVc (80.17–88.35 m) (cooling units 16.05 to 18.02) is a light-grey, sparsely phyric, pillowed lava with about 80 cm of volcanic breccia at the base. Individual pillows range from 30 cm to 1 m in diameter. Pillows are generally aphyric and altered but some fresh glass is present in the chilled margins. The subunit is cut by numerous calcite veins 1–2 cm wide. The breccia consists of fragments of aphyric basalt and altered glass in a finer-grained matrix containing calcite and clay.

Unit V

Upper contact:	88.35 m, depositional
Lower contact:	114.90 m, depositional
Thickness:	26.55 m
Lithology:	Massive basalt flows
Cooling units:	18.03 to 23.01

Unit V is a composite unit composed of three massive lava flows, one of which has thin pillowed sequences at the top. Each of the massive lava flows exhibits a marked concentration of olivine at or near its base. Three subunits are recognized on the basis of the massive flows.

Subunit Va (88.35–96.33 m) (cooling unit 18.03) consists of a massive lava flow. The flow depositionally underlies the pillows of Unit IV without a clear chill zone, but the lower contact of the flow is marked by minor altered glass and carbonate-cemented breccia. The flow is brownish-grey at the top, gradually becoming darker grey at 95.20 m and then dark brownish-grey at 96.00 m. Phenocrysts of olivine make up about 5% of the upper part of the subunit, and have a maximum size of 1 mm. Olivine is absent in the interval between 90.00 and 90.50 m but then increases rapidly in size and abundance below 95.20 m. In the most porphyritic part of the flow at 96.00 m, olivine comprises about 60% and has a maximum size of 1 cm. It decreases again to about 5% in the bottom chill zone where it has a maximum diameter of about 5 mm. All of the olivine is altered to clay minerals and iron oxides. Sparse crystals of fresh clinopyroxene, up to 2 mm across, are present throughout but are most obvious

in the olivine-poor zones. Vesicles comprise about 10% of the rock at the top of the subunit, increasing to about 15% between 90.00–90.50 m, and thereafter decreasing to 5% at 95.00 m and to less than 1% in the most prophyritic section. They increase again to about 10% at the very base of the subunit. The maximum vesicle size varies from about 1 mm in the upper and lower parts of the flow to about 5 mm between 90.00 and 90.50 m. The vesicle filling is carbonate. Minor thin veinlets occur throughout and several unusually persistent longitudinal carbonate- and clay(?)-filled veins occur between 88.60–89.50 m, 90.70–91.20 m, 91.60–92.60 m, and 93.30–96.00 m. Altogether, the veins total about 2% of the rock and have a maximum thickness of 1 cm. Thin veins are filled with carbonate, but thicker veins appear to be filled chiefly with clay minerals accompanied by minor amounts of carbonate, mostly as tiny stringers within the clays.

Subunit Vb (96.33–111.62 m) (cooling units 20.01 to 21.01) is a massive basalt flow with a pillowed top. The upper 2.19 m of subunit Vb consist of sparsely olivine-phyric pillows with green altered glassy rinds, locally separated by altered glass breccia with a carbonate matrix. The pillows have 5–10% vesicles with a maximum diameter of about 4 mm. They are filled chiefly with carbonate and minor clay. Underlying the pillows is a single massive basalt flow, about 13 m thick, displaying marked olivine accumulation in the lower part. The upper 10 m of the flow are brown to reddish-brown, medium-grained, aphyric basalt. In the lower 3 m olivine phenocrysts are abundant, increasing from about 2% at 109.30 m to 15% at 110.70 m, and then decreasing again to zero at about 110.00 m. The maximum size of the crystals is about 4 mm. All of the olivine is altered to clay minerals and iron oxides. Minor spinel forms inclusions in some of the olivine crystals. Vesicles are present throughout but occur in irregular zones, some of which are parallel to the core axis; the largest and most abundant vesicles occur near the top of the subunit. From 98.60 to 102.20 m vesicles comprise up to 15% of the rock and have a maximum size of 3 mm; below 102.20 m the vesicles decrease to about 5% and the size decreases to an average of 1 mm or less. About half of the vesicles are filled with carbonate and sparse zeolites, and some open vesicles are lined with bluish-grey clay. Veins average about 5% of the core and have a maximum width of 1.5 cm. Vein fillings are dominantly carbonate, with minor clay(?) and zeolites. Excellent dog-tooth spar occurs in a cavity at 118.50 m. Locally, pervasive carbonate alteration occurs in the groundmass.

Subunit Vc (111.62–114.90 m) (cooling unit 23.01). Subunit Vc is a massive lava flow, 3.28 m thick, with a thin autobrecciated zone at the top. This greyish-green, medium-grained basalt contains sparse clinopyroxene and altered olivine phenocrysts, which generally comprise less than 1%, but up to 30% in the lower 20 cm of the flow. Vesicles increase in abundance upward and generally make up about 2% of the subunit. They are filled mainly with calcite and white zeolite. The basalt is cut by veins 1 to 3 mm wide which comprise about 5% of the unit. Many have colour variations suggesting several stages of calcite deposition. The groundmass of the rock appears to be moderately altered to brown limonite.

Unit VI

Upper contact:	114.90 m, depositional
Lower contact:	158.60 m, depositional
Thickness:	43.70 m
Lithology:	Pillowed lava and minor sediment
Cooling units:	23.02 to 31.03

Unit VI is a thick sequence of pillowed lavas with a thin sediment layer at the base. The unit is divided into four subunits based on various features such as colour, cooling rind thickness, mineralogy, and lithology.

Subunit VIa (114.90–130.55 m) (cooling units 23.02 to 26.04) consists of buff-coloured, sparsely to highly phyric pillowed lavas. Pillow margins consist of fractured glass and glassy breccia cemented by carbonates. The glass is completely replaced by dark green layer silicates and minor carbonate. The rocks are variably olivine phyric (1–5%) with major olivine accumulation near the base of the largest pillow (121.50–121.70 m). Olivine crystals are generally less than 2 mm across but can be up to 10 mm. All olivine is replaced by clay minerals and iron oxides. The groundmass is glassy to aphanitic at pillow margins, and fine grained in pillow interiors. Vesicles comprise 0–20% of the rock, are 0.5–3 mm across, and are subspherical to subangular. They are normally concentrated just below the upper pillow margins, but there are also thinner vesicle-rich zones just above the lower margin. Vesicles are lined or infilled by clays and carbonates. Veins comprise from 1 to 20% of individual pillows, are 1–5 mm wide, and are filled with clay minerals, zeolites, and carbonate. Some oxidation along the veins has produced reddening of vein material and iron oxide-rich patches in the adjacent rock.

Subunit VIb (130.55–138.30 m) (cooling units 26.05 to 27.07) consists of medium-grey, fine-grained, aphyric to very sparsely olivine-phyric, pillowed lavas. The pillow margins are marked by chilled, fine-grained zones and thin layers of green altered glass. The glassy rinds are much thinner (average 1 cm) than on pillows above and below. The average pillow thickness is about 0.5 m. Olivine phenocrysts comprise less than 1% of the rock, range from 1 to 2 mm in diameter, and are altered to reddish-brown clay minerals and iron oxides. Vesicles comprise 1 to 3% and are most abundant in the upper one-third of each pillow. They range from 1 to 3 mm across, are sub-spherical, and filled with white carbonate. The rock is coherent but is cut by many narrow veins, hairline to 3 mm wide, which are filled with white carbonate. A few larger veins and vugs are lined with euhedral crystals of carbonate and zeolite. One glassy pillow rind from 135.80 to 136.09 m is brecciated, with fragments of green altered glass

in a carbonate matrix. One thick vein at 137.70 m has altered glass fragments in a carbonate matrix. At 137.30 m and 137.60 m large veins or vugs are filled with reddish-brown carbonate that looks somewhat like sediment.

Subunit VIc (138.30–157.80 m) (cooling units 28.01 to 31.02) is a brownish-grey, fine-grained, very sparsely olivine-phyric, pillowed lava unit with a brecciated top (138.60–138.98 m). Pillow margins are much thicker (1–4 cm) than those in the preceding subunit and they have bleached to reddish-brown alteration halos with pronounced spherulitic textures. Individual pillows range from 0.3 to 1.3 m in thickness and average about 0.5 m. The groundmass has a mottled appearance in some pillows. Vesicles range from 1 to 3% of the rock and are concentrated generally near the tops of individual pillows although some occur in pillow centres. Most vesicles are 2 to 4 mm across and are partly filled with white carbonate. Veins comprise 2 to 5% of most pillows, are irregular, and are filled with calcite. Near relatively thick pillow margins (1.5 cm), the veins are filled with a white secondary mineral. Several 1- to 4 cm-thick veins consist of altered glass fragments in a matrix of carbonate, clay, zeolite, and silica. The pillows are less coherent than in the preceding subunit.

Subunit VId (157.80–158.60 m) (cooling unit 31.03) is a poorly recovered, 80 cm-thick layer of coarse-grained, reddish-brown, poorly bedded sediment.

Unit VII

Upper contact:	158.60 m, depositional
Lower contact:	177.51 m, depositional
Thickness:	18.91 m
Lithology:	Pillowed lava
Cooling units:	31.04 to 35.01

Unit VII consists of a sequence of brownish-grey, aphyric to sparsely olivine-phyric, pillowed lavas with abundant interpillow sediment in the lower third (172.80–177.51 m). Pillows range in vertical thickness from 2.5 to 0.3 m and have an average size of 0.45 m. The pillows have an aphanitic to fine-grained groundmass which is slightly mottled and which contains brown, irregularly-shaped clay patches. A large 2.5-m-thick pillow is olivine phyric with a medium-grained groundmass. Pillow margins are generally thick (2–10 cm) and contain glass fragments altered to green clay, along with calcite, gypsum(?), and black sedimentary material. The pillow margins have reddish-brown alteration halos. At 169.10 m a yellowish-white carbonate sediment is present in an inter-pillow area. Reddish-brown inter-pillow sediment consists of fine-grained clayey material and medium- to coarse-grained volcanic breccia with small black fragments in a carbonate matrix. Pillow interiors are coherent with about 10% round vesicles, many of which are lined with blue and brown smectite and partly filled with calcite. Veins comprise about 2% of the unit and range from 1 to 5 mm wide. Most are filled with calcite.

Unit VIII

Upper contact:	177.51 m, depositional
Lower contact:	232.40 m, depositional
Thickness:	54.89 m
Lithology:	Pillowed lavas cut by several thin dykes
Cooling units:	35.02 to 44.08

Unit VIII is a thick sequence of slightly olivine-phyric, pillowed lavas with 1- to 3 cm-thick pillow margins. The rocks are buff-coloured at the top of the unit from 177.51 to 195.20 m, then slate-grey in colour to 224.50 m, and finally buff-coloured again to the bottom of the unit at 232.40 m. Sparse olivine phenocrysts, ranging from 1 to 7 mm across, occur irregularly throughout the unit and are locally concentrated in the lower parts of individual pillows. In total, the olivine phenocrysts comprise considerably less than 1% of the unit. Green, glassy clinopyroxene phenocrysts comprise less than 1% and are sparsely distributed throughout the unit. They average about 1 mm across and are rarely visible megascopically. Vesicles make up about 2 to 3% and are concentrated in the upper parts of pillows. They have a maximum diameter of about 8 mm but most are less than 3 mm across. They are generally filled with carbonate but many are open. White, carbonate-filled net veining is present throughout the unit generally forming about 2 to 3 % of the core. A brownish spotting also occurs throughout the unit, particularly around clusters of small, discrete vesicles. The walls of the brown spots are generally gradational into the surrounding rock, as opposed to those of the vesicles, suggesting that the alteration spread into the host rock from the spot centre. Some of these may be segregation vesicles with a higher iron content than the rock as a whole. The lower buff-coloured (oxidized?) part of the unit contains a number of friable breccia zones, one or two of which may be sedimentary in origin although composed totally of volcanic materials. The most notable of these occur between 227.10–227.40 m, 230.25–231.19 m, and 231.60–232.40 m. The dykes occur in the following intervals: 188.25–188.64 m (cooling unit 37.01), 189.33–189.97 m (cooling unit 37.04), 201.23–201.53 m (cooling unit 39.05), 204.01–204.87 m (cooling unit 39.12), 206.37–207.15 m (cooling unit 40.03), and 207.55–207.78 m (cooling unit 40.05). These dykes are composed of very-fine-grained aphyric basalt and average about 50 cm in vertical thickness. Most are inclined to the core axis at angles of about 45 to 50 degrees. The dykes generally have narrow chill zones without glass and most are weakly vesicular.

Unit IX

Upper contact:	232.40 m, depositional
Lower contact:	246.60 m, depositional
Thickness:	14.20 m
Lithology:	Massive lava flows
Cooling units:	45.01 to 47.03

Unit IX consists of four massive, aphyric, basaltic flows, the thickest of which is cooling unit 45.01. The flows are light grey to brownish grey in the upper parts, becoming darker grey toward the base of the unit. The grain size is greatest in the centres of cooling units and decreases to less than 0.5 mm in the chilled margins. Irregular fine-grained 'schlieren' are randomly distributed within the coarser-grained zones. Individual flows have small vesicles throughout, but become increasingly vesicular toward their tops. Vesicles have a maximum size of about 5 mm and average about 1 mm. Except in cooling unit 47.01, 60 to 80% of the vesicles are carbonate filled; in 47.01, about 80% are open, but here they are usually lined with blue-green celadonite. Orange gmelinite occurs in the centres of some vesicles in cooling unit 47.02. Very thin veinlets occur throughout the unit, but their number and thickness increase in the upper parts of individual flows. Veins are sparse between 235.20 and 243.30 m and absent between 238.00 and 240.30 m. The maximum thickness of veins is about 1 cm. Most are filled with carbonate but zeolites and gypsum also occur in the central parts of some veins. No obvious alteration occurs in the wall rocks adjacent to veinlets. The groundmass is locally weakly-altered to layer silicates and carbonate, and the glassy flow margins are replaced by green clay minerals.

Unit X

Upper contact:	246.60 m, depositional
Lower contact:	257.70 m, depositional
Thickness:	11.10 m
Lithology:	Pillowed lava
Cooling units:	48.01 to 50.03

About 11 m of weakly and irregularly olivine-phyric, buff to reddish-grey or light-grey, pillowed basalt make up Unit X. Pillow rinds are moderately thick (1–4 cm) and consist of dark green smectite and pale grey clays(?). One 7 cm-thick layer of altered and highly friable hyaloclastite occurs between 248.13 and 248.20 m. Olivine phenocrysts average about 1% of the pillow lavas, and are generally less than 2 mm long. All are altered to clay minerals and iron oxides. Vesicles average 2 to 3% of the entire unit but are concentrated near the tops of pillows, where they may make up 10 to 15% of the rock. Vesicles average about 1 mm in diameter but range up to 3 mm. About half of them are empty; the remainder are filled with white carbonate. Net veining is moderately abundant, averaging 5 to 7% of the rock. The veins are filled with carbonate, minor clay minerals, and gypsum. Brown spotting in the groundmass is present throughout. It is evidently related to vesicles but individual spots have gradational boundaries with the enclosing rock.

Unit XI

Upper contact:	257.70 m, depositional
Lower contact:	260.85 m, depositional
Thickness:	3.15 m
Lithology:	Pillow lobe breccia
Cooling units:	50.04 to 50.06

Unit XI is a pillow lobe breccia largely consisting of smoothly rounded lava masses ranging from 5 to about 20 cm in vertical thickness. Most of the lobes have chilled surfaces but some are fractured such that they are only partially surrounded by a chilled margin. The groundmass consists of altered glass fragments and some angular lithic fragments with intersticies filled with white carbonate. Vesicularity in the pillow lobes is very low with infrequent vesicles distributed in layers parallel to the chilled margins.

Unit XII

Upper contact:	260.85 m, depositional
Lower contact:	309.50 m, depositional
Thickness:	48.65 m
Lithology:	Pillowed lava
Cooling units:	50.07 to 59.03

Nearly 50 m of dark grey, aphyric to very sparsely olivine-phyric, pillowed basalt comprise unit XII. Pillow margins have thin glassy rinds but are commonly marked by broad zones of incipient crystallization where spherulitic nucleation takes place over distances of up to 3 to 4 cm. Olivine phenocrysts occur only between 282.70 and 286.63 m where they form a maximum of about 2%. The groundmass is fine grained and lacks the mottling that is so prevalent in overlying units. Vesicularity is moderate, generally less than 5%, but up to 15% in the upper parts of thick pillows. The average maximum vesicle size is about 3 mm. Less than half of the vesicles are filled with calcite; most of the remainder are empty. Net veining is generally thin and spidery, comprising 2–3% of the unit overall. Most veins are filled with carbonate but some contain minor gypsum. One 10 cm-thick gypsum vein occurs at 262 m. Analcite-lined vugs occur at a few places. Between 272.80 and 273.83 m, the pillows of unit XII are cut by a dyke (cooling unit 53.01) of pale grey, aphanitic basalt containing olivine phenocrysts and megacrysts up to 2 cm long along both margins. No phenocrysts occur in the dyke centre.

Unit XIII

Upper contact:	309.50 m, depositional
Lower contact:	329.60 m, depositional
Thickness:	20.10 m
Lithology:	Massive and pillowed lava flows
Cooling units:	60.01 to 61.03

Unit XIII is composed predominantly of three massive flows with two thin intercalations of pillowed material. The stratigraphic divisions are at the following levels:

Massive flow	309.50–312.95 m (Unit 60.01)
Pillowed member	312.95–314.20 m (Units 60.02 to 60.04)
Massive flow	314.20–317.40 m (Unit 61.01)
Pillowed member	317.40–317.96 m (Unit 61.02)
Massive flow	317.96–329.60 m (Unit 61.03)

The massive flows are dark grey, aphyric, and highly vesicular (15–20%) in their upper parts. The lowest of the massive flows is coarse grained in a zone about 2–6 m from the base whereas the upper two flows and the remainder of the lowest flow are fine- to medium-grained. The lowest flow has distinct flow layering within about 1 m of its base. The layering is due to colour variations and to vesicle stringers lying at an angle of about 25 to 30 degrees to the core axis. Vesicles in the massive flows have an average maximum diameter of 7–8 mm and less than a quarter are filled. The fillings appear to be predominantly gypsum with lesser amounts of calcite. The pillow lavas are also fine grained, aphyric, and dark grey. Some pillow margins show relatively wide zones of spherulitic nucleation. Vesicles comprise 5 to 10% of these lavas and they are most abundant in the upper parts of individual pillows. They are partly filled with calcite and rare gypsum. Veins in general are thin and form less than 1% of the unit. Gypsum predominates in the thicker veins and carbonate in the thinner ones.

Unit XIV

Upper contact:	329.60 m, depositional
Lower contact:	335.20 m, depositional
Thickness:	5.60 m
Lithology:	Pillowed lava
Cooling units:	64.01 to 65.01

Unit XIV consists of about 6 m of fine-grained, aphyric, basaltic, pillowed lava. Individual pillows average 0.5 m in vertical thickness, and have broken and altered glassy rinds, usually less than 1 cm wide. There is very little inter-pillow breccia. Vesicles average 3% but are concentrated in the upper parts of pillows where they may be up to 10% by volume. They have a maximum size of 5 mm and average about 1 mm. About 80 to 90% are empty and unlined; the remainder are filled with carbonate. A few hairline fractures are present, but veins are essentially absent. In the spaces between pillows, glassy fragments are altered to green clay minerals and surrounded by minor carbonate and selenite.

Unit XV

Upper contact:	335.20 m, depositional
Lower contact:	348.70 m, depositional
Thickness:	13.50 m
Lithology:	Massive lava flows and pillows cut by several dykes
Cooling units:	65.02 to 67.06

Unit XV consists of two thick massive lava flows and two thinner units that may be pillows. All of the lavas consist of dark grey to dark brownish-grey, fine-grained, aphyric basalt. The two major flows are in the intervals from 335.20–338.74 m and 339.85–344.45 m. Small dykes cut the flows between 336.78–337.18 m (cooling unit 65.03), 346.85–346.90 m (cooling unit 67.02), and 347.10–347.90 m (cooling unit 67.04). The lava flows are vesicular throughout except at the margins. Vesicles average about 10% but some zones in the massive flows have up to 30% vesicles. The zones of high concentration are not always at or near the tops of individual flows. These highly vesicular zones are also coarser-grained than the average, with feldspar microlites up to 1 mm long. The vesicles average about 1 mm but range up to 5 mm across. About 70% of the vesicles are empty; the remainder are filled with carbonate. Veins are very rare with only ten recorded in the entire 13.50 m-thick unit. Most are hairline veinlets but a few are up to 3 mm wide. Carbonate and selenite are the common fillings. Most glass is altered to dark green clays, but there is some relatively fresh glass at 339.10 and 347.00 m. Minor jasper occurs at 338.80 m. The dykes are narrow, inclined bodies having vertical thicknesses in the core from 0.05 to 0.80 m. They are fine-grained, aphyric, generally non-vesicular bodies with sharply chilled margins.

Unit XVI

Upper contact:	348.70 m, depositional(?)
Lower contact:	369.00 m, depositional
Thickness:	20.30 m
Lithology:	Pillowed lavas cut by two dykes
Cooling units:	67.07 to 71.10

Unit XVI consists of about 20 m of light-grey, fine- to medium-grained, aphyric, pillowed lavas cut by dykes at the intervals between 352.60–352.69 m (cooling unit 68.06) and 360.45–360.60 m (cooling unit 70.05). Individual pillows average 0.55 m in vertical thickness, and have glassy margins 1–2 cm thick. Fresh glass is preserved in cooling unit 67.07 between 348.70 and 349.15 m; the remainder of the glass is altered to smectite and minor zeolite(?). There is little glassy inter-pillow breccia. Vesicles range from 0 to 10% and have a very irregular distribution, being most abundant in the centres and upper parts of cooling units. The vesicles average about 1 mm across but range from 0.5 mm up to vug-like cavities 2 cm or more across. The vesicles are typically open but lined

with clay minerals accompanied by minor heulandite and gypsum. Veins comprise less than 1% of the unit and are hairline fractures filled with zeolite and gypsum. The groundmass is moderately fresh except in highly vesicular zones where it is soft, and presumably replaced by smectite. The dykes are small bodies, 0.09–0.15 m in vertical thickness. They are fine-grained, aphyric, non-vesicular, relatively fresh bodies with sharply chilled margins.

Unit XVII

Upper contact:	369.00 m, depositional
Lower contact:	370.50 m, depositional
Thickness:	1.50 m
Lithology:	Clastic material
Cooling unit:	71.11

Unit XVII consists of 1.50 m of volcanic sedimentary material composed of blocky, irregular fragments of fresh and altered glass, 1–5 mm across, in a silty matrix. The rock is very poorly bedded, poorly sorted, light grey, and moderately indurated. There are no veins. Altered glassy material is soft, possibly replaced by smectite.

Unit XVIII

Upper contact:	370.50 m, depositional
Lower contact:	387.48 m, depositional
Thickness:	16.98 m
Lithology:	Massive lava flows cut by two dykes
Cooling units:	72.01 to 73.02

Two massive flows of light-grey, fine- to medium-grained, aphyric basalt make up Unit XVIII. The flows are cut by an olivine-phyric dyke between 375.67 and 376.20 m (cooling unit 73.01) and by an aphyric dyke between 372.95 and 373.15 m (cooling unit 72.02). No chill zone was recovered from the top of the unit but a glassy zone at 373.80 m is taken as the boundary between the two flows. A glassy zone at 373.20 m appears to be a small offshoot from the nearby dyke. The grain size in the bulk of the massive lavas is medium to coarse and small feldspar laths are clearly visible on the core surface. The grain size decreases gradually toward the top and bottom of the unit but there is no obvious change toward the glassy selvedge separating the two flows. Vesicles are irregularly distributed, ranging from 1–5% of the unit and averaging about 2%. Overall, the rock has a porous aspect. The vesicles average about 1 mm across, are irregular to subspherical, and mostly open. A few contain sparse white zeolites(?). Veins total about 1% of the unit, range up to 2 mm across, and are filled with green smectite and sparse white zeolite. Some celadonite occurs between 378.20 and 378.60 m. The olivine-rich dyke of cooling unit 73.01 is 0.53 m thick and has highly irregular but sharply chilled contacts. Olivine phenocrysts average about 2% of the intrusive unit but are concentrated near the base. They are subhedral to euhedral, up to 3 mm long, and are replaced by green clay minerals and calcite. The groundmass is fine grained with an intersertal texture. Vesicles comprise about 5% of the unit and are up to 3 mm across. About half of the vesicles are open, the other half filled with calcite and smectite. Thin veins less than 1.5 mm wide comprise less than 1% of the unit and contain calcite, celadonite(?) and smectite. The dyke of cooling unit 72.02 is 20 cm thick and dips about 55 degrees. It has sharp chilled margins with minor altered glass. The rock is fine grained, light grey, and very sparsely clinopyroxene-phyric. Vesicles make up less than 1% of the rock and never exceed 2 mm in diameter. Most are open; the remainder have minor smectite and zeolite. Narrow veins comprise about 3% of the rock and are filled with smectite and zeolite.

Unit XIX

Upper contact:	387.48 m, depositional
Lower contact:	409.50 m, ambiguous
Thickness:	22.02 m
Lithology:	Pillowed lava cut by a dyke
Cooling units:	75.01 to 78.03

A sequence of light-grey, fine-grained, aphyric pillowed lavas makes up unit XIX. The unit is cut by an olivine-phyric dyke between 390.40 and 391.50 m (cooling unit 75.04). The pillows are relatively large, averaging 1.16 m in vertical thickness. The glassy pillow margins are 1–2 cm across and are often separated by 2–3 cm of coarse-grained, unsorted, poorly bedded, altered sediment. The glass is mostly altered to smectite. Abundant brecciated glass occurs in the basal cooling unit; some of this glass is fresh but most is altered to layer silicates. Vesicles are irregularly distributed, ranging from 1 to 10%, being most abundant and largest in the pillow centres. Vesicles range from 0.5 to 3 mm and average about 1 mm in diameter. Most are open, some contain smectite and zeolite(?). Veins comprise much less than 1% of the pillows, consisting mostly of fractures coated with smectite. The dyke of unit 75.04 is 1.10 m thick and is bounded by sharp, chilled margins dipping about 20 degrees. The rock is fine grained, light grey, and sparsely olivine- and clinopyroxene-phyric. Phenocrysts average about 3% but are concentrated in the interval between 390.75 and 390.90. They have a maximum size of 2 mm and are subhedral to anhedral. The olivine is replaced by clay minerals but the clinopyroxene is fresh. About 2% of vesicles are present and they have an average diameter of 1 mm. Most are filled with layer silicates and lesser amounts of calcite and hematite. Carbonate veins make up less than 1% of the unit.

Unit XX

Upper contact:	409.50 m, ambiguous
Lower contact:	417.87 m, ambiguous
Thickness:	8.37 m
Lithology:	Massive lava flows or thick pillows
Cooling units:	78.04 to 79.03

Unit XX consists of about 8.4 m of light-grey, fine- to medium-grained, aphyric, massive basalt flows. Both contacts appear to be chilled but some core is missing and the contact relationships are ambiguous. Internal cooling breaks are also ambiguous and are based on glassy pieces in broken intervals. A small amount of glassy breccia is preserved at the contact between cooling units 78.04 and 79.01 (411.87 m). The rocks are fine grained to aphanitic at chilled margins, becoming medium grained toward the centres of cooling units. Small plagioclase and clinopyroxene laths are visible with a hand lens in the coarser-grained portions. Vesicles make up 5–10% of the rock in the upper 1.5 m of the unit; elsewhere they range from 1 to 5%. They are largest in the upper zone, averaging 5 mm across, and decrease in the lower part to about 1 mm. The largest vesicles are irregular in shape; the others subspherical. Most are filled with carbonate and zeolite(?), others are open or lined with clay minerals. Some zones in the centres of cooling units appear to be quite porous. Veins are irregularly distributed and total less than 1% of the unit. All are less than 1 mm wide and are filled with green clay minerals, sometimes slickensided, and minor carbonate. The groundmass is relatively fresh, but glassy zones are partly or completely altered to clay minerals. Some thin breccia zones between cooling units are partly altered to clay minerals.

Unit XXI

Upper contact:	417.87 m, depositional
Lower contact:	423.22 m, ambiguous
Thickness:	5.35 m
Lithology:	Pillowed lavas
Cooling units:	80.01 to 81.01

A thin sequence of greenish-grey, aphyric, pillowed lavas makes up Unit XXI. Individual pillows are up to 1.5 m in vertical thickness, being largest toward the bottom of the unit. Several pillow lobe fragments range from 0.2 to 0.3 m across. Where pillow contacts are sharp, they often have double chill zones 1–2 mm wide. In other zones hyaloclastite accumulations, up to 5 cm across, occur between pillows. Fresh glass is locally preserved in the pillow rinds, particularly where hyaloclastite is present. The pillow interiors are fine- to medium-grained and vesicular. Vesicles average 1 to 3% of the pillows and commonly range from 0.5 to 3 mm, and rarely up to 7 mm in diameter. The largest and most abundant vesicles occur near the upper margins of large pillows. Generally, vesicles are round to oval but some are irregular. Locally, vesicle clusters define diffuse layers 5–6 cm wide, presumably parallel to pillow margins. Vesicles generally are not filled except within 1–2 cm of some pillow margins where they contain green smectite(?). Veins make up about 1% of the unit and occur primarily along contacts between pillow selvedges. The vein material is green smectite, white zeolite(?), and carbonate. Slickensides are common along fractures but probably do not represent any significant movement. The pillows are moderately altered, typically having a greenish-grey colour. Dull surfaces and the lack of a vitreous luster reflects the paucity of fresh glass.

Unit XXII

Upper contact:	423.22 m, ambiguous
Lower contact:	435.38 m, depositional?
Thickness:	12.16 m
Lithology:	Massive lava flows cut by several dykes
Cooling units:	81.02 to 83.02

Unit XXII is composed of three sheet flows cut by thin intrusive units. Cooling units 81.02 and 82.01 are sheet flows which are 5.33 m and 1.25 m thick, respectively. Units 82.02, 82.04, 82.06, and 83.02 have been interpreted to be a single massive flow, 5.25 m thick, cut by small dykes. The flows consist of fine- to medium-grained, grey, aphyric, vesicular basalts. Vesicles make up less than 1% of the rock and are mostly open. A few (2%) are filled with calcite. The unit is highly fractured with very few secondary minerals along the fractures. Gypsum(?) and layer silicates are present on some fracture surfaces. Three dykes cut this unit: cooling unit 82.03 (430.50–430.70 m), cooling unit 82.05 (431.33–431.39 m), and cooling unit 83.01 (432.53–432.60 m). All are fine-grained to aphanitic with distinct chilled margins. Cooling unit 82.03 has plagioclase microlites in an aphanitic to glassy groundmass and is very weakly vesicular. In contrast, cooling units 83.01 and 82.05 are markedly vesicular with about 5% vesicles, averaging about 0.5 mm across. Most of these are filled with clay and chlorite. All three intrusions have contacts dipping about 50 degrees to the core axis.

Unit XXIII

Upper contact:	435.38 m, depositional
Lower contact:	438.05 m, ambiguous
Thickness:	2.67 m
Lithology:	Pillowed lava
Cooling units:	83.03 to 84.02

This unit comprises a sequence of seven pillows with vertical thicknesses on the order of 0.5 m. The contact with the overlying massive sheet flow is very sharp and is defined by a 1- to 2 cm-thick zone of hyaloclastite. The lower contact is placed at a shear zone marked by about 30 cm of

intensely slickensided fault gouge. This fault contact is probably not the base of a flow unit and the unit thickness has little stratigraphic significance. Individual pillows are medium greenish-grey to grey, aphyric, and aphanitic to fine-grained. The pillow margins are marked by altered glass rims, 0.5 to 1 cm thick, and separated by 2- to 4 cm-wide zones of hyaloclastite. Fresh glass is locally present. The lavas are essentially non-vesicular although some pillows contain up to 1% of fine vesicles. Greenish-grey to green smectite fills sparse fractures. One pillow in the lower part of the unit contains about 3% fractures filled with white zeolite and calcite. The rocks are only slightly to moderately altered.

Unit XXIV

Upper contact:	438.05 m, ambiguous
Lower contact:	439.42 m, ambiguous
Thickness:	1.37 m
Lithology:	Clastic material
Cooling unit:	84.03

Unit XXIV consists of 1.37 m of highly fragmented material that varies from yellowish-green, intensely slickensided clay at the top to blocky grit near the base. The coarse-grained material is composed of greenish-grey to grey fragments of basalt in a grit- to clay-size matrix. Clasts range from 2 mm to 2 cm (one block is 4 cm across), and nearly all are slickensided. The upper and lower boundaries are drawn at the end of the sheared and intensely broken material. Because of the extensive slickensiding this unit is interpreted as fault gouge in the basalt pillow lava succession.

Unit XXV

Upper contact:	439.42 m, ambiguous
Lower contact:	445.35 m, depositional
Thickness:	5.93 m
Lithology:	Pillowed lava cut by a possible dyke
Cooling units:	84.04 to 85.09

Unit XXV is a 5.93 m-thick sequence of pillowed lava separated from unit XXIV by a probable fault. The upper contact is ambiguous and is drawn at the base of the fragmental material of cooling unit 84.03. The lower contact is drawn where the pillow lavas overlie volcaniclastic material but it is not accurately defined because only part of the lowest pillow is preserved. The unit consists of 11 pillows and one possible dyke. Pillow rims are marked by brecciated and altered glassy rinds, 1–2 cm thick, minor hyaloclastite, and fine breccia which occurs in zones up to 4 cm wide between pillows. Individual pillows are composed of pale grey-green to dark grey, aphyric basalt. Dark grey, aphanitic rims grade into mottled light and dark margins and then into greenish-grey massive cores that are coarser grained than the margins. Textures are microporphyritic intersertal with microphenocrysts of plagioclase and clinopyroxene(?) in an altered vitric matrix. Vesicles average less than 1% of the rock, and range up to 1 mm across. Carbonate and celadonite(?) fill sparse vesicles in some pillow margins. Moderate pale green groundmass alteration has produced mottled textures near the pillow margins and a pale green colour in the cores of pillows. Smectite, celadonite(?), minor zeolite, and carbonate fill sparse veins and heal fractures. Cooling unit 84.05 is a possible dyke, 0.45 m thick, composed of pale greenish-grey, sparsely porphyritic, olivine basalt. Altered olivine crystals, 0.5 mm across, occur in the lower 10 cm of the unit. The unit contains 1–2% vesicles, all less than 0.5 mm across.

Unit XXVI

Upper contact:	445.35 m, depositional
Lower contact:	452.90 m, depositional
Thickness:	7.55 m
Lithology:	Pillowed lava
Cooling units:	85.10 to 86.08

Unit XXVI is a 7.55 m-thick sequence of pillowed lava separated from the overlying unit by 20 cm of volcaniclastic material and from the underlying unit by 30 cm of hyaloclastite. The unit consists of ten closely packed pillows or parts of pillows ranging from 30 to 160 cm in vertical thickness. Pillow margins are clearly marked by altered glass rims, 2–3 cm thick, and only minor hyaloclastite occurs between pillows. The pillows consist of greyish-green, aphanitic, aphyric basalt. Dark grey, altered, glassy margins contain only minor fresh glass. The margins of some pillows show a mottled alteration pattern. All of the pillows are vesicular containing 3 to 10% vesicles, commonly 1–3 mm across, that are concentrated within 3–6 cm of the pillow rims (45 cm of one large pillow is vesicular). Smectite and a transparent to white zeolite(?) fill vesicles within pillow margins. Sparse veins, filled with smectite and zeolite, up to 0.5 mm wide, are restricted to fractured margins of some pillows. The basalt is moderately altered and pillow rims appear less altered than cores. The 30 cm-thick hyaloclastite marking the base of this unit contains parts of pillows in a matrix of altered glassy fragments. Units XXV and XXVI perhaps should be considered a single depositional unit because they are lithologically similar and because it is not clear that the clastic volcanic material separating the two represents a significant break. The hyaloclastite pillow breccia at the base of Unit XXVI could be considered the base of a major effusive unit 13.5 m thick.

Unit XXVII

Upper contact:	452.90 m, ambiguous
Lower contact:	455.35 m, ambiguous
Thickness:	2.45 m
Lithology:	Massive flow
Cooling units:	87.01

Unit XXVII is 2.45 m-thick sequence of poorly recovered core interpreted as a single massive flow of greyish-green, aphyric basalt. The upper contact is drawn at the base of the overlying hyaloclastite and the lower contact is marked by a 19 cm-thick zone of hyaloclastite overlying a sequence of pillow lavas. A thin zone of dark grey altered glass near 454.10 m suggests an internal cooling break. The basalt is dark grey near the contacts and greyish-green in the centre. Vesicularity varies from 15% in upper parts to 2% in middle and lower parts of the unit. Vesicles range from 1 to 3 mm across, and contain clay minerals and a white zeolite(?). The flow is unveined but contains smectite and chlorite along fractures. The rock is moderately altered and only a small amount of fresh glass is preserved at the contacts.

Unit XXVIII

Upper contact:	455.35 m, depositional
Lower contact:	457.12 m, depositional
Thickness:	1.77 m
Lithology:	Pillowed lava
Cooling units:	87.02 to 87.05

Unit XXVIII is a thin sequence of pillowed lavas separated from the overlying and underlying units by thin clastic layers. The upper contact is marked by a zone of hyaloclastite, 5–10 cm thick, and the lower contact is drawn at a 5 cm-thick layer of volcanic grit. This unit comprises four closely packed pillows (or parts of pillows) that have friable, altered glassy rinds and minor hyaloclastite. Individual pillows consist of dark greyish-green, aphanitic to fine-grained, aphyric basalt. Vesicles are largest (up to 2 mm) and most abundant (up to 10%) within 10 cm of the pillow margins. Most vesicles within 5 cm of the pillow margins are filled with very dark green chlorite(?) and white to greenish-grey zeolite(?). Minor irregular veins, ranging up to 1 mm in width, occur in the pillow margins and contain iron-stained white zeolite(?), chlorite(?), and some gypsum. Pillows are moderately- to highly-altered and fresh glass is rare in the pillow rinds.

Unit XXIX

Upper contact:	457.12 m, depositional
Lower contact:	466.95 m, ambiguous
Thickness:	9.83 m
Lithology:	Massive flows
Cooling units:	87.06 to 88.08

Unit XXIX is a 9.78 m-thick sequence of broken and rubbly core interpreted as a series of thin massive lava flows. At the top the unit is separated from the overlying pillowed lavas of Unit XXVIII by a thin layer of volcaniclastic material. The lower contact is defined by the presence of altered glass at the top of the underlying pillows. Individual cooling units average about 1.5 m in vertical thickness and most are bounded by chilled margins with fresh or altered glass. Many contacts are poorly defined because of the broken nature of the core, and some may be intrusive. The flows are composed of greyish-green, fine-grained, generally aphyric basalt. Clinopyroxene phenocrysts make up 1–2% of several units and a few contain traces of a red secondary mineral that may be altered olivine. The groundmass varies from aphanitic at the margins of cooling units to medium grained in the centres. Vesicles are usually less than 1% of the rock but may range up to 15% in the upper parts of some cooling units. They range from 1 mm to 3 cm across and are partly filled with dark green clay minerals, zeolites, and minor carbonate. Veins are small and sparse, averaging about 1% of the unit and rarely exceeding 1 mm in width. They are filled with slickensided clay minerals and minor zeolites. Except for the altered glassy zones the rock is relatively fresh, exhibiting only minor alteration to clay minerals.

Unit XXX

Upper contact:	466.95 m, ambiguous
Lower contact:	474.88 m, unknown
Thickness:	7.93 m
Lithology:	Pillowed lavas
Cooling units:	88.09 to 90.01

Unit XXX consists of about 8 m of rubbly and broken core interpreted as a sequence of pillowed lavas. The nature of the cooling unit contacts is difficult to define because of the rubbly character of the material. Up to 14 pillows or parts of pillows are recognized and they range from 0.2 to 1.7 m in vertical thickness. Zones of altered glass and hyaloclastite up to 2 cm wide define the pillow margins. Individual pillows are greyish-green, aphanitic, aphyric to very sparsely phyric basalt. Phenocrysts and microphenocrysts of green clinopyroxene and olivine(?) comprise 1 to 2% of the rock, and are generally less than 1 mm across. Fresh olivine was not identified but many of the iron oxide specks may be olivine pseudomorphs. Vesicles make up less than 1% of the rock, and are 1–2 mm across. Most are open but some are lined with green clay minerals. Veins are not preserved but slickensided, clay-lined surfaces are common in the rubbly core.

Cyprus Crustal Study Project Hole CY-1A: Lithologic Unit Summaries

P.T. ROBINSON[1], I.L. GIBSON[2], AND L.V.-B. HORNE[1]

[1]Centre for Marine Geology, Dalhousie University, Halifax, Nova Scotia, Canada
[2]Department of Earth Sciences, University of Waterloo, Waterloo, Ontario, Canada

Robinson, P.T., Gibson, I.L., and Horne, L.V.-B., 1991: Cyprus Crustal Study Project Hole CY-1: lithologic unit summaries; in Cyprus Crustal Study Project: Initial Report, Holes CY-1 and 1A, eds. Gibson, I.L., Malpas, J., Robinson, P.T., and Xenophontos, C.; Geological Survey of Canada, Paper 90–20, p. 17–28, 1991.

Abstract

Hole CY-1A is located at Lat. 35°02′10″N, Long. 33°10′29″E in the Akaki Canyon, on the north side of the Troodos ophiolite, Cyprus. It lies about 1 km south of Hole CY-1, and was spudded at a stratigraphic level approximately equal to that at which CY-1 was terminated. CY-1A was drilled to a depth of 701.19 m with a core recovery of 94.5%. Coolings units were recognized on the basis of contact relationships, grain size variations, thickness, mineralogy, and differing degrees of alteration (Horne and Robinson, 1986). The cooling units are numbered sequentially down the core and the numbers designate the core box in which the unit first appears. The recognized cooling units have been grouped into 34 major lithologic units that represent relatively homogeneous sequences. The lithologic units range in thickness from 0.30 m (Unit XXXIII) to 70.43 m (Unit XXX). For each of these major units, the following information is given: the position and nature of the upper and lower contact, the unit thickness, the dominant lithology, and the identification numbers of the cooling units grouped within the major lithologic unit. For each lithologic unit, this heading is followed by a description detailing the lithology, texture, alteration mineralogy, and major megascopic features.

Résumé

Le trou CY-1A est situé à une latitude de 35°02′10″N et à une longitude de 33°10′29″E dans le canyon d'Akaki, sur le côté nord de l'ophiolite de Troodos en Chypre. Il s'étend à environ 1 km au sud du trou CY-1 et a été foré jusqu'à un niveau stratigraphique approximativement égal à celui ou on a mis fin à CY-1. Le forage de CY-1A a été effectué jusqu'à une profondeur de 701,19 m avec une récupération de 94,5%. Les unités de refroidissement ont été identifiées selon les rapports de contact, les variations granulométrique, l'épaisseur, la minéralogie, et les degrés différents d'altération (Horne et Robinson, 1986). Les unités de refroidissement sont numérotées en séquence jusqu'à la carotte et les numéros indiquent la boîte dans laquelle l'unité paraît en premier. Les unités de refroidissement identifiées ont été groupées en trente quatre unités lithologiques majeures qui représentent des séquences relativement homogènes. L'épaisseur des unités lithologiques varie de 0,30 m (unité XXXIII) à 70,43 m (unité XXX). Pour chacune de ces unités majeures, les renseignements suivants sont donnés : la position et la nature du contact supérieur et inférieur, l'épaisseur de l'unité, la lithologie dominante et les numéros d'identification des unités de refroidissement groupées à l'intérieur des unités lithologiques principales. Une description détaillée de la lithologie, de la texture, de la minéralogie d'altération et des principaux aspects mégascopiques suit le titre de chaque unité lithologique.

Site Data

Location:	Lat. 35°02′10″N, Long. 33°10′29″E
Date occupied:	23 July 1984
Drilling started:	30 July 1984
Note:	Drilling was interrupted from 06 September 1984 to 20 February 1985
Drilling ended:	28 February 1985
Date departed:	04 March 1985
Depth drilled:	701.19 m
Recovery:	94.5%
Lithology:	Pillowed and massive lava flows and dykes

Unit I

Upper contact:	0.0 m, top of hole
Lower contact:	15.10 m, depositional
Thickness:	15.10 m
Lithology:	Pillowed lavas
Cooling units:	1.01 to 3.06

Lithologic Unit I is a 15.10 m-thick sequence of greenish-grey, aphyric to sparsely olivine-phyric, pillow lavas. Twenty-eight separate pillows are recognized, ranging from 0.16 to 1.70 m and averaging 0.50 m in vertical thickness. Individual pillows are recognized by the presence of curved glassy rinds. Phenocrysts of clinopyroxene and altered olivine make up 1–5% of most pillows and are irregularly distributed. Olivine crystals are completely replaced, mostly by green smectite, whereas the clinopyroxene is fresh, green, and glassy in appearance. Vesicles average 1–2% by volume and range up to 5%. They are irregularly distributed in most pillows, and usually have a zonal arrangement. Most are 1–2 mm across but some are up to 5 mm in diameter. They are partly to completely filled with smectite and analcime with lesser amounts of calcite. Veins form less than 1% of the rocks and are hairline to 1 mm in width. Most are filled with analcime with lesser amounts of calcite and light-green smectite. A few veins filled with white, slickensided palygorskite are also present. The glassy pillow margins are almost completely replaced by smectite and analcime and only traces of fresh glass remain. The crystalline pillow interiors are only weakly altered to smectite.

Unit II

Upper contact:	15.10 m, depositional
Lower contact:	57.93 m, depositional
Thickness:	42.83 m
Lithology:	Massive flows
Cooling units:	3.07 to 15.02

A 42.83 m-thick sequence of thin massive lava flows makes up Unit II. Twenty five cooling units were identified as lava flows based on contact relations, grain size variations and vesicle content and size. These units range from 0.23 to 8.58 m and average 1.64 m in vertical thickness. This sequence is cut by three thin dykes (cooling units 11.04, 14.01, and 15.01) which range from 0.03 to 0.21 m in vertical thickness. The dykes are identified by steeply dipping, chilled margins, a homogeneous appearance and a paucity of vesicles. In addition, there are three cooling units (13.02, 14.01, and 14.05) whose origin could not be determined.

The lava flows are dark greenish grey, fine- to very fine-grained, aphyric to very sparsely olivine-phyric rocks. Most of the flows have low-dipping, brecciated glassy margins and some have thin, discontinuous glassy zones, particularly in the upper parts of thick flows. A few flows have a partly brecciated character in which fragments of rock are separated by patches and streaks of smectite, celadonite, and zeolite. The thickest flows show distinct grain size variations from aphanitic at the margins to fine-grained in the interiors. Vesicles range from about 1 to 10% and average about 3–5%. The average vesicle size is about 2 mm and the maximum about 5 mm but a few flows have large (3–5 cm) vesicles. Most vesicles are filled with smectite but a few are open and these are lined with celadonite and zeolite. Veins are rare, generally constituting less than 1% of the rock and are hairline to about 1 mm across. Most are filled with heulandite and mordenite. Some fractures are coated with thin films of celadonite and rarely, dark brown, waxy-appearing sepiolite(?). Groundmass alteration is on the order of 25–35% and is chiefly smectite, replacing glass in the margins, and interstitial material in the flow interiors.

The three unidentified cooling units are also composed of greyish-green, fine-grained aphyric material with sparse vesicles. They typically have brecciated glassy margins and are probably thin flows.

Two of the dykes are similar lithologically to the flows and consist of fine- to very fine-grained, aphyric material. One very narrow dykelet (cooling unit 11.04) consists of black

glass. All of the dykes are marked by distinct, steeply-dipping chilled margins, commonly with thin glassy zones. Vesicles and veins are completely absent. Groundmass alteration is confined largely to the glassy margins, which are partly altered to smectite and zeolite.

Unit III

Upper contact:	57.93 m, depositional
Lower contact:	70.65 m, truncated
Thickness:	12.72 m
Lithology:	Pillowed lavas and sheet flows
Cooling units:	15.03 to 18.01

Unit III consists of twelve cooling units marked by glassy margins. Many of the glassy margins are poorly preserved, being either broken during drilling or by disintegration when the samples were immersed in water. The cooling units range in vertical thickness from 0.17 to 2.85 m and average 1.06 m. On a number of units, particularly the thinner ones, the glassy margins are curved suggesting that these are pillows. Other units, such as 16.02, 17.02, and 18.01, have flatter margins and are considerably thicker than the average pillow. These are interpreted as massive flows. This interpretation is supported by the size and distribution of vesicles in these units.

The pillows are composed of dark greenish-grey, very fine-grained, aphyric rock with 5–15% vesicles. Most vesicles are spherical or ovoid and range from 3 to 5 mm in diameter. They are typically filled with smectite. Hairline veins filled with zeolite are locally present but make up much less than 1% of the rock. The glassy rinds are almost completely replaced by smectite and rare zeolite. Smectite also replaces interstitial material in the crystalline pillow interiors.

The thicker units, which are interpreted as massive flows, consist of greenish-grey, fine- to very fine-grained, aphyric, vesicular rock with about 5–15% vesicles. On average, the vesicles in the flows are larger than those in the pillows and they occur in distinct layers or bands. They are partly filled with smectite, celadonite and zeolite. Hairline veins make up much less than 1% of the rock and consist chiefly of zeolite and minor silica. Some fractures are coated with a thin film of slickensided clay. The glassy margins are only partly replaced by smectite and some fresh glass is preserved. Interstitial material in the crystalline flow interiors is also replaced by smectite.

Unit IV

Upper contact:	70.65 m, intrusive
Lower contact:	78.82 m, intrusive
Thickness:	8.17 m
Lithology:	Dyke
Cooling unit:	18.02

A single dyke, 8.17 m-thick, makes up Unit IV. Both the upper and lower contacts are marked by chilled glassy margins. The upper margin is nearly horizontal but the lower one dips 70 degrees. The upper 30 cm of the unit consist of black, perlitic glass with a zone of flow(?) brecciation 1–5 cm wide along the upper and lower margins. The glassy zone passes rather sharply into a crystalline portion composed of greenish-grey, aphyric rock with distinct variations in grain size. Adjacent to the glassy margins, the rock is very fine grained. The grain size increases gradually toward the center of the unit which is uniformly medium grained. Overall vesicles make up less than 1% of the rock but they are concentrated in distinct zones or layers. Within these zones, which may be up to 50 cm-thick, vesicles range from about 5 to 15 modal percent. Most vesicles are round and they have a maximum diameter of about 5 mm. Some are open but most are filled with mixtures of smectite, carbonate and minor zeolite. A few hairline veins are filled with calcite and zeolite and some fractures are coated with dark greenish-brown, slickensided clay. A few narrow fractures between 71.10 and 72.55 m have narrow oxidized rims. Alteration in the glassy zones is concentrated along perlitic cracks where the glass is partly replaced by smectite. Much of the glass is still fresh. In the crystalline portions smectite replaces interstitial material but rarely exceeds 10 to 15 modal percent.

Unit V

Upper contact:	78.82 m, truncated
Lower contact:	97.68 m, depositional(?)
Thickness:	18.86 m
Lithology:	Massive flows
Cooling units:	20.01 to 25.01

An 8.86 m-thick sequence of relatively thin sheet flows makes up Unit V. Thirteen individual flows are recognized, ranging from 0.53 to 2.17 m and averaging 1.45 m in vertical thickness. Most flows are marked by black glassy margins but these are commonly brecciated and poorly recovered so that attitudes are difficult to determine. Where preserved the contacts dip 20 to 40 degrees. The crystalline flow interiors consist of greenish-grey, fine-grained, aphyric rock which also shows varying degrees of brecciation. Where highly brecciated, the flows consist of angular to subrounded fragments of crystalline material in a glassy matrix. In some cases the glassy material may make up as much as 50% of the flow. Vesicles are relatively abundant, averaging about 10% of individual units but ranging up to 25% in some sections. Most are 3–5 mm in diameter but a few range up to 1 cm across. They are partly to completely filled with smectite and minor celadonite. Only a few hairline veins are present and these are filled with zeolite. The glassy material is about 40% altered to smectite whereas the crystalline portions are considerably fresher. In the crystalline zones celadonite is also a common secondary mineral.

Unit VI

Upper contact:	97.68 m, depositional(?)
Lower contact:	114.32 m, depositional
Thickness:	16.64 m
Lithology:	Pillowed lavas and sheet flows
Cooling units:	25.02 to 29.04

Unit VI is a 16.64 m-thick sequence of 23 thin cooling units tentatively identified as pillows and thin flows. Individual units range from 0.15 to 1.88 m and average 0.69 m in vertical thickness. Some of the units, such as 26.03, 26.04, 26.05, and 26.06, which have curved glassy margins and very fine-grained size, are interpreted as definite pillows. Thicker units such as 27.02 and 29.01 have flat glassy rims, slightly coarser grain sizes, and larger and more abundant vesicles than the pillows. These units are interpreted as thin massive flows although some could be large flat pillows. For the other units the lithologic and petrographic data are insufficient to distinguish between pillows and flows.

The definite pillows consist of greyish-green, fine- to very fine-grained, aphyric rock. Small patches, 2–3 mm wide, of clay minerals may be altered olivine or may be zones of groundmass alteration. Vesicle abundance ranges from 0 to 4% overall but reaches 15% in some thin zones. The vesicles are round to irregular in shape and rarely exceed 2 mm in diameter. Sparse zeolite veins less than 1 mm wide are present locally and some fractures are coated with clay minerals. The glassy margins are completely altered to smectite whereas the crystalline portions contain 20–25% smectite.

The probable lava flows (e.g. cooling units 27.02 and 29.01) are lithologically similar to the pillows except for being somewhat coarser grained and having distinct zones and layers of vesicles. One flow has patches and streaks of smectite, possibly reflecting a flow structure. The vesicle-rich zones are normally 15–40 cm-thick and contain up to 15% of vesicles. The vesicles are spherical to irregular in shape and rarely exceed 5 mm in diameter. About half are filled with smectite. Glassy flow margins are completely replaced by smectite whereas the crystalline flow interiors contain 15–25% of smectite and celadonite, commonly in patches and stringers.

The remaining cooling units have some features of both pillows and flows and their origin is not clear.

Unit VII

Upper contact:	114.32 m, depositional
Lower contact:	117.00 m, depositional
Thickness:	2.68 m
Lithology:	Massive flows
Cooling units:	29.05 to 30.01

Unit VII consists of two massive flows which are 0.70 and 1.98 m-thick, respectively. Thin glassy margins occur at the flow boundaries, but these are commonly broken up and are difficult to locate unambiguously. The flows consist of greenish-grey, fine-grained, aphyric rock which is slightly brecciated in several intervals. Cooling unit 29.05 has narrow streaks of smectite parallel to the upper contact suggesting some flow structure. Vesicle abundance is less than 1% overall but ranges up to 7% in several narrow zones. The vesicles are typically spherical, have a maximum diameter of about 5 mm and are completely filled with smectite. Rare hairline veinlets are filled with smectite and calcite. Groundmass alteration is moderate except in the glassy margins where the material is completely replaced by smectite.

Unit VIII

Upper contact:	117.00 m, depositional
Lower contact:	118.63 m, ambiguous
Thickness:	1.63 m
Lithology:	Massive flow
Cooling units:	30.02

Unit VIII is a single massive flow of greenish-grey, fine- to very fine-grained, locally phyric basalt. It is treated as a separate unit because of the presence of olivine and pyroxene phenocrysts. The upper contact is marked by a thin glassy margin that dips about 45 degrees. The lower contact is ambiguous but is probably truncated by the dyke of cooling unit 30.03. The flow shows alternations in grain size and there are several poorly developed chilled margins near the base of the unit. Most of the flow is aphyric but olivine and pyroxene phenocrysts make up 5–10 modal percent in a 25 cm-thick zone in the lower part of the unit. The phenocrysts increase in size and abundance downward in this layer suggesting gravity settling. Both olivine and pyroxene crystals are subhedral to euhedral and range up to about 5 mm across. The olivine is completely replaced by calcite and smectite whereas the pyroxene crystals are partly replaced by smectite alone. Vesicles comprise about 2% of the unit but are concentrated in layers and bands up to about 30 cm-thick. They are mostly spherical and average 2–3 mm in diameter. Most are completely filled with mixtures of smectite, calcite and minor zeolite. A few hairline veinlets of calcite cut the flow at a depth of 117.15 m. Groundmass alteration consists chiefly of patches and streaks of smectite which dip 5–15 degrees.

Unit IX

Upper contact:	118.63 m, ambiguous
Lower contact:	125.60 m, intrusive
Thickness:	6.97 m
Lithology:	Dyke
Cooling units:	30.03

A single dyke, 6.97 m in vertical thickness, makes up Unit IX. The upper contact is ambiguous but the lower one is marked by a glassy chill zone dipping at 45 degrees, which appears to truncate medium-grained rock of cooling unit 32.01. Unit IX

consists of dark greenish-grey, aphyric rock with zonal variations in grain size and vesicle content. The grain size varies from aphanitic at the contacts to fine-grained in the central 6 m. Vesicles comprise about 3% of the unit but the abundance reaches 10% in some zones. These vesicle-rich zones range from about 50 cm to 2 m in thickness. Individual vesicles average about 2 mm and range up to 5 mm in diameter. They are mostly filled with smectite and minor calcite. Rare hairline veinlets of zeolite, carbonate and smectite occur throughout, and some fractures are coated with hematite and celadonite. Groundmass alteration is expressed in irregular streaks and patches of calcite and possibly zeolite.

Unit X

Upper contact:	125.60 m,truncated(?)
Lower contact:	162.90 m, ambiguous
Thickness:	37.30 m
Lithology:	Massive flows
Cooling units:	32.01 to 41.04

A series of nineteen massive flows makes up Unit X. Individual flows range from 0.19 to 11.05 m and average 1.96 m in vertical thickness. Many flow contacts are ambiguous and poorly preserved in drilling rubble but are recognized from glassy margins or sharp changes in grain size. The flows are light green to greenish grey, uniform, generally massive, aphyric, and moderately vesicular. Several flows (e.g. cooling units 34.01, 35.02, 38.01, and 40.02) have alternating zones of glassy and crystalline material a few centimeters thick. The thickest flow (cooling unit 35.03) has some planar zones suggesting possible flow structure. It also shows systematic variations in grain size from aphanitic at the margins to medium-grained in the interior.

Vesicles constitute 1–2% of the rock but the abundance reaches 10% in zones a few meters thick. They are spherical to irregular in shape and range from 1–10 mm across. They are normally entirely filled with zeolite and calcite with lesser amounts of smectite or celadonite. Sparse veinlets rarely exceed 1 mm in width and are filled with zeolite and calcite. A few fractures are coated with celadonite.

Groundmass alteration is irregular and patchy. It is reflected largely in patches of smectite and celadonite several centimeters across that are concentrated in bands or zones. Alteration in the thick flow (cooling unit 35.03) is more uniformly distributed. Glassy flow margins are completely altered to smectite.

Unit XI

Upper contact:	162.90 m, ambiguous
Lower contact:	191.75 m, ambiguous
Thickness:	28.85 m
Lithology:	Pillowed lavas and massive flows
Cooling units:	42.01 to 49.04

A 28.85 m-thick sequence composed chiefly of pillowed lavas makes up Unit XI. The pillows are recognized by their curved glassy margins, fine grain size, and small vertical thickness. Three cooling units (42.04, 43.01, and 48.01) are tentatively identified as massive flows based on their greater thickness, coarser grain size, and vesicle distribution. It is possible, however, that these could be unusually thick pillows. The 26 cooling units identified as pillows range from 0.30 to 2.00 m and average 0.80 m in vertical thickness. The massive flows average 2.32 m and range up to 4.01 m in thickness.

The pillows are composed of light-grey to greenish-grey or rarely reddish-grey, fine-grained, aphyric rock, some of which is weakly brecciated. Vesicles are sparse, and range in abundance from less than 1%, to up to 10% in some pillows. Most are spherical and range from 1–2 mm in diameter. They are generally filled with mixtures of smectite and calcite. A few vug-like masses of calcite are locally present. Veins make up much less than 1% of the rock and range in thickness from hairline to 2 mm. They are filled with mixtures of smectite, zeolite, and calcite.

The massive flows consist of grey to greenish- or reddish-grey, aphanitic to fine-grained, slightly brecciated material. A few stringers of dark aphanitic material (smectite?) suggest some flow banding. The grain size varies systematically, becoming coarser toward the flow centers. Vesicles are sparse but their abundance reaches 5% in some zones. They are spherical to irregular in shape and generally 1–3 mm in diameter. They are completely filled, mostly with smectite and minor zeolite. Veins make up less than 1% of the unit but are considerably more abundant in some zones. They range up to 3 mm in width and are filled with zeolite and calcite, locally accompanied by smectite or celadonite. Groundmass alteration is highly variable ranging from 100% in glassy margins and breccia zones to about 20% in massive, crystalline zones. Smectite and carbonate occur in irregular patches and blebs and there is minor hematitic staining in some sections.

Unit XII

Upper contact:	191.75 m, ambiguous
Lower contact:	201.27 m, ambiguous
Thickness:	9.52 m
Lithology:	Massive flows cut by dykes
Cooling units:	50.01 to 52.02

The core in Unit XII is rubbly and broken making individual cooling units difficult to identify. Three cooling units (50.01, 51.02, and 52.02) are identified as flows, based on grain size, contact relationships and the lack of curved glassy margins. Cooling units 51.01 and 52.01 are tentatively identified as dykes, based on intrusive contacts observed in some rubble fragments. The three flows range from 1.22 to 3.44 m and average 2.41 m in vertical thickness. Only one flow has a glassy margin; the others have poorly preserved chilled zones at the contacts. The flows consist of light-grey to reddish-

or greenish-grey, aphanitic to fine-grained, aphyric rock with regular zonal grain size variations. Some dark streaks suggest flow banding.

Vesicles average 1–2% in abundance but range up to 7% in some zones. Most are irregular in shape and are up to 5 mm across. They are partly filled with smectite or celadonite and sparse calcite. Discontinuous hairline veins filled with calcite and hematite are randomly scattered through the flows. Smectite is the common groundmass alteration phase, occurring in irregular patches, streaks, and blebs. Variable groundmass alteration has produced a mottled appearance in many of the rocks.

The dykes consist of grey to reddish- or brownish-grey, very fine-grained, aphyric rock with small, sparse vesicles which constitute less than 1% of the rock and rarely exceed 2 mm in diameter. They are partly filled with calcite and zeolite. Sparse veins are discontinuous, hairline stringers of calcite, rimmed by hematite. Groundmass alteration produces a blotchy appearance to the rock. Lighter-coloured zones are nearly completely altered to hematite and smectite whereas darker zones have only relatively small amounts of smectite.

Unit XIII

Upper contact:	201.27 m, ambiguous
Lower contact:	205.35 m, ambiguous
Thickness:	4.08 m
Lithology:	Pillow lavas and breccia
Cooling units:	52.03 to 53.01

Unit XIII consists of six cooling units tentatively identified as pillows and glassy breccia. The core is rubbly and contact relations are difficult to determine. However, both the thickness and fine-grained nature of the units suggest that they are pillows. Glassy margins are present on most units but they are commonly broken and scattered. Cooling units 52.03 and 52.05 are composed of brecciated glassy material and are designated as hyaloclastites.

The probable pillows range from 0.35 to 1.82 m and average 0.84 m in vertical thickness. The rocks are light greenish grey, fine grained, and aphyric. Cooling unit 53.01 is quite brecciated and contains alternating layers of glass and crystalline material. Vesicles vary in abundance from 1 to 7% of individual units and rarely exceed 2 mm in diameter. Some contain calcite, zeolite, and smectite. There are no specific veins but the spaces between breccia fragments are filled with zeolite, celadonite, hematite, and calcite.

Groundmass alteration is extensive in the glassy pillow margins, which are completely replaced by smectite, and in some of the breccia zones, where both smectite and zeolite are abundant. The hyaloclastites consist of green, brecciated, altered glass with rare fragments of crystalline material. Sparse vesicles, up to 3 mm across, are filled with zeolite. No veins are present but there is some greenish alteration along fractures. The glassy material is completely altered to smectite.

Unit XIV

Upper contact:	205.35 m, ambiguous
Lower contact:	212.83 m, intrusive(?)
Thickness:	7.48 m
Lithology:	Dyke
Cooling units:	53.02

A single cooling unit of light- to medium-grey, aphanitic to very fine-grained, aphyric basalt makes up Unit XIV. The upper contact is ambiguous but is marked by glassy material in drilling rubble. The lower contact is a chilled glassy margin that dips 80 degrees. There are a number of dark patches in the rock that look like chill zones but they are not taken as contacts because they do not cut completely across the core. The unit is interpreted as a dyke because of its thickness, regular grain-size variations, and steep lower contact. However, the unit could also be a massive flow. Vesicle abundance is less than 1% overall but ranges up to 5% in several zones that are up to 30 cm thick. The vesicles are mostly spherical and do not exceed 3 mm in diameter. Most are filled with smectite and zeolite.

Hairline veinlets of zeolite and hematite are concentrated in a few zones up to 45 cm-thick. Groundmass alteration is moderate and is manifested by bleaching and zeolitization which produces a mottled texture. Smectite replaces interstitial groundmass material throughout the core.

Unit XV

Upper contact:	212.83 m, truncated(?)
Lower contact:	221.68 m, truncated(?)
Thickness:	8.85 m
Lithology:	Glassy breccia cut by a thin dyke
Cooling units:	55.01 to 56.02

Unit XV consists of two cooling units composed largely of brecciated glass and one crystalline flow (cooling unit 55.01). The unit is cut by a narrow dyke (cooling unit 56.01) between 215.54 and 216.10 m.

The glassy breccia is grey to reddish-grey in colour and consists of fragments of very fine-grained, crystalline rock surrounded by glassy material with a fragmental appearance. At least some of the fragmentation may be apparent, resulting from differential alteration. Vesicles are visible only in the crystalline pieces where they make up less than 1% of the rock, except in a few narrow zones where abundance reaches 5%. Most are 1–2 mm across, irregular and partly filled with smectite and zeolite. A few discontinuous hairline veins and stringers are filled with zeolite. The glassy zones are completely altered to mixtures of smectite and hematite whereas the crystalline fragments are only weakly altered to mixtures of smectite, zeolite, and hematite.

Steeply dipping chilled margins suggest that cooling unit 56.01 is a dyke. The rock is light grey, aphanitic to very fine grained, and aphyric. Vesicles are small and sparse, making

up much less than 1% of the rock. They are filled with zeolite and minor calcite. Zeolite veins up to 1 mm wide are scattered through the cooling unit. Groundmass alteration is weak except in the chilled margins which are slightly bleached and replaced by smectite and zeolite.

Unit XVI

Upper contact:	221.68 m, intrusive
Lower contact:	238.39 m, intrusive(?)
Thickness:	16.71 m
Lithology:	Dykes and massive flows
Cooling units:	57.01 to 60.03

Unit XVI consists chiefly of dykes with a few cooling units that could be massive flows. The dykes are recognized from steeply dipping chilled margins and a massive, uniform aspect. Cooling units 58.03, 60.01, and 60.02 are tentatively identified as massive flows because they lack steep chilled margins. However, the core is highly broken and such margins may have been present originally.

The dykes consist of very homogeneous, light-greenish-grey, aphryic rock with sparse vesicles. Systematic increases in grain size are observed; aphanitic at the margins to fine-grained in central parts of the dykes. Vesicles are completely absent or make up much less than 1% of the rock. They are spherical to irregular in shape and rarely exceed 1 mm in diameter. Most are filled with smectite, zeolite, and calcite. The only veins present are rare, hairline stringers of zeolite. Groundmass alteration is moderate except in the chilled margins where the glass is completely altered to smectite.

The possible flows are lithologically similar to the dykes except that they are commonly brecciated and have larger and more abundant vesicles. The vesicles occur in zones where they make up as much as 5% of the rock. They range up to 3 mm across, are spherical to irregular in shape and are filled entirely with zeolite. Rare veins are hairline stringers of zeolite. Groundmass alteration to smectite reaches 40% and is highest in the brecciated zones.

Unit XVII

Upper contact:	238.39 m, ambiguous
Lower contact:	242.20 m, depositional
Thickness:	3.81 m
Lithology:	Pillowed lavas
Cooling units:	62.01 to 62.07

A 3.81 m-thick sequence of pillow lavas makes up Unit XVII. The core is broken and rubbly but some pillow margins are still preserved. Others are recognized from glassy rubble in the core. Seven pillows are recognized, ranging from 0.32 to 0.76 m and averaging 0.54 m in vertical thickness. They consist of light- to reddish- or greenish-grey, very fine-grained, aphyric rock. Vesicles make up 0–7% of individual pillows and average about 3%. They are typically spherical in shape and reach 5 mm in diameter. Most are completely filled with zeolite and minor calcite. Veins are absent except in cooling unit 62.07, but most pillows contain a few blebs and stringers of zeolite. The glassy pillow margins are completely altered to smectite. Groundmass alteration in the crystalline portions is 30–40% and involves replacement by smectite.

Unit XVIII

Upper contact:	242.20 m, depositional
Lower contact:	269.85 m, ambiguous
Thickness:	27.65 m
Lithology:	Breccias and flows
Cooling units:	63.01 to 69.01

Unit XVIII consists of a series of interlayered breccias and massive flows. The homogeneous character of cooling unit 68.01 suggests it may be a dyke, but no intrusive contacts are preserved. The eight cooling units in this sequence range from 0.63 to 5.88 m and average 3.45 m in vertical thickness. The breccias consist of crystalline fragments of light-greenish-grey, aphyric material in a comminuted matrix of the same composition. Some slickensides on breccia fragments in cooling unit 67.02 suggest a small fault. In cooling unit 63.01 brecciated glassy material separates several crystalline zones. The glassy breccia consists of brown fragments surrounded by green material, all of which are completely altered.

The lava flows consist of light-greenish-grey, aphanitic to very fine-grained, aphyric rock with sparse vesicles. The vesicles are typically less than 3 mm across and never exceed 3% of the rock. Rare vesicles are also present in the crystalline breccia fragments. Overall, about half of the vesicles are filled, chiefly with smectite or chlorite, zeolite, and calcite. A small amount of pyrite occurs in vesicles in cooling unit 68.01. Veins are absent in most units but locally make up 1% of the rock. They are 1–2 mm wide and are filled chiefly with zeolite and calcite. Veins in cooling unit 67.02 also contain pyrite. Fractures in many of the rocks are coated with smectite/chlorite and hematite. Groundmass alteration is highest in the breccias, where blebs and patches of calcite and zeolite occur between the breccia fragments. Chlorite also replaces both breccia fragments and matrix material, particularly where it was originally glassy. Pyrite is present in the groundmass of cooling unit 67.02. The crystalline material appears to be mostly recrystallized and replaced by mixtures of chlorite, zeolite, and calcite.

Unit XIX

Upper contact:	269.85 m, ambiguous
Lower contact:	351.11 m, ambiguous
Thickness:	81.26 m
Lithology:	Dyke with some massive flows
Cooling units:	69.02 to 86.01

A thick sequence of relatively uniform dykes makes up Unit XIX. Of the 22 cooling units in this sequence, 19 are identified as definite or probable dykes, two as massive flows and one is of unknown origin. The dykes range from 0.26 to 18.98 m and average 3.95 m in vertical thickness. Three of the dykes (cooling units 69.02, 75.01, and 82.02) are unusually thick, ranging between 14 and 19 m. The cooling units identified as definite dykes typically have one or more steeply dipping chilled margins. Such margins are not preserved on six uniform and non-vesicular cooling units classed as probable dykes. Seven 'thin zones' of glassy breccia occur in cooling unit 69.02, an 18.96 m-thick dyke. Because there are no grain size variations in the adjacent rock these are believed to represent material that fell into the hole when the drill rod was changed from HQ to NQ.

The dykes consist of very uniform, light-greyish-green, very fine-grained, aphyric material, typically with aphanitic, non-glassy chilled margins. The core is quite broken and rubbly but in most cases that seems to be due to drilling, not to original brecciation. A few thin breccia zones in cooling units 75.01, 79.04, 79.05, 81.03, 82.01, and 82.02 consist of crystalline fragments in a comminuted matrix and are probably small shear zones. Vesicles make up much less than 1% of the unit and are concentrated in relatively thin zones. Vesicles rarely exceed 2% of the rock. Most vesicles are small, about 2 mm across, and are about half filled with chlorite, zeolite, quartz, and pyrite. Rare vug-like masses of the same minerals are present in a few cooling units. Veins are thin and sparse, consisting chiefly of hairline stringers of quartz, zeolite, and pyrite. Many of these veins have bleached halos 1–3 mm wide. Groundmass alteration is widespread and the rocks appear to be extensively recrystallized to mixtures of chlorite and quartz, with minor amounts of pyrite and zeolite.

Cooling units 78.02 and 81.04 are tentatively identified as flows, largely because they are more variable than the dykes and contain significant amounts of sometimes glassy breccia. The crystalline material consists of light-greenish-grey, very fine-grained, aphyric rock with larger and more abundant vesicles than are found in the dykes. The breccias consist of crystalline fragments in a greenish matrix which may be altered glass. Vesicles are up to 5 mm across, spherical, and mostly filled with mixtures of quartz, zeolite, and pyrite. One large vesicle in cooling unit 81.04 has traces of epidote, the highest known occurrence of this mineral in the hole. Originally glassy material is completely altered to greenish clay minerals, whereas the crystalline portions are recrystallized to mixtures of chlorite and quartz.

Unit XX

Upper contact:	351.11 m, ambiguous
Lower contact:	377.10 m, truncated
Thickness:	25.99 m
Lithology:	Massive flows cut by dykes
Cooling units:	86.02 to 91.04

Unit XX consists of 11 cooling units, most of which are tentatively interpreted as massive flows. The only cooling unit definitely identified as a dyke is 91.02. However, contact relations are ambiguous because the core is highly broken and rubbly and some of the flows could just as easily be dykes. Cooling unit 91.04 is a 70 cm-thick layer of breccia.

The nine cooling units identified as flows range from 0.54 to 7.25 m and average 2.73 m in vertical thickness. They consist of greyish-green, fine-grained, aphyric rock. In the thickest flow (cooling unit 90.02) the grain size increases systematically from the margins to the centre of the flow. Vesicle abundance averages 1–2% throughout but reaches 8% in some thin zones. Vesicles typically range from 1–3 mm across and are spherical. Most are partly to completely filled with quartz, zeolite, pyrite and traces of epidote. Veins are sparse and rarely exceed 2 mm in width. They are filled with quartz, chlorite, zeolite, and pyrite.

The breccia of cooling unit 91.04 is light grey to greyish green and consists of angular fragments of crystalline material up to 5 cm across, in a comminuted matrix of the same composition. Because the upper contact appears to be intrusive this is probably a brecciated dyke.

The dyke of cooling unit 91.02 is composed of greyish-green, aphanitic, aphyric rocks with streaks and bands that dip about 20 degrees. It has no vesicles or veins. The rock appears to be largely replaced by quartz and chlorite.

Unit XXI

Upper contact:	377.10 m, intrusive
Lower contact:	386.22 m, ambiguous
Thickness:	9.12 m
Lithology:	Dykes
Cooling units:	92.01 to 92.03

Three dykes ranging from 1.30 to 5.98 m in vertical thickness make up Unit XXI. Cooling units 92.01 and 92.02 have definite intrusive contacts and 92.03 is interpreted as a dyke on the basis of its uniform, very fine-grained character. Although very rubbly, the core is not obviously brecciated. The dykes consist of light-grey to greyish-green, fine- to very fine-grained, aphryic rock. Cooling unit 92.03 has 2–3% of small patches of chlorite, some of which could be altered olivine crystals or just patchy groundmass alteration. Vesicles make up about 1% of the rock and are randomly distributed. They average about 1 mm but range up to 5 mm across. They are completely filled with chlorite, quartz, epidote, and some zeolite. Rare hairline stringers of quartz are scattered through the unit. Groundmass alteration is extensive and involves recrystallization to quartz, chlorite, and minor jasper.

Unit XXII

Upper contact:	386.22 m, ambiguous
Lower contact:	389.35 m, depositional
Thickness:	3.13 m
Lithology:	Pillow lavas
Cooling units:	93.01 to 94.03

Unit XXII is a 3.13 m-thick sequence of pillows. Four individual pillows are present, ranging from 0.50 to 1.25 m and averaging 0.78 m in vertical thickness. Chilled glassy margins are preserved on all units although the glass is completely altered. The pillows consist of grey to greenish-grey, fine- to very fine-grained, aphryic rock with 2–4% vesicles, some of which are up to 20 mm across. The vesicles are spherical to irregular and are mostly filled with quartz, epidote, pyrite, and zeolite. Rare veins are up to 2 mm wide and are filled with quartz, zeolite, and pyrite. The glassy pillow rinds are completely altered to chlorite and quartz. The crystalline portions are somewhat less altered to the same minerals.

Unit XXIII

Upper contact:	389.35 m, depositional
Lower contact:	403.31 m, sharp
Thickness:	13.96 m
Lithology:	Massive flows and breccias
Cooling units:	94.04 to 97.01

Unit XXIII consists of three massive flows, two of which show considerable brecciation. The three cooling units range from 3.27 to 6.55 m and average 4.65 m in vertical thickness. Most of them have glassy margins but the core is very rubbly and these are not well preserved. The flows consist of light-greenish-grey, fine- to very fine-grained, aphryic rock, which sometimes has inclined planar streaks suggestive of flow banding. The breccias consist of green, angular fragments of crystalline material in a light-coloured, highly-altered matrix composed largely of quartz with minor epidote and pyrite. Vesicles are sparse and largely confined to the unbrecciated zones. They are spherical to irregular in shape and range up to 15 mm across. They are partly filled with quartz and epidote. Very rare veins are hairline stringers of quartz. Groundmass alteration is highest in the breccias which now consist largely of chlorite, quartz, epidote, and pyrite. The massive zones consist mostly of chlorite and quartz.

Unit XXIV

Upper contact:	403.31 m, sharp
Lower contact:	422.88 m, sharp
Thickness:	19.57 m
Lithology:	Dykes
Cooling units:	97.02 to 101.02

Nine dykes make up this 19.57 m-thick unit. Individual dykes range from 0.49 to 3.15 m and average 2.17 m in vertical thickness. Most of the units have one or more intrusive contacts; the others are interpreted as dykes because of their fine-grained, uniform character. Minor breccia zones occur in cooling units 97.02, 98.01, 99.01 and 101.02. The dykes consist of greyish-green, aphanitic to fine-grained, aphyric material with small, sparse vesicles. Most vesicles are less than 1 mm across and they are typically scattered through the rock. They are filled with quartz, pyrite, and in some cases, zeolite. Discontinuous, hairline veinlets filled with quartz and pyrite are scattered through the unit. Groundmass alteration involves extensive replacement by quartz and chlorite.

The breccia zones consist of small, angular fragments of crystalline rock in a comminuted matrix of the same composition. In these zones the rock appears to be completely altered to quartz and chlorite.

Unit XXV

Upper contact:	422.88 m, sharp
Lower contact:	456.08 m, ambiguous
Thickness:	33.20
Lithology:	Flows, breccias and dykes
Cooling units:	101.03 to 107.01

Unit XXV is a heterogeneous sequence composed chiefly of massive and brecciated lava flows cut by a few dykes. The core is very rubbly and contact relations are rarely preserved so cooling unit identification is difficult. Of the 16 cooling units recognized, ten are tentatively identified as massive or partly brecciated flows, one as a breccia, and five as dykes. The dykes are distinguished from flows by their steep, intrusive contacts or by their massive, uniform character.

The flows range from 0.49 to 4.42 m and average 1.88 m in vertical thickness. They consist of light-grey to greyish-green, fine-grained, aphryic material. A few flows have altered glassy margins; other have thin breccia zones either within the cooling unit or along the contacts. Vesicles in the flows range in abundance from about 1–3% and are up to 5 mm across. They are nearly completely filled with chlorite, quartz, epidote, and pyrite. Vein abundance reaches about 5% and they have a maximum width of about 5 mm. They are filled with quartz, epidote, pyrite, and rare zeolite. Groundmass alteration involves nearly complete replacement by quartz and chlorite. The light-greyish-green breccias consist of fragments of aphyric, crystalline rock, and possibly some altered glass, in a fine-grained, completely altered matrix. Vesicles and veins are absent. The groundmass is altered, largely to chlorite with lesser amounts of quartz.

The dykes consist of very uniform, light-grey to greenish-grey, fine-grained, aphyric material with very little brecciation. Vesicles are rare and never exceed 2 mm in diameter. They are filled chiefly with quartz and traces of pyrite.

There are no veins but some fractures are coated with chlorite. Groundmass alteration is extensive and involves replacement by chlorite and quartz. Some dykes have small 'blebs' of dark chlorite but these do not appear to be altered phenocrysts. There is minor bleaching of the rock adjacent to some fractures.

Unit XXVI

Upper contact:	456.08 m, ambiguous
Lower contact:	462.99 m, ambiguous
Thickness:	6.91 m
Lithology:	Massive flows
Cooling units:	108.01 to 109.03

Unit XXVI consists of 6 cooling units tentatively identified as massive flows. The core is broken and rubbly and cooling unit contacts are mostly ambiguous so some units could be dykes. The rocks are light grey to faintly reddish- or greenish-grey, fine- to very fine-grained, and aphyric. Some units have slightly inclined streaks and bands suggestive of flow banding. Cooling unit 109.01 has a narrow zone of brecciation on the side of the core. Vesicle abundance averages about 1% and vesicles are about 1–3 mm across. Some cooling units (e.g. 108.03) have very large vugs up to 4 cm across. Both vesicles and vugs are filled with mixtures of quartz, epidote, calcite, pyrite, and chlorite. Hairline veins filled with quartz and pyrite make up less than 1% of the unit. Groundmass alteration is extensive and involves replacement by chlorite and quartz with traces of pyrite. Traces of epidote are also found in some of the chilled margins.

Unit XXVII

Upper contact:	462.99 m, ambiguous
Lower contact:	475.15 m, ambiguous
Thickness:	12.16 m
Lithology:	Dykes
Cooling units:	110.01 to 112.02

Unit XXVII is 12.16 m-thick sequence of dykes. The six cooling units range from 0.92 to 3.66 m and average 2.43 m in vertical thickness. Although the core is rubbly and broken, most of the dykes have at least one chilled margin preserved. The dykes consist of light-greyish-green, uniform, fine-grained, aphyric rock with sparse vesicles. A few cooling units have light, inclined streaks or bands and small zones of brecciation. Vesicles average 1–2% and range in size up to 3 mm. They are mostly filled with mixtures of quartz, epidote, chlorite, calcite, and pyrite. Rare hairline veins are filled with chlorite, quartz, and pyrite. Groundmass alteration is extensive and involves replacement by chlorite, quartz, and pyrite with traces of epidote.

Unit XXVIII

Upper contact:	475.15 m, ambiguous
Lower contact:	524/80 m, intrusive
Thickness:	59.93 m
Lithology:	Massive flows, breccias and dykes
Cooling units:	113.01 to 122.02

Unit XXVIII is a series of massive lava flows and breccias cut by numerous dykes. Of the 23 cooling units in this sequence, 14 are interpreted as flows or flow breccias and nine as dykes. However, the core is broken and rubbly and contact relations are rarely preserved, making the correct identification of cooling units difficult. The flows and flow breccias range from 0.53 to 5.88 m and average 2.60 m in vertical thickness. They consist of light-grey to purplish-grey and greenish-grey, aphanitic to very fine-grained, aphyric rock. Many of the flows exhibit weak brecciation along their contacts and some, such as cooling units 113.03, 114.03, 119.01, and 120.01, are extensively brecciated. In the breccias, grey crystalline fragments, up to about 5 cm across, are surrounded by a fine-grained, highly altered matrix. Little or no glass is recognized in these rocks. Vesicle abundance typically averages 1–2% and vesicles are visible only in the crystalline fragments in the breccias. They are irregular to ovoid in shape and range up to 15 mm across. Most are completely filled with epidote, quartz, pyrite, and some chlorite. Veins are extremely rare in this unit. Where present they are up to 2 mm wide and filled with quartz and pyrite. Groundmass alteration is 100% in the breccias, but less in the massive flows. Chlorite, epidote, and quartz are the most common secondary minerals; pyrite is present in a few flows.

The nine definite or probable dykes range from 0.63 to 2.97 m and average 1.45 m in vertical thickness. The dykes have steep chilled margins and a uniform, non-vesicular character. They consist of light-greenish-grey, fine-grained, aphyric rock with some systematic grain size variations. Vesicle abundance averages about 1% and vesicles rarely exceed 2 mm in diameter; a few are up to 12 mm across. They are filled with chlorite, quartz, epidote, and pyrite. Veins are almost non-existent in the dykes but rare hairline stringers are filled with quartz and pyrite. A few fractures are coated with pyrite and hematite. Groundmass alteration is largely to chlorite, epidote, and quartz. A few dykes (e.g. cooling unit 121.02) have a mottled appearance due to white, presumably quartz-rich, patches up to 15 mm across.

Unit XXIX

Upper contact:	524.80 m, truncated
Lower contact:	535.08 m, ambiguous
Thickness:	10.28 m
Lithology:	Massive and brecciated flows
Cooling units:	122.03 to 124.02

Four cooling units, tentatively identified as brecciated lava flows, make up Unit XXIX. The core is broken and rubbly and contact relations are poorly preserved. These units are identified as flows, mainly because of their brecciated and vesicular character. The lavas consist of light-grey to greyish-green, fine- to very fine-grained, aphyric rock with variable degrees of brecciation. In most units the brecciation is confined to thin zones, 10–50 cm thick, but in others (e.g. cooling unit 124.02) it is more extensive. The breccias are generally greyish-green and consist of irregular fragments and clasts of crystalline material, 5–6 cm across, in a highly altered, comminuted matrix. Vesicles make up 1–2% of the massive rock but are not recognized in the breccia. They are irregularly distributed and make up as much as 10% in some narrow zones. Most are less than 5 mm across and are filled with quartz, epidote, and pyrite with minor chlorite. Hairline veins of quartz, chlorite, epidote, pyrite, and zeolite are common but make up less than 1% of the rock. Groundmass alteration is high, particularly in the breccia. It involves replacement by chlorite, quartz, pyrite, and rare hematite. The alteration is variable, producing a mottled or patchy texture in some units. In the breccias the clasts are normally rich in epidote, whereas the matrix consists largely of chlorite.

Unit XXX

Upper contact:	535.08 m, ambiguous
Lower contact:	605.51 m, ambiguous
Thickness:	70.43 m
Lithology:	Dykes and massive flows
Cooling units:	124.03 to 137.01

Unit XXX is a heterogeneous sequence composed of dykes and massive flows. Of the 24 cooling units in this sequence 14 are tentatively identified as dykes, largely on the basis of steep, chilled margins or their uniform, non-vesicular character. The dykes range from 0.29 to 15.19 m and average 2.87 m in vertical thickness. They consist of light-grey to greenish-grey, fine-grained, homogeneous, aphyric rock. Vesicle abundance averages less than 1% and vesicles are more or less uniformly distributed. They are partly or completely filled with epidote, quartz, chlorite, and pyrite. Veins are sparse, typically up to 1 mm wide and filled with pyrite, quartz, chlorite, and zeolite. Groundmass alteration is extensive, at least 60–70%, and involves of replacement by chlorite and quartz. Many of the rocks have a spotted appearance due to the presence of round, white, presumably quartz-rich, patches.

The lava flows range from 0.40 to 8.09 m and average 3.03 m in vertical thickness. They consist of light-greyish-green, aphanitic to fine-grained, aphyric material. The brecciated zones consist largely of green fragments of altered material in an altered quartz-rich matrix. Some of the fragments may originally have been glassy and a few curved margins are suggestive of pillow structures. Vesicle abundance averages about 1–2% and ranges up to 7 or 8% in some zones. Most vesicles are about 3 mm across but a few larger ones are also present. They are about half filled with chlorite, epidote, quartz, pyrite, and minor zeolite. Hairline veins or stringers of quartz, with or without pyrite, are scattered throughout.

Groundmass alteration in the breccias is very extensive and involves replacement by quartz, epidote, chlorite, and pyrite. The same secondary minerals occur in the massive flows, where they are less abundant.

Unit XXXI

Upper contact:	605.51 m, faulted
Lower contact:	606.01 m, faulted
Thickness:	0.50 m
Lithology:	Fault breccia
Cooling units:	138.01

Unit XXXI consists of 0.50 m of grey to reddish-grey fault breccia. The breccia is composed of angular fragments, 2–30 mm across, of fine-grained, aphryic rock in a comminuted matrix of the same composition. There are no vesicles or veins. The breccia matrix is completely replaced by chlorite, epidote, quartz(?), and hematite. The clasts are partly altered to quartz and chlorite.

Unit XXXII

Upper contact:	606.01 m, faulted
Lower contact:	631.05 m, faulted
Thickness:	25.04 m
Lithology:	Dykes and flows
Cooling units:	138.02 to 142.01

Unit XXXII is a 25.04 m-thick sequence of dykes and probable lava flows between two faults. The core is broken and rubbly, making cooling unit identification difficult. Half of the 10 cooling units in this interval are tentatively identified as dykes, the other half as flows. Only one dyke (cooling unit 139.01) has clearly intrusive contacts; the others are identified on the basis of their massive, uniform character.

The five dykes range from 0.84 to 3.45 m and average 2.23 m in vertical thickness. They consist of greenish-grey, very fine- to medium-grained, aphryic material with rare vesicles. Vesicles make up much less than 1% of the unit and are randomly distributed. They have a maximum diameter of about 4 mm and most are spherical. Quartz, epidote, chlorite, and pyrite are the common vesicle fillings. Rare hairline veinlets are filled with various mixtures of the same minerals, along with some zeolite. Groundmass alteration averages about 60% and involves replacement by chlorite and quartz, locally accompanied by epidote and pyrite.

The five probable flows range from 0.82 to 8.35 m and average 2.77 m in vertical thickness. They consist of light-grey to greenish-grey, aphanitic to fine-grained, aphyric material with varying degrees of brecciation. The most highly brecciated

cooling units (139.02 and 141.03) are grey, reddish-grey, or green in colour and are highly altered. The breccias consist of highly altered fragments in a comminuted matrix of the same composition. Vesicles range from 1–2% and are up to about 4 mm across. They are mostly filled with epidote, chlorite, quartz, and pyrite. Sparse hairline veins are filled with the same minerals.

Groundmass alteration is highly variable, being 100% in the brecciated zones and 60–70% elsewhere. The rock is replaced largely by mixtures of chlorite, quartz, epidote, and pyrite. Some hematite occurs in the breccias and gives them their reddish-grey colour.

Unit XXXIII

Upper contact:	631.05 m, faulted
Lower contact:	631.35 m, ambiguous
Thickness:	0.30 m
Lithology:	Fault breccia
Cooling units:	143.01

A 30 cm-thick sequence of light-green fault breccia makes up Unit XXXIII. The breccia consists of angular crystalline fragments of aphanitic material, 2–30 mm across, in a comminuted matrix of the same composition. No vesicles or veins are present. The groundmass material is completely replaced by quartz and chlorite.

Unit XXXIV

Upper contact:	631.35 m, faulted
Lower contact:	701.19 m, base of hole
Thickness:	69.84 m
Lithology:	Dykes and flows
Cooling units:	144.01 to 156.03

Unit XXIV consists of a 69.84 m-thick sequence of dykes and lava flows, very similar to those of Unit XXXII. Flows and probable flows make up 11 of the 19 cooling units in this sequence. They range from 0.24 to 7.64 m and average 3.13 m in vertical thickness. Most are heterogeneous units consisting of greenish-grey, fine-grained, aphyric rock, accompanied by variable amounts of breccia. The brecciated zones are typically green and highly altered. Vesicles average about 2% of the flows but range up to nearly 10% in some zones. One flow (cooling unit 148.01) has many vesicle zones or bands up to a meter thick. Most vesicles are in the range of 1–3 mm across but some are up to 2 cm. Rare vugs up to 4 cm across are present locally. The vesicles and vugs are almost completely filled with mixtures of chlorite, epidote, quartz, and pyrite. Sparse hairline veinlets are filled with the same minerals and a few fractures are coated with hematite. Groundmass alteration is extensive, particularly in the breccia zones. Most of the rock is replaced by mixtures of chlorite, quartz, and epidote but there are some zones (e.g. in cooling unit 148.01) composed almost entirely of epidote.

The eight dykes of Unit XXXIV range from 0.26 to 17.46 m and average 4.43 m in vertical thickness. They are recognized on the basis of steeply dipping chilled margins or on their massive, uniform character. They consist of greenish-grey, fine-grained, aphyric rock with very few vesicles. Veins make up much less than 1% of the rock and are filled with chlorite, epidote, pyrite, and quartz. Some fractures are coated with hematite. Groundmass alteration is between 60 and 80% and involves replacement by chlorite, epidote, and quartz. Some of the dykes have a spotted appearance due to the presence of small white patches, presumably rich in quartz.

ACKNOWLEDGEMENTS

This summary was produced by the first and third authors from the detailed core descriptions prepared in Cyprus by Lech Lewczuk, Angela Dobson, Louisa Horne and Paul T. Robinson. The assistance of these individuals is gratefully acknowledged. The second author was responsible for the preparation of the typeset material at the University of Waterloo, Waterloo, Ontario, Canada.

Geology of the Area Surrounding the CY-1 and CY-1A Boreholes

J. MALPAS AND D. WILLIAMS

Department of Earth Sciences, Memorial University
of Newfoundland, Canada AIB 3X5

Malpas, J. and Williams, D., 1991: Geology of the area surrounding the CY-1 and CY-1A boreholes; in Cyprus Crustal Study Project: Initial Report, Holes CY-1 and 1A, eds. Gibson, I.L., Malpas, J., Robinson, P.T., and Xenophontos, C.; Geological Survey of Canada, Paper 90–20, p. 29–40, 1991.

Abstract

Drillholes CY-1 and CY-1A of the Cyprus Crustal Study Project are situated in the Akaki River canyon on the northern flank of the Troodos ranges, in an area underlain by the higher portions of the ophiolitic succession. The basement rocks of the area consist of a series of pillow lavas and thin flows, hyaloclastites and an underlying sequence of diabase dykes with lava screens. The cover to these igneous rocks forms part of the Circum-Troodos succession and consists of marls, chalks, minor cherts and intermittent occurrences of ferromanganiferous shales and umbers.

The igneous rocks comprise two distinct geochemical types which developed in cycles of tectonic, hydrothermal and volcanic activity. Only tenuous correlation can be made with *in situ* oceanic crust.

Résumé

Les trous de forage CY-1 et CY-1A du project d'étude de la croûte chypriote sont situés dans le canyon de la Rivière Akaki sur le flanc nord des chaînes de montagnes Troodos, au-dessous laquelle est située les plus grands constituants de la succession ophiolitique. Les soubassements de la zone consistent d'une série de coussinets de laves et de minces écoulements, d'hyaloclastites ainsi qu'une séquence au-dessous de dykes de diabase avec une interstratification de laves. L'enveloppe de ces roches ignées forme une partie de la succession des Circum-Troodos et consiste de marnes, de calcaire, d'une quantité moindre de cherts ainsi que quelques gisements intermittents de schistes argileux et de lignites terreuses ferromanganifères.

Les roches ignées comprennent deux types géochimiques distinctifs qui se sont dévelopés dans les cycles d'activité tectonique, hydrothermique et volcanique. Seulement une corrélation ténue peut être faite avec une croûte océanique *in situ*.

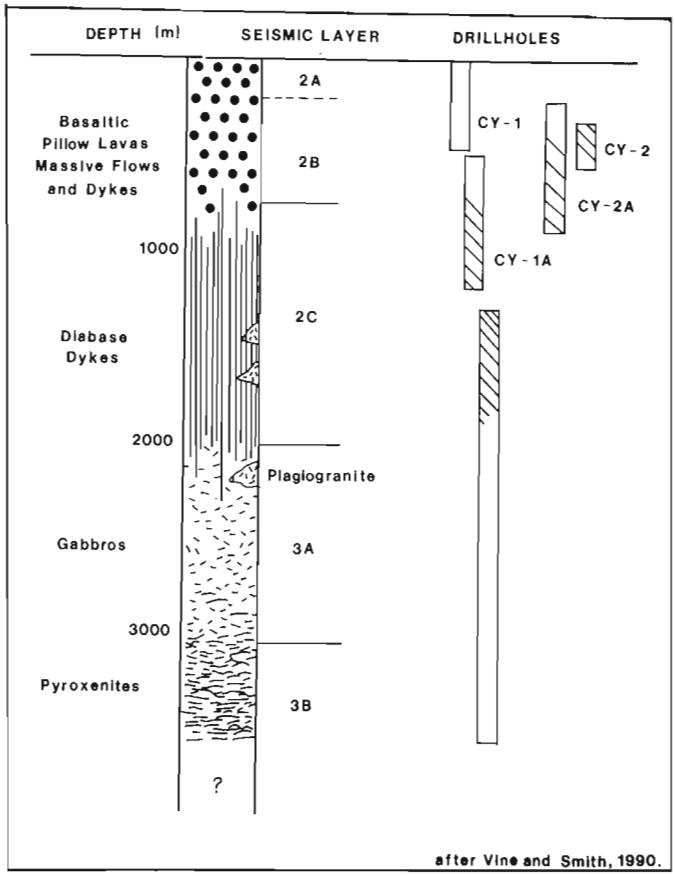

Figure 1: Relative depths of penetration of the ICRDG boreholes of the Cyprus Crustal Study Project and the representative stratigraphic horizons sampled.

INTRODUCTION

The Cyprus Crustal Study Project (CCSP) was designed to investigate the structure and evolution of the Troodos ophiolite complex by a combined program of field mapping and deep crustal drilling. The drilling component consisted of a sequence of five holes designed to sample, by offset drilling, the igneous portion of the ophiolite sequence from the upper pillow lava-sediment interface to the lower plutonic series (Figure 1). Initial results from the holes sampling the deeper portions of the ophiolite are reported in earlier publications (Robinson et al., 1987; Gibson et al., 1989). Holes CY-1 and CY-1A, the results of which are reported in this volume, sampled the volcanic carapace of the ophiolite.

The Troodos massif exposes the ophiolite stratigraphy in an annular form, with the volcanic sequence surrounding a core of lower plutonic rocks (Figure 2). The northern exposures of volcanic rocks are generally less affected by deformation events that took place both on the seafloor and subsequently during emplacement. The Arakapas Fault and Limassol Forest Complex, represent a presumed fossil transform fault (Simonian and Gass, 1978; Murton and Gass, 1986) that traverses the southern margin of the ophiolite and complicates the stratigraphy in that region. For this reason CCSP boreholes CY-1 and CY-1A were sited in the Akaki-Maroulena River canyon on the northern flank of Troodos (Figure 3).

Hole CY-1 was spudded at the sediment/lava interface and was intended to sample the entire volcanic sequence in that locality. However, due to hole instability, drilling was terminated at 474 m with 91% recovery. The core sampled aphyric and olivine/clinopyroxene-phyric lavas. Both pillowed and massive flows occur and these are similar to those exposed in the canyon walls (Figure 4).

CY-1A was sited approximately 2 km further south in the canyon (Figure 4). Drilling started at a stratigraphic horizon approximately equivalent to the base CY-1 and penetrated to a depth of 700 m with 95% recovery. High water pressure prevented further drilling. Surprisingly, it has proved difficult to correlate in detail units from the drill core with exposures in the canyon wall. Both show pillowed and massive lava units and these are cut by diabase dykes. The latter become more common with increasing stratigraphic depth. CY-1A terminates in a sheeted dyke swarm, presumably in the Basal Group (Xenophontos and Malpas, 1987).

REGIONAL GEOLOGY

The Akaki canyon lies within the Akaki-Lythrodonda map area of Bear (1960). The regional geology is summarized in Figure 3. Roughly equal proportions of sediments and the underlying igneous rocks are exposed in the area. However the boundary is complex and marked by numerous inliers and outliers along a line between Mitsero and Analyonda villages. The sedimentary succession comprises the Peraphedi Formation and the overlying Lapithos Group (Figure 5). Although there are significant differences in thickness of this sedimentary pile, even in closely adjacent areas, sedimentation of marls and chalks with chert horizons appears to have been continuous through the Upper Cretaceous to Lower Miocene.

The Circum-Troodos sedimentary cover succession

The Troodos ophiolite was produced during a phase of supra-subduction spreading that was abruptly terminated in the Maastrichtian by collision with the Mamonia Complex microplate (Malpas et al., submitted). The resulting tectonic activity involved the counter-clockwise rotation of the Troodos block. Major strike slip faults and local transpressional and transtensional regimes were also developed along the terrane boundary. A period of tectonic quiescence following the collision allowed for the deposition of a thick series of pelagic carbonates. Subsequent gradual shallowing of the sea was emphasized in the Middle Miocene by more rapid uplift of

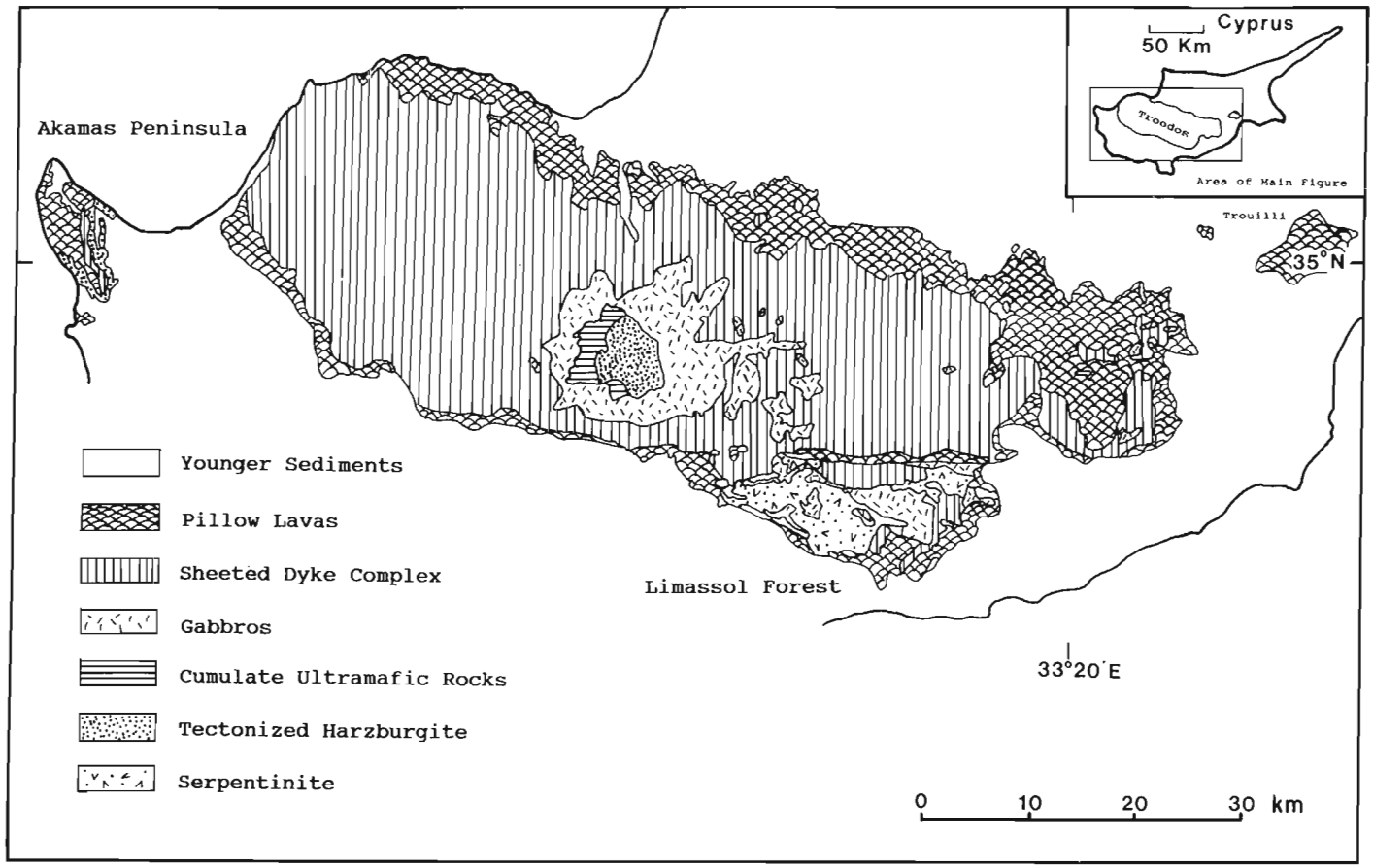

Figure 2: Geology of the Troodos ophiolite, Cyprus.

the ophiolite and its eventual exposure above sea level. In the late Middle to Upper Miocene, sedimentation of evaporitic deposits was widespread both here and elsewhere in the Mediterranean (Hsu et al., 1978). The Pliocene was a period of renewed marine transgression with marl sedimentation in fault controlled basins; coarser arenaceous sediments surround points of positive relief. Renewed episodic uplift continued throughout the Pleistocene with the concomitant deposition of very immature coarse sediments or fanglomerates that cover most of the older sediments.

(a) The Peraphedi Formation

In the present discussion, the Peraphedi Formation is defined as including only the manganiferous sediments, radiolarites, and radiolarian mudstones that immediately overly the ophiolitic extrusive rocks. The overlying bentonites and arenaceous sediments (Bear, 1960) are now considered to be a separate formation. The umbers are homogeneous fine-grained rocks with a conchoidal fracture, consisting of argillaceous material mixed with hydrated ferric- and manganese-oxides. They were formed by precipitation from hydrothermal waters venting onto the ocean floor and grade into manganiferous shales that are by far the most widespread member of the formation. These shales are typically fissile rocks with a pronounced slaty cleavage, chocolate-brown colour, and in places slumped bedding accompanied by the development of thin interbeds of jasper. There is some lateral facies variation into rocks with more clay in places with increased amounts of concentrated pyrolusite and psilomelane. The uneven distribution of these sediments is a result of their confinement to hollows or depressions in the lava surface. The iron/manganese- and trace-element-enriched fine-grained sediments have an average thickness of a few metres but in some areas may reach as much as 35 m.

The almost total absence of detrital and calcareous sedimentation at this time slowly gives way to the deposition of radiolarites and radiolarian mudstones. These are in turn overlain by discontinuous deposits of bentonitic clays and sediments of the Kannaviou Formation (previously the Moni Formation). The radiolarian fauna of the Peraphedi Formation are Campanian, whereas the overlying bentonitic clays have been dated as Maastrichtian (Robertson and Hudson, 1974).

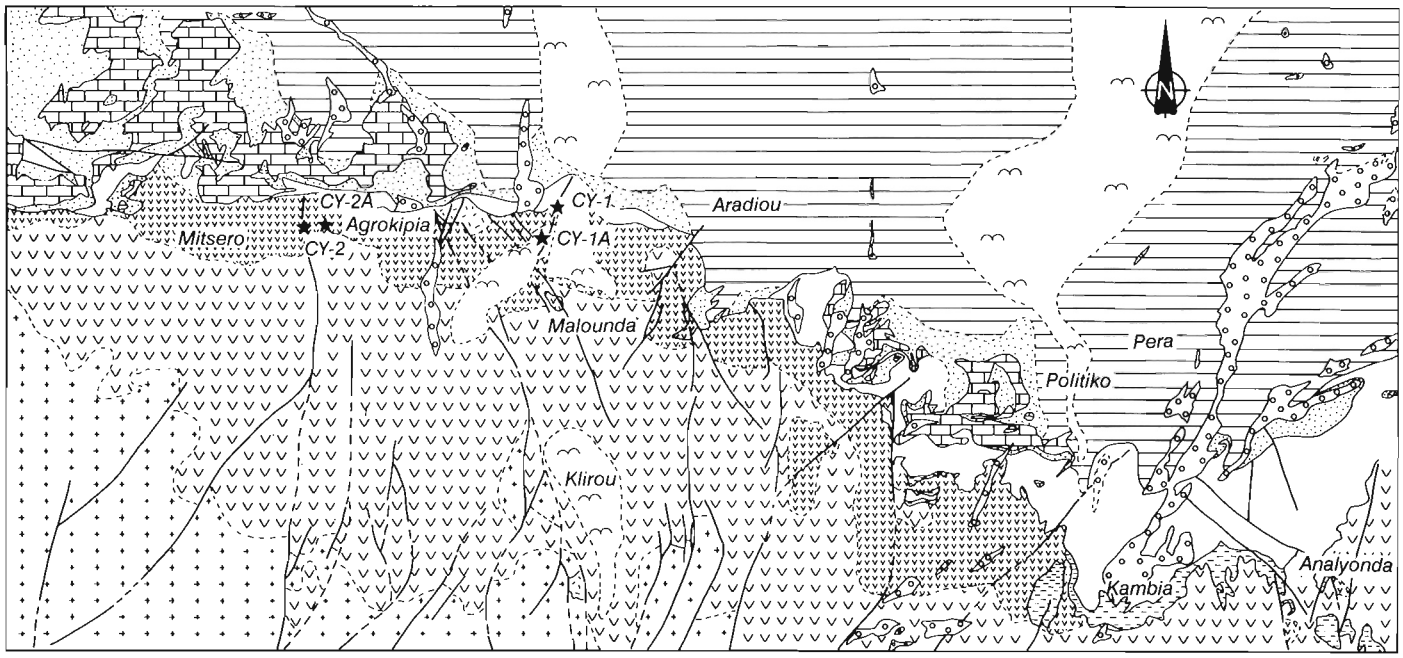

LEGEND

SEDIMENTARY ROCKS

RECENT — Alluvium

PLEISTOCENE — Boulder beds & secondary limestone

PLIOCENE — Buff & grey marl, sands & calcareous siltstones

MIOCENE — Reef limestone

MIOCENE — Chalks, marls & limestones

MIOCENE TO UPPER CRETACEOUS — White flaggy & cleaved chalk. Chalk with chert bands & pink marls

MIOCENE TO UPPER CRETACEOUS — Umberous shales, radiolarian shales & radiolarites

VOLCANIC ROCKS

Pillow lavas. Olivine-basalt, picrite-basalt, glassy basalt, mugearites & limburgites

Pillow lavas & contemporaneous intrusives. Andesites, dacites & keratophyres

Diabase intrusives with screens of pillow lava

INTRUSIVES

High level intrusives

Figure 3: Geology of the area around CY-1 and CY-1A between Analyonda and Mitsero on the northern slopes of the Troodos ranges.

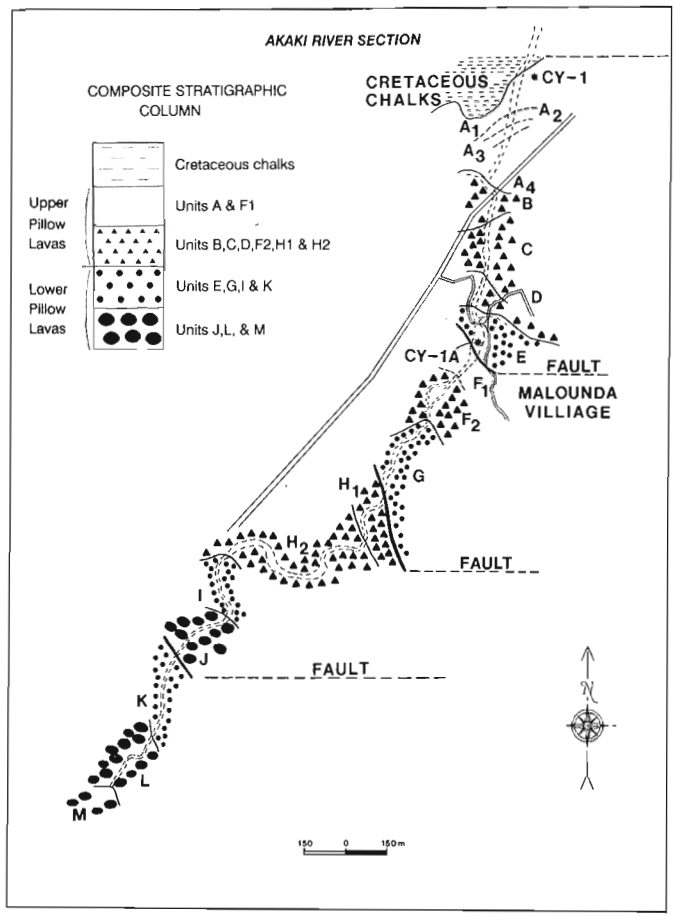

Figure 4: Volcanic units of the Akaki River canyon section in the vicinity of CY-1 and CY-1A.

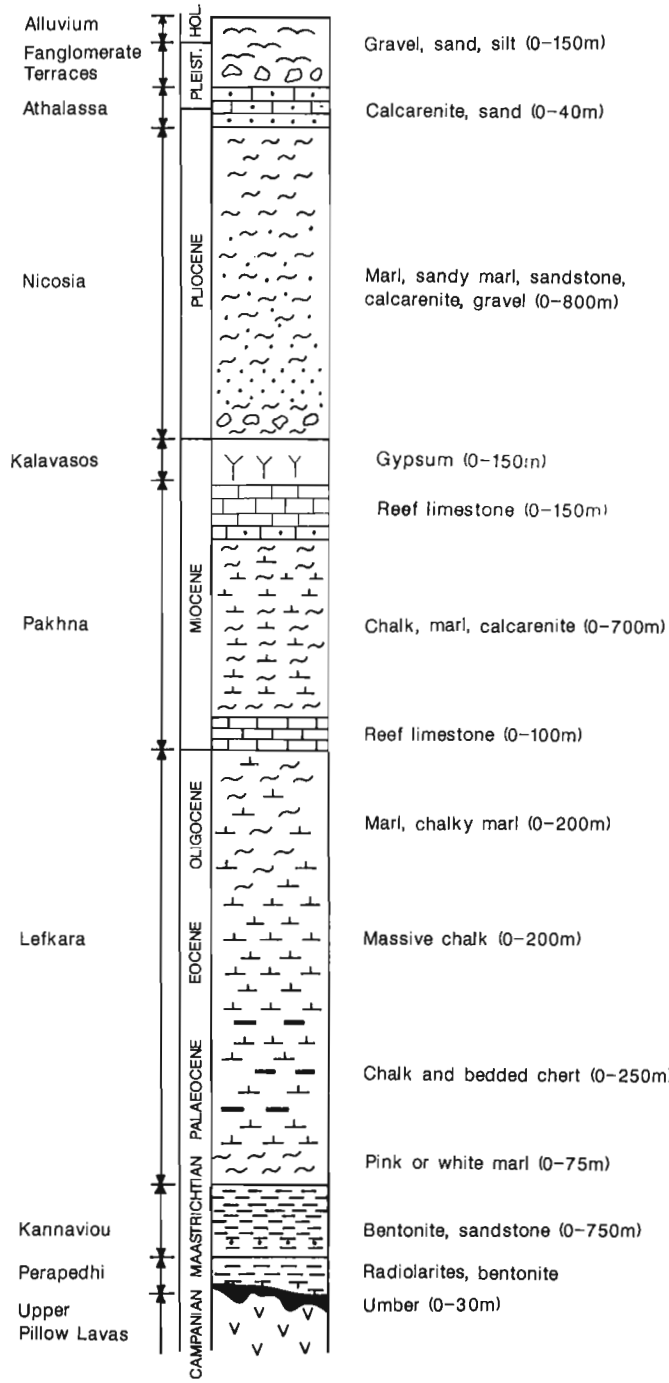

Figure 5: Stratigraphic column of the Circum-Troodos sedimentary succession.

(b) The Kannaviou Formation

The unusual Kannaviou Formation warrants a brief description, although essentially absent in the area surrounding the CY-1 and CY-1A boreholes. These sediments are thickest southwest of the Troodos massif, in the Paphos region, where they reach a thickness of over 700 m.

A thin bed of bentonitic clay is exposed in the Pedieos River canyon near Kambia, resting directly on the pillow lavas. At this locality it is directly overlain by radiolarites and marls and is equated with the Kannaviou bentonite that is better-developed elsewhere. In southwest Cyprus the pillow lavas of the Troodos ophiolite are directly overlain by up to 750 m of Kannaviou Formation sediments of Lower Campanian to Mid-Maastrichtian age. The basal sediments are essentially bentonitic clays and radiolarian mudstones, indicating slow deposition below the calcium-carbonate compensation depth. Stratigraphically higher bentonitic clays are calcareous and are interbedded with siltstones and sandstones of volcanic origin. They appear to have been deposited by turbidity currents at a much more rapid rate than the lower sediments. These higher sequences contain abundant fine-grained clasts of pumice and acid volcanics, and terrigenous material that appears to have been derived from an area not represented in the geology of Cyprus. Possibly the Kannaviou Formation contains deposits derived from active arc volcanism during late Cretaceous times, although such an arc is not preserved in the immediate area.

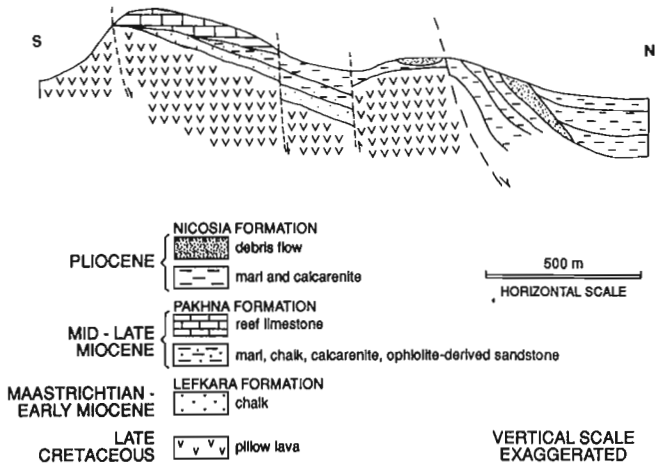

Figure 6: Cross-section (N-S) of the upper volcanic rocks and sedimentary cores on the north front of the Troodos massif near Mitsero village (after Follows and Robertson, 1990).

(c) The Lefkara Formation

The Lefkara Formation (Lapithos Group of previous studies) immediately overlies Peraphedhi (or locally Kannaviou) sediments. In the area of the drillholes it is exposed in a discontinuous belt running east-west immediately north of the igneous rocks. The formation is traditionally divided into Lower, Middle, and Upper units that are dated by planktonic foraminifera.

The Lower Lefkara is Maastrichtian in age and consists of thin-bedded, pinkish to off-white marls and chalks with local chert nodules. It rarely exceeds 50 m in thickness. Where manganiferous sediments and/or bentonitic clays are missing, it directly covers the lavas of the underlying volcanic topography. Near the CY-1 and CY-1A boreholes, the Lower Lefkara is missing and the Middle Lefkara sediments may be faulted against the volcanic rocks, although the contact is not exposed in the Akaki River canyon.

The overlying Upper Lefkara Formation, of mid-late Oligocene age, comprises more uniform pelagic chalk, up to several hundred metres thick (Zomenis, 1972). In the study area, the Lefkara Formation is disconformably overlain by the mid-late Miocene Pakhna Formation (Pantazis, 1967).

(d) The Pakhna Formation

Along the northern margin of Troodos, the Pakhna Formation is composed of chalk, bioclastic limestone, sandstones, and marls. Reefal limestones occur at the base (Terra member) and top (Karonia member) of the formation (Figures 5 and 6). Marked changes in thickness are apparent, especially in the area of the Akaki River canyon. The thickness variations are in places accompanied by lithological changes (e.g. chalk deposition on blocks of higher elevation and marl and reef detritus at lower levels; Follows and Robertson, 1990) and may result from faulting during the deposition of the Pakhna sediments.

(e) The Kalavasos Formation

Evaporite successions several tens of metres thick outcrop between the reefal limestones of the upper Pakhna to the south, and Pliocene rocks of the Mesaoria basin to the north. Large (one metre long) selenite crystals occur with laminated alabaster and gypsiferous marl: carbonate laminae occur within the alabaster. The base of the succession contains large tilted selenite blocks.

(f) The Nicosia Formation

The Messinian erosional surface is unconformably overlain by pink and white foraminiferal chalks and the succeeding brown mudstones of the Nicosia Formation. Lower horizons of this formation are marked by debris flows containing blocks of selenite and other evaporites in carbonate matrix. More widespread debris flows, or megabreccias, up to tens of metres in thickness, contain blocks of reefal and detrital limestone.

(g) Stratigraphic summary

Early Miocene to Early Pliocene sedimentation in the area of the CY-1 and CY-1A boreholes was dominated by local areas of uplift in a tensional regime. As a result, in the Early Miocene, large debris flows developed containing reefal debris. By Late Miocene time the area had become emergent, shedding clastic sediments into the Pakhna basin. After the Messinian salinity crisis, renewed tensional faults resulted in the redeposition of older carbonates and evaporites and their incorporation into the basal Pliocene clastics of the Nicosia Formation (Figure 6).

The Volcanic succession of the Troodos ophiolite

(a) Field relationships

The extrusive sequence of the Troodos ophiolite as exposed along the Akaki River canyon is approximately 1100–1700 m-thick. It may be divided on the basis of both field observations and the chemistry of the volcanic rocks into a lower lava sequence dominated by island-arc tholeiitic basalts and derivatives, and an upper lava sequence of highly depleted arc tholeiites of boninitic affinity. Both lava sequences are made up of a variety of volcanic forms: pillow lavas, sheet flows and breccia flows.

Pillow volcanoes, as described by Schmincke and Bednarz (1990) are comprised of mainly basaltic andesites. Large 3 m × 6 m bulbous megapillows (Figure 7A), related to long-lived trunk feeder systems, make up the basal core facies. The bulk of the pillow volcano, the main facies, has somewhat smaller lava tubes. The discontinuous top facies is made up of isolated minipillows and slope debris. The latter was often oxidized by seafloor weathering.

A

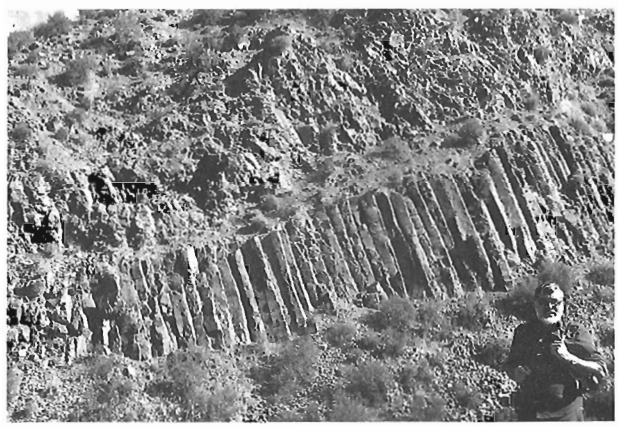

B

C

Figure 7: (A) Massive pillow lavas in the core facies of a pillow volcano. (B) Basal colonnade of sheet flow. (C) Glassy breccia unit of near-vent facies of a breccia volcano. All photographs from Akaki River canyon.

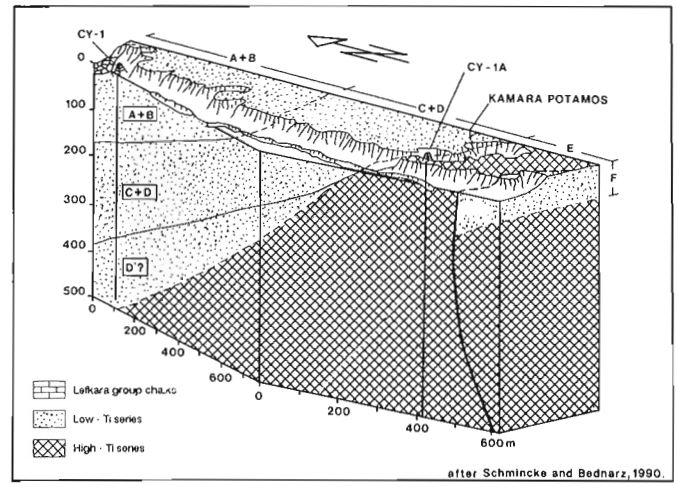

Figure 8: Representative cross-section of the Akaki River section showing distribution of volcanic units and relative positions of CY-1 and CY-1A. (After Schmincke and Bednarz, 1990).

Sheet flow volcanoes contain ponded flows that may extend upwards in tubular protrusions. More extensive sheet flows with well developed colonnades (Figure 7B) grade marginally into pillows and breccias. The sheet flows are thought to have formed at high eruptive rates (Schmincke and Bednarz, 1990).

Breccia volcanoes formed only from the most viscous magmas, and are therefore dominated by andesitic, dacitic, and rare rhyolitic compositions. As such they are found most commonly in the lower part of the volcanic succession. Breccia flows form dome-like masses with irregular extrusive breccias in the vicinity of an eruptive vent (Figure 7C), and glassy sheet flows further away.

Strike and dip of the volcanic rocks along the Akaki River canyon appear to be uniform at 90°/20°N. Thirteen volcanic units have been recognized in the upper portion of the canyon in the region of the CY-1 and CY-1A boreholes (Figures 4, 8 and Schmincke and Rautenschlein, 1987). These are designated A to M and represent examples of both the upper depleted tholeiitic series with low in Ti contents (units A, B, C, D, F, and H), and the lower basalt-andesite-dacite-rhyolite series with relatively higher Ti concentrations (units E, G, I, J, K, L, and M) (Robinson et al., 1983). The thickness of each volcanic units varies between 50 and 400 metres and averages 120 m (Schmincke and Bednarz, 1990). Units consist of volcanic rocks with similar characteristics, i.e. dominantly pillows or sheet flows etc., and boundaries are drawn where one major lithological type changes abruptly. However, within one unit the lithologies may grade into one another, indicating gradual changes in eruptive conditions.

Unit A1 consists of grey, low-Ti, olivine-phyric pillow lavas with calcite and manganese-oxide veining. Unit A2 is a primary extrusive breccia. Unit A3 consists of pillow lavas which show concentrations of cumulate olivine crystals in the lower third of each pillow. Much of the olivine is

replaced by Fe-hydroxide-stained calcite. Unit A4 is made up of large lava tubes with interpillow breccia formed from altered pillow rinds.

Unit B is characterized by a series of pillowed, low-Ti basalts with sparse green clinopyroxene phenocrysts. These are underlain by megapillows that are thought to be the feeders to this unit.

Sheet flows dominate Unit C. The sheet flows have a basal colonnade overlain by massive coarse-grained basalt, becoming progressively more vesicular upward, and a top zone of glass-rich breccia.

Units D and F are composed of pillows, large tubes, and dykes, and Unit H is made up of large irregularly shaped bodies, pillow lavas, dykes, sills, and large tubes. These three units are found interleaved with units that have the chemical characteristics of the Lower Lava Series.

Unit E (the highest unit cored in CY-1A) consists of pillow lavas and sheet flows. Unit G is an unusually light-coloured flow consisting of vesicular spatter-like wispy clasts tightly welded together.

Units I and K comprise sheet flows, extrusive breccia and hyaloclastites, dykes and sills, and locally large tubes. Unit J is similar but lacks the breccias and hyaloclastites. Units L and M are pillow lava units with local hyaloclastites, dykes, and sills.

The apparent interbedding of lavas of high-Ti and low-Ti affinity is probably the result of normal faulting which has down dropped a number of blocks of the Upper Lava Series higher in the canyon (Figure 7).

Schmincke and Bednarz (1990) estimate that the total extrusive crust above the Sheeted Dyke Complex on the northeastern flank of Troodos is made up of between five and ten individual volcanoes. There is very little interstratified sediment and therefore time gaps between the construction of the individual volcanoes appear to have been relatively short. Normal faults suggest that the volcanism was accompanied by crustal extension and subsidence. The general volcanic and structural evolution was marked by a series of volcano-tectonic-hydrothermal cycles, where non-volcanic extension markedly increased the permeability of the upper crust leading to enhanced circulation of seawater (Figure 9).

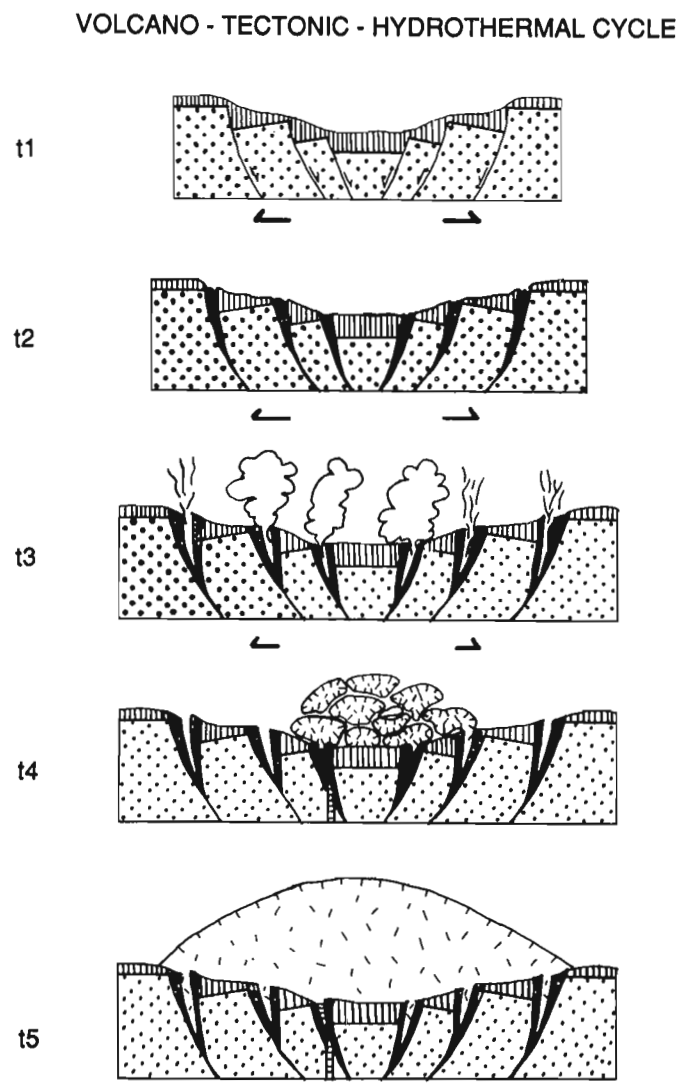

Figure 9: A schematic volcano-tectonic-hydrothermal cycle as represented by extrusive rocks of the Akaki River canyon section. (After Schmincke and Bednarz, 1990). Initial volcanic extension is followed by extensive hydrothermal activity and subsequent extrusion and building of the volcanic edifice.

(b) Chemistry of the lava series

Early workers divided the extrusive section of the Troodos ophiolite into two units, the Upper Pillow Lavas and the Lower Pillow Lavas, locally separated by an angular unconformity and by thin layers of ochreous sediment or haematitic shales (Wilson and Ingham, 1959; Carr and Bear, 1960; Bear, 1960; see Figure 10). After studying the alteration and metamorphism of the lavas, Gass and Smewing (1973) and Smewing et al. (1975) modified this early subdivision and defined axis and off-axis sequences. The boundary between the two sequences was based upon a relative lack of secondary mineralization in the younger off-axis sequence.

Studies by Robinson et al. (1983), Gillis (1987), and Gillis and Robinson (1985) suggest that this interpretation is incomplete and based on erroneous data. The volcanic sequence, as exemplified by the outcrops in the Akaki canyon, has not been pervasively metamorphosed but contains widespread occurrences of fresh volcanic glass. The glass persists down to the top of the sheeted dykes, and the distribution of zeolites and other secondary minerals such as celadonite is not stratigraphically controlled but reflects variations in permeability, lithology (e.g. pillowed vs. massive sheet flows), and proximity to intrusions (Gillis and Robinson, 1985). Glass compositions allow the division of the volcanic pile into two distinct

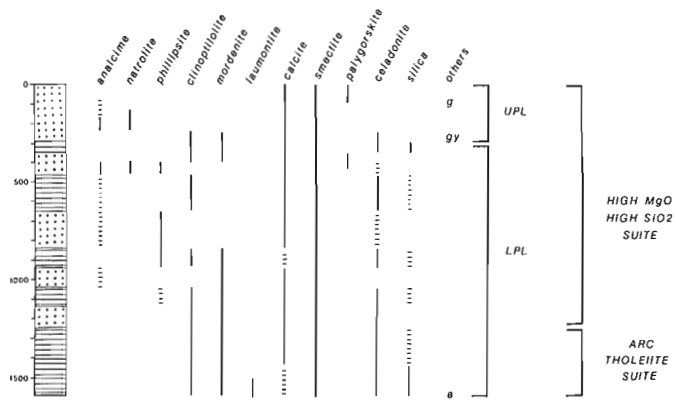

Figure 10: Metamorphic mineral zonation, stratigraphic and geochemical subdivision of the Troodos extrusives (After Gillis and Robinson, 1985).

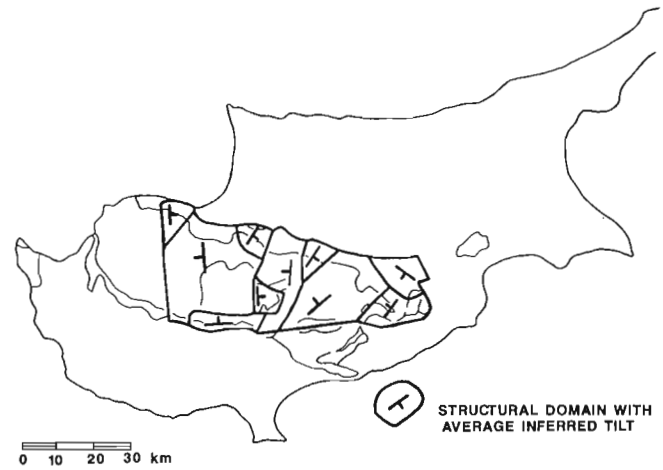

Figure 11: Structural domains of the Troodos ophiolite inferred from orientation of dykes within the Sheeted Complex.

magmatic suites, a lower basalt-andesite-dacite-rhyodacite assemblage with high-Ti contents, and an upper picrite-basalt-basaltic andesite assemblage with much lower Ti concentrations. These upper flows are highly depleted rocks with boninitic affinities (Robinson et al., 1983). Only rarely do the previously defined stratigraphic units correspond to these lava suites. The picrite-basalt basaltic andesite assemblage includes not only the olivine-phyric Upper Pillow Lavas of previous workers but a significant section of aphyric lavas previously included in the Lower Pillow Lavas (Figure 10). Thus this major geochemical boundary in the Akaki River canyon is some distance lower in the section than the classic Upper/Lower lava boundary.

Within the more depleted suite, the predominance of picritic lavas in the upper part of the section suggests that they were derived from the lower parts of fractionated magma chambers, whereas the underlying aphyric basalts and basaltic andesites were presumably drawn from higher levels (Malpas and Langdon, 1984).

Although at times indistinguishable in the field, the two assemblages have clear mineralogical differences. The basalt-andesite-dacite-rhyolite assemblage contains rare silicic differentiates, is fine grained throughout, and is aphyric to very sparsely phyric with microphenocrysts of plagioclase, clinopyroxene, orthopyroxene, and iron-titanium oxides. The overlying high-MgO high-SiO_2 low-Ti suite consists of dark grey to greenish-grey, fine-grained, aphyric to highly olivine-phyric basalts. Porphyritic olivine is commonly accompanied by smaller amounts of clinopyroxene and spinel. In the most magnesian rocks orthopyroxene is also common. The groundmass contains abundant microlites of clinopyroxene, accompanied by plagioclase laths and some iron-titanium oxides.

The Basal Complex and Sheeted Dykes

The extrusive section of the Troodos ophiolite grades downwards into the Sheeted Complex through a zone of intermixed diabase dykes and pillow screens known as the Basal Group. This zone is several hundred metres thick in the Akaki River canyon, but the transition from lavas to dykes is particularly rapid over a 100 m-thick vertical interval where the proportion of dykes increases from 50% to 95%. Above this level the dykes that are present are irregular in strike and dip.

Numerous dykes and the uncertain eruptive morphology of the irregularly shaped breccia volcanoes of the more differentiated basalt-andesite-dacite-rhyolite series make volcanic units difficult to define in the Basal Group. Faulting and alteration are more pervasive in this zone, adding further complications.

The Sheeted Complex ranges from about 1 to 1.2 km thick beneath the Basal Group. It forms a concentric belt around the plutonic core, and throughout most of its thickness, dykes intrude dykes in a classic sheeted fashion. Individual dykes within the Sheeted Complex range from a few centimetres to approximately 5 m-wide but most are less than 2 m. They consist of fine- to medium-grained, generally aphyric basalt and andesite with small amounts of olivine- and pyroxene-phyric basalt. Many dykes are hydrothermally altered to greenschist assemblages but the original igneous textures are preserved and one-sided chilling is commonly observed.

Verosub and Moores (1981) have identified structural domains within the Sheeted Complex in which the dykes have similar attitudes (Figure 11). They have postulated that these domains are bounded by listric normal faults that developed during crustal construction. Such deformation contemporaneous with volcanism is also suggested by the truncation of early sets of dykes by one or more later sets.

COMPARISON WITH OCEAN CRUST

The Troodos ophiolite readily allows study of ocean-crust forming processes. A realistic comparison must, however,

recognize the physical and chemical differences between the Troodos lavas and typical tholeiitic MORB. High vesicularity suggests that Troodos magmas had a much higher primary volatile content than MORB magmas (Rautenschlein, 1987). This is not surprising as the suprasubduction zone Troodos magmas are thought to have been generated by partial melting under hydrous conditions. The high primary volatile (mainly water) contents of the magmas probably influenced their extrusive behaviour, reduced the density of the crust with increased vesicularity, and increased the proportion of glassy lavas (Schmincke and Bednarz, 1990). The higher volatile content may also have offset increased viscosity resulting from the more siliceous nature of the Troodos lavas. However, the abundance of these more siliceous differentiated magmas, particularly in the lower lavas, suggests longer magma chamber residence times and thus more efficient fractionation processes. This may indicate relatively slow spreading of the Troodos ocean basin. Unfortunately there are many factors, including the compositional nature of the primary melts, that make this argument tenuous. Nevertheless, the Troodos crust likely formed in a small ocean basin above a subduction zone and integrated spreading rates were probably small.

REFERENCES

Bear, L.M.
1960: The geology and mineral resources of the Akaki-Lythrodondha area; Cyprus Geological Survey Department Memoir, v. 3, 222 p.

Carr, J.H. and Bear, L.M.
1960: The geology and mineral resources of the Peristerona-Lagoudhera area; Cyprus Geological Survey Department Memoir, v. 2, 79 p.

Follows, E.J. and Robertson, A.H.F.
1990: Sedimentology and structural setting of Miocene reefal limestones in Cyprus; *in* Malpas, J., Moores, E.M., Panayiotou, A., and Xenophontos, C., Ophiolites — Oceanic Crustal Analogues. Proceedings of the Symposium 'TROODOS 1987,' Cyprus Geological Survey Department, Nicosia, p. 185–206.

Gass, I.G. and Smewing, J.D.
1973: Intrusion, extrusion, and metamorphism at constructive margins: evidence from the Troodos massif, Cyprus; Nature, v. 242, p. 26–29.

Gibson, I.L., Malpas, J., Robinson, P.T., and Xenophontos, C., eds.
1989: Cyprus crustal study project: Initial Report, Hole CY-4; Geological Survey of Canada, Paper 88–9, 393 p.

Gillis, K.M.
1987: Multistage alteration of the extrusive sequence, Troodos ophiolite, Cyprus; (PhD Thesis), Dalhousie University, Halifax, 387 p.

Gillis, K.M. and Robinson, P.T.
1985: Low temperature alteration of the extrusive sequence, Troodos ophiolite, Cyprus; Canadian Mineralogist, v. 23, p. 431–441.

Hsü, K.J., Montadert, L., Bernoulli, D., Cita, M.B., Erickson, A., Garrison, R.E., Kidd, R.B., Mélières, F., Müller, C. and Wright, R.
1978: History of the Mediterranean salinity crisis; *in* Hsu, K.J., Montardert, L., et al., Initial Reports of the Deep Sea Drilling Project, v. 42 (Part 1), U.S. Government Printing Office, Washington, p. 1053–1078.

Malpas, J. and Langdon, G.
1984: Petrology of the Upper Pillow Lava suite, Troodos ophiolite, Cyprus; *in* Gass, I.G., Lippard, S.J., and Shelton, A.W., Ophiolites and Oceanic Lithosphere, Geological Society of London, Special Publication, No. 14, p. 155–167.

Malpas, J., Xenophontos, C., and Williams, D.
The Ayia Varvara Formation of S.W. Cyprus: A product of complex collisional tectonics; Tectonophysics, ms submitted.

Murton, B.J. and Gass, I.G.
1986: Western Limassol Forest Complex, Cyprus: part of an Upper Cretaceous leaky transform fault; Geology, v. 14, p. 255–258.

Pantazis, T.M.
1967: The geology and mineral resources of the Pharmakas-Kalavasos area; Cyprus Geological Survey Department Memoir, v. 8, 100 p.

Rautenschlein, M.
1987: Geology and geochemistry of Akaki volcanics, Cyprus; (PhD Thesis), Ruhr-Universität Bochum, 222 p.

Robertson, A.H.F. and Hudson, J.D.
1974: Pelagic sediments in the Cretaceous and Tertiary history of the Troodos Massif, Cyprus; International Association of Sedimentologists, Special Publication, v. 1, p. 403–436.

Robinson, P.T., Gibson, I., and Panayiotou, A., eds.
1987: Cyprus Crustal Study Project: Initial Report, Holes CY-2 and CY-2A; Geological Survey of Canada, Paper 85–29, 381 p.

Robinson, P.T., Melson, W.G., O'Hearn, T. and Schmincke, H.-U.
1983: Volcanic glass compositions of the Troodos ophiolite, Cyprus; Geology, v. 11, p. 400–404.

Schmincke, H.-U. and Bednarz, U.
1990: Pillow, sheet flow and breccia flow volcanoes and volcano-tectonic-hydrothermal cycles in the Extensive Series of the northeastern Troodos ophiolite (Cyprus); *in* Malpas, J. et al., eds., Ophiolites: Oceanic Crustal Analogues, Cyprus Geological Survey Dept., p. 185–206.

Schmincke, H.-U. and Rautenschlein, M.
1987: Volcanology along the Akaki River canyon; *in* Xenophontos, C. and Malpas, J., Field Excursion Guidebook. Troodos 87: Ophiolites and Oceanic Lithosphere, Cyprus Geological Survey Department, Nicosia, p. 36–91.

Simonian, K.O. and Gass, I.G.
1978: Arakapas fault belt, Cyprus: a fossil transform belt; Geological Society of America: Bulletin, v. 89, p. 1220–1230.

Smewing, J.D., Simonian, K.O., and Gass, I.G.
1975: Metabasalts from the Troodos massif, Cyprus; genetic implications deduced from petrography and trace element geochemistry; Contributions to Mineralogy and Petrology, v. 51, p. 49–64.

Verosub, K.L. and Moores, E.M.
1981: Tectonic rotations in extensional regimes and their paleomagnetic consequences for oceanic basalts; Journal of Geophysical Research, v. 86, p. 6335–6349.

Vine, F.J. and Smith, G.C.
1990: Structure and physical properties of the Troodos crustal section at ICRDG drillholes CY-1, 1-a and 4; *in* Malpas, J., Moores, E.M., Panayiotou, A., and Xenophontos, C., Ophiolites — Oceanic Crustal Analogues. Proceedings of the Symposium 'TROODOS 1987,' Cyprus Geological Survey Department, Nicosia, p. 113–124.

Wilson, R.A.M. and Ingham, F.T.
1959: The Geology of the Xeros-Troodos area with an account of the mineral resources; Cyprus Geological Survey Department Memoir, No. 1, 184 p.

Xenophontos, C. and Malpas, J.G.
1987: Field Excursion Guidebook. Troodos 87: Ophiolites and Oceanic Lithosphere, Cyprus Geological Survey Department, Nicosia, p. 260–285.

Zomenis, S.L.
1972: Stratigraphy and hydrogeology of the Neogene rocks in the northern foothills of the Troodos massif; Cyprus Geological Survey Department Bulletin, No. 5, p. 22–90.

Alteration of the ICRDG CY-1 and CY-1A Drill Cores, Troodos Ophiolite: Mineralogical and Geochemical Studies

K.M. GILLIS[1] AND P.T. ROBINSON[2]

[1]Department of Geology, Dalhousie University, Halifax, Nova Scotia, B3H 3J5, Canada
[2]Center for Marine Geology, Dalhousie University, Halifax, Nova Scotia, B3H 3J5, Canada

Gillis, K.M. and Robinson, P.T., 1991: Alteration of the ICRDG CY-1 and CY-1A drill cores, Troodos ophiolite: mineralogical and geochemical studies; in Cyprus Crustal Study Project: Initial Report, Holes CY-1 and 1A, eds. Gibson, I.L., Malpas, J., Robinson, P.T., and Xenophontos, C.; Geological Survey of Canada, Paper 90–20, p. 41–60, 1991.

Abstract

The Cyprus Crustal Study Project drillholes CY-1 and CY-1A sampled a continuous section through the extrusive sequence of the Troodos ophiolite. Four alteration zones are recognized: (1) The Seafloor Weathering Zone (SWZ, 0–275 m depth) is characterized by pervasive alteration, intense oxidation, temperatures $\leq$50°C, high water/rock ratios, and Fe-hydroxides, smectite, K-feldspar, calcite, and palygorskite. Rocks are enriched in K_2O, Rb, Ba, Sr, and CO_2 and depleted in SiO_2 and Na_2O; (2) The Low-Temperature Zone (LTZ, 275–675 m depth) is characterized by large variations in the pervasiveness of alteration, temperatures $\leq$100°C, high to moderate water/rock ratios, and smectite, celadonite, Na-Ca zeolites, and calcite. Rocks are enriched in N_2O, K_2O, Rb, and Ba and depleted in SiO_2 and Sr; (3) The Transition Zone (TZ, 675–750 m depth) is characterized by temperatures $\geq$100 – $\leq$200°C, moderate to low water/rock ratios, and mixed-layer smectite/chlorite, laumontite, quartz, and pyrite; (4) The Upper Dyke Zone (UDZ, 750–1176 m depth) is characterized by complete recrystallization of the groundmass, temperatures $\geq$200°C, low water/rock ratios, and chlorite, quartz, pyrite, albite, and epidote. Rocks are enriched in Na_2O, MnO, Cu, and Zn and depleted in CaO, K_2O, Rb, and Sr.

Four stages of alteration are proposed. Stages 1 through 3 were continuous from crustal accretion to >20 Ma; Stage 4, restricted to the SWZ and upper tens of meters of the LTZ, is related to a later seawater circulation event. The sharp boundary between the low- and high-temperature zones implies that the thermal gradient in the Troodos oceanic crust was stepped during the early stages of alteration.

Résumé

Les trous de forage CY-1 et CY-1A du projet d'étude de la croûte chypriote présentent un échantillon d'une section continue à travers la section extrusive de l'ophiolite de Troodos. On y observe quatre zones d'altération : (1) La zone d'altération désagregée de la couche océanique (de 0–275 m de profondeur) est caractérisée par une profonde altération, une intense oxidation, des températures $\leq$50°C, des rapports élevés eau/roches, et des hydroxides de fer, de la smectite, du feldspaths potassiques, de la calcite et du palygorskite. Les roches sont enrichies en K_2O, Rb, Ba, Sr et CO_2 et pauvres en SiO_2 et Na_2O. (2) La zone de basse température (275–675 m de profondeur) est caractérisée par une très grande diversité de la zone d'altération, des températures $\leq$100°C, des rapports eau/roche allant de hautes à modérés, de la smectite, de la celadonite, des zéolites Na-Ca et de la calcite. Les roches sont riches en N_2O, K_2O, Rb et Ba et pauvres en SiO_2 et Sr. (3) La zone de transition (675–750 m de profondeur) est caractérisée par des températures $\geq$100 – $\leq$200°C, des rapports eau/roche allant de modérées à basse, et des couches alternées de smectite/chlorite, de laumonite, de quartz et de pyrite. (4) La zone supérieure du dyke (750–1176 m de profondeur) est caractérisée par une recrystalisation complète de la matrice, des températures $\geq$200°C, de faible rapports eau/roche, du chlorite, du quartz, du pyrite, de l'albite et de l'épidote. Les roches sont riches en Na_2O, MnO, en cuivre et en zinc, et pauvre en CaO, K_2O, Rb et Sr.

On propose quatre étapes d'altération. Les étapes 1 à 3 étaient continues allant de l'accrétion crustale à 20 m. a; l'étape 4, limitée à la zone d'altération océanique et aux dix mètres supérieurs de la zone de basse température, est reliée à un phénomène tardif de la circulation de l'eau de mer. La séparation très abrupte entre les zones de basse et haute températures implique que le gradient thermale de la croûte océanique de Troodos s'est accrue très tôt au cours de l'étape d'altération.

INTRODUCTION

One of the primary objectives of the Cyprus Crustal Study Project was to investigate the evolution of hydrothermal systems within the Troodos ophiolite. Prior to the on-set of drilling in 1982, studies of hydrothermal recharge zones (e.g., Gass and Smewing, 1973; Smewing, 1975; Spooner et al., 1977) led to the development of supposedly regional metamorphic zones whose grade and intensity of alteration were believed to increase with depth. Recent investigations of the extrusive sequence (Gillis, 1987) and the sheeted dyke complex (Baragar et al., 1987; Richardson et al., 1987; Schiffman et al., 1987) demonstrate that such metamorphic zones are not appropriate to describe alteration in Troodos or *in situ* oceanic crust (Alt et al., 1986).

The CY-1/1A drill cores sampled a continuous section through the extrusive sequence, from the lava/sediment boundary to the transition into the sheeted dyke complex. The alteration profile of these cores, which records the transition from a low- to high-temperature environment, has proved to be an excellent reference section for field studies (Gillis, 1987) and drilled sections of *in situ* oceanic crust (Gillis and Robinson, 1988). This paper describes the mineralogical and geochemical characteristics of four alteration zones recognized in these drill cores. A sequence of four alteration stages is proposed which reflect progressive changes in physical and chemical conditions in the Troodos ocean crust.

HOLES CY-1 AND CY-1A

The CY-1 and CY-1A drill cores represent a continuous stratigraphic section through the extrusive sequence and the transition into the sheeted dyke complex, allowing for 50–75 m of overlap. CY-1 was spudded in at the lava-sediment interface 1.5 km northwest of Malounda and penetrated the upper 475 m of the section. Thirty lithologic units, which vary in thickness from 5 to 50 m, have been defined (Robinson and Gibson, 1990). Pillowed lavas comprise 42%, massive and thin flows 32%, pillow fragment breccias 12%, and intrusions 2% of the recovered cores. A few dykes, 5–20 cm wide, intrude the section below 350 m and a 1.4 m fault breccia cuts the section at 438.0 m. Reddish-green, olivine- to sparsely olivine-phyric and picritic pillows and breccias in the upper 250 m of the section grade downward into greenish-grey to grey, aphyric to sparsely olivine-phyric pillows and flows.

CY-1A, drilled due west of Malounda, penetrated 702 m. Thirty lithologic units have been defined that are dominated either by pillows, glassy and crystalline flows, massive flows, or dykes (Horne and Robinson, 1986). Pillows comprise 7.2%, massive and sheet flows 45.5%, undifferentiated flows and dykes 6.6%, dykes 34.2%, and hyaloclastites 5.0% of the recovered core. Greyish-green, aphyric to sparsely olivine- and clinopyroxene-phyric pillows and flows comprise the upper 200 m. Aphyric dykes increase in abundance below this depth and interfinger with aphyric to sparsely plagioclase- and clinopyroxene-phyric flows and glassy breccias.

The rock types and their distribution in the CY-1 and CY-1A drill cores are similar to the equivalent stratigraphic section exposed along the Akaki River. The thickness of the recovered section is thinner than the field exposures (Schmincke et al., 1983) but is comparable to other studied sections along the northern flank of the ophiolite (Mehegan, 1988). In the remainder of this paper, CY-1 and CY-1A are considered a continuous depth profile with no stratigraphic overlap.

ALTERATION ZONES

Four alteration zones are recognized in the CY-1/1A drill cores and field exposures throughout the northern flank of the ophiolite on the basis of secondary mineral assemblages (Table 1; Figure 1) and field appearance: a Seafloor Weathering Zone (SWZ), a Low-Temperature Zone (LTZ), a Transition Zone (TZ), and an Upper Dyke Zone (UDZ). A fifth, Mineralized Zone (MZ), which includes massive sulfide deposits, mineralized stockwork zones, and smaller zones of mineralization, is located throughout the extrusive sequence (e.g., the zone of mineralization in CY-2A, see Robinson et al., 1987).

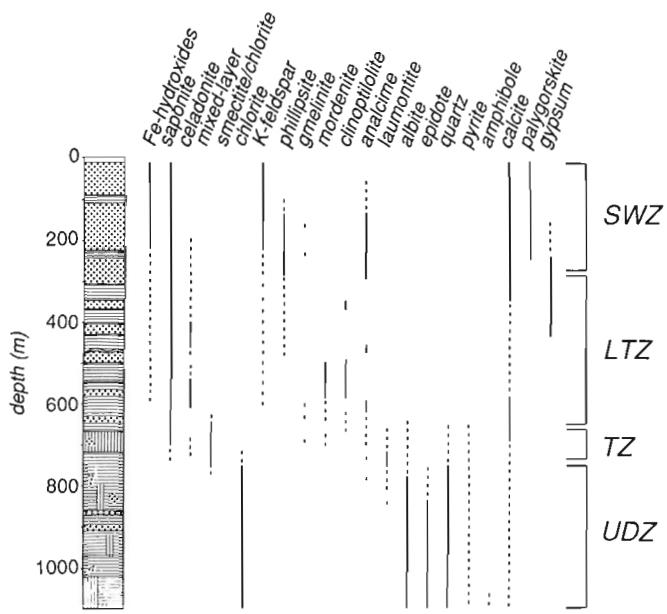

Figure 1: Distribution of secondary minerals in the CY-1/1A drill cores. Stratigraphic column on the left shows the major lithologic units: small dots represent pillows; horizontal lines represent massive and sheet flows; vertical lines represent dykes; open triangles represent breccias and hyaloclastites. Alteration zones are outlined on the left. Solid vertical lines indicate that the phase is found throughout the unit; dashed lines indicate that the phase is locally present.

Zone*	Primary minerals	Groundmass	Glassy Margins	Void–filling+	Chemical changes++
SWZ	Oliv → goet + calc (T) Cpx → smec (F–M) Spinel (F)	Cpx → smec (S) Plag → smec (S–M) Plag → K–spar (T) Timag — maghem (S–M) Mesos → smec, calc (M–T)	Smec ± phil (T)	1. Smec + Fe hydro 2. Anal, adularia 3. Calc 4. Paly	+K_2O, CO_2, Rb, Ba, $Fe_2O_3/(FeO+Fe_2O_3)$, Sr –SiO_2
LTZ	Oliv → goet + calc (T) Cpx → smec (F–S) Plag → smec, celad, calc (F–M) Spinel (F) Timag (F)	Cpx → smec (S) Plag → smec, celad, calc (F–M) Timag → maghem (S–M) Mesos → smec, celad, calc (M–T)	1. Smec ± phil ± anal 2. Smec ± celad ± clino	1. Smec + celad 2. Na–Ca zeolites, qtz, chal 3. Calc 4. Paly	+K_2O, Na_2O, Rb, Ba –CaO, SiO_2
TZ	Cpx → smec, smec/chl (S–M) Plag → albite (M–T) Timag (F)	Cpx → smec, smec/chl (S–M) Plag → smec, smec/chl (S–M) Plag → albite (M–T) Timag (F) Mesos → smec, smec/chl qtz (M–T)	Smec ± smec/chl ± laum ± qtz ± pyr	1. Smec ± smec/chl 2. Laum + qtz + pyr 3. Calc	+Na_2O, K_2O, Ba, (MnO, Zn, Cu) –CaO, Rb
UDZ	Cpx → chl (S–M) Plag → albite (T) Plag → epi, chl (M–T)	Cpx → chl (S–M) Plag → albite (T) Plag → epi + chl (M–T) Timaq → sphene (S–M) Mesos → chl, qtz, epi, pyr (T)	Chl ± qtz ± pyr ± epi	1. Chl ± epi ± qtz ± pyr 2. Qtz ± pyr 3. Calc	+Na_2O, (MnO, Cu, Zn) –CaO, K2O, Sr, Ba,
MZ#	Plag → ill + qtz (T) Timag → sphene (T)	Mesos → chl + qtz + pyr + sphene (T)	Chl + qtz + pyr	1. jasper + pyr + qtz 2. pyr ± chal ± pyrrh	

Table 1: Characteristics of the alteration zones. Note: F = fresh; S = slightly altered; M = moderately altered; T = totally altered; oliv = olivine; cpx = clinopyroxene; plag = plagioclase; Timag = titanomagnetite; mesos = mesostasis; smec = smectite; celad = celadonite; chl = chlorite; smec/chl = mixed–layer smectite/chlorite; paly = palygorskite; Fe hydro = Fe hydroxides; goet = goethite; maghem = maghemite; calc = calcite; anal = analcime; phil = phillipsite; clino = clinoptilolite; laum = laumontite; epi = epidote; chal = chalcedony; qtz = quartz; pyr = pyrite; chalco = chalcopyrite; pyrrh = pyrrhotite; ill = illite; K–spar = potassium feldspar. * SWZ = seafloor weathering zone; LTZ = low temperature zone; TZ = transition zone; UDZ = upper dike zone; MZ = mineralized zone. + Numbers indicate order of deposition, from oldest to youngest. # Summarized from Constantinou and Govette (1973) and Lydon (1984). These characteristics generally describe the zone of most intense alteration and mineralization in the MZ; for details of specific deposits see original references. ++ Calculated by comparing altered whole rock composition to unaltered equivalent (Gillis, 1987).

The Seafloor Weathering Zone is characterized by its reddish 'oxidized' halos along fractures and pillow margins, pervasive alteration, and an abundance of interpillow sediment. It extends downward from the lava-sediment boundary to 275 m depth in CY-1.

Thick glassy pillow margins and interpillow hyaloclastites are pervasively altered. Round to irregular palagonitized glass spalls, elongate parallel to the pillow margins, generally contain spherical granules of phillipsite, and perlitic cracks are filled with phillipsite. These spalls are enclosed within a green smectite - Fe hydroxide - phillipsite - analcime - calcite - palygorskite matrix. Yellowish-brown pillow margins, which owe their colour to the concentration of Fe-hydroxides, grade into greyish-green to greenish-grey pillow interiors.

Original groundmass textures are commonly preserved but may be obscured by the reddish-brown, fibrous to amorphous smectite which replaces the mesostatis; local concentrations of this clay mineral within segregation vesicles give the rocks a spotty appearance.

Several episodes of secondary mineral deposition are recognized from cross-cutting relations and depositional sequences within filled voids. The following generalizations may be made:

1. Smectite, mixed with Fe-hydroxides, lines vesicles, vugs, cracks, and fractures, and was the earliest phase to form (Figure 2A);
2. Where present, zeolites and adularia line voids and project inward toward open cavities;
3. Calcite was deposited in re-opened or cross-cutting veins (Figure 2A). Successive layers of euhedral crystals, mantled by a light dusting of smectite, indicate several stages of growth;
4. Composite veins of buff to white palygorskite and calcite, commonly with thin zeolite-rich zones, cut across and re-open the earlier veins (Figure 2B).

The Low-Temperature Zone extends from 275 to 675 m depth in the boreholes (Figure 1). It is characterized by significant variations in alteration intensity between, and within, individual lithologic units, distinctive assemblages of secondary minerals for pillows and flows, and the random preservation of fresh volcanic glass.

Greyish-green to greenish-brown pillows and breccias generally lack the pronounced colour zonation seen in the SWZ. Chilled margins are pale-green where pillows are highly altered and are dark green to black where pillows are relatively fresh. Glass is variably altered to smectite ± phillipsite ± analcime. Interpillow sediment, hyaloclastite, or breccia fill the pillow interstices.

The degree of alteration within the massive and sheet flows is quite variable. Most flows are relatively fresh with minor surficial celadonite and/or hematite staining. Zones of intense alteration locally occur along flow margins and to a lesser

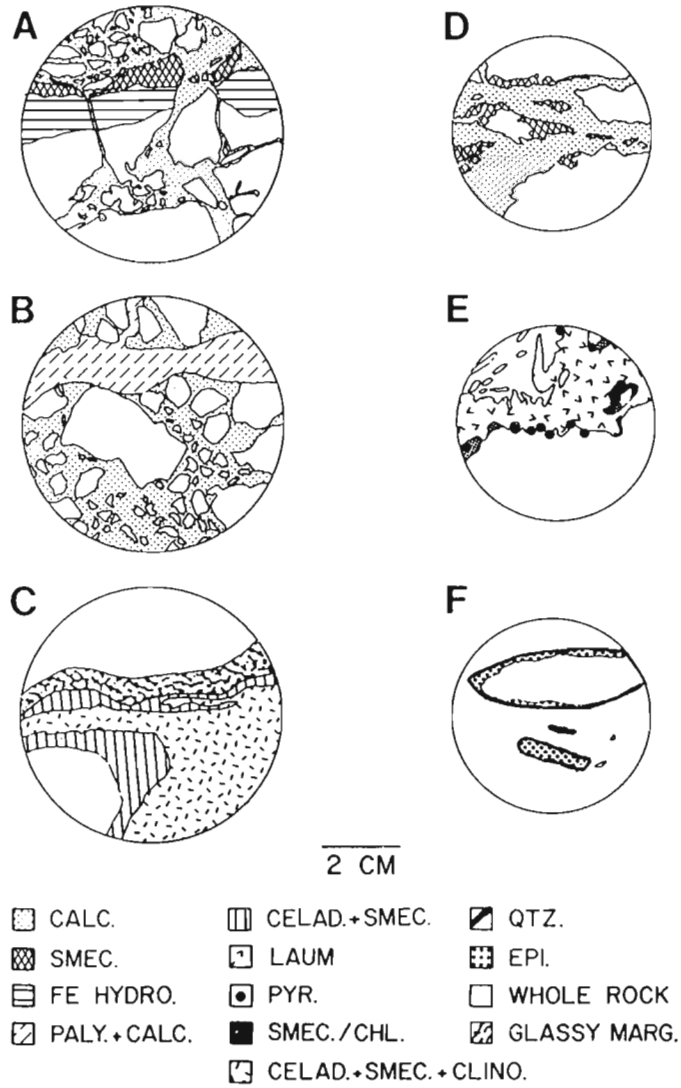

Figure 2: Precipitation sequences in each of the alteration zones. A. (SWZ) Calcite stringers with inclusions of basalt fragments cross-cut a chilled pillow margin. An oxidized halo rims the outer margin of the sample (sample CY1 : 58.50 m). B. (SWZ) Late-stage palygorskite + calcite vein cross-cuts a heterolitic breccia in a calcite matrix (sample CY1 : 25.95 m). C. (LTZ) Upper flow margin altered to celadonite + smectite + clinoptilolite. Glassy margin is partially palagonitized (sample CY1A : 45.80 m). D. (LTZ) Calcite, with minor analcime, fill re-opened smectite-filled fracture (sample CY1 : 256.20 m). E. (TZ) Laumontite filled vug is lined with mixed layer smectite/chlorite and pyrite (CY1A : 300.45 m). F. (UDZ) Chlorite-lined vug is coated with quartz and partially filled with epidote (CY1A : 432.72 m). Glassy Marg. = glassy margin; other abbreviations are given in Table 1.

extent along joint surfaces. These zones consist of celadonite mixed with smectite, clinoptilolite, mordenite, and calcite and may contain massive jasper nodules.

Joint surfaces of flows, lined with mixtures of celadonite and smectite, are thinly coated with platy-brown sepiolite, calcite rhombs, bluish-white opal, or pyrite. Hematite locally stains fracture surfaces and penetrates inward along flow margins which have not been 'celadonitized.' Concentric clay and Fe-hydroxide-rich rings, 2–3 mm wide and spaced 5–20 mm apart, are generally parallel to the outer 3–10 cm of columnar joints. Alteration of the groundmass is more pervasive within these rings than in other parts of the flow.

Discontinuous stringers of smectite and celadonite, with or without zeolite or calcite, form within individual flow units. In some cases these stringers appear to replace aphanitic or glassy patches within the crystalline portion, whereas in others they fill cracks. Stringers rarely have alteration halos in the adjacent groundmass.

Primary igneous textures are preserved within all cooling units and pale brown to yellowish-green smectite replaces the mesostasis. Celadonite and quartz are also part of the groundmass alteration assemblage in flow units. Alteration within segregation vesicles is similar to that in the SWZ. Miarolitic voids, most common in thick flow units, are variably filled with clay minerals.

The diversity and discontinuous nature of the vein systems reflect the heterogeneous style of alteration characteristic of the LTZ. Despite this heterogeneity, some generalizations may be made:

1. In all cooling units, smectite ± Fe-hydroxides is the first phase to form, lining cracks, fractures, vesicles, and vugs (Figure 2D);

2. Assemblages of analcime, phillipsite, gmelinite, natrolite, and chabazite fill vesicles and fractures in pillowed units. Where analcime and phillipsite occur together, phillipsite is the earliest phase to form;

3. Assemblages of celadonite, smectite, clinoptilolite, mordenite, and silica replace glassy zones and fill fractures and cracks in massive and sheet flows (Figure 2C). Where clinoptilolite and mordenite occur together, clinoptilolite is generally the first phase to form;

4. Calcite fills re-opened or cross-cutting veins (Figure 2D). Successive layers of euhedral crystals, mantled by a light dusting of clay, indicate several stages of growth.

5. Palygorskite + calcite ± zeolite veins and stringers of gypsum re-open pre-existing veins and fill clay-lined fractures. Gypsum is restricted to the LTZ.

The Transition Zone has characteristics of both the overlying LTZ and the underlying UDZ. Its upper boundary, at 675 m, is marked by the appearance of laumontite; its lower boundary at 750 m, is marked by the dominance of chlorite-quartz-pyrite in the groundmass and the appearance of epidote. In CY-1A, it is also marked by the disappearance of laumontite. In field exposures, however, laumontite commonly overprints epidote in the UDZ (Gillis, 1987).

Light to dark green pillow and flow margins and glassy brecciated zones are variably altered to smectite, mixed-layer smectite-chlorite, laumontite, and quartz. Clinoptilolite, mordenite, and celadonite with smectite locally replace glassy zones in the upper few tens of meters.

Ovoid, clay-lined vugs are either open or partially to totally filled with assemblages of quartz, laumontite, calcite, pyrite, and clay minerals (Figure 2E). Prismatic quartz radiates inward from the vug walls; laumontite fills the interstices. Where present, calcite is the latest phase to form and locally appears to replace laumontite. Vesicles are locally filled with mixtures of gmelinite, chabazite, and calcite.

Smectite, mixed-layer smectite-chlorite, or rarely, chlorite line fractures and cracks which are locally filled with assemblages of pyrite, laumontite, calcite, analcime, and quartz. Light grey, 1–2 mm-thick-halos, rich in quartz and very fine-grained pyrite, commonly rim narrow pyrite + quartz + chlorite stringers. Analcime is restricted to the upper half of the zone.

The Upper Dyke Zone extends from 750 m to the base of the CY-1A drill core where dykes and massive units are the dominant lithologies. The mesostasis of these rocks is completely recrystallized to chlorite + quartz ± pyrite ± epidote. Where present, pyrite is disseminated throughout the groundmass. Epidote is generally concentrated in irregular patches which do not appear to be fracture- or crack-controlled. Distinctive, irregular, mauve to light-green zonation reflects the relative proportions of quartz and chlorite, respectively, in the groundmass.

Flow and dyke margins are completely altered to chlorite, quartz and epidote assemblages; no fresh glass is preserved. The initial brecciated textures in flow tops are generally preserved although the fragments are completely recrystallized. Discontinuous, angular, jasper-rich zones appear to overprint earlier quartz + chlorite + epidote assemblages.

Epidosites which contain dominantly epidote with minor quartz, chlorite, magnetite, and jasper are erratically distributed. These irregular zones range from cms to tens of cms in size and appear to fill voids and replace the surrounding groundmass.

Igneous textures are generally preserved although in areas of most intense alteration, as in the epidosites, they are obliterated. Textures in segregation vesicles are obscured because the groundmass is completely altered to very fine-grained epidote, quartz, and chlorite. Chlorite-lined vesicles and vugs are rimmed with quartz and filled with assemblages of epidote, pyrite, calcite, chlorite, and prehnite (Figure 2F).

Veins are much less abundant than in the overlying zones. Fractures and cracks are lined with mixtures of chlorite, albite, quartz, and pyrite and are locally coated with Fe-stained calcite. Narrow pyrite and quartz stringers are rimmed by light-green, chlorite-rich halos whereas randomly distributed veins of pyrite, 10–15 mm wide, lack halos.

SECONDARY MINERALS

Methods of Identification

The secondary minerals were identified, either as single phases or as assemblages of phases, using a Phillips X-ray diffractometer with Cu Kα radiation. Clay minerals were gently crushed in water in an agate mortar, pipetted onto a frosted glass slide, and air-dried. These oriented smear mounts were scanned from 3–30° 2θ at a scanning speed of 1° 2θ per minute, treated with ethylene glycol at 60°C for 36 to 48 hours, and re-scanned under the same conditions. Selected samples were heated at 500°C for two hours, slowly cooled, and rescanned. Smear mounts of the remaining secondary minerals were scanned from 3–45°. Quartz was periodically added to samples for internal calibration.

Mineral analyses were obtained using a fully automated JEOL JXA-50A wavelength dispersive microprobe at Memorial University of Newfoundland, a JEOL 733 microprobe at Dalhousie University, and a MARKV Cambridge EDS micro-probe at Dalhousie University. The operating conditions were: (1) JEOL JXA-50A: 22 na, 20 kv accelerating voltage, 10 sec. counting time; (2) JEOL 733: 15 kv, 5 na, 10 sec.; (3) Cambridge: 15 kv, 5 na, 100 sec. To minimize loss due to volatilization in the hydrous phases, Na, Ca, and K were analyzed first and counted for 10 seconds on the wavelength dispersive systems.

Due to the high volatile content of most secondary phases and the heterogeneity of most clay minerals, the quality of the data is difficult to access. Structural formulas were calculated for all analyses; if these were stoichiometric the analyses were deemed good.

Structural formulas for saponite, celadonite, and mixed-layer smectite/chlorite were calculated assuming 22 (O,OH) following the method of Ross and Hendricks, (1945). Si and the necessary Al were assigned to the tetrahedral site to total 8.00. The excess Al, Mg, Fe, and Ti were assigned to the octahedral site. Ca, Na, and K were assigned to the interlayer position. Structural formulas for chlorite were similarly calculated using 28 (O, OH).

Clay Minerals

Smectite

Smectite is the most abundant secondary mineral, being characteristic of three of the five alteration zones. It is a 2:1 layer silicate, identified by its broad basal peak at 1.6 nm and the subsequent shift to 1.8 nm upon treatment with ethylene glycol (Brindley and Brown, 1980). Two types of smectite have been distinguished on the basis of calculated structural formulas: saponite and Al-saponite.

	1	2	3	4	5	6
SiO_2	42.51	46.94	38.32	55.86	47.71	14.25
TiO_2	0.13	–	0.06	0.40	0.11	0.04
Al_2O_3	10.01	8.86	7.91	17.77	15.88	5.15
FeO^T	12.60	6.75	22.21	10.74	14.39	55.44
MnO	0.18	0.08	0.02	0.11	0.18	0.19
MgO	19.68	21.40	10.56	5.71	8.77	2.62
CaO	0.98	1.38	2.40	0.78	0.76	0.72
Na_2O	0.63	0.07	0.09	0.59	0.46	–
K_2O	1.16	0.17	1.57	2.00	3.02	0.08
Total	87.88	85.65	83.14	93.96	91.28	78.49
	Cation Proportions on the basis of 22 (O,OH)					
Si	6.43	6.94	6.55	7.49	6.90	
Al^{iv}	1.57	1.08	1.45	0.51	1.10	
Total	8.00	8.00	8.00	8.00	8.00	
Al^{vi}	0.22	0.48	0.14	2.30	1.61	
Fe	1.60	0.83	3.17	1.20	1.74	
Mn	0.02	0.01	–	0.01	0.02	
Mg	4.44	4.72	2.69	1.14	1.89	
Ti	–	–	0.01	–	0.01	
Total	6.28	6.04	6.02	4.69	5.27	
Ca	0.16	0.22	0.44.	0.11	0.12	
Na	0.18	0.02	0.03	0.15	0.13	
K	0.22	0.03	0.34	0.34	0.56	
Total	0.56	0.27	0.81	0.66	0.81	

Table 2: Representative smectite analyses. – not detected; FeO^T = Total Fe as FeO; (1) orange-brown saponite, groundmass (KG:83:018); (2) orange-brown saponite, vein (KG:82:022); (3) orange-brown, Fe-rich saponite, groundmass (KG:83:176); (4) yellowish-green Al-saponite, vesicle (CY1:72.75 m); (5) yellowish-green Al-saponite, groundmass (CY1:75.25 m); (6) goethite-saponite mix (KG:82:062).

Saponite, a trioctahedral smectite, is characterized by a theoretical octahedral occupancy of 6.0 (Ross and Hendricks, 1945). It is generally orange-brown to brown with 1st to 2nd order birefringence. A plot of the molar proportions of Al_2O_3-FeO-MgO shows that the saponites are generally Mg-rich with low Al_2O_3 contents (Figure 3A). Within individual samples, FeO/(FeO+MgO) ranges from 0.2 to 0.8. The range of FeO/(FeO+MgO) narrows with increasing depth. The MnO content of saponite is generally <0.5 wt.% (Figure 4; Table 2).

Groundmass varieties are finely crystalline, fibrous, radiating, or globular. Saponite that fills voids is usually fibrous to platy and radiates out from the wall of the cavity.

The octahedral occupancy of Al-saponites ranges from 4.4–5.3 indicating either that its structure is intermediate or that it is a mixture of dioctahedral and triocthedral smectite (Alt and Honnorez, 1984). Al-saponite is pale yellow to pale brown

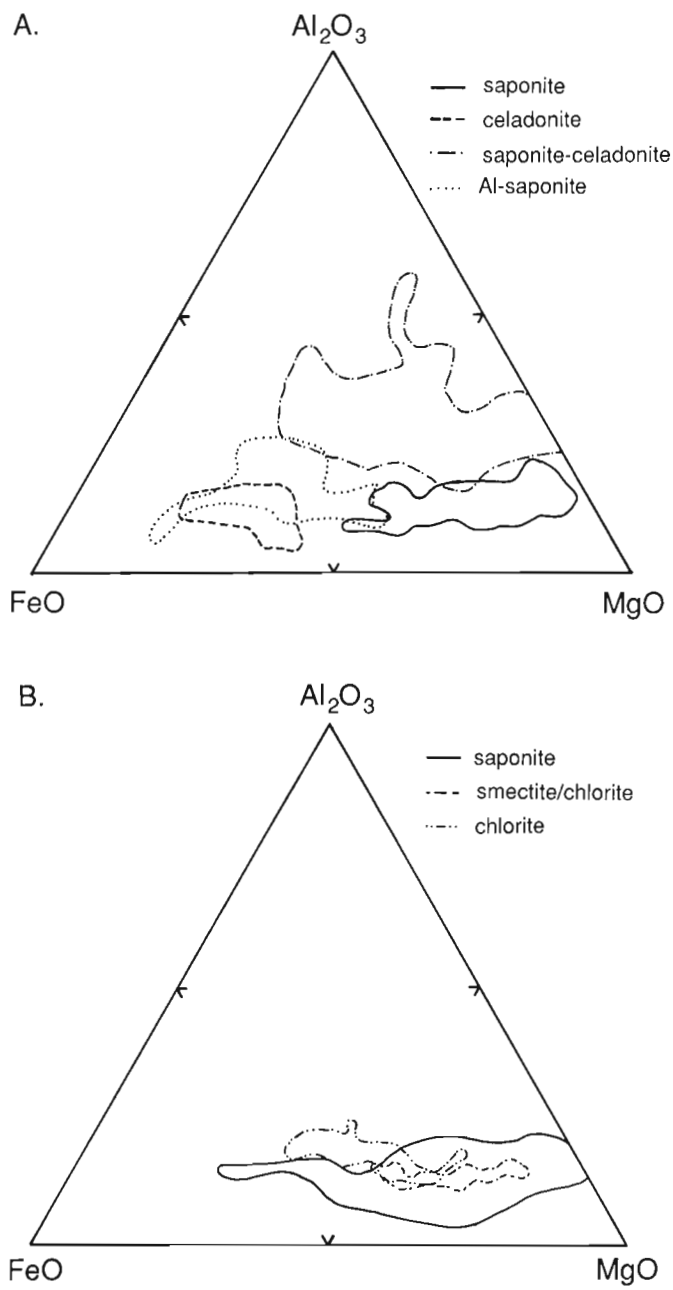

Figure 3: Molar Al_2O_3-FeO-MgO (AFM) proportions of clay minerals from the CY-1/1A drill cores. A. Saponite, Al-saponite, celadonite, and celadonite-saponite. B. Saponite, mixed-layer smectite/chlorite, and chlorite.

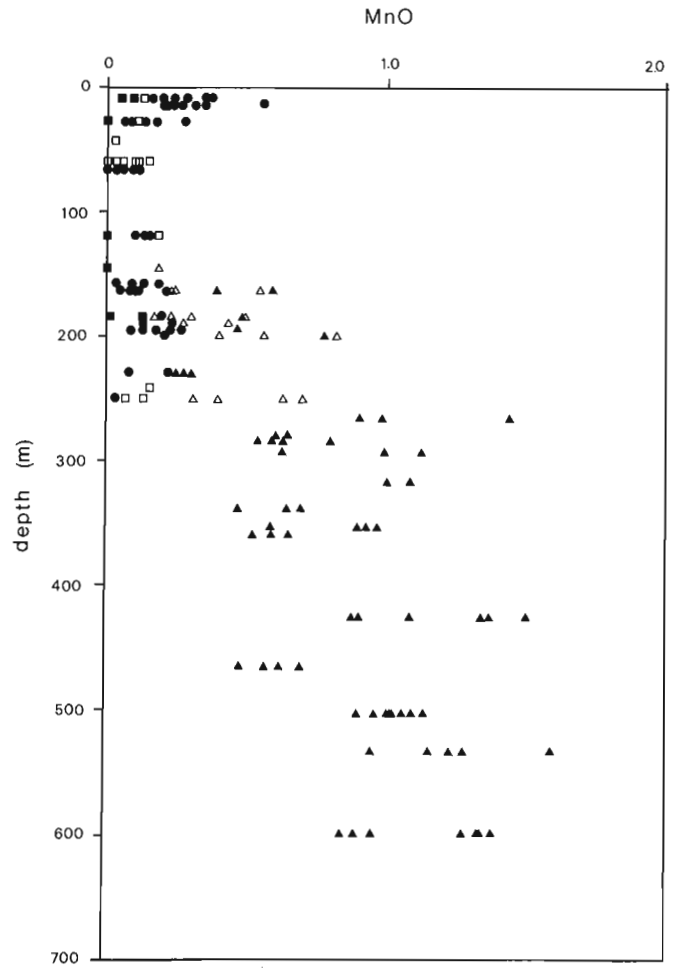

Figure 4: Variation in MnO content (wt.%) of the clay minerals with depth in the CY-1A drill core. Symbols: closed circles: saponite; open squares: celadonite; closed squares: celadonite-saponite; open triangles: mixed-layer smectite/chlorite; closed triangles: chlorite.

with 1st order birefringence and has the same range in habit as saponite.

Al-saponites are more aluminous and slightly more Fe-rich than saponite (Figure 3A; Table 2), suggesting that substitution of Al^{3+} for Mg^{2+} in the octahedral site resulted in an intermediate structure (Alt and Honnorez, 1984). It is also possible that Al-saponite may be a mixture of beidellite, an Al-rich, dioctahedral smectite, with saponite. The compositional continuity between saponite and Al-saponite (Figure 3A) and the absence of pure beidellite, however, make the former explanation preferable. More detailed XRD studies using non-oriented powdered mounts are required to differentiate between these possibilities. The FeO/(FeO+MgO) ratios of Al-saponites are variable within individual samples; there are no consistent compositional trends with depth. MnO contents are similar to saponite.

Al-saponite is generally restricted to the upper 500 m of the studied section and is most abundant in the SWZ.

Nontronite, a dioctahedral smectite, has been identified in the SWZ by X-ray analyses (Elsbree, 1985). Calculated structural formulas from this study did not confirm its presence. However, low-K celadonite may in fact be nontronite.

	1	2	3	4	5	6
SiO_2	55.85	49.57	52.32	55.80	52.55	(56.05–47.23)
TiO_2	0.16	0.23	0.11	–	0.14	(0–0.58)
Al_2O_3	2.32	8.14	6.16	0.77	3.90	(0.82–6.88)
Fe_2O_3T	19.69	15.16	18.70	22.24	19.12	(12.42–22.08)
MgO	6.18	10.59	6.64	6.13	6.34	(4.28–9.00)
CaO	–	0.43	0.17	0.07	0.21	(0.04–0.68)
Na_2O	0.10	1.35	0.13	0.04	0.15	(0–0.81)
K_2O	9.44	2.37	8.41	8.80	9.07	(7.69–10.28)
Total	94.17	87.58	92.54	93.78	91.48	–
	Cation Proportions on the basis of 22 (O,OH)					
Si	7.95	7.25	7.65	8.22	7.92	(7.66–8.18)
Al^{iv}	0.05	0.75	0.35	–	0.10	(0–0.34)
Total	8.00	8.00	8.00	8.22	8.02	
Al^{vi}	0.34	0.65	0.71	0.14	0.58	(0.04–8.18)
Fe	2.12	1.67	2.06	1.35	1.40	(0.09–2.16)
Mg	1.33	2.30	1.45	2.47	2.00	(1.42–2.54)
Ti	0.02	0.03	0.01	–	0.00	(0–0.02)
Total	3.81	4.65	4.23	3.96	3.98	
Ca	–	0.07	0.03	0.01	0.06	(0–0.20)
Na	0.03	0.04	0.04	0.02	0.02	(0–0.10)
K	1.73	0.44	1.56	1.66	1.75	(1.46–1.94)
Total	1.76	0.55	1.63	1.69	1.83	

Table 3: Representative celadonite analyses. – not detected; FeO^T = Total Fe as Fe_2O_3 (1) celadonite, vesicle (CY1A : 8.78 m); (2) celadonite-saponite, groundmass (CY1A : 49.57 m); (3) celadonite-saponite, vein (CY1A : 52.32 m); (4) celadonite, groundmass (KG : 82 : 165); (5) average and (6) range of 13 celadonites from Buckley et al., (1978).

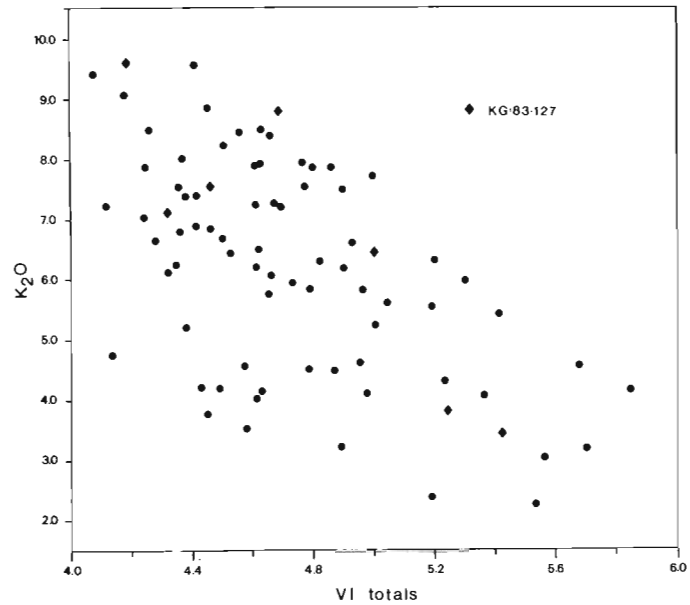

Figure 5: Relationship between K_2O contents (wt.%) and octahedral totals for celadonite and celadonite-saponite mixtures. Sample KG : 83 : 127 (diamond symbol) illustrates the variation within a single sample.

Celadonite

Celadonite, an Fe-rich dioctahedral mica, is commonly identified by its distinctive bluish-green color. X-ray analyses of celadonite indicate that most samples are intimate mixtures of celadonite and smectite. The observed d-spacings of pure celadonites correspond closely to those of Wise and Eugster, (1964).

Representative analyses of celadonite are shown in Table 3. For comparison, the average and range in composition of celadonites from the study of Buckley et al., (1978) are shown. Octrahedral totals generally range from 4.0–5.6, indicating that they are not true dioctahedral clays. A mixture of celadonite with trioctahedral saponite would result in an octahedral total intermediate between dioctahedral and trioctahedral. Further support for this interpretation is the systematic decrease in K_2O content with increasing octahedral totals and thus saponite component (Figure 5). The proportions of celadonite and saponite may be quite variable within a single sample as seen in Figure 4 where the K_2O and octahedral totals of sample KG : 83 : 127 vary from 9.6–3.4 wt.% and 4.2–5.4, respectively. An increase in FeO and K_2O contents characterizes the transition from saponite through celadonite-saponite to celadonite. High octahedral totals reported for celadonites from DSDP Leg 37 were also attributed to saponite interlayering (Andrews, 1980).

Petrographically identified celadonite has therefore been subdivided into two clay types: celadonite and celadonite-saponite, the latter type being a physical mixture, in varying proportions, of saponite and celadonite. This should not be considered a strict subdivision, as the compositions and structures are continuous between the two endmember components.

Chlorite and Mixed-layer Smectite / Chlorite

Trioctahedral chlorite has been identified by X-ray peaks at 1.42 nm and .71 nm that do not shift after treatment with ethylene glycol (Brindley and Brown, 1980). Physical and structural mixtures of smectite and chlorite have been identified by X-ray analyses and calculated structural formulas. The proportion of these mixtures varies from smectite with minor chlorite to chlorite with minor smectite, although mixtures dominated with smectite are most common. Identification of these mixed-layer clays is based upon the common basal 001 and 002 reflections at 1.4 nm and .7 nm of smectite and chlorite, respectively. The 002 peak is most intense for chlorite; the 001 peak is most intense for smectite. Treatment with ethylene glycol further differentiates the two minerals because smectite is an expandable clay mineral and chlorite is not. The proportion of each clay mineral in the mixture is therefore estimated by comparing the 001 and 002 peak intensities and their shift toward larger d-spacings after treatment

	1	2	3	4	5	6
SiO_2	27.37	27.05	25.97	38.11	39.19	33.98
Al_2O_3	17.87	16.64	20.31	9.47	11.77	12.50
FeO^T	25.10	30.52	24.45	17.66	19.12	8.08
MnO	0.86	0.42	1.10	0.24	0.28	0.23
MgO	15.98	13.13	13.82	18.31	16.88	26.01
CaO	0.08	0.13	0.09	1.18	0.34	0.32
Na_2O	0.18	–	0.32	1.08	0.68	0.09
K_2O	0.01	0.05	–	0.33	1.89	0.09
Total	87.45	87.94	86.06	86.14	89.87	81.30
	Cation Proportions					
Si	5.80	5.87	5.58	6.09	6.03	5.48
Al^{iv}	2.20	2.12	2.42	1.78	1.97	2.28
Total	8.00	8.00	8.00	7.87	8.00	7.86
Al^{vi}	2.26	2.13	2.73	–	0.17	–
Fe	4.45	5.53	4.40	2.36	2.65	1.09
Mg	5.05	4.24	4.43	4.36	3.87	6.26
Mn	0.15	0.08	0.20	0.03	0.04	0.03
Ca	0.02	–	0.02	0.20	0.06	0.06
Na	0.07	–	0.13	0.33	0.06	0.03
K	–	0.01	–	0.07	0.37	0.02
Total	12.00	12.01	11.91	7.32	7.18	7.49
0	28	28	28	22	22	22

Table 4: Representative chlorite and mixed-layer smectite/chlorite analyses. – not detected; FeO^T = Total Fe as FeO; (1) chlorite, groundmass (CY1A : 266.60 m); (2) chlorite, groundmass (CY1A : 464.00 m); (3) chlorite, groundmass (CY1A : 598.15 m); (4) smectite/chlorite, groundmass (CY1A : 188.75 m); (5) smectite/chlorite, groundmass (CY1A : 250.20); (6) smectite/chlorite, groundmass (CY1A : 141.52 m).

with ethylene glycol. Compositionally, the transition from saponite to chlorite is marked by a decrease in SiO_2 and an increase in Al_2O_3 (Bettison and Schiffman, 1988). On the basis of 22 (0,0H), the cation proportions of Si and Al in saponite range from 6.4 to 7.0 and 1.6 to 1.9, respectively and in chlorites from 4.4 to 4.9 and 3.2 and 3.4, respectively. Thus, clays with Si and Al proportions intermediate between smectite and chlorite are considered mixed-layer smectite/chlorite. This approach, however, does not indicate the abundance of the two end-member clays.

The majority of chlorites are ferroan clinochlores although there are a few occurrences of magnesian chamosites (Bayliss, 1975). Chlorites are slightly more Fe-rich than smectite/chlorite mixtures (Figure 3B) and show a slight tendency toward increasing Fe content with increasing depth. Within individual samples of both clay types, there is very little variation in FeO/(FeO+MgO). Chlorite contains up to 1.5 wt.% MnO (Table 4; Figure 4), with individual samples varying by up to 1 wt.%. MnO-rich chlorite occurs in the CY-2A drill core where alteration is equivalent to the UDZ (Herzig and Friedrich, 1987). The MnO contents of smectite/chlorite are

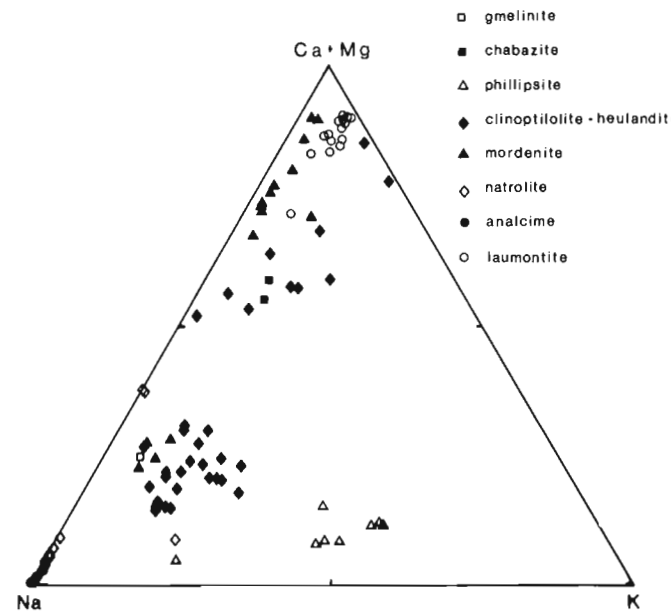

Figure 6: Molar Na-K-Ca+Mg proportions of zeolites from the CY-1/1A drill cores, the Akaki River section, and the Pediaeos River section.

intermediate between chlorite and saponite (Figure 4). The compositions of void-filling and groundmass-replacing phases are indistinguishable.

In this section, chlorite is generally cryptocrystalline to fibrous and pale-green. Most chlorites have anomalous blue interference colours although a few display 1st order birefringence. Groundmass-replacing smectite/chlorite is usually indistinguishable from co-existing saponite or celadonite-saponite. Void-filling varieties, however, are commonly fibrous to platy and pale-green to brownish-green with 1st to 2nd order bifringence.

Zeolites

Several varieties of zeolites form as void-filling or, rarely, groundmass-replacing phases in the SWZ, LTZ, and TZ. They have been identified petrographically and on the basis of their XRD patterns.

In the LTZ, clear, well-formed trapezohedral crystals of analcime, commonly accompanied by radiating aggregates of phillipsite, line fractures and vesicles and replace glassy pillow margins. Phillipsite is generally the earliest of these two phases to form. Radiating prisms of natrolite are commonly associated with analcime and occur chiefly in vesicles and vugs. Hexagonal clusters of pinkish-orange gmelinite are finely mixed with assemblages of chabazite, phillipsite, and analcime. Analcime also forms as a single phase in the SWZ and in the lower portion of the LTZ; it is associated with laumontite in the TZ.

Analcime is uniform in composition with only minor substitution of Ca and K for Na whereas phillipsite is Na- and

K-rich with minor Ca (Figure 6; Table 5). Natrolite analyses are close to the ideal formula with minor substitution of Ca for Na (Figure 6). Gmelinite is Na-rich; chabazite is Ca- and Na-rich (Table 5). With the exception of natrolite, the Si content of all these phases is slightly higher than usual (Deer et al., 1962; Bohlke et al., 1980). Low Na contents for many of the Na-rich zeolites may be due to volatilization of alkalis during microprobe analyses.

Yellowish-green rosettes of tabular clinoptilolite line the edges of fractures and vesicles in massive and sheet flows and replace hyaloclastite-rich zones in the LTZ and in the upper part of the TZ. Clay inclusions are common and partial replacement by calcite is locally evident. Clinoptilolite was distinguished from heulandite by its larger molar Si/Al ratio (8.5–10 compared to 6) (Mumpton, 1960), higher (Na+K)/Ca, and the constancy of the 020 peak upon heating (Boles, 1972) (Figure 6, Table 6).

Fibrous mordenite is typically associated with cliniptilolite in vesicles and in glassy margins where it is the last of the two phases to form. Mixing with quartz, particularly in the TZ, resulted in higher Si contents for the mordenite than those reported in the literature (Deer et al., 1962). Samples from CY-1A are Na-rich whereas Ca is the dominant cation in the samples from the Akaki River section (Figure 6; Table 6).

Pinkish-white prisms of laumontite primarily fill voids and replace glassy margins. Laumontite is commonly associated with quartz, either intermixed or as the latest phase to form. XRD analyses indicate that many samples are actually leonhardite, a partially dehydrated variety of laumontite (Coombs, 1952). Laumontite compositions are close to the ideal formula, with minor substitution of Na and K for Ca (Figure 6; Table 6).

Carbonates

Calcite is common throughout the SWZ and is locally abundant in the other alteration zones. Generally the latest phase to be deposited in primary cavities, calcite also forms irregular patches in the groundmass and replaces phenocrysts. Several stages of growth are commonly indicated by successive layers of euhedral crystals, some of which are mantled by clay minerals.

Calcite is generally pure in composition with <1 mole% $MgCO_3$ (Table 7). Manganiferous calcite, containing up to 3.5 wt.% MnO, is present throughout the drill core but is most common in the TZ and UDZ. Both manganiferous and pure calcites occur within the same veins and vesicles.

Silica

Secondary jasper, chalcedony, opal, and clear colourless quartz form chiefly in the voids of massive flows and dykes. Jasper is commonly associated with celadonite in zones of intense alteration within massive flows. Clear, colourless chalcedony and quartz line or fill vesicles, vugs, and fractures, particularly in the TZ and UDZ. White to bluish opal-C and

	1	2	3	4	5	6
SiO_2	59.36	55.33	47.54	57.59	50.16	53.22
Al_2O_3	22.61	23.24	28.77	22.24	18.64	19.39
FeO^T	0.01	–	0.16	0.08	0.04	0.96
MgO	–	–	–	–	0.06	0.05
CaO	–	–	0.61	0.96	3.63	4.63
Na_2O	12.54	11.65	9.22	2.93	11.20	2.63
K_2O	0.01	–	–	4.28	1.46	1.36
Total	94.53	90.22	86.30	88.08	85.19	82.24
	Cation Proportions					
Si	2.43	2.38	24.43	11.43	16.15	25.53
Al	1.09	1.18	17.43	5.20	7.07	10.96
Fe	–	–	0.07	0.01	0.01	0.39
Mg	–	–	–	–	0.03	0.04
Ca	–	–	0.34	0.20	1.25	2.38
Na	1.00	0.97	9.19	1.13	6.99	2.45
K	–	–	–	1.08	0.60	0.83
Total	4.52	4.53	51.46	19.05	32.10	42.58
0	7	7	80	32	48	72

Table 5: Representative zeolite analyses. – not detected; FeO^T = Total Fe as FeO; (1) analcime (KG : 82 : 076); (2) analcime (CY1A : 138.0 m); (3) natrolite (KG : 83 : 012); (4) phillipsite (CY1 : 87.4 m); (5) gmelinite (KG : 83 : 204); (6) chabazite (KG : 83 : 204).

	1	2	3	4	5	6	7
SiO_2	63.99	62.92	66.35	69.10	66.25	56.85	54.91
Al_2O_3	11.26	12.75	13.59	11.99	9.36	20.19	20.51
FeO^T	0.06	0.04	0.03	0.06	–	0.62	–
MgO	0.05	0.19	0.20	0.29	0.04	0.05	–
CaO	1.96	1.50	2.90	3.47	1.62	6.95	7.75
Na_2O	7.32	4.20	3.77	0.93	4.84	1.90	0.34
K_2O	0.98	1.81	1.87	0.90	0.98	1.06	0.97
Total	85.62	83.41	88.71	86.74	83.09	87.62	84.48
	Cation Proportions						
Si	29.19	29.13	28.95	20.08	20.36	17.18	16.60
Al	6.05	6.96	6.99	4.11	3.39	7.19	7.54
Fe	0.02	0.02	0.01	0.01	–	0.16	–
Mg	0.03	0.13	0.13	–	–	0.02	–
Ca	0.96	0.74	1.36	1.08	0.53	1.93	2.59
Na	6.47	3.77	3.19	0.52	2.88	1.11	0.21
K	0.57	1.07	1.04	0.33	0.38	0.41	0.39
Total	43.29	41.82	41.67	26.13	27.54	28.00	27.33
0	72	72	72	48	48	48	48

Table 6: Representative zeolite analyses. – not detected; FeO^T = Total Fe as FeO; (1) clinoptilolite (KG : 82 : 156); (2) clinoptilolite (CY1A : 31.25 m); (3) clinoptilolite (KG : 83 : 085); (4) mordenite (KG : 83 : 166); (5) mordenite (CY1A: 43.45 m); (6) laumontite (CY1A : 241.4 m); (7) laumontite (CY1A : 266.6 m).

	1	2	3	4	5	6
FeO^T	–	–	–	–	0.06	0.11
MnO	0.02	1.23	0.07	0.01	0.04	0.23
MgO	–	0.23	0.57	0.79	0.88	0.84
CaO	64.79	62.90	57.39	61.20	61.39	65.07
Total	64.81	64.36	58.03	62.00	62.37	66.25

Table 7: Representative calcite analyses. – not detected; FeO^T = Total Fe as FeO; (1), (2) CY1A: 145.30 m; (3) CY1: 72.75 m; (4) CY1: 104.70 m; (5) CY1: 197.80 m; (6) CY1: 256.21 m.

opal-CT (classification after Jones and Segnit, 1971) form very thin layers on fractures and cooling-joint surfaces in massive and sheet flows. Quartz is abundant in the groundmass throughout the TZ and UDZ.

Epidote

Yellowish-green, blocky to radiating epidote is a common void-filling phase whereas granular epidote is locally distributed in the groundmass of rocks from the UDZ. It is associated with quartz and chlorite, either mixed or as the latest phase to form. Analyzed epidotes are uniform in composition with a narrow range in pistacite component, from 10 to 30 ($Fe/Fe+Al^{iv}$). No compositional differences between groundmass and void-filling phases were noted (Figure 7; Table 8); moreover, there is no compositional trend depth. MnO contents range from 0.03 to 0.70 wt.%.

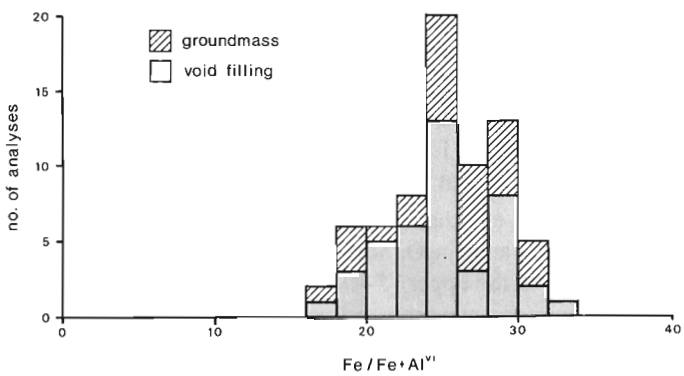

Figure 7: Pistacite component ($Fe/(Fe+Al^{vi})$) of groundmass-replacing and void-filling epidote.

Amphibole

Pale-green, prismatic to fibrous actinolite was identified petrographically in the lower 50 m of Hole CY-1A. It is commonly intergrown with chlorite in the groundmass and epidote - quartz assemblages in vesicles and vugs. No reaction relationship with clinopyroxene was observed in these samples.

	1	2	3
SiO_2	37.81	38.08	38.79
Al_2O_3	25.17	24.38	22.91
FeO^T	8.87	9.43	10.71
MnO	0.17	0.18	0.20
MgO	–	–	0.05
CaO	24.46	24.05	23.34
Total	96.48	96.12	96.00
	Cation Proportions on the basis of 12.5 (O, OH)		
Si	3.07	3.11	3.18
Al^{iv}	–	–	–
Total	3.07	3.11	3.18
Al^{vi}	2.41	2.34	2.22
Fe	0.60	0.64	0.73
Total	3.01	2.98	2.95
Mn	0.01	0.01	0.01
Ca	2.14	2.10	2.05
Total	2.15	2.11	2.06
Fe	0.20	0.22	0.25
$Fe+Al^{iv}$			

Table 8: Representative epidote analyses. – not detected; FeO^T = Total iron as Fe_2O_3; (1) CY1A: 632.25 m, vesicle; (2) CY1A: 632.25 m, groundmass; (3) CY1A: 339.26 m, vesicle.

Other Minerals

Adularia, a K-feldspar, lines fractures and vesicles in the SWZ. A few anhedral grains, which resemble quartz and analcime, were identified by microprobe.

Prehnite showing second order birefringence and occurring as tabular grains have been identified in two samples in the UDZ. These grains are associated with quartz in vesicles; a few occurrences in the groundmass were identified petrographically.

Fe-hydroxides and oxides are present in every alteration zone but are most abundant in the SWZ where they give the rocks their characteristic 'oxidized' appearance. These phases were identified visually because poor crystallinity prevented XRD identification in most cases. Microprobe analyses indicate that they are mixed with clay minerals (Table 2, column 6).

Pyrite is the only secondary sulfide identified in this study. It is most common in the TZ and UDZ where it is associated with quartz, chlorite, and epidote in the groundmass and with quartz, albite, and chlorite or smectite/chlorite on fracture surfaces. Veins of euhedral to subhedral pyrite, up to 2 cm wide, cut massive units in the UDZ and are locally abundant in field exposures.

Gypsum is the only sulfate identified outside the MZ. In field exposures, it is primarily associated with gossans, whereas in the LTZ of CY-1 it forms clear, massive crystals in late-stage veins.

ALTERATION OF PRIMARY MINERALS

Olivine is partly to totally replaced by an assemblage of clay minerals, calcite, and goethite. The clay minerals present in the alteration assemblage are compositionally similar to coexisting groundmass clays.

Plagioclase is variably altered in all zones except the UDZ where it is completely replaced by albite. In the SWZ, LTZ, and TZ, plagioclase may be partly altered to calcite, clay minerals, or totally replaced by K-feldspar. In addition, plagioclase is locally albitized in the TZ. There is no consistent pattern in the distribution of these types of alteration. For example, within one thin section, K-feldspar, plagioclase partly replaced by smectite, and fresh plagioclase may be present.

Clinopyroxene remains essentially fresh in all the alteration zones. Celadonite or saponite locally line fractures and coat grain boundaries.

Red staining adjacent to titanomagnetite in the SWZ and LTZ indicates that the opaque minerals have expelled iron and are cation deficient (Hall et al., 1987). Sphene locally rims titanomagnetite in the UDZ.

ALTERATION OF VOLCANIC GLASS

Fresh volcanic glass is present in the LTZ and TZ. The degree of preservation of glass is quite variable within a single outcrop, from slightly altered with a thin clay coating to totally replaced by authigenic minerals.

Glassy pillow margins are initially altered to palagonite (residual glass) whereas cracks and vesicles are lined with smectite and phillipsite. As alteration proceeds, palagonite is replaced *in situ* by smectite and phillipsite until there is no longer evidence of the residual glass. In many locations, analcime is also associated with glassy pillow margins, where it fills intergranular voids. Where associated with phillipsite, it is the latest phase to form. The typical paragenic sequence of secondary minerals replacing glassy pillow margins is, from oldest to youngest: palagonite, smectite, phillipsite, and analcime. In a few cases, a thin layer of Fe hydroxides separates the palagonite and smectite.

Glassy margins of massive flows are progressively altered in the same stages as pillows but with a different authigenic mineral assemblage. The characteristic paragenic sequence of secondary minerals replacing glassy flow margins is, from oldest to youngest: palagonite, celadonite, smectite, clinoptilolite, and mordenite. As with the pillowed units, Fe-hydroxides are locally present.

The alteration of glass fragments in hyaloclastite units produces mixtures of smectite, clinoptilolite, celadonite, and phillipsite, in decreasing abundance. It was not possible to determine the relative age of the phillipsite and clinoptilolite.

BULK COMPOSITIONAL CHANGES

Two geochemical suites have been recognized in the lavas along the northern flank of the Troodos ophiolite: a lower andesite-dacite-rhyodacite suite of arc tholeiite affinity and an upper picritic basalt to basaltic andesite suite of depleted arc tholeiite affinity (Robinson et al., 1983; Schmincke et al., 1983). The lower suite, referred to as the arc tholeiite suite, contains aphyric to plagioclase- and clinopyroxene-phyric lavas. The upper suite, referred to as the high MgO-high SiO_2 suite, contains aphyric, olivine-, clinopyroxene-, and plagioclase-phyric, and picritic lavas. The CY-1/1A drill cores show the same depth distribution of the geochemical suites seen in field exposures. The boundary between the two suites occurs in the upper part of the CY-1A drill core (475–500 m depth). Dykes, concentrated in the lowermost 300 m of CY-1A, generally belong to the high MgO-high SiO_2 suite.

Variations in the major and trace element composition of crystalline rock samples in the CY-1/1A drill cores (Figures 8, 9, and 10) reflect the variable primary composition and mineralogy of the two lava suites as well as the effect of alteration. Comparison of fresh glass (Robinson et al., 1983; Rautenschlein et al., 1986) and whole rock compositions (Robinson et al., 1983; Mehegan, 1988) with the compositions of altered samples collected for the ICRDG from the CY-1/1A drill cores shows that each alteration zone has distinct compositional trends (Table 9). The co-variance of the CY-1/1A compositions with indicators of alteration (CO_2, H_2O, $Fe_2O_3/(FeO+Fe_2O_3)$) and fractionation trends (Robinson et al., 1983; Mehegan, 1988) combined with their variation with depth indicate qualitative trends of enrichment and depletion. Because the degree of alteration is variable within all zones, samples from each zone do not show the same degree of enrichment or depletion.

The SWZ is enriched in K_2O, Rb, Ba, Sr, and CO_2 and depleted in SiO_2 and Na_2O. Scatter in MgO, Cr, and Ni contents, particularly in the upper 75–100 m where picrites and olivine-phyric lavas are common, primarily reflects the variation in the modal abundance of olivine and clinopyroxene (Figures 8 and 10). Bulk rock $Fe_2O_3/(FeO+Fe_2O_3)$ ratios are higher than in the underlying zones (Figure 8B). Co-variance of major and trace elements with $(Fe_2O_3/FeO+Fe_2O_3)$ ratios and CO_2 content (Gillis, 1987) indicates that most compositional changes occurred during an early oxidative phase of alteration. Pervasive replacement of plagioclase by K-feldspar led to enrichment of K_2O and depletion in Na_2O and CaO. A later, CO_2-metasomatic event led to the enrichment of CaO and CO_2 and dilution of the other elements.

The LTZ is also enriched in K_2O, Rb, and Ba and depleted in SiO_2, but to a lesser extent than the SWZ. $(Fe_2O_3/FeO+Fe_2O_3)$ ratios and CO_2 contents are lower than in the SWZ (Figure 8B). Random replacement of plagioclase

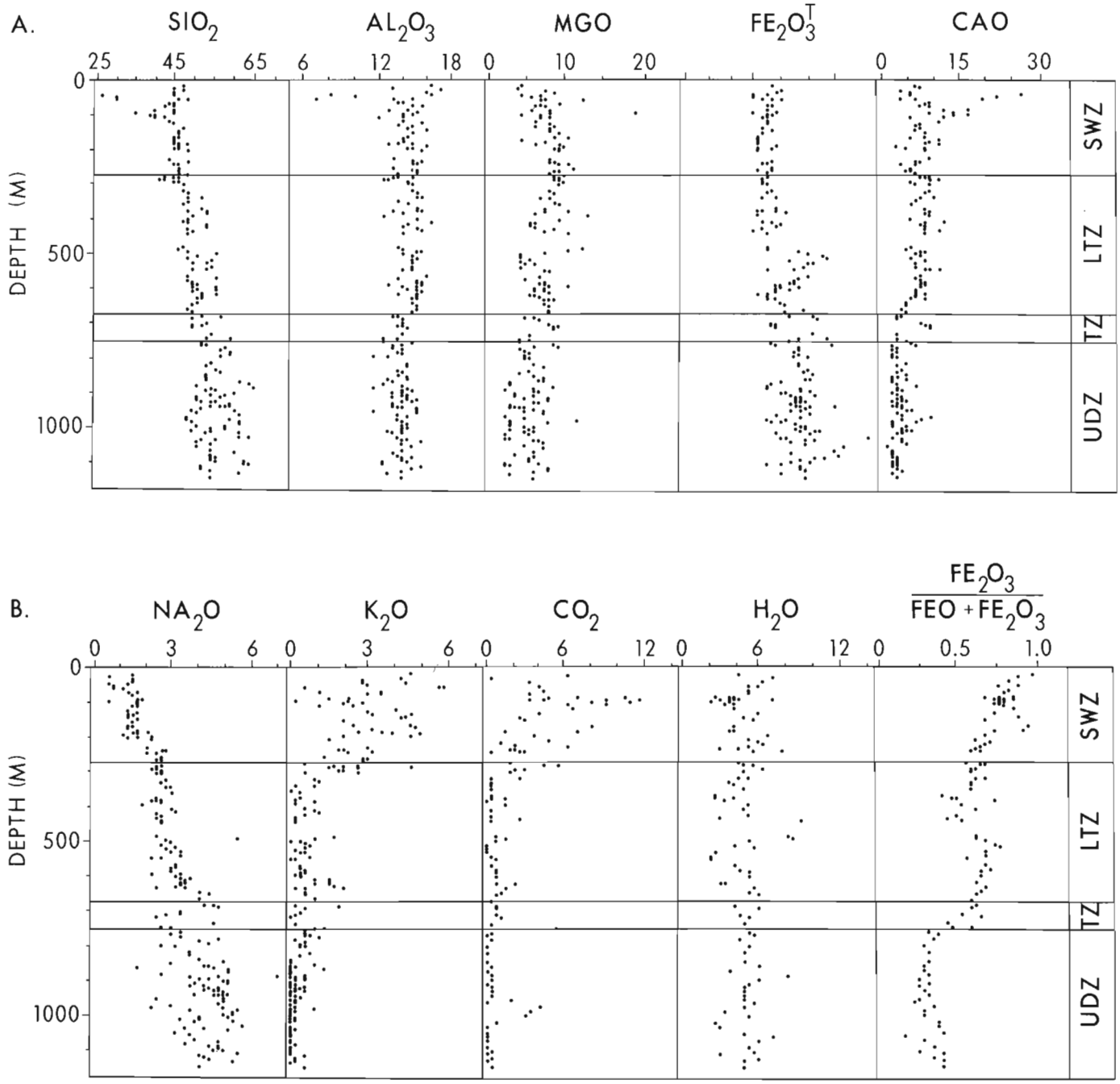

Figure 8: Major element (wt.%) and trace element (ppm) contents versus depth in the CY-1/1A drill cores (continued in Figure 9). A: SiO_2, Al_2O_3, MgO, $Fe_2O_3^T$, and CaO. B: Na_2O, K_2O, CO_2, H_2O, and $Fe_2O_3/(FeO+Fe_2O_3)$. Alteration zones are outlined on the right, abbreviations are the same as Figure 1. Samples were collected for the ICRDG. Major elements were measured at the Geological Survey of Canada (XRF) and Memorial University of Newfoundland (AA). Trace elements were measured at Memorial (XRF). CO_2 and H_2O were measured by C-H-N gas chromotography and ferric iron by titration at the Geological Survey (CY-1) and L'Université de Montreal (CY-1A). Data points do not distinguish lithologic types and include pillows, flows, and dykes.

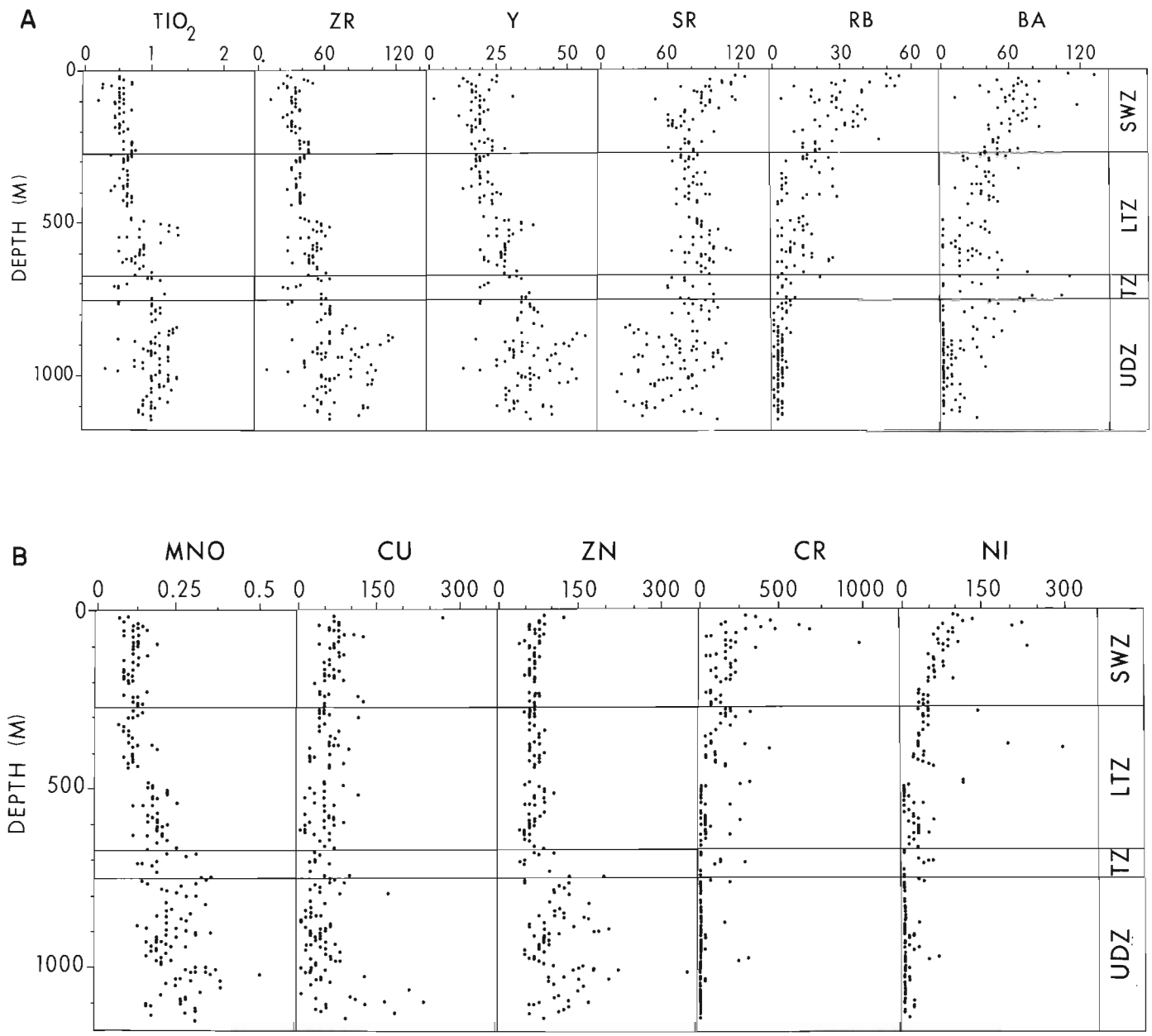

Figure 9: Continuation of major element (wt.%) and trace element (ppm) contents versus depth in the CY-1/1A drill cores. A: TiO_2, Zr, Y, Sr, Rb, and Ba. B: MnO, Cu, Zn, Cr, and Ni. Alteration zones are outlined on the right, abbreviations are the same as Figure 1.

Alteration Zone	Stage*	Mineralogy	Compositional Changes
SWZ	1	Fe-hydroxides, K-feldspar, Al-saponite, saponite	$+Fe_2O_3/(FeO+Fe_2O_3)$ $+K_2O$, Ba, Sr, Rb $-SiO_2$, Na_2O
	2	analcime	??
	3	calcite	$+CaO$, CO_2
	4	palygorskite, calcite	??
LTZ	1	saponite, celadonite, Fe-hydroxides	$+K_2O$, Rb, Ba, Na_2O $-SiO_2$
	2	zeolites	??
	3	calcite	$+CaO$, CO_2
	4	palygorskite, calcite, gypsum	??
TZ	1	saponite, smectite/chlorite, quartz	$+Na_2O$, MnO, Zn $-CaO$
	2	laumontite, quartz, analcime	??
	3	calcite	??
UDZ	1	chlorite, quartz, pyrite, epidote, albite	$+Na_2O$, MnO, Cu $-CaO$, K_2O, Rb
	2	epidote, quartz, pyrite	??
	3	calcite	??

Table 9: Summary of alteration stages. * Stages are listed from oldest to youngest.

by K-feldspar and the local abundance of celadonite led to the scatter in K_2O contents and depletion in CaO. The rocks are enriched Na_2O although no Na-bearing, groundmass-replacing secondary phases have been recognized.

K_2O, Rb, and Sr contents are either depleted or show no change in the UDZ. Na_2O is consistently enriched; CaO is depleted. Ba is generally depleted except for a few samples in the upper half of the zone. Variable TiO_2, Cr, Ni, Zr, and Y contents in this zone (Figures 9A, 9B, and 10) reflect the intercalation of dykes of the high MgO-high SiO_2 suite with lavas from the arc tholeiite suite. $(Fe_2O_3/FeO+Fe_2O_3)$ ratios and CO_2 contents are lower than in the overlying zones. Higher CO_2 contents between 940–1020 m depth occur in an interval where narrow shear zones are common. Albitization of plagioclase in the TZ and UDZ resulted in Na-enrichment and Ca-depletion. Traces of epidote in the groundmass and laumontite-filled voids suggest that some of the released CaO was locally redistributed.

The UDZ and, to a lesser extent, the TZ are enriched in MnO, Cu, and Zn (Figures 9B and 10). Mn-rich chlorites and mixed-layer smectite/chlorite reflect the enrichment of Mn (Figure 4). Similar zones of metal-enrichment are locally distributed throughout the sheeted dyke complex. Outside of these zones, the rocks are slightly metal-depleted (Baragar et al., 1987).

SiO_2, Al_2O_3, MgO, $Fe_2O_3^T$, and TiO_2 generally follow the fractionation trends of the geochemical suites (Figures 8A and 9A; Gillis, 1987) suggesting that these elements were essentially immobile in all alteration zones. Small enrichments or depletions, however, would not be detected using our approach. Ti, Zr, and Y also follow fractionation trends, indicating that these elements are immobile during alteration. A detailed study of chemical variation within several cooling units from the SWZ and LTZ of CY-1 indicates that Y may be depleted in the margins of some pillows (Baragar et al., 1989).

Rocks from the TZ share the geochemical signatures of both the overlying LTZ and underlying UDZ.

ALTERATION STAGES

Depositional sequences and cross-cutting vein relations in each of the alteration zones suggest a sequence of four alteration stages (Table 9). The boundaries separating Stages 1–3 do not necessarily represent a significant change in alteration conditions but, rather, mark changes in the style of alteration, from dominantly groundmass-replacing to void-filling. Isotopic age dating of secondary phases from the SWZ and LTZ show that Stages 1 through 3 were continuous for >20 Ma in the extrusive sequence whereas Stage 4 was restricted to the upper 500 m of the crust and significantly postdates crustal formation (Staudigel and Gillis, 1990).

Stage 1

Reaction with ambient seawater during construction of the volcanic pile marks the initiation of submarine alteration. In most cases, evidence of this incipient alteration and deuteric alteration has been obscured by subsequent alteration. Reaction with oxygenated, chemically unmodified seawater characterized early Stage 1 throughout the extrusive sequence. Oxidation of host-rock Fe and the formation of Fe-hydroxides, expecially in zones of high permeability, such as pillow margins and breccias, produced acidic conditions (Seyfried et al., 1978; Alt and Honnorez, 1984). As seawater migrated inward toward the cores of cooling units, it became chemically modified. Progressive O_2-depletion inhibited the formation of Fe-hydroxides and led to an increase in pH, conditions which favour the formation of saponite over Fe-hydroxides (Bass, 1976; Seyfried et al., 1978; Andrews, 1980) and the replacement of plagioclase by K-feldspar (Alt and Honnorez, 1984). Concentration of Fe-hydroxides along the margins of cooling units produced a pronounced colour zonation particularly diagnostic of the SWZ.

Decreases in the abundance of Fe-hydroxides (Figure 1) and lower whole-rock $Fe_2O_3/(FeO+Fe_2O_3)$ ratios with depth (Figure 8B) show that O_2 was progressively depleted as seawater migrated downward. Initial acidic fluids rapidly became more alkaline, favouring the formation of saponite over Fe-hydroxides. Therefore, pillows in the LTZ typically lack pronounced mineralogic or chemical zonation.

The association of celadonite primarily with massive and sheet flows and intrusive contacts suggests that conditions in these units were different from those in pillows. High SiO_2(aq) concentrations coupled with low pH and oxidative

conditions favour the formation of celadonite (Wise and Eugster, 1964). The distribution of alteration in flows and intrusives suggests that fluid flow was focused along the boundaries of these units. In contrast, radial fracture patterns in pillows led to more diffuse fluid flow. It may be inferred, therefore, that the composition of fluids along flow margins were primarily controlled by the alteration of glass whereas fluids altering pillows contained both glass and crystalline rock components. Because glass alteration produces fluids more Si-rich than crystalline rocks (Seyfried, 1987), celadonite was favoured over saponite.

Celadonite generally forms at temperatures <40°C whereas saponite forms at temperatures <50–200°C (Kristmannsdottir, 1975; Seyfried et al., 1978; Stakes and O'Neil, 1982; Bohlke et al., 1984). The replacement of plagioclase by K-feldspar at normal seawater Na^+/K^+ ratios indicates temperatures less than 140°C (Munha et al., 1980). Oxygen isotopic compositions of chalcedonic quartz associated with celadonite from the Akaki River section indicate temperatures of 20°C (Heaton and Shepperd, 1977). Therefore, temperatures in the extrusive sequence during Stage 1 were probably <50°C.

The TZ, located where the dykes increase in abundance in Hole CY-1A, marks a change in alteration conditions. Because of lower water/rock ratios and previous reaction with the overlying rocks, MgO and O_2 were depleted in the altering fluid, producing near neutral pH and low fO_2. The only evidence of early acidic conditions is minor metal-depletion in the dykes (Rosenbauer and Bischoff, 1983).

Replacement of the mesostasis and volcanic glass by mixed-layer smectite-chlorite + quartz + pyrite (Table 1) and the partial albitization of plagioclase dominate in Stage 1. Decreased Si contents in mixed-layer smectite/chlorite with increasing depth in the TZ and from rim to core in clay aggregates suggest an increased chloritic component (Bettison and Schiffman, 1988). This may reflect a rise in temperature, a change in fluid composition, or both.

Stage 1 in the UDZ is characterized by the complete replacement of the mesostasis and volcanic glass by chlorite + quartz + pyrite ± epidote. Complete albitization of plagioclase and whole-rock Na_2O enrichment suggest the rocks were altered by a SiO_2-rich fluid under low water/rock conditions. The abundance of pyrite and the scarcity of epidote indicate low fO_2. Small zones of epidosite-like alteration, where rocks are totally recrystallized to epidote + quartz ± chlorite, indicate that zones of high permeability maintained high fO_2 (Richardson et al., 1987).

The transition from saponite to mixed-layer smectite/chlorite in the Icelandic geothermal fields occurs at temperatures between 100–200°C and from mixed-layer smectite/chlorite to chlorite between 200–240°C (Kristmannsdottir, 1975). Epidote is stable at temperatures >200°C (Kristmannsdottir, 1975; Bird et al., 1984; Liou et al., 1985); amphibole, restricted to the base of the UDZ, indicates temperatures >300°C (Mottl and Holland, 1978). This sharp rise in temperature, from <100 to >200°C, across the TZ suggests that the thermal gradient was stepped during Stage 1.

In all alteration zones, reduction in permeability by glass hydrolysis and lining of voids by clay deposition eventually restricted the access of seawater to the interior of all cooling units, limiting the deposition of secondary minerals to voids and reducing the contribution of host rock components to the altering fluid. This marks the beginning of Stage 2.

High permeability and close proximity to the source of unaltered seawater ensured the maintenance of an oxidative environment in the upper tens of meters of the volcanic pile. High whole-rock $Fe_2O_3/(FeO+Fe_2O_3)$ ratios and the pronounced mineralogic zonation in the SWZ suggest that Stage 1 continued for a prolonged period of time. After crustal accretion, this oxidative alteration front migrated downward into the volcanic pile overprinting earlier, less oxidative alteration. The lower limit of this alteration front is marked by the lower boundary of the SWZ.

Stage 2

Precipitation of zeolites in voids characterize Stage 2. Zeolite precipitation is generally favoured by the alkaline, O_2- and Mg-depleted, Si-enriched fluids similar to those produced during late Stage 1 (Hay, 1966; Alt and Honnorez, 1984). In the extrusive sequence, zeolites are most abundant in the LTZ. Their scarcity in the SWZ may be attributed to the maintenance of high fO_2 and, thus, low pH conditions. A characteristic feature of the LTZ is the association of specific zeolites and clay minerals with either pillows or flows. The formation of each zeolite group is favoured by fluids with different Si/Al ratios and pH (Hay, 1966; Surdam and Sheppard, 1978; Donahoe and Liou, 1985). Phillipsite and other Si-undersaturated zeolites precipitate from fluids with lower Si activities and higher pH than Si-saturated zeolites, such as clinoptilolite and mordenite (Mariner and Surdam, 1970; Iijima, 1974). Because acidic conditions were probably maintained along flow margins longer than along pillow margins, reduction in permeability and depletion of O_2 and MgO in seawater resulted in Stage 2 fluids with lower pH and higher $SiO_2(aq)$ in flows than in pillows. These conditions led to the assocation of Si-undersaturated and Si-saturated zeolites with pillows and flows, respectively. Other variables, such as cation ratios in the solution and temperature, control which zeolites of each group form.

Low temperatures continued in the SWZ and LTZ during Stage 2. Stable temperature ranges for all the zeolites indicate that temperatures ≤50–100°C were maintained (Iijima and Utada, 1971; Liou, 1971b, Honnorez, 1978; Kristmannsdottir and Tomasson, 1978; Bohlke et al., 1984).

Laumontite, analcime, albite, quartz, and pyrite were deposited in the TZ and UDZ during Stage 2. Their deposition is favoured by Ca- and Si-rich, alkaline fluids.

Laumontite and albite are stable at temperatures between 100 and 200°C (Iijima and Utada, 1971; Liou, 1971a; Kristmannsdottir, 1975; Evarts and Schiffman, 1983). The presence of these minerals in the TZ suggests that the stepped thermal gradient prevalent during Stage 1 continued.

Epidote, quartz, and pyrite were deposited in voids in the UDZ during Stage 2. Similar compositions of both void-filling and groundmass-replacing epidote (Figure 7), however, suggest that epidote precipitated from similar fluids at similar temperatures (Liou et al., 1985). In the UDZ of field exposures epidote is locally overprinted by laumontite.

No bulk compositional changes result from Stage 2 because zeolite deposition was not pervasive and was restricted to voids.

Stage 3

Carbonate precipitation characterizes Stage 3. Several stages of growth are commonly evident but these do not reflect any change in fluid composition. Low Mg/Ca ratios in the carbonates indicate that they precipitated from Mg-depleted seawater because calcite which has precipitated from normal seawater has 8 mole % $MgCO_3$ (Mucci and Morse, 1983). Temperatures calculated from oxygen isotopic data range from 4–15°C in the SWZ, 10–41°C in the LTZ, 40–50°C in the TZ, and 60–90°C in the UDZ (Table 10). Thus, during Stage 3, temperatures increased gradually from those of Cretaceous bottom water (5–15°C, Brass et al., 1982) with depth in the ophiolite. Carbon isotopic data indicate that the carbonates precipitated from solutions with an inorganic component (Muehlenbachs, 1979).

Pervasive calcite deposition in the SWZ led to whole rock enrichment of Ca and CO_2.

Stage 4

Stage 4 was restricted to the SWZ and the upper few tens of meters of the LTZ. Palygorskite and calcite were deposited in veins which cross-cut all previous alteration. Gypsum veins, restricted to the LTZ of CY-1, re-opened and filled earlier veins.

SUMMARY

Four alteration zones with distinct mineralogical and geochemical characteristics are recognized in the CY-1/1A drill cores: a Seafloor Weathering Zone, a Low-Temperature Zone, a Transition Zone, and an Upper Dyke Zone. The depth distribution of these zones in CY-1/1A is comparable to field exposures along the northern flank of the ophiolite; however, the thickness of the zones varies laterally (Gillis, 1987).

Four alteration stages are proposed which reflect changes in physical and chemical conditions. Stage 1 marks the initiation of submarine alteration. Reaction with seawater during crustal construction led to the replacement of mesostatis and volcanic glass by Fe-hydroxides and clay minerals. Temperatures in the dyke section were ≥200°C; in contrast, high permeability in the extrusive sequence resulted in temperatures ≤50°C. The precipitation of clay minerals along fracture surfaces and vesicle walls eventually restricted access of seawater into the hostrock. This led to a change in the style of alteration from groundmass-replacing to void-filling and marks the transition from Stage 1 to 2. Calcite precipitation marks the on-set of Stage 3. Temperatures remained unchanged in the SWZ and LTZ during Stage 3; in the UDZ, temperatures decreased to <100°C. Stage 4 is restricted to the SWZ and upper few meters of the LTZ. Isotopic age dating of secondary minerals from each stage of alteration indicates that Stages 1 through 3 continued from crustal formation for ≥20 Ma. Stage 4 significantly post-dates Stages 1–3 and may be related to the emplacement of the ophiolite (Staudigel and Gillis, 1990).

Depth(m)	Alteration Zone	$^{13}C_{PDB}$	$^{18}O_{SMOW}$	Temp. °C* 1	2
CY-1					
58.35	SWZ	2.3	31.50	9.3	5.3
86.30	SWZ	1.8	30.43	13.7	9.6
123.30	SWZ	2.0	31.54	9.2	5.3
291.00	LTZ	2.7	30.37	14.0	9.8
299.00	LTZ	2.8	30.87	11.8	7.8
410.43	LTZ	2.4	29.46	16.1	13.6
CY-1A					
36.35	LTZ	1.2	26.34	32.8	27.8
138.75	LTZ	0.8	24.79	41.1	35.6
242.09	TZ	-0.9	22.77	53.0	46.9
314.05	TZ	1.7	18.36	84.6	76.6
390.00	UDZ	1.4	19.87	72.7	65.5
406.00	UDZ	2.7	17.85	88.8	80.6
434.00	UDZ	0.9	20.20	70.3	63.2
518.00	UDZ	3.0	18.40	84.2	76.3
617.00	UDZ	3.3	17.82	89.0	80.8

Table 10: Oxygen and carbon isotopic data and calculated temperatures of formation for carbonate. * Calculated following method of O'Neil et al. (1969) using (1) Present seawater value and (2) Cretacious seawater value (Savin, 1977).

Comparison of these zones with zones of alteration recognized in several DSDP basement holes suggests the recharge zones of Troodos are equivalent to *in situ* oceanic crust (Gillis and Robinson, 1988). Hole 504B, drilled in 5.9 m.y.-old crust, approximately 200 km south of the Costa Rica Rift, is the only hole that has sampled the transition between lavas and the underlying sheeted dyke complex (Shipboard Scientific Crew, Leg 69, 1983; Shipboard Scientific Crew, Leg 83, 1985). As in Troodos, the boundary between the low- and high-temperature environments is sharp and is located at the lithologic transition zone (Alt et al., 1986). This implies that the thermal gradient was stepped during the early stages of alteration. The areal distribution of the alteration zones in Troodos

(Gillis, 1987) shows that the boundary between the low- and high-temperature zones varies from <150 to >1400 m depth.

ACKNOWLEDGMENTS

We thank C. Xenophontos, A. Panayiotou, G. Constantinou, and the Cyprus Geological Survey for their support of the Cyprus Crustal Study Project. Discussions with J. Mehegan, D. Bailey, H. Staudigel, and many members of the ICRDG greatly added to this work and made life in the corelab much more enjoyable. Our friends in Mitsero are thanked for their warm hospitality. G. Brown produced excellent thin sections of extremely altered material and R. MacKay assisted with the probe analyses. M. Sulanowska assisted with the figures. Financial support from J.N. Ludden during a post-doctoral fellowship at L'Université de Montreal is acknowledged by K.M.G. This work is part of a Ph.D. thesis by K.M.G. and was supported by Natural Sciences and Engineering Council grants to P.T. Robinson.

REFERENCES

Alt, J.C. and Honnorez, J.
1984: Alteration of the upper oceanic crust, DSDP Site 417: mineralogy and chemistry; Contributions to Mineralogy and Petrology, v. 87, p. 149–169.

Alt, J.C., Honnorez, J., Laverne, C., and Emmermann, R.
1986: Hydrothermal alteration of a 1 km section through the upper oceanic crust, Deep Sea Drilling Project Hole 504B: mineralogy, chemistry, and evolution of seawater-basalt interactions; Journal of Geophysical Research, v. 91, p. 10309–10335.

Andrews, A.J.
1980: Saponite and celadonite in layer 2 basalts, DSDP Leg 37; Contributions to Mineralogy and Petrology, v. 73, p. 323–340.

Baragar, W.R.A., Lambert, M.B., Baglow, N., and Gibson, I.
1987: Sheeted dykes of the Troodos ophiolite, Cyprus; *in* Hall, H.C. and Fahrig, W.F., Mafic Dyke Swarms, Geological Association of Canada, Special Paper 34, p. 257–272.

Baragar, W.R.A., Ludden, J.N., and Auclair, F.
1991: Alteration effects in pillow lavas from the CY-1 drillhole: upper volcanic sequence, Troodos ophiolite; *in* Gibson, I.L., Malpas, J., Robinson, P.T., and Xenophontos, C., Cyprus Crustal Study Project: Initial Report, Holes CY-1 and 1A, Geological Survey of Canada, Paper 90–20.

Bass, M.N.
1976: Secondary minerals in oceanic basalt, with special reference to Leg 34, Deep Sea Drilling Project; *in* Yeats, R.S., Hart, S.R., et al., Initial Reports of the Deep Sea Drilling Project, v. 34, U.S. Government Printing Office, Washington, p. 393–432.

Bayliss, P.
1975: Nomenclature of the trioctahedral chlorites; The Canadian Mineralogist, v. 13, p. 178–180.

Bettison, L.A. and Schiffman, P.
1988: Compositional and structural variations of phyllosilicates from the Point Sal ophiolite, California; American Mineralogist, v. 73, p. 62–76.

Bird, D.K., Schiffman, P., Elders, W.A., Williams, A.E., and McDowell, S.D.
1984: Calc-silicate mineralization in active geothermal systems; Economic Geology, v. 79, p. 671–695.

Böhlke, J.K., Honnorez, J., and Honnorez-Guerstein, B.M.
1980: Alteration of basalts from Site 396B DSDP: petrographic and mineralogical studies; Contributions to Mineralogy and Petrology, v. 73, p. 341–369.

Böhlke, J.K., Honnorez, J., Honnorez-Guerstein, B.M., Muehlenbachs, K., and Petersen, N.
1981: Heterogeneous alteration of the upper oceanic crust: correlation of rock chemistry, magnetic properties, and O isotope ratios with alteration patterns in basalts from Site 396B, DSDP; Journal of Geophysical Research, v. 86, p. 7935–7950.

Boles, J.R.
1972: Composition, optical properties, cell dimensions, and thermal stability of some heulandite-group zeolites; American Mineralogist, v. 57, p. 1463–1493.

Brass, G.W., Southam, J.R., and Peterson, W.H.
1982: Warm saline bottom water in the ancient ocean; Nature, v. 296, p. 620–623.

Brindley, G.W. and Brown, G.
1980: Crystal structures of clay minerals and their XRD identification; Mineralogic Society of London, 495 p.

Buckley, H.A., Bevan, J.C., Brown, K.M., and Johnson, L.R.
1978: Glauconite and celadonite: two separate mineral species; Mineralogical Magazine, v. 42, p. 373–382.

Constantinou, G. and Govette, G.J.S.
1973: Geology, geochemistry, and genesis of Cyprus sulfide deposits; Economic Geology, v. 68, p. 843–858.

Coombs, D.S.
1952: Cell size, optical properties and chemical composition of laumontite and leonhardite; American Mineralogist, v. 37, p. 812–830.

Deer, W.A., Howie, R.A., and Zussman, J.
1962: Rock forming minerals, v. 1–5. Longmans, Green, London.

Donahoe, R.J. and Liou, J.G.
1985: An experimental study on the process of zeolite formation; Geochimica et Cosmochimica Acta, v. 49, p. 2349–2360.

Elsbree, H.C.
1985: Clay alteration in three ore deposits and associated volcanics of the Troodos ophiolite, Cyprus; (MSc Thesis), University of Illinois at Urbana-Campaign, 132 p.

Evarts, R.C. and Schiffman, P.
1983: Submarine hydrothermal metamorphism of the Del Puerto ophiolite, California; American Journal of Science, v. 283, p. 289–340.

Gass, I.G. and Smewing, J.D.
1973: Intrusion, extrusion, and metamorphism at constructive margins: evidence from the Troodos Massif, Cyprus; Nature, v. 242, p. 26–29.

Gillis, K.M.
1987: Multistage alteration of the extrusive sequence, Troodos ophiolite, Cyprus; (PhD Thesis), Dalhousie University, Halifax, 387 p.

Gillis, K.M. and Robinson, P.T.
1988: Distribution of alteration zones in the upper oceanic crust; Geology, v. 16, p. 262–266.

Hall, J.M., Walls, C., Williamson, M., and Wang, B.-X.
1987: Depth trends in magnetic properties in an area of prolonged cold seawater drawdown in uppermost Troodos-type oceanic crust; Canadian Journal of Earth Sciences, v. 24, p. 941–952.

Hay, R.L.
1966: Zeolites and zeolitic reactions in sedimentary rocks; Geological Society of America, Special Paper 85, 134 p.

Heaton, T.H.E. and Sheppard, S.M.F.
1977: Hydrogen and oxygen isotope evidence for sea-water-hydro-thermal alteration and ore deposition, Troodos complex, Cyprus; Volcanic processes in ore genesis, Geological Society of London, Special Publication no. 7, p. 42–57.

Herzig, P.M. and Friedrich, G.H.
1987: Sulfide mineralization, hydrothermal alteration and chemistry in the drill hole CY-2a, Agrokipia, Cyprus; *in* Robinson, P.T., Gibson, I., and Panayiotou, A., Cyprus Crustal Study Project: Initial Report, Holes CY-2 and CY-2a, Geological Survey of Canada, Paper 85–29, p. 103–138.

Honnorez, J.
1978: Generation of phillipsites by palagonitization of basaltic glass in sea water and the origin of K-rich deep-sea sediments; *in* Sand, L.B. and Mumpton, F.A., Natural zeolites: occurrence, properties, use, Pergamon Press, New York, p. 245–258.

Horne, L.V.B. and Robinson, P.T.
1986: Cyprus Crustal Study Project, Hole CY-1A: Edited core descriptions; Dalhousie University, Halifax, 700 p.

Iijima, A.
1974: Clay and zeolitic alteration zones surrounding Kuroko deposits in the Hokuroku District, Norther Akita, as submarine hydrothermal-diagenetic alteration products; *in* Ishihara, S., Kanehira, K., Sasaki, A., Sako, T., and Shimazaki, Y., Geology of Kuroko Deposits, Mining Geology Special Issue, v. 6, 267–289.

Iijima, A. and Utada, M.
1971: Present-day zeolitic diagenesis of the Neogene geosynclinal deposits of the Niigata oil field, Japan; Molecular sieve zeolites-I, Advances in Chemistry Series, v. 101, American Chemical Society, Washington, p. 342–349.

Jones, J.B. and Segnit, E.R.
1971: The nature of opal: I. Nomenclature and constituent phases; Journal of the Geological Society of Australia, v. 18, p. 57–68.

Kristmannsdottir, H.
1975: Hydrothermal alteration of basaltic rocks in Iceland geothermal areas; Proceedings, 2nd U.N. Symposium on the development and use of geothermal resources, 20–29 May, 1975, San Francisco, p. 441–445.

Kristmannsdottir, H. and Tomasson, J.
1978: Zeolite zones in geothermal areas in Iceland; *in* Sand, L.B. and Mumpton, F.A., Natural zeolites: occurrence, properties, use, Pergamon Press, Oxford, p. 277–284.

Liou, J.G.
1971a: Stilbite-laumontite equilibrium; Contributions to Mineralogy and Petrology, v. 31, p. 171–177.

Liou, J.G.
1971b: Analcime equilibrium; Lithos, v. 4, p. 389–402.

Liou, J.G., Maruyama, S., and Cho, M.
1985: Phase equilibria and mineral parageneses of metabasites in low-grade metamorphism; Mineralogical Magazine, v. 49, p. 321–333.

Lydon, J.W.
1985: Some observations on the mineralogical and chemical zonation patterns of volcanogenic sulfide deposits of Cyprus; Current Research Geological Survey of Canada, Paper 84–1A, p. 611–616.

Mariner, R.H. and Surdam, R.C.
1970: Alkalinity and formation of zeolites in saline alkaline lakes; Science, v. 170, p. 977–980.

Mehegan, J.M.
1988: Temporal, spatial, and chemical evolution of the Troodos ophiolite lavas, Cyprus: Supra-subduction zone volcanism in the Tethys Sea; (PhD Thesis), Dalhousie University, Halifax, 700 p.

Mottl, M.J. and Holland, H.D.
1978: Chemical exchange during hydrothermal alteration of basalt by seawater—I. Experimental results for major and minor components of seawater; Geochimica et Cosmochimica Acta, v. 42, p. 1103–1115.

Mucci, A. and Morse, J.W.
1983: The incorporation of Mg^{2+} and Sr^{2+} into calcite overgrowths: influences of growth rate and solution composition; Geochimica et Cosmochimica Acta, v. 47, p. 217–233.

Muehlenbachs, K.
1979: The alteration and aging of the basaltic layer of sea floor: oxygen isotope evidence from DSDP/IPOD Legs, 51, 52, and 53; *in* Donnelly, T., Francheteau, J., Bryan, W., Robinson, P., Flower, M., Salisbury, M., et al., Initial Reports of the Deep Sea Drilling Project, v. 51, 52, 53, U.S. Government Printing Office, Washington, p. 1159–1167.

Mumpton, F.A.
1960: Clinoptilolite redefined; American Mineralogist, v. 45, p. 351–369.

Munhá, J., Fyfe, W.S., and Kerrich, R.
1980: Adularia, the characteristic mineral of felsic spilites; Contributions to Mineralogy and Petrology, v. 75, p. 15–19.

O'Neil, J.R., Clayton, R.N., and Mayeda, T.K.
1969: Oxygen isotope fractionation in divalent metal carbonates; Journal of Chemical Physics, v. 51, p. 5547–5558.

Rautenschlein, M., Jenner, G., Hertogen, J., Hofmann, A.W., Kerrich, R., Schmincke, H.-U., and White, W.M.
1986: Isotopic and trace element composition of volcanic glass from the Akaki Canyon, Cyprus: implications for the origins of the Troodos ophiolite; Earth and Planetary Science Letters, v. 75, p. 369–383.

Richardson, C.J., Cann, J.R., Richards, H.G., and Cowan, J.G.
1987: Metal-depleted root zones of the Troodos ore-forming hydrothermal systems, Cyprus; Earth and Planetary Science Letters, v. 84, p. 243–253.

Robinson, P.T., Gibson, I., and Panayiotou, A., eds.
1987: Cyprus Crustal Study Project: Initial Report, Holes CY-2 and CY-2A; Geological Survey of Canada, Paper 85–29, 381 p.

Robinson, P.T., Melson, W., O'Hearn, T., and Schmincke, H.-U.
1983: Volcanic glass compositions of the Troodos ophiolite, Cyprus; Geology, v. 11, p. 400–404.

Rosenbauer, J.R. and Bischoff, J.L.
1983: Uptake and transport of heavy metals by heated seawater: a summary of the experimental results; *in* Rona, P.A., Bostrom, K., Laubier, L., and Smith Jr., K.L., Hydrothermal processes at seafloor spreading centers, IV Marine Sciences, v. 12, Plenum Press, New York, p. 177–198.

Ross, C.S. and Hendricks, S.B.
1945: Minerals of the montmorillonite group: their origin in relation to soils and clays; U.S. Geological Survey, Professional Paper 205B, p. 23–79.

Savin, S.M.
1977: The history of the earth's surface temperature during the past 100 million years; Annual Review of Earth Planetary Sciences, v. 5, p. 319–355.

Schiffman, P., Smith, B.M., Varga, R.J., and Moores, E.M.
1987: Geometry, conditions and timing of off-axis hydrothermal metamorphism and ore-deposition in the Solea graben; Nature, v. 325, p. 423–425.

Schmincke, H.-U., Rautenschlein, M., Robinson, P.T., and Mehegan, J.M.
1983: Troodos extrusive series of Cyprus: a comparison with oceanic crust; Geology, v. 11, p. 405–409.

Seyfried Jr., W.E., Shanks III, W.C., and Dibble Jr., W.E.
1978: Clay mineral formation in DSDP Leg 34 basalt; Earth and Planetary Science Letters, v. 41, p. 265–276.

Shipboard Scientific Parties of Leg 68 (Site 501), Leg 69, and Leg 70
1983: Sites 501 and 504: sediments and ocean crust in an area of high heat flow on the southern flank of the Costa Rica Rift; *in* Cann, J.R., Langseth, M.G., Honnorez, J., Von Herzen, R.P., White S.M., et al., Initial Reports of the Deep Sea Drilling Project, v. 69, U.S. Government Printing Office, Washington, p. 31–173.

Shipboard Scientific Party, Leg 83
1985: Hole 504B, Leg 83; *in* Anderson, R.N., Honnorez, J., Becker, K., et al., Initial Reports of the Deep Sea Drilling Project, v. 83, U.S. Government Printing Office, Washington, p. 13–118.

Smewing, J.
1975: Metamorphism of the Troodos Massif, Cyprus; (PhD Thesis,) Open University, Great Britain, 132 p.

Spooner, E.T.C., Chapman, H.J., and Smewing, J.D.
1977: Strontium isotopic contamination and oxidation during ocean floor hydrothermal metamorphism of the ophiolitic rocks of the Troodos Massif, Cyprus; Geochimica et Cosmochimica Acta, v. 41, p. 873–890.

Stakes, D.S. and O'Neil, J.R.
1982: Mineralogy and stable isotope geochemistry of hydrothermally altered oceanic rocks; Earth and Planetary Science Letters, v. 57, p. 285–304.

Staudigel, H. and Gillis, K.M.
1990: The timing of hydrothermal alteration in the Troodos ophiolite; *in* Malpas, J., Moores, E.M., Panayiotou, A., and Xenophontos, C., Ophiolites—Oceanic Crustal Analogues. Proceedings of the Symposium 'TROODOS 1987,' Cyprus Geological Survey Department, Nicosia, p. 665–672.

Surdam, R.C. and Shepperd, R.A.
1978: Zeolites in saline, alkaline-lake deposits; *in* Sand, L.B. and Mumpton, F.A., Natural zeolites: occurrence, properties, use, Pergamon Press, Oxford, p. 145–174.

Wise, W.S. and Eugster, H.P.
1964: Celadonite: synthesis, thermal stability and occurrence; American Mineralogist, v. 49, p. 1031–1083.

Secondary Minerals in the CCSP Drillholes CY-1 and CY-1A

O.V. CHUDAYEV, V.B. KURNOSOV, E.D. PETRACHENKO, I.V. KHOLODKEVICH[1], AND P.T. ROBINSON[2]

[1]Far East Geological Institute, Vladivostok, 690022, USSR
[2]Center for Marine Geology, Dalhousie University, Halifax, Nova Scotia, B3H 3J5, Canada

Chudayev, O.V., Kurnosov, V.B., Petrachenko, E.D., Kholodkevich, I.V., and Robinson, P.T., 1991: Secondary minerals in the CCSP Drillholes CY-1 and CY-1A; in Cyprus Crustal Study Project: Initial Report, Holes CY-1 and 1A, eds. Gibson, I.L., Malpas, J., Robinson, P.T., and Xenophontos, C.; Geological Survey of Canada, Paper 90–20, p. 61–80, 1991.

Abstract

Holes CY-1 and CY-1A sampled the extrusive section and upper sheeted dykes of the north flank of the Troodos ophiolite. Four alteration zones can be recognized based on the secondary mineral assemblages: (1) an upper oxidized zone (0–225 m in Hole CY-1) characterized by pervasive alteration and an abundance of smectite, calcite, Fe-hydroxides, and K-feldspar; (2) a zone of discontinuous alteration, about 500 m thick, characterized by clay minerals, zeolites, and minor carbonates and locally by the presence of fresh volcanic glass; (3) a transition zone between about 238 and 270 m in Hole CY-1A that contains mixed-layer clay minerals and laumontite; and (4) a subgreenschist facies in the lower part of Hole CY-1A, characterized by assemblages of epidote, quartz, albite, and chlorite. The two upper zones reflect relatively low-temperature alteration whereas the lower two indicate somewhat higher temperatures. The sharp transition between the two types suggests a stepped geothermal gradient at the time of formation, perhaps related to the presence of a dyke swarm at a relatively shallow level.

Résumé

Les forages CY-1 et CY-1A échantillonnent la section extrusive du flanc nord de l'ophiolite de Troodos, et les groupes de complex de dykes supérieurs de ce même flanc. L'assemblage des minerais secondaires permet de reconnaître quatre zones d'altération : (1) une zone supérieure oxidée (0–225 m dans le forage CY-1) caractérisée par une altération profonde et une abondance de smectite, calcite, hydroxides de fer et de feldspaths potassiques. (2) une zone d'altération discontinue d'environ 500 m d'épaisseur caractérisée par des mineraies d'argile, du zéolite et une quantité moindre de carbonates ainsi que localement par la présence de verres volcanique frais. (3) une zone de transition entre 238 et 270 m environ, dans le trou de forage CY-1A qui contient des couches mixes de minerais d'argile et de laumonite et (4) un faciés shiste sous-vert dans la partie inférieure du trou de forage CY-1A caractérisé par un assemblage d'épidote, de quartz, d'albite et de chlorite. Les deux zones supérieures reflètent une altération à une température relativement basse, tandis que les deux zones inférieures indiquent une température quelque peu plus élevée. La transition abrupte entre ces deux types révèlent une augmentation du gradient géothermal au moment de la formation, ce qui peut-être expliquerait la présence d'un essaim de dykes à un niveau relativement peu profond.

INTRODUCTION

A primary goal of the Cyprus Crustal Study Project was to sample the extrusive sequence of the Troodos ophiolite by drilling a single hole from the top of the lava section into the sheeted dykes. Hole CY-1 was spudded in at the sediment-lava contact in the Akaki River canyon and drilled to a depth of 475 m with a recovery of 92%. It penetrated a sequence of pillowed and massive flows that had previously been assigned to both the Upper and Lower Pillow Lavas.

When this hole was terminated because of poor drilling conditions, the rig was moved about 1 km to the south. CY-1A was then spudded in at about the same stratigraphic level at which CY-1 was terminated. Hole CY-1A penetrated a total of 700 m with 94.5% recovery. Pillowed and massive lava flows make up the upper part of the sequence in this hole and these are underlain by massive lava flows cut by numerous dykes.

All of the lavas and dykes have been altered to some degree by interaction with seawater although fresh glass is locally preserved. The purpose of this study was to identify the secondary mineral assemblages in the lavas, to characterize the nature and extent of the alteration and to identify the alteration zones.

Methods of Investigation

Secondary minerals in Holes CY-1 and 1A replace groundmass material and fill fractures and vesicles. Groundmass minerals were separated by crushing the rock and separating the less than two micron fraction. Secondary minerals filling fractures and vesicles were hand picked under a binocular microscope. Mineral identification was based on optical properties and X-ray diffraction analysis. Smear slides were prepared for X-ray analysis from powdered material. After analysis, all samples were saturated with ethylene glycol, reanalyzed, and then ignited for 1–2 hours at 550° C. Major oxides and selected trace elements were analyzed to determine the chemical variations resulting from alteration. The major oxides were analyzed by R.N. Gritsai using wet chemical methods and the trace elements were analyzed by flame spectroscopy.

Lithology and Petrography

Hole CY-1 was spudded at the top of the extrusive sequence in the Akaki River canyon and penetrated 474.88 m. It sampled a sequence composed largely of pillow lavas and breccias with subordinate massive flows. Individual cooling units were grouped into 30 larger scale lithologic units (Robinson and Gibson, this volume). Hole CY-1A is also located in the Akaki River canyon about 1 km south of CY-1. It was spudded at about the stratigraphic level reached in Hole CY-1 and penetrated 700 m. Thirty four lithologic units were recognized (Robinson and Gibson, this volume) and these consist chiefly of massive lava flows and dykes with less abundant pillow lavas and breccias. Although the exact stratigraphic and structural relationships between Holes CY-1 and 1A are unclear, the two holes are treated as continuous in this report.

Figure 1: Basalt with an intersertal texture, Hole CY-1, 348.1 m, magnification × 150.

The lithology and secondary minerals of the rocks examined in this study are summarized in Appendices I–V. Pillows were recognized from their small thickness, curved glassy rinds and fine-grained textures. Locally, particularly in the upper parts of the section, pillows pass abruptly into breccias composed largely of pillow fragments. Massive lava flows are usually thicker and coarser grained than pillows. Many have glassy margins but these are typically thin and relatively flat. Dykes and sills are recognized on the basis of their sharp, chilled intrusive contacts and uniform, massive character. In the lower part of Hole CY-1A the core is highly broken and rubbly, making it difficult to distinguish dykes from massive lava flows.

The pillow lavas and breccias are fine-grained, sparsely to moderately phyric rocks with hyalopilitic to intersertal groundmass textures (Figure 1). Phenocrysts are chiefly altered olivine and lesser clinopyroxene. They average less than 5% of most rocks but locally make up 50% of some picritic pillows. The groundmass minerals are plagioclase and clinopyroxene with small amounts of iron-titanium oxide and some olivine (Figure 1). Hyalopilitic specimens consist chiefly of crystallized or altered glass with sparse microlites of plagioclase and clinopyroxene (Figure 2). Secondary minerals replace both groundmass material and phenocrysts, particularly olivine (Figure 3), and fill abundant vesicles and veins (Figure 4). The glassy pillow rinds are commonly brecciated (Figure 5) and partly to completely replaced by clay minerals, carbonates, and zeolites.

Massive lava flows are chiefly aphyric, fine- to medium-grained rocks with intersertal textures. Vesicles are usually

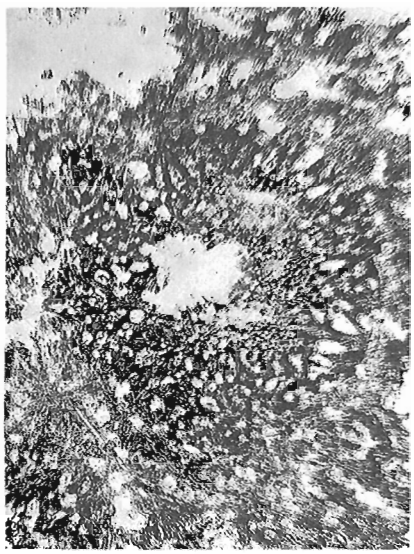

Figure 2: Basalt with hyalopilitic texture, Hole CY-1, 168.8 m, magnification × 150.

Figure 3: Altered olivine phenocryst in basalt, Hole CY-1, 58.35 m, magnification × 150.

Figure 4: Calcite-zeolite vein in basalt, Hole CY-1, 19.97 m, magnification × 60.

Figure 5: Fractured rock, glassy pillow rind, Hole CY-1, 188.05 m, magnification × 150.

less abundant but larger than those in pillows and are concentrated in distinct bands or zones. Rare porphyritic flows have accumulations of olivine and clinopyroxene in their lower parts, presumably reflecting crystal settling. Many of the flows have chilled glassy margins and some contain variable proportions of breccia consisting of crystalline fragments in a glassy matrix (Figures 6 and 7). Many of the glassy margins have well developed variolitic textures (Figure 8). Hyaloclastite layers are rare. The massive flows and particularly the glassy breccias (Figure 9) are moderately to extensively altered. Vesicles are commonly filled with a variety of secondary minerals (Figure 10) and small veins are common.

In the upper part of the section the rocks contain mostly smectite and celadonite, whereas in the lower part the flows have been recrystallized to a subgreenschist facies assemblage.

The dykes and sills are typically fine- to medium-grained, very homogeneous, aphyric rocks with sparse vesicles. Most have well developed chilled margins, some of which have altered glass. Where intrusive contacts are not preserved, dykes are difficult to distinguish from flows but are generally less vesicular. Alteration is most pronounced in the chilled, glassy margins. However in the lower parts of the section, the rocks have been extensively recrystallized to a subgreenschist facies mineral assemblage.

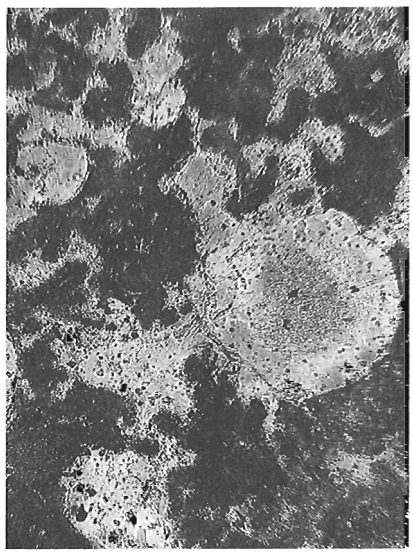

Figure 6: Unevenly crystallized massive flow, Hole CY-1A, 140.0 m, magnification × 150.

Figure 7: Crystalline fragments in altered glass, glassy breccia, Hole CY-1A, 455.2 m, magnification × 150.

Figure 8: Variolitic texture, chilled margin of massive lava flow, Hole CY-1A, 148.65 m, magnification × 150.

Figure 9: Glassy fragments within altered material, massive lava flow, Hole CY-1A, 47.52 m, magnification × 150.

Secondary Minerals

Secondary minerals fill open spaces such as vesicles, fractures, and vugs. They also replace both phenocrysts and groundmass minerals as well as glassy or poorly crystallized interstitial material (Appendices I–V). The most common secondary phases are clay minerals and calcite with lesser amounts of phillipsite, opal, pyrite, and quartz (Tables 1, 2, and 3). [Note: Tables are grouped at the end of this paper, before the appendices.] Potassium feldspar replaces plagioclase, particularly the calcic cores of zoned crystals, in the upper few hundred metres of CY-1. Albite, epidote, and locally actinolite occur in the lower 300 m of Hole CY-1A. Phenocrystic and groundmass olivine is totally to partly replaced by calcite, Fe-hydroxides and smectite whereas pyroxene is commonly fresh, even when other minerals are completely replaced. Most groundmass secondary minerals also occur as open space fillings (Tables 4, 5, and 6) but the proportions are commonly different. In addition to phillipsite, a number of other zeolites, such as mordenite, heulandite, laumontite, herschelite, analcime, and chabazite are also present in veins and vesicles.

Figure 10: Smectite-filled vesicle, brecciated lava flow, Hole CY-1A, 79.05 m, magnification × 150.

Many veins and vesicles show distinct zonations in secondary mineralogy. Vesicle walls are commonly lined with smectite and hydrous iron oxides and the cores filled with mixed-layer clay minerals, carbonate and/or zeolite. Carbonates and zeolites, locally accompanied by clay minerals, are the most common vein fillings.

Amongst the clay minerals, smectite, celadonite, and chlorite are the most common but swelling chlorite, palygorskite, and various mixed-layer species are also present. Both dioctahedral and trioctahedral smectites are represented. Dioctahedral varieties have b-spacings between 9.05 and 9.15 Å, whereas trioctahedral smectites all have b-spacings greater than 9.20 Å (Table 7). Dioctahedral celadonite (b = 9.05–9.15 Å) is a 1M polytype with a high iron content.

Both normal and swelling chlorites have been identified. Normal chlorites are trioctahedral, iron-magnesium varieties. Swelling chlorites are recognized by an expansion of the basal spacing to about 17 Å when saturated with ethylene glycol. The structure then collapses back to about 14.2 Å when heated at 550°C. Spacing on the b axis is about 9.30 Å.

Two types of mixed-layer clay minerals are present; chlorite-smectite and celadonite-smectite. Chlorite-smectite varieties are recognized by non-rational repetitions of the basal reflections, which indicate alternating chlorite and smectite layers. The celadonite-smectite mixed-layer varieties are distinguished by a significant shift of the basal reflection to about 10 Å when heated to 550°C.

Distribution of Secondary Minerals

Hole CY-1. The principal secondary minerals in Hole CY-1 are smectite, mixed-layer smectite-celadonite, K-feldspar, and calcite, which indicate formation by low temperature seawater/rock interaction. The uppermost lavas are intensely altered: they are reddish-brown in colour and highly oxidized. Dioctahedral, iron-rich smectite, carbonate, and zeolite are the most common secondary minerals in this part of the section (Tables 1, 2, and 3). Glassy pillow margins are replaced by smectite, iron oxides, phillipsite, analcime, and calcite. Groundmass alteration involves replacement by smectite, mixed-layer chlorite-smectite, calcite, and K-feldspar. Olivine phenocrysts are altered to iddingsite and calcite. Veins and vesicles are filled largely with smectite, phillipsite, analcime, calcite, and iron oxides. A few late veins are filled with palygorskite and gypsum. Lower in the section, below about 225 m, oxidative alteration diminishes and the rocks contain mostly smectite and mixed-layer smectite-chlorite in the groundmass and zeolites, particularly analcime, in the interpillow spaces (Tables 1, 2, and 3). Celadonite is commonly present, particularly in massive flows, where it is associated with phillipsite and heulandite. Potassium feldspar locally replaces groundmass plagioclase, though to a lesser degree than in the upper part of the section, and smectite replaces rare olivine. Veins are filled with mixed-layer clay minerals, carbonates, and zeolites. These minerals persist to the base of the hole.

Hole CY-1A. Hole CY-1A starts at or near the stratigraphic level reached in Hole CY-1. As expected, the secondary mineral assemblages in the upper part of CY-1A are similar to those in the lower part of CY-1. Glassy material is largely replaced by smectite accompanied by minor iron oxides (Appendices III–V) but a considerable amount of fresh glass is preserved. Very sparse olivine is only partly replaced by smectite. Plagioclase is generally fresh or partly replaced by smectite and analcime (Table 4). Smectite, celadonite, and calcite fill veins and vesicles (Tables 5 and 6). Below lithologic unit XVII, at about 238 m, somewhat higher temperature secondary minerals are encountered. Small quantities of laumontite, chlorite, and epidote appear in veins and vesicles and chlorite replaces smectite and mixed-layer smectite-chlorite as the major groundmass phase (Table 4). Celadonite also disappears below about 238 m. In the transition zone between the rocks containing mostly smectite and those containing mostly chlorite is a zone where corrensite, a mixed-layer clay mineral with smectite and chlorite in a 1:1 ratio, becomes a major groundmass phase (Table 7). The pervasiveness of the alteration increases downhole until the rocks attain a subgreenschist facies assemblage of chlorite, quartz, albite, and epidote at about 270 m. Actinolite is absent but pyrite is common, both in veins and vesicles and as a groundmass phase (Tables 4, 5, and 6). A few late veins contain lower temperature assemblages, particularly mixtures of calcite and zeolite. Many of the veins and vesicles show pronounced mineral zonation. Vesicles in a sample from 148.65 m are rimmed with smectite and filled with mixed-layer celadonite-smectite and analcime. A vein at 216.75 m has alternating bands of chlorite, smectite, iron oxide, and a core filled with quartz.

Chemical Changes During Alteration

Fourteen new major oxide and trace element analyses of variably altered rocks from Hole CY-1 are presented in Table 8. Fresh rocks from this sequence are largely high-SiO_2/high-MgO basalts and basaltic andesites with some picritic pillows in the upper parts of the section (Robinson et al., 1983; Schmincke et al., 1983). Correlation coefficients have been calculated between all major oxides and trace elements (Table 9).

Most of the analyzed rocks have very high water contents (up to 10.37 wt.%), indicating high degrees of alteration and hydration. A positive correlation is evident between H_2O+, Fe_2O_3, and K_2O; all indices of alteration. The very high K_2O contents of the rocks reflect the presence of abundant K-feldspar to a depth of about 280 m. This is also reflected in the strong negative correlation between Na_2O and K_2O as K-feldspar replaces plagioclase. Very high Fe_2O_3 / FeO ratios (up to 10) in the uppermost lavas reflect oxidative alteration and the presence of iron hydroxides that stain the rocks brown to reddish-brown in colour. A negative correlation between H_2O+, SiO_2, and Na_2O suggest some loss of the latter two oxides during alteration. However, a negative correlation between H_2O and CaO suggests a post-hydration addition of calcite because there is a strong positive correlation between CaO and CO_2 (Gillis and Robinson, this volume). A strong negative correlation between CaO and MgO presumably may reflect the breakdown of olivine and other MgO-rich minerals and their replacement by carbonate and Fe-rich smectite. Alternatively, it may simply reflect dilution of other oxides by the addition of $CaCO_3$. The presence of high CO_2 in the upper lavas supports this interpretation. Marked positive correlations among some trace elements are probably inherited from the fresh rocks rather than being due to alteration.

SUMMARY AND CONCLUSIONS

Holes CY-1 and CY-1A penetrated a combined depth of 1190 m into the extrusive sequence of the Troodos ophiolite. Study of the secondary mineral assemblages indicates four major zones of alteration in the cored sequence:

(1) **An upper zone** of intense oxidative alteration extending from the top of the lava pile to about 225 m. This zone is characterized by very pervasive alteration and contains abundant smectite, calcite, iron oxides, and K-feldspar. Temperatures in this zone probably did not exceed 50°C (Gillis and Robinson, 1985; Gillis, 1987). This sequence corresponds to the seafloor weathering zone defined by Gillis and Robinson, (1985; 1990), and presumably formed by long exposure of the upper lavas to seawater. On Troodos this zone is best developed where the impermeable umbers at the top of the lava pile are thin or absent.

(2) **A low temperature zone** of interaction between rock and seawater that extends from about 225 to 713 m below the top of the lava pile (from 225 m in CY-1 to 238 m in CY-1A). Alteration is irregular and patchy in this zone and fresh volcanic glass is commonly preserved. Pillow lavas and their glassy rinds are partly altered to smectite, analcime, and minor carbonate, whereas massive flows have a characteristic assemblage of celadonite, heulandite, and phillipsite. Although the alteration in this zone was generally oxidative there are few iron oxides present and the rocks are generally grey to greenish-grey. This is believed to reflect less-pervasive alteration and the general absence of olivine, the breakdown of which accounts for some of the reddish-brown colour in the seafloor weathering zone. This sequence corresponds to the low temperature zone of Gillis and Robinson (1988) and reflects penetration of cold seawater into the cooling crust. The absence of higher temperature zeolites, such as laumontite, suggests that the temperatures in this zone probably were less than 100°C (Kristmannsdottir and Tomasson, 1978; Gillis and Robinson, 1988; 1991). The distribution of alteration in this zone is largely a function of permeability (Gillis, 1987).

(3) **A transition zone** between about 238 and 270 m in Hole CY-1A (713–745 m below the top of the lava pile) that separates the low temperature zone from the deeper subgreenschist facies zone. This zone is characterized by mixed-layer smectite-chlorite and laumontite, suggesting temperatures between about 100 and 150°C. This zone corresponds to the transition zone defined by Gillis and Robinson, 1985; 1989).

(4) **A higher temperature zone** of hydrothermal alteration. Beginning at about 745 m below the top of the lava piles, the rocks show the effects of higher temperature hydrothermal alteration. Mixed-layer smectite-chlorite is replaced by chlorite and laumontite disappears. Epidote first appears at about 241 m in Hole CY-1A (716 m below the top of the lava pile) and but does not become a major phase until about 540 m (1015 m below the top of the lava pile). Pervasive alteration in this zone produced a subgreenschist facies assemblage consisting of epidote, chlorite, albite, and quartz. Pyrite is common both in veins and vesicles and as a groundmass mineral. Based on the abundance of epidote and the absence of actinolite, the temperatures of alteration are estimated to have ranged from 250–300°C (cf. Anderson et al., 1982, Evarts and Schiffman, 1983). This low grade greenschist assemblage corresponds to the upper dyke zone of Gillis and Robinson (1988).

The sharp boundary between the rocks altered at low temperatures and those altered under subgreenschist facies conditions suggests a stepped thermal gradient (Gillis and Robinson, 1990), and may be related to the abundance of dykes encountered in the lower part of Hole CY-1A.

REFERENCES

Anderson, R.N., Honnorez, J., Becker, K., Adamson, A.C., Alt, J.C., Emmermann, R., Kempton, P.D., Kinoshita, H., Laverne, C., Mottl, M.J., and Newmark, R.L.

1982: DSDP Hole 504B, the first reference section over 1 km through layer 2 of the oceanic crust; Nature, v. 300, p. 589–594.

Evarts, R.C. and Schiffman, P.
1983: Submarine hydrothermal metamorphism of the Del Puerto ophiolite, California; American Journal of Science, v. 283, p. 289–340.

Gillis, K.M.
1987: Multistage alteration of the extrusive sequence, Troodos ophiolite, Cyprus; (PhD Thesis), Dalhousie University, Halifax, 387 p.

Gillis, K.M. and Robinson, P.T.
1985: Low-temperature alteration of the extrusive sequence, Troodos ophiolite, Cyprus; The Canadian Mineralogist, v. 23, p. 431–441.

Gillis, K.M. and Robinson, P.T.
1988: Distribution of alteration zones in the upper oceanic crust; Geology, v. 16, p. 262–266.

Gillis, K.M. and Robinson, P.T.
1990: Patterns and processes of alteration in the lavas and dykes of the Troodos Ophiolite, Cyprus; Journal of Geophysical Research, v. 95, p. 21523–21548.

Kristmannsdottir, H. and Tomasson, J.
1978: Zeolite zones in geothermal areas in Iceland; *in* Sand, L.B. and Mumpton, F.A., Natural zeolites: occurrence, properties, use, Pergamon Press, Oxford, p. 277–284.

Robinson, P.T., Melson, W.G., O'Hearn, T., and Schmincke, H.–U.
1983: Volcanic glass compositions of the Troodos ophiolite, Cyprus; Geology, v. 11, p. 400–404.

Schmincke, H.-U., Rautenschlein, M., Robinson, P.T., and Mehegan, J.M.
1983: Troodos extrusive series of Cyprus: a comparison with oceanic crust; Geology, v. 11, p. 405–409.

Depth (m)	1	2	3	4	5	6	7	8	9	10
13.00	x									
19.97	x									
20.10	o?									
44.40	o				x			+	+	
45.30	x								x	
52.50	x								+	+?
58.35					x					
58.80	x				+					
79.50	x				+					
83.85	x					x				
87.55	x					x		+		
87.90					x	x			x	
91.00		o		+				+	x	
95.42	x								x	
107.45	x									
111.60			+		+?					
117.80			+		+?			+	+	
124.00					x					
124.90	x									
137.70	+		+							
138.90					x					
143.85	x								x	
168.80	x									
176.50	x									
178.00	+			+						
209.50	x				+			+		
212.10	+?				x			+		
212.50									x	
219.20	+?				x			+	x	
229.30					x					
240.30	x									
248.70	x			x						
248.74	x									
250.13								+		
260.60			x		+					
261.53					x			+		
262.00							x			
266.10					x					
281.68					x			+		
298.80	x									
310.10	x							+		
317.95					x					
338.70							x			
348.10	x	+?						+?		
348.70	x									
351.80	x							+?		
360.65	x									
369.10	x									
374.60	x									
378.50	x	+?								
387.20	x									
425.60	x									+
428.70	x	+								
440.70	x	+								
449.20	x									
452.05	x									
459.70	x									
465.80	x	+								
473.05	x							+?		

Table 1: Secondary minerals from the groundmass of volcanic rocks of Hole CY-1. 1 = Smectite; 2 = Celadonite; 3 = Chlorite; 4 = Swelling chlorite; 5 = Mixed-layer clay minerals; 6 = Palygorskite; 7 = Gypsum; 8 = K-feldspar; 9 = Calcite; 10 = Phillipsite. Note: x = abundant; + = moderately abundant; o = trace amount.

Depth (m)	1	2	3	4	5	6	7	8	9	10	11	12	13	14	15	16	17	18	Nature of Sample
13.00	x								x										Red inclusions
	+																		White crust
	+							x								+			Black crust
	x			o															Yellow material
13.80						x													White vein
19.97	+?					+?		o?		o		+				x	o		Grey vein
20.10	+					o		+?		+						x			Vein
23.80				+		x										+			Red material
39.90						x										+			White material
52.50					x														Brown material
	+?									o						o			Green clay
																x			Crust
58.35																x			Vein
					x					o						o			Green crust
79.50		+?	o?		+					o						x			Green crust
	o		+?		+					+						x			Red crust
					+														Vesicle filling
83.85	+?				+					o									Green material
	x			o?						x						x			White crust
					+														Green crust
87.55																x			White vein
87.90	+				x														White vein
				x		x										x			Green material
91.00							x?									o			White vein
95.42	o															x			White vein
	+															x			Brown material
107.45	o															x			Pink crust
111.60					x							+				x			White vein
					o											x			White vein
117.80					x														Green vein
																x			White vein
124.35					+					o									Green crust
124.90						x													White material
137.70																x			White vein
								+		o?									Violet crystals
138.90																x			White crust
143.85	x																		Green material
168.80	+																	+	Yellow vein
	x																		Light material
	o																	+	Red crust
	+		o																Green vesicles
176.50	+								x										White inclusions
	x																		Light clay
	x																		Green clay
	x																		Brown clay

Table 2: (Continues in Table 3.) Secondary minerals in veins and vesicles of the rocks from Hole CY-1. 1 = Smectite; 2 = Chlorite; 3 = Celadonite; 4 = Mixed-layer Celadonite-Smectite; 5 = Mixed-layer Chlorite-Smectite; 6 = Palygorskite; 7 = Sepiolite; 8 = Analcite; 9 = Mordenite; 10 = Phillipsite; 11 = Heulandite; 12 = Laumontite; 13 = Herschelite; 14 = Chabasite; 15 = Gypsum; 16 = Calcite; 17 = Epidote; 18 = Goethite.

Depth (m)	1	2	3	4	5	6	7	8	9	10	11	12	13	14	15	16	17	18	Nature of Sample
178.00					+					+									Green crust
	o									x									White crust
	o?									+		x							White crust
	+	o?																	Pink crust
	+																		Dark material
209.50					o?											x			White vesicles
	+				x														Dark vesicles
	+				+														Bluish vesicles
212.10																x			White crust
								x								o			Red crystals
	o?				+			x											Transparent material
212.50																x			White material
219.20	o?	+														x			White material
	+?				+											o			Green material
229.35								+								x			Transparent vein
	x									o?									Yellow crust
240.35	x															o			Green crust
		+			+														Green crust
248.70	x																		Light crust
248.75	+	+																	Green crust
250.13	o?	+						x								x			Transparent vein
260.60					+								x						White material
266.10	+?				+			x								x			White crust
298.80	+				o?					x									White veinlets
310.10	x																		Light grey material
338.70	x																		Green clay
348.70	x		+																Light green material
	x		+																Green material
	x																		Brown material
351.70	+														x				White crust
	x																		Light material
360.65	x																		Vesicle filling
378.50	x		+								+								Green material
	x		+								x								Vein
387.95				+															Light crust
425.60	+		x																Blue material
428.70	x?		o													+			Vein
440.70	o		o													x			White crust
449.20	+										o								Dark material
465.80	x																		Light crust

Table 3: (Completion of Table 2 data.) Secondary minerals in veins and vesicles of the rocks from Hole CY-1. 1 = Smectite; 2 = Chlorite; 3 = Celadonite; 4 = Mixed-layer Celadonite-Smectite; 5 = Mixed-layer Chlorite-Smectite; 6 = Palygorskite; 7 = Sepiolite; 8 = Analcite; 9 = Mordenite; 10 = Phillipsite; 11 = Heulandite; 12 = Laumontite; 13 = Herschelite; 14 = Chabasite; 15 = Gypsum; 16 = Calcite; 17 = Epidote; 18 = Goethite.

Depth (m)	1	2	3	4	5	6	7	8	9	10	11	12	13
2.45	x		+			+						o	
23.00	x	o											
23.05	x												
40.35	x												
47.52	x	+											
49.85	+	+						+					
61.85	x												
77.78	x												+
86.95	x	o											
29.24	x												
101.85	x												
132.95	x												
140.00	x	o		+									
156.65	x												
160.95	x												
165.60		o			+							+	o
178.05	x												
202.30	x		o										
241.30				+			+						o
254.00	x												
266.00			x						+	o			o
311.52					x								
331.33			x						+				o
361.00			x										o
367.80	x		+										o
380.35			x										+
394.40			x		x				+				
406.00	+				+								
410.45			+										o
421.80			x										+
423.00			x										o
438.20			x										+
455.20			x										+
462.70			x						o				+
481.40			x									o	
498.00			x									o	+
516.85			x										+
542.55			x										+
566.40			x										+
579.90			+							+			x
593.65			x										+
623.35			x						o?				+
631.20			x										
658.25			x										+
659.60			x							+			+

Table 4: Secondary minerals in the groundmass of rocks from Hole CY-1A. 1 = Smectite; 2 = Celadonite; 3 = Chlorite; 4 = Swelling chlorite; 5 = Mixed-layer smectite chlorite; 6 = Analcite; 7 = Laumontite; 8 = Heulandite; 9 = Pyrite; 10 = Epidote; 11 = Actinolite; 12 = Calcite; 13 = Quartz. Note: x = abundant; + = moderately abundant; o = trace amount.

Depth (m)	1	2	3	4	5	6	7	8	9	10	11	12	13	14	15	Type of material
8.45							x									Transparent crystals
	x			+												Clay
23.00	x							x								Lamellar crystals
	x															Clay in vesicles
31.30	x															Clay in vesicles
	x							x								Transparent crystals with clay
	+	x														Green material
	+	x														Dark green material
	+	x						x								Dark green material
40.35	x															Vesicle filling
	x					+?										Clay crust
49.85	x															Brown clay crust
	+	x														Green material
61.85	+	+				+?										Vein
	x	o														Green material
77.78	x					o?										Brown vein filling
79.05	x															Brown material
	x	+														Green material
	+	+						+								Transparent crystals in green material
86.95	x	o														Green material
89.24	x	o														Green crust
	x															Black material
101.85	x															Green crust
	x															Vesicle filling
113.95	x							x								White crystals in clay
	x															Black material
140.00	x	+	o													Green material
	+	o	o													White material
	+	o		o												White material
148.65	x			+			+									White crust
	x			+			o									Clay
156.65	x						o?									Green clay
160.95	x			+												White crust
	+			x												Dark crust
	+											x				White vein
165.60	o?			+	x											Light grey crystals
178.05	x			o												Clay
	x		+													Vesicle fillings
188.05	x		o				o?									Clay
238.45		x			x										x	Clay with hematite
		o		x												Green crust
				+					+							White material
				+					o							Grey material in veins
241.30				+					x							White material in vesicles
				x					+							Clay

Table 5: (Continues in Table 6.) Secondary minerals in veins and vesicles of the rocks from Hole CY-1A. 1 = Smectite; 2 = Celadonite; 3 = Chlorite; 4 = Mixed-layer Chlorite-Smectite; 5 = Mixed-layer Celadonite-Smectite; 6 = Vermiculite; 7 = Analcite; 8 = Heulandite; 9 = Laumontite; 10 = Amphibole; 11 = Epidote; 12 = Calcite; 13 = Quartz; 14 = Pyrite; 15 = Hematite. Note: x = abundant; + = moderate amount; o = trace amount.

Depth (m)	1	2	3	4	5	6	7	8	9	10	11	12	13	14	15	Type of material
245.80			x						x			o				White veinlet
	x		x													Green material
254.00	x			+								o?				Clay
	+											x				White veinlet
282.80	+											x	o			White vein
	x			+												Green material
311.52	x															Green material
331.33			x										o			Grey clay
361.00			x										o	o?		Vein
			+										x	o?		White material
			+										x			Vesicle fillings
367.80	x			+												Coating on crystals
380.35			+									x	o	o?		White vein
394.40			+	+										o?		Green clay
406.00	+		+	+								x				Vein
	x		+	+?					o?	o?		o				Oxidized crust
	x			o?												Black material
421.80			x										o	+?		Clay in veins
438.20			x										+	+		White material
			+										+	+?		Transparent crystals
			o									o	x	+		Transparent crystals
			+										o	+		Vesicle fillings
			x										o	+		Black material
455.20			x										o	+		Brown vein
			o									o?	x	o?		White vein
481.40			x									o				Clay in veins
498.63			x									+	o			Clay
			x									x	x			Brown vein
516.85			x										o			Green vein
566.40			+								+		o			Green material
			+								+	o?	x			White material with clay
			x								o		o			Grey material in vesicles
593.65			x								o		o	o		Grey vein
			+								o		o	+		Vein filling
599.00			+									o	o	+		Fracture filling
			x									o	x			Grey material
			x								o?		+	+		Vesicle fillings
623.35			x								o?		+	+		Vein
			x										+	o		Grey material
659.60				+							o					Green material in vesicles
			x	o							o					Dark green material
			x									o			+	Oxidized sulphides

Table 6: (Completion of Table 5 data.) Secondary minerals in veins and vesicles of the rocks from Hole CY-1A. 1 = Smectite; 2 = Celadonite; 3 = Chlorite; 4 = Mixed-layer Chlorite-Smectite; 5 = Mixed-layer Celadonite-Smectite; 6 = Vermiculite; 7 = Analcite; 8 = Heulandite; 9 = Laumontite; 10 = Amphibole; 11 = Epidote; 12 = Calcite; 13 = Quartz; 14 = Pyrite; 15 = Hematite. Note: x = abundant; + = moderate amount; o = trace amount.

Depth (m)	b Parameter	Polytype	Minerals	Depth (m)	b Parameter	Polytype	Minerals
CY-1				CY-1A			
13.00	9.04		Smectite	8.45	9.25; 9.11		Smectite; chlorite
44.40	9.31; 9.09		Smectite; mixed-layer chlorite-smectite	23.00	9.23		Smectite
				40.35	9.22; 9.08		Smectite
58.35	9.30		Mixed-layer chlorite-smectite	140.00	9.30; 9.08	1M	Smectite; celadonite; swelling chlorite
91.00	9.27		Swelling chlorite	241.30	9.34		Swelling chlorite
107.45	9.13		Smectite	367.80	9.29		Smectite; chlorite
137.70	9.15; 9.12	1M	Smectite; chlorite; celadonite?	423.88	9.34		Chlorite
143.85	9.27		Smectite	481.40	9.30		Chlorite
229.30	9.26		Mixed-layer celadonite-smectite	498.63	9.30		Chlorite
				566.40	9.30		Chlorite
240.30	9.30, 9.15	1M	Smectite; celadonite	623.30	9.32		Chlorite
248.70	9.25; 9.08		Smectite; celadonite	659.60	9.26		Chlorite
298.80	9.09; 9.23		Smectite; celadonite				
348.10	9.24; 9.08		Smectite; celadonite				
360.65	9.30; 9.10		Smectite; celadonite				
378.50	9.20; 9.11	1M	Smectite; celadonite				
428.70	9.25; 9.11	1M?	Smectite; celadonite				
440.70	9.24; 9.09	1M?	Smectite; celadonite				
465.80	9.05	1M?	Smectite; celadonite				
473.05	9.06		Smectite				

Table 7: Crystallographic parameters of clay minerals in the rocks from Holes CY-1 and 1A.

Depth (m)	44.40	58.35	87.55	91.00	212.10	240.30	250.10	281.68	310.10	360.65	374.60	428.70	359.70	473.05
SiO_2	44.64	49.02	46.51	41.93	45.72	50.65	45.68	44.90	47.90	48.42	52.30	53.31	49.26	48.97
TiO_2	0.68	0.66	0.60	0.63	0.78	0.80	0.78	0.74	0.76	0.60	0.68	0.68	0.70	0.69
Al_2O_3	16.86	14.95	17.04	14.99	15.04	15.26	15.22	14.38	16.67	14.68	16.54	15.56	15.75	15.10
Fe_2O_3	7.86	7.43	7.76	6.64	8.68	4.34	6.52	1.63	7.18	6.24	5.39	6.11	6.90	6.16
FeO	0.76	1.56	1.08	1.84	1.02	2.63	1.64	3.43	1.48	2.87	2.46	2.31	1.79	2.34
MnO	0.11	0.11	0.11	0.11	0.06	0.04	0.14	0.13	0.06	0.08	0.10	0.08	0.06	0.11
MgO	7.65	7.89	6.99	5.94	11.00	7.62	8.42	8.79	7.89	10.18	6.60	4.58	8.40	9.28
CaO	6.21	3.57	6.67	14.15	1.85	6.26	6.53	7.81	5.20	5.05	9.25	9.24	6.42	6.32
Na_2O	1.23	0.98	1.16	1.70	1.35	2.66	1.69	2.18	2.40	2.96	2.28	3.00	2.80	2.90
K_2O	3.20	5.62	3.77	2.54	3.69	2.06	3.80	3.61	1.56	0.44	0.29	1.24	0.74	0.91
P_2O_5	0.09	0.07	0.09	0.10	0.10	0.13	0.11	0.09	0.13	0.10	0.09	0.08	0.09	0.09
CO_2	2.34	-	1.21	5.24	-	0.27	1.93	2.41	-	-	-	0.57	-	-
H_2O+	5.32	5.45	5.19	2.62	6.22	2.91	4.93	3.66	3.13	2.12	1.68	0.83	1.83	2.36
H_2O-	3.09	2.24	1.92	1.21	.15	4.05	2.17	2.84	5.54	5.91	2.20	2.05	5.06	4.80
Total	100.04	99.55	100.10	99.64	99.66	99.68	99.56	99.54	99.81	99.65	99.82	99.64	99.85	100.03
B	91	11	79	50	79	34	60	42	48	16	14	15	29	13
Zr	56	36	38	34	50	69	43	68	51	38	30	29	48	46
Cr	93	250	60	100	107	72	140	200	48	48	100	126	118	59
Ni	66	89	44	46	60	29	50	45	50	36	50	35	76	34
Sc	33	40	40	26	38	26	35	37	46	25	38	48	42	42
V	210	270	160	160	250	200	190	200	300	220	320	260	280	170
Co	26	28	20	21	28	25	25	28	37	24	43	20	45	22
Cu	71	80	66	43	71	36	70	59	71	45	130	52	95	38
Zn	48	79	35	32	79	48	40	40	80	60	120	49	87	60
Mo	n.d.	n.d.	n.d.	n.d.	n.d	n.d.	n.d.	n.d.	n.d.	n.d.	n.d.	1.5	n.d.	n.d.
Sn	3	3	3	2	2	3	5.5	4	6	1	4	5	3	2
Ag	n.d.	0.07	0.20	n.d.	n.d.	n.d.	0.69	0.35	0.83	n.d.	0.21	0.22	n.d.	n.d.

Table 8: Major and trace element compositions of rocks from Hole CY-1.

	SiO_2	Fe_2O_3	FeO	Al_2O_3	TiO_2	CaO	MgO	MnO	Na_2O	K_2O	P_2O_5	H_2O+	Zn	Sn	B	Cu	Co	Ni	V	Cr	Zr
SiO_2																					
Fe_2O_3	-0.36																				
FeO	0.33	-0.89																			
Al_2O_3	0.13	0.35	-0.57																		
TiO_2	-0.04	0.20	-0.03	-0.15																	
CaO	-0.14	-0.41	0.28	-0.02	-0.32																
MgO	-0.26	0.21	-0.06	-0.38	0.27	-0.72															
MnO	-0.43	-0.07	-0.02	-0.09	-0.29	0.32	-0.11														
Na_2O	0.57	-0.61	0.68	-0.22	-0.08	0.18	-0.03	-0.42													
K_2O	-0.50	-0.38	-0.42	-0.13	0.12	-0.28	-0.09	0.42	-0.85												
P_2O_5	0.11	-0.20	-0.03	-0.08	0.57	-0.06	0.17	-0.46	0.23	-0.21											
H_2O+	-0.56	0.61	-0.64	-0.08	0.18	-0.54	0.41	0.27	-0.87	0.85	-0.03										
Zn	0.25	0.33	-0.49	0.17	0.60	-0.33	0.33	-0.01	-0.18	0.13	0.46	0.38									
Sn	-0.20	0.43	-0.35	0.24	-0.10	-0.23	0.24	0.10	-0.55	0.28	-0.06	0.51	-0.06								
B	-0.37	-0.06	0.13	-0.28	-0.32	0.39	-0.11	-0.03	-0.01	-0.07	-0.25	-0.14	-0.30	-0.03							
Cu	-0.54	0.31	-0.39	0.21	0.29	-0.02	0.17	0.31	-0.30	0.18	0.39	0.35	0.77	0.30	-0.03						
Co	-0.33	-0.51	-0.51	0.14	0.42	-0.39	0.37	-0.09	0.20	0.16	0.53	0.40	0.82	0.26	-0.20	0.79					
Ni	-0.52	0.47	-0.55	0.49	-0.02	0.14	-0.09	-0.03	-0.20	-0.02	0.24	0.16	0.40	0.01	-0.12	0.56	0.46				
V	0.25	0.52	-0.58	0.30	0.37	-0.30	0.36	-0.03	-0.30	-0.04	0.27	0.37	0.86	0.38	-0.30	0.71	0.78	0.42			
Cr	-0.11	0.26	-0.28	0.52	-0.48	-0.03	-0.10	-0.60	-0.11	-0.77	-0.06	-0.02	-0.03	0.18	-0.18	0.23	- 0.06	0.58	0.16		
Zr	-0.15	0.27	-0.03	-0.38	0.34	-0.28	0.32	-0.30	-0.11	0.18	-0.05	0.13	-0.23	-0.02	0.31	-0.28	- 0.05	-0.10	-0.20	-0.03	
Sc	-0.12	-0.05	-0.05	0.27	0.44	-0.15	0.29	-0.30	-0.09	-0.13	0.51	0.16	0.33	0.55	-0.13	0.34	0.27	0.23	0.47	0.17	-0.21

Table 9: Matrix of correlation coefficients for samples from Hole CY-1. (n = 14, significant coefficients of correlation are r >0.48)

Sample Depth(m)	Lithology	Secondary Minerals						
		Glass	Olivine	Pyroxene	Plagioclase	Groundmass	Fractures & Veins	Vesicles
13.00	Basalt; intersertal texture	Smectite	-	-	Smectite	Smectite	-	Smectite
19.97	Basalt; highly altered	Smectite	-	Fe oxides	Smectite	-	Smectite, Analcite?, Calcite, Phillipsite, Laumontite	Smectite, Ore Minerals
44.40	Basalt; intersertal texture	Smectite	-	Fresh	Smectite K-feldspar	-	Calcite Laumontite	Smectite, Chlorite-smectite
45.30	Breccia; basalt fragments in carbonate matrix	-	-	Fresh	-	-	Carbonate	Apatite?, Smectite
52.50	Breccia; glassy fragments in carbonate matrix	Oxidized	-	-	-	-	Calcite	Chlorite-smectite, Smectite, calcite
58.35	Basalt; highly altered, plagioclase and olivine	Chlorite-smectite	Fresh	Fresh	K-feldspar, Chlorite-smectite	-	-	Chlorite-smectite
58.80	Basalt; olivine-phyric intersertal texture	Smectite	Chlorite-smectite, Carbonate	-	Smectite	-	Calcite	Chlorite-smectite,
79.50	Basalt; hyalopilitic texture	Mostly fresh	-	Fresh	Mostly fresh	Smectite Chlorite-smectite	- -	Calcite, Smectite
83.85	Basalt; hyalopilitic texture	Oxidized	-	-	-	Hydrous iron-oxides	-	Smectite on rim, Mixed-layer chlorite-smectite in centre
87.55	Basalt; sparsely phyric, hyalopilitic texture	Smectite	-	Fresh	K-feldspar	-	Calcite	Smectite Chlorite-smectite
91.00	Basalt, intersertal texture	Oxidized, Swelling chlorite-smectite	-	Fresh	K-feldspar	-	-	Calcite, Smectite, Celadonite
95.42	Basalt; intersertal to pilotaxitic texture, siderite segregations	Smectite	-	Fresh	Smectite	-	Carbonate	Carbonate, Smectite
107.45	Hydrothermal smectite	-	-	-	-	-	-	-
111.60	Glass, some pyroxene	Fresh	-	Fresh	-	-	Chlorite, Chlorite-smectite	Chlorite, Smectite, Actinolite
117.80	Basalt;intersertal	Oxidized	-	Fresh	K-feldspar	Chlorite,	Calcite	Chlorite-smectite
124.33	Basalt; highly altered, filled vesicles	-	-	-	-	-	-	Chlorite-smectite, Phillipsite
137.70	Basalt; glassy	Smectite	-	Fresh	Smectite	-	-	Smectite-chlorite
168.80	Basalt glass; partly crystallized	Oxidized	-	Fresh	Fe-oxides	-	-	Smectite-goethite
176.50	Basalt; hyalopilitic	Smectite	-	Fresh	Fresh	-	-	Smectite, Mordenite
178.00	Basalt; highly altered	-	-	-	-	-	Swelling chlorite, Chlorite-smectite, Smectite	Chlorite-smectite, Calcite, Smectite, Phillipsite, Herschelite
209.50	Basalt; intersertal texture	Smectite	-	Smectite	K-feldspar	-	Calcite Chlorite-smectite	Chlorite-smectite, Smectite, Calcite

Appendix 1: (Continues in Appendix 2.) Lithology and secondary mineralogy of the rocks from Hole CY-1. The secondary minerals were determined optically and checked with X-ray diffraction techniques (see Tables 1, 2, and 3).

Sample Depth(m)	Lithology	Secondary Minerals						
		Glass	Olivine	Pyroxene	Plagioclase	Groundmass	Fractures & Veins	Vesicles
212.10	Basalt; hyalopilitic texture	Smectite, Chlorite-smectite	-	Fresh	K-feldspar	-	-	Calcite, Smectite
219.20	Basalt, hyalopilitic texture, very altered	Chlorite-smectite	-	Fresh	K-feldspar	-	-	Calcite, Smectite
229.35	Basalt, glassy with hyalopilitic texture	Celadonite-smectite	-	Fresh	Fresh	-	Calcite	Calcite, Analcite
240.35	Basalt; porphyritic with intersertal texture	Smectite	-	Weakly altered	K-feldspar,Smectite	-	-	Calcite, Smectite
250.13	Basalt; intersertal texture	Chlorite, Chlorite-smectite	-	Fresh	K-feldspar, Chlorite	-	Calcite, Analcime	Chlorite, Smectite Calcite
261.53	Basalt; intersertal texture	Oxidized	Fresh	Fresh	K-feldspar	-	-	Chlorite-smectite, Calcite
266.10	Basalt; glassy with hyalopilitic texture	Oxidized	-	-	Chlorite-smectite	-	Chlorite-smectite	Calcite, Analcime
281.68	Basalt; intersertal texture	Chlorite-smectite	-	Fresh	K-feldspar Chlorite-smectite	-	-	Chlorite-smectite, Calcite
310.10	Basalt; glassy with intersertal texture	Smectite	-	Fresh	Smectite, K-feldspar	-	-	Smectite, Calcite
348.10	Basalt; pyroxene-phyric, variolitic to intersertal texture	Smectite,	-	Fresh	K-feldspar, Smectite?	-	Smectite, Calcite	Smectite, Calcite
348.70	Hydrothermal minerals; smectite, celadonite	-	-	-	-	-	-	-
351.85	Basalt; intersertal texture	Smectite	-	Smectite?	K-feldspar,	-	Smectite, Gypsum	Smectite
360.65	Basalt; glassy with variolitic texture	Oxidized	-	Smectite	Smectite, Calcite	-	Smectite	Smectite
374.65	Basalt; pyroxene-phyric, intersertal texture	Smectite	-	Fresh	Smectite	-	-	Calcite, Smectite
378.50	Basalt; pyroxene- and plagioclase-phyric, intersertal texture	Smectite, Celadonite	-	-	-	-	-	Smectite, Laumontite
425.60	Basalt; intersertal texture	Smectite	Smectite	Fresh	Smectite	-	-	Smectite, Celadonite
428.70	Basalt; intersertal texture	Oxidized	-	Fresh	Albite?	-	Smectite, Calcite, Celadonite	Smectite, Calcite
440.70	Basalt; variolitic texture	Oxidized	-	Fresh	Smectite?	-	Smectite, Celadonite	Smectite, Calcite, Celadonite
459.70	Basalt; glassy, very altered	Smectite	-	Fresh	Celadonite, Smectite	-	Smectite	Smectite
475.05	Basalt; glassy, very altered	Smectite	-	Fresh	Celadonite, Smectite	-	Smectite	Smectite

Appendix 2: (Completion of Appendix 1 data.) Lithology and secondary mineralogy of the rocks from Hole CY-1. The secondary minerals were determined optically and checked with X-ray diffraction techniques (see Tables 1, 2, and 3).

Sample Depth(m)	Lithology	Secondary Minerals						
		Glass	Olivine	Pyroxene	Plagioclase	Groundmass	Fractures & Veins	Vesicles
8.45	Basalt glass; variolitic texture	Smectite	Fresh	-	Smectite, Analcite	-	Smectite	Smectite, Calcite, Chlorite
23.00	Basalt; glassy	Fe-oxides	-	-	Fresh	-	-	Smectite
31.30	Basalt; glassy	Minor smectite	-	-	Fresh	-	Smectite, Amphibole	Smectite Amphibole
40.35	Basalt; intersertal texture	Smectite	-	Smectite	Fresh	-	-	Smectite
47.52	Basalt; glassy	Fresh	-	-	Fresh	-	Smectite, Calcite Celadonite	-
49.85	Unknown	-	-	-	-	-	-	-
61.85	Basalt; intersertal texture	Fe-oxides	-	-	Fresh	-	Smectite	Smectite, Celadonite
77.78	Basalt; intersertal texture	Fe-oxides	-	-	Smectite	-	Smectite, Calcite, Celadonite(?)	Smectite
79.05	Basalt; glassy	Fe-oxides	-	-	Fresh	-	Smectite	Smectite
86.95	Basalt; hyalopilitic, fragmental	-	-	-	Smectite	-	Smectite, Celadonite	Smectite
89.29	Basalt; glassy	Fe-oxides	-	-	Fresh	-	-	Smectite, Quartz
101.85	Basalt; glassy with intersertal texture	Fe-oxides	-	-	Fresh	-	-	Smectite
113.95	Basalt; hyalopilitic texture	Smectite	-	-	Fresh	-	-	Smectite, Heulandite
132.95	Basalt; highly altered, intersertal texture	Smectite	-	Fresh	Albite(?)	-	Smectite, Limonite	Smectite
140.00	Basalt; intersertal texture	Smectite, Chlorite, Swelling chlorite, Celadonite	-	Fresh	Chlorite, Albite(?)	-	-	Chlorite, Celadonite
148.65	Basalt; variolitic texture	Fe-oxides	-	-	-	-	-	Analcite, Smectite-celadonite
156.65	Basalt; ophitic texture	Smectite	-	Zoisite?	Smectite	-	-	-
160.95	Basalt; intersertal to variolitic texture	Smectite Chlorite-smectite	-	-	Chlorite-smectite, Smectite	-	-	Chlorite-smectite, Smectite
165.60	Basalt; fragmental, glassy	Celadonite-smectite Chlorite-smectite, Celadonite	-	-	-	-	-	-
178.05	Basalt; glassy, variolitic texture	Chlorite-smectite Smectite	-	-	-	-	Chlorite-smectite	Chlorite-smectite
188.05	Basalt?	Chlorite, Smectite	-	-	-	-	Chlorite, Smectite	-
202.30	Basalt glass	Smectite, Chlorite Calcite	-	-	-	-	Chlorite	Smectite, Chlorite

Appendix 3: (Continues in Appendices 4 and 5.) Lithology and secondary mineralogy of the rocks from Hole CY-1A. The secondary minerals were determined optically and checked with X-ray diffraction techniques (see Tables 4, 5, and 6).

Sample Depth(m)	Lithology	Secondary Minerals						
		Glass	Olivine	Pyroxene	Plagioclase	Groundmass	Fractures & Veins	Vesicles
216.75	Glass; altered	Fe-oxides	-	-	-	-	Smectite, Quartz, Fe-oxides	Chlorite, Smectite
238.45	Basalt; glassy, plagioclase-phyric	Chlorite	-	-	K-feldspar(?)	-	Gypsum	Celadonite, Celadonite-smectite, Epidote, Gypsum, Chlorite(?)
241.30	Basalt; variolitic to intersertal texture	Swelling chlorite	-	-	K-feldspar, Swelling chlorite	Epidote	Swelling chlorite, Epidote, Quartz, Laumontite	Chlorite-smectite, Swelling chlorite, Epidote, Gypsum, Laumontite
245.80	Basalt; glassy	Fe-oxides	-	-	-	-	-	Laumontite, Calcite
254.00	Basalt; glassy, brecciated	Chlorite-smectite	iddingsite	-	-	-	Chlorite-smectite, Smectite, Epidote	Quartz
266.00	Basalt breccia with ore minerals	Chlorite	-	-	Chlorite, Epidote	Epidote, Amphibole	-	Chlorite, Quartz, Pyrite
282.80	Basalt glass; highly altered	Fe-oxides	-	-	-	-	Smectite, Calcite, Quartz	-
331.33	Basalt breccia; glassy	Chlorite, Quartz	-	-	Chlorite, Epidote, Albite(?)	-	-	Quartz, Chlorite
347.00	Basalt; glassy with intersertal texture	Epidote, Chlorite	-	Chlorite	Epidote, Chlorite, Quartz, Albite(?)	-	Quartz, Chlorite	Quartz, Chlorite
361.00	Basalt; intersertal texture	-	-	Fresh	Chlorite, Epidote, Albite(?)	-	Quartz, Chlorite	Quartz, Chlorite
367.80	Basalt; glassy	Fe-oxides, Smectite, Epidote	-	-	-	-	Smectite, Chlorite, Epidote, Calcite	Calcite
380.35	Andesite; trachytic texture	Epidote	-	-	Epidote, Calcite	-	-	Chlorite, Quartz, Calcite
394.40	Basalt; variolitic, highly altered	Chlorite, Epidote	-	-	-	Epidote	Corrensite, Chlorite, Calcite	Chlorite, Calcite, Corrensite
406.00	Basalt; intersertal texture	Chlorite, Smectite	-	Amphibole?	Chlorite-smectite	Chlorite, Epidote	-	Smectite, Chlorite, Calcite
410.45	Basalt; glassy, many ore minerals	Epidote, Chlorite	-	-	Epidote, Chlorite, Albite	-	Chlorite	Chlorite, Quartz
421.80	Basalt hyaloclastite	Epidote, Chlorite	-	-	Epidote, Chlorite, Quartz, Albite	Epidote, Chlorite	Quartz, Chlorite, Epidote	Quartz
423.00	Andesite	Chlorite	-	-	Albite	-	Chlorite, Quartz	Chlorite, Quartz, Epidote
438.20	Basalt; pilotaxitic texture	Chlorite	-	-	Epidote, Albite(?)	Chlorite, Epidote	-	Chlorite, Quartz
455.20	Andesite?; brecciated	Chlorite	-	Fresh	-	-	Quartz, Chlorite, Epidote, Pyrite	Chlorite, Quartz
462.70	Andesitic basalt; pilotaxitic texture	Chlorite	-	-	Albite	Chlorite, Epidote, Quartz	Pyrite, Quartz, Epidote	Chlorite, Quartz

Appendix 4: (Continues Appendix 3 data.) Lithology and secondary mineralogy of the rocks from Hole CY-1A. The secondary minerals were determined optically and checked with X-ray diffraction techniques (see Tables 4, 5, and 6).

Sample Depth(m)	Lithology	Secondary Minerals						
		Glass	Olivine	Pyroxene	Plagioclase	Groundmass	Fractures & Veins	Vesicles
481.40	Silicic rock; felsitic texture	Chlorite	-	-	Albite	-	Chlorite, Calcite	Chlorite, Calcite
498.63	Basalt; intersertal texture	Chlorite Calcite, Quartz	-	-	Epidote, Albite	Chlorite, Quartz, Calcite	Chlorite, Quartz, Calcite	Chlorite, Quartz Calcite
516.85	Basalt; intersertal texture	Chlorite Calcite, Quartz	-	-	Epidote, Albite	Chlorite, Epidote, Quartz	Chlorite, Pyrite, Quartz	Quartz, Epidote Pyrite
542.55	Basalt; intersertal texture	Chlorite, Epidote, Quartz, Calcite	-	-	Albite	-	-	Chlorite, Epidote, Calcite
566.00	Basalt; intersertal texture	Chlorite, Epidote	-	Fresh	Albite	-	Chlorite, Epidote, Quartz, Sulphide	Chlorite, Quartz Sulphide
579.30	Epidosite	-	-	-	-	-	-	-
593.65	Basalt; intersertal texture	Chlorite, Epidote	-	Fresh	Epidote, K-Feldspar	Chlorite, Epidote	Chlorite, Pyrite, Quartz, Calcite	Chlorite, Quartz
599.00	Basalt; intersertal and variolitic textures	Chlorite, Calcite, Epidote	-	Fresh	Chlorite, Albite, Epidote, Calcite	-	Epidote, Chlorite Quartz, Calcite	Quartz, Chlorite, Pyrite
623.35	Andesite; pilotaxitic texture	-	-	-	Albite	-	Epidote, Chlorite, Pyrite, Calcite	Quartz, Calcite, Pyrite
631.20	Basalt; glassy texture	Chlorite	-	-	Chlorite, Albite	-	Calcite	Chlorite, Calcite, Epidote
658.25	Basalt; many veinlets	Epidote, Chlorite	-	Fresh	Albite	Epidote, Quartz, Chlorite	Epidote, Quartz, Actinolite	Chlorite, Quartz, Epidote
659.60	Basalt; intersertal texture	Chlorite Epidote, Quartz	-	Fresh	Albite,	Chlorite, Epidote, Amphibole, Quartz	Quartz, Epidote	Quartz, Epidote

Appendix 5: (Completes Appendices 3 and 4 data.) Lithology and secondary mineralogy of the rocks from Hole CY-1A. The secondary minerals were determined optically and checked with X-ray diffraction techniques (see Tables 4, 5, and 6).

Geochemistry of Altered Lavas of the Troodos Ophiolite, Cyprus Crustal Study Project, Hole CY-2A

J. ERZINGER, R. EMMERMANN, AND M. MANDLER

Institut für Geowissenschaften und Lithosphärenforschung, Justus-Liebig University, Giessen, F.R.G.

Erzinger, J., Emmermann, R., and Mandler M., 1991: Geochemistry of altered lavas of the Troodos ophiolite, Cyprus Crustal Study Project, Hole CY-2A; in Cyprus Crustal Study Project: Initial Report, Holes CY-1 and 1A, eds. Gibson, I.L., Malpas, J., Robinson, P.T., and Xenophontos, C.; Geological Survey of Canada, Paper 90–20, p. 81–94, 1991.

Abstract

Drillhole CY-2A was drilled 685 m into the Troodos ophiolite complex (Cyprus) and provides a complete section of the oceanic layer 2. The geochemical data supports an earlier conclusion that the Troodos ophiolite was formed in a subduction zone environment. Our studies established the existence of three significantly different, depth-related alteration zones that formed under very specific alteration conditions. Alteration within the uppermost 154 m has been caused by oxidative low-temperature rock / seawater interaction. Alteration of the lowest portion of the section (300 m–685 m) is very clearly the result of upflowing, highly concentrated and reducing hydrothermal fluids depositing sulfides on their way upwards, and producing a greenschist facies mineral assemblage in the host rocks. The very spectacular middle alteration zone with its pervasive sulfide mineralization and its drastic mineralogical and chemical changes is a zone of mixing of upflowing acidic, reducing hydrothermal fluids with lower temperature oxidizing seawater solutions circulating in the lava pile. From our data we propose a genetic model with respect to the formation of the Agrokipia 'A' and 'B' ore bodies.

Résumé

Le sondage CY-2A a été foré sur 685 m dans le complexe ophiolitique de Troodos et présente une section complète du niveau océanique 2. Les données géochimiques confirment une conclusion précédente, proposant pour la formation des ophiolites de Troodos, un contexte de zone de subduction. Selon la profondeur, nos travaux établissent trois zones distinctes d'altération formées sous des conditions d'altération très spécifiques. Pour les 154 premiers mètres, l'altération résulte d'une interaction oxydante basse température roche-eau de mer. Dans la partie inférieure du sondage (300–685 m), elle résulte très clairement de circulations ascendantes, des fluides hydrothermaux très enrichis et réducteurs déposant sur leurs passages des sulfures et donnant naisance à un assemblage minéralogique du facies schiste vert dans la matrice. Avec une minéralisation sulfurée disséminée et une transformation chimique et minéralogique sévère, la très spectaculaire zone d'altération intermédiaire est une zone de mélange pour des fluides hydrothermaux acides et réducteurs et les solutions d'eau de mer oxydantes de plus basse temperature qui circulent dans l'amas de laves. Sur la base de nos données, nous proposons un modèle génétique pour les formations minéralisées Agrokipia 'A' et 'B.'

INTRODUCTION

The purpose of this study was to provide a detailed geochemical characterization of a paleo-hydrothermal discharge zone that gave rise to the formation of sulfide ore deposits. This discharge zone occurs within the volcanic pile of the Troodos ophiolite complex (Cyprus) and was sampled by borehole CY-2A, one of five holes drilled by the 'International Crustal Research Drilling Group' within the frame of the Cyprus Drilling Project (Robinson et al., 1987). The hole was devoted to the study of the Agrokipia 'A' and 'B' ore bodies two of a number of irregularly-shaped sulfide deposits scattered throughout the volcanic section of the Troodos Massif. These ore bodies are the result of hydrothermal processes operating in newly-formed oceanic crust and occur either at the boundary between the so called Upper and Lower Pillow Lavas (UPL and LPL, respectively) or within the Lower Pillow sequence.

The major objectives of our investigations were:

- to establish the primary chemical compositions and variations of the rocks recovered from Hole CY-2A
- to define the chemical effects of water/rock interaction
- to study the downhole variation in alteration chemistry
- to interpret the geochemical behaviour of alteration-sensitive elements
- to evaluate the alteration patterns
- to establish a model for the alteration processes and alteration conditions
- to combine the chemical findings with the results of the analysis of the downhole distribution of ore-forming elements and ore paragenesis and
- to clarify the origin, transport conditions and deposition mechanisms of ore-forming elements.

SAMPLING AND ANALYTICAL PROCEDURE

Drillhole CY-2A is situated immediately above the Agrokipia 'B' ore body, some 300 m east of the now exhausted Agrokipia 'A' ore body (Figure 1), a near-surface cupriferous sulfide lens developed at the UPL/LPL contact. The 'B' ore body had been traced by mining exploration some 120 m below the present surface and is completely within the LPL. Drilling started in the lowermost portion of the UPL and penetrated through the LPL into the underlying sheeted dyke complex. The hole reached a depth of 685 m and was completely cored. In order to collect a well-defined and complete set of samples from Hole CY-2A, two members of our working group spent some time in the field laboratory near Agrokipia (in December 1983) and carried out detailed petrographic and mineralogical studies on the core material. Based on these macroscopic investigations a total of 120 rock samples were selected which represent all lithological units and comprise relatively fresh, as well as completely altered material, and all transitions in between. Out of this collection, 92 samples were finally chosen for geochemical and petrographical analysis. After the samples were cleaned with distilled water, dried, and crushed, they were powdered in an agate mill to a grain size (<40 µm) suitable for analysis. The following analytical techniques were used:

1. The major oxides (SiO_2, TiO_2, Al_2O_3, Fe_2O_3, MnO, MgO, CaO, Na_2O, K_2O, and P_2O_5) were analyzed by X-ray fluorescence (XRF) on samples prepared as fused glass discs of lithium metaborate (sample-to-flux ratio 1:4). Analyses were performed on a Philips PW 1400 computerized spectrometer, and the Philips 'alphas' program was used to calculate concentrations.

2. Ferrous iron was analyzed by manganometric titration.

3. H_2O^+ was determined by coulometric Karl Fischer titration after thermal decomposition of the basalts at 1,200°C.

4. CO_2 was measured coulometrically following thermal decomposition at 1,200°C.

5. Sulfur analyses were performed on a Leco sulfur determinator SC132.

6. Measurements of Co, Cr, Cu, Ni, Rb, Sr, Y, Zn and Zr were conducted by XRF on pressed powder pellets. The Rh-compton peak of the X-ray tube was used for matrix correction.

7. Fluorine was analyzed with a fluoride-sensitive electrode, following a pyrohydrolytic decomposition and enrichment method (Erzinger and Puchelt, 1982).

8. The rare earth elements (REE) were determined by optical emission spectroscopy using an inductively coupled plasma for excitation (ICP-OES). For this purpose, the REE had to be quantitatively separated from rock dissolution and concentrated by a chromatographic technique (Zuleger and Erzinger, 1988).

9. Following the development of analytical methods suitable for the analysis of traces of Cd, Pb and Mo in basalts, these elements were determined by flameless atomic absorption spectrometry (AAS) in acidic rock dissolution.

Precision of the determinations was tested by multiple measurements of selected samples; accuracy was checked by analyzing different international reference rocks.

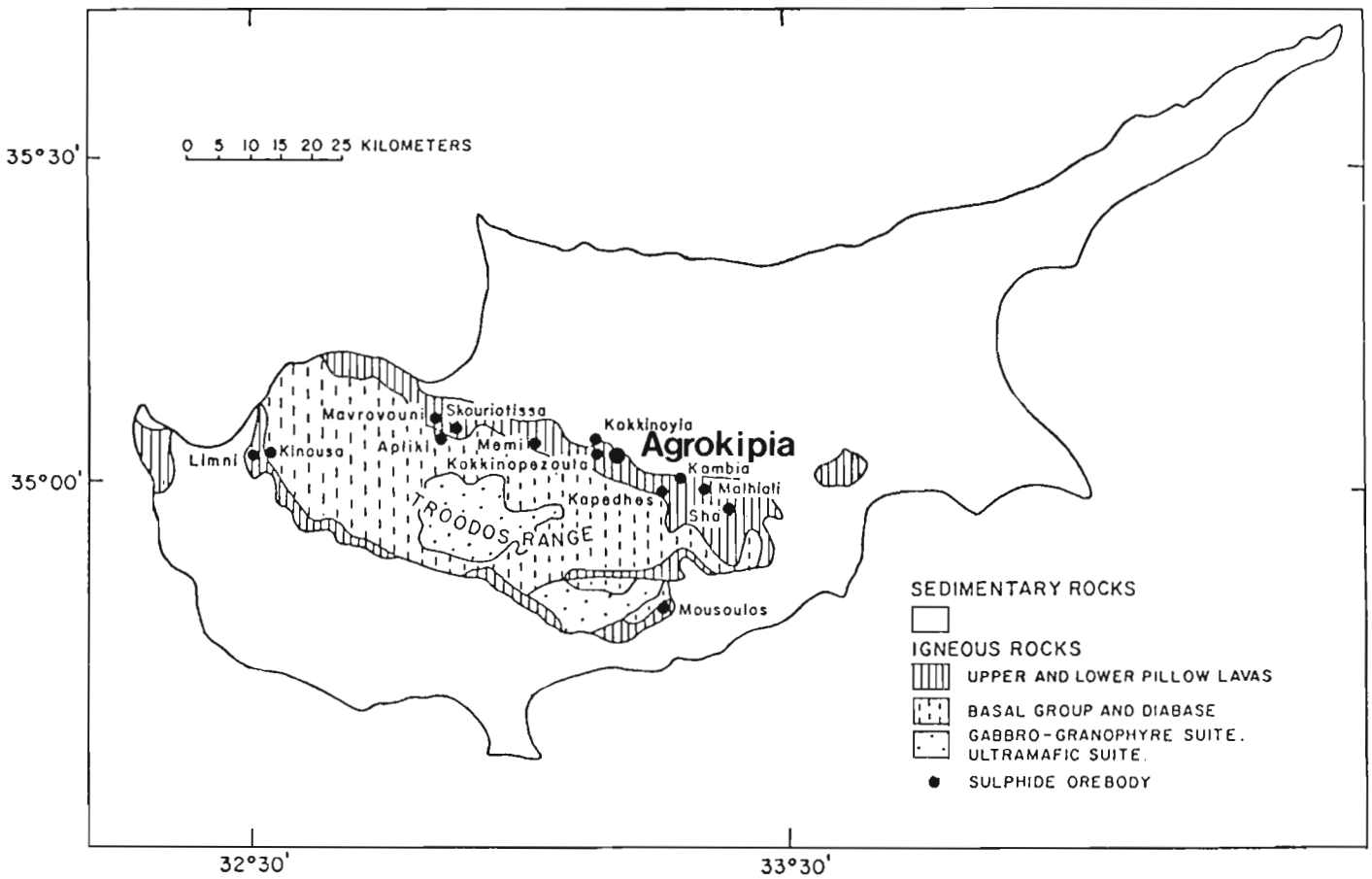

Figure 1: Map of the Troodos ophiolite complex. Drillhole CY-2A is marked by an asterix.

RESULTS AND DISCUSSION

The analytical data obtained on the CY-2A samples are summarized in Tables 1–4 (see Appendix). The samples are identified by their depth. The rare earth element data are presented for 24 samples in Table 5 (see Appendix). The samples were selected for analysis according to their major and trace element characteristics.

Stratigraphically, the section penetrated by drillhole CY-2A can be divided into three zones (Figure 2):

1. The uppermost 295 m represent a volcanic sequence. This zone is made up predominantly of massive lava flows, with some interlayered pillowed flows and breccias, sometimes containing thick intercalations of glass;

2. the volcanic sequence zone is underlain by a 234 m transition zone consisting of steeply-dipping dykes, cross-cutting pillowed and massive lavas;

3. below 529 m, down to the bottom of the hole, only dykes were encountered. This zone is, therefore, regarded as the upper portion of a sheeted dyke complex.

Petrographically and chemically, the recovered rocks can be assigned to two compositionally significantly different rock series. These can be, for example, unequivocally discriminated on the basis of their Ti and Cr contents (Figure 3). The uppermost 32 m of the sequence is made up of olivine-phyric lavas, characterized by relatively high silica and MgO contents, and very low abundances of TiO_2 (Figures 3 and 4). These rocks, which according to their chemical characteristics belong to the Upper Pillow Lavas, have been variously referred to as high-magnesian andesites or boninites. They overlie a less-magnesian rock series higher in Ti, ranging from basaltic to dacitic with the majority of the rocks being andesitic in composition. This series comprises the Lower Pillow Lavas and the underlying dykes. The entire drilled sequence is more or less strongly affected by alteration. Macroscopically, three depth-related alteration zones can be distinguished which differ in colour and do not coincide with stratigraphically defined zones (Figure 2).

1. Rocks from the uppermost 154 m are characterized by a brownish alteration colouring;

2. between 154 and 297 m, light-grey colours predominate, and most lavas are extremely bleached;

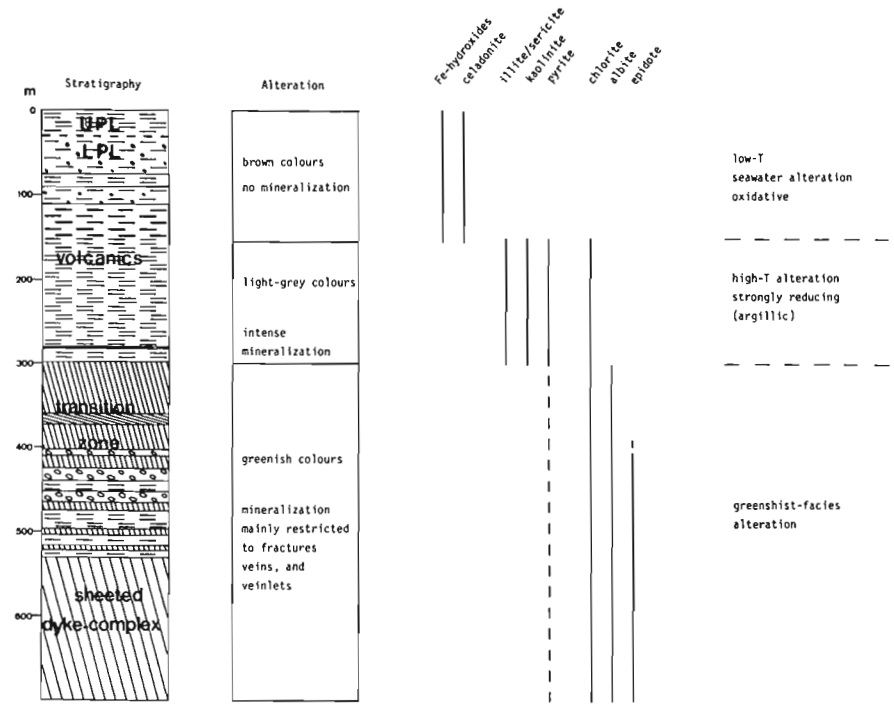

Figure 2: Downhole changes in CY-2A in lithostratigraphy, alteration type, and mineralogy.

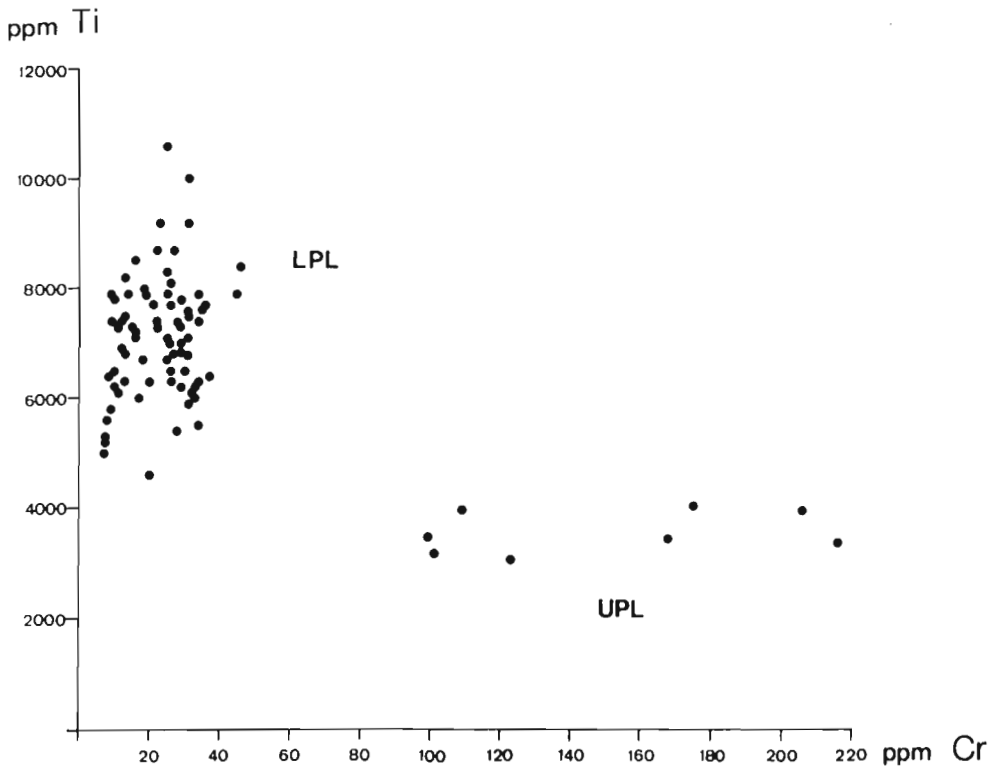

Figure 3: Plot of TiO_2 vs. Cr for CY-2A samples.

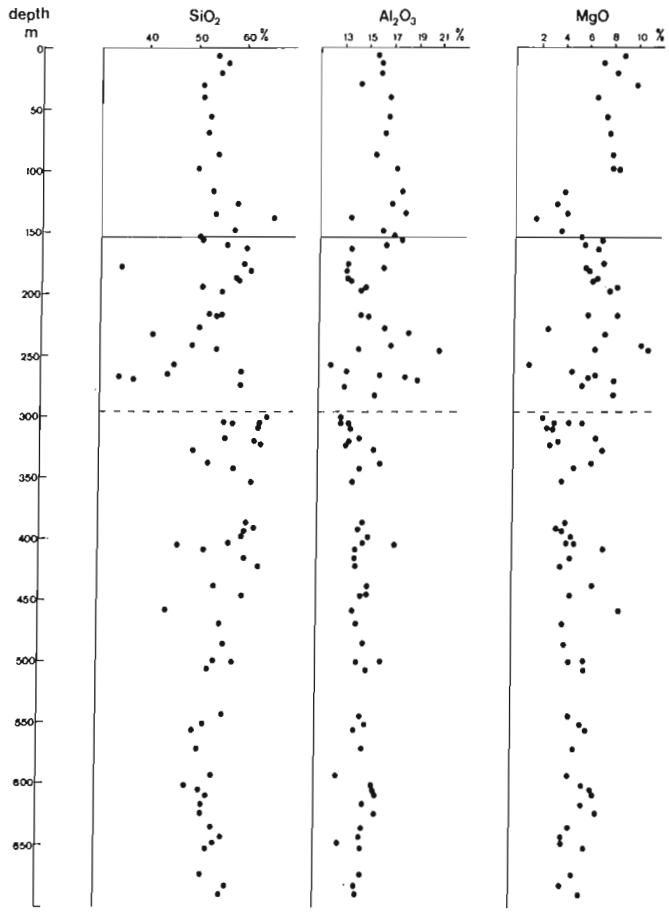

Figure 4: CY-2A downhole variation of SiO_2, Al_2O_3, and MgO.

3. greenish colours mark the beginning of the lowermost alteration zone, and they grade into an intense green below 400 m.

This change in alteration colouring reflects significant downhole variations in the alteration mineralogy. The alteration minerals and mineral assemblages define three significantly different alteration zones (see Figure 2), and provide some information as to the alteration conditions. Characteristic alteration minerals of the upper alteration zone are iron-hydroxides and celadonite which have commonly been observed in ocean floor basalts as typical products of submarine alteration. Their disappearence and the first occurrence of illite/sericite, kaolinite, and chlorite together with pyrite, mark the beginning of the second alteration zone. This type of alteration can be classified as argillitization and typically occurs as a result of plagioclase breakdown and calcium and sodium removal under the influence of hot acidic solutions. Alteration in the lowermost zone occurred under greenschist facies conditions as indicated by the presence of albite, chlorite, and epidote (for further details see Alt and Emmermann, 1985, and Alt et al., 1986). The high temperature alteration of the middle and lower section was closely connected with intense sulfide mineralization. Occurrence, style, and degree of mineralization follow the same three-fold subdivision. The uppermost alteration zone is virtually free of any visible sulfides. However, a pervasive pyritic mineralization starts in the top 15 m of the second alteration zone, and reaches concentrations of up to 30% in brecciated and highly-bleached lavas. Occasionally, massive pyrite bands occur as intercalations. Altogether, 11 such intervals of massive, silicified pyrite ore, ranging up to 3.5 m in thickness, were encountered. Mineralization in the lowermost zone is mainly restricted to fissures, veins, and veinlets. Groundmass mineralization seldom exceeds 1%. The main ore mineral is pyrite, followed by sphalerite and lesser amounts of chalcopyrite, both of the latter being very irregularly distributed (Figure 5).

Alteration and mineralization of the drilled segment of the Troodos ophiolite complex caused significant and spectacular changes of the original chemical composition of the rocks. Evaluation of major and trace element data supports the existence of three distinct chemical alteration zones which are more or less sharply set off from each other, and enables quantitative description of the alteration effects.

Rocks from the uppermost 154 m are characterized by the highest iron oxidation ratios, the lowest sulfur contents (Figure 6), and a considerable potassium enrichment of up to 4% in samples whose primary potassium content was less than 0.3%. At about 154 m, there is a sharp decrease in the degree of oxidation, indicating alteration under extremely reducing conditions. At the same time, sulfur exhibits a strong enrichment. Potassium, as well as rubidium, is still enriched in this zone. The pervasive nature of this alteration is documented by a strong increase in whole-rock water contents from about 2% to more than 5%. Below 300 m, potassium and rubidium decrease significantly, and the sulfur concentrations are also much lower. Iron oxidation remains low but shows a certain scatter, due to the different degrees of alteration.

This obviously drastic change in alteration conditions with depth is also portrayed in the downhole distribution of many of the analyzed elements. Sodium and calcium (Figure 6) are almost completely leached, and strontium is considerably depleted in the second alteration zone. On average, however, sodium appears to be slightly enriched in the lowermost alteration zone, whereas calcium is slightly depleted. Barium exhibits a very specific behaviour (Figure 5). It is strongly enriched in the second alteration zone and obviously depleted in the lower section. The greenschist-facies altered rocks suffered a Mn-enrichment, whereas Mn is slightly depleted or enriched in the middle alteration zone, and obviously not affected in the uppermost portion. Recalculations of the major oxides to a dry and reduced base and a normalization to 100% reveals that magnesium and aluminium are enriched in the second alteration zone. On average, silicon could also be slightly enriched within this zone.

The extent and character of the sulfide mineralization can be estimated from the occurrence of pyrite. Pyrite is absent in the upper alteration zone, shows a strong enrichment in

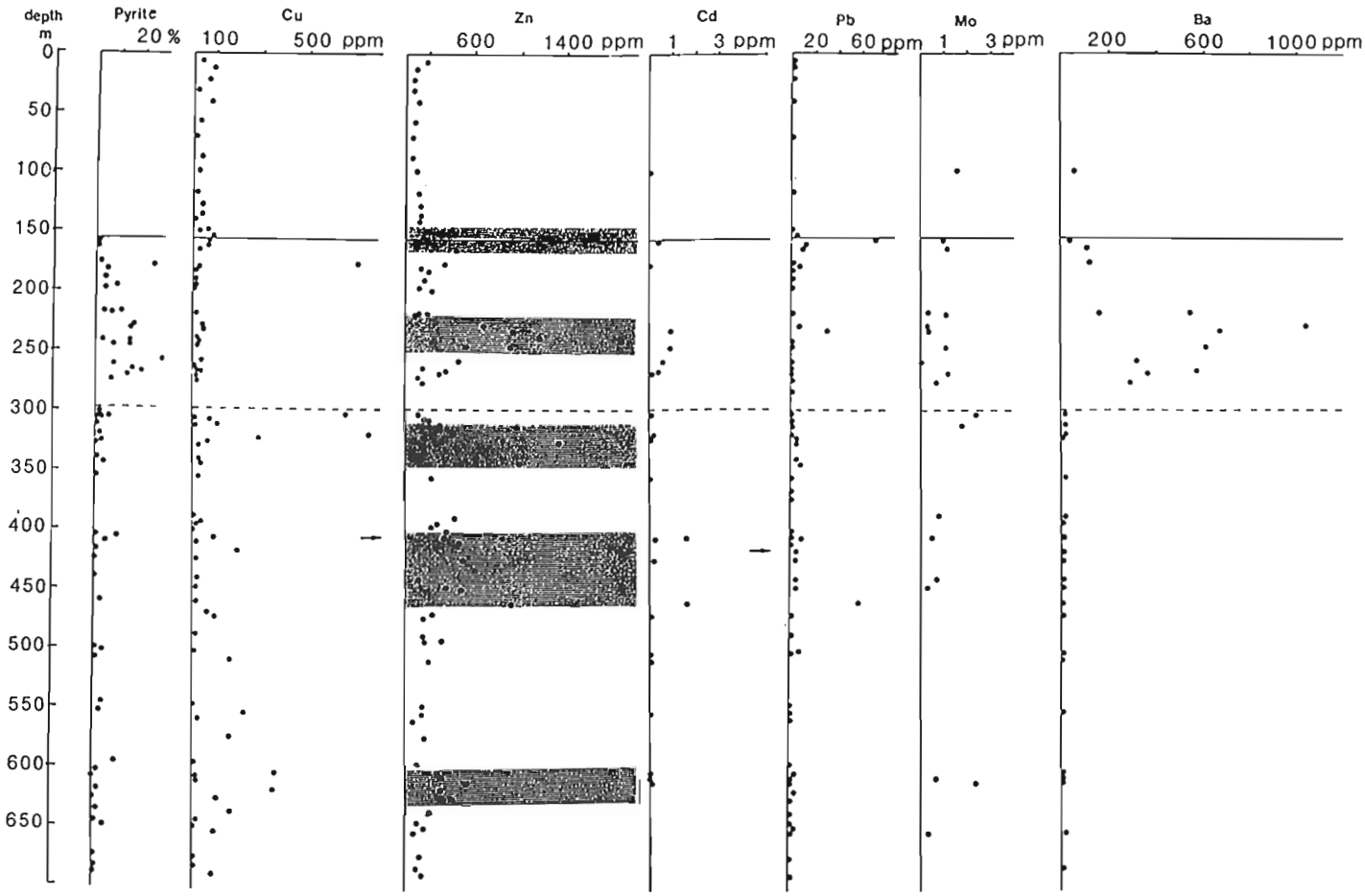

Figure 5: CY-2A downhole variation of pyrite, Zn, Cu, Cd, Ba, Pb, and Mo contents.

the second zone with a maximum concentration of more than 30%, and exhibits a much lesser and rather irregular enrichment averaging 1% in the lowermost alteration zone (Figure 5). The chalcophile elements, zinc, cadmium, copper, and lead, vary considerably with depth and show either zonal or irregular point-like enrichments. Zinc is the most abundant of these elements and varies between 80 and 4,000 ppm. On average, it is enriched in the second and third alteration zone, developing concentration maxima at five distinct intervals. Cadmium whole-rock contents vary between 0.04 and 6 ppm, and are closely correlated with the zinc contents. Copper ranges from less than 5 to 150 ppm, aside from irregular point-like enrichments, is relatively low throughout the entire drilled section. With one exception, it even appears to be depleted in the strongly mineralized second alteration zone. Lead contents are low, 'with only a few enrichments, and molybdenum does not show any systematic variations, although it is among the elements whose geochemical behaviour are thought to be of importance for the understanding of the formation of hydrothermal ore deposits.

CONCLUSIONS

Summarizing all available data and observations, the following statements and conclusions can be made. Drillhole CY-2A provides a complete section from the Upper Pillow Lavas through the Lower Pillow sequence to the underlying sheeted dyke complex. This section is built up of two compositionally different rock series. The Upper Pillow Lavas are high magnesium andesites with a very low content of incompatible elements. This is especially well documented by the respective chondrite-normalised REE distribution patterns (Figure 7), which show a strong depletion in LREE and very low overall REE abundances. The Lower Pillow sequence and most dykes are basalt-andesitic to dacitic rocks, that according to their chemical characteristics (for example the REE patterns), resemble evolved island-arc tholeiites. These chemical data, therefore, support the conclusion of Robinson et al. (1983) that the Troodos ophiolite complex was formed in a subduction zone environment. he occurrence of two distinct magma series indicates that the processes of magma generation and crustal accretion were much more complex than those associated with present-day mid-ocean ridge systems.

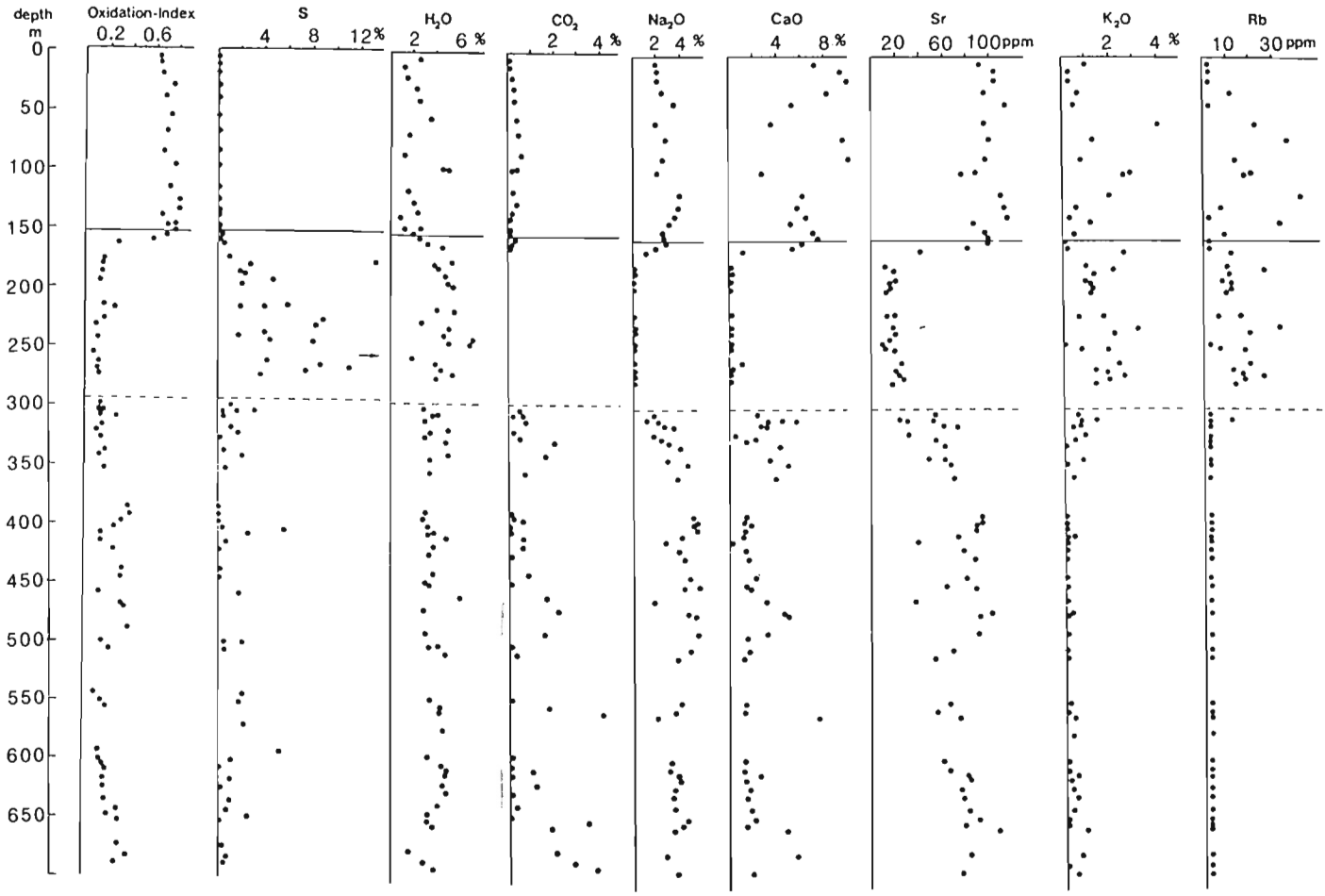

Figure 6: CY-2A downhole variation of alteration sensitive chemical parameters (Oxidation-Index is calculated as $Fe_2O_3 \times 100/Fe_2O_3 + FeO$).

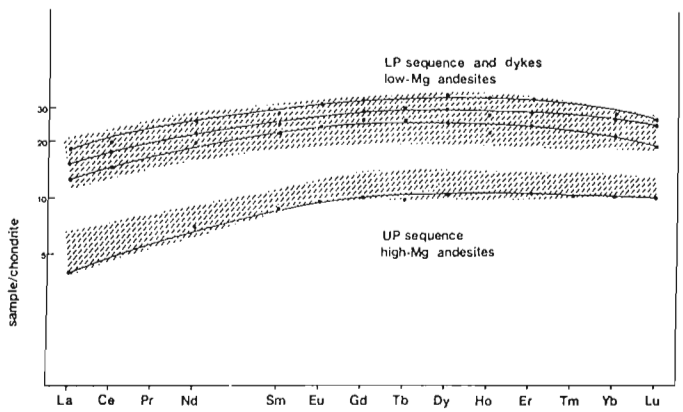

Figure 7: Chondrite-normalized rare earth element distribution patterns of CY-2A samples.

However, because of an intense alteration and mineralization of the drilled section, a more detailed genetic evaluation of the data appears to be impossible.

Mineralogical and chemical studies establish the existence of three significantly different, depth-related alteration zones that formed under very specific alteration conditions. Alteration within the uppermost 154 m has been undoubtedly caused by low temperature rock/seawater interaction which resulted in a considerable potassium and rubidium uptake, a strong iron oxidation, and an almost complete sulfur loss through sulfide oxidation, because of the high oxidation ability of seawater. This type of alteration has been encountered in many ocean-floor basalts recovered from DSDP drillholes. Alteration of the lowest portion of the section is very clearly the result of upflowing, highly concentrated and reducing hydrothermal fluids that used fractures, veins, and veinlets as pathways, depositing sulfides on their way upward, and producing a greenschist facies mineral assemblage in the host rocks. Chemically, this type of alteration is characterized by a slight sodium enrichment and a concomitant calcium depletion, a significant increase in the manganese whole-rock concentrations, and a pronounced leaching of potassium, rubidium, and barium.

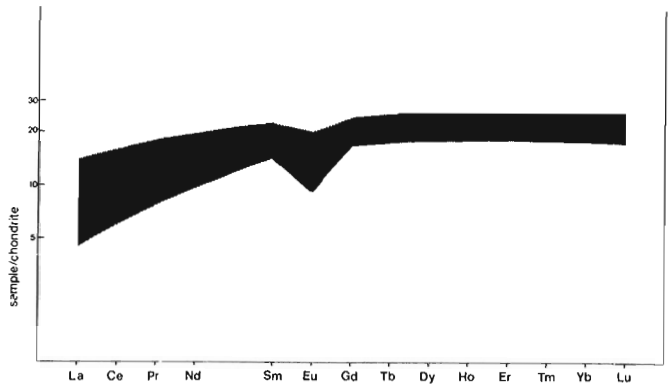

Figure 8: Chondrite-normalized rare earth element distribution patterns of highly bleached lavas from the second alteration zone.

We interpret the very spectacular middle alteration zone with its pervasive sulfide mineralization and its drastic mineralogical and chemical changes as being a zone of mixing of upflowing acidic, reducing hydrothermal fluids with low temperature oxidizing seawater solutions circulating in the lava pile. Such ore precipitations and element enrichments would be expected to occur where highly-concentrated metal and sulfur-rich hydrothermal fluids came into contact with solutions lower in temperature and complexing anions, and with different redox properties. Sulfide precipitation drastically changed the elemental concentrations of the solution, and thereby strongly enhanced its ability to leach other elements like calcium and sodium. The dominant effect of plagioclase breakdown is underlined by the REE patterns of the highly-bleached rocks that show a pronounced negative Eu-anomaly (Figure 8).

GENETIC MODEL

With respect to the formation of the Agrokipia 'A' and 'B'ore bodies, the following picture emerges (Figure 9). Both deposits are genetically closely related, and were formed at different levels within a hydrothermal discharge zone. The 'B' ore body is a replacement deposit developed by subsurface mixing of these fluids with seawater circulating within the lava pile, and constitutes a mineralized stockwork. The 'A' ore body is a massive, tectonically controlled sulfide deposit, thought to have precipitated in a depression on the ancient seafloor from solutions that discharged through the stockwork beneath. The enrichment of copper in the massive ore and its obvious depletion in the stockwork, suggests a close chemical interrelationship between these two types of deposits. Sulfide formation definitely took place before the deposition of the Upper Pillow sequence, as is proved by the occurrence of differently altered and non-mineralized feeder dykes of Upper Pillow Lavas encountered deeper in the hole.

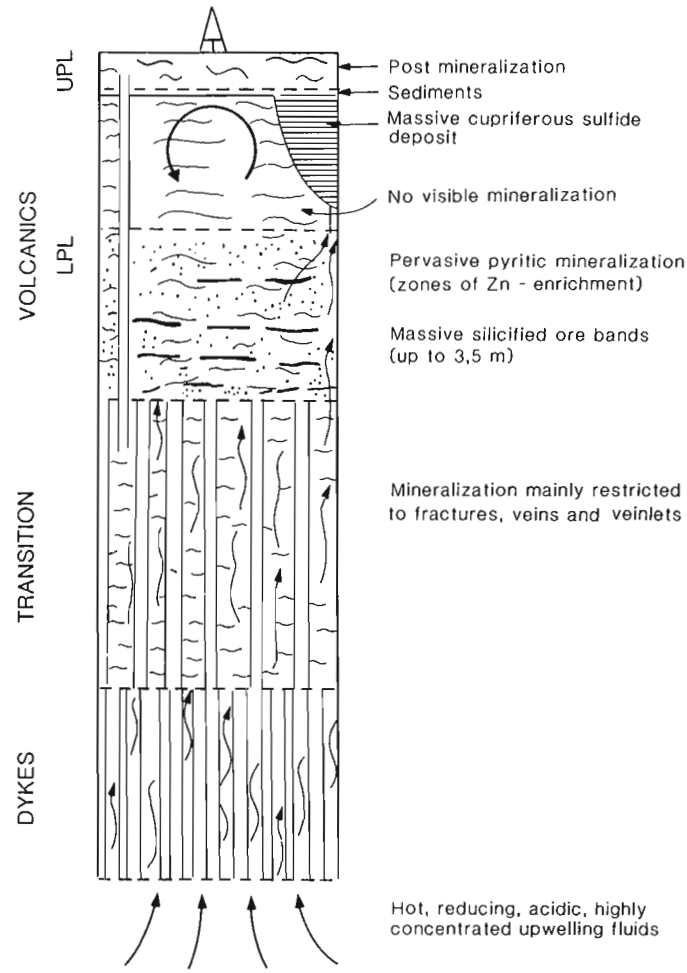

Figure 9: Drillhole CY-2A Agrokipia: Mineralization pattern and fluid motion.

ACKNOWLEDGEMENTS

This work was funded by the European Community contract MSM-17D.

REFERENCES

Alt, J.C. and Emmermann, R.
1985: Geochemistry of hydrothermally altered basalts: Deep Sea Drilling Project Hole 504B, Leg 83; *in* Anderson, R.N., Honnorez, J., Becker, K., et al., Initial Reports of the Deep Sea Drilling Project, v. 83, U.S. Government Printing Office, Washington, p. 249–262.

Alt, J.C., Honnorez, J., Laverne, C., and Emmermann, R.
1986: Hydrothermal alteration of a 1 km section through the upper oceanic crust, Deep Sea Drilling Project Hole 504B: mineralogy, chemistry, and evolution of seawater-basalt interactions; Journal of Geophysical Research, v. 91, p. 10309–10335.

Auclair, F. and Ludden, J.N.
1987: Cyclic geochemical variation in the Troodos Pillow Lavas: evidence from the CY-2A Drill Hole; *in* Robinson, P.T., Gibson, I.L., and Panayiotou, A., Cyprus Crustal Study Project: Initial Report, Holes CY-2 and 2a, Geological Survey of Canada, Paper 85–29, p. 221–235.

Erzinger, J. and Puchelt, H.
1982: Methoden zur Bestimmung umweltrelevanter Spurenelemente in geologischem Material.-Erzmetall, v. 35, p. 173–179.

Robinson, P.T., Melson, W.G., O'Hearn, T., and Schminke, H.-U.
1983: Volcanic glass compositions of the Troodos ophiolite, Cyprus; Geology, v. 11, p. 400–404.

Zuleger, E. and Erzinger, J.
1988: Determination of the REE and Y in silicate materials with ICP-AES; Fresenius Zeitschrift für Analytische Chemie, v. 332, p. 140–143.

APPENDIX – TABLES 1–5

See the next five pages.

Depth(m)	SiO_2	TiO_2	Al_2O_3	Fe_2O_3	FeO	MnO	MgO	CaO	Na_2O	K_2O	P_2O_5	H_2O	CO_2	Pyrite
5.95	54.3	0.5	15.7	5.45	2.91	0.11	8.79	7.09	1.99	0.99	0.05	2.52	0.12	-
11.65	55.8	0.6	16.0	5.25	2.84	0.08	7.13	9.41	2.14	0.31	0.06	1.23	0.11	-
20.85	54.4	0.6	15.9	4.95	2.42	0.08	8.18	10.00	2.13	0.29	0.05	1.39	0.16	-
30.00	51.2	0.6	14.3	8.10	2.43	0.11	9.83	8.29	2.48	0.68	0.05	2.17	0.29	-
39.90	51.3	1.5	16.7	8.19	3.43	0.10	6.62	5.33	3.45	0.53	0.13	2.48	0.32	-
55.90	52.5	0.7	16.7	7.01	2.33	0.09	7.39	3.62	2.04	4.08	0.10	3.45	0.39	-
69.10	52.3	0.7	16.3	6.52	2.25	0.11	6.77	9.57	2.78	1.32	0.07	1.62	0.47	-
85.65	53.7	0.7	15.5	5.60	2.65	0.10	6.87	10.10	2.65	0.81	0.07	1.25	0.64	-
96.60	50.3	1.1	17.1	8.23	2.13	0.16	7.85	2.90	2.19	2.88	0.14	4.49	0.39	-
97.65	50.2	1.1	17.3	7.92	2.41	0.16	8.35	2.66	2.00	2.57	0.14	5.01	0.24	-
115.90	53.1	1.3	17.7	7.59	2.71	0.20	3.98	6.21	4.61	1.98	0.17	1.50	0.22	-
125.80	58.3	1.3	16.9	6.37	1.47	0.18	3.28	5.72	3.89	0.63	0.21	2.00	0.39	-
134.10	53.6	1.4	18.0	8.29	1.89	0.29	4.22	6.52	4.07	0.30	0.15	2.26	0.24	-
138.40	65.4	1.2	13.5	5.14	2.45	0.21	1.75	5.22	3.25	1.19	0.13	0.92	0.13	-
147.40	50.1	1.2	16.8	10.60	2.88	0.25	5.95	7.06	2.58	0.18	0.09	2.56	0.14	-
147.90	57.4	1.2	16.1	7.29	2.80	0.22	3.73	7.33	2.91	0.49	0.12	1.25	0.19	-
152.50	50.6	1.3	17.1	10.50	2.86	0.29	5.37	7.54	2.74	0.07	0.10	2.03	0.13	-
156.45	50.7	1.2	17.7	7.62	2.65	0.11	7.06	6.18	2.89	0.14	0.10	2.52	0.32	0.82
160.15	56.1	1.1	16.4	6.05	3.68	0.18	5.73	5.43	2.01	0.20	0.09	3.25	0.19	0.39
162.85	59.9	1.2	13.6	2.46	5.53	0.43	6.77	1.18	1.06	2.58	0.11	4.49	0.14	0.90
174.90	59.5	1.2	13.3	1.82	7.90	0.34	7.19	0.18	0.17	1.04	0.11	5.26	0.07	1.81
178.10	34.5	1.2	16.2	4.15	3.50	0.07	5.82	0.29	0.33	2.29	0.21	3.79	-	2.47
181.40	60.8	1.1	13.2	1.50	5.00	0.13	5.98	0.28	0.32	1.32	0.15	4.06	-	5.31
187.00	58.1	1.2	13.7	1.84	7.24	0.20	6.67	0.24	0.29	1.03	0.12	4.70	-	3.63
189.05	58.4	1.2	13.6	1.67	6.83	0.25	6.35	0.25	0.24	1.16	0.11	4.61	-	4.27
194.10	51.1	1.3	14.7	1.77	6.41	0.17	8.26	0.14	0.22	1.32	0.10	4.87	1.14	8.87
197.25	55.2	1.3	14.4	1.83	8.32	0.31	7.77	0.14	0.16	1.16	0.10	5.40	-	3.95
216.35	52.6	1.4	14.4	2.26	5.09	0.13	6.04	0.20	0.22	1.67	0.13	4.02	-	1.00
216.50	55.3	1.3	14.5	7.59	2.94	0.23	8.39	0.23	0.11	0.69	0.11	5.52	-	3.52
216.60	53.7	1.4	15.0	3.53	4.94	0.13	6.05	0.20	0.24	1.84	0.12	3.95	-	7.48
227.00	50.5	1.5	16.3	2.43	1.70	0.04	2.74	0.11	0.34	3.23	0.08	2.69	2.40	6.50
231.50	40.8	1.8	18.3	1.58	5.27	0.12	7.36	0.20	0.28	2.22	0.14	5.02	1.98	5.30
240.60	48.8	1.2	16.9	1.44	8.88	0.44	0.40	0.21	0.13	0.03	0.13	7.12	-	3.29
244.75	53.9	1.1	14.3	1.92	7.33	0.15	6.55	0.17	0.12	0.77	0.10	4.97	-	8.16
244.90	29.1	1.7	20.9	2.02	8.21	0.17	1.00	0.20	0.24	1.94	0.15	6.89	-	5.00
257.15	45.5	1.0	12.0	1.79	1.67	0.10	1.22	1.09	0.29	2.35	0.11	1.85	-	8.80
262.30	59.0	1.1	13.2	1.50	5.42	0.20	4.74	0.29	0.22	1.44	0.12	3.78	-	7.93
265.25	44.0	1.3	16.0	2.05	5.58	0.12	6.74	0.17	0.21	1.90	0.13	4.31	-	5.90
269.70	36.9	1.5	19.1	2.25	7.10	0.14	8.17	0.22	0.29	1.95	0.15	5.33	-	3.90
274.00	59.3	1.0	13.1	1.50	5.24	0.17	5.55	0.25	0.20	1.42	0.12	3.91	-	7.02
282.30	55.5	0.5	15.6	5.84	2.50	0.24	8.14	7.23	2.18	0.42	0.05	2.49	0.32	-
300.45	64.5	0.8	12.8	1.40	6.83	0.59	2.39	2.43	1.88	0.63	0.13	2.90	0.53	2.13
304.25	55.6	0.9	13.5	1.80	7.97	0.70	4.48	1.67	1.16	1.38	0.08	4.05	0.68	6.08
304.60	57.6	0.9	12.9	2.13	8.37	0.42	5.67	0.85	2.06	0.81	0.07	4.29	0.22	3.26
305.25	62.9	0.9	13.5	1.22	7.45	0.36	3.28	2.54	2.28	0.70	0.13	3.58	0.58	0.75
309.35	62.6	0.9	13.6	1.40	6.75	0.35	2.75	2.70	2.82	0.72	0.13	3.10	0.75	1.22
310.40	63.1	0.9	13.8	2.35	5.45	0.27	3.21	2.66	3.52	0.43	0.13	2.88	0.66	0.64

Table 1: Major element oxides and pyrite (wt.%); '-' = not determined.

Depth(m)	SiO_2	TiO_2	Al_2O_3	Fe_2O_3	FeO	MnO	MgO	CaO	Na_2O	K_2O	P_2O_5	H_2O	CO_2	Pyrite
317.15	56.2	0.9	14.4	1.87	8.43	0.68	6.74	0.49	1.80	0.91	0.08	5.00	0.17	2.34
319.95	62.2	0.9	13.5	1.06	6.86	0.46	3.61	2.30	2.50	0.46	0.12	3.39	0.32	2.40
322.85	63.2	0.9	13.3	1.06	5.88	0.40	2.97	1.52	3.13	0.49	0.13	2.97	0.50	3.14
326.55	49.6	1.2	15.6	1.67	8.53	0.36	7.34	4.30	4.02	0.10	0.10	4.81	2.00	0.44
338.45	52.5	1.2	16.1	1.74	7.37	0.38	6.36	3.50	3.04	0.80	0.10	4.98	1.55	0.86
341.95	57.8	1.1	14.4	1.19	5.84	0.27	4.98	1.35	4.57	0.13	0.11	3.37	0.62	3.95
353.30	61.6	0.9	13.9	1.53	5.99	0.28	4.00	1.91	3.83	0.36	0.12	3.37	0.73	1.31
363.80	51.0	1.2	14.7	4.84	6.98	0.23	5.54	6.75	2.68	0.19	0.09	3.67	2.04	-
364.00	50.0	1.3	15.3	5.52	7.27	0.27	5.83	6.53	2.54	0.22	0.09	3.77	2.17	-
365.25	52.6	1.3	15.4	8.60	3.69	0.29	5.42	7.16	2.52	0.04	0.09	2.41	1.00	-
370.55	53.0	1.3	15.2	8.89	3.61	0.35	6.00	6.43	2.63	0.05	0.08	2.44	0.65	-
385.95	60.4	1.0	14.7	3.82	5.74	0.31	4.31	1.46	5.08	0.05	0.12	3.01	0.13	-
390.85	62.0	1.0	14.5	3.73	5.08	0.28	3.63	1.35	5.44	0.08	0.12	2.68	0.21	-
393.35	60.3	1.0	14.3	3.77	5.52	0.25	4.04	1.88	5.15	0.06	0.12	2.88	0.65	-
397.90	59.5	1.1	15.2	3.30	6.21	0.33	4.68	1.37	5.41	0.10	0.12	3.21	0.06	-
403.20	57.0	1.1	14.8	3.53	8.49	0.41	4.35	1.16	4.08	0.37	0.11	3.73	0.12	0.82
407.70	52.3	1.3	14.2	2.10	8.36	1.08	7.52	0.29	2.77	0.11	0.10	4.82	0.64	4.83
414.80	59.7	1.1	14.1	1.42	7.01	0.44	4.74	1.45	3.92	0.15	0.15	3.68	0.59	1.29
421.62	61.8	1.1	14.2	2.37	6.48	0.47	4.03	1.66	4.26	0.00	0.15	3.27	0.09	0.11
438.45	54.0	1.3	15.2	4.02	7.17	0.26	6.59	2.30	4.83	0.06	0.11	3.75	0.78	0.17
445.20	59.5	1.3	15.1	3.15	5.96	0.32	4.68	1.47	5.61	0.05	0.13	3.05	0.11	-
446.20	59.8	1.2	14.6	3.19	6.31	0.41	4.79	1.90	4.32	0.13	0.14	3.32	0.10	-
458.28	44.4	1.4	14.0	2.37	12.00	0.64	8.76	3.16	1.76	0.03	0.12	6.05	1.59	3.31
467.70	55.6	1.0	14.3	3.52	6.55	0.24	4.23	4.71	4.66	0.25	0.09	2.90	2.07	-
469.85	54.8	1.0	14.3	3.71	6.29	0.29	4.06	5.15	5.27	0.12	0.09	2.79	2.14	-
484.70	55.9	1.2	14.9	4.25	6.26	0.24	4.31	3.31	5.51	0.10	0.11	2.97	1.50	-
499.25	54.0	1.4	16.3	2.09	8.44	0.40	5.90	1.58	4.88	0.04	0.14	4.14	0.13	0.95
499.70	58.0	1.3	14.3	1.63	6.34	0.26	4.72	1.81	4.05	0.03	0.11	3.31	0.21	3.95
505.58	52.7	1.2	15.1	3.50	10.30	0.33	6.00	1.29	3.82	0.03	0.11	4.69	0.30	1.07
544.30	55.8	1.2	14.7	1.22	8.56	0.28	4.73	1.47	4.07	0.20	0.13	3.43	0.10	3.87
550.55	51.8	1.2	15.1	2.32	10.20	0.32	5.72	1.39	3.58	0.12	0.10	4.34	1.73	3.46
556.12	50.2	1.0	14.2	2.17	8.12	0.18	6.07	7.66	2.09	0.43	0.08	4.17	4.06	-
593.25	53.9	1.2	12.8	2.17	7.29	0.26	4.70	1.39	3.27	0.08	0.10	3.22	0.14	9.67
601.18	48.6	1.1	15.7	2.66	13.30	0.53	5.90	1.34	3.13	0.08	0.09	5.39	0.06	2.04
604.70	51.6	1.1	15.8	2.19	9.40	0.40	6.63	2.85	3.88	0.50	0.09	4.78	1.03	0.11
608.75	52.9	1.1	16.0	2.53	9.63	0.46	6.83	1.55	3.96	0.21	0.10	4.73	0.09	0.11
616.55	52.4	1.0	15.0	2.87	10.40	0.41	5.76	1.77	3.46	0.28	0.09	4.49	1.15	1.80
624.25	51.9	1.1	16.0	2.49	10.00	0.45	6.99	1.64	3.35	0.51	0.09	4.85	0.13	0.39
635.48	53.7	1.1	14.9	3.02	10.30	0.46	4.79	2.05	3.53	0.26	0.08	4.00	0.28	1.80
643.45	56.0	1.3	14.7	4.23	7.89	0.25	4.24	2.26	4.62	0.06	0.13	3.16	0.05	1.35
648.16	54.5	1.1	13.0	2.80	6.43	0.29	4.22	1.65	4.13	0.04	0.10	3.11	3.36	4.75
652.05	53.1	0.8	14.9	3.41	6.92	0.19	6.14	5.03	3.40	0.89	0.07	3.62	1.78	-
672.55	52.1	1.2	14.9	3.78	7.13	0.32	5.10	5.86	2.75	0.66	0.10	1.62	2.01	0.60
682.18	57.2	1.3	14.4	5.03	6.62	0.25	4.14	2.24	4.89	0.04	0.13	2.84	0.90	1.37
688.50	55.8	1.3	14.5	3.66	7.92	0.33	5.71	2.08	3.70	0.46	0.10	3.75	0.51	0.82

Table 2: Major element oxides and pyrite (wt.%); '-' = not determined.

Depth(m)	Rb	Sr	Y	Zr	Zn	Cu	Pb	Cd	Mo	Co	Ni	Cr	Ba
5.95	<5	92	11	42	187	42	-	-	-	48	35	101	28
11.65	<5	104	14	46	90	86	-	-	-	38	30	99	30
20.85	<5	104	11	45	68	74	-	-	-	25	45	168	23
30.00	12	96	11	41	69	19	-	-	-	40	113	216	23
39.90	<5	114	37	98	110	82	-	-	-	44	14	27	-
55.90	23	96	18	47	84	29	-	-	-	32	37	109	59
69.10	36	100	17	55	58	15	-	-	-	32	60	206	-
85.65	14	97	19	57	58	36	-	-	-	32	58	175	22
96.60	21	89	23	77	104	30	-	-	-	36	21	25	15
97.65	18	77	27	71	96	26	1.4	n.d.	1.6	36	22	26	64
115.90	42	110	37	95	114	19	-	-	-	24	6	18	43
125.80	8	113	53	97	128	39	-	-	-	15	<5	10	24
134.10	<5	116	37	94	136	41	-	-	-	23	5	16	-
138.40	33	87	29	77	128	12	-	-	-	13	<5	11	37
147.40	<5	97	27	66	200	66	-	-	-	34	13	29	-
147.90	9	97	26	66	292	31	-	-	-	26	11	25	29
152.50	<5	100	26	68	157	91	5	-	-	36	14	29	-
156.45	<5	100	27	66	521	75	72	440	1.0	32	15	28	55
160.15	<5	82	26	62	105	73	12	-	-	26	11	27	-
162.85	12	42	31	77	449	32	10	-	1.2	14	<5	12	116
174.90	10	12	32	81	352	712	-	n.d.	-	22	<5	13	139
178.10	26	19	52	124	143	33	7	-	-	16	<5	22	-
181.40	11	20	37	98	211	15	-	-	-	11	<5	9	319
187.00	8	21	34	87	178	11	-	-	-	15	<5	12	244
189.05	12	16	33	85	170	23	-	-	-	22	<5	16	240
194.10	12	16	30	75	135	15	-	-	-	22	7	45	-
197.25	10	13	28	75	239	11	-	-	-	21	<5	26	269
216.35	16	20	31	86	129	20	3.7	-	0.4	18	<5	26	544
216.50	6	14	31	81	201	13	0.9	-	1.2	20	<5	19	193
216.60	17	21	34	86	87	19	-	-	-	19	<5	25	829
227.00	33	19	38	95	684	45	7	-	0.3	28	<5	22	1204
231.50	20	20	42	102	1030	50	32	960	0.4	28	<5	25	673
240.60	<5	9	31	80	1878	30	-	-	-	24	11	31	-
244.75	7	12	29	71	533	24	-	-	-	29	<5	30	-
244.90	18	20	48	118	914	21	-	900	1.1	40	<5	31	614
257.15	20	26	32	90	471	38	-	580	n.d.	91	<5	32	320
262.30	13	21	33	96	161	13	-	-	-	20	<5	13	437
265.25	17	20	36	97	373	19	-	380	-	31	<5	25	569
269.70	18	28	41	105	121	15	-	-	-	35	<5	23	-
274.00	14	18	33	95	156	17	-	-	0.7	18	<5	17	377
282.30	<5	74	12	41	88	68	0.4	60	0.6	30	39	123	49
300.45	<5	55	38	93	119	657	1.8	100	2.4	11	<5	7	24
304.25	12	24	24	61	172	11	-	-	-	34	<5	34	-
304.60	<5	31	19	59	207	12	-	-	-	21	<5	28	21
305.25	<5	53	37	96	172	79	-	-	-	14	<5	7	-
309.35	<5	62	38	96	970	107	1.0	-	1.8	13	<5	7	23
310.40	<5	74	37	99	306	12	-	-	-	13	<5	8	27

Table 3: Trace element data (all values in ppm; Cd in ppb); '-' = not determined; n.d. = not detectable.

Depth(m)	Rb	Sr	Y	Zr	Zn	Cu	Pb	Cd	Mo	Co	Ni	Cr	Ba
317.15	<5	32	19	59	419	757	3.4	160	-	25	10	34	28
319.95	<5	55	37	94	185	292	5.0	80	-	13	<5	8	22
322.85	<5	56	38	97	1326	74	6.0	-	-	13	<5	8	28
326.55	<5	63	30	74	155	34	5.0	-	-	31	10	29	-
338.45	<5	63	28	76	145	43	5.0	-	-	32	7	28	27
341.95	<5	68	35	82	989	37	9.0	-	-	22	<5	13	-
353.30	<5	71	37	89	242	34	2.9	60	-	12	<5	8	24
363.80	<5	78	27	66	110	52	-	-	-	35	8	34	-
364.00	<5	77	28	67	100	49	-	-	-	39	11	35	-
365.25	<5	99	26	67	146	46	-	-	-	35	9	34	-
370.55	<5	97	26	63	111	52	0.9	100	-	38	10	36	11
385.95	<5	95	35	85	423	<10	-	n.d	0.8	21	<5	10	5
390.85	<5	95	37	91	286	36	2.5	n.d.	-	21	<5	9	8
393.35	<5	90	39	87	243	19	-	-	-	21	<5	11	-
397.90	<5	90	37	93	363	<10	-		-	19	<5	10	-
403.20	<5	74	33	76	849	1512	2.0	1620	0.5	22	<5	20	14
407.70	<5	40	15	78	475	19	-	-	-	31	<5	31	-
414.80	<5	79	42	111	4045	197	5.0	5800	-	15	<5	10	5
421.62	<5	89	42	116	504	22	5.0	180	-	19	<5	8	11
438.45	<5	82	30	83	123	25	5.0	-	0.7	36	8	31	12
445.20	<5	65	40	108	365	20	6.0	-	0.3	19	<5	9	9
446.20	<5	90	39	110	492	21	5.0	-	-	18	<5	9	-
458.28	<5	38	34	91	935	20	59.0	1650	-	36	5	46	n.d.
467.70	<5	103	27	70	248	73	1.6	n.d.	-	30	10	29	10
469.85	<5	93	27	67	169	100	-	-	-	26	11	33	-
484.70	<5	92	32	87	169	20	-	-	-	20	<5	15	-
499.25	<5	70	40	111	329	17	9.0	-	-	24	<5	13	-
499.70	<5	84	32	80	177	<10	1.6	n.d.	-	24	<5	13	11
505.58	<5	55	30	83	218	172	1.2	100	-	34	7	29	7
544.30	<5	68	36	98	157	<10	-	-	-	21	<5	16	-
550.55	<5	57	30	78	160	227	0.9	n.d..	-	29	11	29	6
556.12	<5	77	25	62	82	28	-	-	-	38	13	31	-
593.25	<5	63	29	83	115	14	-	-	-	32	<5	25	-
601.18	<5	68	26	69	283	365	5.0	40	n.d	41	12	37	3
604.70	<5	84	27	73	317	18	0.7	n.d.	0.7	30	12	26	13
608.75	<5	86	26	73	531	23	0.6	100	2.4	34	13	31	4
616.55	<5	79	27	70	307	355	5.0	-	-	33	10	33	-
624.25	<5	80	27	74	407	107	-	-	-	32	11	29	-
635.48	<5	85	25	63	212	169	-	-	-	30	7	34	-
643.45	<5	94	38	101	114	20	-	-	-	22	<5	19	-
648.16	<5	82	31	84	173	<10	5.0	-	-	21	<5	18	-
652.05	<5	111	18	52	82	104	-	-	0.4	36	8	20	20
672.55	<5	87	30	78	141	10	-	-	-	31	6	22	-
682.18	<5	69	37	102	103	14	-	40	-	16	<5	14	9
688.50	<5	80	28	80	153	87	-	-	-	21	<5	21	-

Table 4: Trace element data (all values in ppm; Cd in ppb); '-' = not determined; n.d. = not detectable.

Depth(m)	La	Ce	Pr	Nd	Sm	Eu	Gd	Tb	Dy	Ho	Er	Tm	Yb	Lu
11.65	1.4	4.0	-	3.3	-	0.61	-	0.50	2.6	0.54	1.6	-	1.7	0.25
30.00	1.4	2.2	-	3.1	-	-	-	-	-	0.44	-	0.17	1.1	0.19
96.60	3.2	7.4	-	7.2	2.3	1.05	-	0.64	4.3	0.92	2.6	-	2.6	0.38
125.80	4.5	11.9	-	12.2	4.2	1.79	-	-	8.9	1.94	5.6	0.62	4.6	0.66
160.15	2.2	5.2	-	5.8	1.5	0.88	3.0	-	3.4	0.82	2.3	-	2.3	0.36
178.10	3.4	8.9	1.7	9.0	3.4	1.13	4.6	-	6.0	1.27	4.5	-	3.9	0.62
216.60	2.3	6.1	-	5.7	2.1	0.71	3.3	-	4.3	0.91	2.7	0.40	2.7	0.42
231.50	2.3	5.0	1.6	7.3	3.0	1.90	4.8	-	6.3	1.38	-	-	4.0	0.62
240.60	2.1	6.5	1.5	7.8	3.0	0.56	3.8	0.71	5.0	1.02	3.3	-	2.9	0.47
244.90	1.6	4.7	1.4	7.2	4.0	0.78	5.9	1.11	7.6	1.51	5.2	0.71	4.8	0.73
265.25	1.1	-	1.0	4.4	2.1	0.51	3.5	0.67	4.9	0.98	3.3	-	3.0	0.51
282.30	1.0	2.3	-	2.9	-	0.55	2.0	0.32	2.6	0.44	1.8	0.26	1.8	0.26
300.45	3.2	9.2	-	9.3	3.4	1.37	5.3	0.96	6.4	1.24	4.0	-	3.6	0.47
317.15	1.6	3.7	-	4.8	1.6	0.54	2.5	-	2.7	0.52	1.8	-	1.8	0.29
326.55	2.4	6.8	-	8.6	2.8	-	4.2	0.83	5.2	1.70	3.1	0.46	3.0	0.43
364.00	2.4	6.7	-	7.2	2.5	1.25	4.7	0.68	5.6	1.14	3.7	-	3.6	0.52
403.20	2.7	7.9	-	9.0	3.0	1.31	5.3	0.86	6.6	1.34	4.3	-	4.1	0.60
414.80	3.8	11.4	-	10.4	3.7	1.82	6.0	1.12	7.6	1.54	4.8	0.62	4.3	0.62
438.45	2.7	6.0	-	7.7	2.6	1.03	4.8	0.88	5.8	1.22	3.7	0.49	3.5	0.51
467.70	2.4	5.7	-	6.8	2.0	0.82	3.7	0.75	4.5	0.93	2.9	-	3.0	0.44
499.70	2.4	5.9	-	7.3	2.4	1.29	4.1	0.64	4.8	1.03	3.1	0.45	3.1	0.45
593.25	2.6	6.2	1.5	7.5	-	1.20	3.7	0.66	4.1	1.08	3.2	-	2.6	0.34
604.70	2.5	5.4	-	7.2	-	0.95	4.0	0.70	5.3	1.10	3.3	-	-	0.42
652.05	1.7	3.5	-	4.4	1.7	0.67	2.9	0.38	3.7	0.71	2.3	0.28	2.3	0.32

Table 5: Rare earth element data (values in ppm); '-' = not determined

The Petrography of Altered Submarine Lavas and Major Element Mobility in Drillholes CY-1 and CY-1A, Cyprus

ULRICH BEDNARZ, PETRA GÖTTE, AND HANS-ULRICH SCHMINCKE

Institut für Mineralogie, Ruhr-Universität Bochum Postfach 102148, D-4630 Bochum, F.R.G.

Bednarz, U., Götte, P., and Schmincke, H.-U., 1991: The petrography of altered submarine lavas and major element mobility in Drillholes CY-1 and CY-1A, Cyprus; in Cyprus Crustal Study Project: Initial Report, Holes CY-1 and 1A, eds. Gibson, I.L., Malpas, J., Robinson, P.T., and Xenophontos, C.; Geological Survey of Canada, Paper 90–20, p. 95–116, 1991.

Abstract

Rocks of Drillholes CY-1 (478.88 m deep) and CY-1A (701.19 m deep) belong to the two series: (a) the andesitic to rhyodacitic High-Ti Series (HTS) in the lower part of the sequence and (b) the basaltic andesitic to andesitic Low-Ti Series (LTS) in the upper part. Changes in the major element concentrations of the lavas due to reaction with convecting seawater and hydrothermal solutions were calculated.

Four alteration zones were distinguished: (A) Highly oxidative cold seawater alteration (CSW) with inferred extremely high seawater/rock ratios (>100). This zone, which is present in the uppermost 220 m of Hole CY-1 is characterized by strong enrichment in K_2O and depletion in Na_2O. Temperatures probably were in the range between 80 and 4°C. (B) Low temperature hydrothermal alteration (LTA) with abundant smectite, smectite-chlorite mixed layer clay minerals, and celadonite extends down to a crustal depth of about 700 m. Two- to three-fold enrichment in K_2O and moderate enrichment in Na_2O are discriminators for the LTA-zone. Inferred temperatures are <170°C, mean seawater/rock ratios around 20 (<350°C). (C) High temperature hydrothermal alteration (HTA) is reflected by the paragenesis of epidote, sphene, and chlorite and is characterized by almost complete K_2O removal and moderate to strong Na_2O uptake. It occurs in Hole CY-1A below 271.20 m in a dyke swarm extending upward into the extrusive rocks. Mean seawater/rock ratios were estimated to be below 15. (D) A transitional zone (TZ) with characteristics of low temperature hydrothermal alteration overprinted by cold-seawater alteration was distinguished in the range of 240 to 340 m depth in CY-1.

Résumé

Les roches du trou de forage CY-1, à 478,88 mètres de profondeur et CY-1A, à 701,19 mètres de profondeur, appartiennent à deux séries: (a) les séries andésitiques à rhyodacitique, avec un contenu très élevé en Titane situées dans la partie inférieure de la séquence, et (b) les séries andésitique basaltique à andésitique, de faible contenu en Titane, dans la partie supérieure. Les modifications dans les principales concentrations d'éléments des laves causées par les réactions avec les courants de convection de l'eau de mer et les solutions hydrothermales ont été calculées.

On a ainsi établi quatre zones d'altération: (A) une altération hautement oxydante de l'eau de mer froide avec des rapports inférés extrêmement élevées eau de mer/roche (>100). Cette zone qui se trouve dans les 220 mètres supérieurs du trou CY-1 est caractérisée par un fort enrichissement en K_2O et un appauvrissement en Na_2O. Les températures y étaient probablement de l'ordre de 80 à 4°C; (B) une altération hydrothermale de basse température avec une abondance de smectite, des couches amalgamées de minéraux d'argile et de smectite-chlorite et de celadonite jusqu'à une profondeur de 700 m de la croûte. Les discrimants pour la zone de basse température sont l'apport en K_2O, qui est de deux à trois fois plus élevé, et un apport modéré en Na_2O. Les températures inférées sont inférieures à 170°C, les rapports moyens eau de mer/roche sont de 20 à 350°C. (C) La paragenèse de l'épidote, du sphène et du chlorite reflètent une altération hydrothermale à haute température. Elle est aussi caractérisée par une disparition presque complète de K_2O et une remontée modérée ou forte de Na_2O. Elle a eu lieu dans le trou CY-1A au-dessous de 271,20 m dans un esssaim de dykes qui se prolonge en hauteur dans les roches extrusives. On estime que la moyenne des rapports eau de mer/roche est inférieure à 15. (D) une zone de transition (ZT) dotée des caractéristiques d'une altération hydrothermale à basse température surimpressionnée par une altération d'eau de mer froide a été observée entre 240 et 340 m de profondeur dans CY-1.

INTRODUCTION

Four holes with a total depth of 2.2 km and a mean core recovery of 90% were drilled in Cyprus into the Extrusive Series on the flanks of the Troodos ophiolite complex (Cyprus, Eastern Mediterranean) by the Cyprus Crustal Study Project. A fifth site (CY-4) was located near the base of the Sheeted Dyke Complex and reached a final depth of 2263 m within ultramafic cumulates in the lowermost parts of the ophiolitic crust. In Holes CY-2 (Figure 1, depth: 226.16 m) and CY-2A (depth: 689.15 m), which were drilled directly into the stockwork-like ore bodies Agrokipia A and B, low- (<50°C) to high- (>300°C) temperature alteration zones were distinguished (Sunkel et al., 1987; Herzig and Friedrich, 1987). Holes CY-1, 478.88 m deep (35°02′12″N, 33°10′38″W), and CY-1A, 701.19 m deep (35°02′10″N; 33°10′29″E) were drilled in the Akaki River Canyon in an attempt to recover a complete profile of the Extrusive Series from the contact with the overlying Lefkara Group chalks of Maastrichtian age (Blome and Irwin, 1985) to the highly irregular lower boundary with the Sheeted Dyke Complex ('Basal Group').

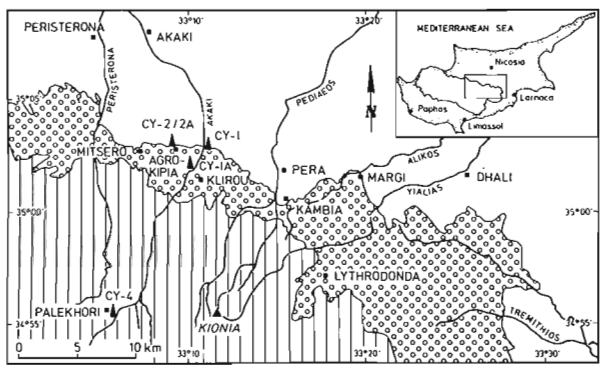

Figure 1: Simplified geological map of the northeastern Troodos ophiolite complex (Cyprus) showing locations of river canyons, Holes CY-1 to CY-4 and Mt. Kionia. Vertical hatching: High level plutonics and Sheeted Dyke Complex; Open circles: Extrusive Series; Blank: Sedimentary Cover.

Hole CY-1 can be divided into three volcanic units (A, B, C), each about 150 m thick (Figure 2; Bednarz, 1988) based on modal compositions and on major extrusive rock types. The upper two units correlated with field units A and B in the Akaki River which were mapped earlier (Schmincke et al., 1983; Rautenschlein, 1987; Schmincke and Rautenschlein, 1987). Field unit C was not reached by Drillhole CY-1, which is located about 1 km to the north of the upper boundary of Unit C in the field.

The Akaki section is disturbed by at least two normal NE-SW trending faults which may represent the flanks of a regional graben structure (Figure 3, probably the eastern extension of the Mitsero graben of Varga and Moores, 1985). Faulting makes extrapolation of individual units between the two holes and of drillhole and field units impossible. In this report, however, we discuss the alteration patterns of CY-1 and CY-1A as reflecting a single stratigraphic profile.

	High-Ti Series	Low-Ti Series
Rock Types	andesite - rhyodacite	basaltic andesite-andesite
Stratigraphic position	low	high
Thickness	300–600 m	200–500 m
Composition at 57 wt.% SiO_2	1.1 wt.% TiO_2 11.5 wt.% FeO° 350 ppm V	0.6 TiO_2 7.5 wt.%FeO° 175 ppm V
Phenocryst content (vol. %)	plag <1 cpx <1 opx/pig <1 Fe-Ti oxides <1	ol <50 cpx <10 plag <1 chromite <1

Table 1: Summary of chemical and petrological characteristics of High- and Low-Ti Series.

Two magmatic series where distinguished in Drillholes CY-1/CY-1A and in Holes CY-2/CY-2A (Bednarz et al., 1987) differing in mineralogy and concentrations of stable elements and bulk composition of glass separates (Table 1): (1) a High-Ti Series (HTS), mostly andesites and dacites; and (2) a Low-Ti Series (LTS), mostly basaltic andesites. Major characteristics are summarized in Table 1. These two series are dominant in the northeastern section of the Troodos ophiolite complex. In the field two more magmatic series can be recognized (Bednarz, 1988), whose abundance is, however, comparatively rare.

(a) Relatively mafic (mostly pillowed) lavas with low TiO_2 concentrations (0.7 to 1 wt.%) are found in small screens between dyke swarms in the transitional zone between the extrusive part of the crust and the Sheeted Dyke Complex (Lo-LTS). Little is known about the original chemical composition of this series because of pervasive alteration, but it is suspected that the magmas of this series may have been related to the HTS-lavas (Bednarz, 1988).

(b) Lavas with essentially the same major element concentrations as the LTS, but different trace element characteristics, built isolated volcanic edifices at the top of the extrusive section (Bednarz, 1988). They differ from the LTS by having lower absolute concentrations of rare earth elements (REE), large ion lithophile elements (LILE) and high-field strength elements (HFSE), as well as by differences in discriminating trace element ratios. A low Ce/Ta-ratio averaging around 34.0, for instance, reflects the lack of a negative Ta-anomaly distinctive for the other Troodos magmatic series (Bednarz, 1988) and for arc-related magmas in general (e.g. Ewart and Hawkesworth, 1987).

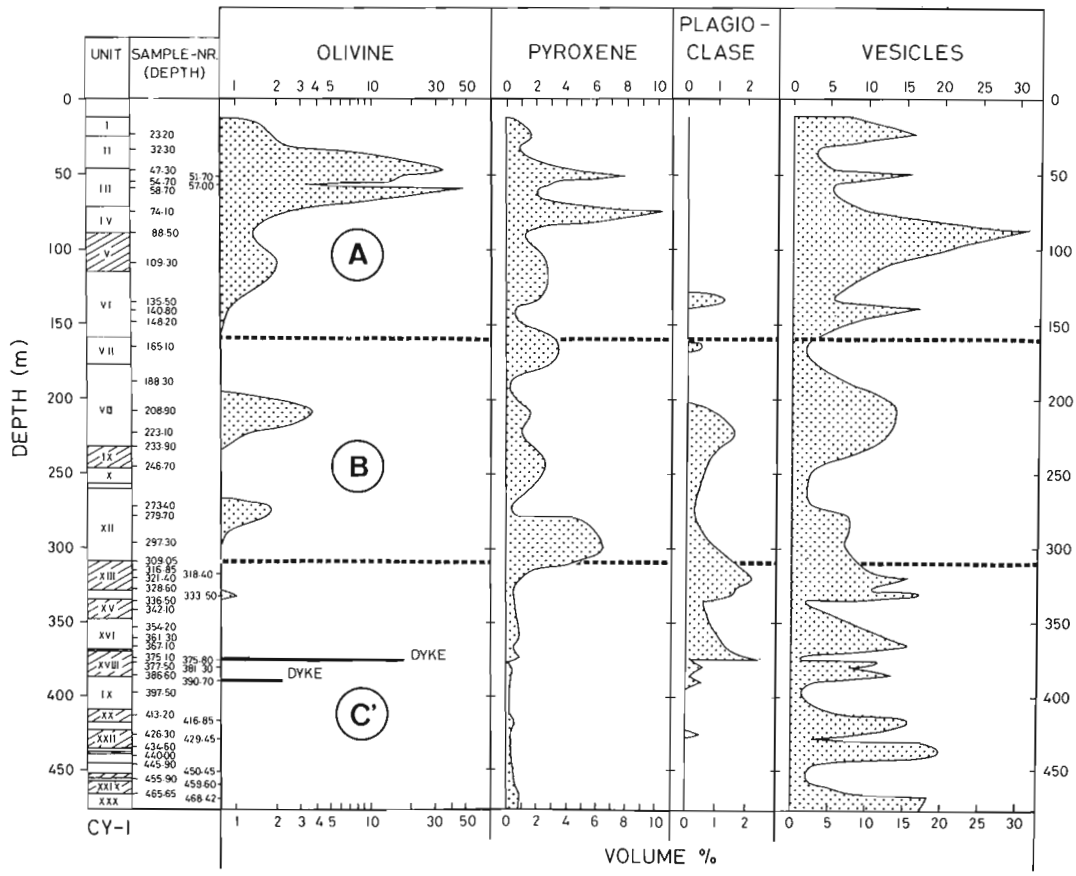

Figure 2: Modal content (vol.%) of phenocrysts and vesicles in lavas from CCSP Hole CY-1. Units A and B (each about 150 m thick) are correlated to field units A and B of Schmincke et al. (1983). Note logarithmic scale for olivine content.

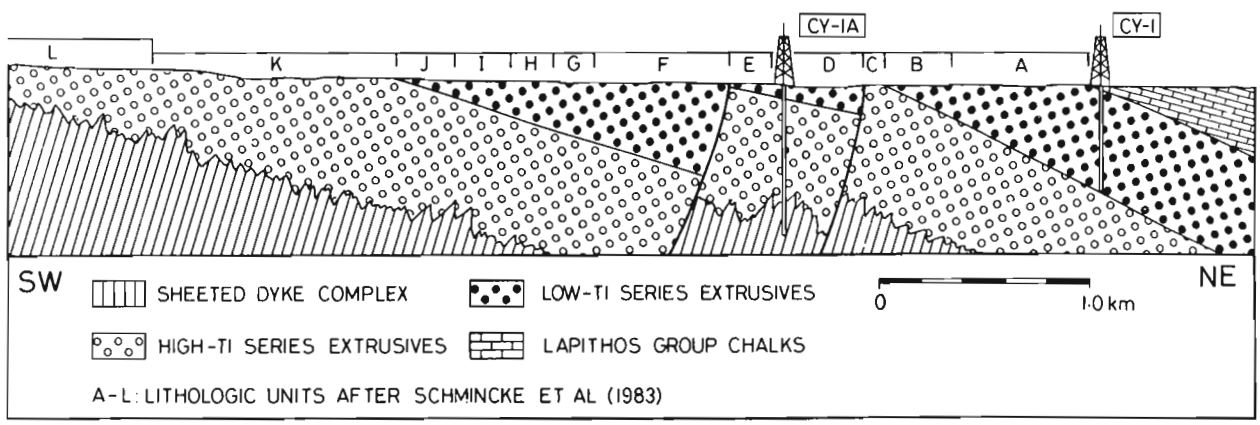

Figure 3: Interpretation of the structure of the extrusive sequence and the upper part of the Sheeted Dyke Complex in the Akaki Canyon from Hole CY-1/CY-1A and field evidence.

ANALYTICAL METHODS

Seventy-four samples from CY-1 and 50 samples from CY-1A were chemically analyzed by X-ray fluorescence methods on glass fusion beads, using a fully automated Philips PW 1400. In addition, 22 handpicked glass samples of pillow rinds, brecciated and massive sheet flows from the Akaki River section, from the drill core of CY-2 and from the Pediaeos River area were analyzed by the same methods.

The fusion beads consist of rock powders (dried at 100°C overnight) and flux (lithium metaborate and lithium tetraborate, Merck A 12) in the ratio 1:4, melted at 1000°C for 10 minutes and poured into a 34 mm diameter pellet mold. Fe^{2+} was determined by semi-automatic potentiometric titration of the hydrofluoric acid-silver perchlorate digested sample, with standard potassium bromide solution. CO_2 was determined by closed system coulometric titration of a barium perchlorate solution into which were passed the gases produced by passing oxygen over the sample roasted in a tube furnace. H_2O^+ was measured by closed system coulometric titration of a nonaqueous Karl Fischer reagent into which was passed the carrier gas (N_2) containing water stripped from the sample by heating in a Pt-crucible to 1,300°C with an induction furnace.

Glass samples were crushed with a steel mortar. The <1 mm fraction was handpicked and cleaned repeatedly in an ultrasonic bath. Grain sizes of the samples prior to grinding ranged from 0.5 to 2 mm. 'Contamination' of the glasses by adhering alteration products ('palagonite,' clay minerals) was estimated to be <10% and, in many samples, <5%. Fifty-two thin sections of CY-1 rocks and 36 thin sections of CY-1A rocks were studied petrographically. Modal amounts of primary and secondary phases were determined by point-counting. About 150 microprobe analyses were carried out (primary and secondary mineral phases) on 10 polished thin sections from CY-1 and CY-1A cores using a wave dispersive automatic microprobe CAMEBAX. A defocused beam (5 × 5 µm) with a filament current of 14 nA, an acceleration voltage of 15 kV, and a counting time of 10 seconds were used. Secondary phases from veins and vesicles were also analyzed by XRD - methods.

MODAL COMPOSITION AND IGNEOUS TEXTURES

The description of modal compositions and igneous textures is mainly based on Bednarz (1988) and includes evidence from rock samples taken in the Pediaeos River area west of Kambia village which is adjacent to the Akaki River Canyon.

High-Ti Series (HTS)

The aphyric to slightly phyric-glomerophyric rocks of the HTS vary texturally and include hyalopilitic, intersertal, hyalo-ophitic, subophitic and ophimottled textures. The modal ratio of groundmass plagioclase to clinopyroxene (as determined by point-counting) is in the range of 50 to 100, whereas Fe-Ti oxides contents in the groundmass range from 5 to 10 vol.%. Augite and plagioclase are common phenocrysts throughout the HTS, but hypersthene is mainly restricted to the more mafic members such as basaltic andesites and andesites. Low-Ca pyroxenes which occur in the more evolved HTS-lavas include Mg-, intermediate- and Fe-pigeonites and, in some rocks, subcalcic ferroaugites. Accessory titanomagnetites are common whereas phenocrysts of ferrian ilmenite are sparse. The following phenocryst assemblages were observed:

1. Basaltic andesites and andesites:
   - augite + plagioclase + magnetite
   - augite + hypersthene + plagioclase + magnetite
   - augite + ferriferous pigeonite + hypersthene + plagioclase + magnetite
2. Dacites and rhyodacites:
   - ferriferous pigeonite + subcalcic ferroaugite + plagioclase + magnetite + ilmenite
   - augite / ferroaugite + magnesium pigeonite / intermediate pigeonite + plagioclase + magnetite
   - intermediate pigeonite / ferriferous pigeonite + augite / subcalcic ferroaugite + bronzite + plagioclase + magnetite

The total phenocryst content rarely exceeds 1 vol.%, relative abundances are normally plagioclase > clinopyroxene > low-Ca pyroxene > magnetite > ilmenite. Plagioclase seems to have been precipitated before pyroxene, based on evidence from glomerophyric clusters.

Some plagioclase crystals are >1.5 mm long, with slightly elongate to tabular appearance. Small crystals are frequently twinned. The outermost rim, compositionally different from the core of the crystal, may form very elongate spikes, typical of strong undercooling and commonly associated with vitric textures. Morphologies are euhedral to strongly corroded with all transitions in individual samples. Corrosion and/or rapid crystal growth is obvious from sieve-like textures with glass 'inclusions'. Skeletal structures of plagioclase crystals are interpreted as selective corrosion which only affected distinct compositions in zoned crystals. Many larger phenocrysts, when intact, show patchy extinction and normal, reverse, complex or oscillatory zonation.

Euhedral to anhedral augite phenocrysts rarely exceed 1 mm in size and have a slightly elongate to tabular appearance. Very patchy, irregular optical extinction is typical, especially in anhedral phenocrysts. Hypersthene phenocrysts, mostly euhedral, may reach 2.8 mm in length, and are easily recognized by their extremely elongate, needle-like shape with aspect ratios of up to 12. Some orthopyroxenes with

rounded contours show evidence for resorption. Pigeonites are mostly euhedral to subhedral and are distinguished from Ca-rich pyroxenes by characteristic elongate, wedge-shaped forms and lower birefringence. Evidence for compositional instability is common. Euhedral, subhedral, dendritic and corroded opaque phenocrysts, some reaching up to 0.5 mm in diameter, occur as isolated grains or in glomerophyric clusters with plagioclase and augite. Fe/Ti-oxides belong mainly to the ulvöspinel - magnetite solid solution series. Members of the ilmenite - hematite solid solution series are rare (microprobe data from Bednarz, 1988) as in other arc-related lavas, probably due to the generally low TiO_2-concentrations in these magmas (Ewart, 1976).

Low-Ti Series (LTS)

Igneous textures of these aphyric and slightly to strongly phyric-glomerophyric rocks are normally hyalopilitic, hyalophitic, subophitic and ophimottled. Vitric groundmass textures are mainly restricted to the chilled margins of pillow tubes and pillow-rind breccias. The groundmass assemblage is essentially the same as in the HTS, however with a noticeably higher clinopyroxene (modal ratio plag : cpx <5) and lower Fe-Ti-oxide content (<5 vol.%).

Observed phenocrysts assemblages are:

- olivine + clinopyroxene ± chromian spinel
- clinopyroxene ± plagioclase

Where present, olivine is generally the dominant phenocryst phase with volume ratios of up to 50 over clinopyroxene and modal concentrations of up to 50 vol.% in some rare picritic samples. However, these extreme concentrations, where observed in the field (Bednarz and Schmincke, 1987), can all be related to post-eruptive settling of crystals in lava flows or sills (concentrations in the lower part of the bodies) or to flow differentiation in pillow tubes and dykes (concentration in the central portions of the lava bodies). 'Normal' modal olivine contents rarely exceed about 4 vol.%. Fresh olivine is rarely preserved and is restricted to fresh glassy rinds of pillow tubes or as relics in picritic megacrysts. Preserved outlines of olivine crystals, generally <500 µm in diameter, suggest predominant euhedral to subhedral shapes. In picrites, single olivine grains may be up to 5 cm across. Olivine has abundant inclusions of chromian spinel especially in picrites, and also partly crystallized glass inclusions up to 0.8 mm in diameter. Crystals in these were identified optically as cpx ± opx ± chromian spinel.

Clinopyroxene, rarely exceeding 0.7 mm in diameter, is euhedral to subhedral, occasionally anhedral. It is light green and commonly exhibits a patchy, irregular optical extinction. Modal concentrations rarely exceed about 4 vol.% but may reach up to 10 vol.% in picritic cumulates. Plagioclase is generally absent as a phenocryst phase in LTS rocks. Euhedral to subhedral lath-shaped crystals, generally less than

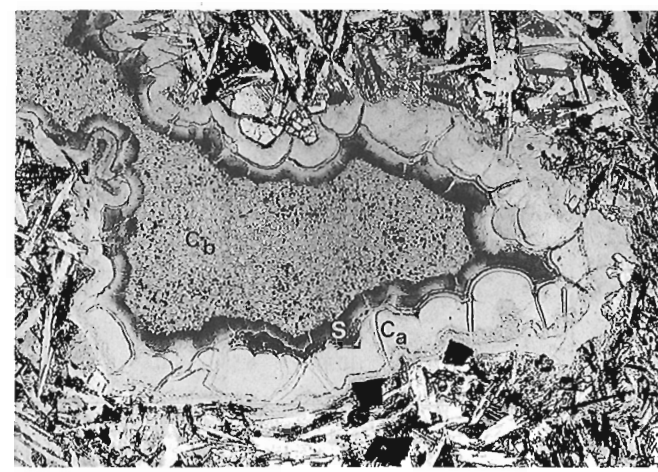

Figure 4: Photomicrograph of concentric growth of celadonite and smectite (S) in a vesicle of sample 27.70 m (CY-1A). Celadonite (C_a): yellow-green; celadonite (C_b): turquoise; dark patches: fresh titanomagnetite; (from: Götte, 1986). Long side of photomicrograph: about 1.2 mm.

500 µm in length, may constitute up to 2 vol.% in some volcanic units. Chromian spinel occurs as inclusion in olivine (here also frequently in glass inclusions) or is intergrown with olivine mainly close to the olivine grain boundaries. It forms euhedral, equant grains, though rounded contours are also common. The size of chromian spinels appears to have a bimodal distribution with one set of larger crystals reaching about 0.6 mm in diameter and a second set rarely exceeding 100 µm in diameter. The colours range from translucent dark reddish/brownish to dark brownish/blackish to almost opaque. Microprobe analyses of Bednarz (1988) suggest that the variation of colour intensity correlates positively with the chromium concentration in the spinels.

OCCURRENCE AND CHEMISTRY OF SECONDARY MINERALS

Celadonite

Celadonite occurs only locally in the lower 250 m of Hole CY-1. It is a common vesicle-filling mineral from 10.5 to 185.7 m in Hole CY-1A, and locally also replaces interstitial glass and primary phases. Colour variations in the normally cryptocrystalline to fibrous aggregates range from distinct bluish-green or turquoise, to grass- or yellow-green. Potassium contents generally exceed 3 wt.% (Table 2). High FeO concentrations of 21.97 to 24.04 wt.% in yellow-green celadonites may be due to a nontronite component. Bluish-green celadonites are characterized by lower FeO concentrations of 11.63 to 17.11 wt.% with Al_2O_3 ranging from 3.23 to 9.98 wt.% and SiO_2 ranging from 50.08 to 55.44 wt.% (Figure 4, Table 2).

	Celad. +	Celad. ⋆	Celad. ×	Celad. ×	Beidel. +	Palyg. ×	Sapon. +	Sapon. ⋆	Sapon. +	Nontr. o	mixed ⋆	mixed +	mixed o	mixed ×
Depth	CY-1 286.6m	CY-1 286.6m	CY-1A 10.5 m	CY-1A 10.5m	CY-1A 10.5m	CY-1 54.7m	CY-1 430.6m	CY-1A 10.5 m	CY-1A 27.7m	CY-1A 27.7m	CY-1A 10.5m	CY-1A 224.4m	CY-1A 224.4m	CY-1A 641.7m
SiO_2	57.16	54.46	55.45	48.44	53.20	43.97	48.59	43.47	44.80	41.69	35.43	30.89	38.15	34.36
TiO_2	0.29	n.d.	0.10	0.27	0.14	0.22	0.13	0.18	n.d.	n.d.	0.05	0.03	n.d.	0.07
Al_2O_3	2.50	2.43	3.78	6.89	23.72	14.83	4.38	8.64	5.72	5.83	11.05	11.87	9.95	14.39
FeO	21.20	19.06	18.02	21.62	1.46	13.17	8.59	12.50	16.57	18.46	12.91	21.25	17.51	12.16
MnO	0.02	0.02	0.10	0.02	0.08	0.17	0.09	0.27	0.08	0.11	0.38	0.25	0.20	0.57
MgO	6.90	5.87	5.49	4.51	1.92	10.72	19.54	18.48	16.04	13.83	21.06	14.04	17.28	22.23
CaO	0.52	0.36	n.a.	n.a.	8.06	0.41	0.93	0.71	0.13	0.67	0.34	0.39	0.97	0.83
Na_2O	1.42	0.52	0.13	0.68	4.35	0.57	1.73	2.35	2.44	2.89	1.05	1.21	2.52	0.21
K_2O	4.02	6.88	10.75	6.58	0.69	2.77	0.21	0.38	0.20	0.04	0.04	0.02	0.09	0.01
Total	94.03	89.60	93.82	89.01	93.62	86.83	84.19	86.98	85.98	83.52	82.31	79.95	86.67	84.83
	Numbers of ions on the basis of 22 oxygens													
Si	8.289	8.367	8.240	7.659	7.051	6.700	7.407	6.642	7.031	6.876	5.800	5.510	6.082	5.433
Ti	0.032	n.d.	0.011	0.032	0.014	0.025	0.015	0.021	n.d.	n.d.	0.006	0.004	n.d.	0.008
Al	0.427	0.440	0.662	1.284	3.705	2.663	0.787	1.556	1.058	1.133	2.132	2.496	1.870	2.681
Fe^{2+}	2.571	2.449	2.239	2.859	0.162	1.679	1.096	1.597	2.174	2.547	1.768	3.171	2.334	1.607
Mn	0.002	0.003	0.013	0.003	0.009	0.022	0.012	0.035	0.011	0.015	0.053	0.038	0.027	0.076
Mg	1.491	1.344	1.216	1.063	0.379	2.435	4.440	4.208	3.752	3.400	5.139	3.733	4.106	5.239
Ca	0.081	0.059	n.a.	n.a.	1.145	0.067	0.152	0.116	0.022	0.118	0.060	0.075	0.166	0.141
Na	0.399	0.155	0.037	0.208	1.118	0.168	0.511	0.696	0.742	0.924	0.333	0.419	0.779	0.064
K	0.744	1.348	2.038	1.327	0.117	0.538	0.041	0.074	0.040	0.008	0.008	0.005	0.018	0.002
Total	14.036	14.165	14.456	14.435	13.700	14.297	14.461	14.945	14.830	15.021	15.299	15.451	15.382	15.251

Table 2: Electron microprobe analyses of clay minerals from Drillholes CY-1 and CY-1A. n.a. not analyzed; n.d. not detected; ⋆ in vesicle;o replacing plagioclase; × replacing pyroxene; + replacing interstitial glass.

Smectite

Smectite is the most abundant alteration mineral in all rocks of CY-1 and from 10.5 to 288.55 m in CY-1A. It replaces interstitial glass, plagioclase and pyroxenes and is a major vesicle-filling phase.

Crystals are non- to weakly pleochroic, varying from dark- to pale-brown or pale olive-brown. Smectites which replace interstitial glass usually occur as cryptocrystalline aggregates with low refractive index and low first order birefringence, whereas a scaly texture is typical of those which replace plagioclase.

The MgO content of smectite ranges between 20.2 wt.% in the dark-brown saponites and <16 wt.% in the olive brown nontronites (Table 2). The Si/Al and Fe/Mg ratios of the smectites vary rather systematically, depending on the chemical composition of the whole rocks. Both ratios are lower in smectites from basaltic andesites of the LTS, than in those of the more silicic rocks of the HTS.

Smectite-Chlorite Mixed Layer Minerals

The term mixed mineral is used for sheet-silicates which have optical properties and chemical compositions intermediate between smectite and chlorite. Mixed layer minerals in CY-1 replace clinopyroxene below 273.4 m and occur as vesicle fillings below 336.5 m. They are common in vesicles of CY-1A between 10.5 and 288.5 m and decrease in abundance below 357.7 m. They are, however, the dominant alteration product of clinopyroxenes, especially below 641.7 m. Generally strongly pleochroic mixed layer minerals are distinguished from smectites by their higher refractive index and higher birefringence. Colours vary from dark olive-green, slightly bluish in vesicles, to pale olive, and slightly brownish in clinopyroxene pseudomorphs. Mixed layer minerals filling vesicles usually form fibrous radiating aggregates whereas those replacing clinopyroxenes are characterized by a more platy appearance. Mixed minerals differ chemically from chlorite in having higher Si and lower Al concentrations (Figure 5) and lower totals. Atomic Si+Al is generally <8 (on the basis of 22 oxygens), not sufficient to fill the tetrahedral position in the crystal structure (Table 2), unlike smectites.

Chlorite

Chlorite is the most widespread alteration mineral below 254 m of Hole CY-1A. It mainly replaces interstitial glass, minor plagioclase and clinopyroxene and also occurs as a vesicle filling. Two different types of chlorite were distinguished:

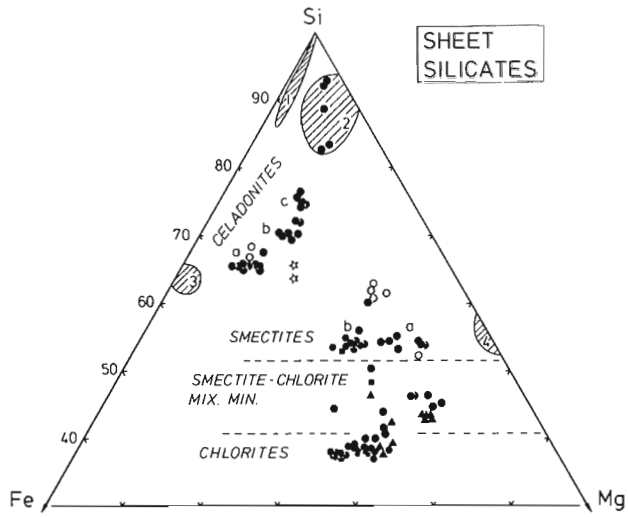

Figure 5: Atomic proportions of Fe, Si, and Mg of sheet-silicates from Holes CY-1 (circles and stars) and CY-1A (solid dots, squares and triangles). Shaded areas indicate fields of reference analyses from Deer et al. (1977): (1) = beidellite; (2) = illite/montmorillonite; (3) = nontronite; (4) = saponite. Celadonite: (a) = yellow green; (b) = olive brown; (c) = pale green. Smectite: (a) dark brown; (b) olive brown. Dots: in vesicles and replacing interstitial glass; triangles: replacing pyroxene; square: replacing plagioclase; stars: palygorskite, beidellite.

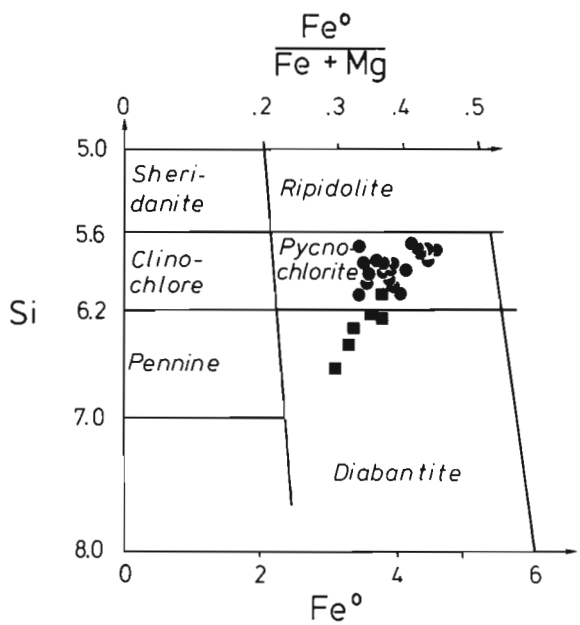

Figure 6: Variation of total Fe [p.f.u.], Si [p.f.u.] and Fe/(Fe+Mg) for chlorites from Hole CY-1A in vesicles and replacing interstitial glass. Nomenclature after Hey (1954). Squares: in basaltic andesite; dots: in evolved andesite.

(m)	+ 288.6	⋆ 288.5	⋆ 347.7	⋆ 410.1	⋆ 641.7	+ 641.7	+ 652.8	⋆ 652.8
SiO_2	33.22	30.82	28.15	27.14	27.81	28.14	26.75	26.41
Al_2O_3	14.49	16.24	17.93	17.01	17.84	17.37	18.20	18.06
FeO	18.05	20.76	21.84	24.94	22.22	22.07	23.65	24.01
MnO	0.37	0.35	0.80	0.83	0.66	0.69	0.93	0.70
MgO	20.27	19.38	18.67	15.97	17.78	18.38	16.33	16.10
CaO	1.06	0.27	0.08	0.11	0.05	0.07	0.05	0.06
Na_2O	0.16	0.17	0.12	0.03	0.03	0.04	0.05	0.06
Total	87.62	87.99	87.59	86.03	86.39	86.76	85.96	85.40
	Number of ions on the basis of 28 (O).							
Si	6.693	6.283	5.840	5.852	5.860	5.900	5.731	5.709
Al	3.441	3.902	4.384	4.323	4.430	4.292	4.596	4.601
Fe^{2+}	3.041	3.539	3.789	4.497	3.915	3.870	4.238	4.340
Mn	0.063	0.060	0.141	0.152	0.118	0.123	0.169	0.128
Mg	6.087	5.889	5.773	5.132	5.584	5.744	5.215	5.187
Ca	0.229	0.059	0.018	0.025	0.011	0.016	0.011	0.014
Na	0.063	0.067	0.048	0.013	0.012	0.016	0.021	0.025
Total	19.617	19.799	19.993	19.994	19.930	19.961	19.981	20.004

Table 3: Electron microprobe analyses of chlorites from Drillhole CY-1A. ⋆ in vesicle; + replacing interstitial glass.

Chlorite (I) is the most common. It is pleochroic from bluish-green to pale yellow-green with characteristic anomalous metallic blue interference colours and plots in the pycnochlorite field of Hey (1954; Figure 6). It generally forms fibrous radiating crystals; irregular aggregates are less abundant. Type (I) chlorite is characterized by high SiO_2 of 30.8 to 33.2 wt.% and MgO of 19.4 to 20.3. wt.% with FeO ranging between 18.1 and 20.8 wt.% (Table 3).

Chlorite (II) is pale to yellow-green with grey to pale yellow interference colours. It is a diabantite, close to the field of pycnochlorite (Hey, 1954; Figure 6), assuming all Fe to be divalent. Compared to Type (I) chlorite, SiO_2 (26.4 to 28.2 wt.%) and MgO concentrations (16.0 to 18.7 wt.%) are slightly lower and FeO-concentrations (21.8 to 24.9 wt.%) significantly higher. Fe/Mg ratios in chlorites from the mafic HTS andesites are slightly higher than in chlorites from silicic HTS-andesites, which may indicate a positive correlation between the compositions of chlorites and of the whole rocks.

Zeolites

Zeolites occur sporadically throughout CY-1 and are slightly more abundant from 10.5 to 288.55 m in CY-1A.

Analcite is found in colourless to dusty brownish, slightly rounded patches and is mostly isotropic but locally weakly birefringent. It occurs generally as a late precipitate, filling veins and vesicles. Analcite replaces some plagioclase below 208.9 m in CY-1; in CY-1A in a sample from 10.5 m and in the interval between 175.6 and 202.6 m. Representative microprobe analyses of analcite are listed in Table 4.

Depth (m)	⋆ 10.5	# 10.5	o 10.5	o 10.5	# 224.4	# 224.4	# 224.4
SiO_2	52.50	54.24	54.87	55.56	59.17	56.75	58.41
Al_2O_3	23.30	24.07	23.11	22.87	23.01	22.94	23.06
CaO	0.29	0.31	0.03	0.06	0.01	0.01	0.01
Na_2O	11.29	9.49	10.32	9.91	11.01	11.51	10.95
Total	87.38	88.11	88.33	88.40	93.20	91.21	92.43
Si	2.000	2.027	2.047	2.065	2.091	2.060	2.082
Al	1.046	1.060	1.016	1.002	0.958	0.982	0.969
Ca	0.012	0.012	0.001	0.002	0.000	0.000	0.001
Na	0.827	0.687	0.747	0.714	0.754	0.810	0.745
Total	3.885	3.786	3.811	3.783	3.803	3.852	3.797

Table 4: Electron microprobe analyses of analcites from Drillhole CY-1A. ⋆ in vesicle; # in vein; o replacing plagioclase.

Gismondine, determined by XRD, replaces interstitial glass (or smectites?) and plagioclase. Colourless to very pale brownish or greenish, fine-grained aggregates with a low refractive index and low first order birefringence show radiating optical extinction.

Gmelinite occurs as pinkish, round or hexagonal clusters (<20 µm) in smectite which has replaced interstitial glass (111.9–129.20 m; CY-1A).

Epidote

Epidote is common below 254.0 m in CY-1A and becomes increasingly abundant downsection. It occurs dominantly as a late filling of veins and vesicles with sulfides, chlorite, and quartz, or replaces plagioclase.

Yellow pleochroism, a high refractive index, and very low birefringence frequently with anomalous bluish-grey to 'lemon'-yellow interference colours are characteristic. In vesicles and veins, dark yellow, slightly brownish epidotes occur as prismatic crystals or fibrous aggregates (Figure 7) with radiating extinction. Anhedral, nearly colourless patches of epidote are intergrown with quartz, whereas pale yellow, prismatic crystals generally replace plagioclase.

The major substitution in the octahedral position is Al^{3+} for Fe^{3+} (Figure 8).

Vein and vesicle filling epidote shows slight Al enrichment downsection (Table 5).

Pumpellyite

Pumpellyite fills vesicles and replaces plagioclase between 288.55 and 464.55 m in CY-1A. It is typically pleochroic from dark/bluish-green to pale-green/colourless with anomalous brown to purple-bluish interference colours and a refractive index between that of chlorite and epidote.

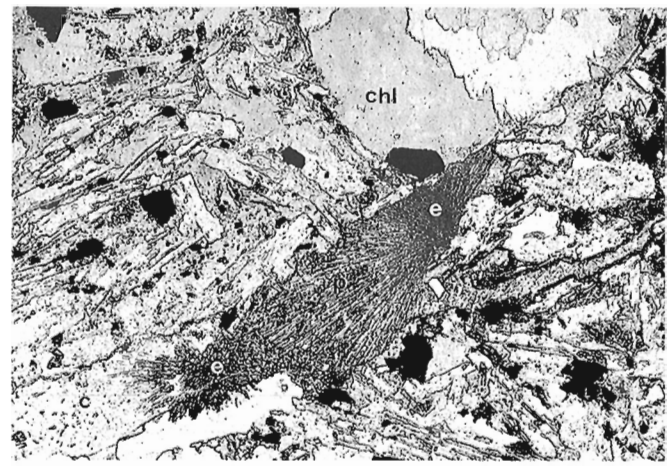

Figure 7: Photomicrograph of radiating aggregate of green pumpellyite (p) and pale yellow epidote (e), platy dark yellow epidote, and calcite (c); chl: chlorite (type I), dark patches are oxides which are replaced by Fe-Cu sulfides and sphene (Götte, 1986). Long side of photomicrograph: about 3 mm.

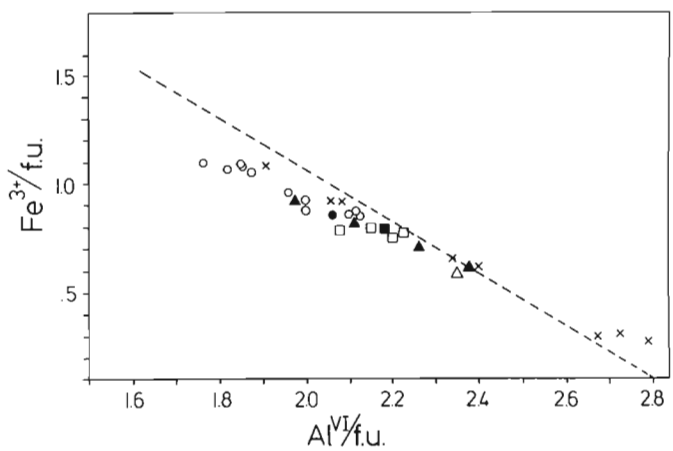

Figure 8: Atomic proportions of Al and Fe^{3+} in the octahedral position of epidotes from Hole CY-1A. Open symbols: in vesicles; filled symbols: in plagioclase; o/●: 410.1 m; △/▲: 641.7 m; □/■: 652.8 m; x indicates reference analyses of epidotes from the del Puerto ophiolite (from: Evarts and Schiffman, 1983); dashed line indicates ideal substitution of Fe^{3+} for Al in the octahedral position.

Pumpellyite in vesicles forms radiating aggregates (Figure 7) whereas it occurs as prismatic crystals when replacing plagioclase. Pumpellyite differs from epidote chemically by having higher MgO- (<2.5 wt.%) and lower FeO^o-concentrations (9.1–10.2 wt.%; Table 5).

Prehnite

Prehnite was identified between 310.4 and 357.45 m in CY-1A in colourless anhedral to platy patches, replacing plagioclase and filling vesicles together with quartz, chlorite, calcite and

	Epidote ⋆	Epidote o	Epidote ⋆	Epidote ⋆	Epidote +	Epidote o	Pump. o	Pump. ⋆	Prehn. o	Prehn. ⋆	Sphene #	Sphene	Sphene	Sphene –
Depth	410.1m	410.1m	641.7m	652.8m	652.8m	652.8m	410.1m	410.1m	347.7m	347.7m	347.7m	410.1m	410.1m	652.8m
SiO_2	36.95	37.40	38.26	36.93	37.53	37.61	37.80	35.80	42.80	43.01	30.83	30.36	30.93	30.59
TiO_2	n.a.	n.a.	n.a.	n.a.	n.a.	n.a.	n.a	n.a.	n.a.	n.a.	35.09	34.97	34.65	35.30
Al_2O_3	19.50	21.48	25.14	21.14	23.54	23.13	22.20	20.88	21.87	20.77	2.28	2.10	2.45	1.76
Fe_2O_3	17.21	13.97	9.83	13.91	12.92	12.98	7.54	11.38	3.41	4.08	1.73	1.47	1.89	1.21
MnO	0.12	0.21	0.33	0.26	0.23	0.07	0.10	0.23	0.02	0.02	0.06	n.d.	0.17	n.d
MgO	0.03	0.19	0.09	0.12	0.03	0.03	2.53	1.89	n.a.	n.a.	0.15	0.08	n.d.	n.d
CaO	23.12	22.76	23.10	23.25	23.06	23.53	21.53	22.26	26.85	26.23	28.29	27.85	28.24	28.77
Total	96.93	96.01	96.75	95.61	97.31	97.35	91.70	92.44	94.95	94.11	98.43	96.83	98.33	97.63
	Number of ions the basis of (O, F, OH, H_2O)													
	13	13	13	13	13	13	28	28	24	24	20	20	20	20
Si	3.023	3.051	3.047	3.026	3.003	3.009	5.874	5.604	5.997	6.103	2.688	2.692	2.698	2.692
Ti	n.a.	n.a.	n.a.	n.a.	n.a.	n.a.	n.a	n.a.	n.a.	n.a.	2.300	2.332	2.273	2.335
Al	1.880	2.065	2.360	2.042	2.221	2.182	4.064	3.852	3.611	3.473	0.234	0.220	0.252	0.182
Fe^{3+}	1.059	0.857	0.589	0.858	0.778	0.782	0.881	1.340	0.360	0.435	0.113	0.098	0.124	0.080
Mn	0.008	0.015	0.022	0.018	0.016	0.005	0.013	0.030	0.002	0.002	0.004	n.d.	0.013	n.d
Mg	0.004	0.023	0.011	0.015	0.004	0.004	0.585	0.441	n.a.	n.a.	0.019	0.011	n.d.	n.d
Ca	2.026	1.989	1.971	2.041	1.978	2.018	3.583	3.733	4.030	3.987	2.642	2.647	2.640	2.711
Total	8.000	8.000	8.000	8.000	8.000	8.000	15.000	15.000	14.000	14.000	8.000	8.000	8.000	8.000

Table 5: Electron microprobe analyses of epidote, pumpellyite, prehnite, and sphene from Drillhole CY-1A. n.a. not analyzed; n.d. not detected; ⋆ in vesicle; o replacing plagioclase; + replacing interstitial glass; # intergrown with Fe-Ti oxide; – intergrown with chlorite and albite.

pumpellyite. Interference colours range from grey to dark yellow or are anomalous brownish. The prehnites are chemically characterized by low FeO of 3.1 to 3.7 wt.% and relatively high CaO-concentrations averaging around 26.5 wt.% (Table 5).

Prehnite was observed in the following mineral assemblages:

1. prehnite + pumpellyite + quartz + calcite (in vug at 310.1 m)
2. prehnite + pumpellyite (in albite at 341.2 m)
3. prehnite + chlorite + quartz + calcite (vesicle at 347.7 m)
4. prehnite + chlorite + quartz + sphene (vesicle at 7.7 m)

Sphene and Leucoxene

Sphene occurs only sporadically in the upper part of CY-1A but is more widespread below 271.2 m, replacing interstitial glass, Fe-Ti-oxides and less commonly plagioclase and clinopyroxene. It is characterized by dark brown or greenish-brown colours, high refractive index and birefringence. It usually forms 'cauliflower' aggregates or rosettes up to 50 µm in diameter. In two samples (142.0 m, 410.1 m), sphene forms nearly colourless, chequered crystals with an oxidized rim. The chemical composition of sphene is relatively uniform with SiO_2 of 30.24–30.93 wt.%, TiO_2 of 30.04–35.87 wt.%, CaO of 27.24–28.77 wt.%, Al_2O_3 of 1.32–2.99 wt.% and Fe_2O_3 of 1.00–1.99 wt.%). No systematic variation in chemical composition with depth was observed.

Leucoxene appears as a brownish to opaque mass, mainly replacing Ti-magnetite which has grown as fine-grained 'dust' in the groundmass.

Plagioclase Alteration

Almost pure K-feldspar dominantly replaces plagioclase in the upper 223.1 m of Hole CY-1 (Table 6) decreasing in abundance in the transition zone below (240.0 to 336.9 m).

Albitization of plagioclase starts below 185.70 m in CY-1A and becomes increasingly abundant downhole. Feldspars are essentially Or-free with An contents ranging from 1 to 4 mole% (Table 6).

Others

Dark yellow to red-brown and dark brown Fe-hydroxides occur dominantly as alteration product of olivine in CY-1 and also appear in the upper 120 m of CY-1A, coating smectites or rarely replacing groundmass clinopyroxene.

Beidellite, which occurs in the upper part of CY-1 (CSW-alteration zone), is characterized by high Al_2O_3 (23.7 wt.%) and SiO_2 (53.2 wt.%) concentrations and very low FeO concentrations (1.5 wt.%; Table 2).

Depth	K-fsp CY-1 54.7m	K-fsp CY-1 54.7m	Albite CY-1A 347.7m	Albite CY-1A 410.1m	Albite CY-1A 641.7m
SiO_2	64.51	64.04	66.87	66.17	67.71
Al_2O	18.28	18.94	19.77	20.18	19.37
Fe_2O_3	0.19	0.20	0.16	0.38	0.13
CaO	0.03	0.00	0.88	1.02	0.20
Na_2O	0.28	0.17	11.65	11.09	11.34
K_2O	16.55	16.74	0.03	0.19	0.00
Total	99.84	100.09	99.36	99.03	98.75
	Number of ions on the basis of 32 (O).				
Si	11.962	11.841	11.749	11.709	12.003
Al	3.995	4.127	4.094	4.209	4.047
Total	15.957	15.968	15.843	15.918	16.050
Fe^{3+}	0.021	0.023	0.017	0.041	0.014
Ca	0.006	0.000	0.166	0.193	0.038
Na	0.101	0.061	3.969	3.805	3.898
K	3.915	3.948	0.007	0.043	0.000
Total	4.043	4.032	4.159	4.082	3.950
Or	97.35	98.48	0.16	1.06	0.00
Ab	2.50	1.52	95.84	94.15	99.03
An	0.15	0.00	4.00	4.79	0.97

Table 6: Electron microprobe analyses of secondary feldspars from Drillholes CY-1 and CY-1A.

Palygorskite, which also occurs in the CSW-zone of CY-1, has intermediate Al_2O_3 concentrations (14.8 wt.%) and slightly increased K_2O concentrations when compared to saponite (around 2.8 wt.%; Table 2).

Calcite occurs throughout the section in variable amounts as a late vesicle filling or alteration product of primary phases and is extremely abundant in the interval between 50 and 150 m of CY-1. In alteration zones I and II, calcite dominantly occurs as fibrous crystals with radiating extinction or in cryptocrystalline aggregates. It forms euhedral to subhedral crystals in vesicles in the hydrothermal alteration zone.

Anhydrite, occurring sporadically in both holes, is colourless and forms anhedral patches, having crystallized in plagioclase and in vesicles. Anhydrite has low first order birefringence but shows the same orientation-dependant refractive index typical of calcite.

SiO_2 phases are mostly missing in the upper part of the crust but quartz becomes increasingly dominant in the hydrothermal alteration zone, generally growing as euhedral but undulose crystals into pore spaces and vesicles. Anhedral undulose quartz has replaced interstitial glass together with chlorite, calcite and epidote, or grew as patches in plagioclase.

Fe-Cu-sulfides occur throughout the section below 271.2 m of Hole CY-1A. They occur as euhedral to subhedral crystals in vesicles, together with chlorite, quartz and epidote, or as fine-grained patches in the groundmass. They probably replaced primary Ti-magnetite as well. In the high temperature alteration zone of CY-2A, sulfides are dominantly pyrite with minor amounts of chalcopyrite, sphalerite and pyrrhotite (Herzig and Friedrich, 1987).

METHODS TO CALCULATE MASS BALANCE OF CHEMICAL EXCHANGE BETWEEN ROCK AND SEAWATER

A common method to estimate mass balances of hydrothermally altered and fresh submarine extrusives is to compare bulk compositions of altered rocks with average compositions of either fresh bulk rocks or fresh glasses (e.g. Donnelly et al., 1980; Alt et al., 1986). However, this method can not be applied to the northwestern Troodos extrusive rocks because of the large range of original chemical compositions from basaltic andesites to dacites occurring in the two different series (Table 1). Moreover, the chemical evolution of the High-Ti Series in the Troodos lavas is spatially distinctly different on a scale of 10 km (Bednarz, 1988).

Therefore, we calculated the linear regression lines of SiO_2 and the elements of interest for glass separates of the Low-Ti Series and the High-Ti Series. The resulting relations are expressed in the following equations:

Low-Ti Series:

(1) $FeO^{\circ}_{SiO_2 > 54\ wt.\%} = 27.23 - (SiO_2 \times 0.35)$

(2) $CaO_{SiO_2} = 32.83 - (SiO_2 \times 0.41)$

(3) $Na_2O_{SiO_2} = -7.48 + (SiO_2 \times 0.18)$

FeO°- values for SiO_2 contents <54 wt.% were not calculated because of high data scatter in this range. K_2O concentration in the Low-Ti Series was assumed to have a mean concentration of 0.25 wt.% because of data scatter and the small overall variation. MgO was omitted in the calculations, because its original concentration depends largely on the abundance of olivine phenocrysts.

High-Ti Series:

Regression lines of Zr with the elements of interest were calculated in addition to those of SiO_2 because of the large variation of Zr within the High-Ti Series.

(4a) $FeO_{SiO_2} = 36.77 - (SiO_2 \times 0.44)$

(4b) $FeO_{Zr} = 14.49 - (Zr \times 0.049)$

(5a) $MgO_{SiO_2} = 25.71 - (SiO_2 \times .38)$

(5b) $MgO_{Zr} = 6.76 - (Zr \times 0.043)$

(6a) $CaO_{SiO_2} = 23.41 - (SiO_2 \times 0.29)$

(6b) $CaO_{Zr} = 8.61 - (Zr \times .030)$

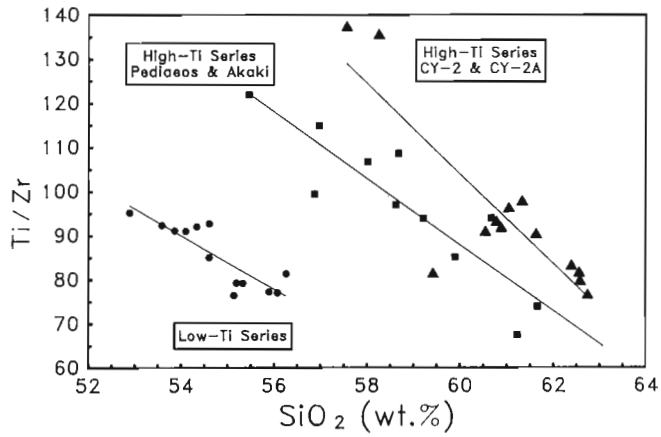

Figure 9: SiO_2 - Ti/Zr for glass separates from the northwestern Troodos Extrusive Series.

(7a) $Na_2O_{SiO_2} = -12.50 + (SiO_2 \times 0.26)$

(7b) $Na_2O_{Zr} = 0.63 + (Zr \times 0.027)$

A mean concentration of 0.32 wt.% K_2O was assumed in the range of the High-Ti Series.

We used the ratio of Ti and Zr (Figure 9), two high field strength elements whose concentrations are relatively unaffected by seawater alteration in order to calculate the original SiO_2 concentrations of the altered whole rocks (Figure 10). The ratio of these 'immobile' elements is also unaffected by passive accumulation. Thus, we get for the Low-Ti Series:

(8) $SiO_2 = 65.23 - (Ti/Zr \times 0.122)$

For the High Ti Series we restricted the calculation of the regression line to glass samples from the Akaki and the Pediaeos area because of different SiO_2 - Zr trends in the samples from the Agrokipia area (CY-2, CY-2A; Bednarz et al., 1987). We also calculated the Zr regression for these samples as a control of the results. Thus, we obtain for the High-Ti Series:

(9a) $SiO_2 = 69.33 - (Ti/Zr \times 0.107)$

(9b) $SiO_2 = 52.13 + (Zr \times 0.092)$

The SiO_2 values resulting from the two different approaches (Equations 9a and 9b) have a mean difference of only 0.18 wt.% and a standard deviation of only 1.17. Below we take the average of both methods.

We take the average of the SiO_2- and Zr-method results in a similar way for the elements FeO°, MgO, CaO, and Na_2O. The mean difference between both methods here is 0.10 wt.% for FeO° (Std.Dev.: 0.30), 0.16 wt.% for MgO (Std.Dev.: 0.27), 0.04 wt.% for CaO (Std.Dev.: 0.18), and 0.06 wt.% for Na_2O (Std.Dev.: 0.16). Even assuming that errors add up, we believe the results to be of sufficient precision for practical interpretation.

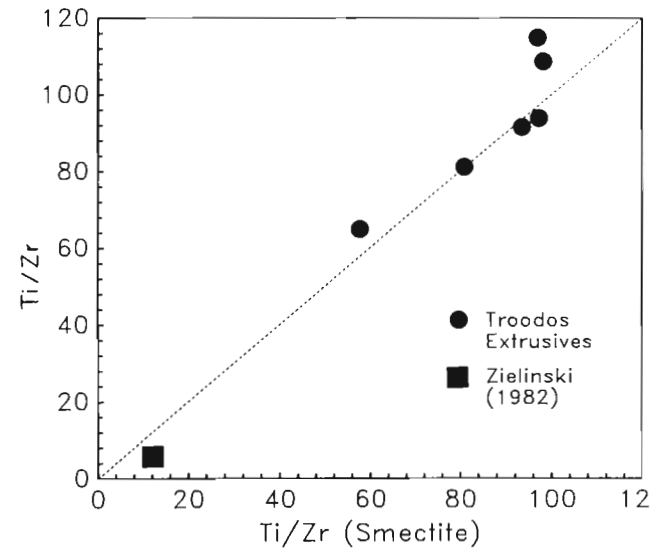

Figure 10: Ti/Zr - ratio for glass separates vs. Ti/Zr ratio of adhering smectites.

Unfortunately, we cannot use Zr variation as a control for the Low-Ti Series, because it varies unsystematically by only about 20 ppm. For further interpretation we calculated Δ-values for these elements which is simply the difference between the analyzed concentration in the altered whole rock and the assumed original pre-alteration concentration calculated from fresh glass compositions.

ALTERATION ZONES

We divided the Drillholes CY-1 and CY-1A into four different alteration zones, based on characteristic element changes and secondary mineral parageneses.

1. Cold seawater alteration zone above 223.1 m in Hole CY-1.
2. Transition zone at 240.0 to 336.9 m in Hole CY-1.
3. Low temperature hydrothermal alteration zone below 390.7 m in Hole CY-1 and above 259.0 m in Hole CY-1A.
4. High temperature hydrothermal alteration zone below 271.2 m in Hole CY-1A.

All boundaries between zones are somewhat arbitrary because alteration did not affect the rocks pervasively, but is strongly dependant on the permeability and thus the lithology and location, width and vertical extent of fracture zones (Figure 11).

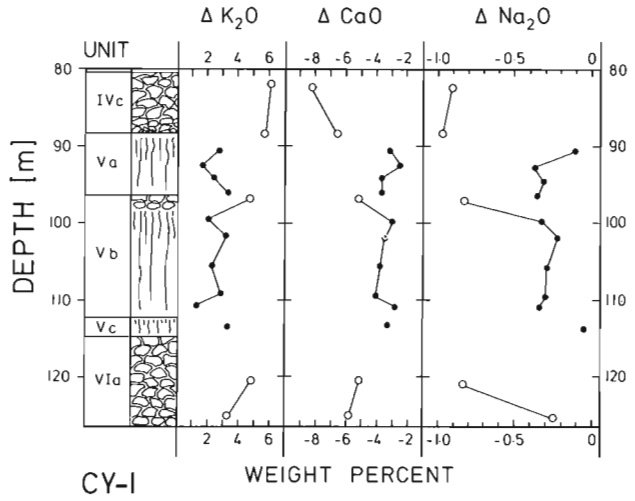

Figure 11: Detail of Δ-K_2O, Δ-CaO, and Δ-Na_2O variations in the cold seawater alteration zone of CY-1, showing higher depletion/enrichment values in pillow lavas and pillowed tops of massive flows.

Also, criteria based on secondary mineralogy and calculated element changes overlap to some degree.

GENERAL CHARACTERISTICS OF ALTERATION ZONES

Cold seawater alteration (CSW)

The partial to complete replacement of groundmass plagioclase by potassium feldspar (adularia?) is the most characteristic petrographic criterion for this zone. The degree of replacement decreases downhole towards the lower boundary of the alteration zone.

Olivine is always altered to iron-hydroxides and calcite, the abundance of Fe-hydroxides being also characteristic of the CSW alteration zone. Clinopyroxene phenocrysts are optically relatively fresh throughout this zone (Figure 12), whereas replacement of groundmass clinopyroxene generally increases downhole.

Groundmass glass is completely altered to brownish, greenish and yellowish smectites (mainly saponites and less commonly beidellite). Smectites are also the main void-filling material apart from calcite and minor amounts of iron-hydroxides and zeolites. The dominant vein filling mineral is Mg-poor calcite (Gillis, 1987).

The alteration of plagioclase to potassium feldspar is reflected in the good correlation of Δ-K_2O (enrichment) with Δ-CaO (depletion) and Δ-Na_2O (depletion) values (Figures 13, 14). Moreover, the mole proportions of (Ca+Na)/K of Δ-values are only slightly larger than unity in the upper part of the drillhole, indicating that only slightly more Ca and Na than that released by plagioclase is removed from the rocks.

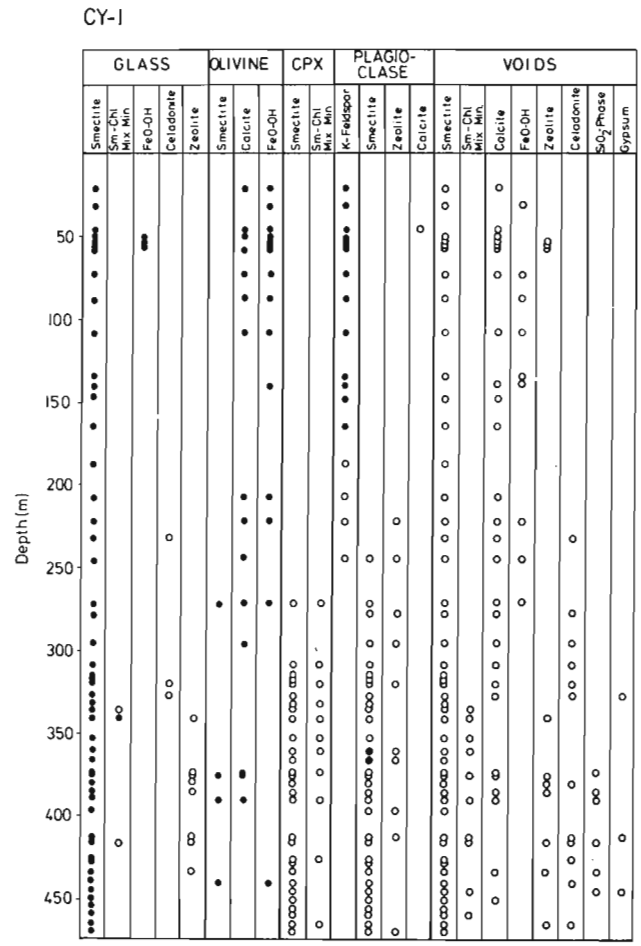

Figure 12: Alteration products of interstitial glass, olivine, clinopyroxene, plagioclase and void-filling secondary minerals in Hole CY-1. Dots: Generally thorough to complete alteration; Circles: Generally incomplete alteration/void-filling.

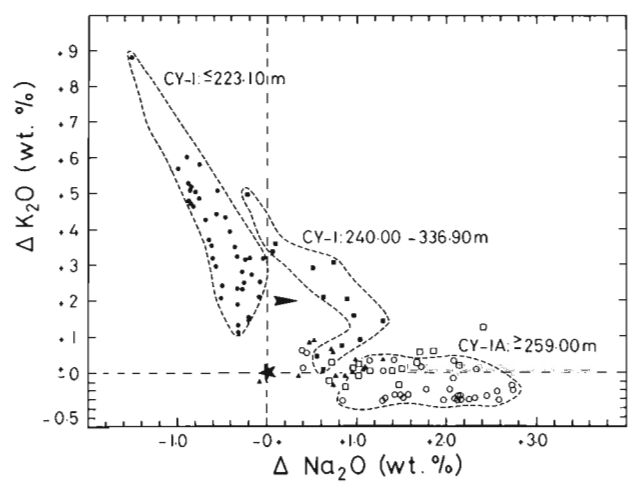

Figure 13: Δ-Na_2O vs. Δ-K_2O variation diagram for Holes CY-1 and CY-1A discriminating the different alteration zones.

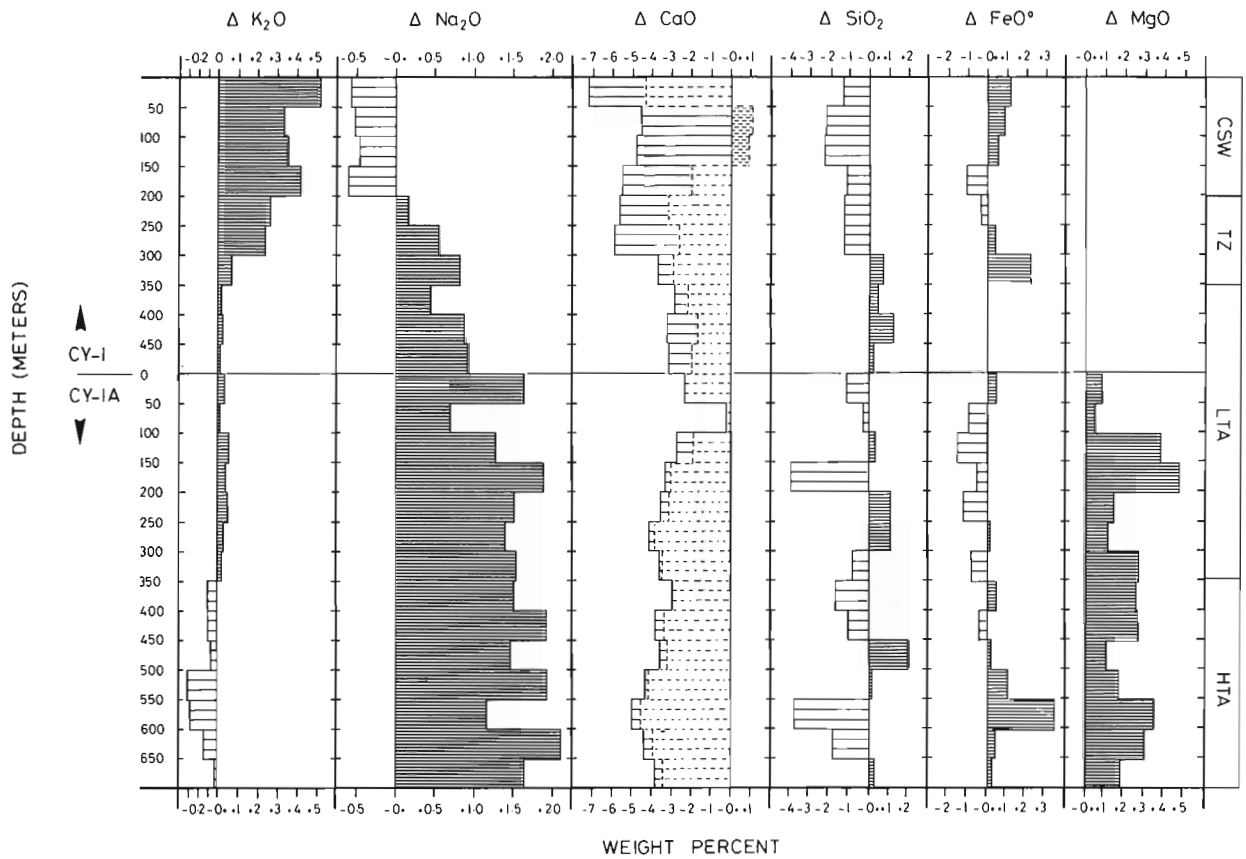

Figure 14: Variation of Δ-K_2O, Δ-Na_2O, Δ-CaO, Δ-SiO_2, Δ-FeO°, and Δ-MgO for Holes CY-1 and CY-1A and distribution of alteration zones. Data are presented as averages of 50 m intervals. Different hatching in the CaO column indicates CaO including carbonate and carbonate-free analyses. Note different scale for negative and positive Δ-K_2O-values.

High seawater/rock ratios ranging from 114 (0–50 m) to 58 (200–250 m) are inferred, assuming complete removal of 380 ppm K dissolved in seawater judging from the high absolute K_2O enrichment in zone (I), averaging 5.2 wt.% (43,200 ppm K) in the uppermost 50 m and 2.67 wt.% (22,200 ppm K) in the interval from 200 to 250 m.

Much of the calcium released from the rocks was probably not transported very far by the solutions, but precipitated as carbonate in voids. Calcite also replaced the bulk of the olivine phenocrysts probably when downwards increasing temperature reduced the solubility for calcium carbonate. This is obvious from the large difference of Δ-CaO for CaO calculated carbonate free and Δ-CaO for CaO including $CaCO_3$ of the rocks. There is even a slight overall enrichment of CaO including carbonate in the depth range from 50 to 150 m (Figure 4).

The exact values of Δ-MgO are difficult to estimate because of the abundance of mafic phenocrysts and non-unique SiO_2 - MgO trends. Judging from the MgO contents of phenocryst-poor rocks, we estimate a general enrichment of MgO around 1 wt.%. This is in agreement with experimental results of Mottl (1983) who reports removal of Mg from seawater at high seawater/rock ratios over a wide range of temperatures. Wolery and Sleep (1976) found complete removal of 1,300 ppm Mg from the seawater at water/rock ratios ranging from 1 : 3 to 1 : 30. As seawater/rock ratios were most probably much higher in all of CSW zone, this corresponds to a maximum MgO increase in the rocks of 3.8 wt.% Mg (6.33 wt.% MgO). XRF-analyses of glass and smectite separates from Hole CY-2A (Sunkel et al., 1987) indicate 2.3 times as much MgO in the smectites as in adhering glass in these least altered rocks of CY-2A. Smectites are probably the only major sink for MgO, as void-filling calcite in the Troodos extrusives has average MgO concentrations of only 0.5 wt.% (Gillis, 1987).

The calculated FeO° changes (Δ-FeO°) in the CSW zone are subtle. The iron content of seawater (0.002 to 0.02 ppm) cannot significantly contribute to the calculated increase in FeO° from 0.64 to 1.18 wt.% in the upper 150 m. If not the result of methodological errors, the Δ-FeO° may be the result of passive accumulation or be related to (late)syn-volcanic to

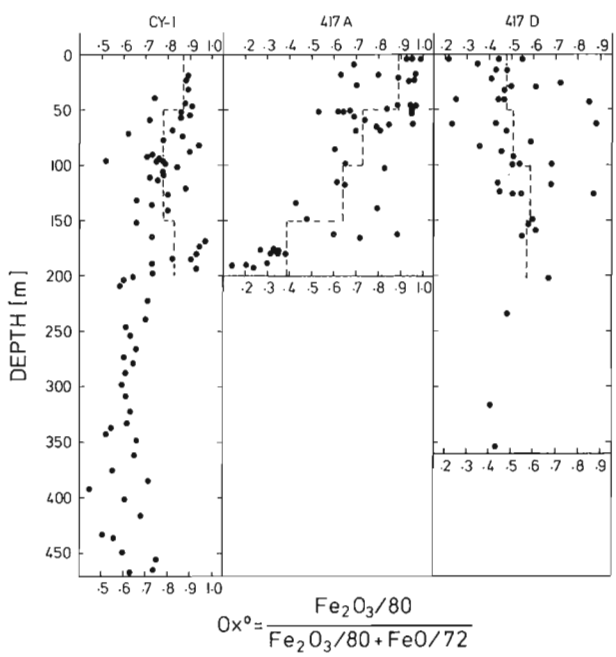

Figure 15: Downhole variation of $Fe^{3+}/(Fe^{3+}+Fe^{2+})$ [Ox°] in CCSP Hole CY-1 and DSDP Holes 417A and 417D. Dashed line indicates mean values of 50 m intervals. DSDP data from Donnelly et al. (1980).

post-volcanic precipitation of Fe/Mn-rich metalliferous sediments (umber and ochre).

The $Fe^{3+}/(Fe^{3+}+Fe^{2+})$ ratio (average values are 0.7 to 0.9; Figure 15) is considerably higher than in fresh glasses of the Low-Ti Series which is around 0.4 (Bednarz, 1988).

SiO_2 changes are also rather subtle compared to the bulk rock compositions. There is a general tendency, however, for SiO_2 depletion of the rocks by 1 to 2 wt.%.

The temperature of cold seawater alteration probably did not significantly exceed that of Cretaceous ocean bottom water. Assuming Mg/Ca ratios close to seawater for late stage solutions from which these carbonates were precipitated, their temperature may have been as low as 4.5°C (Füchtbauer and Hardie, 1980). Pertsev and Boronikhin (1983), on the other hand, estimate temperatures for K-feldspar formation from plagioclase in submarine basalts to be in the interval between 30 and 80°C. This suggests very late formation of secondary calcite.

Cold seawater alteration is thought to be effective until intense percolation of seawater through the rocks is prevented; the lava surface becomes effectively sealed by the sediment burden, or parts of the crust become effectively sealed by secondary sheet-silicates. Thus, the deepest penetration of cold seawater alteration is to be expected when morphological highs such as seamounts are exposed to seawater for a long time. In the western Pediaeos area, where the submarine topography at the volcanic/sedimentary interface is very well preserved, intense red oxidative alteration occurs

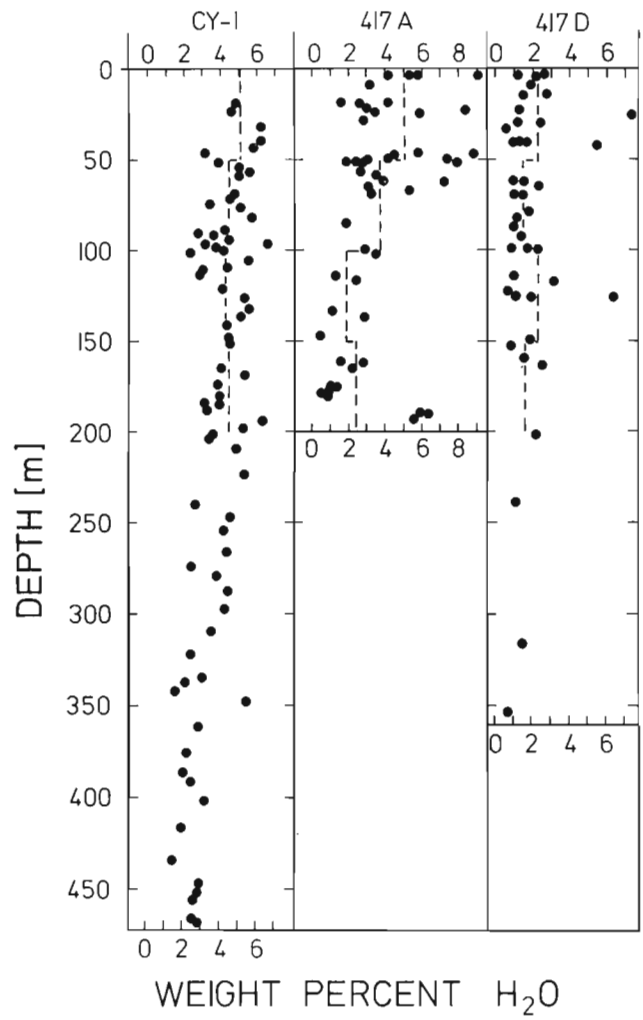

Figure 16: Downhole variation of K_2O in CCSP Hole CY-1 and DSDP Holes 417A and 417D. Dashed line indicates mean values of 50 m intervals. DSDP data from Donnelly et al. (1980).

on submarine hills, whereas oxidative alteration is much less pervasive in topographic lows which were sealed early by umber precipitation. This is why the upper part of the Akaki extrusive section, penetrated by CY-1, was interpreted as a small seamount which rose above the seafloor by about 200 m (Schmincke et al., 1983; Rautenschlein, 1987). At DSDP Hole 417A, interpreted as a topographic high (Donnelly et al., 1980), K-enrichment, oxidation, and H_2O-uptake of the rocks (Figures 15, 16, 17) decreases faster with increasing depth than in Hole CY-1. We thus speculate that the Akaki River area may have formed a regional scale topographic high on the Troodos seafloor. This is confirmed by a maximum thickness of the Low-Ti Series of 500 to 600 m in the Akaki River section, compared to about 280 m near Agrokipia, and about 200 m in the western Pediaeos area, whereas Low-Ti rocks are completely missing in the Analiondas area (about

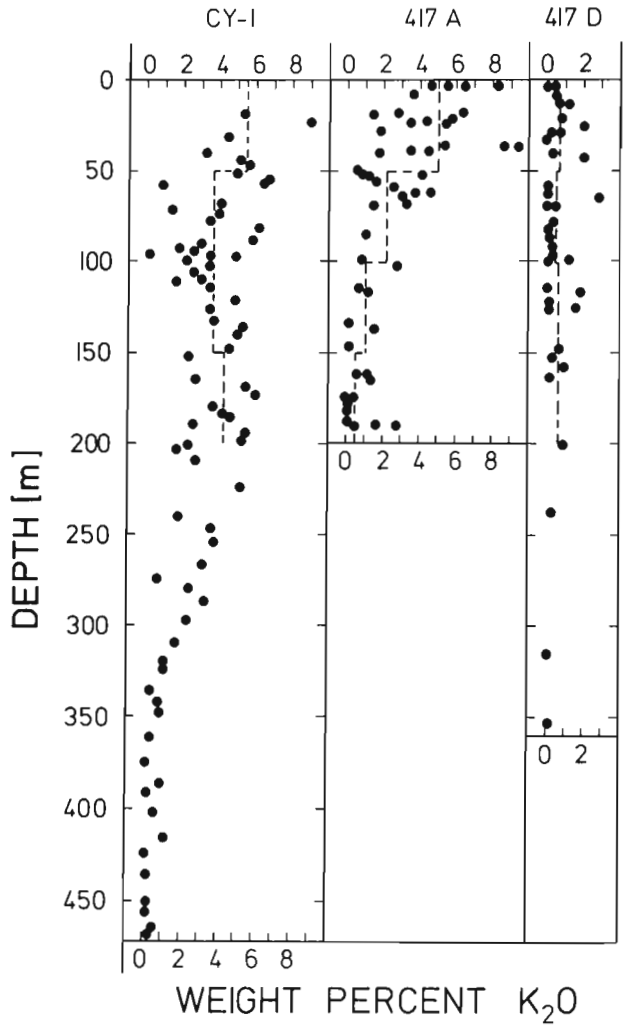

Figure 17: Downhole variation of H_2O in CCSP Hole CY-1 and DSDP Holes 417A and 417D. Dashed line indicates mean values of 50 m intervals. DSDP data from Donnelly et al. (1980).

4 km to the east of Kambia). Furthermore, the oldest circum-Troodos sediments (Perapedhi shales and Middle Lapithos marls and cherts) are missing at the Malounda/Akaki River volcanic/sedimentary contact (Bear, 1960).

Another reason for the deep extent, intensity and pervasiveness of the CSW alteration zone in the Troodos crust is the high porosity of the Troodos lavas, averaging around 19% in CY-1/CY-1A (Smith and Vine, this issue). This is 4 to 15 times higher than average values from DSDP Hole 504B (Wilkens et al., 1983; Karato, 1983; Salisbury et al., 1984).

Transition Zone (TZ)

Plagioclase is only partially replaced by K-feldspar and also partly altered to smectite in the transition zone. There is still a significant enrichment in K_2O (Δ-K_2O up to 4 wt.%), which, however, rapidly decreases downhole (Figure 14).

The main chemical signature of the Transition Zone (II) is the changeover from Na_2O-depletion to Na_2O-enrichment, characteristic of increasing temperature and/or lower water/rock ratios (e.g. Mottl and Holland, 1978; Seyfried and Bischoff, 1981; Mottl, 1983).

We interpret this zone to be slightly influenced by low temperature hydrothermal alteration (with decreasing effect upsection), which was later overprinted by long-lived cold seawater alteration with rapidly decreasing intensity downhole.

Low Temperature Hydrothermal Alteration Zone (LTA)

The upper boundary of this zone was defined at a depth around 350 m in Hole CY-1A, below which rocks are distinctly less enriched in K_2O.

There are no significant petrographic changes in the upper part of the LTA alteration zone (III), except that pyroxene is partly replaced by smectite and analcite (Figure 12). Celadonite and silica phases locally, partially or completely fill voids, but calcite is less abundant than in the CSW zone (I). In the lower half of the LTA zone (III) (upper part of Hole CY-1A) celadonite becomes more abundant and also replaces interstitial glass in addition to smectite. Pyroxene is locally replaced by smectite-chlorite mixed layer minerals. Plagioclase is mostly fresh but rare phenocrysts may be replaced by smectite and smectite-chlorite mixed layer minerals. Analcite pseudomorphs after plagioclase occur in some intervals (e.g. 208.9–468.42 m of CY-1; 10.5 and 208.9–202.6 m of CY-1A). Albitization of plagioclase is observed below 175.6 m in CY-1A (Figures 18, 19), indicative of further increase of alteration temperatures down-section.

Vesicles are either rimmed or completely filled by clay minerals which have grown concentrically from the vesicle rim towards the center in the order: celadonite — smectite → smectite/chlorite mixed minerals (Figure 4). The latest vesicle fills are generally zeolites ± calcite ± silica phases.

The trend of the elemental changes is the same as in the transitional zone (TZ), the rocks become increasingly enriched in Na_2O downhole. SiO_2 changes from very slight enrichment to slight depletion to reach a maximum depletion of about −4 wt.% at 150 and 200 m depth in CY-1A. In the same range, Na_2O and MgO show maximum enrichment of almost 2 wt.% and 4.5 wt.%, respectively. The minimum elemental mobility indicated by calculated Δ-values in the whole profile of CY-1 and CY-1A (i.e. the least altered, 'freshest' rocks) are in the range between 50 and 100 m of CY-1A.

Low temperature hydrothermal alteration is the most common and widespread type of alteration in the northwestern Troodos Extrusive Series. In the upper part of the section

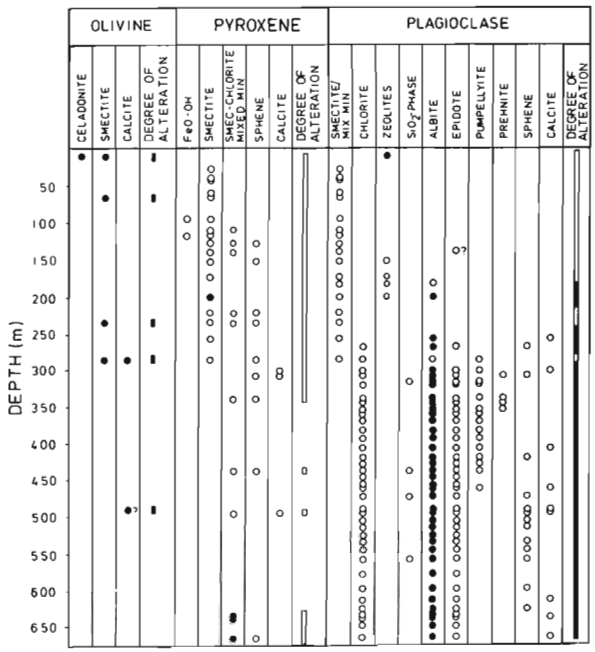

Figure 18: Alteration products of olivine, pyroxene and plagioclase in Hole CY-1A. Dots / black bars: generally thorough to complete alteration; Circles/white bars: generally incomplete alteration.

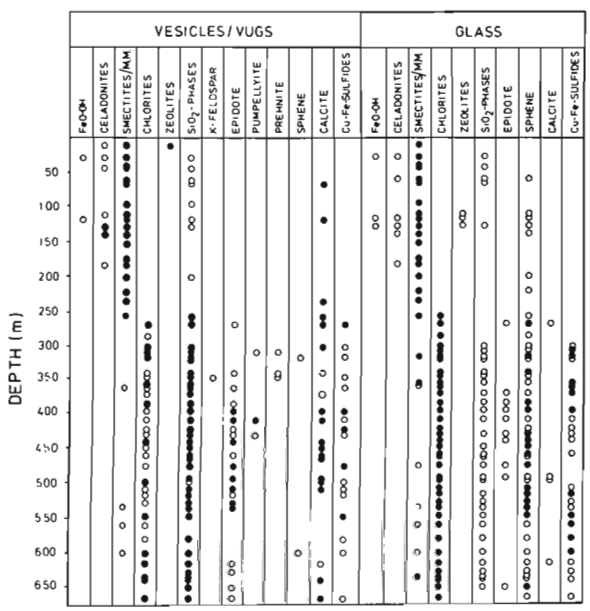

Figure 19: Alteration products of interstitial glass and void-filling secondary minerals in Hole CY-1A. Dots: generally thorough to complete alteration; Circles: generally incomplete alteration / void-filling.

it may overlap with the cold seawater alteration, and it normally reaches down into the Sheeted Dyke Complex (e.g. Pediaeos area, Bednarz and Schmincke, 1989a, b). The degree of alteration within this zone is highly inhomogeneous and strongly dependant on the lithology and permeability of the rocks (e.g. generally weakest in brecciated glassy flows and strongest in pillow lavas and pillow breccias), and the proximity to local volcanic eruptive centers. These are central areas, commonly synvolcanically intensely faulted, and often showing intensive hydrothermal alteration. Episodes of increased hydrothermal activity are clearly genetically related to periods of increased spreading rates and episodes of volcanic activity (Schmincke and Bednarz, 1990).

This contrasts with K/Ar and Rb/Sr age determinations by Staudigel et al. (1986) which suggest that celadonite-formation in the Troodos crust was also a long-lasting process, probably still active 7 to 15 m.y. after crustal formation, an interpretation consistent with isotopic ages of secondary phases from DSDP sites (e.g. Hart and Staudigel, 1978; 1983). This interpretation is equivocal for the following reasons: (1) estimates of basement age are uncertain; (2) the rates and duration of crustal formation are unknown; (3) differences in crustal age between Akaki River Canyon and the Pediaeos area may be on the order of 1 m.y., assuming slow spreading rates; (4) the diffusive loss of ^{40}Ar may lead to celadonite ages that are too low. (5) Furthermore, celadonites in the Troodos crust do not occur in the uppermost alteration zone (in contrast to DSDP Holes 417A, 417D, and 504B; Alt and Honnorez, 1984; Alt et al., 1986).

We suggest that celadonite forms at least in part from K-enriched hydrothermal solutions and is thus not necessarily indicative for direct influence of cold seawater from above.

High Temperature Hydrothermal Alteration Zone (HTA)

Elevated alteration temperatures are evident from petrographic evidence, such as complete albitization of plagioclase, abundance of chlorite and epidote and common alteration of Fe-Ti oxides to sphene (Figures 18, 19). Pumpellyite and minor prehnite locally replace plagioclase. Fe-Cu sulfides are common in vesicles and in the former glassy groundmass. Most vesicles are completely filled by an irregular mixture of minerals, whereas concentric growth of secondary phases, which is especially common in the lower part of the low-temperature alteration zone, is rare. Veins are dominantly filled by mixtures of quartz, epidote and sulfides.

The most characteristic elemental change in the high temperature zone is the thorough, locally almost complete, depletion of K_2O in the rocks. Na_2O and MgO are continuously enriched by up to 2, and 3.5 wt.%, respectively, whereas CaO is depleted by up to 5 wt.%. SiO_2 and FeO^o alternate frequently from slight to moderate enrichment to depletion and vice versa. The mobility of these two elements seems to show a slight negative correlation, i.e. parts which are enriched in

SiO_2 are depleted in FeO° and vice versa. There is no obvious relation of silica enrichment and abundances of silica phases in the rocks, whereas strong Fe enrichment is characteristic of rocks containing abundant sulfides.

High temperature alteration zones are not widespread within the northwestern Troodos Extrusive Series but are restricted to local zones of short-lived upwelling of hot hydrothermal fluids related to major eruptive centers. These centers have local dyke swarms which protrude into the extrusive section and generate high temperature alteration and mineralization zones like those of Hole CY-2A, and/or major fault zones. The high frequency of dykes downhole in CY-1A in this HTA alteration zone indicates a similar volcano-stratigraphic position, although the interpretation of lithologies in the core is difficult and this conclusion is tentative.

BULK ELEMENTAL MASS TRANSFER

The bulk elemental mass transfer for Holes CY-1 and CY-1A summed up to a total thickness of 1200 m can be calculated from the estimates of Δ-values, neglecting parts of the stratigraphy that are most likely tectonically repeated.

Thus, a total of 2.6×10^7 g K per m^2 of exposed seafloor is transferred from the seawater to the rocks. For the upper 200 m of CY-1 we obtain 1.8×10^7 g/m^2, while the same portion of DSDP hole 417A (positioned also on a stratigraphic high) is only a sink for 0.9×10^7 g/m^2. The upper 200 m of DSDP Hole 417D — positioned on 'normal' ocean floor — gained only 0.2×10^7 g/m^2 K. We assumed a concentration of 0.15 wt.% K_2O for MORB (Pearce et al., 1981).

Na gain of the rocks in the upper 1,200 m is similar to that for potassium, totalling about 2.4×10^7 g/m^2 ocean floor. This figure is already corrected for the Na-depletion in the CSW-zone and thus represents the total mass of Na transferred from seawater to the rocks. Assuming that the 10,600 ppm Na from seawater are totally transferred to the rocks we obtain an average seawater/rock-ratio of 1 in the zones of Na-enrichment, with average values of enrichment of 8,500 ppm in the LTA-zone and 12,390 ppm in the HTA-zone. Higher water/rock ratios in the less-permeable rocks downhole are not reasonable, and thus the general increase in Na-enrichment is thought to be controlled by higher temperatures. Generally, low water/rock ratios are in good accordance — especially if not all of the Na is removed from the seawater — with findings of Hajash, (1975) Mottl and Holland (1978), and Seyfried and Bischoff (1981) who report removal of Na from seawater at water/rock ratios <5 and temperatures >200° C.

We have to assume considerably higher water/rock-ratios of 19 and 14 respectively, judging from high Mg-enrichment at an average of 24,000 ppm in the LTA-zone and 18,300 ppm in the HTA-zone (IV) and Mg concentrations in seawater of 1,300 ppm. These have to be considered as minimum numbers, because fluids which are active so far down in the crust had probably already lost a substantial amount of their original Mg to the extrusive rocks upsection.

Calcium is generally leached from the rocks, totalling 9.0×10^7 g/m^2 seafloor in Holes CY-1 and CY-1A. However, about 3.1×10^7 g/m^2 are precipitated as carbonate in voids and vesicles, thus holding about 3.4×10^7 g/m^2 of CO_2. The general flux of Ca into the convecting seawater is in good agreement with the findings of Bischoff and Dickson (1975) and Albarede and Michard (1983).

Changes in Fe are unsystematic. A general enrichment of Fe in the lower part of CY-1A is supported by the occurrence of Fe-Cu sulphides and suggest a total addition of Fe of 0.6×10^7 g/m^2 seafloor. Due to the minute amounts of Fe in seawater this must have been leached from the rocks in deeper-seated parts of the crust.

Silica enrichment and depletion are also unsystematic. This is supported by field observations of intense silification and almost fresh glassy brecciated flows, side by side on the scale of decimetres. Whereas the solubility of silica in the hydrothermal fluid is strongly dependant on pH and temperature, the amount of silica released from the rocks may depend on the abundance of fresh glass and its silica content, as the clay minerals generally have lower Si concentrations than the original glass. This is in accordance with the observation of a common, close, spatial relationship of brecciated glassy flows (matrix altered to smectite) and silification of neighbouring massive lavas. Thus, Si leached from the rocks totals 0.9×10^7 g/m^2 seafloor, probably reflecting the general abundance of glassy rocks and the glassy matrix of differentiated Troodos extrusive rocks.

SUMMARY AND CONCLUSIONS

Rock Types

Holes CY-1 and CY-1A together penetrated 1180 m, i.e. almost the complete section through the extrusive crust and the upper part of the Sheeted Dyke Complex of the Troodos ophiolite. Pillow lavas make up about 35% of the total thickness but about 70% of the LTS rocks in Drillhole CY-1 (Robinson and Gibson, 1982). Less than 30% of the LTS lavas were erupted as massive sheet flows, the dominant rock type in the central portion of the extrusive crust, i.e. the upper part of the HTS sequence. Brecciated glassy flows which are widespread in the lower parts of the Troodos extrusives, as in the Pediaeos area (Bednarz, 1988; Schmincke and Bednarz, 1990) and Drillholes CY-2/CY-2A (Bednarz et al., 1987), are not common in CY-1A (Horne and Robinson, 1986). We interpret Drillhole CY-1A to be positioned right above a local dyke swarm which reaches upwards into the lavas. Similar dyke swarms, several tens of metres wide are widespread in the Pediaeos area in the lower part of the extrusive crust (Bednarz, 1988).

Crustal Structure in the Akaki River Canyon

Schmincke and Rautenschein (1987) found major faults as boundaries between volcanic units C/D and E/F in the Akaki River Canyon. The scale of these faults can be approximately reconstructed (in the order of 200 to 300 m) based on the stratigraphy of Drillholes CY-1 and CY-1A. It is also evident (see Figure 3) that the absolute thickness of the extrusive section (and especially the LTS-lavas) along the Akaki River is easily overestimated by about 30% due to tectonic repetition of the LTS. This illustrates the general difficulty in estimating realistically the thickness of alteration zones, volcanic units etc., which are also characterized by highly variable thicknesses, even from three-dimensional outcrops in the field.

Sub-Seafloor Alteration

The high core recovery in an almost complete profile of the extrusive part of fossil oceanic crust, along with the chance to calibrate the composition of altered lavas against fresh glass compositions, allows us to quantify the chemical exchange between rocks and convecting fluids.

Our interpretations about the direction of element exchange between extrusive crust and seawater are generally in accordance with findings from the recent oceanic crust (e.g. Donnelly et al., 1980; Alt et al., 1986), but the scale of exchange is normally larger in the Troodos section (Figure 20). Our

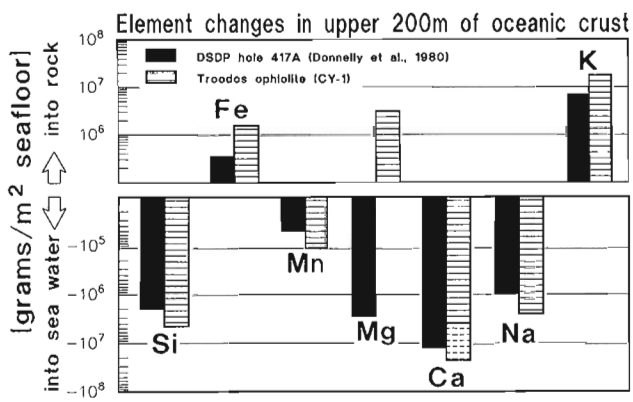

Figure 20: Cumulative major element mass transfer in CCSP Holes CY-1 and CY-1A for the upper 200 m of the crust compared to mass transfer in the same portion of DSDP Hole 417A as estimated by Donnelly et al. (1980). The broken hatching in the Ca-bar for Troodos indicates the amount of Ca which precipitated as calcite in veins and vesicles.

data are also mostly consistent with chemical changes in the Troodos crust found by Gillis and Robinson (1988). Below we highlight some major differences and implications of our study mostly concerning the direction and scale of chemical exchange in the uppermost, cold seawater alteration zone.

1. The enrichment of K (and other LIL-elements such as Rb) in the Troodos extrusive crust is considerably larger than in all sections of present-day oceanic crust. Net fluxes of K (estimated by Bednarz and Schmincke, 1989a, b), which take into account K-depletion in the rocks in high temperature alteration zones of the Sheeted Dyke Complex are almost an order of magnitude larger than estimates by Alt et al. (1986) for DSDP Hole 504B and Hart and Staudigel (1982) for Hole 418A. As discussed above this is interpreted as resulting from the position of the Akaki section on a seafloor topographic high exposed to percolating seawater for a long period of time, and to the higher porosity and permeability of the Troodos lavas compared to mid-ocean ridge basalts.

2. Enrichment of Mg in the rocks of the uppermost alteration zone is only reported by Alt et al. (1986) for Hole 504B. Increased Mg reactivity and Mg enrichment in the rocks with high seawater/rock ratios was found experimentally by Seyfried (1987) and is consistent with extreme seawater/rock mass ratios which are estimated for the upper part of CY-1.

3. Changes in Na concentrations during cold seawater alteration of oceanic crust are generally not included in recent estimates. Flux of Na into the seawater during low temperature alteration is, however, consistent with findings of Hart (1973), Maynard (1976) and Donnelly et al. (1980) and probably reflects replacement of groundmass plagioclase by K-feldspar.

4. The formation of oceanic crust is normally considered as a major contributor to the global CO_2-cycle, of the order of 2.6×10^{14} g/a, mainly by magmatic degassing (e.g. Holser et al., 1988). Bednarz and Schmincke (1989) estimate that the massive carbonate precipitation in the upper part of CY-1 corresponds to an annual flux of about 10^{14} g, the same order of magnitude as the value for CO_2-release, consistent with findings from Staudigel et al. (1990) for North Atlantic oceanic crust.

ACKNOWLEDGEMENTS

Drilling costs were supported financially by the VW foundation grant No. I 38488. U.B. was initially supported by European Community grant No. MSM 018 D and later by the Deutsche Forschungsgemeinschaft grant No. Schm 250/33-1. Thin sections were prepared by G. Olesch, chemical analyses were performed by H. Niephaus, and figures were photographed by A. Fischer. Glass samples from the Akaki River were kindly provided by Martina Rautenschlein. Special thanks are expressed to ou/ colleagues from the Geological Survey Department, Nicosia, especially Costas Xenophontos, Andreas Panayiotou and George Constantinou, for abundant logistical and organizational aid. We thank Paul Robinson and an anonymous reviewer for their helpful comments on the manuscript.

REFERENCES

Albarede, F. and Michard, C.R.P.G.
1983: Chemical exchanges at the mantle/seawater boundary along ridge crests; *in* Duncan, M.A, Grove T.L., and Hildreth, W., Proceedings of the DSEM Field Conference on open magmatic systems, Institute for the Study of Earth and Man, Southern Methodist University, Dallas, p. 1–2.

Alt, J.C. and Honnorez, J.
1984: Alteration of the upper oceanic crust; DSDP Site 417: mineralogy and chemistry; Contributions to Mineralogy and Petrology, v. 87, p. 149–169.

Alt, J.C., Honnorez, J., Laverne, C., and Emmermann, R.
1986: Hydrothermal alteration of a 1 km section through the upper oceanic crust, Deep Sea Drilling Project Hole 504B: mineralogy, chemistry, and evolution of seawater-basalt interactions; Journal of Geophysical Research, v. 91, p. 10309–10335.

Bear, L.M.
1960: The geology and mineral resources of the Akaki-Lythrodondha area; Cyprus Geological Survey Department Memoir, v. 3, 222 p.

Bednarz, U.
1988: Volcanological, geochemical and petrological evolution, and sub-seafloor alteration in the northeastern Troodos ophiolite (Cyprus); (PhD Thesis), Ruhr-Universität Bochum, 295 p.

Bednarz, U. and Schmincke, H.-U.
1987: Volcanology in the Pediaeos-, Onouphrios-, Kokkinovrysi-, and Mazovounous River System; *in* Xenophontos, C. and Malpas, J.G., Field Excursion Guidebook. Troodos 87: Ophiolites and Oceanic Lithosphere, Cyprus Geological Survey Department, Nicosia, p. 260–285.

Bednarz, U. and Schmincke, H.-U.
1990: Chemical patterns of seawater and hydrothermal alteration in the northeastern Troodos extrusive series and sheeted dyke complex, Cyprus; *in* Malpas, J., Moores, E.M., Panayiotou, A., and Xenophontos, C., Ophiolites — Oceanic Crustal Analogues. Proceedings of the Symposium 'TROODOS 1987,' Cyprus Geological Survey Department, Nicosia, p. 639–654.

Bednarz, U. and Schmincke, H.-U.
1989: Mass transfer during sub-seafloor alteration of the upper Troodos crust (Cyprus); Contributions to Mineralogy and Petrology, v. 102, p. 93–101.

Bednarz, U., Sunkel, G., and Schmincke, H.-U.
1987: The basaltic andesite-andesite and the andesite-dacite series from the ICRDG Drill Holes CY-2 and CY-2a. I. Lithology, petrology and geochemistry; *in* Robinson, P.T., Gibson, I.L., and Panayiotou, A., Cyprus Crustal Study Project: Initial Report, Holes CY-2 and 2A, Geological Survey of Canada, Paper 85–29, p. 183–204.

Bischoff, J.L. and Dickson, F.W.
1975: Seawater-basalt interaction at 200°C and 500 bars: implications for origin of sea-floor heavy-metal deposits and regulation of seawater chemistry; Earth and Planetary Science Letters, v. 25, p. 385–397.

Blome, C.D. and Irwin, W.P.
1985: Equivalent radiolarian ages from ophiolitic terrains of Cyprus and Oman; Geology, v. 13, p. 401–404.

Deer, W.A., Howie, R.A., and Zussman, J.
1977: An introduction to the rock-forming minerals, Longmans, Green, London, 528 p.

Donnelly, T.W., Thompson, G., and Salisbury, M.H.
1979: The chemistry of altered basalts at Site 417, Deep Sea Drilling Project Leg 51; *in* Donnelly, T., Francheteau, J., Bryan, W., Robinson, P., Flower, M., Salisbury, M., et al., Initial Reports of the Deep Sea Drilling Project, v. 51, 52, 53, U.S. Government Printing Office, Washington, p. 1319–1330.

Evarts, R.C. and Schiffman, P.
1983: Submarine hydrothermal metamorphisms of the Del Puerto ophiolite, California; American Journal of Science, v. 283, p. 289–340.

Ewart, A.
1976: Mineralogy and chemistry of modern orogenic lavas — some statistics and implications; Earth and Planetary Science Letters, v. 31, p. 417–432.

Ewart, A. and Hawkesworth, C.J.
1987: The Pleistocene-Recent Tonga-Kermadec Arc lavas: interpretation of new isotopic and rare earth data in terms of a depleted mantle source model; Journal of Petrology, v. 28, p. 495–530.

Füchtbauer, H. and Hardie, L.A.
1980: Comparison of experimental and natural magnesian calcites (abstract); International Association of Sedimentologists 1st European Meeting, Bochum (Germany), p. 167–169.

Gillis, K.M.
1987: Multistage alteration of the extrusive sequence, Troodos ophiolite, Cyprus; (PhD Thesis), Dalhousie University, Halifax, 387 p.

Gillis, K.M. and Robinson, P.T.
1988: Distribution of alteration zones in the upper oceanic crust; Geology, v. 16, p. 262–266.

Götte, P.
1986: Petrology of volcanic rocks of drill hole CY-1A, Troodos ophiolite (Cyprus); (Diplom-thesis), Ruhr-Universität Bochum, 67 p.

Hajash, A.
1975: Hydrothermal processes along mid-ocean ridges: an experimental investigation; Contributions to Mineralogy and Petrology, v. 53, p. 205–226.

Hart, S.R.
1973: A model for chemical exchange in the basalt-seawater system of oceanic layer II; Canadian Journal of Earth Sciences, v. 10, p. 799–816.

Hart, S.R. and Staudigel, H.
1978: Oceanic crust: age of hydrothermal alteration; Geophysical Research Letters, v. 5, p. 1009–1012.

Hart, S.R. and Staudigel, H.
1982: The control of alkalies and uranium in seawater by ocean crust alteration; Earth and Planetary Science Letters, v. 58, p. 202–212.

Hart, S.R. and Staudigel, H.
1983: Age of hydrothermal circulation on the Rio Grande Rise: Deep Sea Drilling Project Site 516; *in* Barker, P.F., Carlson, R.L., and Johnson, D.A.; Initial Reports of the Deep Sea Drilling Project, v. 72, U.S. Government Printing Office, Washington, p. 471–474.

Herzig, P.M. and Friedrich, G.H.
1987: Sulphide mineralization, hydrothermal alteration and chemistry in the drill hole CY-2a, Agrokipia, Cyprus; *in* Robinson, P.T., Gibson, I.L., and Panayiotou, A.; Cyprus Crustal Study Project: Initial Report, Holes CY-2 and 2a, p. 103–138.

Hey, M.H.
1954: A new review of the chlorites; Mineralogical Magazine, v. 30, p. 277–292.

Holser, W.T., Schidlowski, M., Mackenzie, F.T. and Maynard, J.B.
1988: Biogeochemical cycles of carbon and sulfur; in Gregor, C.B., Garrels, R.M., MacKenzie, F.T., and Maynard, J.B. Chemical cycles in the evolution of the earth, John Wiley, New York, p. 105–173.

Horne, L.V.B. and Robinson, P.T.
1986: Cyprus Crustal Study Project, Hole CY-1A: edited core descriptions; Dalhousie University, Halifax, 700 p.

Karato, S.
1983: Physical properties of basalts from Deep Sea Drilling Project Hole 504B, Costa Rica Rift; *in* Cann, J.R., Langseth, M.G., Honnorez, J., Von Herzen, R.P., White, S.M., et al., Initial Reports of the Deep Sea Drilling Project, v. 69, U.S. Government Printing Office, Washington, p. 687–695.

Maynard, J.B.
1976: The long-term buffering of the oceans; Geochimica et Cosmochimica Acta, v. 40, p. 1523–1532.

Mottl, M.J.
1983: Hydrothermal processes at seafloor spreading centers: application of basalt-seawater experimental results; *in* Rona, P.A., Boström, K., Laubier, L., and Smith Jr., K.L., Hydrothermal processes at seafloor spreading centers, IV Marine Sciences, v. 12, Plenum Press, New York, 796 p.

Mottl, M.J. and Holland, H.D.
1978: Chemical exchange during hydrothermal alteration of basalt by seawater–I. experimental results for major and minor components of seawater; Geochimica et Cosmochimica Acta, v. 42, p. 1103–1115.

Pearce, J.A., Alabaster, T., Shelton, A.W., and Searle, M.P.
1981: The Oman ophiolite as a Cretaceous arc-basin complex: evidence and implications; Philosophical Transactions of the Royal Society of London, v. A300, p. 299–317.

Pertsev, N.N. and Boronikhin, V.A.
1983: Secondary K-feldspar in basalts at Deep Sea Drilling Project Hole 504B and the problem of K-feldspathization in oceanic basalts; *in* Cann, J.R., Langseth, M.G., Honnorez, J., Von Herzen, R.P., White, S.M., et al., Initial Reports of the Deep Sea Drilling Project, v. 69, U.S. Government Printing Office, Washington, p. 589–592.

Rautenschlein, M.
1987: Geology and geochemistry of Akaki volcanics, Cyprus; (PhD Thesis), Ruhr-Universität Bochum, 222 p.

Robinson, P.T., Gibson, I.L., and Horne, L.V.-B.
1991: Cyprus Crustal Study Project Hole CY-1: lithologic unit summaries; *in* Gibson, I.L., Malpas, J., Robinson, P.T., and Xenophontos, C., Cyprus Crustal Study Project: Initial Report, Holes CY-1 and 1A, Geological Survey of Canada, Paper 90–20.

Salisbury, M.H., Christensen, N.I., Becker, K. and Moos, D.
1985: The velocity structure of layer 2 at Deep Sea Drilling Project Site 504 from logging and laboratory experiments; *in* Anderson, R.N., Honnorez, J., Becker, K., et al. Initial Reports of the Deep Sea Drilling Project, v. 83, U.S. Government Printing Office, Washington, p. 529–539.

Schmincke, H.-U., and Bednarz, U.
1990: Pillow, sheet flow and breccia flow volcanoes and volcano-tectonic-hydrothermal cycles in the Extrusive Series of the northeastern Troodos ophiolite (Cyprus); *in* Malpas, J., Moores, E.M., Panayiotou, A., and Xenophontos, C., Ophiolites—Oceanic Crustal Analogues. Proceedings of the Symposium 'TROODOS 1987,' Cyprus Geological Survey Department, Nicosia, p. 185–206.

Schmincke, H.-U. and Rautenschlein, M.
1987: Volcanology along the Akaki River Canyon; *in* Xenophontos, C., Malpas, J.G., Field Excursion Guidebook. Troodos 87: Ophiolites and Oceanic Lithosphere, Cyprus Geological Survey Department, Nicosia, p. 36–81.

Schmincke, H.-U., Rautenschlein, M., Robinson, P.T., and Mehegan, J.M.
1983: Troodos extrusive series of Cyprus: a comparison with oceanic crust; Geology, v. 11, p. 405–409.

Seyfried Jr., W.E.
1987: Experimental and theoretical constraints on hydrothermal alteration processes at mid-ocean ridges; Annual Review of Earth and Planetary Science, v. 15, p. 317–335.

Seyfried Jr., W.E. and Bischoff, J.L.
1981: Experimental seawater-basalt interaction at 300°C, 500 bars, chemical exchange, secondary mineral formation and implications for the transport of heavy metals; Geochimica et Cosmochimica Acta, v. 45, p. 135–147.

Smith, G.C. and Vine, F.J.
1991: The physical properties of basalts from CCSP Drillholes CY-1 and CY-1A, Akaki Canyon, Cyprus; *in* Gibson, I.L., Malpas, J., and Robinson, P.T. Cyprus Crustal Study Project: Initial Report, Holes CY-1 and 1A, Geological Survey of Canada, Paper 90–20.

Staudigel, H., Hart, S.R., Schmincke, H.-U., and Smith, B.M.
1989: Creataceous ocean crust at DSDP Sites 417 and 418: carbon uptake from weathering versus loss by magmatic outgassing; Geochimica et Cosmochimica Acta, v. 53, p. 3091–3094.

Sunkel, G., Bednarz, U., and Schmincke, H.-U.
1987: The basaltic andesite-andesite and the andesite-dacite series from the ICRDG Drill Holes CY-2 and CY-2A. II. Alteration; *in* Robinson, P.T., Gibson, I.L., and Panayiotou, A., Cyprus Crustal Study Project Initial Report, Holes CY-2 and 2a, Geological Survey of Canada, Paper 85–29, p. 205–219.

Varga, R.J. and Moores, E.M.
1985: Spreading structure of the Troodos ophiolite, Cyprus; Geology, v. 13, p. 846–850.

Wilkens, R.H., Christensen, N.I., and Slater, L.
1983: High-pressure seismic studies of Leg 69 and 70 basalts: *in* Cann, J.R., Langseth, M.G., Honnorez, J., Von Herzen, R.P., White, S.M., et al.; Initial Reports of the Deep Sea Drilling Project, v. 69, U.S. Government Printing Office, Washington, p. 683–686.

Wolery, T.J. and Sleep, N.H.
1976: Hydrothermal circulation and geochemical flux at mid-ocean ridges; Journal of Geology, v. 84, p. 249–275.
Zielinski, R.A.
1982: The mobility of uranium and other elements during alteration of rhyolitic ash to montmorillonite: a case study in the Troublesome formation, Colorado, U.S.A.; Chemical Geology, v. 35, p. 185–204.

Alteration Effects in Pillow Lavas from the CY-1 Drillhole, Upper Volcanic Sequence, Troodos Ophiolite

W.R.A. BARAGAR[1], J.N. LUDDEN,[2] AND F. AUCLAIR[2]

[1]Geological Survey of Canada, Lithosphere and Canadian Shield Division,
588 Booth Street, Ottawa, Ontario, K1A 0E4, Canada
[2]IREM/MERI, Départment de Géologie, Université de Montréal, Montréal, CP 6128 'A,' H3C 3J7, Canada

Baragar, W.R.A., Ludden, J.N., and Auclair, F., 1991: Alteration effects in pillow lavas from the CY-1 drillhole, upper volcanic sequence, Troodos ophiolite; in Cyprus Crustal Study Project: Initial Report, Holes CY-1 and 1A, eds. Gibson, I.L., Malpas, J., Robinson, P.T., and Xenophontos, C.; Geological Survey of Canada, Paper 90–20, p. 117–132, 1991.

Abstract

Rim to core sampling traverses across five pillows taken at successively deeper levels of the CY-1 drillhole have been used to evaluate element mobility and fluid migration within the Upper Pillow Lavas of the ophiolite. Four regimes of alteration can be identified. Two represent pillow rims and interiors respectively of an upper zone that was severely conditioned by reaction with cold circulating seawater. Relative to fresh basalt, pillow interiors are marked by enrichment in K_2O, Fe_2O_3/FeO, Ba, and Sr coupled with depletion in CaO, Na_2O, and to lesser degree SiO_2 and MgO. The rims relative to interiors show increases in Na_2O, iron, Fe_2O_3/FeO, and to minor degree, Cu and Zn, and decreases, generally, in K_2O, Ba, Sr, Y, LREE, and Cr. The alteration diminishes downward. A third regime, immediately below the upper zone, of low-temperature alteration shows impoverishment of the pillow interior in SiO_2 and enrichment in MgO and Na_2O. The rims are glassy. The fourth regime represents long-term fracture and void filling with mainly calcite of seawater provenance. Rim to core compositional differences in upper-zone pillows are variously attributed to different water/rock ratios, oxidation environments, crystallinity, and for Cr, flow differentiation. 'Immobile' elements (e.g. LREE and Y) are variably, but mostly little, leached from 'glassy' rims and interior mesostases, hence, generally retain reliability as petrogenetic indicators.

Résumé

Un échantillonage systématique, de la marge au centre des coussins, a été effectué sur cinq coussins à des profondeurs croissantes du forage CY-1. Ces échantillons ont été utilisé pour évaluer la mobilité des éléments de même que la migration des fluides dans les laves coussineées supérieures de l'ophiolite. On peut y identifier quatre régimes d'altération. Deux de ceux-ci sont représentés par des marges et des cœurs de coussins, respectivement, dans une zone supérieure fortement altérée par une réaction avec l'eau de mer froide et circulant. Par rapport au basalte frais, les cœurs des coussins sont caractérisés par un enrichissement en K_2O, Fe_2O_3/FeO, Ba et Sr aussi bien que un appauvrissement en CaO, en Na_2O et de façon moindre, en SiO_2 et en MgO. Les marges, par rapport aux cœurs accusent des enrichissements en Na_2O, en Fe, en Fe_2O_3/FeO, et de façon moindre, en Cu et en Zn. Ils accusent généralement des appauvrissements en K_2O, en Ba, en Sr, en Y, en ETR légers et en Cr. L'altération décroit vers le bas. Un troisième régime, situé directement sous la zone supérieure, d'altération hydrothermale de faible température cause un appauvrissement en SiO_2 à l'intérieur des coussins et un enrichissement en MgO et en Na_2O. Les marges des laves coussinées dans ce régime sont vitreuses. Le quatrième régime représente un remplissage des fractures et des pores par la calcite provenant surtout de l'eau de mer. Les différences de composition des marges aux centres des coussins de la zone supérieure sont attribuées à des rapports différents eau/roche, à des environnements d'oxidation, à des cristallinités et, pour le Cr, á la différenciation d'écoulement. Les éléments "immobile" (e.g. les ETR légers et le Y) sont généralement peu lessivés des marges vitreuses et des mésostases d'intérieurs, donc sont assez fiables en tant que moniteurs pétrogénétiques.

INTRODUCTION

The CY-1 drillhole of the International Crustal Research Drilling Group's (ICRDG) Cyprus Project is located at the upper contact of the Troodos ophiolite and provides a nearly continuous section of the uppermost 475 m of the ophiolite's volcanic sequence. Thus, it transects much of the 'Upper Pillow Lava' division of the volcanic sequence and the lavas intersected are of the high-MgO/high-SiO_2 suite of Robinson et al. (1983). More importantly, from the point of view of the alteration of oceanic crust, CY-1 passes through the zone of low temperature alteration related to the prolonged circulation of cold seawater (Gillis, 1987). The object of this study is to detail the total effects of sub-seafloor alteration on the compositions of pillows. Assuming that pillows were altered from their rims inward, the present variations in composition across a pillow can be expected to record the gains and losses of elements resulting from the alteration. By systematically analyzing successively deeper pillows we should be able to discriminate between the diminishing influence of cold water circulation from above and the higher temperature effects associated with spreading ridge hydrothermal activity. Five pillows at varying depths between 136 and 347 m were sampled from their lower to upper margins and the samples analyzed for major, trace, and rare earth elements (REE). In proposing to relate changes in composition across a pillow to secondary effects we must make the assumption that the pillows were originally uniform in composition; this may not be strictly true. Staudigel et al. (1979), Staudigel and Bryan (1981), and Flower et al. (1979) have shown that phenocryst concentration in pillow interiors, possibly by flow differentiation, can result in significant primary differences between rim and interior compositions. However, in the five pillows of this study, the phenocryst content is rarely more than 1–2%, so the effect of phenocryst concentration is negligible. Of greater significance are complications imposed by the heterogeneity of alteration effects caused by the irregular distribution of veins, fractures, and porous zones through the individual pillows.

SAMPLING AND ANALYTICAL METHODS

The samples are minicores bored from the main core of CY-1 at intervals through each of the five pillows selected. We attempted to include what had been the glassy rim from both margins, but in most cases it was too friable to be drilled and samples had to be selected instead from whatever broken chips of the rim were available. Nothing remained of the lower rim of pillow 2 and the upper rim of pillow 4, so in these cases samples had to be taken from the area immediately adjoining the rim. Detailed sample descriptions are given in the Appendix.

The major elements were determined in the Geological Survey of Canada laboratories by wave-length dispersion XRF. FeO was analyzed by the Wilson or Pratt methods and CO_2, H_2O and S by infrared spectrometry. Estimated probable error for the major elements in absolute terms are as follows: SiO_2 and Al_2O_3 1.5%, Fe_2O_3, MgO, CaO, TiO_2, P_2O_5 and K_2O 1%, FeO and MnO 2%, Na_2O 2.5%, H_2O and S 5%, CO_2 3% of the amounts present. Trace elements were analyzed at both the Geological Survey of Canada (by optical emission spectrometry with estimated probable error of ±15% of value reported) and at Université de Montréal (by XRF, techniques adapted from Schroeder et al., 1980; estimated probable error 5–10%). The two sets of trace element analyses generally agree and, since the G.S.C. analyses are more complete, they were chosen for the present study. Analyses of samples taken routinely through the length of CY-1 are used in this paper as background data. All such analyses were made in the Geological Survey of Canada Laboratories by the same methods as outlined above.

The REE, Co, Cs, Hf, Sc, Ta, Th, and U were analyzed at the Université de Montréal by instrumental neutron activation techniques. The samples were irradiated in a Slowpoke II reactor for 2 hours at a flux of 10^{12} n/cm/sec. Counting was done over a six month period on a coaxial detector having a 1.2 Kev resolution at 122 Kev and on a planar detector of 0.6 Kev resolution at 122 Kev. The estimated error for La, Sm, Eu, Yb, Sc, and Co is ± 5% and for all other elements between ± 5 to ± 10%.

Electron microprobe analyses were conducted by M. Bonardi in the Geological Survey of Canada laboratories using a Cameca Camebac electron micro-probe equipped with four automated wave-length dispersive spectrometers. The estimated probable error is 1–2%.

CHEMICAL VARIATION WITH DEPTH IN CY-1

The span in composition for the major elements in each of the five pillows plotted against depth in CY-1 is shown in Figures 1 and 2. The average depth of each of the pillows plotted in Figure 1 is as follows: pillow 1 – 136.43, pillow 2 – 152.43, pillow 3 – 167.94, pillow 4 – 292.63, and pillow 5 – 346.38 m (individual sample depths are given in Tables 1 and 2). Also shown are plots of the analyses of samples taken systematically through the drillhole, most of which are from pillow interiors. All the analyses have been recalculated to 100% volatile-free. Of principal interest in Figure 1 is that: (1) generally the variability of compositions in individual pillows exceeds that in the lava succession at the same stratigraphic level and (2) the four uppermost pillows are distributed through the zone of alteration that is obviously attributable to influences from seawater alteration. Demarcation of this zone is evidenced particularly by the decline in K_2O and Fe_2O_3 contents to levels consistent with that of fresh glasses from the same sequence at about 300 to 325 m depth. Pillow 5, which is the only one of the sampled pillows with fresh glassy rims, lies just below this zone of alteration.

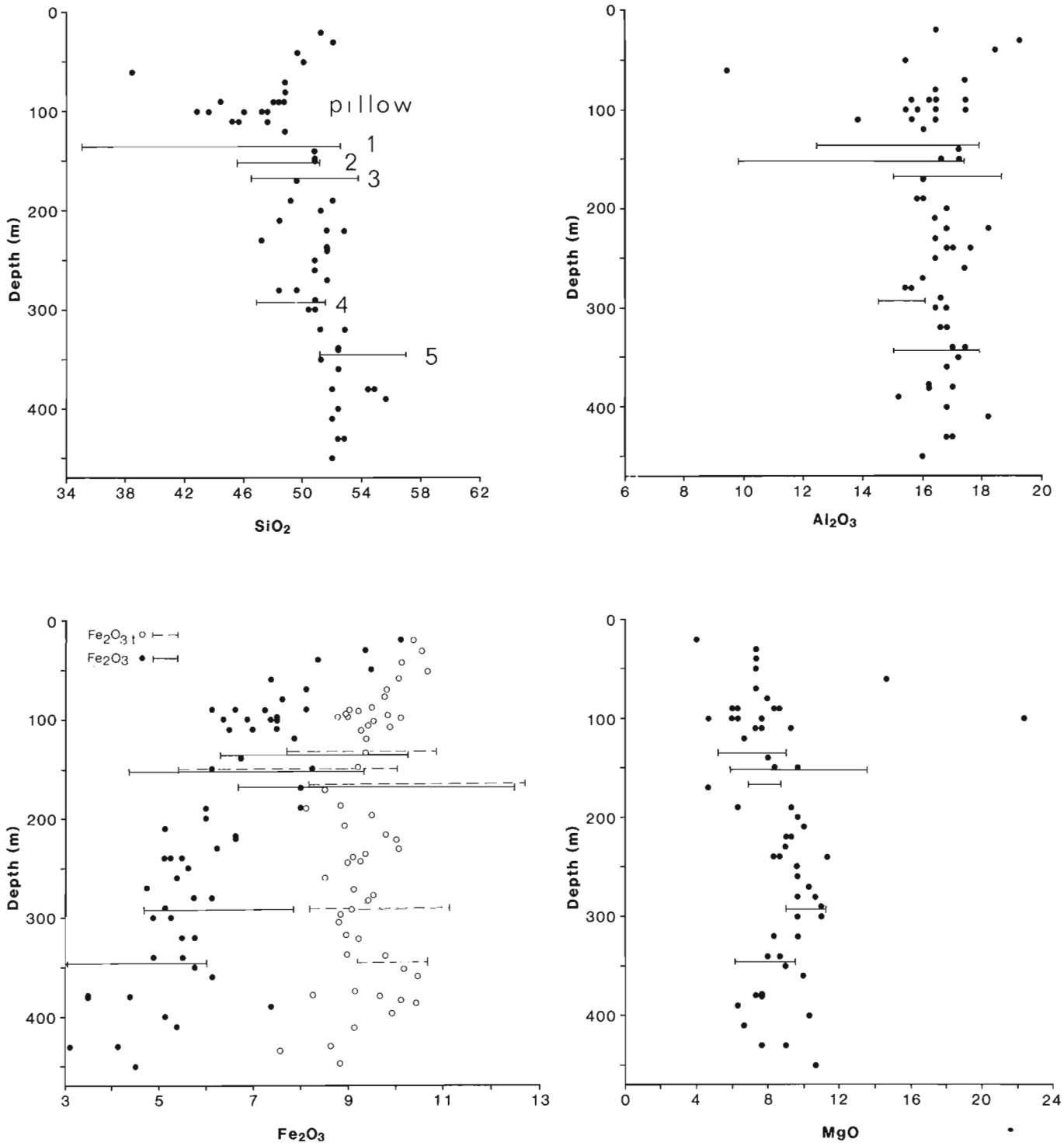

Figure 1: Routine analyses for SiO_2, Al_2O_3, Fe_2O_3, and MgO for the CY–1 drill core plotted against depth. The compositional range of each pillow is shown as a solid or dashed line at the appropriate depth. Analyses all recalculated to 100% and are (H_2O + CO_2 + $CaCO_3$)-free.

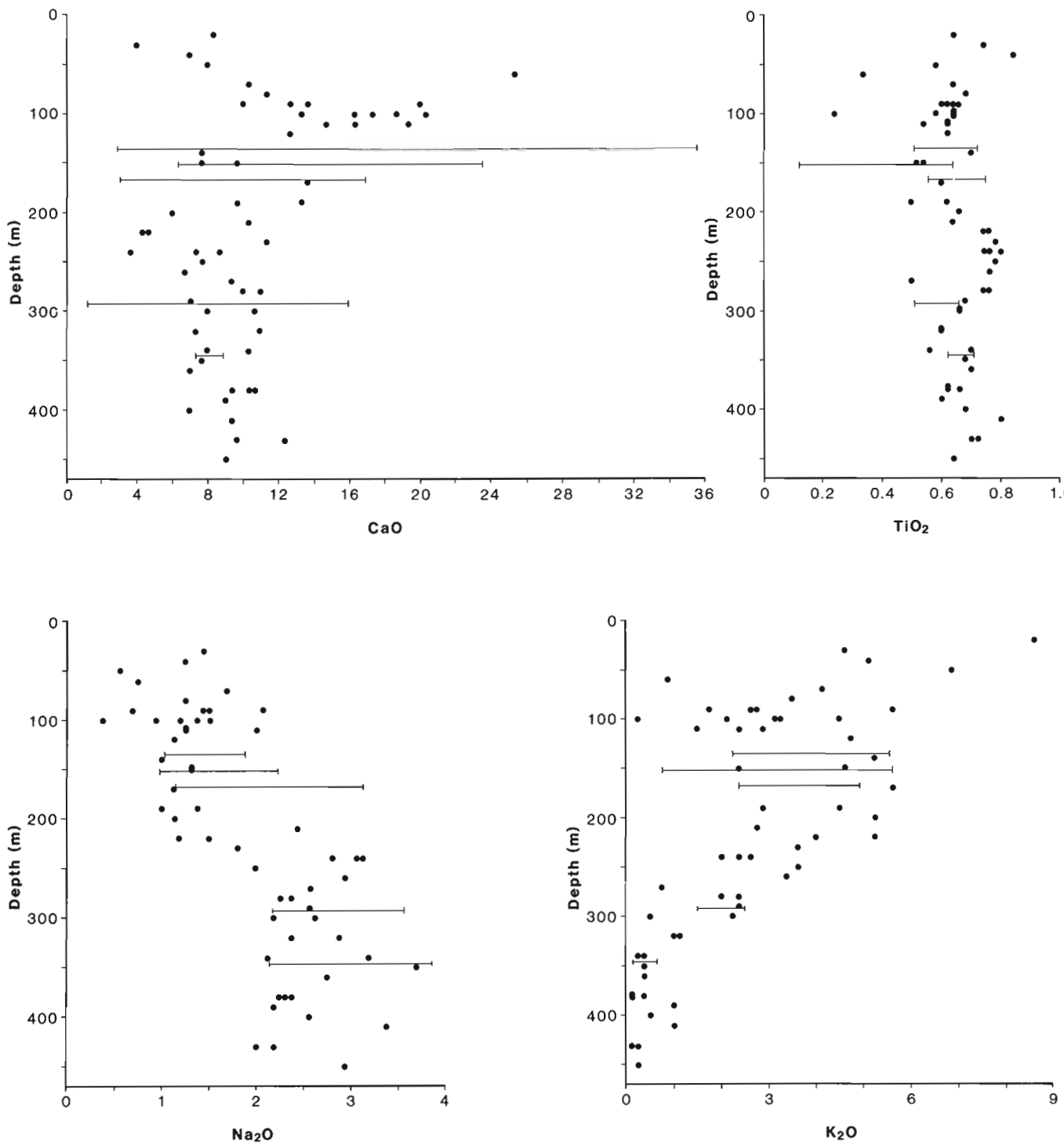

Figure 2: Routine analyses for CaO, TiO_2, Na_2O, and K_2O for the CY–1 drill core plotted against depth. The compositional range of each pillow is shown as a solid or dashed line at the appropriate depth. Analyses all recalculated to 100% and are (H_2O + CO_2 + $CaCO_3$)-free.

	136.08	136.10	136.22	136.37	136.59	136.65	136.72	136.78	151.65	151.71	151.75	152.20	152.45	152.46
SiO_2	51.36	53.05	53.36	53.52	52.84	52.87	52.27	52.20	54.91	52.29	53.54	52.75	52.96	52.11
Al_2O_3	18.27	17.83	18.46	18.25	17.73	18.07	17.64	17.25	11.84	15.97	16.47	18.27	16.70	16.89
Fe_2O_3	10.10	7.50	6.95	6.68	7.16	7.30	7.32	11.94	5.26	7.72	7.04	6.09	7.30	7.15
FeO	1.07	2.39	2.02	2.22	2.35	2.36	2.09	.59	1.15	2.26	2.60	2.76	2.74	2.60
MgO	7.61	9.16	7.30	7.63	8.16	8.63	8.89	7.83	16.31	6.79	7.42	8.48	8.37	8.30
CaO	5.63	2.92	3.57	3.12	3.30	3.13	3.72	4.01	7.50	6.54	5.22	5.56	6.26	6.25
Na_2O	1.50	1.30	1.77	1.78	1.53	1.70	1.62	1.48	1.48	2.00	1.95	1.72	1.04	2.08
K_2O	3.24	4.87	5.50	5.79	5.80	5.41	5.30	3.48	.92	5.51	4.80	3.50	3.78	3.79
TiO_2	.75	.73	.72	.73	.74	.73	.71	.66	.15	.53	.56	.56	.53	.52
MnO	.19	.15	.15	.13	.15	.16	.16	.15	.26	.16	.11	.14	.16	.16
P_2O_5	.06	.04	.11	.06	.16	.15	.09	.06	.05	.11	.10	.07	.06	.05
S	.19	.04	.08	.09	.08	.08	.12	.21	.16	.13	.17	.08	.08	.09
Sr	131.	78.	140.	124.	122.	109.	115.	66.	84.	128.	106.	108.	124.	116.
Ba	64.	76.	101.	67.	94.	90.	78.	44.	33.	93.	87.	92.	91.	91.
Rb	84.	47.	53.	55.	50.	47.	51.	81.	21.	44.	36.	32.	40.	35.
Zr	52.	41.	44.	46.	47.	47.	44.	41.	13.	25.	31.	32.	30.	27.
Y	32.	16.	25.	21.	32.	29.	26.	18.	21.	23.	18.	16.	25.	23.
Cu	200.	79.	83.	96.	82.	85.	91.	153.	182.	57.	44.	46.	55.	55.
Co	47.	52.	39.	39.	48.	58.	47.	50.	56.	43.	42.	39.	40.	39.
Cr	58.	101.	94.	110.	89.	106.	89.	80.	44.	214.	286.			
Ni	99.	55.	49.	53.	43.	46.	51.	100.	66.	52.	55.	55.	73.	73.
Zn	123.	83.	73.	80.	80.	79.	81.	121.	64.	69.	72.	80.	85.	84.
	152.76	152.96	153.20	153.21	167.45	167.51	167.60	167.70	167.89	168.03	168.23	168.36	168.36	168.41
SiO_2	52.74	53.39	52.78	52.66	50.97	53.81	53.11	54.03	51.88	52.55	54.20	52.19	51.56	52.81
Al_2O_3	15.59	17.22	17.15	17.17	18.16	17.22	16.63	16.68	16.78	16.60	16.15	16.87	18.74	17.56
Fe_2O_3	7.14	8.04	9.90	9.48	9.43	7.32	7.00	7.00	8.00	8.36	7.23	10.53	8.15	11.95
FeO	1.69	1.72	.66	.90	.84	1.29	1.38	1.40	1.29	1.19	1.35	1.02	1.40	.36
MgO	6.60	7.20	7.80	7.73	7.79	7.23	7.42	7.67	7.98	7.83	7.66	7.63	8.84	6.90
CaO	6.40	5.52	5.83	5.75	6.71	5.73	6.22	5.84	7.03	6.48	6.07	5.95	5.87	3.12
Na_2O	2.34	2.30	2.11	2.56	2.53	1.94	2.29	1.51	1.42	1.79	1.58	2.04	2.33	3.23
K_2O	6.56	3.60	2.86	2.87	2.56	4.53	5.08	5.00	4.53	4.23	4.76	2.86	2.10	3.19
Ti_2	.58	.67	.66	.67	.70	.67	.61	.62	.63	.62	.62	.60	.76	.60
MnO	.13	.10	.13	.13	.15	.07	.10	.07	.17	.10	.10	.12	.12	.10
P_2O_5	.16	.14	.07	.03	.03	.12	.07	.09	.13	.13	.07	.06	.03	.01
S	.10	.09	.05	.06	.10	.07	.08	.07	.15	.11	.21	.12	.12	.18
	152.76	152.96	153.20	153.21	167.45	167.51	167.60	167.70	167.89	168.03	168.23	168.36	168.36	168.41
Sr	109.	106.	57.	54.	76.	100.	104.	96.	125.	117.	100.	82.	63.	41.
Ba	78.	57.	53.	26.	84.	65.	80.	75.	77.	96.	102.	68.	58.	60.
Rb	53.	37.	63.	59.	54.	47.	52.	43.	39.	39.	0.	44.	0.	0.
Zr	38.	39.	41.	40.	46.	41.	39.	38.	41.	39.	42.	36.	45.	38.
Y	25.	22.	20.	17.	21.	23.	24.	17.	30.	25.	19.	11.	15.	7.
Cu	64.	59.	110.	108.	108.	55.	64.	73.	93.	55.	71.	117.	90.	91.
Co	35.	30.	45.	42.	38.	34.	30.	30.	34.	31.	37.	42.	43.	49.
Cr					390.	421.	391.	435.	281.	371.	381.	343.	455.	145.
Ni	62.	56.	100.	99.	84.	66.	71.	70.	66.	68.	73.	79.	91.	99.
Zn	51.	67.	92.	88.	82.	62.	70.	68.	72.	72.	78.	91.	79.	111.

Table 1: Analyses recalculated to 100% H_2O–CO_2–$CaCO_3$ free. The procedure is as follows: The projected base levels of CaO in each pillow (i.e. the intercept value on the zero CO_2 axis of Figure 3) is assumed to be the CaO content of the pillow prior to carbonate introduction. Hence, using this base level of CaO the analysis is summed without volatiles and recalculated to 100%. The raw data set can be obtained from the authors.

	168.42	291.95	292.55	293.02	293.22	293.31	345.86	345.98	346.12	346.49	346.69	346.85	346.90	346.91
SiO_2	53.53	52.36	52.97	52.73	52.97	56.06	57.05	52.75	51.93	51.79	51.68	52.66	55.19	55.15
Al_2O_3	17.00	16.71	16.42	16.44	16.54	15.73	15.03	16.32	16.87	16.73	17.94	16.58	15.30	15.87
Fe_2O_3	12.45	5.65	5.30	5.67	5.94	8.88	4.57	5.52	6.06	5.82	4.77	5.17	3.63	3.02
FeO	.24	3.76	3.58	3.63	3.36	2.04	5.56	4.11	4.22	4.10	4.03	3.98	6.21	6.48
MgO	7.05	11.88	10.21	11.10	10.34	9.63	6.46	8.52	8.23	8.39	7.62	8.57	6.61	6.10
CaO	3.27	4.37	4.98	4.18	4.78	1.16	7.32	8.26	8.47	8.88	8.87	8.32	8.91	8.82
Na_2O	2.40	2.59	3.05	2.61	2.58	3.60	2.28	3.14	2.92	3.02	3.71	3.34	2.56	2.91
K_2O	3.21	1.60	2.30	2.56	2.29	1.98	.69	.26	.20	.17	.28	.25	.46	.51
TiO_2	.61	.69	.69	.68	.70	.52	.62	.69	.70	.71	.70	.69	.66	.66
MnO	.10	.14	.21	.15	.15	.13	.16	.11	.11	.11	.10	.11	.19	.18
P_2O_5	.02	.09	.09	.07	.09	.02	.04	.08	.06	.05	.06	.09	.04	.04
S	.12	.14	.20	.18	.26	.24	.22	.24	.23	.23	.23	.24	.24	.26
	168.42	291.95	292.55	293.02	293.22	293.31	345.86	345.98	346.12	346.49	346.69	346.85	346.90	346.91
Sr	47.	89.	121.	104.	107.	35.	75.	103.	107.	103.	115.	109.	111.	119.
Ba	48.	35.	66.	57.	52.	48.	44.	43.	54.	54.	42.	32.	53.	65.
Rb	0.	0.	0.	0.	0.	0.	0.	0.	0.	0.	0.	0.	0.	0.
Zr	41.	42.	45.	42.	44.	37.	37.	39.	42.	43.	44.	46.	43.	45.
Y	7.	25.	24.	20.	26.	8.	15.	18.	21.	21.	22.	29.	22.	25.
Cu	92.	73.	53.	42.	48.	226.	124.	94.	75.	73.	76.	89.	92.	95.
Co	54.	45.	40.	41.	36.	46.	34.	45.	43.	42.	38.	43.	39.	39.
Cr	148.	225.	207.	249.	238.	139.	86.	93.	89.	93.	99.	90.	73.	82.
Ni	99.	39.	38.	42.	39.	55.	25.	35.	32.	32.	32.	36.	27.	30.
Zn	111.	79.	79.	74.	72.	90.	76.	94.	91.	91.	86.	93.	91.	92.

Table 2: Analyses recalculated to 100% H_2O–CO_2–$CaCO_3$ free. The procedure is as follows: The projected base levels of CaO in each pillow (i.e. the intercept value on the zero CO_2 axis of Figure 3) is assumed to be the CaO content of the pillow prior to carbonate introduction. Hence, using this base level of CaO the analysis is summed without volatiles and recalculated to 100%. The raw data set can be obtained from the authors.

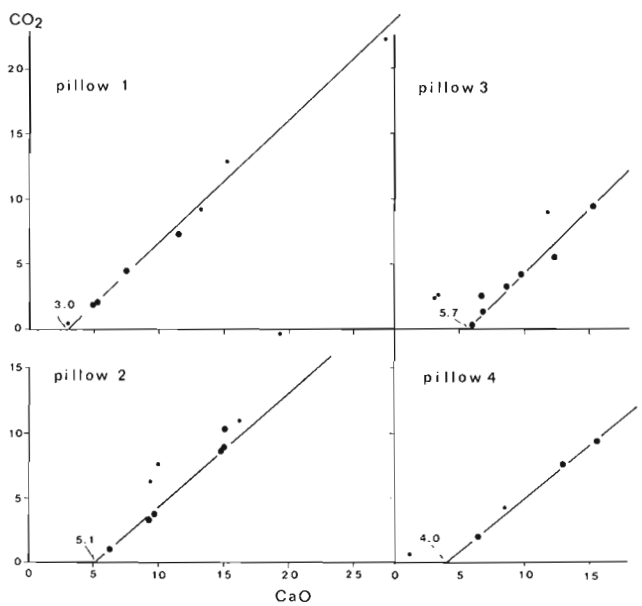

Figure 3: CaO vs. CO_2 for each of pillows 1 to 4. Small circles are marginal or near marginal samples; large circles are interior samples. Trend lines based on interior samples project to values indicated on the plot at 0% CO_2. These are interpreted as the CaO content of the pillow prior to the late phase of carbonate deposition.

This uppermost zone of alteration, termed the Seafloor Weathering Zone (SWZ) by Gillis and Robinson (1988), has been interpreted as the result of prolonged exposure of basalt to circulating cold seawater (Gillis, 1987). Such a process might occur on a topographic high without protective sediment covering. Where the lava sequence is overlain by umbers the SWZ is very thin or lacking (Gillis, 1987). In both cases this zone grades laterally and downward into a zone of variable intensity of alteration termed by Gillis and Robinson the Low Temperature Zone (LTZ). In this zone the development of secondary minerals tends to be controlled by the porosity of the rock. Pillow 5 and the lower part of the CY-1 drillhole are in the LTZ.

PETROGRAPHY

According to Robinson et al. (1983), basalt and basaltic andesite from the upper part of the volcanic sequence are typically olivine- and clinopyroxene-phyric. Rarely did they find plagioclase present as a phenocryst phase and then only in intergrowths with clinopyroxene. The five pillows sampled contain <2% phenocrysts and only pillow 2 is olivine-phyric. The others are either plagioclase/clinopyroxene- or clinopyroxene-phyric, yet chemically all pillows belong to the high-MgO/high-SiO_2 suite of Robinson et al. (1983).

The groundmass comprises principally plagioclase, clinopyroxene, and glassy mesostasis in various proportions, depending on the degree of crystallinity. Although best developed in pillow centres, the crystallinity is rarely well developed and as much as 30% mesostasis is common in the pillow interiors. Iron oxide is present only as intermittent particles or as secondary phases in the mesostasis. Vesicles range in abundance from 5 to 25% through various parts of the pillows and from pillow to pillow. They are empty or variously filled with carbonate, smectite, and magma residue (segregation vesicles).

VERTICAL COMPOSITIONAL PROFILES OF THE PILLOWS

Introduction

The considerable variation in the content of secondary diluents (notably H_2O and CO_2) within individual pillows requires some means of restoring the analyses to a diluent-free basis so that compositions of the less mobile elements can be compared on the same basis. Recalculating the analyses to 100% volatile-free (i.e. H_2O + CO_2-free) does not address the fact that most of the CO_2 is present as calcite in veins and vesicles and must surely have been added as such. Hence, the CaO equivalent of the CO_2 should be removed in addition to H_2O. The adjusted analyses are given in Tables 1 and 2 and the procedure of adjustment is given in the captions. The unadjusted data are available on request from the authors.

The relations between CaO and CO_2 in each of pillows 1 to 4 are illustrated in Figure 3. Pillow 5 has a negligible CO_2 content and no adjustment for carbonate is necessary. In pillows 1 to 4, CaO and CO_2 show excellent co-variation above some minimum level of CaO which can be interpreted as marking the content in the rock prior to the introduction of calcite. We note, however, that the content ranges from 3 to 5.7%, considerably lower than the CaO level typical of the high-MgO/high-SiO_2 suite. Robinson et al. (1983) report CaO contents in glasses of this suite as ranging between about 8 and 12% and that of the glassy rim of pillow 5 (Tables 1 and 2) is 9.6%. As noted earlier the calcite veins and vesicle fillings appear to post-date the major alterations that permeate these rocks (see also Gillis, 1987). Hence, the comparatively low CaO content remaining in pillows 1 to 4 after CO_2 has been reduced to zero (Figure 3) may represent the depleted levels of lime that existed in these rocks after the bulk of the alteration had taken place. Although the major phase of alteration is believed to follow closely the formation of the crust at a spreading ridge, cross-cutting vein material may be emplaced as much as 15–20 Ma later (Staudigel and Hart, 1985; Staudigel et al., 1986).

Results

Chemical variations through pillows 1 to 5 are shown in the profiles of Figures 4a (major elements) and 4b (trace elements). The heavy lines in Figure 4a represent the analyses recalculated to 100% water- and calcite-free according to the method outlined in the captions to Tables 1 and 2, whereas the light lines are plotted from the original data. For the trace elements (Figure 4b), only the recalculated data are plotted. For purposes of comparison the range of analyses from glasses of the same suite are shown by the columns between pillows 1 and 2, and 4 and 5. The major elements are from Robinson et al. (1983) and the trace elements from Rautenschlien et al. (1985) and Rautenschlein (1987).

Pillow 5 seems to be comparable in geochemistry to the fresh glass and is therefore below the influence of the alteration system affecting pillows 1 to 4. It is reasonable to conclude that compositions of pillows 1 to 4 were modified by the effects of prolonged exposure to cold circulating seawater from above.

From Figures 1, 2 and 4 taken together, changes attributable to the alteration are interpreted to be as follows:

- The enrichment in K_2O, Ba and Sr declines systematically with depth; generally pillow margins are less enriched than the interiors;
- The oxidation of iron decreases with depth and consistently increases at pillow margins with respect to cores;
- The content of iron also increases (with the exception of pillow 2) at the pillow margins;
- Although less systematic, Na_2O increases downward and has a tendency towards enrichment at pillow rims;
- SiO_2 shows a slight general increase in composition downward but no systematic change at the pillow margins;
- MgO, TiO_2, and Al_2O_3 are all variably enriched or depleted at pillow rims, although MgO, except for pillow 2, seems to be generally depleted at the margins. MgO may on average increase slightly downward to pillow 4 (Figures 1 and 2) but neither Al_2O_3 nor TiO_2 show any systematic variation with depth;
- CaO was not plotted in profile in pillows 1 to 4 since it was a factor in reducing the other analyses to a volatile- and carbonate-free base (see caption to Table 1). However, from Figure 3 it is apparent that the carbonate- free values of CaO in each of pillows 1 to 4, as noted earlier, are well below fresh rock values and considerable CaO must have been lost prior to the introduction of carbonate. Also, the increasing base-level CaO content from pillows 1 to 3 may be indicative of its generally systematic depletion upward in the sequence. Note in Figure 3 that the rims tend to be more depleted in CaO than the

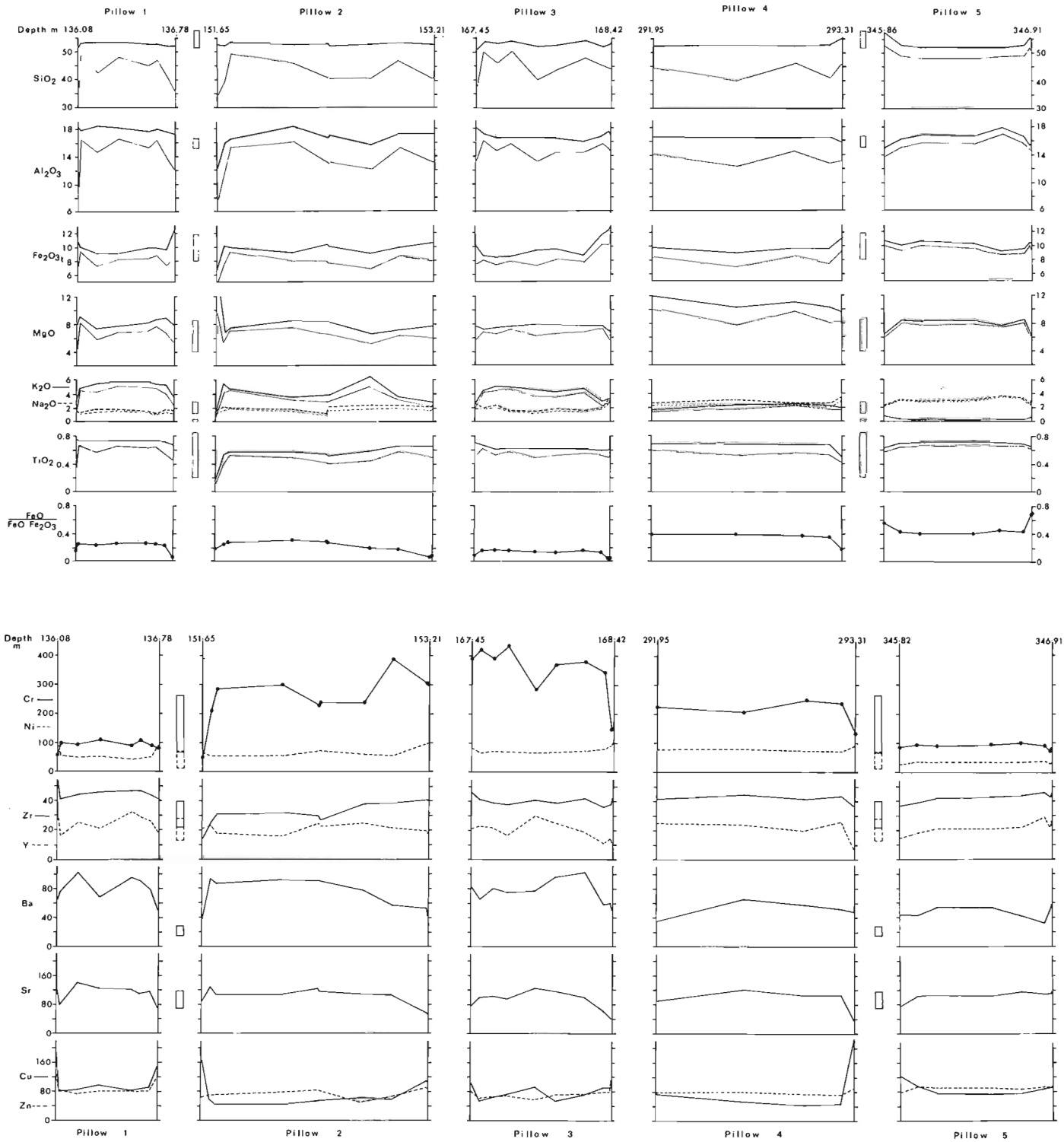

Figure 4: Compositional profiles across pillows 1 to 5: a Major elements; b Trace elements. Note that for pillows 2 and 4 the lower and upper rims respectively are absent and the end of the profile in each case is represented by a near rim specimen only. This undoubtedly accounts for the asymmetry of these profiles. Columnar boxes opposite each profile between pillows 1 and 2 and again between pillows 4 and 5 represent the range of compositions of glasses from the high MgO-high SiO_2 suite analyses by Robinson et al., 1983 and by Rautenschlein (1987) and Rautenschlein et al. (1985). Analyses recalculated to 100% $H_2O + CO_2 + CaCO_3$–free (Tables 1 and 2).

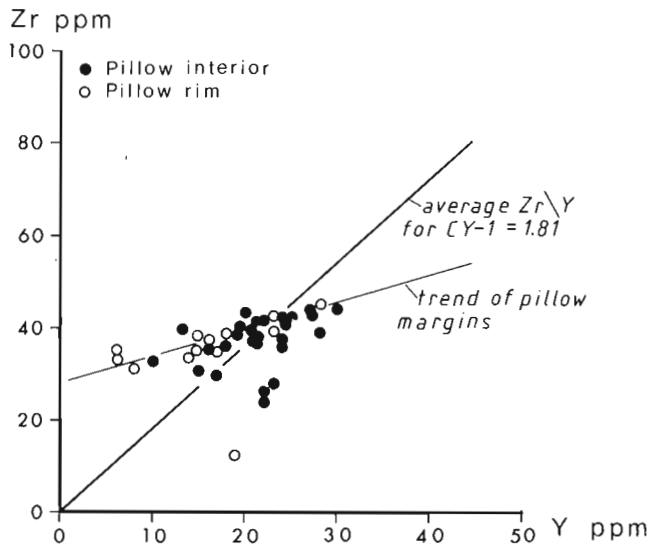

Figure 5: Zr vs. Y plot of pillows 1 to 5. Rim and near rim samples are marked by open circles, interior samples by closed circles. The trend of the marginal samples differs markedly from that of the routinely-taken CY-1 samples which define an average Zr/Y ratio for the succession of 1.81. The marginal samples are interpreted as having lost Y relative to Zr in comparison with the interior samples and the routinely-taken samples.

	La	Ce	Nd	Sm	Eu	Tb	Ho	Yb	Lu
Pillow 1									
M-136.1	1.41	4.02	3.15	1.65	.58	.35	.7	1.48	.24
C-136.37	1.56	4.12	2.78	1.67	.6	.47	nd	1.56	.19
C-136.59	1.47	4.11	4.93	2.23	.8	.61	1.03	2.47	.32
M-136.78	.88	2.21	2.21	1.18	.49	.29	.62	2.26	.29
Pillow 2									
C-152.54	1.46	3.32	2.66	1.54	.56	.39	.86	2.09	.37
C-152.76	2.13	2.00	4.40	1.72	.68	.47	.89	2.33	.36
M-152.96	1.84	6.32	3.33	1.44	.71	.61	.63	1.41	.31
Pillow 3									
M-167.45	1.02	2.18	2.18	1.18	.52	.36	nd	2.18	.39
C-167.70	1.41	3.89	3.14	1.14	.55	.45	nd	1.62	.23
C-167.89	2.21	5.85	2.99	.96	.73	.64	nd	2.7	.49
M-168.41	.36	1.91	.36	.32	.19	nd	nd	1.19	.13
Pillow 4									
M-291.95	1.28	3.72	4.07	2.02	.73	.49	.91	1.74	.29
C-293.02	1.23	1.79	3.14	1.55	.59	nd	.66	1.59	.28
M-293.31	.3	.55		.26	.19	.1	.2	1.1	.24
Pillow 5									
C-346.49	1.3	2.81	3.68	1.6	.52	nd	.7	1.62	.28
M-346.90	1.07	2.68	2.25	1.39	.52	nd	.57	2.03	.31

Table 3: Rare earth analyses (ppm) of pillow samples from the CY-1 drillhole. Data are normalized as described in Tables 1 and 2. The raw data set can be obtained from the authors.

interiors of pillows; in pillows 2 and 4 in particular, the margin and near margin samples plot on the low CaO side of the trend line;

- Cr is markedly depleted in the pillow margins whereas Ni is slightly enriched with the degree of enrichment seemingly declining downward;
- Cu and Zn are both enriched at the margins of pillows.
- Zr and Y show variable patterns but, as illustrated in the Zr-Y plot of Figure 5, the marginal samples tend to be preferentially depleted in Y relative to Zr. This is evident in the trend line along which most of the rim samples lie and which intersects the Zr axis at about 29 ppm. Compare this with the average trend line for the routinely taken samples of CY-1 (not plotted in Figure 5) which passes through the zero point of the plot and defines a Zr/Y ratio of 1.81.

Sixteen of the samples were analyzed for REE. These data were normalized in the same fashion as the major and trace elements, and the normalized data are presented in Table 3. Where enough material was available the margins were analyzed; these are represented as (C)-core or (M)-margin in chondrite-normalized diagrams in Figure 6.

Analyses of four glass samples from surface exposures of the Upper Pillow Lavas are given as a comparison in Figure 6. These glasses are characterized by light-REE depleted profiles, with flat heavy-REE at 5–10 times chondrites, and small negative Eu anomalies in the most evolved glasses (e.g. TR-1b). A characteristic of the Troodos Upper Pillow Lava is the slight enrichment of La over Ce - Nd, resulting in a concave REE profile from La - Sm. This must represent a primary characteristic of the source region of these lavas and may reflect LIL-element enrichment of a strongly light-REE depleted (La/Sm 0.2–0.3) peridotite source (Thy et al., 1985, Auclair and Ludden, 1987).

Correlating REE abundance with MgO and Zr, a reasonable approximation of the abundances of the fresh pillows in CY-1 would be those of Tr-12. The abundances of pillow 5 are comparable to those of Tr-12, and given the analytical uncertainty in these REE-poor samples, the variation in pillow 5 reasonably approximates the total analytical error.

The margins can be visually normalized relative to the cores in the figure and all samples can be compared with pillow 5 or Tr-12. Generally it is only the highly altered margin samples that show extreme REE mobility. However, if the normalization for H_2O and CO_2 has successfully eliminated dilution effects due to vesicle and fracture filling by REE-poor solutions, the overall decrease in total-REE for pillows 1 to 3 (Table 3) may reflect REE leaching associated with reaction with seawater. Given the fairly high proportion of an originally glassy mesostasis in these pillows relative to such phases as clinopyroxene, which would be expected to represent the major REE reservoir in a crystalline basaltic rock, much of

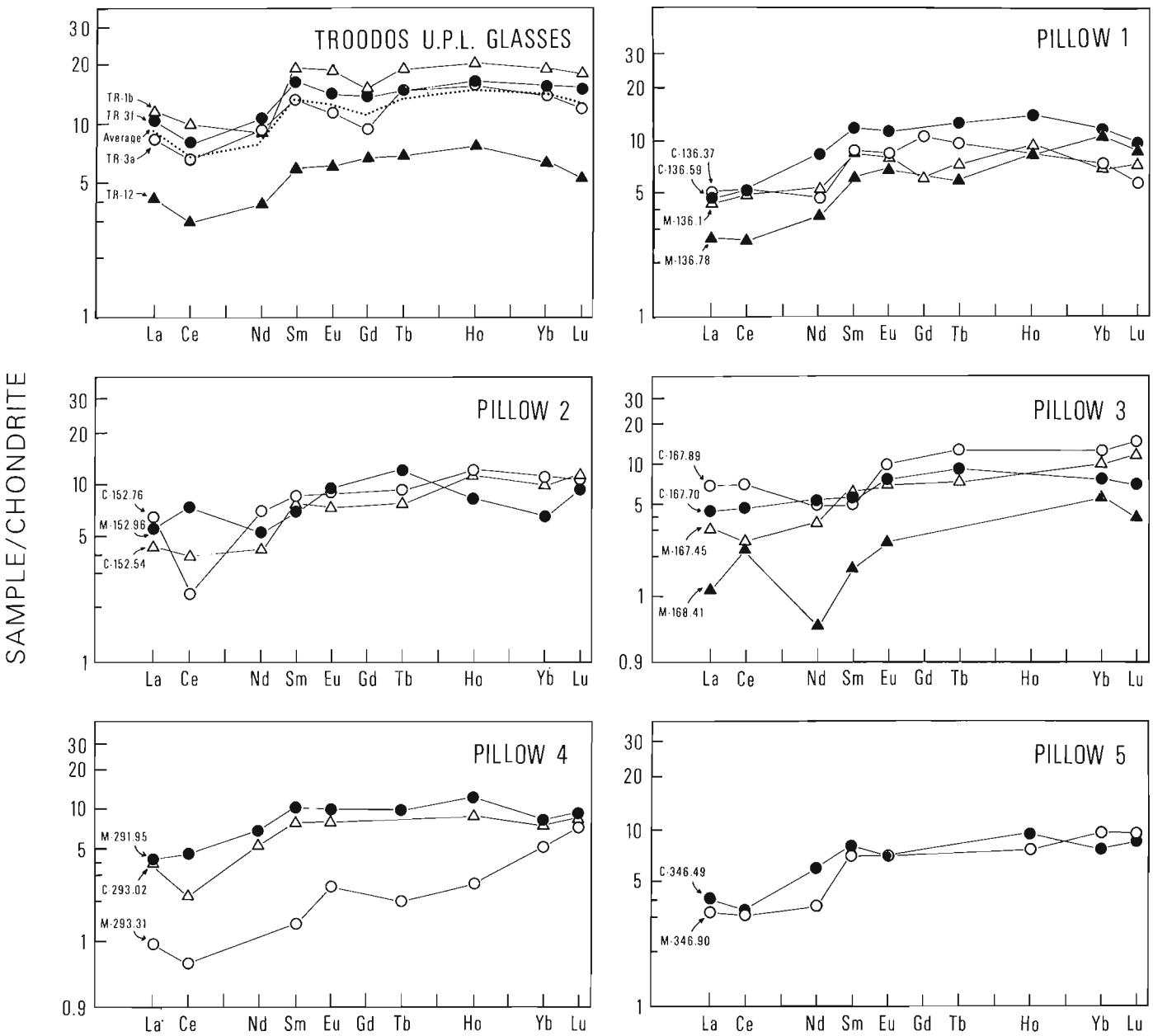

Figure 6: Chondrite normalized REE plots of the CO_2 and H_2O normalized data. The fresh glass analyses are taken from Auclair and Ludden (1987). The primary composition of these pillow lavas is approximately that of TR-12 and pillow 5. The difference in the two analyses presented for pillow 5 approximates the analytical error. Anomalies in samples with 1 to 2 times chondritic abundances have been reevaluated by repeat spectral analyses, but must be interpreted with caution.

the REEs are expected to be located in the glass. The rapid breakdown of this glass during seawater alteration would release REE and may account for significant differences in the mobility of REE and other trace elements in basalt of differing states of crystallinity (Humphries, 1984). The REE may reprecipitate in smectite veins or may be lost to the fluid. Similar arguments may be invoked for the preferential leaching of Y over Zr.

In the altered margins it appears that the light-REE are leached preferentially to the heavy-REE. This would be consistent with their relative ionic radii where the smaller heavy-REE might be expected to be more tightly bound in the glass, resulting in preferential leaching of the light-REE. The pillow margins are also leached of K_2O (Figure 4a). Possibly this event is responsible for the leaching of the light-REE. Both positive and negative Ce anomalies are observed (pillows 3 and 2 and 4 respectively). One must be prudent in interpreting these data given the precision of Ce analyses by INAA at 1–2 ppm. Nonetheless, careful examination of the spectra indicate that these anomalies are probably real and may reflect a seawater signature on the one hand (Ludden and Thompson, 1979), and incorporation of Ce by metalliferous enrichments at the pillow margin on the other. The higher total iron, Ni, and Zn contents of marginal sample M-168.41 is supportive of the latter process.

The fresh glassy margins and unaltered primary minerals of pillow 5 would seem to indicate that it has undergone very little alteration. Yet its compositional profiles are difficult to explain by primary processes alone. The compositional profiles are shown in Figure 4 and for the major elements again in Figure 7 where they are compared with microprobe analyses of glass of the lower rim and of the smectite blebs of the interior.

For a number of the elements the profiles in pillow 5 are remarkably symmetrical and signify systematic differences in composition between rims and interior of pillow 5. Assuming the rims represent the lava composition the interior has been depleted in SiO_2 and enriched in Al_2O_3, MgO, TiO_2, and moderately enriched in Na_2O. For the trace elements we do not have the pure glass analysis for comparison, but from the shape of the profiles (Figure 4b) we can judge that the interior has been slightly enriched in Cr and depleted in Mn and Cu. The interior is more oxidized than the rims, but is still less oxidized than that of any of the four pillows in the sequence above.

Note that the microprobe and XRF analyses of the lower rim are significantly different for CaO and Fe_2O_3 (total). Minor differences might be expected between the glass alone and the whole rock sample because of the minor palagonitization which would have been included in the latter. The slight increase in K_2O at the margins is probably attributable to this effect. However the larger differences are most likely due to differences in the analytical methods. If so a better comparison of these elements between the glass of the lower rim and pillow interior would be given by the short dashed lines in the CaO and Fe_2O_3 (total) profiles of Figure 7 which assume coincidence of the whole rock and glass compositions.

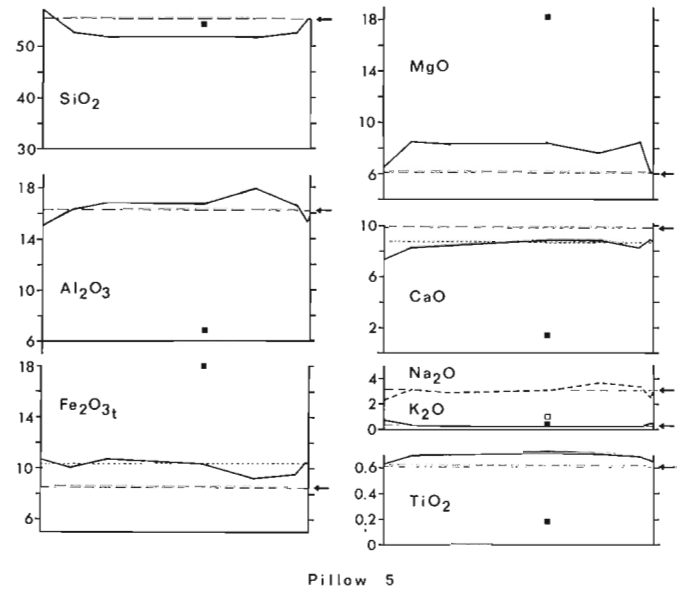

Figure 7: Compositional profiles of pillow 5 showing, in addition, the average microprobe analysis of glass at the lower rim (arrow and broad dashed line) and of the groundmass smectite blebs in one of the interior samples (solid square). Probably the differences in lower rim compositions between the microprobe and XRF analyses are largely due to differences in analytical methods. If so, the short dashed line, which assumes their equivalence for these elements, is a better basis of comparison between the glass and profile. Analyses recalculated to 100% $H_2O + CO_2 + CaCO_3$-free.

DISCUSSION

Compositional variation within both the upper part of the lava sequence and individual pillows distributed through it can be interpreted in terms of four regimes of alteration which involve respectively: (1) the rims of pillows 1 to 4; (2) the interiors of pillows 1 to 4; (3) pillow 5; (4) late open-space fillings. The first two regimes are within a zone severely and pervasively conditioned by reaction with circulating seawater but the third is just below this zone in a region of fairly uniform composition and little apparent alteration. The fourth regime postdates the others and can be interpreted as the long-term filling of voids by cold groundwaters of oceanic provenance. Gillis (1987) subdivided the alteration of the Troodos lava sequence into four chronological stages of which the first three were continuous and the fourth distinctly later. The regimes of this study are not chronological and not equivalent to Gillis' stages. However, parts of her third stage (calcite deposition in voids) and fourth stage (late calcite, palygorskite, and gypsum veins) may be represented here by the fourth regime.

The significance of the four regimes is interpretable in terms of a spreading environment by relation to the model of Gillis and Robinson (1988). In this model the upper part of the oceanic crust responds to the spreading centre thermal regime with development of four successively deeper zones; the SWZ and LTZ already noted, the Transitional Zone (TZ), and the Upper Dyke Zone (UDZ). They result from a stepped geothermal gradient that rises sharply at the TZ: above this zone, the permeable, mainly pillow lavas are effectively cooled (<50–100°C) by vigorous circulation of seawater; below in the less permeable dykes and lavas, an impeded circulation and restricted water content permits higher temperatures to be attained (>200°C). The SWZ, resulting from continuing reaction with cold oxygenated seawater, migrates downward with crustal aging.

Regimes 1 and 2 are within the SWZ, and Regime 3 in the LTZ of Gillis and Robertson (1988). The method of recalculating the analyses to 100% without H_2O, CO_2, $CaCO_3$, (caption Table 1) essentially removes the effects of the fourth regime. Hence, the compositional profiles of Figures 4 and 7 reflect mainly the effects of the first three regimes.

The compositional differences between the rims and the cores of pillows 1 to 4 may be attributed to contemporaneous but distinct alteration environments, to successively imposed environments, or to both. Generally the differences are attributed to the differences in water/rock ratios between margins and cores arising from the greater permeability at the margins (e.g. Spooner et al., 1977; Humphries and Thompson, 1978; Seyfried et al., 1978). However, other factors may include the greater reactivity of the glassy rim in comparison with the crystalline interior (Seyfried and Bischoff, 1979; Seyfried and Mottl, 1982; Seyfried, 1987) and the greater potential for oxidation at the rim where oxygen-bearing seawater is more accessible (Spooner et al., 1977; Seyfried, 1987).

Gross changes in composition of the upper four pillows as manifested by their interiors, are principally as follows (Figure 1, Figure 4): enrichment in K_2O, Ba and Sr; depletion in CaO, Na_2O, and to a lesser degree SiO_2 and MgO; and increased oxidation of iron. These are all changes that diminish with depth in the sequence and are obviously related to the influence of downward moving seawater. Changes of a similar nature were reported by Thompson (1973) and related by him to seafloor weathering as opposed to hydrothermal activity. Even in very low temperature hydrothermal alteration (less than 70°C) the principal effect on basalt is a marked increase in MgO and reduction in CaO (Seyfried and Bischoff, 1977, 1979). That is very different from seafloor weathering, where MgO is typically depleted. Seyfried and Bischoff (1979) attribute the difference, in the case of seafloor weathering, to the availability of a vast body of seawater which buffers the pH at a level below that at which appropriate clay minerals can form at seabottom temperatures. Thus, CaO, Na_2O, MgO, MnO, and SiO_2 could all be leached directly from basalt by seawater under conditions of seafloor weathering (Seyfried and Bischoff, 1979). Similar conditions can probably be extended to the very permeable upper few hundred metres of ocean crust where it is not protected by sedimentary cover and is, therefore, subject to unimpeded access by seawater. Just such a case exists at the site of CY-1. Hall et al. (1987) have shown that the absence of impermeable sedimentary units overlying the lava sequence at this site exposed the lava surface to seawater penetration for at least 25 Ma. At low temperatures seawater invariably loses its K_2O (and probably Ba) to any basalt with which it is in contact, whereas at higher temperatures (about 150°C) the flux reverses and basalt loses K_2O to seawater (Seyfried and Bischoff, 1979). Hence, the enrichments of K_2O and Ba, the depletion of CaO, Na_2O, MgO, and SiO_2, and the oxidation of iron in the upper 300 m of the volcanic sequence can all be related to the convective circulation of cold seawater. Since Sr does not correlate with CO_2 it is unlikely to be related to the late regime of carbonate void filling; therefore, it too probably owes its current distribution to a prolonged regime of seawater convection.

At least some of the compositional differences between pillow rims and interiors are attributable to the higher water/rock ratios which must generally have existed at the pillow rims during seawater circulation. CaO, and where applicable MgO, depletions at the pillow rims would be consistent with their tendency to be leached by cold seawater and to its probable greater flux there. Similarly the enhanced oxidation of iron at pillow margins must relate to the better accessibility along margins of oxygenated seawater. By precipitation of hydrous iron oxides, this in turn can lower the pH of seawater locally and lead to greater solubility of some elements (Seyfried and Bischoff, 1979) (e.g. Mg, Ca, Sr?). Of less certainty are explanations for the relative depletions at pillow rims of K_2O and Ba and enrichments of iron, Cu, Zn and to lesser degree Ni.

Since K_2O, and presumably Ba, are characteristically lost from cold seawater in contact with basalt they might be expected to be enriched at the pillow rims relative to interiors. Pillows sampled at DSDP Site 417 do show just such systematic enrichment in K_2O at their rims (Alt and Honnorez, 1984). Moreover, a more oxidizing environment such as exists at pillow margins would tend to promote the precipitation of celadonite with consequent enrichment of K_2O (Seyfried et al., 1978). Its relative impoverishment, therefore, is not readily explained. What may be an analogous relationship between adjoining alteration zones was described by Alt and Honnorez (1984) from Site 417. Although these were zones within the interiors of pillows, rather than between rim and interior, their explanation could have application here. Between brown zones, marginal to fractures in pillow interiors, and adjoining light grey zones farther from the fracture, K_2O is consistently lost from the brown relative to the light grey zone and FeO (total) consistently gained. The presence of K-feldspar in the light grey zone and in its place in the brown zone the smectite, beidellite, is the basis for the explanation. K-feldspar in the presence of excess H^+ alters to beidellite

with release of K^+. At least part of the H^+ required may have come from the oxidation of iron in the brown zone to Fe hydroxide. Moreover, the oxidizing environment of this zone should maintain a low level of iron in solution thereby creating a sink into which Fe ions, released by alteration of the grey zone, would migrate. Thus, the relative impoverishment of K_2O in the zone adjoining the seawater-rich interface (fracture) together with enrichment of FeO (total) is explained. The parallel with pillows 1 to 3 of this study is obvious. The pillow rim would be equivalent to the brown zones and the interior, to the grey zones of Site 417. If this is so, the pillow rims must have been fairly rich in plagioclase microlites which could have been replaced by K-feldspar during an early stage of alteration. Then the breakdown of the feldspar (or other K-bearing secondary minerals) by the more acidic environment of the pillow rims would start the process described. Cu, Zn, and Ni enrichment at the pillow margins probably reflects an earlier enrichment of sulphides since all three are chalcophile but not otherwise closely similar chemically. Sulphide enrichment at pillow margins relative to their interiors is not uncommon in oceanic basalts (Keays and Scott, 1976, Moore and Fabbi, 1971, and Baragar et al., 1977) and is generally attributed to selective leaching of metal sulphides from the pillow interiors after their rims cool and fracture. It seems possible that in the more severely altered pillows 1 to 4 such concentration is exaggerated by oxidation of the sulphides. Note that in pillow 5, Cu and Zn, at least, show some measure of increase at the margins which would suggest that whatever the process responsible for this distribution it must have acted at an early stage of alteration.

The impoverishment of Cr at most of the pillow rims is difficult to relate to any of the secondary processes since Cr is virtually insoluble in either cold or hot seawater (Seyfried and Mottl, 1982). It may be the one element in these pillows that could have been concentrated in the interiors by flowage differentiation, as advocated by Staudigel and Bryan (1981) for pillows at IPOD sites 417 and 418. Even pillow 5 with very little alteration shows a similar, although more subdued, profile. Chromite is present as a phenocryst phase in pillow 2 and although very sparse is a sufficiently concentrated source of Cr that very little imbalance in its distribution would be required to effect the profiles shown.

Pillow 5, below the zone of prolonged cold water convection, shows the effects of only very mild, presumably hydrothermal alteration. Except for minor palagonite development, which might account for the slight increase of K_2O at the pillow margins, the rims are glassy. Thus, the major part of the alteration shown by the compositional profile must be attributed to changes in the interior of the pillow. Its most obvious manifestation is the cryptocrystalline smectite which forms some 20 to 25% of the pillow interior. Its average composition, determined by microprobe on one of the specimens, is plotted at the location of the specimen on each of the profiles of Figure 7. As can be seen from the position of the plotted value relative to that of the profiles, the addition of this smectite to the interior composition is consistent only with its higher MgO and lower SiO_2 values relative to those of the glassy rim. It is definitely inconsistent with the higher Al_2O_3, Na_2O and TiO_2 of the pillow interior and seems to have had little effect on the profiles of CaO and total Fe_2O_3, despite its higher iron content. The only conclusion that seems tenable, therefore, is that the smectite development in the pillow interior resulted from a complex exchange with fairly low temperature hydrothermal fluids with a resulting net gain of mainly MgO and loss of SiO_2. Both Al_2O_3 and TiO_2 are generally immobile and probably show gains only because of their relative concentration with SiO_2 loss.

ACKNOWLEDGEMENTS

W.R.A.B. acknowledges support from the Geological Survey of Canada for laboratory and logistic support. J.N.L. and F.A. were supported by a NSERC-Canada collaborative special project grant. G. Gauthier and O. Stecher are acknowledged for help with analyses. We are grateful for the helpful reviews provided by K. Gillis and by U. Bednarz and H.-U. Schmincke. The logistic framework provided in Cyprus by ICRDG led by P.T. Robinson and J.M. Hall enabled this study to be undertaken and is gratefully acknowledged.

REFERENCES

Alt, J.C. and Honnorez, J.
1984: Alteration of the upper oceanic crust, DSDP Site 417: Mineralogy and Chemistry; Contributions to Mineralogy and Petrology, v. 87, p. 149–169.

Auclair, F. and Ludden, J.N.
1987: Cyclic geochemical variation in the Troodos Pillow Lavas: evidence from the CY-2a Drill Hole.; *in* Robinson, P.T., Gibson, I.L., and Panayiotou, A., Cyprus Crustal Study Project: Initial Report, Holes CY-2 and 2a, Geological Survey of Canada, Paper 85–29, p. 221–235.

Baragar, W.R.A., Plant, A.G., Pringle, G.J., and Schau, M.
1977: Petrology and alteration of selected units of Mid-Atlantic Ridge basalt sampled from sites 332 and 335, DSDP; Canadian Journal of Earth Sciences, v. 14, p. 837–874.

Flower, M.F.J., Pritchard, R.G., and Puchelt, H.
1979: Variation in single cooling units at Deep Sea Drilling Project Hole 418A: effects of alteration and phenocryst redistribution; *in* Donnelly, T., Francheteau, J., Bryan, W., Robinson, P., Flower, M., Salisbury, M., et al., Initial Reports of the Deep Sea Drilling Project, v. 51, 52, 53, U.S. Government Printing Office, Washington, p. 1021–1035.

Gillis, K.M.
1987: Multistage alteration of the extrusive sequence, Troodos ophiolite, Cyprus; (PhD Thesis), Dalhousie University, Halifax, 387 p.

Gillis, K.M. and Robinson, P.T.
1988: Distribution of alteration zones in the upper oceanic crust; Geology, v. 16, p. 262–266.

Hall, J.M., Wall, C., Williamson, M., and Wang, B.-X.
1987: Depth trends in magnetic properties in an area of prolonged cold seawater drawdown in uppermost Troodos-type oceanic crust; Canadian Journal of Earth Sciences, v. 24, p. 941–952.

Humphries, S.E.
1984: The mobility of the rare earth elements in the crust; *in* Henderson, Rare Earth Element Geochemistry, Elsevier, p. 317–340.

Humphries, S.E. and Thompson G.
1978: Hydrothermal alteration of oceanic basalt by seawater; Geochimica et Cosmochimica Acta, v. 42, p. 107–125.

Keays, R.R. and Scott, R.B.
1976: Precious metals in ocean ridge basalts; implications for basalts as source rocks for gold mineralization; Economic Geology, v. 71, p. 705–720.

Ludden, J.N. and Thompson, G.
1979: An evaluation of the behavior of the rare earth elements during the weathering of sea-floor basalt; Earth and Planetary Science Letters, v. 43, p. 85–92.

Moore, J.G. and Fabbi, B.P.
1971: An estimate of the juvenile sulphur content of basalt; Contributions to Mineralogy and Petrology, v. 33, p. 118–127.

Rautenschlein, M.
1987: Geology and geochemistry of Akaki volcanics, Cyprus; (PhD Thesis), Ruhr-Universität Bochum, 222 p.

Rautenschlein, M., Jenner, G.A., Hertogen, J., Hofmann, A.W., Kerrich, R., Schmincke, H.–U., and White, W.M.
1985: Isotopic and trace element composition of volcanic glasses from the Akaki Canyon, Cyprus: implications for the origin of the Troodos ophiolite; Earth and Planetary Science Letters, v. 75, p. 369–383.

Robinson, P.T., Melson, W.G., O'Hearn, T., and Schmincke, H.–U.
1983: Volcanic glass compositions of the Troodos ophiolite, Cyprus; Geology, v. 11, p. 400–404.

Schroeder, B., Thompson, G., Sulanowska, M., and Ludden, J.N.
1980: Analysis of geologic materials using an automated X-ray fluorescence system; X-ray Spectrometry, v. 9, p. 198–205.

Seyfried Jr., W.E.
1987: Experimental and theoretical constraints on hydrothermal alteration processes at mid-ocean ridges; Annual Review of Earth and Planetary Science, v. 15, p. 317–335.

Seyfried Jr., W. and Bischoff, J.L.
1977: Hydrothermal transport of heavy metals by seawater: The role of seawater/basalt ratio; Earth and Planetary Science Letters, v. 34, p. 71–77.

Seyfried Jr., W.E. and Bischoff, J.L.
1979: Low temperature basalt alteration by seawater: an experimental study at 70°C and 150°C; Geochimica et Cosmochimica Acta, v. 43, p. 1937–1947.

Seyfried Jr., W.E. and Mottl, M.J.
1982: Hydrothermal alteration of basalt by seawater under seawater-dominated conditions; Geochimica et Cosmochimica Acta, v. 46, p. 985–1002.

Seyfried Jr., W.E., Mottl, M.J., and Bischoff, J.L.
1978: Seawater/basalt ratio effects on the chemistry and mineralogy of spilites from the ocean floor; Nature, v. 275, p. 211–213.

Spooner, E.T.C., Beckinsale, R.D., England, P.C., and Senior, A.
1977: Hydration, ^{18}O enrichment and oxidation during ocean floor hydrothermal metamorphism of ophiolitic metabasic rocks from E. Liguria, Italy; Geochimica et Cosmochimica Acta, v. 41, p. 857–871.

Staudigel, H. and Bryan, W.B.
1981: Contrasted glass-whole rock compositions and phenocrysts redistribution, IPOD Sites 417 and 418; Contributions to Mineralogy and Petrology, v. 78, p. 255–262.

Staudigel, H. and Hart, S.R.
1985: Dating of ocean crust hydrothermal alteration; strontium isotope ratios from Hole 504B carbonates and reinterpretation of Sr isotope data from Deep Sea Drilling Project Sites 105, 332, 417 and 418; *in* Anderson, R.N., Honnorez, J., and Becker, K., et al., Initial Reports of the Deep Sea Drilling Project, v. 83, U.S. Government Printing Office, Washington, p. 297–303.

Staudigel, H., Bryan, W.B. and Thompson, G.
1979: Chemical variation in glass-whole rock pairs from individual cooling units in Holes 417D and 418A; *in* Donnelly, T., Francheteau, J., Bryan, W.B., Robinson, P., Flower, M., Salisbury, M., et al.; Initial Reports of the Deep Sea Drilling Project, v. 51, 52, 53, U.S. Government Printing Office, Washington, p. 977–986.

Staudigel, H., Gillis, K., and Duncan, R.
1986: K/Ar and Rb/Sr ages of celadonites from the Troodos ophiolite, Cyprus; Geology, v. 14, p. 72–75.

Thompson, G.
1973: A geochemical study of the low-temperature interaction of seawater and oceanic igneous rocks; Transactions of the American Geophysical Union, v. 54, p. 1015–1019.

Thy, P., Brooks, C.K., and Walsh, J.N.
1985: Tectonic and petrogenetic implications of major and rare earth element chemistry of Troodos glasses, Cyprus; Lithos, v. 18, p. 165–178.

APPENDIX – SAMPLE DESCRIPTIONS

Pillow 1

0.7 m thick. Comprises sparse well-formed phenocrysts of plagioclase and clinopyroxene in a groundmass of poorly crystallized plagioclase needles, clinopyroxene anhedra and an indistinct, turbid mesostasis. The combined phenocryst content ranges from 0.75 to about 2Śmectite is well developed in the mesostasis and plagioclase is generally recrystallized to a fine mosaic of probable alkali feldspar. Clinopyroxene is fresh. Vesicles, composing from 7 to 25 of the rock, are filled to a varying degree with carbonate and smectite.

Pillow 2

1.56 m thick. Olivine, clinopyroxene, and a single cluster of chromite phenocrysts together total about 2 of the rock. Some degree of gravity settling is indicated by the presence in the lower part of the pillow of the coarsest (1.3 mm) olivine and the only clinopyroxene and chromite. The olivine is entirely

replaced by carbonate, smectite, and iron oxide. The groundmass comprises a framework of plagioclase needles, intersertial and poorly developed clinopyroxene, and from about 15 to 60% indistinct brownish mesostasis much replaced by smectite. Vesicles are minor (5–15%) and variously empty or partially to completely filled with carbonate and magma residue. Minor veins are filled with carbonate and in one case also zeolite.

Pillow 3

0.97 m thick. Small (0.2–0.5 mm), sparse (0.5–1%) clinopyroxenes are the only phenocryst phase present. They are generally euhedral, blocky crystals and some show pronounced sector zoning. The groundmass, as in the case of the other pillows, comprises a poorly developed framework of plagioclase needles and interstitial clinopyroxene anhedra contained in an interconnecting turbid, reddish brown to pale green mesostasis charged with minute needles and particles of opaque. Vesicles form about 20 to 30% of the rock of which the majority are less than 0.1 mm diameter and occur in the mesostasis of the groundmass. These are generally empty except for smectite rims, but the sparse larger vesicles are filled with carbonate. In addition the rock is cut by a few carbonate-rich stringers. Clinopyroxene is invariably fresh, plagioclase is either recrystallized to a fine, clear mosaic or has been replaced by smectite, and the mesostasis is both oxidized, as evidenced by its reddish colour, and partly replaced by smectite.

Pillow 4

1.36 m thick. The pillow is sparsely clinopyroxene–plagioclase phyric (0.5–3.5%) with slight concentrations of both phenocryst types in the lower part of the pillow suggestive of a minor degree of gravity settling. Clinopyroxene phenocrysts commonly show marked sector zoning. The groundmass is an ill-defined mix of poorly crystallized plagioclase and clinopyroxene and a pervading mesostasis of uncertain composition. Vesicles comprise 20 to 30% of the rock, but as in pillow 3, a high proportion are in the interstices of the groundmass. Those of less than about 0.2 mm diameter are filled with a fibrous smectite; above this size they have hollow centres or are empty. A few of the larger vesicles contain carbonate centres. Alteration is less severe than in pillows 1 to 3. Nevertheless plagioclase shows patchy replacement by a clear isotropic mineral (analcite?) or is clouded with an indeterminable clay mineral and the mesostasis is much replaced with pale green smectite.

Pillow 5

1.05 m thick. Both margins of this pillow are composed of clear glass with generally less than 10% palagonite in vesicles and fractures. It is very sparsely phyric with both clinopyroxene and plagioclase forming less than 0.5% of the rock in all parts of the pillow. The interior is semi-crystallized with bundles of minute plagioclase needles and patchy clinopyroxene rather poorly segregated from the mesostasis. About 20 to 25% of the pillow interior comprises curious, small (less than 0.5 mm), rounded blebs and irregular interstitial masses of a uniform, pale yellow-brown, cryptocrystalline material which probe analyses (Table 4) suggest is iron-rich smectite.

Many of the masses are dissected by curved fractures reminiscent of syneresis cracks in gel deposits. The blebs are presumably void fillings but differ from the groundmass vesicles of the other pillows in that their boundaries with the enveloping mesostasis are abrupt but not sharp and they lack any suggestion of concentric layering. Apart from these blebs the lava of pillow 5 shows little alteration. Both primary crystal phases present are wholly fresh. Probe analyses of the groundmass plagioclase (Table 4), gives compositions ranging from An_{62} to An_{75}.

Smectite	(1)	(2)	(3)	(4)	(5)	Av. of 17
SiO_2	45.37	42.65	45.54	51.70	44.87	45.61
Al_2O_3	5.77	4.56	5.69	8.74	4.58	5.80
FeO*	13.80	15.87	15.24	10.78	15.95	14.34
MgO	14.90	16.03	15.90	11.30	17.38	15.29
CaO	1.21	1.34	1.34	1.40	1.07	1.23
Na_2O	0.97	1.00	0.73	0.70	1.23	0.89
K_2O	0.43	0.23	0.29	0.79	0.43	0.40
TiO_2	0.20	0.07	0.13	0.27	0.07	0.15
MnO	0.08	0.08	0.00	0.17	0.08	0.12
Cr_2O_3	0.08	0.08	0.00	0.00	0.00	0.02
Total	82.81	81.96	84.86	85.85	85.66	83.85
Glasses	(1)	(2)	(3)	(4)		Av. of 10
SiO_2	54.83	53.56	54.05	53.12		54.12
Al_2O_3	16.15	15.79	15.91	15.68		15.94
FeO*	8.59	8.42	8.32	8.31		8.42
MgO	5.91	6.20	6.09	5.74		6.04
CaO	9.97	9.59	9.66	9.53		9.69
Na_2O	3.07	3.15	3.09	2.76		3.08
K_2O	0.23	0.19	0.29	0.29		0.27
TiO_2	0.61	0.62	0.60	0.58		0.60
MnO	0.15	0.13	0.12	0.17		0.15
Cr_2O_3	0.10	0.02	0.12	0.04		0.06
Total	99.61	97.67	98.25	96.22		98.38
Plagioclase	(1)	(2)	(3)			Av. of 6
SiO_2	51.42	52.58	50.94			51.84
Al_2O_3	30.38	29.49	31.03			30.40
FeO*	0.97	0.97	0.72			0.89
CaO	14.36	12.82	14.92			14.09
Na_2O	3.11	4.12	2.72			3.24
K_2O	0.14	0.10	0.04			0.08
Total	100.38	100.08	100.37			100.54
Or	0.84	0.55	0.21			0.44
Ab	27.95	36.60	24.77			29.27
An	71.21	62.84	75.02			70.30

Table 4: Representative microprobe analyses of plagioclase, smectite, and glass of pillow 5. Analyst: M. Bonardi.

Major and Trace Element Geochemistry of Holes CY-1 and CY-4: Implications for Petrogenetic Models

J. TARNEY AND N.G. MARSH

Department of Geology, University of Leicester, Leicester LE1 7RH, UK

Tarney, J. and Marsh, N.G., 1991: Major and trace element geochemistry of Holes CY-1 and CY-4: implications for petrogenetic models; in Cyprus Crustal Study Project: Initial Report, Holes CY-1 and 1A, eds. Gibson, I.L., Malpas, J., Robinson, P.T., and Xenophontos, C.; Geological Survey of Canada, Paper 90–20, p. 133–176, 1991.

Abstract

Major and trace element XRF analyses are presented for samples collected at regular intervals from the lavas in the upper part of Hole CY-1 and from the dyke section of Hole CY-4. In CY-4 the range in abundance of incompatible elements is larger than could be achieved by fractional crystallization, considering the limited volume of cumulates in the Troodos complex. Instead three broad groups can be recognized, and a coherent picture emerges by accepting some degree of source heterogeneity. These mantle sources appear to be more refractory (i.e. higher Y/Zr, Ti/Zr, etc.) than the mantle sources feeding most present-day mid-ocean ridges. Interestingly, the Mg-rich Upper Pillow Lavas in CY-1 seem to be higher degree melts of a less-refractory source. The range of compositions is best explained by interaction between asthenosphere and more-refractory lithosphere in a supra-subduction zone environment, with the sources being contaminated by subduction zone fluids. The closest compositional analogues are found in the Western Pacific arc/back-arc systems. Careful analysis of Cr-Mg and Ni-Mg relationships suggest there may have been as many as ten individual batches of magma feeding the dyke suite at this locality; thus there were a series of individual magma pulses, the data offering no support for the classic model of a single continuously fractionating magma chamber. Plagiogranites seem to have evolved mainly from one of the three main magma groups. Some exotic external factors such as access by hydrothermal fluids or rafts of hydrothermally-altered sheeted dykes falling into the magma, were perhaps responsible for precipitation of titanomagnetite and initiating the fractionation trend toward plagiogranite.

Résumé

Les observations faites aux rayons X des échantillons d'éléments trace et d'éléments majeurs, prélevés à des intervalles réguliers, et provenant des laves situées dans la partie supérieure du trou de forage CY-1 et de la section du dyke du trou CY-4. L'abondance et la variété de la gamme des éléments incompatibles dans le trou CY-4 sont bien trop grandes pour être le résultat d'une cristalisation fractionnelle, considérant le volume limité de cumulat dans le complexe filonien de Troodos. Ainsi, partant de l'hypothèse d'un certain degré d'hétérogénéité de la source, on peut reconstituer un schéma cohérent et distinguer trois larges groupes. Ces sources mantellique semblent être plus réfractaires (c'est à dire avec des rapports plus élevés Y/Zr, Ti/Zr, etc.) que les sources mantelliques alimentant les crêtes medio-océaniques actuelles. Il est intéressant de noter que les couches supérieures des laves en coussinet riche en magnésium dans CY-1 semblent être des fusions de degrés plus élevés, provenant de sources moins réfractaires. La meilleure explication que l'on puisse offrir pour cette gamme de compositions est celle de l'interaction entre l'aesthénosphère et une lithosphère plus réfractaire dans le contexte d'une zone de super-subduction dont les sources sont contaminées par des fluides provenant de la zone de subduction. Les compositions analogues qui se rapprochent le plus de celles-ci se trouvent dans les systemes de l'arc et du dos de l'arc de l'ouest du Pacifique. Une analyse détaillée des relations Cr-Mg et Ni-Mg suggère qu'il aurait pu y avoir jusqu'à dix groupes magmatiques individuels alimentant la suite de dykes à cet endroit précis; il y a ainsi eu des séries de poussées magmatiques individuelles, car les données n'appuient pas le modèle classique d'une chambre magmatique unique qui se serait fractionnée continuellement. Les plagiogranites semblent s'être développés principalement à partir de l'un des trois principaux groupes de magma. Certains facteurs externes exotiques tels que la pénétration des fluides hydrothermaux ou la tombée de radeaux de groupes de dykes altérés hydrothermallement dans le magma seraient peut-être à l'origine des précipitations de titanomagnetite et du déclenchement du fractionnement vers le plagiogranite.

INTRODUCTION

This paper concentrates on the major and trace element chemistry of samples from two of the Troodos drillholes, CY-1 and CY-4, using element concentrations determined by X-ray fluorescence spectrometry at the University of Leicester. These holes together provide a section through part of what is traditionally (e.g. Smewing et al., 1975) termed the Upper Pillow Lavas and the Sheeted Dyke Suite. In total 68 samples were analyzed from Hole CY-1 through the depth range 20–468 m (the upper part of the Pillow Lavas) and 174 samples from Hole CY-4 in the depth interval 9 to 626 m (most of the Sheeted Dyke Suite). The major elements determined were Si, Ti, Al, Fe, Mn, Mg, Ca, Na, K, P (all as oxides, with Fe being reported as total Fe_2O_3, and LOI (the total loss on ignition observed during preparation of fused discs for XRF analysis). Trace elements determined were Cr, V, Ni, Zn, Rb, Sr, Y, Zr, Nb, Ga, Ba, La, Ce, Nd, Pb, and Th, although the levels of some of these elements (particularly Nb, La, Ce, and Th) were near or below the limit of detection by XRF techniques in many samples. Nonetheless despite the problem of low concentrations, and the added problem of element mobility due to hydrothermal alteration, a number of key, relatively immobile, elements can be determined with sufficiently high precision by XRF methods to enable clear deductions to be made concerning the petrogenesis of the Troodos Complex.

Consideration will be given below to four aspects:

1. A preliminary assessment of the extent of chemical mobility within the sample suite resulting from hydrothermal activity. Although the degree of alteration in these two holes may be considerably less than in CY-2, it is important to try to assess the magnitude of the chemical effects attending alteration before any reliance can be placed on element abundances as a guide to petrogenesis.

2. An assessment of the chemical character of the main rock groups within the lava/dyke sequence, to emphasize the chemical differences between the broad petrological-chemical units, and to identify any differences between the Upper Pillow Lavas of CY-1 and the Sheeted Dykes of CY-4. The latter may feed just the Lower Pillow Lavas (e.g. Smewing et al., 1975), and perhaps the upper lava units as well (Baragar et al., 1987).

3. The geochemical data from the CY-4 dykes, where there is a greater range of variation than the CY-1 lavas, will then be examined in more detail to determine the processes involved in the petrogenesis of the various magmatic groups and sub-groups, including the silicic plagiogranites. None of the gabbro samples drilled were available to us in this study, hence our conclusions are based entirely on the presumed liquid or liquid + crystal intrusive dykes and extrusive components of the complex.

4. Troodos has long been regarded as the type ophiolite, but it has been debated whether the ophiolite represents true ocean basin crust, back-arc basin crust, or the roots or fore-arc of an island arc. Objective comparisons will be made with drill- and dredge-sample data from modern ocean basins, back-arc basins, and island arcs to ascertain the probable tectonic setting of the Complex. The data used in this exercise has all been analyzed in the same laboratories using the same techniques and standards.

Sampling

Figure 1 illustrates the location of samples used in this study in relation to the drillholes and the standard section. The freshest possible samples were selected, to represent a particular cooling unit, or the visible extremes of such units. At each sample point about five one-inch diameter minicores were extracted from the main drill core. After washing, the samples were coarse-crushed (to <2 mm) using a Fritsch jaw crusher fitted with hardened tool steel jaw plates. A Fritsch planetary ball mill fitted with agate barrel and balls was used for final crushing, and representative splits were taken and sealed for distribution.

Analytical Techniques

Major and trace element analysis of the samples was carried out using a Philips PW1400 X-ray fluorescence spectrometer. Analytical techniques used were closely comparable to those used during the study of DSDP basalt samples (Legs 49, 58, 59, 69, 70, 72, and 83). Major elements were determined on fusion discs (1 : 5 mixture of pre-ignited sample and JM100B lithium tetraborate/metaborate flux) using a Rh anode, the count data being processed using the de Jongh style, a coefficient correction model (de Jongh, 1973). Trace elements were determined on 46 mm pressed powder discs using a Rh anode for Nb, Zr, Y, Sr, Rb, Th, Ga, Zn, and Ni, and a W anode for V, Cr, Ba, La, Ce, and Nd. Appropriate corrections were made for peak overlaps of Sr on Zr, Rh (Rayleigh) on Rb, Rb on Y, Ti on Ba, Ti on V, V on Cr, and the mutual overlap of Ce on Nd and Nd on Ce. Corrections for mass absorption were made using tube scatter lines RhKα (Compton) or WLβ (Rayleigh), and corrections across the Fe absorption edge (for V, Cr, Ba, La, Ce, and Nd) were made using the method of Walker (1973). Table 1 (page XX) gives relevant information on precision and accuracy.

Analytical data for major and trace elements and calculated C.I.P.W. norms are given in Table 2 for Hole CY-1 and in Table 3 for Hole CY-4 (see end of paper for these tables). Because measured concentrations of Th, U, and Pb in CY-1 and the upper part of CY-4 were considered too low to be reliable, these elements were not determined in samples from the lower part of CY-4. Some samples contain appreciable quantities of secondary hydrous minerals. Values for the observed loss on ignition (LOI) are given in the tables. This represents the total loss observed during preparation of the fused glass discs for XRF major element analysis. All major

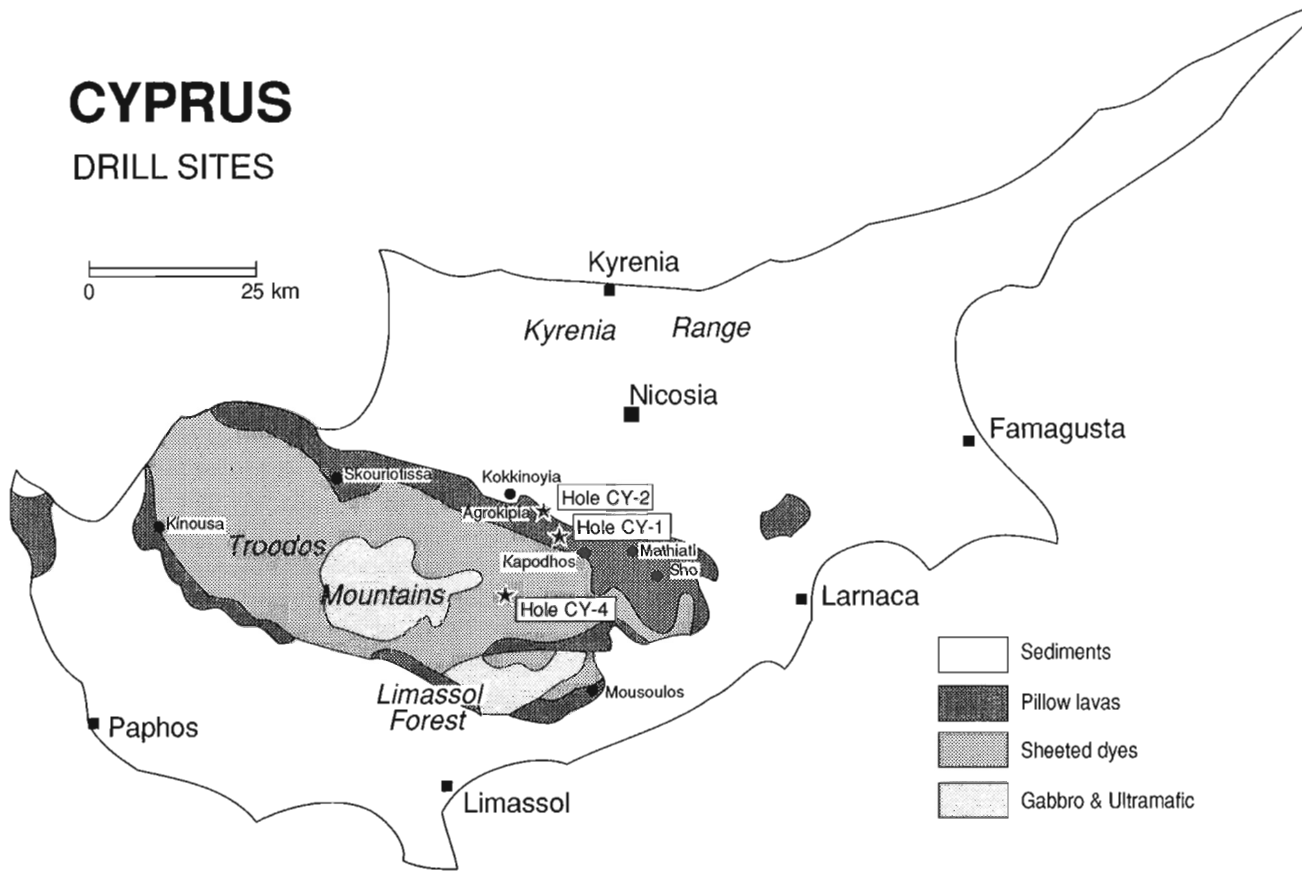

Figure 1: Outline geology of Cyprus showing the location of Drill-Sites CY-1, CY-2, and CY-4 in the Troodos Complex.

element concentrations used in plotting have been recalculated volatile-free to aid comparisons.

GEOLOGICAL BACKGROUND

Following the early geological and geophysical studies (Wilson, 1959; Gass and Masson-Smith, 1963) that established the main features of the Troodos Complex, including the existence of high-Mg pillow lavas (Gass, 1958), the new concepts of seafloor spreading and plate tectonics allowed the Complex to be interpreted as a section of oceanic crust (Gass, 1968; Moores and Vine, 1971; Greenbaum, 1972). Kidd and Cann (1974) for instance used the chilling statistics of the sheeted dykes to predict that the spreading ridge lay to the west. Indeed the exposed upward sequence of harzburgite-tectonite, cumulate ultramafics, gabbro, sheeted dykes, pillow lavas, and the associated Fe-Mn rich sediments and sulphide mineralization, has had a considerable influence on models of ridge spreading processes. Geochemical studies (Smewing et al., 1975; Smewing and Potts, 1976; Kay and Senechal, 1976) confirmed the depleted MORB-like character of the basalts, and isotopic and fluid inclusion studies (Chapman and Spooner, 1977; Spooner, 1977; Spooner and Bray, 1977; Spooner et al., 1977) have confirmed that seawater was the active fluid during hydrothermal alteration and mineralization. Moores and Vine (1971) suggested that the Arakapas Fault in the southern part of the Complex could be interpreted as a fossil oceanic transform, and Simonian and Gass (1978) proposed that the whole of the southern Limassol Forest region may be a transform domain, with the characteristics of a leaky transform (Murton and Gass, 1986). Gass and Smewing (1973) proposed a time gap between the more silicic Lower Pillow Lavas + dykes (the Axis Sequence that had been severely affected by contemporaneous ridge hydrothermal activity and local sulphide mineralization), and the Mg-rich olivine basalts, limburgites, and picrites (Searle and Vokes, 1969) that characterize the Upper Pillow Lavas. They interpreted the Upper Pillow Lavas as later off-axis volcanism.

The controversy sparked by the proposal of Miyashiro (1973, 1975), that the silicic Lower Pillow Lavas might represent the roots of an island arc (see response by Gass et al., 1975), seemed partly resolved by suggestions that Troodos could represent spreading in a back-arc basin (Pearce,

	BOB-1		W-1		BE-N	
	Mean	σ	Mean	σ	Mean	σ
SiO_2	50.20	±0.185	52.09	±0.534	39.25	±0.350
TiO_2	1.28	±0.005	1.08	±0.008	2.66	±0.028
Al_2O_3	16.54	±0.062	14.88	±0.133	10.22	±0.092
Fe_2O_3	8.61	±0.033	11.07	±0.044	13.10	±0.013
MnO	0.14	±0.003	0.17	±0.000	0.20	±0.000
MgO	7.57	±0.004	6.66	±0.104	13.53	±0.021
CaO	11.21	±0.027	11.00	±0.119	14.28	±0.014
Na_2O	3.08	±0.046	2.17	±0.072	3.28	±0.042
K_2O	0.353	±0.003	0.629	±0.007	1.433	±0.009
P_2O_5	0.169	±0.006	0.135	±0.002	1.072	±0.001
LOI	0.73	±0.08	0.52	±0.11	2.73	±0.07
Rh X-ray tube trace element program						
Nb	4.5	±0.26	7.5	±0.50	111.2	±0.67
Zr	102.2	±1.03	93.3	±2.09	280.1	±2.69
Y	27.9	±1.03	22.7	±0.71	29.7	±0.17
Sr	194.8	±1.58	188.5	±1.38	1431.9	±9.43
Rb	6.1	±0.95	22.6	±0.52	50.4	±0.45
T	1.6	±1.21	2.5	±1.29	13.7	±0.65
Ga	15.3	±0.73	18.6	±0.74	18.2	±0.73
Zn	68.1	±0.67	90.1	±1.07	132.1	±1.13
Ni	109.9	±3.02	75.8	±1.18	291.6	±3.42
W X-ray tube trace element program						
V	244.0	±4.48	270.9	±3.45	254.2	±1.61
Cr	305.2	±1.71	133.2	±0.84	374.2	±4.06
Ba	37.5	±0.82	166.9	±3.28	1106.0	±12.26
La	5.8	±0.92	11.8	±1.06	85.3	±1.30
Ce	12.8	±1.97	23.8	±1.35	151.4	±1.45
Nd	10.7	±1.09	12.7	±1.82	64.2	±0.44

Table 1: Precision and accuracy of XRF results based on analyses of three standard rocks: BOB-1, W-1, and BE-N. Data were acquired during analytical runs for CY-1 and CY-4 samples and refer to mean values for seven analyses of each of the standard rocks. In the case of loss on ignition (LOI) the data are based on duplicates only. Major element data for Birmingham Ocean Basalt (BOB-1) refers to seven repeat analyses of the same bead. Major element data for diabase W-1 refers to seven analyses from four separate beads produced at different times. Major element data for BE-N refers to seven analyses from two beads made at the same time. Although the CY-1 basalts and CY-4 diabases were analyzed at different times, no significant analytical differences were observed for the standard rocks analyzed simultaneously with the two sample sets.

1975, 1980). The growing data set on basalts from modern back-arc basins (summarized in Tarney et al., 1977, 1981; Saunders and Tarney, 1984) showed that significant geochemical differences exist between some back-arc basalts and MORB, attributable to the influence of the subducting slab in the back-arc region, and that simple criteria could be erected to distinguish the two (Saunders et al., 1980; Pearce, 1980). The high primary volatile contents of Troodos basaltic glasses (Muenow et al., 1990) are also compatible with a back-arc origin. Nonetheless uncertainties in finding an acceptable tectonic environment for all the component rock types in Troodos remain. Wood (1979) tried to account for the Mg-rich depleted Upper Pillow Lavas in terms of second stage melts following the dynamic melting model of Langmuir et al. (1977), as did Duncan and Green (1980). But such Mg-rich depleted basalt compositions have yet to be located in modern back-arc basins. Moreover the picritic Upper Pillow Lavas on Cyprus have many mineralogical, textural and chemical similarities with boninites (Cameron et al., 1979; Cameron and Nisbet, 1983; McCulloch and Cameron, 1983), which have only been recorded to date in the fore-arc region of modern arcs (see Crawford et al., 1981, 1986; Tarney et al., 1981; Hickey and Frey, 1982). Boninites are regarded by these authors and by Tatsumi (1981) as a product of wet melting of refractory mantle underlying the volcanic arc: this would accord with the generally vesicular nature of the Upper Pillow Lavas on Cyprus. These tholeiite-boninite associations might have developed during splitting of a primitive volcanic arc (Flower and Levine, 1987), as obviously happened during development of the Mariana Arc system (Tarney et al., 1981).

Two more recent studies near the drill site, on the major element compositions of glasses (Robinson et al., 1983) and the whole-rock trace element abundances (Schmincke et al., 1983), have emphasized the lack of a metamorphic discontinuity between the upper and Lower Pillow Lavas. However both studies note the upward change from more silicic Mg-poor basalts to Mg-rich basaltic lavas. The Lower Pillow Lavas are interpreted as a differentiated arc-tholeiite suite, the upper as a boninitic suite, similar to that in the Mariana forearc. There is of course no arc as such: this is regarded as incipient. One problem with this model is that the Lower Pillow Lavas of the Arakapas Fault zone are also Mg-rich, and not easily distinguishable chemically from the Upper Pillow Lavas (Simonian and Gass, 1978). Following trace element and isotopic studies in this region, McCulloch and Cameron (1983) suggested that, whereas a component of seawater Sr could be recognized in the isotopic compositions of the lavas, there was also a large variation in Nd isotopic composition—that did not overlap the MORB field—despite the depleted character of the Troodos basalts. Both the trace element and isotope data indicated heterogeneity in the source, and suggested the presence of two components, one enriched, the other depleted in incompatible elements.

Pb isotopic studies of Troodos lavas by Hamelin et al. (1984) also demonstrated significant source heterogeneity, and a continental Pb component with enhanced $^{207}Pb/^{204}Pb$ isotopic ratios significantly different from normal MORB and strongly suggestive of an island arc environment. Similarly, in their trace element and Sr-, Nd-, Pb- and O-isotopic study of selected fresh volcanic glasses from the Akaki region, Rautenschlein et al. (1985) argued that much of the isotopic data could be explained by contamination of the

Troodos mantle source by about 0.5% subducted oceanic sediment plus a small contribution from seawater Sr, and that this also could account for some variation in the more incompatible LIL-element abundances. On balance they favoured an incipient island arc rather than back-arc origin for the Troodos ophiolite. Interestingly the level of sediment contamination deduced is similar to that proposed for the Mariana Arc (Hole et al., 1984; Whitehead et al., 1984) based on other geochemical evidence.

The problem of 'an arc without an arc' is further confused by the more recent studies of Varga and Moores (1985a, b) along the northern margin of the Troodos Complex. They recognize three structural graben, bounded by listric and normal faults and defined by rotated dykes dipping toward the graben axes, which are the focus of extensive hydrothermal activity and mineralization (Schiffman et al., 1987). The graben are interpreted as fossil axial valleys produced by successive eastward ridge jumps of about 10 km. If substantiated, such a model would imply a considerable variation in thermal input at any particular point with time, which may offer an explanation for the observed differences in basalt compositions. Moores et al. (1984) also proposed a tectonic model for the belt of ophiolite complexes between Cyprus and Oman, drawing analogies with the Andaman Sea, and invoking oblique subduction of the African Plate beneath an oceanic plate to the northeast, resulting in back-arc spreading without significant arc development.

Clearly this supposedly classic section of uplifted ocean floor may turn out to be anything but typical. But it may be possible to reconcile magmatic and tectonic models. A prime objective must be to try to identify and quantify the petrogenetic processes involved. Three immediate observations may be made. First, most basalts/dykes/gabbros are quite depleted in incompatible elements compared with North Atlantic MORB (e.g. Tarney et al., 1979a, b, 1980), implying that the mantle source was also markedly depleted. Second, of the total volume of igneous rocks produced, cumulates form no more than about 15% of the total thickness of about 5 km in most measured sections: there appears to be little scope for fractional crystallization to enhance incompatible trace element levels (which vary by a factor of about 10). Third, a considerable volume of quite high-Mg lavas was erupted, apparently escaping the buffering effects of a continuous magma chamber: there is appreciable primary isotopic, and trace element, heterogeneity amongst the Troodos lavas.

GEOCHEMICAL EFFECTS OF ALTERATION

Whether element mobility occurs during hydrothermal alteration depends on two factors: the nature of the mineral assemblages developed at a particular temperature and the volume of fluids passing through the rock (fluid/rock ratio). Because of the high geothermal gradient at a spreading ridge there is a rapid change in metamorphic facies and mineralogy downward (see Cann, 1979; Stern and Elthon, 1979). But the fluid activity varies according to the proximity of hydrothermal discharge zones. Almost all DSDP drilled samples we have previously studied show the effects of alteration, particularly with respect to Rb and K, and sometimes for other elements such as Ba and Sr (e.g. Floyd and Tarney, 1979). But elements such as Zr, Nb, Ti, Cr, Y, and the REEs are mostly unaffected. Indeed the high field strength elements Zr, Nb, Hf, and Ta are immobile in MORB, even at advanced stages of low-grade alteration (Bienvenu et al., 1990).

Few, if any, of the Troodos drilled samples can be considered really fresh. All have been affected to a greater or lesser extent by hydrothermal fluid activity. As continued hydrothermal activity in the upper sections of ocean crust leads to the development of clays, zeolites and other low-grade hydrous minerals, then the extent to which a sample has been affected can be gauged (to a first approximation) by its total volatile content. This is less valid at deeper levels in the ocean crust because the higher grade assemblages developed (e.g. amphiboles) are not particularly hydrous. Indeed changing mineralogy with depth can completely reverse the behaviour of certain elements in this regard: for instance whereas K and Rb may be readily absorbed by altered glass or zeolite- or clay-dominated secondary assemblages at shallow levels, they may be excluded from amphibole-dominated assemblages at deeper levels. Nonetheless the degree of mobility or loss/gain of a particular element can often be assessed by comparison with other immobile but incompatible elements with which they normally exhibit coherent behaviour in unaltered samples. Figures 2, 3, and 4 are selected plots of more mobile elements against LOI (loss on ignition) for all the samples analyzed in Hole CY-1 and samples from the upper part of Hole CY-4. Note that the element values used in these plots are those recalculated volatile-free to avoid sympathetic changes with the often large volatile content. The results are surprising in that there is almost a complete separation of Holes CY-1 and CY-4 on these plots, a consequence of the consistently much higher volatile content of CY-1 samples, particularly in the vesicular pillow lavas and brecciated material. This arises from the abundance of secondary clays and zeolites (as detailed in the downhole lithologic descriptions).

Curiously, despite this extensive absorption of circulating fluids, there are major changes in abundance in only three elements in the CY-1 samples. Silica shows a smooth and consistent decrease with increasing volatile content (Figure 2). Conversely, K_20 (Figure 3) and Rb (not shown) often display a more erratic but very significant increase, to more than an order of magnitude above likely primary values reported for fresh glasses from this region by Robinson et al. (1983). These systematic changes presumably reflect replacement of glass and infilling of vesicles by zeolites, clays, gypsum, and carbonate. Above 10% total volatile content, Ca concentrations rise systematically in a few samples, a consequence of impregnation by gypsum and carbonate. Apart from these

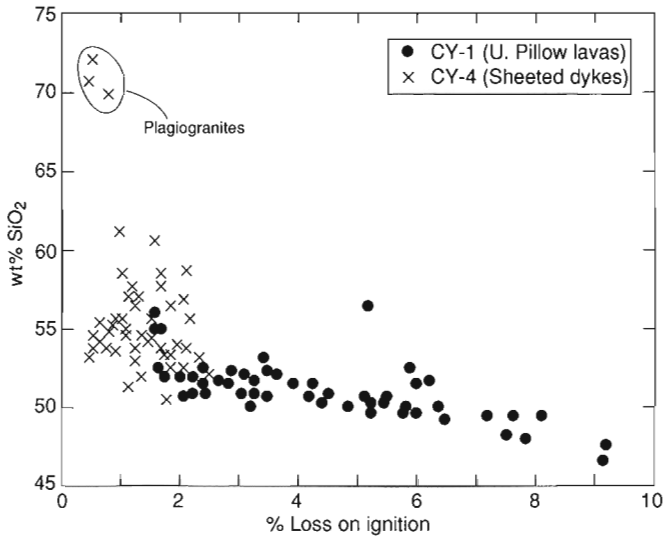

Figure 2: Plot of wt.% SiO_2 (recalculated dry) against LOI for CY-1 Upper Pillow Lavas and for sheeted dykes from the upper part of CY-4.

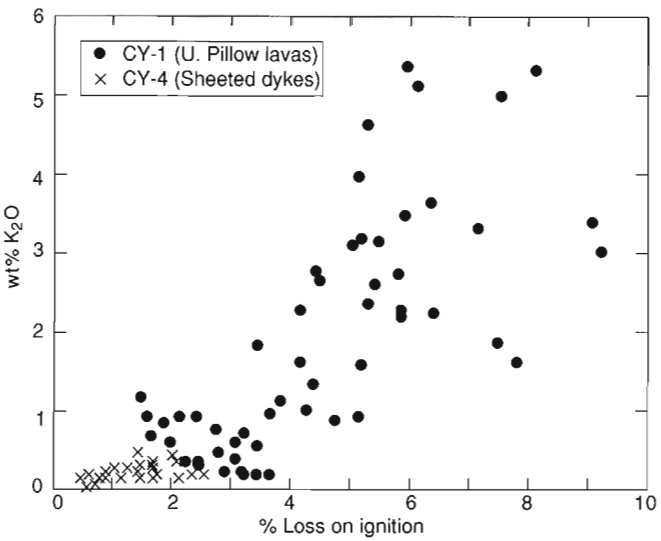

Figure 3: Plot of wt.% K_2O (recalculated dry) against LOI for CY-1 Upper Pillow Lavas and for sheeted dykes from the upper part of CY-4.

systematic changes there are more erratic ones. We stress that the total primary range of chemical variation in Hole CY-1 is considerably less than in Hole CY-4, as judged for instance by the relative range in abundance of 'immobile' elements such as Zr (Figure 5) Ti and P. These elements exhibit coherent behaviour (see below) and we suspect that they have indeed remained immobile, although their abundances may have changed in the more heavily impregnated altered samples. Elements which show a greater relative variation in CY-1 than in CY-4 samples may have been moved locally

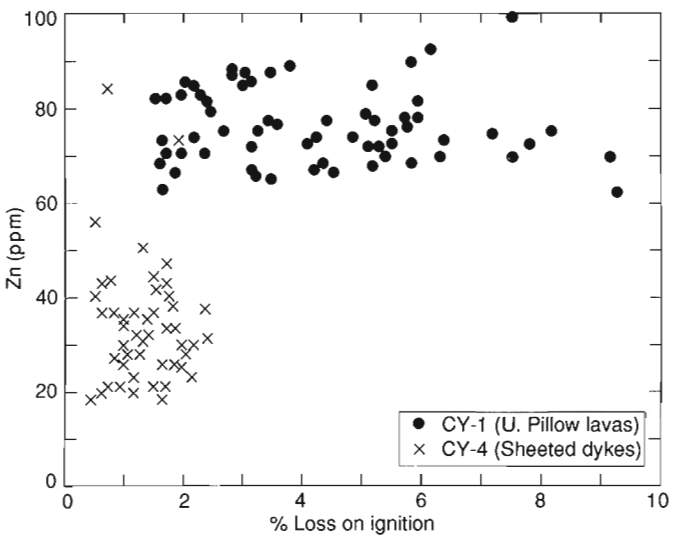

Figure 4: Systematic difference in zinc content between CY-4 Sheeted Dykes and CY-1 Upper Pillow Lavas that is not directly correlated with degree of alteration, as measured by volatile content of the samples.

during alteration, but may not necessarily have been removed from the lava pile. Values for Ca, Al, and Mg show more scatter than predicted, although the scatter for Mg is smaller than for the other two, perhaps because alteration is affecting the glassy mesostasis rather than the Mg-rich crystalline phases. There is appreciable scatter for Ba, suggesting that (as with K and Rb) there may have been up-take of Ba within the lava pile. On the other hand Sr values are surprisingly consistent, suggesting Sr has remained immobile. The systematic difference in Zn (Figure 4) between CY-1 and CY-4 suggest that the upper lavas have been mineralized to a minor extent, although this is not accompanied by any obvious difference in Pb abundance. Whether this might be a primary difference could be resolved by comparison of the Upper and Lower Pillow Lavas in CY-1/CY-1A.

The dyke samples from CY-4 clearly have much lower volatile contents, and there are no consistent trends with any alteration-related parameter, which leads to the conclusion that they may be less altered. It is therefore important to focus first on CY-4 samples in trying to explain primary petrogenetic relationships, and then attempt to integrate the data on CY-1 lavas.

PETROGENETIC RELATIONSHIPS: CY-4 DYKES and CY-1 LAVAS

With the uncertainties concerning element mobility during hydrothermal alteration, it is necessary to focus on elements that are relatively immobile. Zr and Y are probably the most useful elements in this regard. They are amongst the least mobile

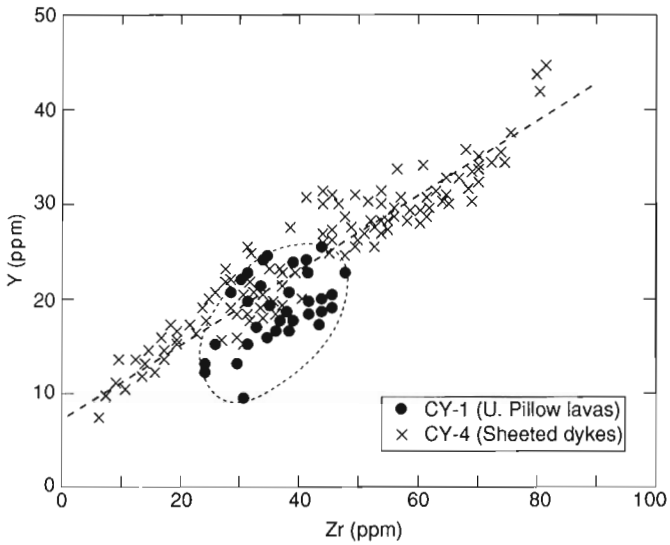

Figure 5: Plot of Y vs. Zr for CY-1 Upper Pillow Lavas and for dyke samples from CY-4. The dashed line represents the best-fit line through CY-4 samples, and intersects the Y axis. CY-1 samples are displaced slightly to higher Zr values.

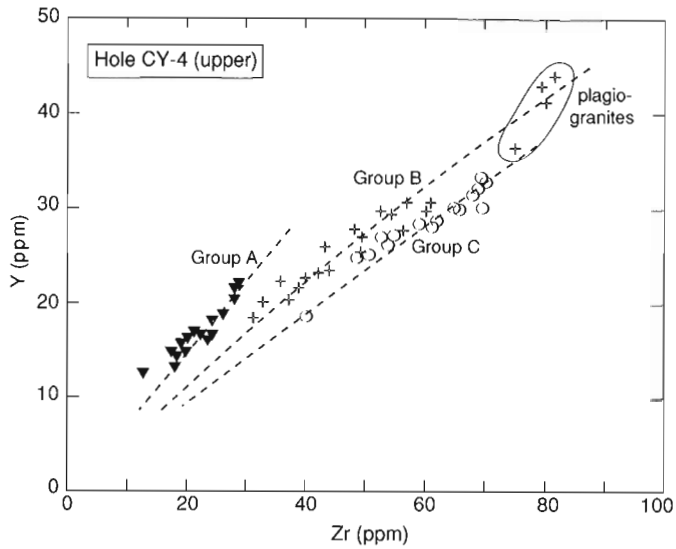

Figure 6: Y-Zr relationships in the upper part of CY-4. There are broadly three main groups, A, B, and C, each with different Y/Zr ratio. Most of the plagiogranites appear to be linked to Group B.

trace elements, they can be determined with high precision by XRF techniques—particularly within the range normally found in basaltic rocks, and their behaviour during magmatic processes is well known. Both remain essentially incompatible within basaltic magma compositions during fractional crystallization. Thus any single magma batch will retain a nearly constant Y/Zr ratio over an appreciable fractionating range (in reality a slight curve, because Y is preferentially incorporated in clinopyroxene). On the other hand, source heterogeneity and differences in the degree of partial melting can cause Y/Zr ratios to vary markedly between different magma batches. For the purposes of comparison in understanding Zr-Y relationships, data for North Atlantic MORB (Reykjanes Ridge, 45°N, FAMOUS; from Tarney et al., 1979), for marginal basin basalts and for primitive island arcs (Scotia Region and West Pacific; summarized in Tarney et al., 1980 and in Saunders and Tarney 1984) are included in Figures 7–9. High precision Zr-Y determinations are a particularly sensitive method of distinguishing different magma batches.

A Zr vs. Y plot for all CY-1 lavas and CY-4 dykes is shown in Figure 5. Each sample represents a different petrographic unit, based on initial examination of the drill core. All are essentially liquid compositions. CY-1 samples fall near the centre of the distribution, but some have slightly lower Y/Zr ratios than CY-4. There is a reasonable linear trend between Zr and Y, but the Zr/Y ratio is continuously variable. In fact the best-fit line through the CY-4 samples intersects the Y axis. Such a relationship is impossible to explain through crystallization of a single magma batch. The range in Zr abundance (from about 6 ppm to almost 80 ppm) would require about 95% crystallization of the most primitive magma, with a complementary volume of cumulate gabbros many times more than is observed on Cyprus. Moreover such cumulates would need to have significantly higher Y/Zr ratios than the dykes: gabbros with these characteristics do not exist on Cyprus as far as we are aware. These simple constraints would not significantly be circumvented by a continuously fractionating, periodically refilled magma chamber model (O'Hara and Matthews, 1981). The observed Zr-Y trend could, at least theoretically, be reproduced by a partial melting model, but would require a large range in the degree of partial melting and the postulating of some strange primary melt compositions, both of which are unrealistic. Moreover, there may be a significant volume of gabbro (representing a possible magma chamber) under the sheeted dykes.

The more realistic solution is shown in Figure 6, where individual dyke samples from the upper part of Hole CY-4 have been divided into three broad groups (A, B, and C) with approximately constant Zr/Y ratios. This implies that there are (at least) three separate magma batches represented in this part of the drilled section. In fact all samples from CY-4 can be assigned provisionally to one of these three groups, and different symbols are used for these subdivisions on subsequent diagrams where appropriate. Many samples from the Upper Pillow Lavas in CY-1 also fall into these groupings, though the majority corresponds with Group C. Most of the plagiogranite compositions have affinities with Group B.

Figure 7 shows how the three groups of Troodos samples compare with mid-ocean ridge basalts from the North Atlantic (DSDP Holes 407–413; data from Tarney et al., 1979) and the

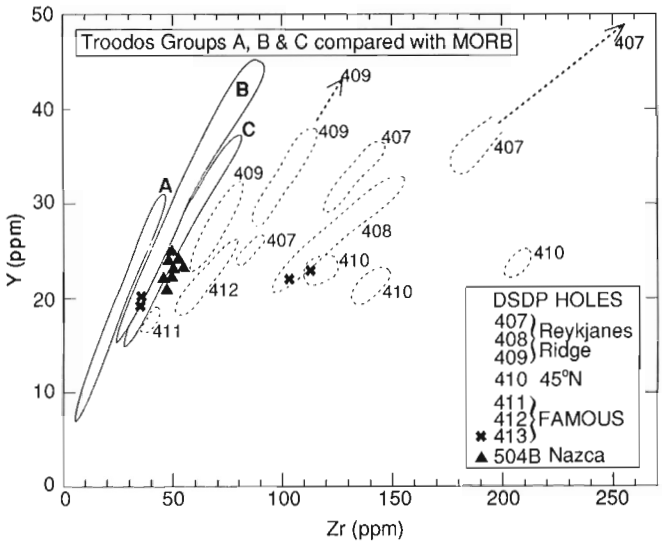

Figure 7: Comparison between Troodos basalts and MORB in terms of Y-Zr relationships. Troodos Groups A, B, and C encompassing all samples in Hole CY-4 are shown. Fields including basalts drilled near Iceland, 45°N, and near the Azores (FAMOUS area) are shown within dashed lines. Each represents a coherent chemical unit with the same Y/Zr ratio. Only the most 'depleted' MORB from the Atlantic and Pacific plot near the Troodos samples. Data from Tarney et al. (1979) and Marsh et al. (1983).

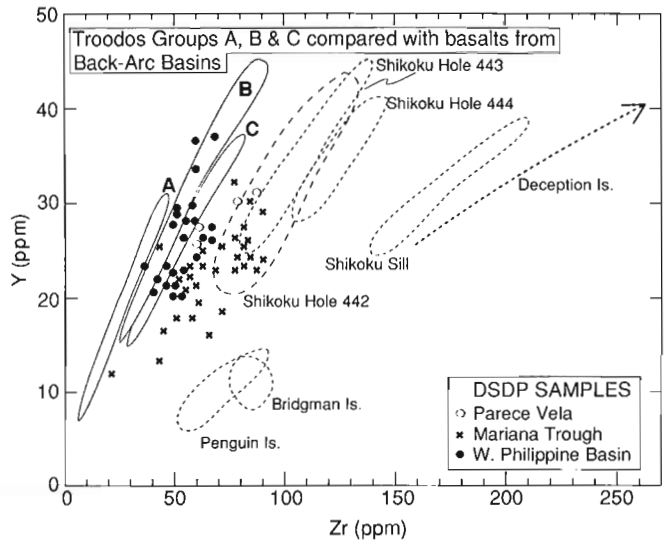

Figure 8: Y vs. Zr, as in Figure 7, comparison of Troodos with basalts from back-arc marginal basins from the Western Pacific and the Scotia Sea area. Individual points are shown only where data overlap Troodos. Data for Deception, Bridgeman, and Penguin Islands from Weaver et al. (1979) and for West Pacific transects from Marsh et al. (1980), Mattey et al. (1980) and Wood et al. (1980a,b; 1982).

Pacific Nazca Plate (Hole 504B; data from Marsh et al., 1983). Note that Y/Zr ratios are constant within each chemical unit, justifying the separation of the Troodos basalts into three geochemical groups. The North Atlantic basalts are mostly 'E-type' or 'T-type' MORB and there is very little overlap with Troodos basalts. In fact only the depleted basalts at Sites 411 and 413 in the FAMOUS area approach the Troodos Y/Zr ratios. Basalts from Hole 504B are amongst the most depleted MORB described, and just overlap with Troodos Group C (and CY-1 basalts). It appears there is little correspondence between Troodos and typical MORB compositions.

Surprisingly, although it has been stressed that Troodos basalts have a supra-subduction zone character, there is only limited overlap with a range of basalts from back-arc basins and island arcs, summarized in Figures 8 and 9 respectively. For clarity, separate points are plotted only where there is reasonably close overlap with Troodos; otherwise fields and trends are shown. Hardly any of the basalt samples from active or recently active back-arc basins overlap with Troodos. The closest correspondence is with the West Philippine Basin, but this basin has not strictly been formed by back-arc spreading. Amongst the arc samples it is only the most primitive intra-oceanic arcs (erupting island-arc tholeiites) that correspond with Troodos. These are tholeiites erupted during the very earliest stages (about 10 Ma) of arc evolution. Even the boninites from the W. Pacific arcs do not overlap with Troodos Upper Pillow Lavas on this diagram.

Similar conclusions can be based on TiO_2 vs. Zr, P_2O_5 vs. Zr, and Nb vs. Zr distributions (Figures 10–13), using the same data set as for Y vs. Zr. Ti/Zr ratios in Troodos samples are consistent, with a typical 'spur' towards plagiogranite (Figures 10 and 11). Compared with most MORB (Figure 10) there is very little Ti enrichment, and it is significant that the only appreciable overlap is with the most depleted MORB samples from the Atlantic and Pacific. Many Troodos basalts have much lower TiO_2 contents than average MORB. Compared with basalts from primitive island arcs and back-arc basins (Figure 11) there is again significant overlap with basalts from the West Philippine Basin and very primitive island-arc tholeiites, but not with most basins formed by back-arc spreading or more evolved island arcs. Moreover few basalts from these environments contain such low Ti and Zr contents as the Troodos basalts. Similar conclusions can be drawn from the P_2O_5 vs. Zr plot (Figure 12); P/Zr ratios are comparable with many MORB and MBB, but the very low content of P_2O_5 in many Troodos basalts is notable. The Nb vs. Zr plot (Figure 13) clearly shows the divergence between Troodos samples and the vast majority of MORB. Instead there is close correspondence with marginal basin and arc basalt compositions, and with West Philippine Basin and primitive Mariana Arc basalts in particular. High Nb contents and Nb/Zr ratios typically indicate an enriched ocean island (OIB) source component in E-type and T-type

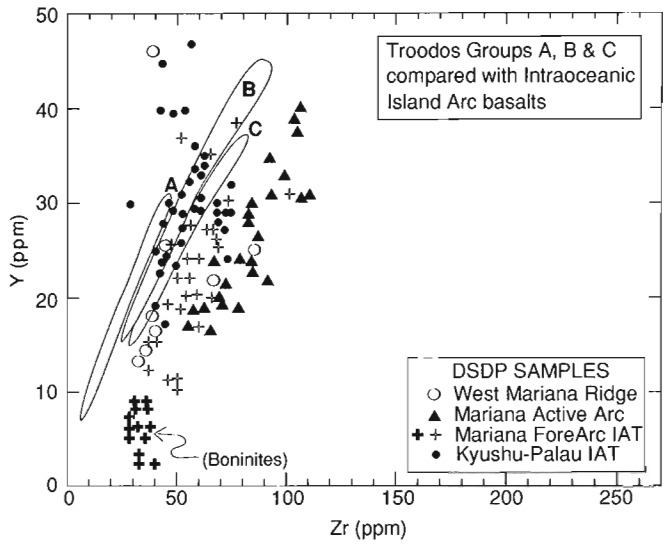

Figure 9: Y vs. Zr, as in Figure 7, comparison of Troodos with primitive West Pacific island arc lavas. Main overlap is with primitive island-arc tholeiites (IAT) erupted at the earliest stages of arc development. Data sources: Marsh et al. (1980), Mattey et al. (1981), Wood et al. (1980a,b; 1982) and Hole et al. (1984).

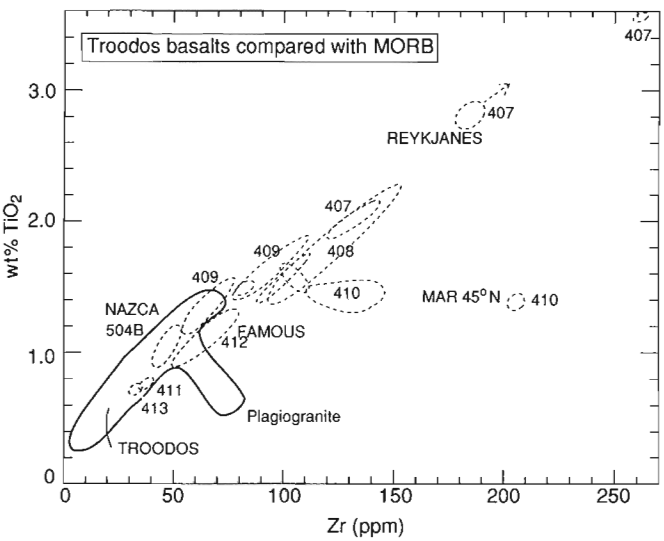

Figure 10: TiO_2 vs. Zr relationships in Troodos basalts and in MORB. Data sources as in Figure 7. Although Ti/Zr ratios are similar, absolute levels of Ti and Zr are much lower than in most MORB.

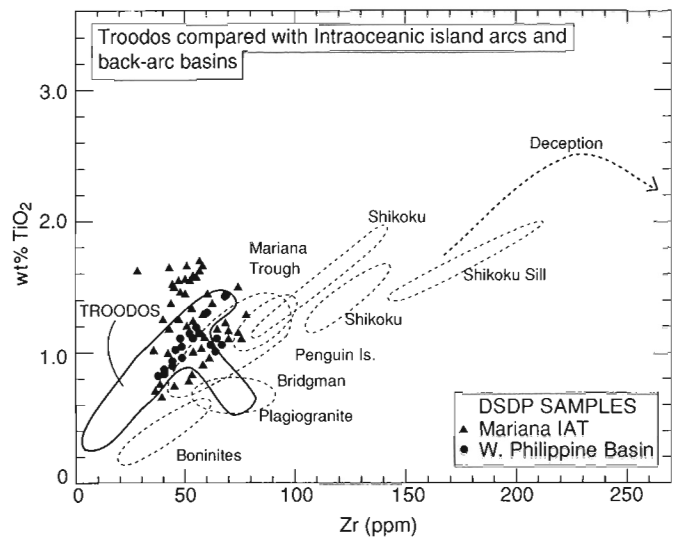

Figure 11: TiO_2 vs. Zr, as in Figure 10, comparison with arc and back-arc basalts. Data sources as in Figures 8 and 9. The rapid fall-off in TiO_2 in Troodos occurs at much lower absolute levels of titanium than in other arc/basin basalts.

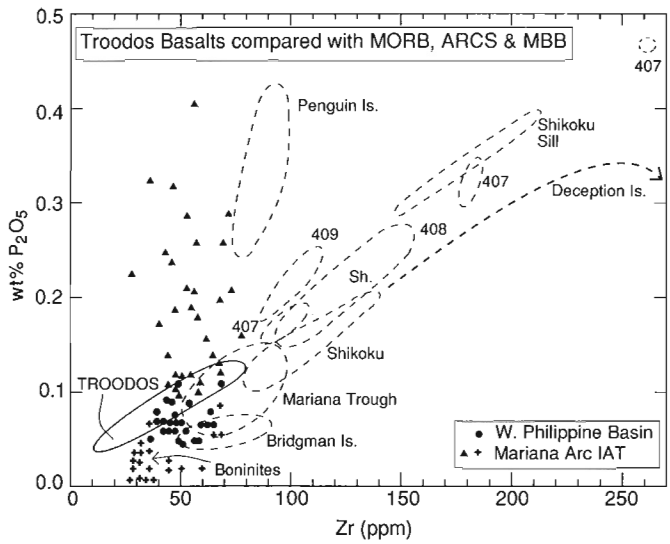

Figure 12: P_2O_5 vs. Zr relationships in oceanic, marginal basin and arc basalts. Data sources as in Figures 7–9.

MORB (Wood et al., 1979; Weaver et al., 1987), and clearly there can be little of this component in the Troodos basalt sources, or the melting conditions have not favoured entry of high field-strength elements like Nb into the melt. This latter solution is unlikely for high-Mg Troodos basalts, which must represent high degrees of melting, allowing little possibility for appeal to residual minor mineral phases.

The separation of three groupings, A, B and C, from the 'cloud' of CY-4 data for trace elements such as Zr-Y (Figure 6) also holds for major elements as well. In MgO vs. Zr for instance (Figure 14) each subgroup shows a progressive increase in Zr abundance with decreasing MgO. A simple interpretation is that there are three separate magma

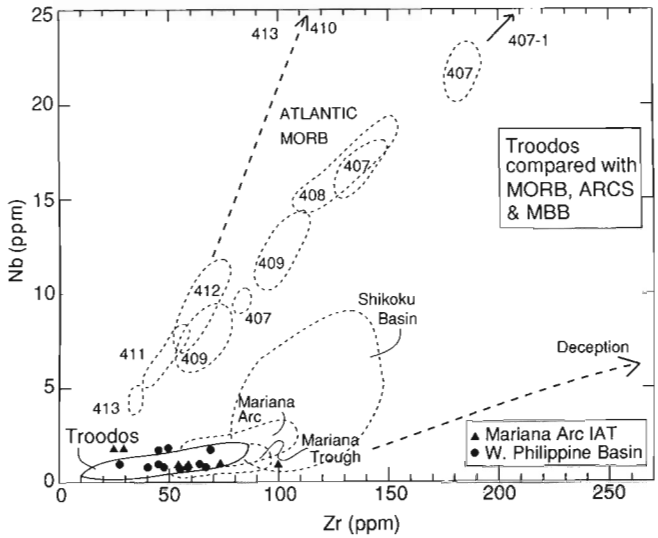

Figure 13: Nb vs. Zr relationships in oceanic, marginal basin and arc basalts. Data sources as in Figures 7–9. Troodos rocks have very low Nb contents and Nb/Zr ratios typical of arc and some marginal basin samples. There is no overlap with MORB.

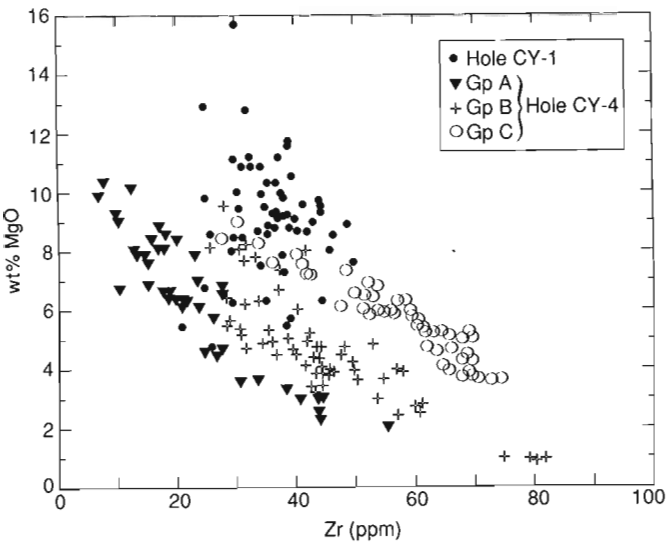

Figure 14: MgO vs. Zr for CY-4 and CY-1 samples, showing how three broad groups can be distinguished (viz. Figure 6). Upper pillow basalts from CY-1 correspond most closely with Group C.

batches with different primary levels of Zr. The CY-1 upper pillow lava samples again show a close correspondence with Group C. All three groups appear to have fractionated over a similar range of MgO, though only Group B seems to more commonly fractionate toward low MgO contents (plagiogranites). The CY-1 Upper Pillow Lavas seem not to have undergone much fractionation. Very similar relations are apparent

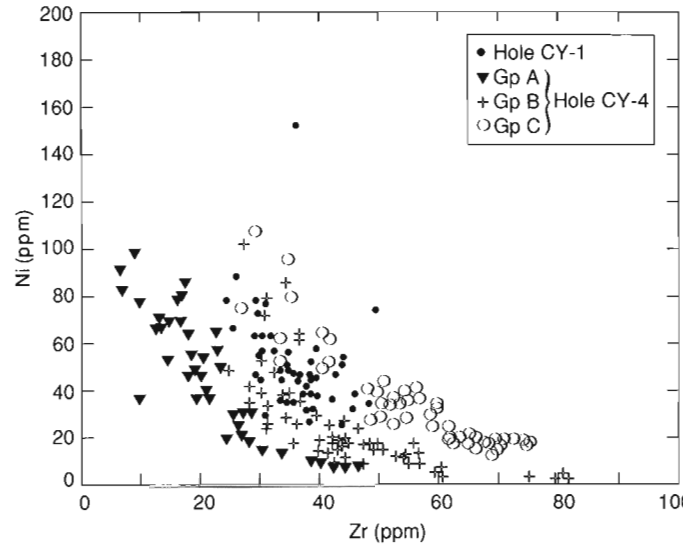

Figure 15: Ni vs. Zr for CY-4 and CY-1 samples. CY-1 corresponds most closely with Group C.

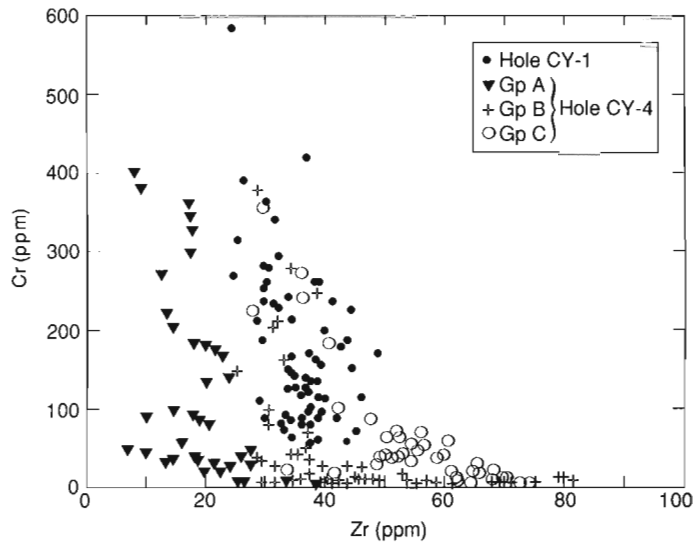

Figure 16: Cr vs. Zr for CY-4 and CY-1 samples. Note the rapid fall in Cr abundance with increasing Zr.

from a plot of Ni vs. Zr (Figure 15) but it is interesting that the curve for each group is not very steep, a feature expected if extensive olivine fractionation had taken place. In this plot CY-1 lavas have similar Ni contents to many CY-4 samples. The picture for Cr-Zr (Figure 16) does show a different relationship in that, although the three groups can be distinguished, there is a very rapid fall in Cr concentration within each group. This would be consistent with extensive early chromite fractionation. CY-1 samples also show this. The essential difference between CY-1 and CY-4 samples can be emphasized by a plot of MgO vs. Cr (Figure 17). This shows that although there is some overlap between the two, and the

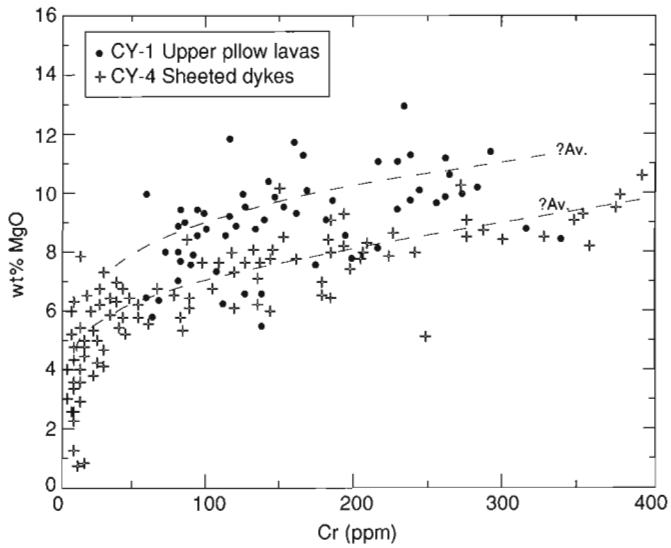

Figure 17: Comparison of CY-1 and CY-4 samples. Dashed lines indicate broad average trends for each group. CY-1 basalts have about 2% higher MgO contents at equivalent Cr concentrations.

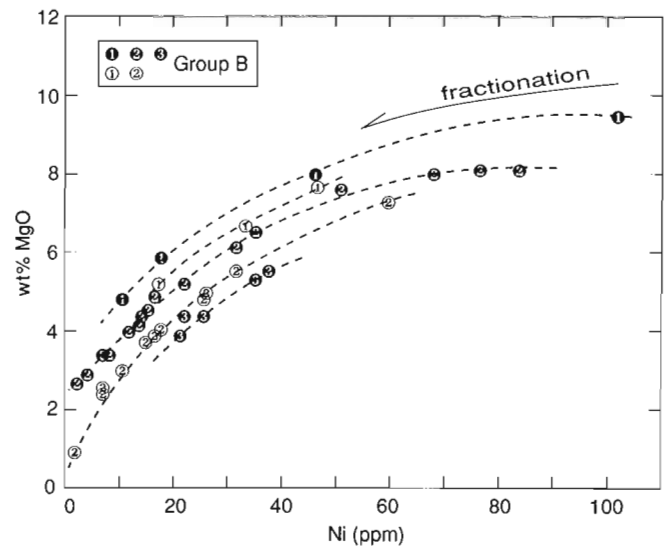

Figure 18: Possible interpretation of MgO-Ni variations in CY-4 Group B samples. The relationships show that Group B could consist of five sub-units.

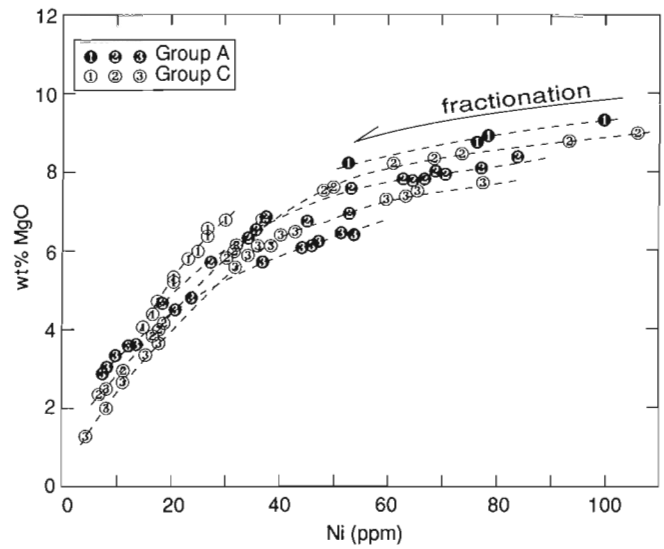

Figure 19: MgO vs. Ni, as in Figure 18, but for CY-4 Groups A and C.

fractionation trends are broadly parallel, the CY-1 samples have about 2% higher MgO at comparable Cr contents. The reason for this is not clear; it may be a result of CY-1 basalts being generated from a similar source, but at greater depth. The large range in Cr abundance is a notable feature of Troodos basalt petrogenesis; clearly chromite has separated from the magmas (giving local chromite ore concentrations), but chromite may have also been a residual mineral in the source regions of Troodos basalts.

There may be not just three main magma types amongst CY-4 dykes, but a whole series of small magma batches, as envisaged by Allen (1975). Each may have followed a slightly different evolutionary path before being emplaced into its present position. Unfortunately dyke swarms by their very nature do not allow links to be made on field criteria. However elements such as Mg, Ni, and Cr are very sensitive to olivine, chromite, and pyroxene fractionation in magma chambers, and the dykes allow monitoring of the progress of each stage of evolution. For instance, plotting Group B samples from CY-4 on a MgO vs. Ni diagram (Figure 18) shows that it is possible to interpret this group as five sub-groups, each with a more coherent behaviour, and each of which began its evolutionary path with a slightly different Mg/Ni ratio. Figure 19 shows the same plot for Group A and C samples, and again several different magma batches can be identified.

Because Cr and Ni abundances are particularly sensitive to chromite and olivine fractionation, a plot of these two elements can act as a sensitive discriminator between magma batches. Figure 20 shows how two separate groups can be distinguished amongst Group B samples in the upper part of Hole CY-4. Figure 21 indicates how (with faith!) other samples in Groups A and C and in CY-1 could potentially be linked. This provides a more coherent interpretation of the wide range in Ni and Cr abundances and Ni/Cr ratios in Troodos basalt samples. Otherwise appeal must be made to alteration.

The major implication from accepting such an interpretation is that the classic picture of Troodos (Moores and Vine, 1971; Moores and Jackson, 1974; Gass, 1980) as a continuous fractionating magma chamber at a mid-ocean ridge must

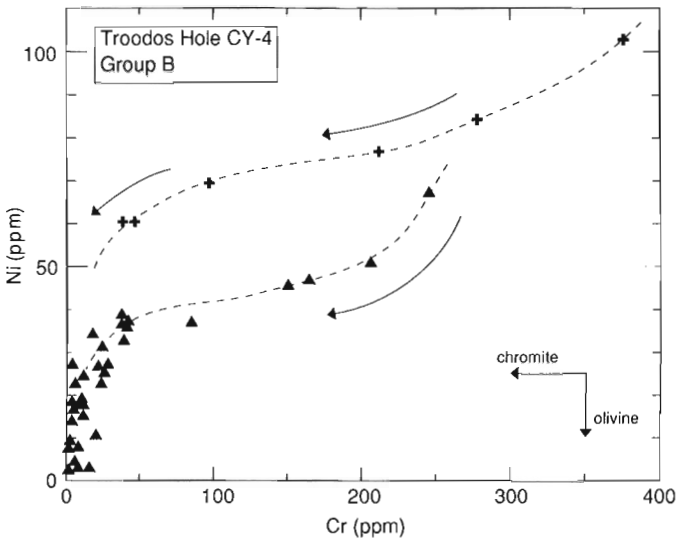

Figure 20: Ni vs. Cr for CY-4 Group B samples. Variations are dominated by chromite fractionation, but at least two distinct trends with different Ni contents can be recognized.

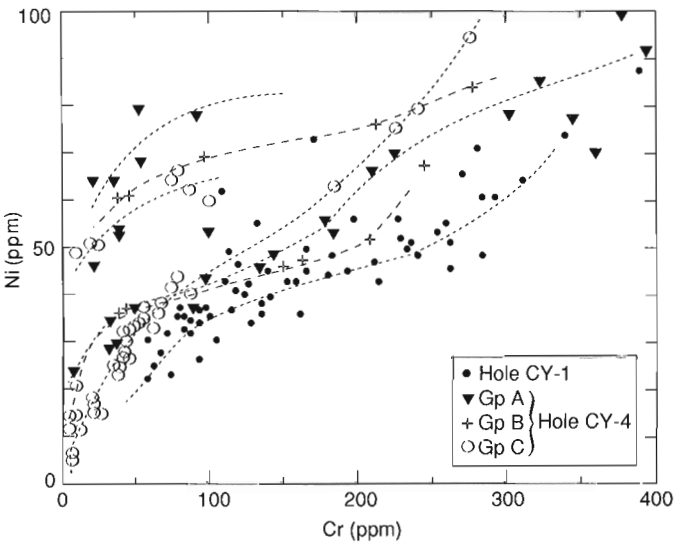

Figure 21: Ni vs. Cr, as in Figure 20, but suggesting that several different small magma batches with varying primary Cr/Ni ratios may account for the dispersion in these two elements.

be wrong. Even in the small section drilled there must be several of discrete magma batches that have not had their compositions smoothed by passing through a large axial magma chamber. There is insufficient volume of olivine and chromite cumulates exposed on Cyprus to account for the variations in Cr, Ni, and MgO. Either the different magma batches represent distinct melts from a mantle source that was heterogeneous with respect to the proportions of olivine and chromite,

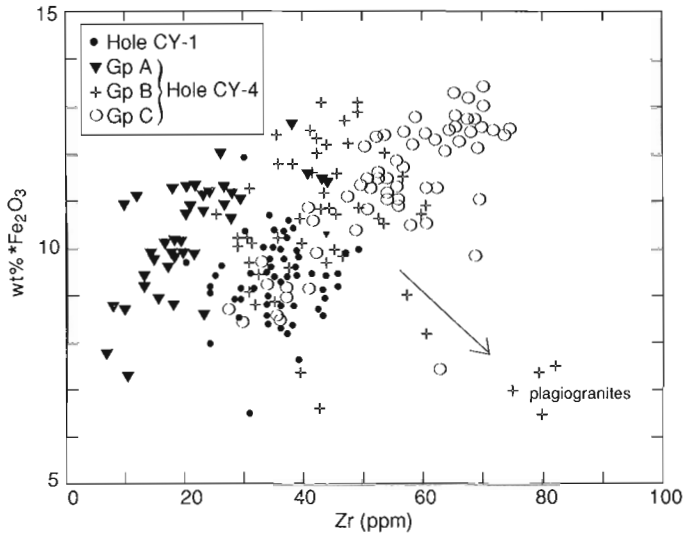

Figure 22: Total iron (as Fe_2O_3) vs. Zr for CY-4 and CY-1 samples.

and/or considerable fractionation involving these two minerals must have taken place within the uprising mantle diapir, before being emplaced at the spreading centre. There are of course discrete bodies of chromitite and dunite within the tectonized harzburgite on Cyprus (and in other ophiolite complexes) that could represent the products of such fractionation (see Figure 3.3 in Lippard et al., 1986). It is notable that Cr/Ni ratios are high in most of the more primitive Troodos basalts, but the rapid fall-off in Cr relative to Ni on Figures 20 and 21 implies that chromite fractionation was more important than olivine fractionation in the early stages of magma evolution. There is some indication from Figure 21 that olivine fractionation is more important in Group C magmas than in Group A ones. It could be that Group A magmas have been derived from a more refractory harzburgitic source, which was also lower in incompatible trace elements. Further detailed examination of CY-4 and CY-1 basalts using high-precision analytical data is necessary before these provisional conclusions could be substantiated.

PLAGIOGRANITE PETROGENESIS

Plagiogranites (Coleman and Peterman, 1975) are a common, though little understood feature of many ophiolite complexes. There were significant numbers of high-silica dykes drilled in the upper part of CY-4 that may provide information on their petrogenesis. The simplest way to encourage a magma to fractionate toward silica-rich compositions is the early precipitation of magnetite or titanomagnetite (Saunders et al., 1979).

Figure 22 shows a plot of total iron (as Fe_2O_3) against zirconium, which discriminates broadly between Groups A, B, and C, and emphasizes the close correspondence between

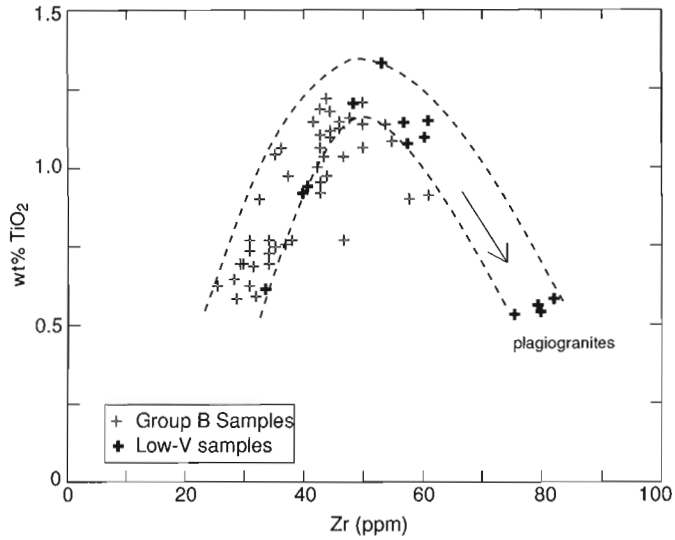

Figure 23: TiO_2 variation in CY-4 Group B samples, showing fall in titanium towards plagiogranites as titanomagnetite is removed. Heavy crosses are linked samples (Figure 20).

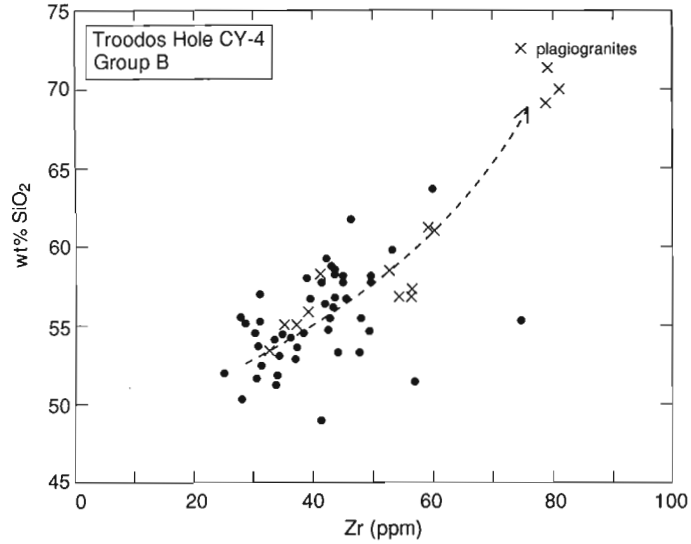

Figure 24: SiO_2 variation in CY-4 Group B samples showing increase in silica as titanomagnetite is removed. Crosses are linked samples (Figure 20).

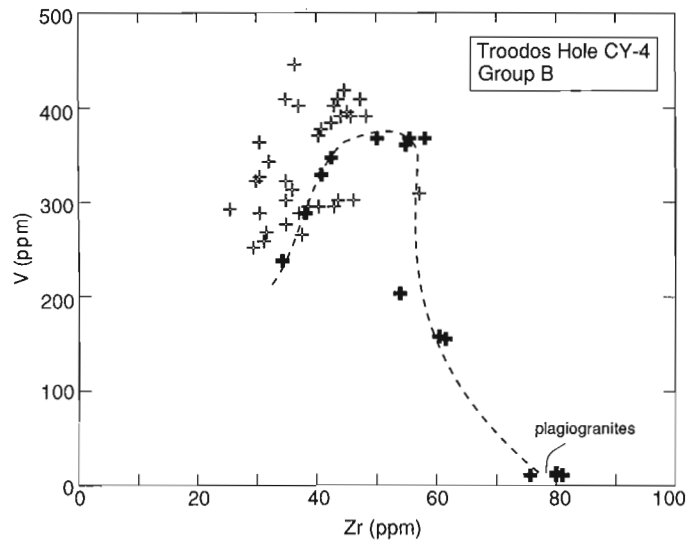

Figure 25: Vanadium variation in CY-4 Group B samples showing rapid depletion in V as titanomagnetite crystallizes. Compare with Ti in Figure 23. Crosses are linked samples (Figure 20).

CY-1 and Group C basalts. In general Group C samples are more iron-rich than those in Group A, which agrees with the suggestion made above that Group C basalts have been derived from a more fertile source. It might have been expected that these Fe-rich basalts were more prone to evolve into plagiogranite because it was easier to achieve titanomagnetite saturation. However, it appears that most plagiogranites (or transitional plagiogranites) can be linked with Group B, and therefore factors other than the initial Fe concentration may have been important.

Figure 23 shows a plot of TiO_2 vs. Zr for Group B samples. The samples with crosses are those that appear to share the same lineage from Figure 20. There is a positive correlation of Ti and Zr, but this rapidly switches to a negative correlation with the development of the plagiogranite trend, indicating that titanomagnetite has been fractionating. Simultaneously (Figure 24) there is an increase in silica. In fact, vanadium (Figure 25) is a much more sensitive indicator of titanomagnetite fractionation than titanium, so there is a very rapid fall in vanadium concentration in the sample group once the trend toward plagiogranite is established. As this does not seem directly correlated with absolute concentration of Fe, Ti, or V (indeed Figures 10 and 11 show that Troodos basalts are distinctly low-TiO_2), the most acceptable explanation is that titanomagnetite precipitation is encouraged by locally increased oxygen fugacity in the magma. This would occur if blocks of hydrothermally-altered basalt fell into the magma chambers (Pederson and Malpas, 1984), or seawater locally gained access. The irregular occurrence of plagiogranite is consistent with Troodos developing as a series of small independent magma chambers, rather than as one large semi-continuous magma chamber.

DISCUSSION

The rather wide dispersion in the compositions of Troodos basalts revealed by drilling in Holes CY-1 and CY-4 would appear to represent the composite evolution of up to a dozen

small batches of magma, rather than the product of differentiation of one single continuous magma chamber. This strongly supports the contention of Allen (1975), based on petrographic evidence. It is consistent with the relatively small volume of undisputed cumulate in Troodos in comparison with the large volume of 'liquid' dykes and lavas. Indeed many Troodos gabbro samples analyzed by Adamides (1984) have liquid rather than cumulate characteristics. A consequence is that the mineral phases responsible for the observed chemical fractionations must be resident in, and have been active in, the upper mantle, and that considerable fractionation must have taken place within the uprising mantle diapir at oceanic spreading centres. Interestingly, it is only through analysis of large numbers of samples, such as has been provided by the Cyprus drilling, that it is possible to begin to elucidate these relationships. It could well be that the popular model of a large semi-continous axial magma chamber at oceanic spreading centres needs to be replaced by one of small discrete and discontinuous magma chambers. For instance, although seismic profiling along the fast-spreading East Pacific Rise has identified reflections that can be interpreted as the top of an axial magma chamber extending for tens of kilometers (Detrick et al., 1987), the evidence is less clear for medium- to slow-spreading ridges. Recently, Smith and Cann (1990) have identified hundreds of seamounts forming the axial zone of a small sector of the slow-spreading North Atlantic, which can be extrapolated to literally tens of millions in the North Atlantic as a whole. They interpret these as representing erupted pulses of magma fed by their individual plumbing systems and not buffered by a large axial magma chamber. Studies of drilled basalts in the North Atlantic have also suggested that their compositions are not buffered by large magma chambers (Tarney et al., 1979a, b, 1980; Wood et al., 1979).

The range of basalt compositions exhibited in CY-4 and CY-1 is too large to be accomplished simply by fractionation in uprising diapirs and in high-level magma chambers. For instance it is notable that Group C magmas not only appear to have higher incompatible trace element abundances than Group A, but are also more iron-rich. This suggests that the mantle source may have been more fertile in terms of major elements as well as trace elements, Group A magmas are unusually low in terms of elements such as Ti, Zr and P, which could indicate they derived from a source that had suffered extraction of basalt at some earlier period. A possible scenario is that the mantle source feeding the Troodos lavas was a mixture of relatively fertile asthenosphere (represented by Group C basalts) with more refractory oceanic lithosphere (represented by Group A basalts). The later Upper Pillow Lavas, sampled in Hole CY-1, have close affinities with Group C, but are on the whole rather more Mg- and Cr-rich. They may represent deeper-seated melts of the same asthenosphere material. As the amount of petrological and geochemical data available for Troodos basalts has increased, various workers have begun to distinguish two, three, or even four distinct magma types (Robinson et al., 1983; McCulloch and Cameron, 1983; Cameron, 1985; Flower and Levine, 1987; Taylor and Nesbitt, 1988; Ohenstetter et al., 1990), some of which have the geochemical characteristics of the four main groups described here. In fact in a model where a MORB asthenosphere is mixing and interacting with a variably more depleted and refractory ocean lithosphere, there could well be a spectrum of 'primary' magma compositions in the Troodos Complex as a whole. The cloud of points seen in the Zr vs. Y diagram (Figure 5), which is real and does not reflect analytical uncertainty, would be consistent with this model. Implicit in this interpretation is that magma compositions have not been buffered by long-lived axial magma chambers.

Troodos magma compositions undoubtedly have a supra-subduction zone signature (Saunders et al., 1980a, b; Pearce et al., 1984), marked particularly by very low contents of high field strength elements, LIL-element values higher than MORB, isotopic evidence of sediment contamination, and generally more siliceous compositions than normal MORB. However, in detail the only close geochemical comparisons that can be made so far are with basalts from the West Philippine Basin and with primitive tholeiites erupted at the very early stages of intra-oceanic arc development. In effect the chemistry indicates that the source is very depleted, but has been contaminated by fluids and by minor subducted components (e.g. sediment), though not necessarily at the time of generation of the Troodos basalts (it could have been during an immediately preceeding subduction phase). The West Philippine Basin analogy is interesting in that although spreading occurred close to a primitive arc (now Kyushu-Palau remnant arc; mainly IAT) it was not strictly linked in terms of back-arc spreading: the spreading centre is oblique to the arc. On the other hand this may be a tectonic situation that (given the high water contents in the back-arc environment: cf. Muenow et al., 1990) would permit mobilization of contaminated refractory ocean lithosphere as well as asthenosphere. The siliceous compositions of many Troodos basalts would be more compatible with the melting, particularly hydrous melting, of harzburgitic lithosphere. The existence of an active arc is not a pre-requisite for 'back-arc' spreading; an arc may develop some time after 'back-arc' spreading has started, and need not develop at all if back-arc spreading is aborted. The Upper Pillow Lavas may then have been erupted after spreading and extension had ceased. Troodos does not conform to a typical oceanic spreading centre.

Finally, plagiogranite development, so common in many ophiolites, appears to reflect local entry of water into the system at a later stage. It does not seem to be connected with primary volatile contents of the magma, or with the Fe content of the melt. Vanadium (more than titanium) is a very sensitive indicator of this process because it is rapidly sequestered by magnetite or titanomagnetite and removed from the melt. Water may have gained access to the magmas through fault activity connected with episodic extension, or through blocks

of hydrothermally altered basalt falling into newly extending/enlarging magma chambers.

REFERENCES

Adamides, N.G.
1984: Cyprus volcanogenic sulphide deposits in relation to their environment of formation; (PhD Thesis), University of Leicester, U.K., 383 p.

Allen, C.R.
1975: The petrology of a portion of the Troodos plutonic complex, Cyprus; (PhD Thesis), University of Cambridge, U.K., 161 p.

Bienvenu, P., Bougault, H., Joron, J.L., Treuil, M., and Dmitriev, L.
1990: MORB alteration: Rare-earth element/non-rare-earth hygromagmaphile element fractionation; Chemical Geology, v. 82, p. 1–14.

Cameron, W.E.
1985: Petrology and origin of primitive lavas from the Troodos ophiolite, Cyprus; Contributions to Mineralogy and Petrology, v. 89, p. 239–255.

Cameron, W.E. and Nisbet, E.G.
1983: Phanerozoic analogues of komatiitic basalts; *in* Arndt, N.T. and Nisbet, E.G., Komatiites, George Allen and Unwin, London, p. 29–50.

Cameron, W.E., Nisbet, E.G., and Dietrich, V.J.
1979: Boninites, komatiites and ophiolitic basalts; Nature, v. 280, p. 550–553.

Cann, J.R.
1979: Results of Deep Sea Drilling in the Atlantic; *in* Talwani, M. et al., Results of Deep Sea Drilling in the Atlantic, Maurice Ewing Series 2, American Geophysical Union, p. 230–238.

Chapman, H.J. and Spooner, E.T.C.
1977: ^{87}Sr enrichment in ophiolitic sulphide deposits in Cyprus confirms ore formation by circulating seawater; Earth and Planetary Science Letters, v. 35, p. 71–78.

Coleman, R.G. and Peterman, Z.E.
1975: Oceanic plagiogranite; Journal of Geophysical Research, v. 80, p. 1099–1108.

Crawford, A.J., Beccaluva, L., and Serri, G.
1981: Tectono-magmatic evolution of the West Philippine-Mariana region and the origin of boninites; Earth and Planetary Science Letters, v. 54, p. 346–356.

Crawford, A.J., Beccaluva, L., Serri, G., and Dostal, J.
1986: Petrology, geochemistry and tectonic implications of volcanics dredged from the intersection of the Yap and Mariana trenches; Earth and Planetary Science Letters, v. 80, p. 265–280.

de Jongh, W.K.
1973: X-ray fluorescence analysis applying theoretical matrix corrections. Stainless Steel; X-ray Spectrometry, v. 2, p. 151–158.

Detrick, R.S., Buhl, P., Vera, E., Mutter, J., Orcutt, J. Madsden, J., and Brocher, T.
1987: Multi-channel seismic imaging of a crustal magma chamber along the East Pacific Rise; Nature, v. 326, p. 35–41.

Duncan, R.A. and Green, D.H.
1980: Role of multistage melting in the formation of oceanic crust; Geology, v. 8, p. 22–26.

Flower, M.F.J. and Levine, H.M.
1987: Petrogenesis of a tholeiite-boninite sequence from Ayios Mamas, Troodos ophiolite: evidence for splitting of a volcanic arc?; Contributions to Mineralogy and Petrology, v. 96, p. 326–342.

Floyd, P.A. and Tarney, J.
1979: First order alteration chemistry of Leg 49 basement rocks; Initial Reports of the Deep Sea Drilling Project, v. 49, U.S. Government Printing Office, Washington, p. 693–708.

Gass, I.G.
1958: Ultrabasic pillow lavas from Cyprus; Geological Magazine, v. 95, p. 241–251.

Gass, I.G.
1968: Is the Troodos Massif of Cyprus a Fragment of Mesozoic Ocean Floor?; Nature, v. 220, p. 39–42.

Gass, I.G.
1980: The Troodos massif: its role in the unravelling of the ophiolite problem and its significance in the understanding of constructive plate margin processes; *in* Panayiotou, A., Ophiolites: proceedings of the International Ophiolite Symposium, Cyprus 1979, Cyprus Geological Survey Department, Nicosia, p. 23–35.

Gass, I.G. and Masson-Smith, D.
1963: The geology and gravity anomalies of the Troodos Massif, Cyprus; Philosophical Transactions of the Royal Society, London, v. A255, p. 417–467.

Gass, I.G. and Smewing, J.D.
1973: Intrusion, extrusion, and metamorphism at constructive margins: evidence from the Troodos Massif, Cyprus; Nature, v. 242, p. 26–29.

Gass, I.G., Neary, C.R., Plant, J., Robertson, A.H.F., Simonian, K.O., Smewing, J.D., Spooner, E.T.C., and Wilson, R.A.M.
1975: Comments on 'The Troodos ophiolitic complex was probably formed in an island arc', by A. Miyashiro and subsequent correspondence by A. Hynes and A. Miyashiro; Earth and Planetary Science Letters, v. 25, p. 236–238.

Greenbaum, D.
1972: Magmatic processes at ocean ridges: evidence from the Troodos Massif, Cyprus; Nature, Physical Science, v. 238, p. 18–21.

Hamelin, B., Dupré, B., and Allègre, C.J.
1984: The lead isotope systematics of ophiolite complexes; Earth and Planetary Science Letters, v. 67, p. 351–366.

Hickey, R.L. and Frey, F.A.
1982: Geochemical characteristics of boninite series volcanics: implications for their source; Geochimica et Cosmochimica Acta, v. 46, p. 2099–2115.

Hole, M.J., Saunders, A.D., Marriner, G.F., and Tarney, J.
1984: Subduction of pelagic sediment: implications for the origin of Ce-anomalous basalts from the Mariana Islands; Journal of the Geological Society, London, v. 141, p. 453–472.

Kay, R.W. and Senechal, R.G.
1976: The rare earth geochemistry of the Troodos ophiolite complex; Journal of Geophysical Research, v. 81, p. 964–970.

Kidd, R.G.W. and Cann, J.R.
1974: Chilling statistics indicate an ocean-floor spreading origin

for the Troodos Complex, Cyprus; Earth and Planetary Science Letters, v. 24, p. 151–155.

Lippard, S.J., Shelton, A.W., and Gass, I.G.
1986: The Ophiolite of Northern Oman; Geological Society of London, Memoir, v. 11, 178 p.

Marsh, N.G., Saunders, A.D., Tarney, J., and Dick, H.J.B.
1980: Geochemistry of basalts from the Shikoku and Daito Basins, Deep Sea Drilling Project Leg 58; Initial Reports of the Deep Sea Drilling Project, v. 58, U.S. Government Printing Office, Washington, p. 805–842.

Marsh, N.G., Tarney, J., and Hendry, G.L.
1983: Trace element geochemistry of basalts from Hole 504B, Panama Basin, Deep Sea Drilling Project Legs 69 and 70; Initial Reports of the Deep Sea Drilling Project, v. 69, U.S. Government Printing Office, Washington, p. 747–763.

Mattey, D.P., Marsh, N.G., and Tarney, J.
1980: The geochemistry, mineralogy, and petrology of basalts from the West Philippine and Parece Vela Basins and from the Palau-Kyushu and West Mariana Ridges, Deep Sea Drilling Project Leg 59; Initial Reports of the Deep Sea Drilling Project, v. 59, U.S. Government Printing Office, Washington, p. 753–800.

McCulloch, M.T. and Cameron, W.E.
1983: Nd-Sr isotopic study of primitive lavas from the Troodos ophiolite, Cyprus: evidence for a subduction-related setting; Geology, v. 11, p. 727–731.

Miyashiro, A.
1973: The Troodos ophiolitic complex was probably formed in an island arc; Earth and Planetary Science Letters, v. 19, p. 218–224.

Miyashiro, A.
1975: Classification, characteristics and origin of ophiolites; Journal of Geology, v. 83, p. 249–281.

Moores, E.M. and Jackson, E.D.
1974: Ophiolites and oceanic crust; Nature, v. 250, p. 136–139.

Moores, E.M., Robinson, P.T., Malpas, J., and Xenophontos, C.
1984: Model for the origin of the Troodos massif, Cyprus, and other mideast ophiolites; Geology, v. 12, p. 500–503.

Moores, E.M. and Vine, F.J.
1971: The Troodos Massif, Cyprus and other ophiolites as oceanic crust: evaluation and implications; Philosophical Transactions of the Royal Society, London, v. A268, p. 443–466.

Muenow, D.W., Garcia, M.O., Aggrey, K.E., Bednarz, U. and Schmincke, H.U.
1990: Volatiles in submarine glasses as discriminant of tectonic origin: application to the Troodos ophiolite; Nature, v. 343, p. 159–161.

Murton, B.J. and Gass, I.G.
1986: Western Limassol Forest complex, Cyprus: part of an Upper Cretaceous leaky transform fault; Geology, v. 14, p. 255–258.

O'Hara, M.J. and Mathews, R.E.
1981: Geochemical evolution in an advancing, periodically replenished, periodically tapped, continuously fractionated magma chamber; Journal of the Geological Society, London, v. 138, p. 237–277.

Ohenstetter, M., Bechon, F., and Ohnenstetter, D.
1990: Geochemistry and mineralogy of lavas from the Arakapas fault belt, Cyprus: consequences for magma chamber evolution; Mineralogy and Petrology, v. 41, p. 105–204.

Pearce, J.A.
1975: Basalt geochemistry used to investigate past tectonic environments on Cyprus; Tectonophysics, v. 25, p. 41–67.

Pearce, J.A.
1980: Geochemical evidence for the genesis and eruptive setting of lavas from Tethyan ophiolites; *in* Panayiotou, A., Ophiolites: proceedings of the International Ophiolite Symposium, Cyprus, 1979, Cyprus Geological Survey Department, Nicosia, p. 261–272.

Pearce, J.A., Lippard, S.J., and Roberts, S.
1984: Characteristics and tectonic significance of supra -subduction zone ophiolites; *in* Kokelaar, B.P. and Howells, M.F., Marginal Basin Geology, Special Publication of The Geological Society, London, v. 16, p. 77–94.

Pedersen, R.B. and Malpas, J.
1984: The origin of oceanic plagiogranites from the Karmoy ophiolite, Western Norway; Contributions to Mineralogy and Petrology, v. 88, p. 36–52.

Rautenschlein, M., Jenner, G.A., Hertogen, J., Hofmann, A.W., Kerrich, R., Schmincke, H.-U., and White, W.M.
1985: Isotopic and trace element composition of volcanic glasses from the Akaki Canyon, Cyprus: implications for the origin of the Troodos ophiolite; Earth and Planetary Science Letters, v. 75, p. 369–383.

Robinson, P.T., Melson, W.G., O'Hearn, T., and Schmincke, H.-U.
1983: Volcanic glass compositions of the Troodos ophiolite, Cyprus; Geology, v. 11, p. 400–404.

Saunders, A.D., Tarney, J., Stern, C.R., and Dalziel, I.W.D.
1979: Geochemistry of Mesozoic marginal basin floor igneous rocks from southern Chile; Geological Society of America: Bulletin, v. 90, p. 237–258.

Saunders, A.D., Tarney, J., and Weaver, S.D.
1980a: Transverse geochemical variations across the Antarctic Peninsula: implications for the genesis of calc-alkaline magmas; Earth Planetary Science Letters, v. 46, p. 344–360.

Saunders, A.D., Tarney, J., Marsh, N.G., and Wood, D.A.
1980b: Ophiolites as ocean crust or marginal basin crust: a geochemical approach; Ophiolites: proceedings of the International Ophiolite Symposium, Cyprus, 1979, Cyprus Geological Survey Department, Nicosia, p. 193–204.

Saunders, A.D. and Tarney, J.
1984: Geochemical characteristics of basaltic volcanism within back-arc basins; *in* Kokelaar, B.P. and Howells, M.F., Marginal Basin Geology, Special Publication of the Geological Society, London, v. 16, p. 59–76.

Schiffman, P., Smith, B.M., Varga, R.J., and Moores, E.M.
1987: Geometry, conditions and timing of off-axis hydrothermal metamorphism and ore-deposition in the Solen graben; Nature, v. 325, p. 423–425.

Schmincke, H.-U., Rautenschlein, M., Robinson, P.T., and Mehegan, J.M.
1983: Troodos extrusive series of Cyprus: a comparison with oceanic crust; Geology, v. 11, p. 405–409.

Searle, D.L. and Vokes, F.M.
1969: Layered ultrabasic lavas from Cyprus; Geological Magazine, v. 106, p. 515–530.

Simonian, K.O. and Gass, I.G.
1978: Arakapas fault belt, Cyprus: a fossil transform fault; Geological Society of America: Bulletin, v. 89, p. 1220–1230.

Smewing, J.D. and Potts, P.J.
1976: Rare earth abundances in basalts and metabasalts from the Troodos Massif, Cyprus; Contributions to Mineralogy and Petrology, v. 56, p. 245–258.

Smith, D.K. and Cann, J.R.
1990: Hundreds of small volcanoes on the median valley floor of the Mid-Atlantic Ridge at 24–30°N; Nature, v. 348, p. 152–156.

Smewing, J.D., Simonian, K.O., and Gass, I.G.
1975: Metabasalts from the Troodos Massif, Cyprus: genetic implications deduced from petrography and trace element geochemistry; Contributions to Mineralogy and Petrology, v. 51, p. 49–64.

Spooner, E.T.C.
1977: Hydrodynamic model for the origin of the ophiolitic cupriferous pyrite deposits of Cyprus; *in* Volcanic Processes in ore Genesis, Institution of Mining and Metallurgy, London, p. 58–71.

Spooner, E.T.C. and Bray, C.J.
1977: Hydrothermal fluids of seawater salinity in ophiolitic sulphide ore deposits in Cyprus; Nature, v. 266, p. 808–812.

Spooner, E.T.C., Chapman, H.J., and Smewing, J.D.
1977: Strontium isotopic contamination and oxidation during ocean floor hydrothermal metamorphism of the ophiolitic rocks of the Troodos Massif, Cyprus; Geochimica et Cosmochimica Acta, v. 41, p. 873–890.

Stern, C. and Elthon, D.
1979: Vertical variations in the effects of hydrothermal metamorphism in Chilean ophiolites: their implications for ocean floor metamorphism; Tectonophysics, v. 55, p. 179–213.

Tarney, J., Saunders, A.D., and Weaver, S.D.
1977: Geochemistry of volcanic rocks from the island arcs and marginal basins of the Scotia Arc region; *in* Maurice Ewing Series 1, American Geophysical Union, p. 367–378.

Tarney, J., Saunders, A.D., Weaver, S.D., Donnellan, N.C.B. and Hendry, G.L.
1979a: Minor-element geochemistry of basalts from Leg 49, North Atlantic Ocean; Initial Reports of the Deep Sea Drilling Project, v. 49, U.S. Government Printing Office, Washington, p. 657–691.

Tarney, J., Wood, D.A., Saunders, A.D., Varet, J., and Cann J.R.
1979b: Nature of mantle heterogeneity in the North Atlantic: evidence from Leg 49; *in* Talwani, M. et al., Results of Deep Sea Drilling in the Atlantic, Maurice Ewing Series 2, American Geophysical Union, p. 285–301.

Tarney, J., Wood, D.A., Saunders, A.D., Cann, J.R., and Varet., J.
1980: Nature of mantle heterogeneity in the North Atlantic: evidence from deep sea drilling; Philosophical Transactions of the Royal Society of London, v. A297, p. 179–202.

Tarney, J., Saunders, A.D., Mattey, D.P., Wood, D.A., and Marsh, N.G.
1981: Geochemical aspects of back-arc spreading in the Scotia Sea and western Pacific; Philosophical Transactions of the Royal Society of London, v. A300, p. 263–285.

Tatsumi, Y.
1981: Melting experiments on a high-magnesian andesite; Earth and Planetary Science Letters, v. 54, p. 357–365.

Taylor, R.N. and Nesbitt, R.W.
1988: Light rare-earth enrichment of supra subduction-zone mantle: evidence from the Troodos ophiolite, Cyprus; Geology, v. 16, p. 448–451.

Varga, R.J. and Moores, E.M.
1985a: Spreading structure of the Troodos ophiolite, Cyprus; Geology, v. 13, p. 846–850.

Varga, R.J. and Moores, E.M.
1985b: Ocean floor structure of the Troodos ophiolite, Cyprus; Geological Society of America Abstracts with Programs, v. 17, p. 415.

Walker, D.
1973: Behavior of X-ray mass absorption coefficients near absorption edges: Reynolds method revisited; American Mineralogist, v. 58, p. 1069–1072.

Weaver, S.D., Saunders, A.D., Pankhurst, R.J., and Tarney, J.
1979: A geochemical study of magmatism associated with the initial stages of back-arc spreading: the Quarternary volcanics of Bransfield Strait, from South Shetland Islands; Contributions to Mineralogy and Petrology, v. 68, p. 151–169.

Weaver, B.L., Wood, D.A., Tarney, J., and Joron, J.L.
1987: Geochemistry of ocean island basalts from the South Atlantic: Ascension, Bouvet, St. Helena, Gough and Tristan da Cunha; *in* Fitton, J.G. and Upton, B.G.J., Alkaline Igneous Rocks, Geological Society of London Special Publication, no. 30, p. 253–267.

Whitehead Jr., J.A., Dick, H.J.B., and Schouten, H.
1984: A mechanism for magmatic accretion under spreading centres; Nature, v. 312, p. 146–148.

Wilson, R.A.M.
1959: The Geology of the Xeros-Troodos Area; Cyprus Geological Survey Department Memoir, v. 1, 136 p.

Wood, D.A.
1979: Dynamic partial melting: its application to the petrogeneses of basalts erupted in Iceland, the Faeroe Islands, the Isle of Skye (Scotland) and the Troodos Massif (Cyprus); Geochimica et Cosmochimica Acta, v. 43, p. 1031–1046.

Wood, D.A., Tarney, J., Varet, J., Saunders, A.D., Bougault, H., Joron, J.L., Treuil, M., and Cann, J.R.
1979: Geochemistry of basalts drilled in the North Atlantic by IPOD Leg 49: implications for mantle heterogeneity; Earth and Planetary Science Letters, v. 42, p. 77–97.

Wood, D.A., Joron, J.L., Marsh, N.G., Tarney, J., and Treuil, M.
1980a: Major- and trace-element variations in basalts from the North Phillippine Sea drilled during Deep Sea Drilling Project Leg 58: a comparative study of back-arc-basin basalts with lava series from Japan and mid-ocean ridges; Initial Reports of the Deep Sea Drilling Project, v. 58, U.S. Government Printing Office, Washington, p. 873–894.

Wood, D.A., Mattey, D.P., Joron, J.L., Marsh, N.G., Tarney, J., and Treuil, M.
1980b: A geochemical study of 17 selected samples from basement cores recovered at Sites 447, 449, 450, and 451, Deep Sea Drilling Project Leg 59; Initial Reports of the Deep Sea Drilling Project, v. 59, U.S. Government Printing Office, Washington, p. 743–752.

Wood, D.A., Marsh, N.G., Tarney, J., Joron, J.L., Fryer, P., J., and Treuil, M.

1982: Geochemistry of igneous rocks recovered from a transect across the Mariana Trough, Arc, Fore-arc and Trench, Sites 453 through 461, Deep Sea Drilling Project Leg 60; Initial Reports of the Deep Sea Drilling Project, v. 60, U.S. Government Printing Office, Washington, p. 743–752.

Pellet	L2457	L2458	L2459	L2460	L2461	L2462	L2463	L2464	L2465	L2466
Core/Sec	32.6	41.7	42.4	43.2	45.1	45.1	45.1	45.1	48.1	49.8
Depth (m)	165.10	214.40	218.00	223.10	233.90	237.50	240.00	244.50	246.70	254.00
SiO_2	47.8	45.5	48.2	48.4	42.5	48.8	49.0	48.7	46.9	46.9
TiO_2	0.57	0.62	0.73	0.70	0.66	0.73	0.76	0.76	0.72	0.70
Al_2O_3	14.9	15.3	16.4	15.7	14.9	15.6	16.0	16.3	15.4	15.2
Fe_2O_3	8.1	8.8	9.2	9.3	8.9	9.0	8.8	9.1	8.4	8.1
MnO	0.11	0.15	0.11	0.09	0.17	0.09	0.08	0.11	0.14	0.13
MgO	10.5	9.2	8.6	8.3	8.1	8.4	7.7	11.1	9.0	8.4
CaO	9.2	5.5	4.3	3.8	9.6	6.7	7.9	3.5	6.8	7.5
Na_2O	1.5	1.1	1.6	1.3	1.9	2.4	2.8	2.1	1.9	1.8
K_2O	2.45	4.88	3.80	5.08	3.07	2.14	1.79	2.50	3.29	3.40
P_2O_5	0.05	0.06	0.06	0.05	0.08	0.07	0.08	0.07	0.08	0.10
LOI	5.45	8.16	5.20	5.90	9.16	4.19	3.43	4.49	5.90	6.34
Total	100.54	99.22	98.25	98.69	99.14	98.14	98.33	98.83	98.39	98.59
Trace elements in parts per million										
Cr	238	146	114	120	89	92	72	159	154	185
V	234	246	319	235	262	272	284	279	249	233
Ni	75	46	49	45	32	36	31	42	51	43
Zn	73	76	85	82	69	74	78	77	78	70
Rb	16.6	30.7	26.9	33.8	46.3	16.6	26.7	12.3	17.4	21.0
Sr	82.7	91.3	82.3	72.8	80.5	81.4	91.5	80.3	83.2	71.6
Y	15.5	17.5	18.5	20.1	17.6	19.2	19.1	16.4	18.8	19.9
Zr	29.4	34.5	39.6	35.9	38.7	41.6	45.7	38.9	44.4	42.9
Nb	1.1	0.6	1.4	1.2	0.5	1.1	0.8	0.8	0.7	0.8
Ga	14	14	16	14	14	15	15	14	14	13
Ba	32.5	19.0	13.5	24.5	27.4	9.7	21.9	12.0	28.9	19.8
La	1.1	0.8	1.5	1.3	2.7	1.7	1.2	0.3	3.3	3.4
Ce	5.2	3.7	9.7	7.2	4.6	6.2	4.2	6.1	3.2	8.2
Nd	5.5	4.8	6.2	5.0	4.1	5.1	5.1	4.4	5.4	7.6
Pb	2	6	3	4	4	3	8	4	4	4
Th	n.d.	n.d.	n.d.	n.d.	n.d.	n.d.	1	2	n.d.	n.d.
U	n.d.	3	2	2	2	3	3	2	5	2
C.I.P.W. norms (calculated using $FeO : Fe_2O_3 = 0.85 : 0.15$)										
Qz	–	–	–	–	–	–	–	–	–	–
Co	–	–	2.00	1.24	–	–	–	3.96	–	–
Or	14.46	28.83	22.44	30.02	18.17	12.65	10.55	14.79	19.44	20.09
Ab	12.32	9.22	13.32	11.31	1.66	20.67	23.29	17.94	15.77	15.61
An	26.77	22.35	21.11	18.46	23.25	25.28	25.94	16.82	23.96	23.24
Ne	–	0.06	–	–	7.68	–	–	–	–	–
Di	14.78	3.71	–	–	19.36	6.18	10.51	–	7.41	10.65
Hy	8.21	–	22.94	16.10	–	15.21	9.40	31.18	3.69	1.25
Ol	15.25	23.29	7.34	11.79	16.09	10.07	11.29	5.67	18.51	17.76
Mt	1.40	1.51	1.59	1.61	1.54	1.55	1.52	1.57	1.44	1.39
Il	1.08	1.19	1.39	1.32	1.26	1.38	1.45	1.45	1.36	1.33
Ap	0.13	0.14	0.14	0.13	0.19	0.17	0.18	0.15	0.19	0.22

Table 2: (part 1 of 7) Hole CY-1 basalt samples: Chemical Analyses.

Pellet	L2467	L2468	L2469	L2470	L2471	L2472	L2473	L2474	L2475	L2476
Core/Sec	50.5	50.7	51.6	52.2	53.1	54.3	54.7	55.10	55.10	55.2
Depth (m)	259.20	261.20	266.30	268.80	273.40	279.70	281.90	287.20	289.20	283.50
SiO_2	48.6	48.2	47.7	48.0	49.5	46.2	47.0	43.4	44.5	44.8
TiO_2	0.65	0.74	0.80	0.79	0.47	0.68	0.73	0.63	0.62	0.67
Al_2O_3	14.1	15.7	15.6	15.6	15.5	14.3	15.1	13.5	13.5	14.1
Fe_2O_3	10.0	8.1	9.3	8.9	8.6	8.8	8.6	8.3	8.3	8.7
MnO	0.11	0.15	0.14	0.14	0.08	0.10	0.13	0.14	0.14	0.11
MgO	11.3	9.2	8.4	8.0	9.7	9.0	8.7	8.9	9.5	9.8
CaO	5.7	6.1	5.4	6.7	8.7	9.0	8.5	9.8	11.7	9.8
Na_2O	2.5	2.3	2.4	2.3	2.6	2.3	2.3	2.4	2.4	2.5
K_2O	1.28	2.95	2.98	2.98	0.67	2.11	2.55	2.73	1.49	1.70
P_2O_5	0.10	0.08	0.10	0.09	0.05	0.09	0.09	0.09	0.08	0.09
LOI	4.42	5.11	5.23	5.47	3.22	6.41	5.76	9.25	7.86	7.54
Total	98.76	98.48	98.07	99.04	99.08	99.07	99.35	99.17	100.19	99.64
Trace elements in parts per million										
Cr	115	186	89	116	285	238	233	265	424	265
V	181	255	230	242	254	221	257	203	218	232
Ni	43	48	33	36	70	51	51	45	151	50
Zn	68	71	78	75	67	72	78	62	72	70
Rb	13.3	17.0	19.2	18.6	8.1	15.3	15.4	22.4	12.8	12.5
Sr	64.0	86.8	78.8	89.4	91.4	77.0	92.1	75.8	84.5	73.8
Y	19.6	17.4	22.4	20.0	13.2	18.2	19.6	18.1	16.3	20.0
Zr	39.0	43.5	48.2	46.5	29.7	41.2	43.8	38.1	36.6	39.0
Nb	0.8	1.0	1.0	2.0	1.3	0.6	0.7	0.6	0.7	0.8
Ga	16	14	14	15	14	13	14	12	12	13
Ba	8.1	43.7	23.7	25.4	15.8	11.6	23.1	17.8	11.7	9.8
La	2.5	1.8	0.9	2.4	1.8	1.6	1.2	1.2	1.3	2.8
Ce	5.7	6.9	4.3	6.1	0.8	5.4	3.8	1.6	2.8	3.5
Nd	5.3	5.1	5.9	6.0	3.0	5.7	5.7	6.3	4.7	5.4
Pb	5	4	3	5	5	2	5	5	5	4
Th	n.d.	n.d.	n.d.	n.d.	n.d.	n.d.	3	n.d.	n.d.	n.d.
U	2	1	2	n.d.	2	3	n.d.	2	n.d.	2
C.I.P.W. norms (calculated using $FeO : Fe_2O_3 = 0.85 : 0.15$)										
Qz	–	–	–	–	–	–	–	–	–	–
Or	7.55	17.46	17.63	17.61	3.98	12.44	15.10	16.14	8.79	10.05
Ab	20.87	19.19	19.97	19.12	21.62	16.78	17.34	3.77	8.06	12.55
An	23.66	23.93	23.17	23.76	28.94	22.47	23.55	17.92	21.76	22.33
Ne	–	–	–	–	–	1.55	0.93	9.10	6.57	4.52
Di	3.16	4.58	2.38	7.38	11.13	17.67	14.42	24.49	29.05	20.69
Hy	23.77	8.55	9.67	6.31	19.03	–	–	–	–	–
Ol	11.27	15.98	15.85	15.38	7.91	17.98	18.44	14.95	14.59	18.23
Mt	1.73	1.39	1.61	1.54	1.49	1.52	1.48	1.43	1.44	1.50
Il	1.23	1.41	1.51	1.51	0.90	1.30	1.38	1.19	1.17	1.26
Ap	0.23	0.18	0.23	0.21	0.11	0.20	0.22	0.21	0.18	0.22

Table 2 (part 2 of 7)

Pellet	L2477	L2478	L2479	L2480	L2481	L2482	L2483	L2484	L2485	L2486
Core/Sec	56.6	57.6	58.3	58.5	59.3	61.3	61.5	61.5	61.5	64.6
Depth (m)	292.80	297.70	301.50	304.50	309.05	316.80	318.10	321.40	328.60	333.50
SiO_2	47.9	47.1	48.8	48.9	47.0	50.5	50.4	48.6	52.0	49.6
TiO_2	0.65	0.62	0.61	0.64	0.65	0.61	0.58	0.56	0.66	0.67
Al_2O_3	15.6	15.2	15.2	16.1	15.5	15.6	15.5	15.6	12.4	15.9
Fe_2O_3	8.4	8.4	8.7	8.5	9.1	6.3	8.6	8.8	9.4	9.9
MnO	0.14	0.14	0.12	0.10	0.09	0.07	0.05	0.07	0.09	0.09
MgO	10.6	10.2	9.6	9.6	8.2	10.6	9.2	8.2	12.9	8.8
CaO	6.3	7.2	6.6	10.0	8.3	7.0	6.8	10.1	7.8	6.2
Na_2O	2.5	2.5	2.3	2.5	2.6	2.6	2.7	2.7	3.1	2.9
K_2O	2.17	2.11	2.68	0.45	1.49	0.78	0.90	0.94	1.27	1.10
P_2O_5	0.06	0.07	0.09	0.06	0.08	0.05	0.04	0.06	0.05	0.06
LOI	5.32	5.85	4.50	3.16	5.14	2.69	3.60	4.25	n.d.	3.84
Total	99.65	99.41	99.31	100.11	98.17	96.81	98.37	99.86	99.66	99.13
Trace elements in parts per million										
Cr	169	217	286	243	80	263	256	194	235	98
V	251	242	214	253	260	262	237	260	263	279
Ni	44	46	48	47	34	54	53	44	50	37
Zn	72	69	66	73	79	76	77	67	72	89
Rb	9.6	12.5	22.0	4.7	11.5	4.6	9.7	14.0	26.3	9.0
Sr	85.3	87.0	67.9	80.4	78.2	69.2	73.6	82.3	79.6	80.8
Y	18.5	17.6	18.3	17.8	21.0	16.6	15.7	16.0	15.1	22.9
Zr	36.9	34.2	34.2	33.8	33.3	30.6	30.0	29.3	31.5	36.9
Nb	1.1	0.7	0.5	n.d.	0.9	0.7	0.4	1.1	0.6	0.9
Ga	13	12	13	13	14	18	14	14	15	15
Ba	11.8	14.8	14.0	7.4	10.4	9.5	7.7	14.4	26.7	7.8
La	0.7	2.0	0.9	2.8	1.0	1.9	0.9	1.2	2.9	1.9
Ce	3.0	2.0	3.2	4.9	4.9	2.1	3.7	1.6	4.0	8.0
Nd	5.1	3.6	4.6	5.6	4.6	4.3	3.7	3.8	3.3	4.5
Pb	4	4	5	4	5	5	4	6	4	4
Th	n.d.	n.d.	n.d.	n.d.	n.d.	n.d.	n.d.	n.d.	n.d.	n.d.
U	1	1	3	1	2	2	n.d.	n.d.	1	n.d.
C.I.P.W. norms (calculated using $FeO : Fe_2O_3 = 0.85 : 0.15$)										
Qz	–	–	–	–	–	–	–	–	–	–
Or	12.80	12.47	15.85	2.65	8.82	4.60	5.29	5.53	7.50	6.51
Ab	21.47	20.87	19.80	21.55	22.07	22.23	23.25	22.93	26.28	24.33
An	24.69	24.22	23.15	31.14	26.24	28.58	27.33	27.77	16.15	27.14
Di	4.93	9.04	7.29	14.79	11.73	4.53	4.99	17.65	17.78	2.73
Hy	6.65	1.73	8.45	12.14	4.88	29.59	28.47	5.94	9.45	23.65
Ol	20.20	21.70	16.63	11.12	15.53	1.66	2.03	12.31	18.66	6.94
Mt	1.46	1.45	1.50	1.47	1.57	1.09	1.48	1.52	1.63	1.71
Il	1.24	1.18	1.16	1.21	1.24	1.16	1.10	1.07	1.26	1.28
Ap	0.15	0.15	0.22	0.13	0.18	0.13	0.09	0.13	0.13	0.14

Table 2 (part 3 of 7)

Pellet	L2487	L2488	L2489	L2490	L2491	L2492	L2493	L2494	L2495	L2496
Core/Sec	65.2	65.3	66.2	67.07	67.03	68.7	70.8	71.8	72.4	73.1
Depth (m)	337.90	336.90	342.40	348.40	347.10	354.20	361.20	367.10	375.10	375.80
SiO_2	50.9	51.0	52.3	53.8	52.0	49.8	50.4	50.9	54.3	50.7
TiO_2	0.70	0.54	0.65	0.59	0.62	0.67	0.69	0.68	0.64	0.53
Al_2O_3	16.4	16.8	16.0	13.2	15.8	16.0	15.8	16.1	15.5	10.7
Fe_2O_3	9.7	8.7	8.1	11.3	8.4	10.0	10.2	9.3	9.3	8.7
MnO	0.08	0.08	0.10	0.15	0.10	0.10	0.11	0.11	0.10	0.18
MgO	8.4	7.8	6.5	7.4	8.1	9.0	9.6	9.2	7.4	15.3
CaO	7.8	9.8	10.3	3.9	9.9	7.1	6.4	7.2	9.1	8.6
Na_2O	2.8	2.4	2.7	2.6	2.4	2.9	2.9	2.9	2.5	2.1
K_2O	0.19	0.33	0.79	0.89	0.12	0.29	0.37	0.51	0.27	0.18
P_2O_5	0.06	0.04	0.07	0.02	0.06	0.07	0.06	0.11	0.06	0.04
LOI	2.81	2.18	1.85	5.17	1.57	3.02	3.11	3.45	1.53	3.17
Total	99.81	99.66	99.27	99.17	98.96	98.94	99.57	100.34	100.68	100.24
Trace elements in parts per million										
Cr	101	216	138	92	153	94	61	84	90	365
V	282	281	234	208	255	265	267	265	244	224
Ni	35	42	36	26	42	33	30	33	35	203
Zn	89	74	67	68	64	86	86	88	69	66
Rb	1.7	6.6	20.6	17.2	0.7	4.3	3.0	5.9	4.2	3.4
Sr	90.1	74.1	93.9	48.3	85.7	86.8	83.2	84.3	86.8	92.3
Y	22.6	16.8	17.3	18.1	17.1	19.4	16.5	24.1	16.9	15.3
Zr	39.8	28.6	37.3	30.6	33.6	35.5	37.7	34.6	33.9	30.2
Nb	1.0	1.1	0.6	0.6	0.8	1.0	0.6	0.7	1.0	0.6
Ga	15	15	14	8	14	14	15	15	14	13
Ba	4.8	14.2	15.0	4.5	17.3	8.5	8.5	3.5	14.9	23.3
La	3.0	1.6	2.2	0.7	2.1	3.1	2.6	1.2	2.1	1.5
Ce	4.2	n.d.	n.d.	0.5	1.6	5.1	9.0	5.9	2.2	2.1
Nd	5.0	3.6	5.7	1.6	4.7	4.4	5.0	5.9	5.6	3.4
Pb	6	5	3	5	4	4	2	2	1	4
Th	n.d.	n.d.	n.d.	n.d.	n.d.	n.d.	n.d.	n.d.	n.d.	n.d.
U	n.d.	1	n.d.	2	1	n.d.	n.d.	n.d.	2	2
C.I.P.W. norms (calculated using $FeO : Fe_2O_3 = 0.85 : 0.15$)										
Qz	0.82	1.13	2.29	8.89	3.35	–	–	–	6.26	–
Co	–	–	–	0.81	–	–	–	–	–	–
Or	1.13	1.98	4.68	5.27	0.68	1.74	2.19	3.03	1.58	1.07
Ab	23.44	20.45	22.51	22.39	20.32	24.62	24.19	24.35	20.75	18.14
An	31.88	34.06	29.49	19.43	32.10	29.61	29.13	29.44	30.48	19.18
Di	5.05	11.56	17.06	–	13.28	4.40	1.78	4.58	11.67	18.39
Hy	30.69	24.93	17.90	33.12	24.17	27.64	32.82	29.54	24.64	27.86
Ol	–	–	–	–	–	3.88	2.26	1.99	–	9.10
Mt	1.68	1.50	1.39	1.95	1.44	1.73	1.76	1.60	1.61	1.50
Il	1.33	1.02	1.23	1.12	1.18	1.27	1.31	1.28	1.22	1.01
Ap	0.14	0.10	0.16	0.05	0.14	0.16	0.14	0.26	0.14	0.08

Table 2 (part 4 of 7)

Pellet	L2497	L2498	L2499	L2500	L2501	L2502	L2503	L2504	L2505	L2506
Core/Sec	73.2	73.2	73.2	75.4	76.3	77.2	78.4	79.2	79.3	81.2
Depth (m)	377.50	381.30	386.60	390.70	397.50	402.20	410.20	413.20	416.85	426.30
SiO_2	52.4	51.2	54.5	50.7	50.1	51.0	47.9	50.0	55.2	54.0
TiO_2	0.60	0.64	0.59	0.41	0.69	0.71	0.66	0.80	0.68	0.64
Al_2O_3	15.3	16.5	14.6	12.8	16.1	16.4	16.7	17.2	14.7	14.7
Fe_2O_3	8.1	9.6	10.4	7.7	9.7	9.1	7.9	9.2	10.2	9.8
MnO	0.13	0.13	0.11	0.20	0.11	0.10	0.11	0.08	0.10	0.11
MgO	7.5	7.6	6.2	12.6	10.1	9.7	5.2	6.2	5.6	6.3
CaO	9.7	10.3	8.5	9.8	6.5	6.1	12.7	8.9	8.4	8.6
Na_2O	2.7	2.4	2.5	1.7	2.8	2.9	3.2	3.2	2.6	2.9
K_2O	0.10	0.13	0.93	0.14	0.52	0.60	0.79	0.90	1.11	0.63
P_2O_5	0.06	0.06	0.05	0.04	0.08	0.06	0.07	0.10	0.07	0.06
LOI	1.95	1.61	1.55	3.49	2.82	3.04	4.81	2.13	1.49	1.63
Total	98.51	100.27	100.11	99.62	99.46	99.69	100.18	98.71	100.13	99.36
Trace elements in parts per million										
Cr	82	82	68	593	142	124	138	61	64	129
V	251	269	206	207	278	260	274	269	220	201
Ni	33	37	27	307	39	40	37	22	25	33
Zn	71	83	73	65	87	88	74	85	83	70
Rb	n.d.	1.8	23.5	1.4	3.1	4.8	17.6	19.1	26.0	10.7
Sr	93.0	92.7	81.4	69.3	81.1	82.0	98.5	100.3	79.6	81.4
Y	18.1	19.4	16.0	12.7	24.5	23.1	20.7	25.6	18.3	17.7
Zr	36.3	37.4	34.4	24.1	34.9	37.5	38.0	43.8	38.8	33.2
Nb	1.0	0.8	0.5	1.0	0.7	0.9	0.7	1.2	0.8	0.5
Ga	15	15	14	12	16	16	16	16	15	15
Ba	12.6	5.6	20.3	22.1	8.9	12.4	15.9	17.6	19.9	15.0
La	2.2	3.0	3.0	2.3	2.0	1.4	2.8	4.0	2.7	1.6
Ce	3.2	4.7	0.6	1.3	5.9	7.2	3.9	5.5	4.7	4.0
Nd	3.0	5.5	4.2	2.8	4.7	6.4	3.6	7.5	4.3	4.4
Pb	4	6	n.d.	4	5	4	4	4	5	6
Th	n.d.	n.d.	n.d.	n.d.	n.d.	n.d.	n.d.	n.d.	n.d.	n.d.
U	n.d.	2	n.d.	1	1	2	2	n.d.	n.d.	2
C.I.P.W. norms (calculated using $FeO : Fe_2O_3 = 0.85 : 0.15$)										
Qz	3.82	1.37	6.04	0.40	–	–	–	–	7.31	5.22
Co	–	–	–	–	–	0.07	–	–	–	–
Or	0.59	0.79	5.47	0.81	3.04	3.53	4.66	5.34	6.54	3.74
Ab	22.73	20.65	21.58	14.54	23.68	24.86	19.86	27.33	22.01	24.22
An	29.47	33.63	25.75	26.81	29.86	29.62	29.05	29.76	25.25	25.33
Ne	–	–	–	–	–	–	3.86	–	–	–
Di	14.99	14.03	13.41	17.44	1.44	–	27.6	11.31	12.99	13.95
Hy	21.59	24.35	22.35	33.28	29.40	32.60	–	11.86	20.45	21.38
Ol	–	–	–	–	5.20	2.12	6.8	6.82	–	–
Mt	1.40	1.66	1.80	1.33	1.67	1.57	1.37	1.59	1.76	1.69
Il	1.14	1.21	1.12	0.77	1.31	1.34	1.25	1.52	1.29	1.21
Ap	0.13	0.13	0.13	0.09	0.18	0.14	0.17	0.24	0.16	0.13

Table 2 (part 5 of 7)

Pellet	L2507	L2508	L2509	L2510	L2511	L2512	L2513	L2514	L2515	L2516
Core/Sec	82.1	83.2	84.5	85.10	87.03	88.01	88.07	89.01	2.4	8.2
Depth (m)	429.45	434.60	440.00	445.90	455.90	459.60	465.65	468.42	19.70	44.50
SiO_2	49.7	49.9	50.2	49.8	50.0	50.8	51.2	51.5	48.4	46.0
TiO_2	0.68	0.68	0.57	0.63	0.62	0.63	0.69	0.73	0.52	0.78
Al_2O_3	16.1	16.0	14.8	15.0	14.8	16.6	16.0	16.3	16.6	16.8
Fe_2O_3	8.6	7.4	10.0	8.9	8.9	9.0	10.0	8.5	9.0	9.2
MnO	0.10	0.13	0.12	0.11	0.11	0.11	0.12	0.10	0.09	0.11
MgO	9.0	7.5	8.3	10.6	10.9	9.1	7.2	9.0	4.6	6.9
CaO	9.3	11.5	9.9	8.4	8.3	8.0	8.5	7.9	7.1	6.2
Na_2O	2.6	2.6	2.5	2.6	2.4	2.8	2.9	2.7	1.4	1.2
K_2O	0.16	0.12	0.90	0.21	0.20	0.26	0.53	0.32	4.80	4.62
P_2O_5	0.07	0.07	0.06	0.08	0.08	0.06	0.06	0.05	0.05	0.11
LOI	1.99	3.25	2.34	2.40	2.35	2.47	1.94	2.32	6.18	7.59
Total	98.22	99.00	99.69	98.80	98.84	99.82	98.98	99.36	98.66	99.59
Trace elements in parts per million										
Cr	141	201	283	229	295	127	106	162	394	174
V	278	285	215	239	248	265	222	238	273	249
Ni	45	55	60	55	61	41	30	36	87	72
Zn	84	76	71	82	82	81	83	83	92	99
Rb	2.7	1.1	20.7	2.2	2.7	2.0	9.7	1.6	47.3	43.6
Sr	86.4	91.7	80.9	73.6	73.8	100.3	88.1	94.9	119.8	124.4
Y	21.2	20.4	16.5	22.6	24.5	17.7	19.1	18.4	14.8	24.8
Zr	36.5	39.5	30.5	31.8	31.8	36.2	37.7	38.5	26.2	49.5
Nb	1.1	0.9	0.7	0.5	1.2	0.6	0.7	0.3	0.9	1.2
Ga	16	16	16	15	14	15	15	15	14	14
Ba	5.3	19.0	17.5	8.5	8.2	7.0	18.4	8.1	93.0	55.3
La	3.3	3.3	3.6	2.2	2.2	2.8	1.6	1.9	0.8	1.3
Ce	4.3	3.1	3.1	3.6	2.6	3.8	2.9	5.5	n.d.	7.9
Nd	5.8	4.8	4.6	5.6	4.9	4.5	5.4	5.0	3.1	7.7
Pb	2	4	5	4	5	3	6	3	5	3
Th	n.d.	1	n.d.	n.d.	n.d.	n.d.	n.d.	n.d.	n.d.	n.d.
U	n.d.	2	n.d.	n.d.	n.d.	2	n.d.	1	2	1
C.I.P.W. norms (calculated using $FeO : Fe_2O_3 = 0.85 : 0.15$)										
Qz	–	0.07	–	–	–	–	0.65	1.21	–	–
Or	0.97	0.73	5.34	1.26	1.17	1.52	3.12	1.90	28.37	27.32
Ab	21.65	21.86	21.40	22.38	20.58	23.69	24.40	22.90	11.83	10.32
An	32.06	31.58	26.38	28.44	29.01	31.92	29.15	31.32	24.92	26.80
Di	10.88	20.31	18.07	10.31	9.40	5.85	10.25	5.97	8.08	2.76
Hy	25.07	17.86	15.73	23.94	29.16	29.16	25.44	30.02	7.30	2.66
Ol	1.94	–	6.60	6.38	3.47	1.52	–	–	8.54	18.03
Mt	1.48	1.27	1.73	1.53	1.54	1.56	1.72	1.47	1.55	1.59
Il	1.28	1.29	1.08	1.20	1.19	1.20	1.30	1.39	0.98	1.47
Ap	0.16	0.16	0.13	0.18	0.19	0.14	0.14	0.13	0.11	0.26

Table 2 (part 6 of 7)

Pellet	L2517	L2518	L2519	L2520	L2521	L2522	L2523	L2524
Core/Sec	8.5	9.5	11.4	20.2	25.11	29.7	30.9	39.9
Depth (m)	47.30	51.70	57.00	96.90	126.20	148.20	152.20	203.50
SiO_2	26.5	31.2	49.7	41.4	46.1	47.7	47.4	49.0
TiO_2	0.24	0.32	0.59	0.48	0.64	0.52	0.49	0.60
Al_2O_3	8.1	10.0	15.3	13.9	16.5	16.5	15.4	16.4
Fe_2O_3	7.6	7.3	9.1	7.7	8.7	8.9	8.7	8.0
MnO	0.13	0.11	0.10	0.09	0.16	0.10	0.12	0.09
MgO	4.3	5.6	7.8	5.6	8.0	8.1	9.3	9.6
CaO	27.4	22.3	4.2	14.0	8.2	6.9	8.8	8.5
Na_2O	0.7	0.9	0.9	1.3	1.7	1.6	1.5	2.1
K_2O	2.23	2.48	6.23	3.67	3.05	4.32	2.06	1.57
P_2O_5	0.14	0.07	0.03	0.08	0.07	0.09	0.02	0.07
LOI	21.95	18.59	5.83	10.80	7.24	5.34	5.85	4.12
Total	99.17	98.85	99.92	98.95	100.29	100.20	99.51	100.18
Trace elements in parts per million								
Cr	1076	692	343	112	133	316	271	168
V	206	194	234	240	207	262	236	265
Ni	205	199	74	61	55	64	77	49
Zn	73	63	90	64	75	70	77	74
Rb	24.9	28.0	53.2	31.3	28.6	34.0	20.6	9.0
Sr	112.8	118.9	99.5	93.5	107.8	64.0	74.9	106.3
Y	16.4	12.6	9.3	20.7	17.4	17.8	12.4	16.8
Zr	20.8	24.3	31.1	29.1	34.8	25.4	24.1	34.0
Nb	0.8	0.8	1.2	0.7	0.8	0.7	1.7	1.1
Ga	7	9	13	12	15	13	13	14
Ba	37.0	43.5	55.3	42.4	47.1	46.9	36.8	28.1
La	1.0	1.9	0.8	1.8	2.2	2.5	1.3	1.4
Ce	0.7	1.0	1.6	3.4	2.7	n.d.	2.6	4.6
Nd	1.1	4.9	2.9	5.8	4.5	2.9	1.6	4.7
Pb	3	6	4	4	3	2	3	4
Th	n.d.	n.d.	1	2	n.d.	n.d.	n.d.	n.d.
U	2	2	2	2	2	1	n.d.	2
C.I.P.W. norms (calculated using $FeO : Fe_2O_3 = 0.85 : 0.15$)								
Qz	–	–	–	–	–	–	–	–
Or	–	–	36.84	–	18.00	25.53	12.20	9.30
Ab	–	–	7.89	–	14.21	12.64	12.43	18.17
An	–	16.12	19.27	21.31	28.43	25.22	29.24	30.41
Lu	–	11.51	–	17.03	–	–	–	–
Ne	–	3.96	–	5.89	–	0.49	–	–
Di	–	-29.74	0.97	33.49	9.58	6.87	11.52	9.09
Cs	–	41.29	–	2.13	–	–	–	–
Wo	–	14.70	–	–	–	–	–	–
Hy	–	–	11.94	–	0.25	–	15.30	15.27
Ol	–	38.09	13.62	5.27	18.94	20.61	9.73	10.42
Mt	–	1.27	1.58	1.32	1.50	1.54	1.50	1.39
Il	–	0.60	1.13	0.91	1.22	0.99	0.93	1.15
Ap	–	0.15	0.07	0.18	0.16	0.21	0.05	0.16

Table 2 (part 7 of 7)

Pellet	L2525	L2526	L2527	L2528	L2529	L2530	L2531	L2532	L2533	L2534
Core/Sec	2.01	2.01	2.01	4.02	4.02	7.01	7.02	9.02	9.02	11.04
Depth (m)	8.80	12.20	15.00	17.20	22.50	23.90	27.10	32.25	34.75	42.40
SiO_2	55.7	56.9	53.8	53.3	53.0	55.7	56.6	53.9	54.6	53.4
TiO_2	1.07	1.10	0.65	0.69	0.71	1.12	1.08	1.20	1.20	0.47
Al_2O_3	14.1	14.5	16.2	16.4	16.2	14.9	14.9	14.8	15.0	15.2
Fe_2O_3	11.7	10.6	9.9	10.5	9.7	11.3	11.3	12.6	11.9	9.7
MnO	0.11	0.12	0.15	0.13	0.14	0.13	0.12	0.13	0.14	0.18
MgO	3.7	3.9	6.3	6.4	6.6	3.9	3.8	4.1	4.6	8.3
CaO	7.6	8.0	10.4	10.7	8.9	7.5	8.3	8.4	8.1	9.6
Na_2O	3.2	3.2	1.6	2.1	3.3	3.6	2.7	2.7	2.8	2.2
K_2O	0.14	0.17	0.11	0.09	0.19	0.10	0.08	0.14	0.23	0.18
P_2O_5	0.12	0.09	0.07	0.07	0.07	0.10	0.11	0.13	0.11	0.05
LOI	1.81	1.61	1.04	0.93	1.98	2.00	1.11	0.99	1.45	1.66
Total	99.17	100.20	100.12	101.14	100.74	100.37	100.23	99.11	100.18	100.73
Trace elements in parts per million										
Cr	8	10	48	36	32	7	10	12	12	327
V	365	371	262	274	267	371	373	374	397	275
Ni	12	13	31	29	28	16	13	15	16	84
Zn	26	26	27	29	29	25	23	34	36	47
Rb	0.7	1.2	0.9	n.d.	n.d.	0.9	0.7	n.d.	1.2	n.d.
Sr	122.1	112.4	108.2	97.9	117.0	112.6	111.6	102.0	101.1	84.2
Y	30.0	26.0	20.5	21.9	22.5	28.0	31.2	27.5	28.5	14.0
Zr	54.1	49.2	27.4	27.5	28.0	56.2	56.9	49.7	47.8	17.8
Nb	0.6	1.0	1.2	0.8	1.5	1.3	1.2	0.7	0.8	0.6
Ga	15	16	15	15	14	15	17	18	17	13
Ba	11.7	13.3	14.3	13.3	17.9	15.9	11.5	8.8	11.8	15.8
La	3.1	0.7	0.7	1.6	0.4	2.5	2.9	0.6	2.0	1.4
Ce	8.5	4.8	0.7	4.9	0.4	6.9	4.3	7.8	5.7	n.d.
Nd	7.1	7.7	3.6	4.7	4.3	6.4	6.4	6.5	4.5	1.5
Pb	4	2	3	5	4	3	5	1	2	5
Th	n.d.	n.d.	1	n.d.	n.d.	n.d.	1	n.d.	n.d.	n.d.
U	n.d.	2	n.d.	n.d.	n.d.	n.d.	1	n.d.	1	n.d.
C.I.P.W. norms (calculated using $FeO : Fe_2O_3 = 0.85 : 0.15$)										
Qz	11.38	12.08	10.12	6.33	2.19	9.31	13.54	9.81	9.56	5.04
Or	0.83	1.00	0.68	0.50	1.14	0.61	0.49	0.84	1.39	1.09
Ab	27.17	27.48	13.31	17.69	27.70	30.10	23.26	22.54	23.43	18.39
An	23.55	24.43	36.81	35.00	28.93	24.40	28.17	28.10	27.87	31.09
Di	11.26	12.21	11.67	14.28	11.93	10.32	10.43	10.62	9.73	13.02
Hy	17.82	16.36	22.53	22.19	22.83	18.32	17.99	20.35	21.11	26.93
Ol	–	–	–	–	–	–	–	–	–	–
Mt	2.02	1.82	1.70	1.81	1.68	1.96	1.95	2.18	2.06	1.67
Il	2.03	2.09	1.24	1.32	1.34	2.12	2.05	2.28	2.28	0.90
Ap	0.27	0.21	0.16	0.17	0.17	0.23	0.26	0.30	0.26	0.13

Table 3: (part 1 of 18) Hole CY-4 basalt samples: Chemical Analyses.

Pellet	L2535	L2536	L2537	L2538	L2539	L2540	L2541	L2542	L2543	L2544
Core/Sec	11.04	13.01	13.01	15.03	15.03	16.01	16.04	17.03	18.01	18.01
Depth (m)	43.55	47.20	49.05	53.65	55.40	55.90	57.95	61.65	62.70	64.55
SiO_2	53.3	53.3	50.9	52.5	54.1	54.2	51.2	60.7	59.9	54.7
TiO_2	0.60	0.49	0.40	0.62	0.67	0.76	0.62	1.08	1.13	0.91
Al_2O_3	14.8	15.3	15.4	16.0	15.3	5.3	16.3	14.5	15.1	15.6
Fe_2O_3	11.1	9.9	10.7	9.2	8.9	8.9	10.6	10.5	10.6	9.8
MnO	0.16	0.15	0.13	0.14	0.14	0.12	0.14	0.08	0.08	0.11
MgO	6.3	8.7	9.9	7.6	7.5	6.5	8.0	2.7	2.7	5.8
CaO	8.8	9.6	8.7	9.8	9.6	8.3	10.3	6.6	6.0	7.7
Na_2O	2.0	1.8	2.0	2.7	2.4	3.9	2.6	3.4	4.3	4.3
K_2O	0.08	0.06	0.17	0.23	0.21	0.20	0.24	0.18	0.26	0.27
P_2O_5	0.06	0.05	0.05	0.07	0.07	0.08	0.06	0.11	0.11	0.09
LOI	1.28	1.68	2.40	1.70	1.34	1.64	1.31	0.94	1.49	2.13
Total	98.44	100.91	100.85	100.67	100.21	99.79	101.45	100.77	101.73	101.44
Trace elements in parts per million										
Cr	185	348	273	163	207	17	150	6	5	9
V	315	284	272	241	255	290	294	164	161	335
Ni	52	76	65	47	51	33	45	3	3	18
Zn	51	42	32	33	32	22	31	22	22	23
Rb	0.6	0.6	n.d.	0.7	0.6	0.7	0.8	0.5	n.d.	1.5
Sr	76.1	84.4	72.3	103.5	101.8	113.6	11.8	181.0	221.8	170.1
Y	16.9	15.0	12.7	20.7	19.0	20.8	18.1	30.6	31.0	23.6
Zr	20.5	16.7	11.8	32.5	30.8	37.0	24.9	59.6	60.4	39.8
Nb	0.9	0.4	0.7	0.5	0.8	0.6	0.7	1.4	1.5	0.8
Ga	14	13	12	14	13	12	15	14	13	12
Ba	15.2	13.3	17.7	17.6	14.8	11.7	9.8	13.9	18.0	19.0
La	0.2	1.2	n.d.	0.2	2.0	1.0	0.1	3.0	3.1	3.2
Ce	n.d.	2.5	n.d.	4.1	4.2	4.8	1.3	7.1	6.5	2.9
Nd	1.6	3.1	n.d.	4.6	4.8	5.7	2.4	6.1	4.2	2.5
Pb	5	4	3	3	1	4	2	2	3	5
Th	1	n.d.	n.d.	n.d.	n.d.	1	n.d.	n.d.	n.d.	n.d.
U	1	4	1	n.d.	n.d.	1	n.d.	2	n.d.	2
C.I.P.W. norms (calculated using $FeO : Fe_2O_3 = 0.85 : 0.15$)										
Qz	9.34	6.48	1.32	2.03	6.33	2.15	–	18.41	13.05	1.62
Or	0.50	0.38	1.03	1.35	1.26	1.20	1.43	1.08	1.56	1.58
Ab	16.87	14.98	16.52	23.04	20.29	32.96	21.88	28.92	36.76	36.19
An	31.11	33.70	32.86	30.86	30.32	23.66	32.25	23.78	20.93	22.72
Di	9.93	11.08	8.11	14.25	13.65	13.81	15.25	6.77	6.97	12.06
Hy	25.25	29.00	34.95	23.70	23.27	20.45	23.17	15.83	15.79	20.64
Ol	–	–	–	–	–	–	2.08	–	–	–
Mt	1.92	1.70	1.85	1.59	1.54	1.53	1.83	1.81	1.83	1.70
Il	1.14	0.93	0.76	1.18	1.27	1.44	1.18	2.05	2.15	1.73
Ap	0.14	0.12	0.11	0.17	0.17	0.19	0.14	0.26	0.26	0.21

Table 3 (part 2 of 18)

Pellet	L2545	L2546	L2547	L2548	L2549	L2550	L2551	L2552	L2553	L2554
Core/Sec	20.03	21.05	22.02	28.02	29.05	30.03	32.02	32.02	34.02	34.02
Depth (m)	72.00	77.35	78.80	102.30	104.55	107.90	118.05	120.55	126.20	128.15
SiO_2	57.5	57.5	51.7	69.7	52.3	54.8	53.7	54.1	71.9	71.0
TiO_2	1.07	1.31	0.58	0.58	1.12	1.05	1.36	1.38	0.53	0.56
Al_2O_3	14.8	15.1	16.2	13.5	15.5	15.9	15.0	15.2	12.4	13.1
Fe_2O_3	10.9	10.4	9.6	7.3	11.8	12.2	12.7	13.1	6.8	7.2
MnO	0.10	0.09	0.12	0.04	0.21	0.18	0.20	0.22	0.04	0.03
MgO	4.6	4.7	8.2	0.9	6.5	4.8	4.4	4.9	0.9	0.8
CaO	5.1	5.8	9.7	2.4	9.1	7.6	8.0	7.2	2.5	3.8
Na_2O	4.7	4.6	2.7	5.7	2.9	3.5	3.2	3.4	5.2	4.4
K_2O	0.41	0.33	0.44	0.18	0.09	0.10	0.10	0.12	0.18	0.13
P_2O_5	0.11	0.11	0.05	0.13	0.09	0.08	0.10	0.11	0.12	0.13
LOI	2.07	1.66	2.03	0.71	1.89	1.01	0.70	1.63	0.57	0.39
Total	101.32	101.58	101.33	101.18	101.48	101.07	99.43	101.38	101.07	101.48
Trace elements in parts per million										
Cr	8	20	184	4	44	12	12	11	5	15
V	306	206	299	16	381	445	406	402	17	17
Ni	15	10	52	2	26	16	12	11	2	3
Zn	26	18	28	20	74	36	85	65	20	18
Rb	1.2	1.6	1.9	0.4	n.d.	n.d.	0.8	0.9	n.d.	0.4
Sr	83.5	117.7	87.7	83.2	115.6	112.9	104.7	110.3	82.7	106.0
Y	29.1	30.2	15.4	44.5	25.0	23.1	32.3	32.7	37.0	43.4
Zr	62.2	52.7	19.4	81.3	49.9	35.6	69.1	69.8	74.8	79.3
Nb	1.3	1.4	0.8	1.4	0.7	0.8	1.4	1.0	1.7	2.1
Ga	14	15	13	14	16	17	19	18	11	13
Ba	11.0	13.2	32.9	28.0	15.8	18.7	14.2	13.2	17.9	19.4
La	2.4	3.4	2.8	3.0	1.6	1.3	5.2	1.7	3.0	3.3
Ce	4.5	4.4	n.d.	7.0	3.9	3.2	7.7	12.2	6.4	7.4
Nd	6.8	6.3	3.6	8.8	6.1	3.1	7.1	7.6	7.5	9.5
Pb	4	5	4	4	4	2	4	3	3	2
Th	n.d.	n.d.	n.d.	n.d.	n.d.	n.d.	1	n.d.	n.d.	n.d.
U	1	3	n.d.	3	n.d.	n.d.	3	2	2	2
C.I.P.W. norms (calculated using $FeO : Fe_2O_3 = 0.85 : 0.15$)										
Qz	6.75	6.53	–	25.35	2.92	6.19	7.07	5.98	31.26	32.54
Or	2.41	1.97	2.59	1.04	0.52	0.62	0.56	0.71	1.08	0.79
Ab	39.36	39.11	22.96	48.65	24.41	29.40	27.06	29.13	43.84	36.84
An	18.22	19.52	30.77	10.58	29.10	27.51	26.37	25.80	10.16	15.76
Di	5.23	7.08	13.77	0.60	12.95	7.93	10.77	7.60	1.07	1.94
Hy	22.15	20.28	24.35	10.98	24.30	23.08	20.80	24.25	10.05	10.00
Ol	–	–	1.14	–	–	–	–	–	–	–
Mt	1.88	1.79	1.66	1.25	2.04	2.10	2.19	2.26	1.18	1.24
Il	2.03	2.48	1.10	1.09	2.12	1.99	2.58	2.62	1.00	1.06
Ap	0.27	0.26	0.12	0.30	0.20	0.18	0.22	0.26	0.28	0.29

Table 3 (part 3 of 18)

Pellet	L2555	L2556	L2557	L2558	L2559	L2560	L2561	L2562	L2563	L2564
Core/Sec	36.01	37.01	37.05	37.05	38.02	38.02	41.01	42.05	43.01	43.02
Depth (m)	130.30	133.05	136.60	138.80	141.70	144.30	150.80	156.70	157.25	157.90
SiO_2	52.7	54.9	56.1	57.9	51.9	49.7	53.6	55.3	53.4	53.7
TiO_2	0.69	1.05	1.19	1.12	1.16	1.15	1.39	1.31	0.80	1.11
Al_2O_3	16.4	16.1	15.1	14.5	15.4	15.4	15.2	14.9	13.9	15.0
Fe_2O_3	11.7	12.1	12.8	11.4	12.0	12.1	12.6	11.9	10.1	11.6
MnO	0.14	0.14	0.15	0.15	0.19	0.19	0.17	0.09	0.15	0.13
MgO	5.6	4.6	4.5	4.7	6.6	6.7	5.1	3.9	7.2	4.9
CaO	7.6	7.4	6.9	7.4	7.1	8.4	6.5	7.9	8.7	8.3
Na_2O	4.3	3.8	3.2	2.9	4.2	3.4	4.1	3.9	3.5	3.7
K_2O	0.17	0.14	0.21	0.19	0.15	0.14	0.19	0.21	0.45	0.26
P_2O_5	0.06	0.09	0.10	0.10	0.10	0.09	0.11	0.12	0.08	0.10
LOI	1.84	0.96	1.14	0.96	2.35	1.78	1.49	0.87	1.39	1.48
Total	101.22	101.31	101.39	101.42	101.18	98.93	100.45	100.37	99.63	100.26
Trace elements in parts per million										
Cr	40	9	10	8	39	42	8	11	32	246
V	277	405	410	354	352	382	396	429	391	305
Ni	27	17	14	16	24	30	10	17	25	67
Zn	33	29	20	26	37	41	44	28	35	42
Rb	1.1	n.d.	n.d.	0.5	n.d.	0.7	0.7	0.9	n.d.	2.2
Sr	264.2	107.5	100.6	97.8	103.2	28.6	116.1	142.3	138.2	111.0
Y	19.2	26.5	23.8	23.7	27.3	26.2	30.0	33.8	24.7	22.5
Zr	25.8	42.8	43.4	41.8	52.3	53.3	68.9	69.1	48.2	38.4
Nb	1.2	1.4	1.0	1.1	0.4	0.7	1.0	1.3	0.5	0.7
Ga	14	18	16	15	16	18	19	17	16	14
Ba	27.7	14.7	10.6	12.5	9.9	9.7	9.8	8.5	7.4	21.4
La	0.9	3.8	3.1	0.8	1.1	0.5	2.9	1.2	3.4	1.7
Ce	6.1	5.2	3.3	7.1	6.7	6.5	8.9	6.6	7.6	3.8
Nd	3.5	5.3	5.5	5.5	6.0	4.8	8.1	7.2	5.0	3.7
Pb	4	4	2	3	2	3	3	2	4	4
Th	n.d.	n.d.	n.d.	n.d.	n.d.	2	n.d.	n.d.	n.d.	n.d.
U	2	n.d.	1	2	n.d.	2	n.d.	n.d.	n.d.	2
C.I.P.W. norms (calculated using $FeO : Fe_2O_3 = 0.85 : 0.15$)										
Qz	–	5.01	9.95	13.60	–	–	3.04	6.29	1.25	3.56
Or	1.02	0.85	1.25	1.13	0.88	0.81	1.15	1.24	2.68	1.56
Ab	36.38	32.02	26.77	24.22	35.53	28.67	34.34	33.05	29.29	31.43
An	25.01	26.51	26.29	26.24	22.71	26.39	22.61	22.59	21.10	23.58
Di	10.34	8.25	6.28	8.27	9.73	11.98	7.47	13.12	17.75	13.89
Hy	17.53	22.38	23.90	21.68	18.89	18.65	24.18	17.36	21.85	19.41
Ol	4.60	–	–	–	5.54	5.11	–	–	–	–
Mt	2.02	2.09	2.22	1.98	2.07	2.09	2.18	2.05	1.74	1.99
Il	1.31	1.99	2.25	2.13	2.21	2.18	2.64	2.49	1.52	2.11
Ap	0.15	0.20	0.22	0.22	0.23	0.21	0.25	0.28	0.18	0.24

Table 3 (part 4 of 18)

Pellet	L2565	L2566	L2567	L2568	L2569	L2570	L2571	L2572	L2573	L2574
Core/Sec	44.05	44.15	45.01	47.02	47.02	47.02	47.02	47.02	53.03	53.03
Depth (m)	162.40	165.30	167.65	176.65	178.85	182.00	185.50	193.60	196.90	201.35
SiO_2	51.2	53.3	54.6	53.4	53.5	53.9	54.4	51.8	55.5	54.1
TiO_2	1.17	1.10	1.35	1.25	1.26	1.23	1.26	0.69	0.67	0.65
Al_2O_3	16.0	15.4	14.7	15.2	15.3	15.0	15.2	16.2	14.9	15.0
Fe_2O_3	11.9	11.3	12.7	12.3	12.2	12.1	12.3	8.9	11.1	10.7
MnO	0.18	0.17	0.16	0.16	0.16	0.15	0.19	0.14	0.17	0.13
MgO	6.3	5.9	4.2	5.2	5.4	5.1	4.9	7.7	6.1	6.9
CaO	9.3	9.6	7.7	9.1	9.1	8.9	9.1	10.6	9.1	8.9
Na_2O	3.2	2.6	3.5	2.9	2.9	2.9	2.8	2.8	2.4	2.7
K_2O	0.07	0.06	0.12	0.06	0.08	0.06	0.05	0.16	0.07	0.19
P_2O_5	0.10	0.09	0.13	0.11	0.10	0.10	0.10	0.07	0.05	0.06
LOI	1.10	0.74	0.80	0.47	0.48	0.61	0.48	1.78	0.59	n.d.
Total	100.51	100.33	99.91	100.01	100.53	100.14	100.86	100.79	100.64	99.33
Trace elements in parts per million										
Cr	40	34	12	21	21	20	20	187	135	179
V	376	342	409	390	387	359	382	253	332	328
Ni	27	25	14	15	17	17	14	62	45	55
Zn	37	44	36	41	41	37	57	37	43	27
Rb	n.d.	0.6	n.d.	n.d.	0.7	1.0	0.9	0.6	0.8	n.d.
Sr	97.7	108.1	116.0	110.2	105.6	118.7	99.3	135.7	81.2	89.6
Y	28.7	27.2	32.8	30.2	28.3	30.0	31.2	18.9	16.5	16.0
Zr	58.4	54.2	69.7	64.2	61.0	65.9	67.9	40.1	20.1	22.7
Nb	0.7	1.0	1.2	0.7	1.1	0.7	0.9	0.9	0.9	1.0
Ga	17	17	18	17	17	17	17	13	14	15
Ba	9.8	10.9	10.5	11.9	9.1	12.2	13.0	13.0	18.0	14.8
La	2.1	1.3	3.2	2.2	2.4	2.4	2.6	2.5	2.8	1.2
Ce	8.1	5.5	9.0	8.9	5.8	4.8	7.6	2.3	4.7	2.5
Nd	6.7	7.3	8.3	6.9	6.4	6.1	9.0	5.1	2.4	3.9
Pb	5	5	3	n.d.	3	4	4	3	1	4
Th	1	2	n.d.	n.d.	n.d.	3	1	n.d.	n.d.	n.d.
U	2	2	n.d.	n.d.	2	3	2	2	2	n.d.
C.I.P.W. norms (calculated using $FeO : Fe_2O_3 = 0.85 : 0.15$)										
Qz	0.05	6.12	7.45	6.21	5.86	6.91	7.69	0.40	9.50	5.86
Or	0.41	0.35	0.69	0.38	0.50	0.36	0.29	0.94	0.41	1.13
Ab	27.28	22.01	29.21	24.34	24.42	24.64	24.09	23.52	20.44	22.42
An	29.10	30.30	24.20	28.27	28.59	27.82	28.58	31.17	29.70	28.56
Di	13.42	13.77	11.23	13.40	13.05	13.20	13.23	17.01	12.49	12.71
Hy	23.58	21.79	20.17	21.12	21.81	20.88	20.67	22.19	23.23	24.52
Ol	–	–	–	–	–	–	–	–	–	–
Mt	2.06	1.96	2.20	2.12	2.11	2.08	2.12	1.53	1.92	1.84
Il	2.22	2.09	2.56	2.38	2.40	2.34	2.40	1.31	1.26	1.23
Ap	0.24	0.21	0.30	0.25	0.23	0.24	0.23	0.17	0.13	0.13

Table 3 (part 5 of 18)

Pellet	L2575	L2576	L2577	L2578	L2579	L2580	L2581	L2582
Core/Sec	53.03	57.02	58.02	58.04	58.04	60.04	60.07	62.01
Depth (m)	204.55	210.35	213.90	214.95	217.85	221.25	226.20	228.70
SiO_2	55.5	52.7	52.5	56.5	53.8	56.9	54.4	69.0
TiO_2	0.70	0.53	0.50	0.77	0.52	1.06	0.64	0.55
Al_2O_3	15.1	16.1	14.9	15.0	15.7	14.2	15.2	12.6
Fe_2O_3	11.1	9.6	10.0	11.0	9.6	12.8	11.1	6.4
MnO	0.18	0.15	0.17	0.12	0.16	0.14	0.19	0.03
MgO	6.1	6.1	6.4	4.5	6.6	3.6	6.4	0.8
CaO	8.9	8.4	9.3	7.5	9.5	6.4	8.3	4.0
Na_2O	2.5	3.5	2.5	3.3	2.9	4.0	3.5	4.2
K_2O	0.10	0.12	0.08	0.13	0.10	0.13	0.08	0.17
P_2O_5	0.06	0.05	0.05	0.06	0.05	0.12	0.07	0.12
LOI	n.d.	2.09	1.20	1.19	1.44	1.17	n.d.	n.d.
Total	100.34	99.38	97.54	100.06	100.35	100.51	99.99	97.90
Trace elements in parts per million								
Cr	143	31	86	24	98	7	180	9
V	315	272	279	379	295	372	329	15
Ni	47	34	36	18	43	14	61	2
Zn	40	29	31	27	23	25	36	11
Rb	0.5	n.d.	n.d.	0.4	0.2	0.1	0.0	0.9
Sr	82.5	98.5	80.4	116.3	99.4	166.7	87.6	111.0
Y	17.1	16.8	15.7	18.6	16.4	31.1	16.9	41.5
Zr	23.5	21.2	18.9	23.9	17.8	49.9	18.1	79.7
Nb	1.0	0.7	0.9	0.9	1.6	2.2	1.5	3.0
Ga	15	13	13	15	17	17	17	15
Ba	16.8	18.5	14.7	16.3	12.8	16.8	18.1	13.1
La	2.1	0.8	n.d.	1.4	0.9	0.7	n.d.	2.6
Ce	1.3	2.2	2.1	2.5	4.4	2.6	2.6	8.5
Nd	2.8	1.9	2.6	2.1	2.4	4.3	1.3	9.6
Pb	3	3	4	4	n.d.	n.d.	n.d.	n.d.
Th	n.d.	n.d.	n.d.	n.d.	n.d.	n.d.	n.d.	n.d.
U	2	n.d.	n.d.	n.d.	n.d.	n.d.	n.d.	n.d.
C.I.P.W. norms (calculated using $FeO : Fe_2O_3 = 0.85 : 0.15$)								
Qz	9.01	2.21	6.01	10.36	4.66	9.70	3.20	31.86
Or	0.57	0.69	0.50	0.75	0.57	0.79	0.48	0.99
Ab	21.32	29.58	21.24	27.84	24.60	33.45	29.70	35.54
An	29.69	27.92	29.12	25.76	29.54	20.62	25.52	15.10
Di	11.83	11.23	13.69	9.04	13.96	8.62	12.55	3.24
Hy	23.58	22.06	22.12	20.65	21.97	20.55	24.28	8.19
Ol	–	–	–	–	–	–	–	–
Mt	1.91	1.65	1.72	1.90	1.66	2.21	1.92	1.10
Il	1.33	1.00	0.96	1.46	0.99	2.01	1.22	1.04
Ap	0.13	0.12	0.12	0.14	0.12	0.28	0.16	0.28

Table 3 (part 6 of 18)

Pellet	L5387	L5388	L5389	L5390	L5391	L5392	L5393	L5394	L5395	L5396
Core/Sec	234.50	236.82	241.26	245.50	249.73	253.66	262.42	266.61	270.63	273.44
Depth (m)	63.01	63.01	65.01	65.01	67.04	67.04	70.06	70.08	70.08	73.01
SiO_2	51.9	51.2	54.0	61.3	61.2	54.3	52.4	53.7	54.5	55.2
TiO_2	1.27	1.23	1.24	0.76	1.02	1.07	0.45	1.32	1.33	0.65
Al_2O_3	15.3	15.0	15.3	13.9	13.2	14.3	16.4	15.1	15.2	15.3
Fe_2O_3	12.4	12.0	12.1	9.7	11.7	11.9	9.6	11.9	12.4	9.9
MnO	0.13	0.15	0.19	0.06	0.07	0.12	0.18	0.13	0.14	0.14
MgO	5.8	5.3	5.2	2.4	2.0	3.8	7.5	4.7	4.7	5.4
CaO	8.2	9.1	9.1	5.6	6.5	8.6	10.0	9.0	8.7	10.0
Na_2O	3.1	2.8	2.8	3.9	2.7	2.4	2.7	2.8	3.0	2.0
K_2O	0.15	0.14	0.06	0.10	0.16	0.09	0.06	0.07	0.08	0.09
P_2O_5	0.16	0.17	0.17	0.16	0.26	0.16	0.11	0.17	0.18	0.13
LOI	1.87	1.01	0.62	0.71	0.43	0.60	1.35	0.62	0.69	0.67
Total	100.21	98.09	100.76	98.65	99.22	97.34	100.77	99.32	100.95	99.52
Trace elements in parts per million										
Nb	1.6	0.9	1.0	1.9	1.6	1.6	1.2	0.7	2.0	1.5
Zr	58.8	62.6	61.8	46.3	55.1	42.8	14.6	63.6	65.2	28.3
Y	28.0	29.9	30.0	30.0	27.6	25.1	14.0	31.1	30.9	18.4
Sr	177.3	123.7	104.3	112.7	121.0	103.0	75.7	123.0	120.8	81.1
Rb	1.4	1.4	1.6	2.3	0.3	1.2	1.9	0.6	1.5	1.0
Th	2.2	2.6	4.6	3.5	1.3	3.8	2.5	3.4	1.8	0.8
Ga	17	18	19	15	16	16	15	18	17	14
Zn	31	34	49	9	19	20	54	29	32	33
Ni	23	20	20	8	8	13	53	18	17	32
Cr	41	17	19	9	7	8	97	13	14	38
Va	377	387	377	120	67	389	294	414	424	326
Ba	10.6	10.1	6.9	17.2	9.1	7.2	11.6	4.9	4.0	9.4
la	2.8	4.2	5.0	2.5	2.2	3.2	2.3	2.0	5.3	1.5
Ce	10.8	7.7	6.5	9.5	5.4	6.4	3.4	7.9	7.8	6.1
Nd	6.8	6.2	7.9	6.7	5.6	3.2	1.2	8.3	6.6	3.1
C.I.P.W. norms (calculated using $FeO : Fe_2O_3 = 0.85 : 0.15$)										
Qz	3.49	4.30	7.15	18.92	23.90	12.44	1.77	8.48	7.73	11.82
Or	0.88	0.81	0.33	0.59	0.94	0.53	0.36	0.39	0.46	0.55
Ab	25.91	23.71	23.80	33.10	22.58	20.61	23.21	23.29	25.55	16.89
An	27.62	28.09	29.01	20.06	23.59	27.70	32.39	28.59	27.74	32.54
Di	9.86	13.25	12.39	5.84	5.76	11.85	13.29	12.26	12.03	13.51
Hy	24.58	21.11	21.58	15.09	16.45	18.09	24.80	19.70	20.58	19.44
Ol	–	–	–	–	–	–	–	–	–	–
Mt	2.14	2.07	2.09	1.68	2.02	2.06	1.66	2.05	2.05	1.71
Il	2.40	2.33	2.36	1.45	1.93	2.04	0.86	2.51	2.51	1.23
Ap	0.37	0.39	0.39	0.36	0.60	0.37	0.26	0.39	0.39	0.31

Table 3 (part 7 of 18)

Pellet	L5397	L5398	L5399	L5400	L5401	L5402	L5403	L5404	L5405	L5405B
Core/Sec	277.58	278.18	281.18	287.92	295.50	300.62	301.00	307.00	309.91	313.01
Depth (m)	73.04	74.01	74.01	76.05	79.01	80.01	80.02	81.03	82.02	83.01
SiO_2	52.4	50.1	58.1	54.9	56.5	53.6	51.9	57.1	65.9	52.6
TiO_2	1.26	0.59	1.32	0.60	0.89	0.61	1.13	0.68	0.72	0.44
Al_2O_3	14.8	15.9	15.3	16.2	15.3	15.4	15.5	15.2	14.3	15.9
Fe_2O_3	12.4	9.8	10.9	9.6	11.1	10.6	11.5	10.8	7.3	8.7
MnO	0.12	0.18	0.10	0.14	0.18	0.16	0.19	0.16	0.07	0.16
MgO	4.0	9.6	2.9	6.1	4.7	6.0	6.3	4.4	1.2	8.0
CaO	7.9	12.5	7.1	10.1	9.0	9.5	10.0	8.9	5.6	10.9
Na_2O	3.5	1.5	3.7	2.3	2.2	2.3	2.8	2.2	3.7	1.9
K_2O	0.07	0.09	0.09	0.07	0.05	0.05	0.07	0.05	0.09	0.09
P_2O_5	0.20	0.13	0.29	0.13	0.14	0.12	0.15	0.13	0.20	0.12
LOI	0.46	0.71	0.18	0.51	0.69	0.75	0.93	0.44	0.46	0.73
Total	97.05	101.08	99.92	100.79	100.81	99.05	100.45	100.05	99.59	99.59
Trace elements in parts per million										
Nb	0.8	1.4	1.9	0.8	0.9	1.7	1.3	1.0	1.9	0.7
Zr	56.2	28.2	69.4	31.3	31.0	19.9	56.0	26.6	62.6	17.4
Y	29.5	16.2	34.1	18.2	21.3	16.2	27.7	20.7	31.8	13.0
Sr	114.5	72.9	123.0	74.2	77.5	65.6	89.0	71.7	124.1	74.5
Rb	1.1	3.7	0.8	2.2	1.4	2.0	1.6	1.6	3.0	2.8
Th	4.0	2.2	2.2	3.2	3.9	3.0	1.8	4.0	1.1	3.1
Ga	19	15	18	14	16	15	15	16	15	13
Zn	18	51	16	23	59	51	65	47	18	48
Ni	15	101	11	31	26	46	41	21	4	77
Cr	13	378	9	25	25	120	72	16	9	302
Va	319	256	162	268	348	334	372	286	26	265
Ba	9.6	13.5	10.3	11.0	8.6	14.3	12.5	16.7	13.7	12.6
la	2.0	1.3	3.6	2.0	2.5	1.1	4.0	3.3	4.3	1.1
Ce	7.0	4.7	10.0	0.8	5.1	5.5	8.2	5.8	6.0	1.9
Nd	6.0	4.4	5.6	2.6	3.6	1.5	6.3	2.6	6.8	1.0
C.I.P.W. norms (calculated using $FeO : Fe_2O_3 = 0.85 : 0.15$)										
Qz	5.66	0.07	13.64	8.51	13.80	8.02	2.91	15.04	27.69	5.13
Or	0.44	0.56	0.53	0.43	0.29	0.27	0.40	0.29	0.51	0.51
Ab	29.40	12.52	30.92	19.62	18.66	19.32	23.39	18.70	31.17	15.88
An	24.48	36.46	25.07	33.58	31.83	31.68	29.70	31.45	22.17	34.70
Di	11.20	19.95	7.10	13.08	10.08	12.07	15.45	9.78	3.81	15.26
Hy	19.34	26.86	16.48	21.13	20.55	22.77	22.17	19.96	10.07	24.03
Ol	–	–	–	–	–	–	–	–	–	–
Mt	2.14	1.70	1.88	1.66	1.92	1.83	1.99	1.86	1.27	1.50
Il	2.40	1.11	2.50	1.13	1.70	1.15	2.15	1.29	1.36	0.83
Ap	0.47	0.29	0.66	0.30	0.33	0.27	0.35	0.31	0.46	0.27

Table 3 (part 8 of 18)

Pellet	L5406	L5407	L5408	L5409	L5410	L5411	L5412	L5413	L5414	L5415
Core/Sec	317.52	321.66	331.02	331.86	336.25	338.10	341.81	346.42	353.95	358.64
Depth (m)	86.02	88.06	90.06	90.07	91.02	92.02	93.01	93.01	94.02	97.03
SiO_2	53.7	51.5	63.2	56.4	60.5	57.1	56.0	53.2	53.1	52.5
TiO_2	0.60	1.05	0.92	1.04	1.08	1.09	0.96	1.03	1.01	1.13
Al_2O_3	14.6	15.3	14.1	15.1	14.6	15.4	15.4	15.5	15.3	15.0
Fe_2O_3	10.0	10.9	9.7	11.5	10.3	10.7	11.1	10.7	10.3	11.4
MnO	0.16	0.16	0.10	0.12	0.13	0.12	0.10	0.17	0.15	0.19
MgO	6.5	6.0	2.3	3.9	2.7	3.3	4.2	5.8	5.5	6.0
CaO	10.0	9.6	6.1	8.0	7.0	8.3	9.2	9.9	9.5	10.4
Na_2O	2.0	2.6	3.5	3.1	3.3	2.9	3.0	2.6	2.7	2.2
K_2O	0.07	0.07	0.15	0.08	0.12	0.17	0.06	0.06	0.06	0.03
P_2O_5	0.20	0.14	0.19	0.16	0.16	0.25	0.16	0.17	0.18	0.25
LOI	0.71	0.80	0.40	0.25	0.42	0.37	0.29	0.67	0.68	0.33
Total	98.55	98.05	100.52	99.70	100.33	99.68	100.44	99.83	98.59	99.41
Trace elements in parts per million										
Nb	1.3	0.3	2.2	1.8	1.8	1.7	1.3	1.0	1.5	1.0
Zr	18.6	53.8	68.1	46.2	57.5	51.3	43.7	56.2	60.3	53.5
Y	16.5	26.9	35.7	27.8	29.7	26.9	25.7	28.3	28.8	27.3
Sr	77.2	87.1	113.6	105.3	103.9	113.5	108.3	95.9	93.4	95.6
Rb	2.3	2.4	2.6	2.6	2.7	2.9	1.4	2.2	1.7	1.6
Th	2.7	3.0	3.1	4.5	3.0	3.8	2.2	1.9	3.2	4.7
Ga	14	17	16	16	16	17	18	16	16	17
Zn	42	52	21	21	22	24	29	56	57	78
Ni	54	36	6	22	7	15	26	34	32	32
Cr	138	54	8	21	6	10	27	55	61	46
Va	337	357	102	354	240	362	412	332	328	358
Ba	14.0	7.9	15.2	13.9	15.7	13.4	18.3	9.1	8.3	6.9
la	1.3	3.2	3.4	1.9	3.1	3.4	3.7	3.2	2.8	3.4
Ce	1.0	7.8	9.3	3.1	8.5	6.8	9.6	10.5	8.3	9.1
Nd	1.6	5.4	7.3	4.1	5.8	6.0	5.0	6.3	6.5	6.7
C.I.P.W. norms (calculated using $FeO : Fe_2O_3 = 0.85 : 0.15$)										
Qz	9.10	4.64	22.64	11.51	18.70	14.27	10.28	6.15	6.65	6.91
Or	0.42	0.41	0.89	0.45	0.69	0.98	0.33	0.36	0.38	0.15
Ab	16.97	21.83	29.33	26.50	27.55	24.28	24.98	22.11	23.20	18.47
An	30.73	29.86	22.41	26.91	24.99	28.64	28.74	30.36	29.27	31.17
Di	14.62	13.96	5.58	9.94	7.16	9.05	13.12	14.72	13.80	15.67
Hy	21.81	21.41	14.58	18.79	15.71	16.68	17.63	20.32	19.59	21.05
Ol	–	–	–	–	–	–	–	–	–	–
Mt	1.73	1.88	1.67	1.99	1.78	1.84	1.91	1.85	1.78	1.96
Il	1.13	2.00	1.74	1.97	2.04	2.06	1.82	1.96	1.92	2.14
Ap	0.45	0.34	0.44	0.38	0.38	0.59	0.37	0.40	0.41	0.57

Table 3 (part 9 of 18)

Pellet	L5416	L5417	L5418	L5419	L5420	L5421	L5422	L5423	L5424	L5425
Core/Sec	365.44	368.50	372.62	373.30	377.36	381.50	383.65	390.10	392.60	396.00
Depth (m)	98.02	99.01	99.01	101.01	101.03	103.01	104.01	104.02	106.01	106.01
SiO_2	51.8	56.6	52.2	52.6	54.9	56.4	53.6	52.0	54.3	54.9
TiO_2	1.16	0.85	1.01	1.03	1.34	1.12	1.02	1.07	1.39	1.37
Al_2O_3	15.3	14.8	15.4	15.5	15.2	14.7	16.3	15.2	14.7	14.5
Fe_2O_3	11.5	10.9	11.0	11.0	12.7	10.8	9.6	11.1	12.6	12.6
MnO	0.18	0.13	0.18	0.18	0.17	0.06	0.10	0.17	0.18	0.19
MgO	5.9	3.5	6.1	6.3	3.6	2.7	4.9	5.9	4.0	3.8
CaO	10.2	8.2	10.2	10.2	8.4	8.0	9.9	9.6	8.4	8.6
Na_2O	2.3	2.9	2.4	2.4	3.0	3.4	3.0	2.7	2.8	2.7
K_2O	0.03	0.05	0.05	0.05	0.03	0.05	0.07	0.07	0.05	0.05
P_2O_5	0.17	0.16	0.16	0.17	0.23	0.28	0.16	0.25	0.27	0.20
LOI	0.42	0.55	0.63	0.41	0.20	0.65	0.96	0.87	0.75	0.25
Total	98.77	98.65	99.31	99.91	99.78	98.08	99.60	98.97	99.46	99.20
Trace elements in parts per million										
Nb	0.8	1.9	0.2	1.9	2.1	1.9	0.6	1.0	1.6	1.1
Zr	51.9	30.0	47.3	28.8	74.9	55.8	34.2	55.1	65.4	67.6
Y	27.5	22.6	24.8	21.7	35.1	31.8	21.3	26.7	32.1	33.7
Sr	97.9	91.8	91.9	83.5	99.1	152.1	108.4	106.0	94.5	96.6
Rb	1.4	0.8	2.0	1.6	1.0	2.0	1.3	1.4	0.6	1.2
Th	2.6	1.3	1.8	2.4	3.3	1.3	1.7	2.2	2.9	4.1
Ga	16	15	16	16	19	16	15	16	17	17
Zn	70	52	63	39	93	19	27	57	56	82
Ni	32	14	39	15	16	11	26	33	14	17
Cr	39	8	88	11	12	15	13	50	28	11
Va	364	338	348	331	404	411	412	355	333	116
Ba	7.1	17.5	10.1	17.0	12.8	7.5	4.2	6.2	12.2	15.8
la	2.3	3.8	3.6	4.2	5.8	5.4	4.6	3.4	4.2	4.4
Ce	7.9	7.7	6.1	7.0	10.0	11.0	10.0	5.5	6.9	9.5
Nd	6.3	4.9	5.6	3.4	8.3	9.1	5.7	5.9	3.8	7.3
C.I.P.W. norms (calculated using $FeO : Fe_2O_3 = 0.85 : 0.15$)										
Qz	5.77	13.75	5.16	5.21	10.25	13.21	6.50	4.89	10.24	11.48
Or	0.21	0.30	0.28	0.29	0.19	0.28	0.40	0.39	0.32	0.28
Ab	19.38	24.24	20.69	20.73	25.50	28.50	25.14	22.73	23.94	22.88
An	31.25	27.43	30.92	31.09	27.80	24.90	30.95	29.33	27.26	27.42
Di	15.02	10.23	15.19	15.27	10.33	11.04	14.26	13.67	10.77	11.76
Hy	21.17	17.34	21.29	21.70	19.16	13.92	16.59	21.60	19.66	18.80
Ol	–	–	–	–	–	–	–	–	–	–
Mt	1.98	1.88	1.89	1.90	2.19	1.86	1.66	1.91	2.17	2.18
Il	2.19	1.61	1.93	1.95	2.54	2.13	1.94	2.03	2.64	2.60
Ap	0.39	0.37	0.38	0.39	0.52	0.65	0.36	0.59	0.62	0.46

Table 3 (part 10 of 18)

Pellet	L5426	L5427	L5428	L5429	L5430	L5431	L5432	L5433	L5434	L5435
Core/Sec	398.30	400.90	404.90	407.40	408.60	411.85	413.25	416.50	419.80	423.80
Depth (m)	107.01	108.01	108.02	110.01	110.01	111.02	111.02	112.03	113.04	113.04
SiO_2	51.2	53.6	55.2	52.6	52.0	52.8	56.0	56.3	52.7	56.2
TiO_2	1.12	1.09	1.40	1.10	1.10	1.41	1.33	0.98	0.76	1.33
Al_2O_3	15.2	15.5	14.9	15.5	15.1	15.4	15.1	14.3	15.8	15.1
Fe_2O_3	11.3	11.1	13.1	11.3	11.2	12.8	12.4	11.0	9.3	12.4
MnO	0.19	0.17	0.18	0.18	0.19	0.17	0.15	0.07	0.15	0.13
MgO	6.0	5.7	4.1	6.4	6.5	4.2	3.6	3.7	7.1	3.7
CaO	10.2	9.8	8.6	10.6	9.7	8.1	8.4	8.4	10.9	7.3
Na_2O	2.6	2.8	2.8	2.4	2.6	3.4	2.9	3.2	2.2	3.2
K_2O	0.06	0.07	0.04	0.04	0.05	0.09	0.07	0.06	0.08	0.07
P_2O_5	0.17	0.21	0.27	0.20	0.22	0.23	0.24	0.24	0.18	0.23
LOI	0.69	0.62	0.47	0.58	1.34	1.85	0.31	0.91	1.64	0.59
Total	98.75	100.73	101.04	100.93	99.97	100.37	100.43	99.13	100.77	100.22
Trace elements in parts per million										
Nb	0.9	1.0	1.3	1.2	1.0	2.3	2.1	2.4	1.1	1.8
Zr	50.3	60.2	64.9	52.2	49.8	67.5	72.1	53.7	37.5	74.0
Y	26.7	28.1	32.0	24.8	25.6	32.5	34.0	27.2	21.9	35.2
Sr	110.9	100.0	88.9	87.3	151.0	104.5	103.9	109.9	81.8	110.3
Rb	1.3	2.1	1.6	1.9	0.8	1.1	1.1	2.3	1.8	2.0
Th	1.7	2.1	4.9	2.8	1.8	4.3	3.0	1.6	3.4	3.1
Ga	16	16	17	16	15	15	17	15	15	17
Zn	77	58	71	68	68	62	56	21	68	57
Ni	32	30	18	36	37	17	17	14	60	16
Cr	44	42	14	65	67	10	13	13	138	12
Va	346	341	435	355	366	446	402	396	264	406
Ba	6.2	9.8	9.3	3.3	13.3	7.2	10.2	12.8	7.5	8.2
la	1.7	4.4	3.8	4.4	4.1	4.6	6.1	2.8	2.1	4.5
Ce	9.6	8.7	11.7	8.9	9.5	9.5	10.9	10.1	5.4	11.2
Nd	6.0	6.4	8.1	6.9	6.6	7.6	6.3	5.6	4.0	8.8
C.I.P.W. norms (calculated using $FeO : Fe_2O_3 = 0.85 : 0.15$)										
Qz	3.33	5.71	10.47	4.65	4.37	5.26	12.06	11.98	5.26	11.72
Or	0.35	0.43	0.25	0.24	0.27	0.54	0.40	0.33	0.50	0.41
Ab	22.10	23.72	23.92	20.53	21.79	28.99	24.63	26.83	18.39	27.09
An	29.54	29.49	27.77	31.29	29.53	26.25	27.92	24.57	33.08	26.64
Di	16.43	14.84	11.14	16.32	14.12	10.27	10.08	13.18	16.01	6.82
Hy	20.84	20.50	20.33	21.83	23.04	20.67	18.76	16.05	21.62	20.67
Ol	–	–	–	–	–	–	–	–	–	–
Mt	1.96	1.91	2.26	1.95	1.93	2.22	2.13	1.90	1.60	2.14
Il	2.13	2.08	2.67	2.10	2.08	2.68	2.52	1.86	1.44	2.53
Ap	0.39	0.48	0.63	0.47	0.52	0.52	0.55	0.56	0.42	0.53

Table 3 (part 11 of 18)

Pellet	L5436	L5437	L5438	L5439	L5440	L5441	L5442	L5443	L5444	L5445
Core/Sec	425.60	429.95	435.70	439.20	441.75	447.20	450.60	453.90	456.90	460.70
Depth (m)	113.04	115.00	117.01	117.01	119.02	119.02	121.02	121.03	121.03	123.01
SiO_2	52.1	59.3	54.1	52.6	51.1	53.3	55.7	55.6	56.3	51.9
TiO_2	0.76	1.12	1.37	1.10	0.71	0.49	1.31	1.34	1.33	0.58
Al_2O_3	15.8	14.6	14.4	14.2	15.3	14.8	14.7	15.0	14.9	15.9
Fe_2O_3	9.6	10.4	12.5	12.0	9.2	9.4	12.3	12.5	12.4	8.6
MnO	0.16	0.06	0.17	0.11	0.16	0.18	0.18	0.17	0.17	0.15
MgO	7.4	3.0	3.9	3.7	8.2	7.9	3.7	3.7	3.8	8.1
CaO	10.7	7.5	7.8	8.5	12.1	10.5	8.2	8.4	8.1	11.5
Na_2O	2.1	3.4	3.2	3.8	1.8	1.9	2.7	2.7	2.7	2.0
K_2O	0.08	0.08	0.08	0.10	0.06	0.08	0.06	0.07	0.09	0.10
P_2O_5	0.19	0.31	0.23	0.25	0.22	0.17	0.23	0.24	0.25	0.22
LOI	1.25	0.70	0.90	1.00	0.62	1.05	0.34	0.24	0.51	0.90
Total	100.20	100.40	98.69	97.30	99.42	99.87	99.36	99.96	100.52	100.03
Trace elements in parts per million										
Nb	1.0	1.5	1.5	0.9	0.7	1.4	1.5	1.4	1.8	0.6
Zr	37.1	53.9	68.2	44.4	34.1	16.6	74.1	68.9	70.0	31.4
Y	21.2	31.5	32.6	26.1	17.9	14.8	34.5	33.0	35.0	17.6
Sr	90.5	132.2	155.3	160.0	96.9	74.7	98.3	103.1	111.5	99.1
Rb	1.7	1.9	0.9	1.6	2.0	2.3	2.0	1.0	0.8	2.4
Th	3.8	4.1	4.1	2.0	1.5	3.1	3.4	0.3	1.4	3.6
Ga	15	16	15	16	13	12	17	18	17	13
Zn	67	16	66	37	72	45	62	53	62	49
Ni	60	10	18	15	84	69	15	16	16	76
Cr	144	10	8	3	279	360	13	11	12	213
V	282	124	415	417	275	264	393	417	413	244
Ba	9.7	13.8	11.3	12.0	9.7	11.3	10.0	5.1	8.1	11.8
La	1.9	3.7	4.5	3.8	2.2	0.0	3.5	7.0	5.0	2.9
Ce	3.5	9.1	8.8	9.9	6.1	3.5	11.0	11.6	12.8	4.7
Nd	3.7	7.1	6.6	6.1	5.3	2.8	8.2	8.8	10.1	3.6
C.I.P.W. norms (calculated using $FeO : Fe_2O_3 = 0.85 : 0.15$)										
Qz	4.71	16.20	9.18	4.67	3.03	6.90	13.15	12.63	13.14	3.21
Or	0.45	0.45	0.49	0.61	0.36	0.49	0.38	0.43	0.53	0.59
Ab	17.63	28.91	27.17	31.83	15.14	15.66	22.69	22.46	23.15	17.28
An	33.54	24.25	24.72	21.58	33.50	31.85	27.92	28.79	28.10	33.98
Di	15.08	9.25	10.33	15.84	20.44	15.72	9.45	9.37	8.88	17.56
Hy	23.16	15.11	19.51	16.00	22.08	24.41	19.22	19.68	19.88	22.65
Ol	–	–	–	–	–	–	–	–	–	–
Mt	1.66	1.79	2.17	2.07	1.59	1.63	2.12	2.16	2.13	1.49
Il	1.44	2.13	2.60	2.09	1.34	0.94	2.48	2.54	2.53	1.11
Ap	0.44	0.71	0.54	0.57	0.51	0.40	0.54	0.56	0.59	0.52

Table 3 (part 12 of 18)

Pellet	L5446	L5447	L5448	L5449	L5450	L5451	L5452	L5453	L5454	L5455
Core/Sec	463.40	466.05	472.05	470.00	473.45	478.10	481.85	485.00	488.70	491.05
Depth (m)	123.01	125.02	125.03	126.01	126.05	128.01	128.01	130.05	131.02	131.08
SiO_2	52.3	53.0	51.4	52.5	50.8	57.3	56.1	53.9	58.8	58.4
TiO_2	0.42	0.46	0.69	0.74	0.91	0.99	0.93	0.74	1.04	1.07
Al_2O_3	15.8	16.4	15.8	15.9	15.4	15.0	14.9	15.5	14.1	14.6
Fe_2O_3	8.8	8.4	9.5	8.8	10.6	10.7	10.4	8.3	10.6	10.6
MnO	0.16	0.16	0.16	0.09	0.17	0.10	0.10	0.09	0.06	0.06
MgO	8.3	7.7	8.0	6.3	7.5	4.0	4.5	6.3	3.2	3.3
CaO	10.9	10.7	11.9	10.9	10.2	8.3	8.7	10.8	9.1	9.0
Na_2O	2.1	2.4	1.6	2.3	2.6	2.6	3.0	2.3	2.4	2.7
K_2O	0.09	0.11	0.08	0.09	0.12	0.10	0.11	0.06	0.09	0.14
P_2O_5	0.16	0.18	0.20	0.06	0.23	0.21	0.21	0.20	0.25	0.21
LOI	1.14	1.10	0.61	0.70	1.19	0.68	0.86	0.49	0.57	0.64
Total	100.26	100.68	99.98	98.37	99.79	100.02	99.81	98.62	100.16	100.66
Trace elements in parts per million										
Nb	0.6	1.2	0.2	0.9	1.3	1.7	0.9	1.4	1.7	1.0
Zr	15.4	22.7	30.6	34.2	40.2	41.4	39.9	34.2	42.5	42.9
Y	11.8	15.7	18.4	18.9	22.9	24.3	24.2	19.7	25.2	25.0
Sr	92.7	86.5	66.8	100.2	78.7	122.0	127.7	103.7	140.8	127.7
Rb	2.3	3.2	1.7	2.8	2.4	2.0	2.3	1.7	1.1	1.7
Th	3.9	4.0	2.0	3.3	4.3	1.2	2.3	1.9	1.4	2.6
Ga	13	13	14	14	15	15	16	15	16	16
Zn	42	42	58	23	67	27	24	28	13	14
Ni	68	64	69	35	48	12	13	36	8	9
Cr	154	120	197	40	109	7	7	39	11	6
V	270	242	290	306	332	382	374	324	300	301
Ba	12.8	16.7	5.3	9.3	3.6	10.9	11.7	10.3	10.1	5.5
La	1.3	1.5	1.6	2.4	2.3	2.5	4.1	1.1	2.8	2.5
Ce	4.8	4.0	3.7	6.6	5.3	6.5	5.3	6.4	6.2	3.8
Nd	1.7	3.4	3.1	3.5	4.2	5.4	4.7	3.9	5.0	5.3
C.I.P.W. norms (calculated using $FeO : Fe_2O_3 = 0.85 : 0.15$)										
Qz	3.15	3.69	4.00	5.78	1.05	14.83	10.81	8.16	18.57	16.16
Or	0.56	0.65	0.45	0.50	0.73	0.57	0.63	0.33	0.52	0.80
Ab	18.15	20.25	13.79	19.33	21.66	22.36	25.42	19.37	20.45	22.87
An	33.34	33.66	35.45	32.94	30.30	28.84	26.84	31.95	27.48	27.25
Di	16.10	14.93	18.34	16.92	15.54	9.31	12.44	16.41	13.32	13.31
Hy	24.38	22.92	23.10	18.35	24.32	18.28	17.84	17.89	13.95	14.35
Ol	–	–	–	–	–	–	–	–	–	–
Mt	1.52	1.46	1.65	1.52	1.83	1.84	1.80	1.43	1.83	1.84
Il	0.79	0.88	1.30	1.41	1.73	1.89	1.77	1.40	1.98	2.04
Ap	0.37	0.41	0.46	0.14	0.53	0.49	0.49	0.46	0.58	0.48

Table 3 (part 13 of 18)

Pellet	L5456	L5457	L5458	L5459	L5460	L5461	L5462	L5463	L5464	L5465
Core/Sec	493.10	497.90	501.35	507.15	510.95	514.35	515.30	516.20	520.15	529.05
Depth (m)	132.03	133.06	134.08	135.06	136.04	136.04	137.01	137.01	138.06	140.02
SiO_2	58.2	54.1	57.5	52.4	52.0	51.2	55.9	53.9	62.0	47.0
TiO_2	1.08	0.75	0.91	0.69	0.68	0.67	0.93	0.96	0.87	1.11
Al_2O_3	14.8	16.4	15.7	16.2	16.2	15.7	14.7	15.4	14.2	16.9
Fe_2O_3	10.7	10.1	7.2	8.9	9.0	8.9	11.8	11.7	10.2	11.9
MnO	0.07	0.18	0.06	0.14	0.15	0.15	0.16	0.13	0.13	0.11
MgO	3.3	5.3	4.6	7.4	7.5	7.3	4.2	4.4	2.3	7.6
CaO	9.3	9.7	9.8	11.5	10.4	10.3	8.6	8.9	6.9	6.3
Na_2O	2.3	2.1	3.1	2.0	2.8	2.9	2.5	2.2	3.0	4.1
K_2O	0.08	0.08	0.08	0.07	0.10	0.10	0.07	0.10	0.08	0.37
P_2O_5	0.22	0.06	0.24	0.20	0.19	0.23	0.24	0.20	0.22	0.18
LOI	0.40	0.44	0.69	0.50	1.35	1.36	0.77	0.46	0.45	3.91
Total	100.48	99.17	99.86	99.97	100.30	98.79	99.75	98.41	100.26	99.56
Trace elements in parts per million										
Nb	1.8	0.4	2.0	0.9	1.1	0.4	1.0	0.5	1.5	1.7
Zr	43.8	35.1	39.2	37.1	33.3	37.1	42.5	36.4	44.0	41.4
Y	26.0	19.3	23.6	18.2	17.3	19.0	26.4	23.1	29.9	26.8
Sr	130.1	97.6	125.1	84.1	109.1	85.1	95.0	91.5	86.6	138.7
Rb	1.8	1.4	2.5	2.0	3.0	1.4	1.1	1.2	1.8	3.7
Th	4.0	3.2	1.2	0.8	3.5	4.7	3.5	1.3	3.6	4.1
Ga	15	15	14	13	13	14	16	17	16	20
Zn	13	19	13	42	13	38	28	21	25	20
Ni	8	37	27	64	50	65	22	24	6	20
Cr	8	43	28	176	126	179	16	19	6	16
V	301	312	293	263	335	263	352	406	151	5
Ba	3.7	13.8	9.2	9.4	5.5	7.7	12.3	8.8	19.3	14.1
La	3.8	1.6	2.8	3.8	3.1	1.6	2.9	3.7	3.7	2.4
Ce	5.1	5.8	4.2	5.3	7.1	4.3	7.6	6.1	6.3	6.4
Nd	4.4	4.1	5.7	4.0	5.1	3.3	5.6	4.3	4.8	3.5
C.I.P.W. norms (calculated using $FeO : Fe_2O_3 = 0.85 : 0.15$)										
Qz	17.80	9.83	12.19	4.64	1.52	0.72	13.18	11.18	22.78	–
Or	0.48	0.47	0.47	0.41	0.59	0.58	0.42	0.58	0.45	2.16
Ab	19.13	18.11	26.14	17.09	23.62	24.62	20.91	19.04	25.02	34.72
An	29.92	34.85	28.62	35.02	31.35	29.37	28.75	31.72	25.27	26.66
Di	12.57	10.74	14.95	16.93	15.37	16.48	10.13	9.48	6.25	2.76
Hy	14.83	20.54	12.65	21.31	22.42	21.53	20.19	20.64	15.23	0.58
Ol	–	–	–	–	–	–	–	–	–	23.17
Mt	1.85	1.74	1.25	1.53	1.55	1.54	2.04	2.01	1.76	2.06
Il	2.04	1.42	1.74	1.30	1.29	1.27	1.77	1.81	1.64	2.10
Ap	0.52	0.15	0.55	0.46	0.45	0.53	0.56	0.47	0.51	0.41

Table 3 (part 14 of 18)

Pellet	L5466	L5467	L5468	L5469	L5470	L5471	L5472	L5473	L5474	L5475
Core/Sec	529.80	530.78	533.18	536.75	539.10	542.15	545.30	548.80	550.80	553.80
Depth (m)	141.05	141.06	142.02	143.05	143.09	144.05	145.05	146.04	146.04	148.02
SiO_2	57.8	54.1	54.0	48.5	55.0	57.6	57.3	54.0	54.1	51.0
TiO_2	0.91	0.79	0.63	0.47	0.68	1.16	1.14	0.45	0.41	0.89
Al_2O_3	15.2	15.3	15.0	14.8	16.0	14.8	15.2	15.6	15.1	14.5
Fe_2O_3	6.3	11.1	10.7	10.8	10.1	9.5	9.8	9.9	9.3	8.8
MnO	0.06	0.08	0.15	0.12	0.09	0.06	0.08	0.16	0.16	0.07
MgO	5.0	4.7	5.7	6.7	5.6	4.0	3.8	6.9	7.9	2.4
CaO	9.2	9.6	9.8	11.5	10.3	8.9	9.6	10.4	10.5	10.6
Na_2O	4.4	2.4	2.3	2.5	2.0	2.7	2.6	1.6	1.6	1.8
K_2O	0.15	0.08	0.07	0.08	0.11	0.19	0.08	0.08	0.05	0.11
P_2O_5	0.19	0.21	0.12	0.19	0.14	0.19	0.19	0.14	0.13	0.23
LOI	2.33	1.06	0.79	1.09	0.62	1.03	0.86	0.64	0.77	0.77
Total	101.48	99.52	99.14	96.80	100.60	100.19	100.55	99.92	99.95	91.22
Trace elements in parts per million										
Nb	1.5	1.5	0.8	0.7	1.3	1.3	1.9	0.9	0.9	1.6
Zr	42.6	26.9	20.5	9.8	29.1	44.0	45.4	14.4	13.0	57.0
Y	26.3	21.2	17.7	13.0	18.7	26.8	26.8	13.9	11.8	33.3
Sr	117.2	115.7	81.0	94.8	104.4	116.3	125.2	64.6	61.8	184.4
Rb	3.7	2.2	1.2	1.8	2.4	2.0	2.9	2.7	2.2	2.0
Th	0.8	2.2	2.4	2.4	2.8	2.8	3.5	3.7	3.4	1.7
Ga	15	17	14	14	16	16	18	14	12	20
Zn	9	17	30	25	15	15	17	46	46	14
Ni	17	24	37	37	38	18	17	52	70	8
Cr	12	16	81	47	37	9	9	137	225	5
V	323	369	322	389	329	398	399	290	266	310
Ba	5.5	11.1	10.7	11.1	4.7	5.8	8.1	9.8	10.1	4.2
La	2.7	2.7	1.1	0.3	2.6	3.9	4.1	0.7	0.0	2.5
Ce	9.4	8.8	6.5	1.1	9.0	5.6	7.2	1.7	0.0	8.5
Nd	4.3	2.8	4.0	1.4	4.1	3.5	4.7	1.4	0.6	6.6
C.I.P.W. norms (calculated using $FeO : Fe_2O_3 = 0.85 : 0.15$)										
Qz	6.78	9.78	8.85	–	10.68	14.93	14.65	9.48	8.96	13.84
Or	0.87	0.49	0.43	0.45	0.67	1.15	0.45	0.49	0.31	0.63
Ab	37.03	20.35	19.39	21.43	16.82	22.61	21.64	13.71	13.52	15.20
An	21.37	30.85	30.33	28.93	34.36	27.89	29.69	35.16	33.92	31.30
Di	18.82	12.98	14.43	22.08	13.14	12.61	13.98	12.91	13.94	16.82
Hy	10.48	19.16	20.66	15.41	20.10	14.86	14.13	23.79	25.04	8.14
Ol	–	–	–	3.28	–	–	–	–	–	–
Mt	1.09	1.91	1.84	1.87	1.74	1.65	1.69	1.71	1.60	1.52
Il	1.73	1.50	1.21	0.90	1.28	2.20	2.17	0.85	0.77	1.70
Ap	0.43	0.48	0.28	0.43	0.32	0.43	0.44	0.32	0.31	0.53

Table 3 (part 15 of 18)

Pellet	L5476	L5477	L5478	L5479	L5480	L5481	L5482	L5483	L5484	L5485
Core/Sec	555.90	557.70	559.70	563.20	565.75	570.00	571.40	575.90	577.30	580.10
Depth (m)	148.03	148.09	149.01	150.05	150.06	152.05	152.07	153.01	154.01	154.04
SiO_2	52.8	63.4	53.2	53.3	50.5	51.7	61.4	59.7	57.3	51.3
TiO_2	0.78	0.91	0.77	0.44	1.14	0.67	0.87	0.79	1.12	0.98
Al_2O_3	15.5	14.5	17.4	15.4	15.5	15.8	13.9	17.0	15.2	15.8
Fe_2O_3	9.7	8.0	10.0	9.7	11.1	9.4	9.7	9.1	10.6	10.4
MnO	0.16	0.05	0.11	0.19	0.15	0.14	0.05	0.04	0.07	0.14
MgO	7.2	2.4	5.2	7.8	6.4	8.1	2.4	1.3	3.8	7.2
CaO	10.6	7.7	10.1	10.3	10.2	9.5	8.1	7.7	9.4	10.5
Na_2O	2.4	2.8	2.4	1.9	2.8	3.0	2.3	2.8	2.4	2.4
K_2O	0.05	0.07	0.11	0.06	0.09	0.18	0.04	0.23	0.09	0.11
P_2O_5	0.18	0.23	0.17	0.13	0.24	0.15	0.20	0.17	0.10	0.16
LOI	0.74	0.45	0.64	1.13	1.59	2.03	0.31	0.52	0.53	1.11
Total	100.16	100.51	100.01	100.35	99.69	100.71	99.28	99.34	100.60	100.10
Trace elements in parts per million										
Nb	0.9	1.7	1.1	1.0	0.7	0.1	1.8	0.8	1.8	0.8
Zr	42.1	60.7	30.7	14.1	51.2	33.0	43.9	23.7	45.3	41.5
Y	22.0	33.8	19.3	12.8	26.2	18.6	29.8	8.2	26.1	23.1
Sr	95.5	123.9	122.7	72.4	106.4	98.4	114.9	175.3	117.6	83.5
Rb	2.0	2.7	3.0	2.4	2.3	3.5	2.2	4.2	2.1	2.6
Th	4.3	3.9	3.8	2.7	4.0	3.1	3.3	2.8	5.3	4.4
Ga	15	15	17	14	15	13	16	18	15	17
Zn	48	14	21	43	29	25	13	12	13	31
Ni	60	7	22	66	43	61	8	12	16	50
Cr	200	9	12	208	77	86	12	11	14	120
V	296	127	369	282	380	271	162	510	391	373
Ba	7.0	8.6	13.2	10.6	8.0	9.0	8.3	4.4	5.7	6.5
La	3.2	3.7	3.2	0.3	2.3	2.0	1.4	1.3	1.9	1.9
Ce	4.8	9.4	6.2	1.1	3.7	5.8	7.4	5.2	7.3	5.7
Nd	4.4	7.2	1.3	2.7	5.3	5.2	5.0	3.4	5.3	3.4
C.I.P.W. norms (calculated using $FeO : Fe_2O_3 = 0.85 : 0.15$)										
Qz	4.55	25.33	7.14	6.58	1.34	–	24.27	20.16	14.87	2.29
Or	0.31	0.39	0.66	0.33	0.52	1.07	0.27	1.39	0.53	0.66
Ab	20.07	23.42	20.01	15.98	23.57	25.70	19.82	23.99	20.71	20.59
An	31.59	27.08	36.43	33.42	29.64	28.93	27.30	33.09	30.12	31.93
Di	16.21	7.95	10.27	13.81	16.08	13.87	9.70	3.42	13.44	15.65
Hy	22.26	11.57	20.42	25.41	21.35	24.06	12.99	12.54	15.29	22.95
Ol	–	–	–	–	–	0.98	–	–	–	–
Mt	1.68	1.38	1.73	1.68	1.91	1.63	1.67	1.56	1.83	1.79
Il	1.49	1.72	1.45	0.85	2.17	1.27	1.65	1.49	2.13	1.86
Ap	0.41	0.53	0.38	0.31	0.56	0.34	0.46	0.39	0.22	0.37

Table 3 (part 16 of 18)

Pellet	L5486	L5487	L5488	L5489	L5490	L5491	L5492	L5493	L5494	L5495
Core/Sec	581.80	585.70	591.85	594.70	596.05	599.90	603.60	606.30	608.10	609.30
Depth (m)	155.03	155.04	157.05	157.00	157.09	159.02	159.02	161.01	161.01	161.02
SiO_2	54.0	57.3	54.1	55.8	53.6	45.6	51.3	49.5	53.0	57.9
TiO_2	0.75	0.98	1.00	0.99	1.02	0.99	0.58	0.59	0.59	0.85
Al_2O_3	16.4	14.8	15.6	15.8	15.7	13.5	16.1	15.9	15.9	14.1
Fe_2O_3	10.0	11.2	11.1	11.2	12.2	10.8	8.5	8.2	8.2	9.6
MnO	0.18	0.14	0.10	0.08	0.11	0.09	0.14	0.11	0.13	0.10
MgO	5.2	2.9	2.9	2.9	3.2	3.8	8.2	8.6	7.6	3.5
CaO	9.7	5.5	4.8	5.7	5.2	6.4	10.4	12.0	10.9	8.5
Na_2O	2.1	4.8	6.4	5.1	6.0	3.8	2.9	2.5	2.6	2.6
K_2O	0.08	0.08	0.08	0.10	0.11	0.16	0.16	0.09	0.13	0.13
P_2O_5	0.06	0.19	0.19	0.18	0.18	0.16	0.05	0.14	0.16	0.22
LOI	0.57	1.35	2.25	2.70	2.56	14.42	2.16	2.36	1.13	0.90
Total	99.17	99.30	98.35	100.51	99.91	99.75	100.56	99.95	100.43	98.49
Trace elements in parts per million										
Nb	0.6	2.2	1.9	1.5	1.6	1.6	0.9	0.0	0.5	2.2
Zr	30.3	43.9	44.5	40.5	38.2	47.5	26.8	35.2	35.4	33.3
Y	20.1	31.1	31.0	30.1	27.3	28.4	15.3	19.6	17.8	24.3
Sr	88.0	90.4	227.7	698.4	77.3	185.7	229.5	135.0	116.2	114.1
Rb	1.7	1.3	1.7	1.3	1.5	1.9	3.8	1.5	3.6	3.5
Th	0.9	2.6	2.6	2.5	3.3	2.3	4.9	2.4	2.1	2.8
Ga	16	14	13	14	14	15	12	14	13	15
Zn	37	31	27	20	24	21	53	35	53	47
Ni	36	7	8	7	9	15	74	94	78	12
Cr	85	3	2	3	1	2	229	277	245	6
V	327	172	190	193	239	411	261	282	242	251
Ba	11.6	11.4	16.6	50.8	3.1	14.0	40.7	6.1	13.5	7.2
La	1.3	2.5	3.7	3.1	2.8	4.1	1.2	3.8	0.3	0.6
Ce	5.7	6.8	9.7	7.2	9.5	9.0	5.5	4.3	3.8	7.0
Nd	3.0	5.6	5.7	6.2	5.7	7.5	1.8	4.4	3.5	4.3
C.I.P.W. norms (calculated using $FeO : Fe_2O_3 = 0.85 : 0.15$)										
Qz	9.82	8.88	–	4.82	–	0.19	–	–	2.75	17.34
Or	0.47	0.50	0.48	0.62	0.68	0.93	0.93	0.55	0.78	0.79
Ab	18.09	40.32	53.85	43.56	50.79	32.44	24.34	21.40	22.42	21.64
An	34.81	18.88	13.77	19.63	15.67	19.11	30.68	31.78	31.16	26.72
Di	10.73	6.15	7.21	6.35	7.44	9.87	16.87	21.54	17.77	11.55
Hy	20.51	18.01	11.03	17.62	11.01	17.73	19.49	11.94	20.79	14.92
Ol	–	–	4.54	–	6.24	–	2.67	6.80	–	–
Mt	1.73	1.93	1.91	1.93	2.11	1.86	1.47	1.42	1.42	1.66
Il	1.42	1.85	1.89	1.88	1.94	1.89	1.10	1.11	1.13	1.62
Ap	0.15	0.44	0.45	0.42	0.41	0.38	0.12	0.33	0.36	0.51

Table 3 (part 17 of 18)

Pellet	L5496	L5497	L5498	L5499	L5500	L5501
Core/Sec	612.94	615.10	617.65	618.85	623.50	625.95
Depth (m)	162.02	163.01	163.05	164.02	164.06	164.06
SiO_2	50.3	49.7	53.1	50.0	53.3	52.5
TiO_2	0.52	0.25	0.23	0.22	0.50	0.34
Al_2O_3	15.7	17.2	16.7	15.4	16.5	15.6
Fe_2O_3	8.2	7.6	7.2	8.5	9.1	8.6
MnO	0.13	0.13	0.13	0.16	0.14	0.14
MgO	8.9	9.7	8.9	10.1	7.8	9.2
CaO	11.1	12.1	12.1	9.2	11.6	12.1
Na_2O	2.6	1.6	1.3	2.5	1.2	1.3
K_2O	0.17	0.10	0.05	0.58	0.08	0.12
P_2O_5	0.13	0.12	0.11	0.10	0.12	0.11
LOI	1.82	1.67	1.02	2.97	0.48	0.81
Total	99.58	100.24	100.85	99.80	100.91	100.86
Trace elements in parts per million						
Nb	0.8	0.9	1.0	0.3	1.5	1.2
Zr	29.4	6.3	9.7	7.5	13.0	9.5
Y	15.2	7.0	9.5	9.0	12.2	10.4
Sr	98.6	222.1	82.3	102.0	54.9	53.9
Rb	3.6	2.8	2.6	4.7	1.2	1.4
Th	3.3	1.1	2.7	0.9	0.8	1.1
Ga	11	10	11	10	13	11
Zn	67	44	52	51	52	44
Ni	107	80	78	91	64	99
Cr	358	153	193	398	134	381
V	237	207	189	201	317	231
Ba	18.3	20.8	10.7	22.3	7.2	9.8
La	2.4	0.5	0.7	1.2	4.6	2.0
Ce	4.4	n.d.	2.6	2.1	1.6	1.3
Nd	5.5	0.9	0.8	1.7	0.3	1.3
C.I.P.W. norms (calculated using $FeO : Fe_2O_3 = 0.85 : 0.15$)						
Qz	–	–	6.34	–	8.08	4.69
Or	1.02	0.59	0.28	3.45	0.46	0.69
Ab	22.02	13.90	11.14	21.51	10.44	11.42
An	30.76	39.29	39.41	28.89	39.37	36.13
Di	19.04	16.05	16.20	13.01	14.23	18.72
Hy	16.47	24.60	23.90	18.83	24.27	25.29
Ol	5.03	1.42	–	8.28	–	–
Mt	1.42	1.31	1.24	1.46	1.57	1.48
Il	0.99	0.47	0.43	0.42	0.95	0.64
Ap	0.31	0.28	0.25	0.24	0.27	0.26

Table 3 (part 18 of 18)

Lava Groups and Volcanic Stratigraphy of the CCSP Boreholes CY-1 and CY-1A, Troodos Ophiolite, Cyprus

JAMES M. MEHEGAN[2] AND PAUL T. ROBINSON

Department of Geology and Centre for Marine Geology, Dalhousie University,
Halifax, Nova Scotia, B3H 3J5, Canada

Mehegan, J.M. and Robinson, P.T., 1991: Lava groups and volcanic stratigraphy of the CCSP Boreholes CY-1 and CY-1A, Troodos ophiolite, Cyprus; in Cyprus Crustal Study Project: Initial Report, Holes CY-1 and 1A, eds. Gibson, I.L., Malpas, J., Robinson, P.T., and Xenophontos, C.; Geological Survey of Canada, Paper 90–20, p. 177–186, 1991.

Abstract

Cluster analysis is used to define magma types in the extrusive rocks of the Troodos ophiolite. Three major groups (A, B, and C) are recognized on the basis of major element geochemistry and these are subdivided further using trace element data. All of the lavas from CCSP borehole CY-1 belong to Group B but there is a regular downhole repetition of Subgroups B1 and B2, reflecting variations in Cr contents. In borehole CY-1A, most of the recovered lavas belong to Group A, but two intervals have lavas of Group B character. The geochemical stratigraphy of this hole thus provides clear evidence for interfingering of the major magma types on the northern flank of Troodos.

Résumé

Afin de pouvoir définir les types de magma dans la partie extrusive des roches de l'ophiolite de Troodos, on a procédé à une étude des fragments utilisant la methode d'analyse des groupes. A la lumière des principaux éléments géochimique, on peut reconnaître trois principaux groupes (A, B et C). Ces derniers peuvent être subdivisés en utilisant le résultat des observations des éléments trace. Toutes les laves du trou de forage CY-1 appartiennent au groupe B, mais il y a toutefois une répétition régulière en profondeur des sous groupes B1 et B2, reflétant les différences de teneur en Cr. Dans le trou de forage CY-1A, la plupart des laves récupérées appartiennent au groupe A, mais deux couches comportent des laves ayant les caractèristiques du groupe B. La stratigraphie géochimie de ce trou offre ainsi une preuve évidente de l'intercroisement des principaux types magmatiques sur le flanc nord de Troodos.

---

[2]Now at Department of Geological Sciences, California State University, San Bernardino, California 92407, USA.

INTRODUCTION

One of the prime objectives of the Cyprus Crustal Study Project (CCSP) was to determine the magmatic evolution of the Troodos ophiolite. We have undertaken a detailed study of the geochemical stratigraphy of the Troodos lavas in order to document compositional changes with time. Early studies by Robinson et al. (1983) and Schmincke et al. (1983) suggested the presence of distinct lava groups on the northern flank of Troodos which in most areas did not correlate with the previously defined Upper and Lower Pillow Lavas (Bear, 1960). A detailed study of the major and trace element geochemistry of the Troodos lavas by Mehegan (1988) demonstrated the presence of three major magmatic events or volcanic cycles in the extrusive sequence. During the first cycle, a suite of arc tholeiite lavas ranging in composition from basalt to rhyodacite (Group A) was erupted. Overlying and interfingering with Group A lavas are two suites of more depleted basalts and basaltic andesites, Group B on the northern flank and Group C on the southern flank. Group B lavas are depleted arc tholeiites whereas Group C lavas are highly depleted arc tholeiites with boninitic affinities.

These three major magma groups have been subdivided into regional and stratigraphic subgroups on the basis of trace element geochemistry; Group A into A1, A2 and As, Group B into B1, B2 and B3, and Group C into C1 and C2. All of the lavas along the southern flank of Troodos (Groups As, C1, C2) are more depleted in incompatible trace elements than their counterparts along the northern flank (Groups A1, A2, B1, B2 and B3).

Based on their distinctive geochemistry, all of the Troodos lavas are believed to have formed in a supra-subduction zone environment, probably in an incipient arc.

Compilation of a detailed geochemical stratigraphy is hampered by poor exposures and commonly by structural complexity. Fortunately, CCSP boreholes CY-1 and CY-1A provide a nearly continuous section through the lavas on the northern flank of Troodos, thus permitting the high-resolution sampling required to determine the relationships among the different magma groups. In this paper, we attempt to identify compositional groups in the recovered rocks and to determine their stratigraphic relationships. Multivariate cluster analyses is used to document the lava groups and to help illustrate the gross geochemical stratigraphy. Five statistically defined Subgroups (A1, A2, B1, B2, and B3)(Table 1) are recognized in the cored section on the basis of major and trace element compositions. These subgroups reflect successive cycles of seafloor volcanism on the northern flank of Troodos.

	TiO_2	Zr	Cr	Ni	Y	V
Group A1	0.76–1.36	55–116	0–13	0–11	31–56	34–608
Group A2	0.72–0.88	44–52	1–25	2–30	25–32	334–434
Group B2	0.51–0.84	25–41	19–97	18–80	15–27	115–313
Group B1	0.49–0.81	27–50	103–226	36–106	13–25	168–283
Group B3	0.16–0.68	11–41	248–968	90–1038	2–25	71–365

Table 1: Trace element characteristics of CCSP CY-1 and CY-1A Lavas.

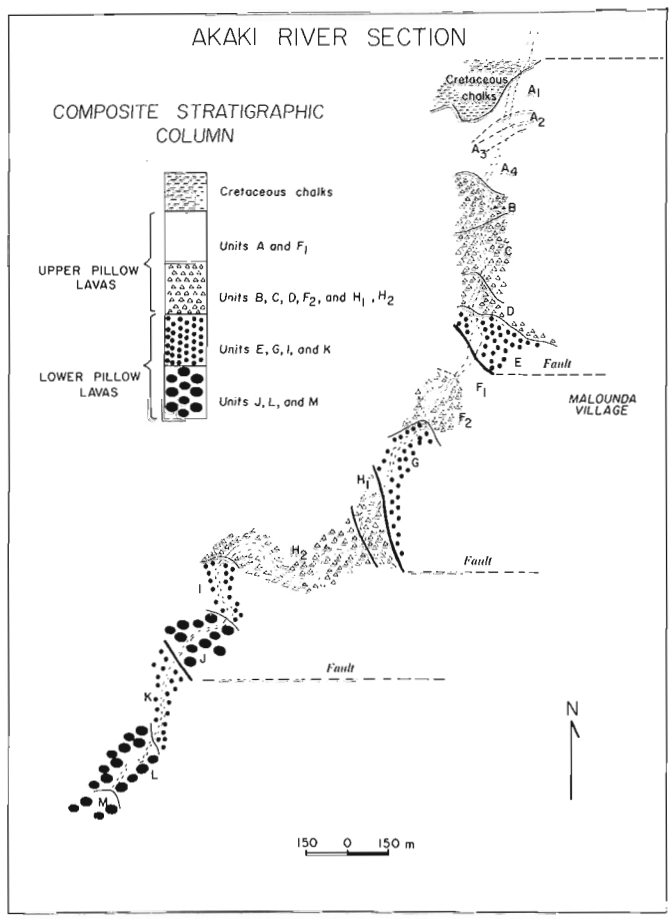

Figure 1: Generalized geologic map of the Akaki River canyon showing stratigraphic subdivision of the Troodos extrusive sequence. Note repetition of lithologic units by faulting. Modified from Schmincke et al. (1983).

GEOLOGY

CCSP boreholes CY-1 and CY-1A are sited in the Akaki-Maroulena canyon on the northern flank of Troodos (Figure 1). Hole CY-1 was spudded at the sediment-lava interface and was intended to sample the entire volcanic sequence. The hole penetrated 474 m with a recovery of just over 90% before it was terminated because of hole instability and drilling difficulties. Thirty lithologic units are recognized in the recovered core (Robinson et al., this volume) and these are similar to the units exposed in the canyon walls. The most common lithologies are aphyric to sparsely olivine- and clinopyroxene-phyric

pillow lavas and sheeted to massive lava flows. Picritic pillows are present in the upper parts of the core and a few dykes cut the lower parts. Fresh glass was observed only in lavas below 330 m where it occurs chiefly as pillow rinds.

Hole CY-1A was spudded about 2 km farther up the canyon at approximately the same stratigraphic level at which Hole CY-1 was terminated. It penetrated 700 m with nearly 95% recovery before being terminated due to high water pressures. The recovered core consists chiefly of aphyric pillowed and massive flows, locally cut by dykes. Thirty four major lithologic units are recognized in the core (Robinson et al., this volume), but these do not correlate closely with the exposed section. The hole terminated in a sheeted dyke swarm.

CLUSTER ANALYSIS AND LAVA GROUPS

Until recently igneous petrologists typically used graphs of element pairs to identify chemical subdivisions within geochemical data sets. However, the subdivision of large data sets into natural clusters, or groups, requires simultaneous evaluation of all the data, something that is difficult to do with traditional variation diagrams. The search for natural clusters within large populations thus requires a multivariate approach. Because geochemical data seldom have normal distributions, non-parametric techniques, such as cluster analysis, must be used to assess the data. With cluster analysis, the geochemical data are evaluated by measuring, in polydimensional space, the Euclidean distance between attributes of samples. Euclidean distance, or the dissimilarity coefficient, measures the literal distance between two objects, or clusters; hence the smaller the Euclidean distance the more similar the two objects. A matrix of Euclidean distances is compiled and then examined to identify the nearest neighbors to each object, or sample, and thus clusters are determined. The clustering procedure continues until no new clusters are formed.

The data set investigated for Holes CY-1 and CY-1A includes major element data on volcanic glasses (Mehegan, 1988) and major and trace element data on bulk rock samples (this volume). The data set was evaluated using the UPGMA (unweighted pair-group method using arithmetic averages) cluster method which displays similarities and dissimilarities between pairs of objects in a set, with the aim of classifying the samples. With this method both the latest and earliest additions to a cluster have equal weight (Romesburg, 1990).

Sample classification is recorded in cluster trees or dendrograms (Figures 2 and 3) which show patterns of similarities between the chemical compositions of the volcanic glasses or bulk-rock samples. The abscissas of the dendrograms lack scale because they are organized with samples evenly spaced near most similar samples, or their most compatible neighbors, from the data set. Euclidean distance is plotted along the scaled ordinate of each dendrogram.

The results of the data analysis for Holes CY-1 and CY-1A (Figures 2 and 3) demonstrate that the sampled lavas can be classified solely on their geochemical characteristics. In the tests for clusters, stratigraphy is excluded as a variable. Figure 2 is a dendrogram for major elements of volcanic glasses from the northern flank of Troodos including the glasses from Hole CY-1. Figure 3 is a dendrogram showing trace element groupings for bulk-rock samples from holes CY-1 and CY-1A.

Glass Data

Dendrograms produced by cluster analysis often contain many clusters which need to be evaluated for their importance and relevance to the geologic as well as the statistical problem. For example, if the dendrogram for the northern Troodos glasses (Figure 2) is cut at the Euclidean distance of 0.6, then five clusters are clearly visible; however, Mehegan (1988) demonstrated that three of these clusters are chemically related through fractionation processes and they thus form one geologic group. The three large branches, or clusters, on the left-side of the dendrogram are composed exclusively of glasses from the lower portions of exposed lava sections. The branch furthest to the left is composed of rhyodacite glasses (PED-5A–TR-5), which are the most evolved samples known from the Troodos lavas (Robinson et al., 1983; Mehegan, 1988). Adjacent to the rhyodacite cluster is a branch which contains dacitic and andesitic glasses (PED-26A–TR-13). The very abundant andesites and basaltic andesites (A-51–A-54) which form the large cluster in the centre of the dendrogram are also from the lower portions of exposed stratigraphic sections. Although the glass compositions from these three clusters form separate branches of the tree, Mehegan (1988) demonstrated that their major element compositions can be related by closed-system fractionation, and thus samples from these three branches combine to form one geochemical group, Group A (Figures 2 and 4).

On the right-side of Figure 2 the thick branch, labelled B1, is composed of glasses sampled from upper stratigraphic levels of the lava pile and from the CY-1 drill core. Between the Group A and B1 branches is a smaller cluster, labelled Group B2 (Figure 2), which is composed of a few glasses sampled from high in the extrusive section, mostly from the Akaki-Maroulena canyon and from Hole CY-1. Although the dendrogram suggests that these seven samples are more similar to glasses of Group A than to Group B1, their mineralogy and phase chemistry are most similar to those of Group B1 (Mehegan, 1988). Group B2 is well defined in bulk-rock samples from both Holes CY-1 and CY-1A (Figure 3).

In summary, cluster analysis applied to compositional data for northern Troodos glasses documents the presence of multiple clusters, or populations (Figure 2). The three recognized populations correspond to lava Groups A, B1, B2, and each successively younger group is more depleted in TiO_2 (Figure 4). Glasses sampled in the CY-1 borehole have major element compositions that cluster with Groups B2 and B1.

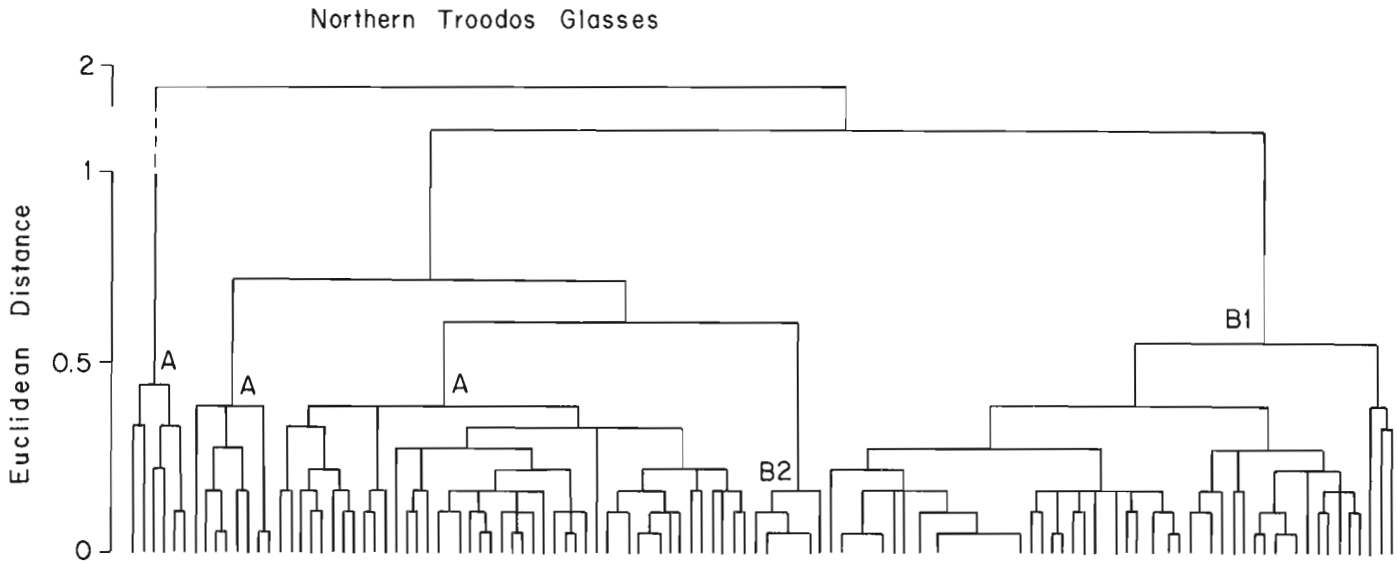

Figure 2: Dendrogram (cluster tree) for major element compositions of volcanic glasses from the northern part of the Troodos ophiolite. After Mehegan (1988).

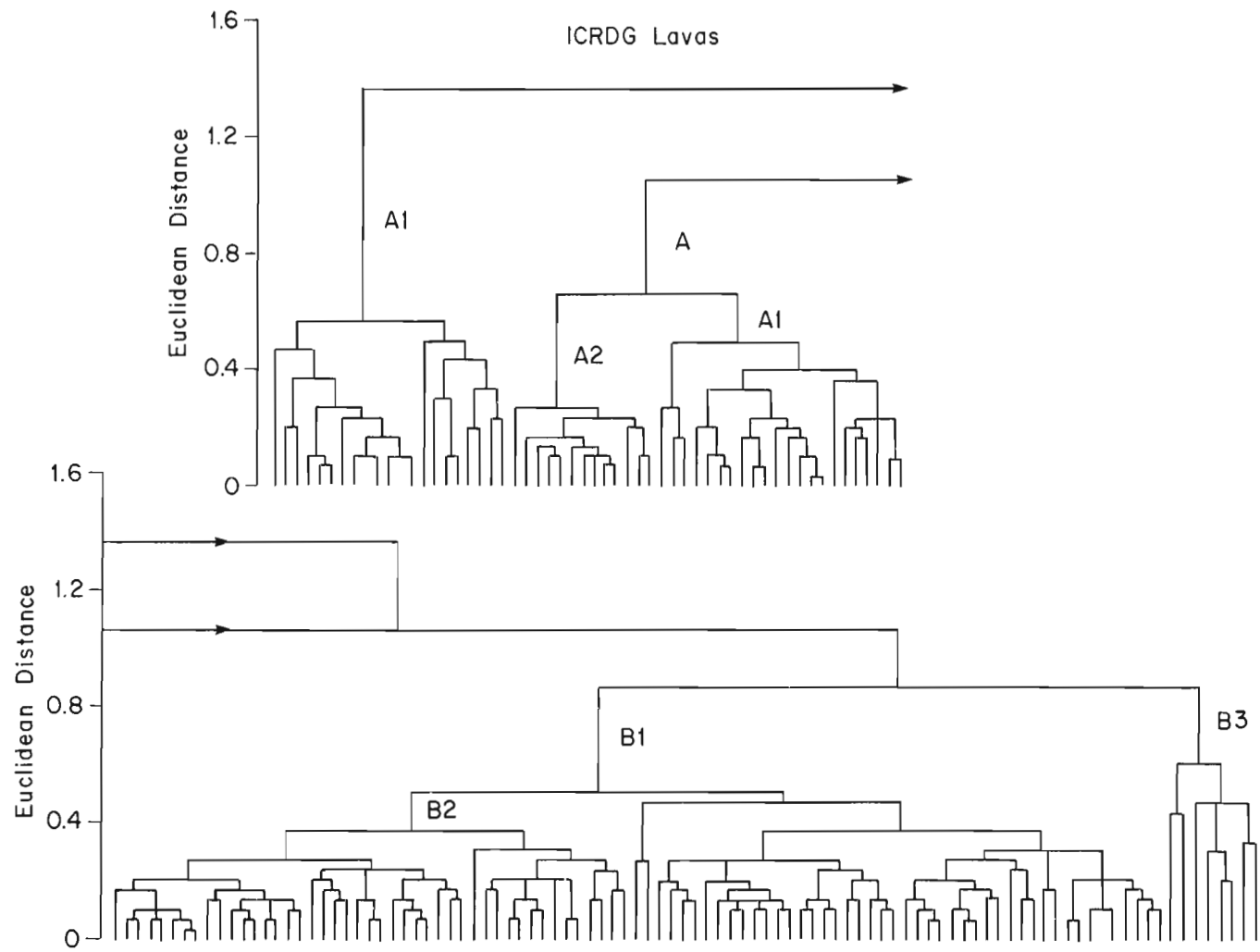

Figure 3: Dendrogram for trace element compositions of bulk rock samples from CCSP boreholes CY-1 and CY-1A. After Mehegan (1988).

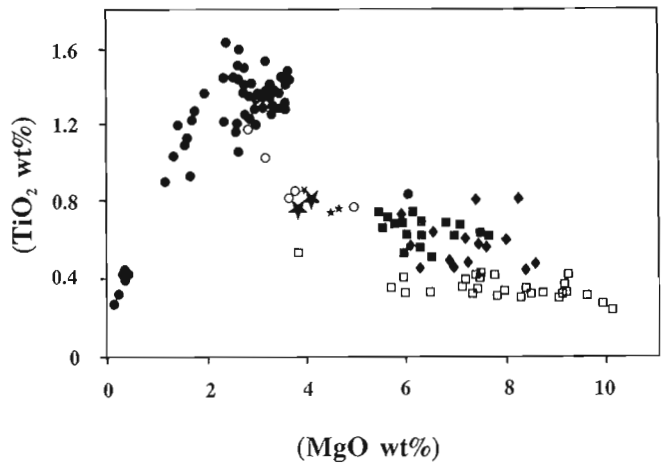

Figure 4: TiO_2 versus MgO for volcanic glasses of the Troodos ophiolite: • = magma Group A from exposed section; o = Group As from the exposed section; ★ = Group B2 from CCSP boreholes CY-1 and 1A; ⋆ = Group B2 from exposed section; ◆ = Group B1 from exposed section; ■ = Group B1 from CCSP boreholes CY-1A and 1A; □ = Group C from exposed section.

Figure 4 also illustrates that glasses from the southern flank of Troodos are more depleted in TiO_2 than those from the northern flank.

Whole Rock Data

Trace element compositions have been used by Mehegan (1988) to support major element classifications and to further subdivide the Troodos extrusive sequence. Important trace elements used as input variables for testing for natural subdivisions by cluster analysis are the compatible elements Cr and Ni and the incompatible elements Y, Zr, Ti, and V (Figures 5 and 6). Figure 3 shows the resultant dendrogram for cluster analysis of samples from Hole CY-1 and CY-1A.

If the tree in Figure 3 is cut at a Euclidean distance of 0.6 there are six major branches. The three branches on the left-side of the upper diagram are composed exclusively of bulk-rock samples from Hole CY-1A. The cluster farthest to the left contains mostly dacites and andesites which have very evolved trace element compositions, whereas the cluster on the right contains andesites and basaltic andesites with less evolved trace element compositions (Figure 3). Both of these first two clusters combine to form one compositional group, Group A1 (Figures 5 and 6). An intermediate cluster contains lavas with trace element compositions that are less evolved than those reported for Group A1, and these form a second subdivision of Group A, Group A2. Mehegan (1988) originally included these lavas in Group B2; however, it is now clear that they are more akin to Group A (Figures 3, 5 and 6).

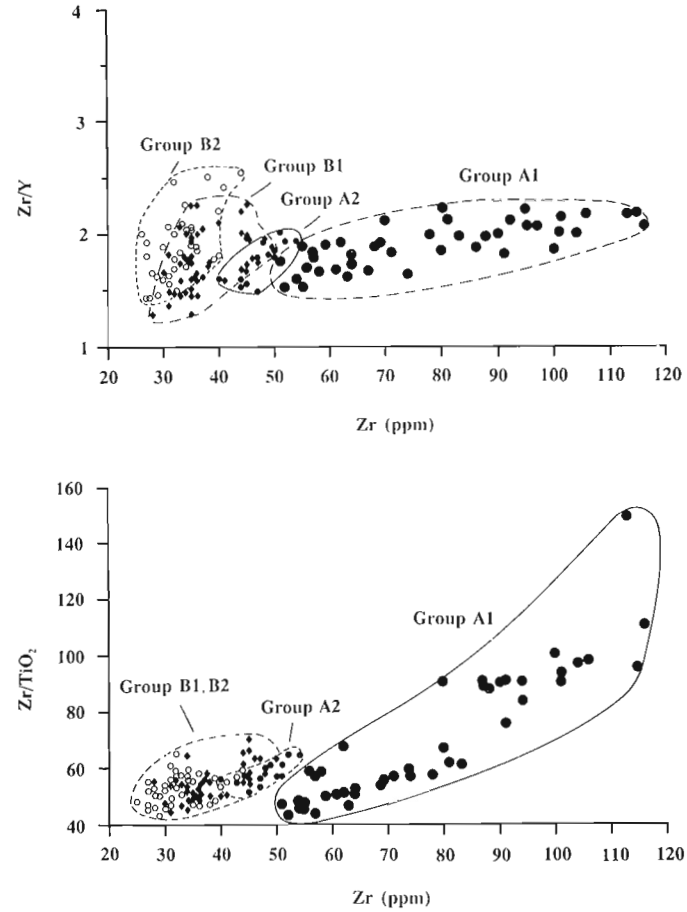

Figure 5: Plots of selected minor and trace elements for lavas of the Troodos ophiolite, showing the various geochemical groups. Plots of Zr versus Zr/Y and Zr versus Zr/TiO_2: ◆ = Group B1; o = Group B2; • = Group A2; ● = Group A1.

All the lavas on the northern flank of Troodos belong to either compositional Group A (an arc tholeiite suite) or Group B (a depleted arc tholeiite suite) (Mehegan, 1988). Five subgroups are recognized in the drill core from Holes CY-1 and 1A, each characterized by specific trace element compositions (Table 1). Subgroup A2 is distinguished from A1 primarily on the basis of lower Zr and TiO_2 contents. Subgroups B1, B2, and B3 differ chiefly in their Cr and Ni contents, with B2 having the lowest and B3 the highest values of these elements (Table 1). Subgroup B3 includes olivine phyric basalts and picrites formed by olivine accumulation.

GEOCHEMICAL STRATIGRAPHY OF HOLE CY-1 and CY-1A

In this section we consider the stratigraphic distribution of the subgroups recognized within the drilled sequence in order to develop a detailed geochemical stratigraphy for the lava pile.

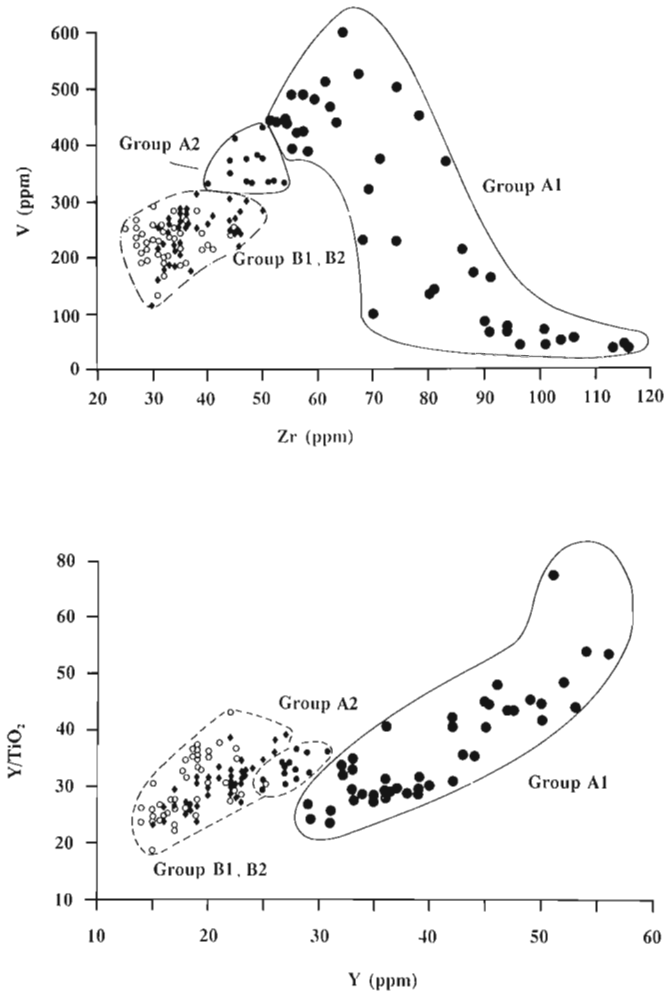

Figure 6: Plots of selected minor and trace elements for lavas of the Troodos ophiolite, showing the various geochemical groups. Plots of Zr versus V and Y versus Y/TiO_2: ◆ = Group B1; o = Group B2; • = Group A2; ● = Group A1.

Hole CY-1

All the analyzed volcanic glasses from Hole CY-1 belong to Group B. These glasses were sampled from a depth interval of 320-440 m in CY-1 and show a repetition of Subgroups B1 and B2. Additional information on the chemical stratigraphy of the CY-1 drill core can be gained from cluster analysis of trace element compositions of crystalline bulk-rock samples (Figure 3). An evaluation of the results of the multivariate analysis demonstrates that most lavas of the CY-1 drill core can be subdivided into chemical units that correspond to a high-Cr subgroup, Group B1, and a low-Cr subgroup, Group B2 (Table 1 and Figures 5, 6 and 7).

A regular repetition of Subgroups B1 and B2 is apparent downhole with a concentration of the rarer, very high-Cr, Group B3 lavas at the top of the sequence (Figure 8). Thin layers of picrites belonging to Group B3 occur between depths of 285 to 312 m. In general, lavas of Group B1 are most voluminous in the upper part of the core and diminish irregularly with depth. There is no apparent correlation between lava type and lithologic unit (i.e. pillowed or massive) in the section.

Mehegan (1988) argued that magma Groups B1 and B2 could not be related to one another by simple fractionation processes and thus were probably not erupted from the same magma chamber. If this interpretation is correct the extrusive sequence sampled in Hole CY-1 must have been formed by alternating eruptions from coexisting magma supply systems. Such a model can be easily accommodated if one or both of the magmas moved laterally through the dyke system before being erupted at the surface. Group B3 lavas (picrites) can be related to those of Subgroup B1 by olivine accumulation (Mehegan, 1988) and, hence, were probably derived from the same supply system.

All of the analyzed volcanic glasses from Hole CY-1 belong to Group B1 except for a few samples at 370 m which have Group B2 compositions (Figures 2 and 8). These Group B2 glasses were recovered from a sequence of aphanitic fine- to medium-grained basalt flows overlain by 1.2 m of volcanic sediments (Robinson et al., this volume). Geochemically and stratigraphically, these lavas correspond to samples from the top of Unit 3 in the Akaki-Maroulena canyon (Figures 1 and 8), suggesting a possible correlation between the drilled and exposed sections (Mehegan, 1988). Similar glasses also occur in stratigraphically lower lithologic units in the canyon (600–700 m) but probably do not correlate with the borehole samples.

Hole CY-1A

In Hole CY-1A the extrusive sequence is cut by three major dyke swarms (210–350 m, 560–620 m and 655–700 m) which obscure the lava stratigraphy (Figure 9). Nonetheless, most of the lavas recovered from this hole belong to Group A. Both Subgroups A1 and A2 are present and these alternate down the hole. Lavas of Subgroup A2 appear to be most abundant in the upper parts of the section whereas those of Subgroup A1 dominate below about 185 m.

Two intervals have lavas of Group B compositions: a 15-m-thick interval of olivine-phyric lavas with high Cr contents typical of Subgroup B3 occurs at the top of the sequence (Figure 9), and lavas of Subgroup B1 alternate with those of Subgroup B2 in the interval between about 115 and 165 m depth. Intercalated with these lavas is a thin layer belonging to Group A2.

Mehegan (1988) demonstrated that magma Group A could not be derived from either Group B1 or B2 by simple fractionation processes, suggesting the presence of a separate parental magma. The intercalation of lavas with Group A and B compositions suggests that the section was built by eruptions from separate magma supply systems.

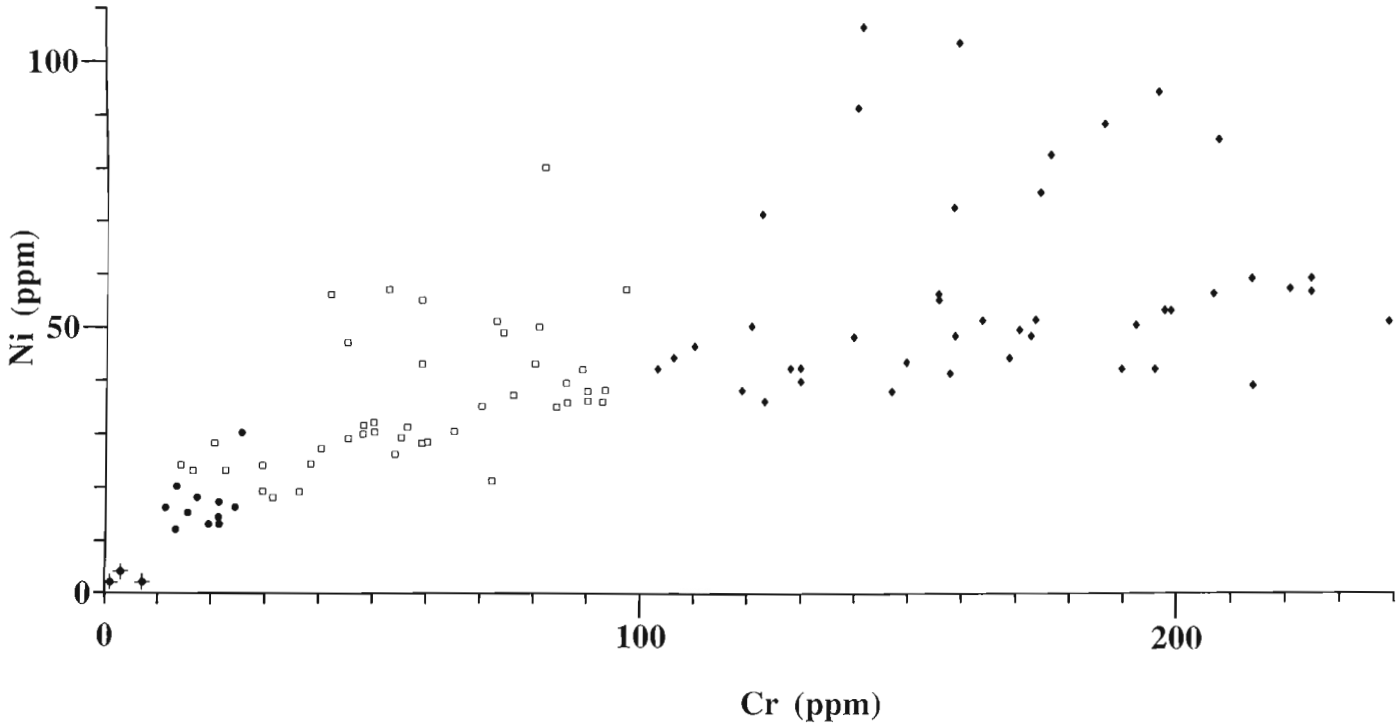

Figure 7: Geochemical variation diagram showing Cr vs. Ni for lavas from CCSP borehole CY-1 and 1A: ✦ = Group A1; • = Group A2; □ = Group B2; ◆ = Group B1.

SUMMARY

In summary, cluster analysis illustrates that northern Troodos lavas sampled in the CCSP drill cores can be subdivided into magma Groups A and B. Group A can be further subdivided into two Subgroups (A1 and A2). Mehegan (1988) originally included lavas of Subgroup A2 in Group B but data from the borehole samples suggest an affinity with Group A. The dendrogram for the CCSP drill core samples differs from those produced for the exposed sections by Mehegan (1988) in that: (1) rhyodacites which occur in the field were not encountered in the CCSP boreholes, (2) the division of Group B lavas into Subgroups B2 and B1 is better illustrated within the CCSP data set than the field samples, and (3) Group A is divided into Subgroups A1 and A2.

The combined CY-1 and CY-1A drill cores and the Akaki-Maroulena canyon section show a complex volcanic and magmatic history. At the base of the sequence are lavas typical of magma Group A and these are overlain by lavas of Group B. Throughout the sequence Groups A and B can be subdivided into a number of Subgroups (A1, A2, B1, B2, and B3) which represent important magma types. The combined geochemical stratigraphy of drill cores CY-1 and CY-1A and the Akaki-Maroulena canyon records the following extrusive history: basalts and some siliceous lavas of Group A2 were extruded, and partially obscured by later dykes which cut the sequence. This was followed by the extrusion of siliceous lavas of lava Group A1 which are represented in the CY-1A drill core between 650 and 390 m. Above 210 m in Hole CY-1A, the uppermost Group A lavas interfinger with relatively basic lavas of Group B. In Hole CY-1, Subgroups B1 and B2 show a regular alternation, with B1 lavas becoming more abundant up section.

The CY-1 and CY-1A drill core is cut by numerous dykes and low angle sills which have compositions of andesite to picritic basalt. As expected, the trace element compositions of the intrusions span those of Groups A and B.

DISCUSSION

Robinson et al. (1983) reported that the analyses of natural volcanic glasses from the Troodos ophiolite indicated multiple cycles of arc volcanism. Mehegan (1988) demonstrated that the Troodos lavas were produced by three cycles of magmatism (Groups A–As, B2–C2, B1–C1) with each cycle marked by a progressive depletion of its lavas in incompatible elements with subsequent enrichment of the more compatible elements. The Troodos lavas from all three cycles are LREE-depleted and have MORB-normalized geochemical profiles similar to those of lavas from the Mariana fore-arc, the Palau-Kyushu Ridge, and the Semail and Point Sal ophiolites. The geochemical data suggest that the Troodos lavas evolved in a supra-subduction zone setting, probably in an incipient arc.

Data presented in this paper supports these earlier conclusions and helps to further clarify the petrogenetic history of Troodos. Interfingering of lavas from the different compositional groups is well documented in the drill cores of

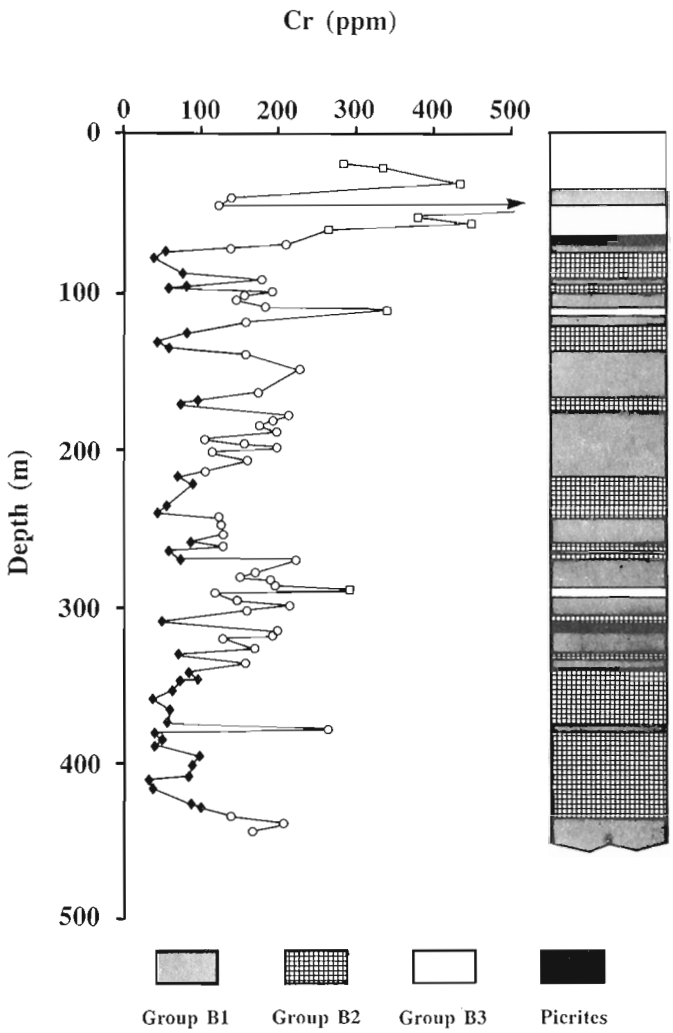

Figure 8: Downhole variation of Cr and simplified geochemical stratigraphy for CCSP Hole CY-1: o = Group B1; ◆ = Group B2; □ = Group B3.

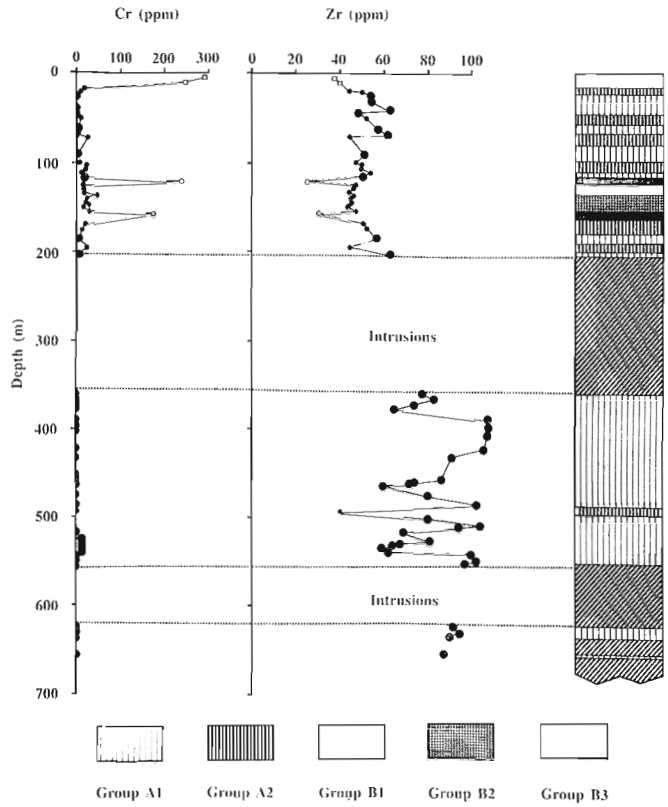

Figure 9: Downhole variation of Cr and Zr and simplified geochemical stratigraphy for CCSP borehole CY-1A: ● = Group A1; • = Group A2; o = Group B1; ◆ = Group B2; □ = Group B3.

the CCSP. This interfingering could indicate that all volcanism was related to one magmatic event through a complex history of open- and closed-system fractionation or that the lavas from each statistically and chemically distinct group were products of separate magmatic cycles. It was demonstrated by Mehegan (1988) that the range of major and trace element compositions within each of the Troodos lavas groups could be explained by low-pressure fractionation. However, modelling demonstrated that the separate groups could not be related by simple low-pressure, closed-system fractionation or by magma mixing.

Mehegan (1988) presented a model suggesting that each cycle of magmatism derived from a separate parental magma, generated at successively shallower mantle depths. He suggested that the earliest volcanic sequence of Troodos, Cycle A–As, was produced by extensive olivine and Cr-spinel fractionation of primary tholeiitic melts. The tholeiitic melts are believed to have formed by about 10% partial melting of a spinel lherzolite at 40–60 km and to have undergone fractionation during diapiric uprise. The range of lava compositions in Cycle A–As can be explained by a combination of low-pressure, closed-system fractionation, with lesser open-system fractionation and magma mixing. Diapiric rise of these melts through a wet peridotite led to production of Cycle B2–C2 melts at depths of around 30–40 km by 10–20% partial melting. Because they were denser, the diapirs forming B2–C2 melts trailed behind the first-cycle diapirs that were producing tholeiitic melts. Heat from these earlier formed diapirs could have caused additional melting (20–30%) at depths as shallow as 25 km, forming Cycle B1–C1.

The net result of these processes would be the formation of a vertical series of diapirs, the uppermost of which would contain the first formed and least dense melts of Cycle A–As. The more recently formed and denser melts (Cycles B2–C2 and B1–C1) would lie at progressively lower levels. These young, dense melts were the most depleted in REE and incompatible trace elements of all the Troodos magmas.

Cycle A–As melts generally arrived in the upper crust prior to those of Group A and Group B lavas observed in the CY-1A drill core indicates that both depleted and relatively enriched magmas co-existed at shallow levels. It is not clear

how these magmas maintained separate identities in such a rifting environment.

REFERENCES

Bear, L.M.
1960: The geology and mineral resources of the Agros-Akrotiri area; Cyprus Geological Survey Department Memoir, v. 7, 104 p.

Mehegan, J.M.
1988: Temporal, spatial, and chemical evolution of the Troodos ophiolite lavas, Cyprus: supra-subduction zone volcanism in the Tethys Sea; (PhD Thesis), Dalhousie University, Halifax, 700 p.

Robinson, P.T., Melson, W.G., O'Hearn, T., and Schmincke, H.-U.
1983: Volcanic glass compositions of the Troodos ophiolite, Cyprus; Geology, v. 11, p. 400–404.

Romesburg, C.H.
1990: Cluster analysis for researchers; Krieger Publishing, Melbourne, Florida, 350 p.

Schmincke, H.-U., Rautenschlein, M., Robinson, P.T., and Mehegan, J.M.
1983: Troodos extrusive series of Cyprus: a comparison with oceanic crust; Geology, v. 11, p. 405–409.

Ultramafic and Related Lavas from the Margi Area, Troodos Ophiolite

D.G. BAILEY[1], G.S. LANGDON[2], J. MALPAS[2], AND P.T. ROBINSON[1]

[1]Centre for Marine Geology, Dalhousie University, Halifax, Nova Scotia, B3H 3J5, Canada
[2]Department of Earth Sciences, Memorial University, St. John's, Newfoundland, A1B 3X5, Canada

Bailey, D.G., Langdon, G.S., Malpas, J., and Robinson, P.T., 1991: Ultramafic and related lavas from the Margi area, Troodos ophiolite; in Cyprus Crustal Study Project: Initial Report, Holes CY-1 and 1A, eds. Gibson, I.L., Malpas, J., Robinson, P.T., and Xenophontos, C.; Geological Survey of Canada, Paper 90–20, p. 187–202, 1991.

Abstract

Massive and pillowed olivine-rich flows form part of the Upper Pillow Lavas of the Troodos ophiolite in the vicinity of Margi, Cyprus. Although originally thought to have crystallized directly from peridotitic melts, these lavas are here shown to result from olivine crystal settling either in high level magma chambers or within the flows. Lithologic units identified in the field correlate with four major geochemical types. Analyses of glasses and 'fresh' basalts from the upper part of the sequence clearly show that these lavas are part of the 'depleted' suite described by earlier workers. The parental magmas of these depleted lavas were derived by low degrees of partial melting of a variably depleted mantle source.

Résumé

Des coulées de lave massive riche en olivine et des coulées en coussinet font partie des couches supérieures de laves en coussinet de l'ophiolite de Troodos, dans les environs du village de Margi. Bien qu'à l'origine ont ait pensé qu'elles se soient directement crystallisées à partir des fusions péridotitiques, ces laves paraissent être ici le produit de crystaux d'olivine, qui se sont établis soit dans les chambres magmatiques supérieures, soit dans les coulées elles-mêmes après extrusion. On peut identifier un certain nombre d'unités lithologique sur le terrain et celles-ci sont rattachées à quatre types géochimiques principaux. Les observations des verres et du basalte frais provenant de la partie supérieure de la séquence indique clairement que ces laves font partie de la suite appauvrie, décrite par des travaux antérieurs, et le magma parent duquel a été obtenu par une fusion partielle à faible degré d'une source mantellique inégalement appauvrie.

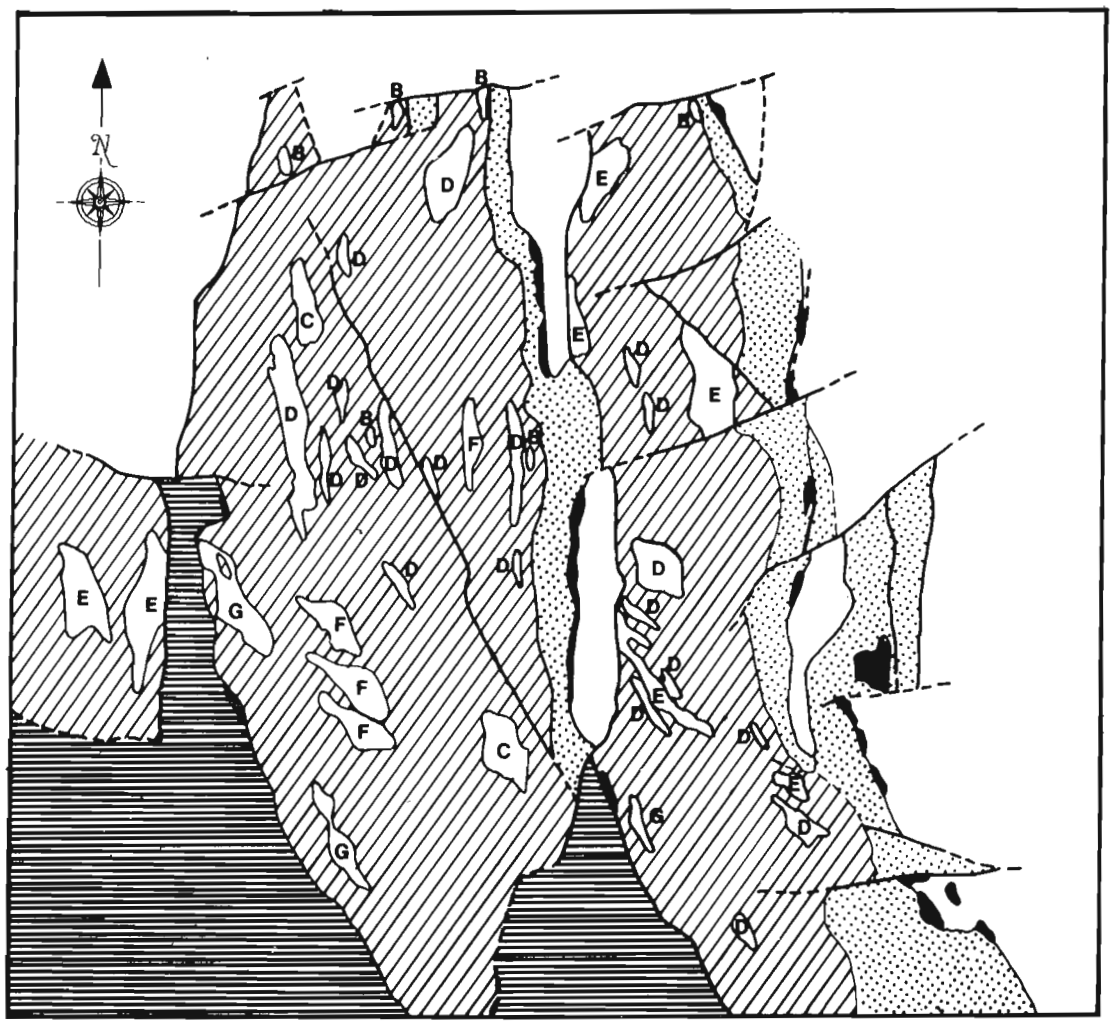

GEOLOGIC MAP OF THE MARGI AREA, CYPRUS

LEGEND

SEDIMENTARY ROCKS

CHALKS

UMBERS/CHERTS

VOLCANIC ROCKS

UPPER PILLOW LAVAS (UPPER SEQUENCE)
H,I

UPPER PILLOW LAVAS (LOWER SEQUNCE)
A,B,C,D,E,F,G

LOWER PILLOW LAVAS
A

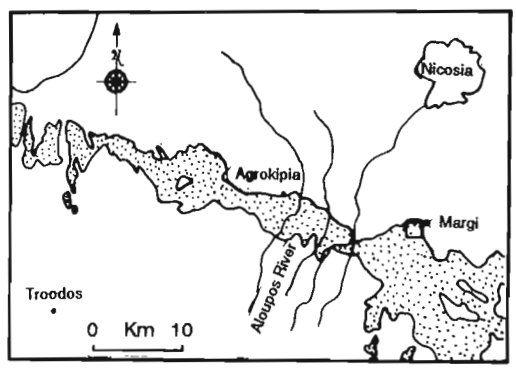

SCALE

0 100 200 300

METERS

Figure 1: General geology of the area around Margi village on the north flank of the Troodos ophiolite.

INTRODUCTION

The petrology and geochemistry of the volcanic rocks of the Troodos ophiolite, Cyprus have been a matter of considerable discussion in recent years (e.g. Robinson et al., 1983; Malpas and Langdon, 1984: Rautenschlein et al., 1985; Schmincke et al., 1983; Cameron, 1985; Taylor, 1990). Of particular interest is a sequence of ultramafic lavas, first described by Gass (1958), near the village of Margi (Figure 1). These occur as olivine-phyric pillowed and massive flows in the Upper Pillow Lavas near the top of the extrusive sequence. Gass (1958) recognized two varieties of ultramafic lavas, which he termed 'vitrophyric' and 'holocrystalline,' reflecting the crystallization state of the groundmass. Because these rocks are compositionally similar to peridotites and peridotitic komatiites, Gass (1958) and Searle and Vokes (1969) suggested that they crystallized directly from high magnesium peridotitic melts.

This origin was questioned by Malpas and Langdon (1984). They noted that these rocks are extremely rare even in Troodos, and that such highly picritic magmas were unlikely to be generated given the geothermal gradient that probably existed at the time of formation of the lava-pile; field and mineralogical evidence cited below suggest an alternate origin.

The current study was undertaken to characterize the ultramafic rocks and to find the source from which these ultramafic lavas were derived. Since olivine-phyric lavas are common throughout the extrusive complex of the ophiolite, it is likely that the processes identified within the Margi area are applicable to other sections of Troodos volcanics.

STRATIGRAPHY AND LITHOLOGY

The Margi area is underlain by a sequence of olivine-phyric lavas some 225 m-thick, traditionally known as Upper Pillow Lavas. These lavas unconformably overlie rocks of the Lower Pillow Lavas, a generally aphyric suite, from which they are separated by a thin sediment horizon. This can be traced from the Mathiati sulphide deposit, 5 km southeast of Margi, to the Ayios Onouphios river, 10 km to the west (Taylor, 1990). The Margi area is one of the few places in Troodos where the Upper and Lower Pillow Lava boundary correlates with the boundary between the compositional groups defined by Robinson et al. (1983, and see below). The Margi lavas are overlain by umbers and calcareous rocks of the Perapedhi and Lefkara Formations.

The Margi area is dissected by several north-south striking normal faults which repeat the lava stratigraphy in east-west transects. The Lower Pillow Lavas comprise aphyric to clinopyroxene- and plagioclase-phyric pillows and thin flows. In the Margi area these rocks are overlain by hyaloclastites and a volcanic breccia. Pillows are variable in size, dark brown, and highly vesicular. Most vesicles have linings of smectite, analcime, or calcite, and in thin section the only primary minerals observed are plagioclase, clinopyroxene, and titanomagnetite.

This paper deals for the most part with the overlying Upper Pillow Lavas.

THE UPPER PILLOW LAVAS

Two major stratigraphic sequences are recognized in the Upper Pillow Lavas of the Margi area: a lower sequence, about 175 m thick, composed chiefly of olivine-phyric lavas and an upper sequence, about 50 m thick, of aphyric and sparsely-phyric lavas (Figure 2).

The Lower Sequence

The lower sequence consists chiefly of crystalline or glassy, olivine-phyric pillows and thin flows, picritic pillows, and thick massive flows with picritic bases. A few aphyric and microphyric massive flows are also present. Locally, the volcanic units are separated by thin layers of breccia and sediment.

Olivine-phyric Pillows (Units A and B, Figure 2)

These rocks are chiefly light brown, light grey, or reddish brown in colour, reflecting variable degrees of alteration. A few pillows have fresh black glassy rinds, but most glass has been altered to green smectite and minor carbonate, which also fill interpillow voids. Olivine, clinopyroxene, and spinel phenocrysts combined rarely exceed ten modal percent. Olivine phenocrysts are subhedral to euhedral and range from 0.5 to 10 mm in diameter. Most are completely altered to mixtures of smectite, iron oxides, and calcite. Clinopyroxene forms equant, subhedral crystals with an average diameter of approximately 0.3 mm. Typically, the clinopyroxene crystals are much fresher than adjoining olivine crystals and are pale green in hand specimen. Dark red to black, euhedral spinel grains occur as inclusions in large olivines or, more rarely, independently within the groundmass.

The groundmass of these rocks is tan to brown in colour, and composed largely of clays, disseminated secondary oxides, and calcite. Poorly formed elongate microlites of clinopyroxene are present in all samples (4–20 modal percent). Minute grains and needles of plagioclase are also common but are generally less abundant than clinopyroxene (3–15 modal percent).

In a few specimens, the groundmass is black, hard, and appears glassy. In these rocks, clinopyroxene microlites with quench morphologies comprise 40–70 modal percent of the groundmass. The remainder is glass, most of which has been altered to dark-brown smectite.

Picritic Pillows (Unit C, Figure 2)

Picritic pillows in the lower sequence occur at two localities and, in both cases, grade vertically and laterally into typical olivine-phyric lavas. The pillows are generally spherical,

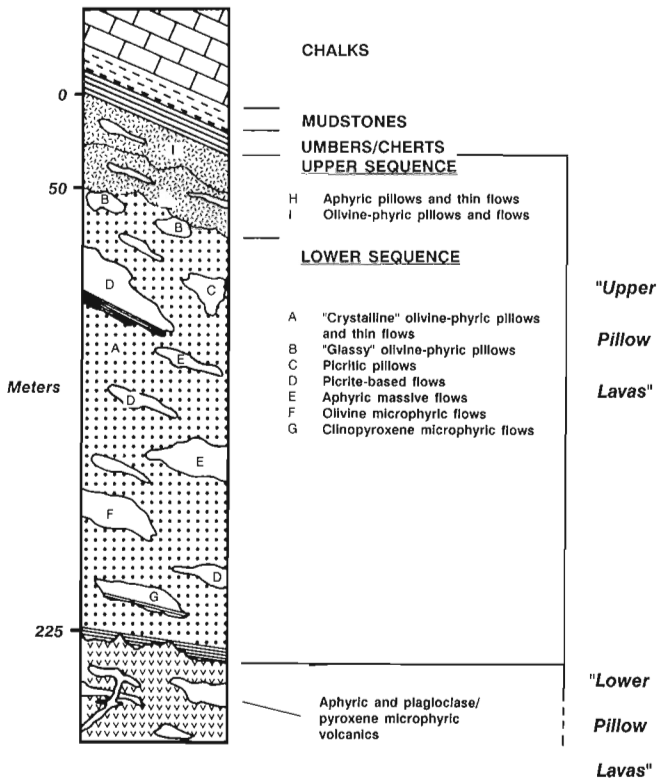

Figure 2: sequence of volcanic rocks and overlying sediments in the Margi area.

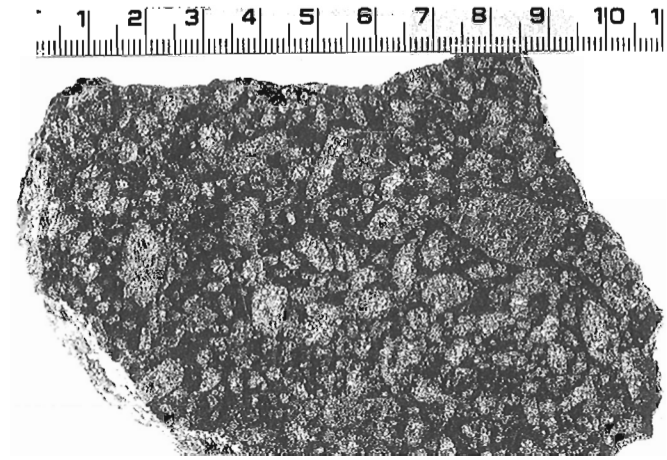

Figure 3: Large olivine phenocrysts in core of picritic pillow.

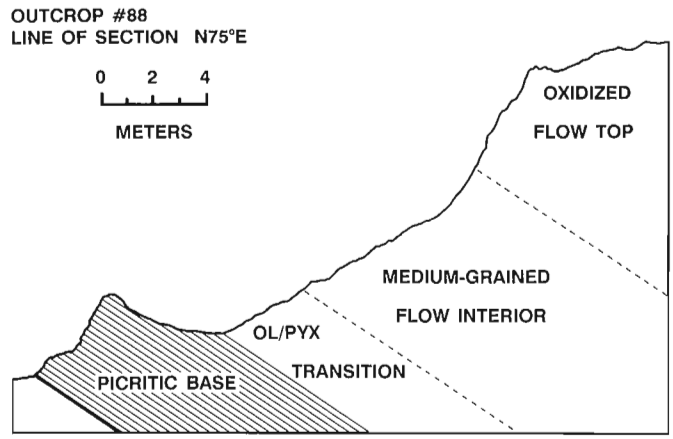

Figure 4: Cross section of thick picritic flow showing lithologic divisions.

with diameters ranging from 20 to 60 cm. Individual pillows are often difficult to discern because chilled margins are indistinct. Locally, however, pillow forms are accentuated by the presence of interpillow sediment. Fresh glass is preserved along some pillow margins, forming a rind that is never more than 2 mm thick.

Fresh porphyritic olivine is abundant (45–65 modal percent) and is distributed within single pillows with only a slight decrease in grain size from pillow core to rim (Figure 3).

Grains are euhedral to subhedral and range from 0.5 to 14 mm in size, with an average of 4 mm. They commonly contain inclusions of spinel and groundmass material and are typically altered to greenish-brown smectite along fractures and grain boundaries.

The groundmass of these pillows is dark brown to black, being largely composed of devitrified and altered glass. Clinopyroxene microlites comprise 20–30 modal percent of most samples and some anhedral olivines are also present. Subhedral, dark-red to black spinels, averaging 2 mm in size, occur in minor amounts (trace to four modal percent).

Massive picritic flows (Unit D, Figure 2)

Massive flows with picritic bases are also common in the lower sequence. Individual flows range from about 1 to 30 m thick and have a lateral extent up to about 200 m. In thin flows (<5 m), olivine is present throughout but is most abundant in the bottom half. A cross-section of a thicker flows is shown in Figure 4. There are four distinct lithologies in such flows: (1) a picritic base, (2) a transition zone, (3) a medium-grained aphyric flow interior, and (4) an olivine-phyric, oxidized flow top.

The picritic base is typically dark green to black and relatively resistant to weathering. Columnar jointing is invariably present, but poorly developed. Layering on a 5–10 cm scale reflects minor variations in the size and modal abundance of the mineral phases. Some flows have a basal chilled zone, 5–30 cm-thick, which is only moderately olivine-phyric. The picritic zone typically contains 20–60 modal percent olivine, 5–25 modal percent clinopyroxene, 4–12 modal percent plagioclase, and trace to four modal percent spinel. Olivines are subhedral to round and have an average diameter of approximately 2 mm. They contain inclusions of spinel and groundmass material, and a few of the largest crystals exhibit strain

features and broad kink-bands. Alteration to light-green smectite ranges from about 10 to 80%. Clinopyroxene grains are subhedral and elongate, with an average diameter of 0.4 mm. Most are diopsidic augite, although trace amounts of Ca-poor pyroxene mantle resorbed olivine grains. Plagioclase varies in size from minute needles to 2 mm-long laths. The largest plagioclase crystals are commonly zoned and intergrown with pyroxene. Groundmass and opaque inclusions are ubiquitous, especially in the cores of crystals. Reddish-brown, subhedral spinel occurs either as inclusions in other phases or as individual groundmass crystals.

The transition zone, rarely more than a few metres thick, marks the interval in which clinopyroxene replaces olivine as the dominant ferromagnesian phase.

The aphyric interior is a light-tan, medium-grained rock, composed chiefly of clinopyroxene and plagioclase. Subhedral clinopyroxenes average 0.4 mm in diameter, are strongly zoned, and commonly twinned. They contain minute opaque inclusions which outline the crystallographic zones in concentric trails. Plagioclases are variable in size and shape, but are typically strongly zoned laths with an average length of 0.25 mm.

The aphyric flow interior grades upward into the oxidized flow top. This uppermost zone is commonly olivine-phyric, but the abundance of the olivine phenocrysts is much less and the grains are a little smaller than lower in the flow. Most of the olivine is altered to smectite and iron oxides.

Aphyric and microphyric massive flows (Units E, F, and G, Figure 2)

Aphyric massive flows occur only near the centre of the lower sequence, although they are apparently not confined to a single stratigraphic horizon. Individual flows vary from 3 to 15 m thick and can be traced laterally for up to 150 m. These flows are aphyric throughout, but the lower portions are coarser-grained and more pyroxene-rich than the upper portions. Columnar jointing is well-developed in the lower parts and vesicles are common in the upper parts. Plagioclase makes up 40–70 modal percent and occurs as strongly zoned subhedral laths up to 1.2 mm long. Clinopyroxene makes up 5–10 modal percent of most flows but may be as much as thirty modal percent in small localized zones along the base of some. The clinopyroxenes are typically subhedral with an average diameter of 0.3 mm. Most are optically zoned, and contain abundant opaque inclusions. The groundmass is totally altered to clays and oxides.

In the lower part of the lower sequence are exposed some thick flows containing olivine and clinopyroxene microphenocrysts. In olivine-bearing flows, olivine varies from trace amounts to ten modal percent and is homogeneously distributed, although grain sizes are somewhat larger toward the base. Olivine grains are anhedral to subhedral, 0.25 mm in diameter, and completely altered to smectite and Fe-oxides. Flows with thick basal concentrations of clinopyroxene range from 5 to 15 m in thickness, and exhibit a gradual decrease in the total abundance of clinopyroxene and a corresponding increase in the relative amount of plagioclase from bottom to top. Pyroxene microphenocrysts average 0.2 mm diameter with occasional grains up to 1 mm long.

The Upper Sequence (Units H and I, Figure 2)

The boundary between the lower and upper sequence is distinct and marked by an abrupt decrease in modal olivine concentrations and an increase in clinopyroxene microphenocrysts. Fresh glass and hyaloclastic material are also more abundant in the upper sequence. Most rocks are aphyric, but sparsely olivine-phyric varieties are present in the top part of the upper sequence. This consists chiefly of pillowed lavas with some thin flows. The pillows range from 30 to 250 cm in diameter and average about 1 m. They are typically light greenish grey but many have tan to reddish-brown margins. Highly oxidized varieties are typically yellowish- to reddish-brown. The thin, non-pillowed flows range from about 10 cm to 2 m in thickness. They are greenish grey in colour and typically are harder and more coherent than the surrounding pillows. Vesicles, 0.3–5 mm in diameter, are concentrated in the upper one-third of individual flows and are predominantly spherical. Many of the thinnest flows have well developed ropey surfaces, whereas the thicker flows typically have a smooth upper surface.

Olivine is the main phenocryst phase in this unit but microphenocrysts of clinopyroxene are also common. The olivine is irregularly distributed, being concentrated in pillow cores and flow bases, but it never exceeds five modal percent. Olivine grains are typically subhedral and small, rarely larger than 1.5 mm in diameter. They are completely altered to mixtures of smectite, iron oxides, and minor carbonate. The clinopyroxene typically forms small equant grains approximately 0.3 mm across with a few up to 1.2 mm long.

Groundmass alteration is extensive in these rocks, ranging from about 60 to 100%. However, despite this high degree of alteration, fresh glassy rinds are preserved on many pillows and flow surfaces. Generally the glass is best preserved where thick layers of umber overlie the volcanic sequence.

MINERALOGY

Olivine

Olivine is the dominant phenocryst phase in the lavas of the Margi area. It ranges from zero to over fifty modal percent in both pillow lavas and massive flows. Although most of the olivine has been altered to smectite, iron oxides, hydroxides, and carbonate, fresh grains are common, particularly in the picritic units and 'glassy' olivine-phyric pillows. In the picritic flows, olivine crystals range up to 12 mm across and are mostly subhedral to round; in picritic pillows they are typically euhedral. Most of these grains contain inclusions of spinel and groundmass material and many

Sample #	DL36	99-5	10-3	DL23	86-6
SiO_2 %	41.66	40.12	39.66	40.64	38.65
Al_2O_3	0.04	-	-	0.19	-
Cr_2O_3	-	0.19	0.05	-	-
FeO*	6.90	7.99	10.75	12.12	15.23
MnO	0.11	0.05	0.11	0.16	0.23
MgO	52.63	50.50	48.80	47.88	45.19
CaO	0.17	0.20	0.18	0.23	0.18
NiO		0.29	0.22	-	0.05
Fo	93	92	89	87.5	84
Si	0.993	0.986	0.982	0.994	0.980
Fe_2	0.138	0.164	0.223	0.248	0.323
Mn	0.002	0.001	0.002	0.003	0.005
Mg	1.869	1.851	1.801	1.746	1.707
Ca	0.004	0.005	0.005	0.006	0.005
Ni	-	0.006	0.004	-	0.001

Table 1: Representative Olivine Analyses. DL36: Ultrabasic pillow lava - phenocryst core; 99-5: Picritic flow base - phenocryst core; 10-3: Glassy olivine-phyric pillow lava - phenocryst core; DL23: Picritic flow base - groundmass grain; 86-6: Olivine-phyric pillow lava - groundmass grain; - = not detected; * = Total iron as FeO.

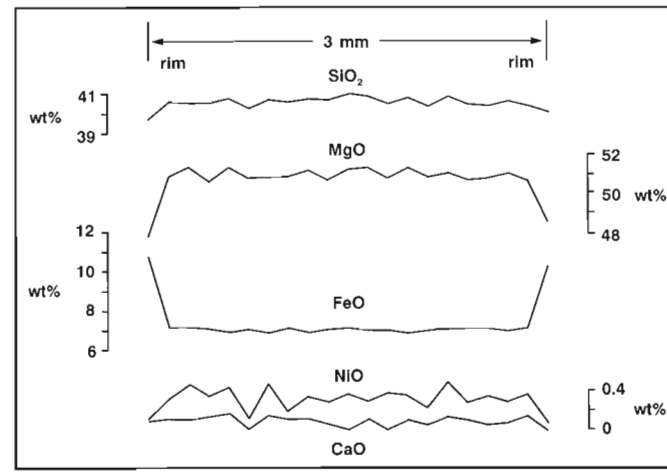

Figure 5: Electron microprobe traverses across a 3 mm olivine phenocryst from a picritic pillow. Composition of grain interior is Fo_{92}, rim composition Fo_{88}.

exhibit broad kink-bands. Such deformation is commonly observed in olivines of mantle peridotites and is the result of high-temperature dislocation creep (Poirier and Nicolas, 1976; Koehlstedt et al., 1976).

Olivines are Mg-rich, ranging in composition from Fo_{86} to Fo_{93} in picritic units (Table 1). In many specimens there is a bimodal assemblage with large, relatively homogeneous, highly magnesian (Fo_{92-93}) phenocrysts and smaller more iron-rich (Fo_{86-88}) groundmass grains. Some large phenocrysts have narrow rims with compositions similar to groundmass olivines (Figure 5). Olivine in the sparsely phyric lavas is typically skeletal to subhedral and rarely exceeds 2.5 mm. These grains are relatively iron-rich compared to those of picritic units, ranging from Fo_{83} to Fo_{89}, and may show the entire range of compositions within a single sample.

The relatively wide range of olivine compositions suggests variable conditions of crystallization. The large olivine phenocrysts in the picrites, with high forsterite contents, spinel inclusions, kink-bands, and rounded grain boundaries, probably crystallized from magnesium-rich liquids at relatively high temperatures. They were probably not in equilibrium with the melts in which they were extruded. Conversely, the relatively iron-rich grains found in the surrounding pillows appear to have been liquidus phases at the time of extrusion.

Pyroxenes

Pyroxenes are the second most abundant phase in the volcanic rocks of the Margi area. Large phenocrysts are rare, but microphenocrysts ranging from 0.2 to 0.6 mm in diameter are common. As with olivine, the crystals are highly variable in both distribution and abundance. Distinct microphenocrysts are particularly abundant in the lowermost and uppermost parts of the sequence but are conspicuously absent in the picritic pillows. Groundmass microlites are abundant in almost all samples and exhibit morphologies typical of rapid growth and quenching, particularly in the pillowed units.

Clinopyroxene makes up 5–20 modal percent of the picritic bases of massive flows. Crystals are typically elongate to bladed, and vary from 0.1 to 3 mm in length. Minute grains of calcium-poor pyroxene rim some large olivines and Ca-rich pyroxenes in these rocks.

In the aphyric, massive flows, clinopyroxene typically occurs as subhedral to euhedral, strongly zoned, equant grains that range from 0.2 to 1 mm in diameter.

Microprobe analyses show the presence of four distinct varieties of pyroxene: Ca/Mg-rich clinopyroxene, Al-rich clinopyroxene, Fe-rich clinopyroxene, and Ca-poor pyroxene (Table 2). Ca/Mg-rich diopsides and endiopsides are the most common pyroxene phenocrysts. These distinctive crystals contain significant amounts of chromium (0.5–1.5 wt.%) and only minor amounts of titanium (<0.5 wt.%). Al-rich clinopyroxenes occur as groundmass microlites and quench crystals. Most of these lie in the diopside or salite fields, although many plot above the diopside-hedenbergite join in the pyroxene quadrilateral (Figure 6). The unusual compositions of these grains (e.g. the high Al and Fe, and low Si, Mg, and Cr contents), are likely the result of rapid cooling (cf. Lofgren et al., 1974 and Coish and Taylor, 1979). Fe-rich clinopyroxenes occur only in aphyric massive flows. These are generally richer in Fe and lower in Al than the Ca/Mg-rich pyroxenes and plot in the augite field. Ca-poor pyroxenes rim many large Ca-rich pyroxenes in the picrite-based flows. Compositions range from hypersthene to magnesian pigeonite (1.5–6 wt.% CaO).

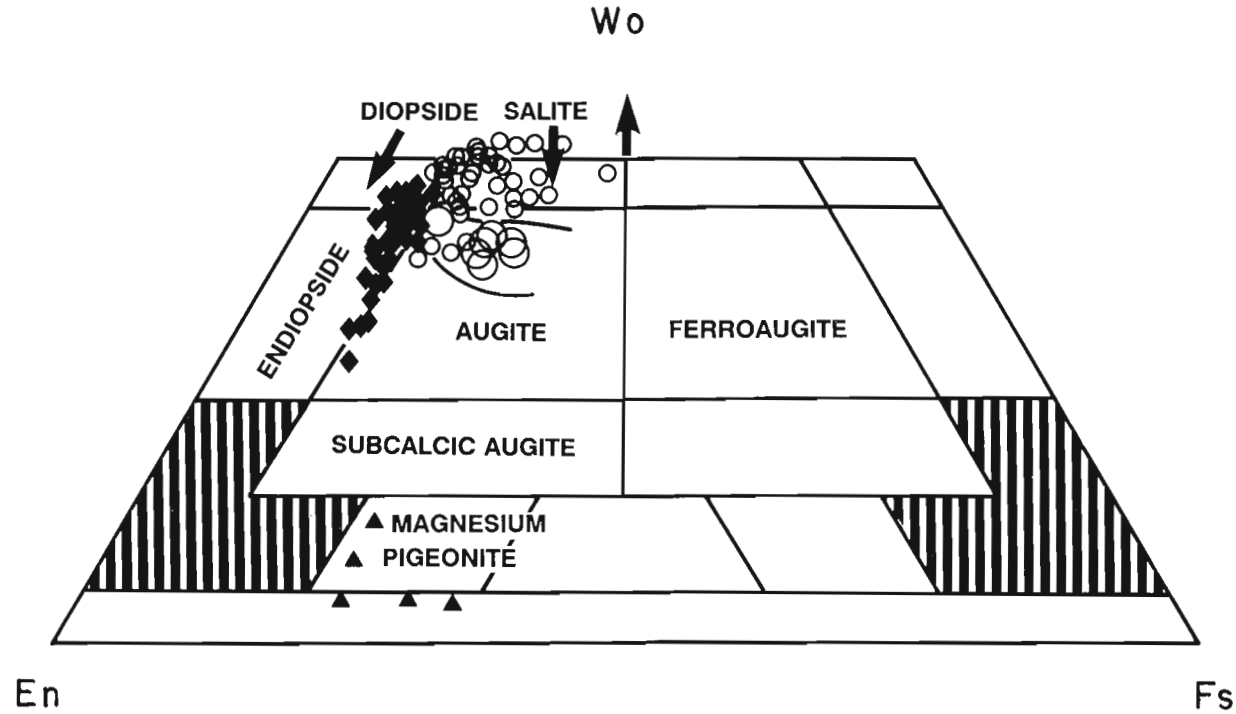

Figure 6: Pyroxene compositions plotted in the pyroxene quadrilateral; o = groundmass grains; ○ = microphenocrysts from aphyric flows; ▲ = Ca-poor groundmass grains in picritic flow bases; ◆ = phenocrysts from picritic flows.

Sample #	14-7	35-6	PL24	KL34
SiO_2 %	52.83	46.06	53.47	56.70
TiO_2	0.18	0.89	0.12	0.04
Al_2O_3	2.61	11.05	1.89	1.81
Cr_2O_3	0.48	-	0.26	-
FeO*	5.71	11.16	7.24	7.64
MgO	16.90	10.55	17.21	31.04
CaO	20.76	20.20	19.38	3.17
Si	1.941	1.731	1.962	1.968
Al_4	0.059	0.269	0.038	0.032
Al_6	0.054	0.220	0.044	0.042
Ti	0.005	0.025	0.003	0.001
Fe_2	0.175	0.351	0.222	0.222
Mg	0.925	0.591	0.941	1.606
Cr	0.014	-	0.008	-
Ca	0.817	0.813	0.762	0.118

Table 2: Representative pyroxene analyses. 14-7: Olivine-phyric flow base - Ca/Mg-rich diopside; 35-6: Glassy olivine-phyric flow - Al-rich groundmass grain; PL24: Aphyric flow - Fe-rich groundmass grain; KL34: Picritic flow base - Ca-poor phenocryst rim; - = not detected; * = total iron as FeO.

Plagioclase

Plagioclase is a groundmass phase in all but the picritic pillows and a few poorly crystallized olivine-phyric pillows. In general the greater the thickness of a flow unit, the larger and more abundant the groundmass plagioclase grains, suggesting that they crystallized after eruption. Most grains are small, lath-shaped microlites, except for those in the thickest flows that are large, anhedral grains commonly intergrown with pyroxene.

Porphyritic plagioclase has not been observed in any of the rocks, although elongate microphenocrysts are locally present.

Much of the plagioclase is 'cloudy,' suggesting incipient alteration to clay minerals, and the cores of some large grains have been replaced by potassium feldspar (adularia). Most plagioclase is highly calcic, with compositions between An_{70} and An_{80} (bytownite) (Table 3). More sodic rims (up to An_{52}) are present on a few grains. No systematic variations in plagioclase composition were detected in the lavas.

Sample #	101-3b	KL23	74-5	101-3c
SiO_2 %	49.32	50.45	53.65	55.94
Al_2O_3	31.20	29.70	28.35	26.46
FeO*	0.39	0.80	0.60	0.62
MgO	-	0.46	-	-
CaO	16.39	15.00	13.16	11.01
Na_2O	2.35	2.65	4.23	5.31
K_2O	-	0.05	0.27	0.10
Or	-	0.40	0.02	0.01
Ab	21.0	24.1	36.0	46.0
An	79.0	75.5	62.0	53.0
Si	9.072	9.303	9.738	10.160
Al	6.763	6.458	6.064	5.663
Fe_2	0.060	0.123	0.091	0.094
Ca	3.230	2.964	2.559	2.142
Na	0.838	0.948	1.489	1.870
K	-	0.012	0.063	0.023

Table 3: Representative plagioclase analyses. 101-3b: Olivine-phyric flow - core of large grain; KL23: Aphyric massive flow - groundmass grain core; 74-5: Aphyric massive flow - groundmass grain rim; 101-3c: Olivine-phyric flow - groundmass grain; - = not detected; * = total iron as FeO.

Sample #	154a-7	127-8	127-2r	154a-5
TiO_2 %	0.82	-	0.18	0.27
Al_2O_3	15.52	12.29	11.19	11.79
Cr_2O_3	43.77	53.16	55.22	57.45
FeO*	26.12	20.53	18.63	16.84
MnO	0.16	0.15	0.16	-
MgO	12.36	12.51	13.78	13.52
CaO	0.05	-	-	0.06
Mg/(Mg+Fe_2)	0.577	0.605	0.658	0.655
Cr/(Cr+Al)	0.654	0.744	0.768	0.766
Ti	0.158	-	0.035	0.052
Al	4.672	3.759	3.394	3.332
Cr	8.841	10.910	11.238	11.547
Fe_3	2.163	1.328	1.296	0.807
Fe_2	3.414	3.126	2.712	2.772
Mn	0.035	0.033	0.035	-
Mg	4.706	4.840	5.287	5.275
Ca	0.014	-	-	0.016

Table 4: Representative Spinel Analyses. 154a-7: Olivine-phyric pillow lava - groundmass grain rim; 127-8: Picritic pillow lava - groundmass grain core; 127-2r: Picritic pillow lava - inclusion in olivine; 154a-5: Olivine-phyric pillow lava - microphenocryst core; - = not detected; * = total iron as FeO.

Spinel

Spinel is a common accessory mineral (trace to five modal percent), particularly in the picritic and highly olivine-phyric rocks. Most grains are subhedral and less than 0.5 mm in diameter, although discrete phenocrysts up to 2 mm are present locally. The smallest typically occur as inclusions within large olivine phenocrysts.

All the spinels are chrome-rich with Cr_2O_3 contents between 40 and 60 wt.% (Table 4). Most analyzed grains fall within the field of spinels from the Troodos plutonic sequence (Cameron et al., 1980).

GEOCHEMISTRY

Major Elements

Whole-rock samples from all major lithologies were analyzed by XRF. Four major compositional types can be distinguished by major element geochemistry: picrites (type 1), olivine phyric lavas (type 2), aphyric massive flows (type 3)(all part of the Upper Pillow Lavas), and the aphyric flows of the Lower Pillow Lavas (type 4). Selected examples are given in Table 5.

Plots of major element chemistry (Figure 7) clearly show the unusual, ultrabasic compositions of the picritic rocks, with MgO contents ranging from 20 to 40 wt.% and SiO_2 contents generally less than 45 wt.%.

The other compositional types are predominantly basalt to basaltic andesite, though it should be noted that types 2 and 3 have unusually low TiO_2, high MgO, and high SiO_2 contents compared to typical MORB, and are therefore similar to boninites and high-Mg andesites (Cameron and Nisbet, 1982). Although major element diagrams cannot be used with confidence to separate the compositional types, samples from type 4 do appear to be distinct from the other types.

Trace Elements

The following trace and minor elements were analyzed by XRF: Rb, Sr, Y, Zr, Nb, Ba, V, Zn, Cu, Ni, Cr, Ti, and P. Niobium and barium are typically at or below detection levels (approximately 3 ppm and 20 ppm, respectively) and are not shown in any of the geochemical plots.

The remaining elements, except for Ni, Cr, and Cu, tend to behave incompatibly in basaltic magmas. Plots between pairs of incompatible elements are often useful for distinguishing magma suites, since the inter-element ratios are not significantly influenced by simple fractional crystallization processes. Unfortunately, the behaviour of incompatible trace elements in basalts subjected to low-temperature, hydrous alteration is highly variable.

Titanium was chosen as a common plotting parameter for the following reasons: (1) it is generally regarded as 'immobile' under conditions of low-temperature seawater alteration and the tight cluster of data points on the TiO_2/MgO diagram (Figure 7) supports this conclusion; (2) it is present in relatively high concentrations that can be analyzed with precision; and (3) samples contain a wide range of titanium concentrations enhancing the separation of chemical types. The resulting variation diagrams are shown in Figure 8.

Sample #	DL36	DL37	25	47	26	PL20	143	145
SiO_2 %	39.30	36.40	47.74	48.79	57.49	54.60	48.99	51.43
TiO_2	-	0.14	0.52	0.68	0.84	0.38	1.34	1.54
Al_2O_3	3.67	3.48	14.31	14.69	15.91	14.60	16.12	16.88
Fe_2O3	2.71	3.22	*7.94	*8.30	*8.65	5.48	*12.68	*13.54
FeO	4.57	4.44	n.d.	n.d.	n.d.	3.12	n.d.	n.d.
MnO	0.11	0.12	n.d.	n.d.	n.d.	0.10	n.d.	n.d.
MgO	35.90	34.35	8.87	6.73	4.26	5.33	6.00	5.76
CaO	4.00	8.77	15.30	16.86	7.58	9.94	9.27	6.15
Na_2O	0.08	0.28	0.48	1.80	2.47	1.05	0.62	2.73
K_2O	0.04	0.08	3.97	1.30	1.71	0.43	3.78	1.16
P_2O_5	-	-	0.02	0.03	0.06	-	0.18	0.15
LOI	9.05	8.61	13.62	7.08	5.10	4.71	15.79	6.74
Total	99.43	99.89	99.16	99.19	98.97	99.74	98.98	99.34
Zr ppm	6	5	29	27	51	8	54	81
Sr	23	51	88	93	105	43	75	105
Rb	2	3	22	22	34	10	21	17
Zn	39	36	57	90	64	63	88	91
Cu	23	3	20	39	64	30	31	26
Ba	-	-	-	-	29	8	66	22
Nb	-	-	-	-	3	-	-	1
Ni	1407	1378	80	82	17	29	12	3
Cr	3025	2951	243	211	18	2	18	26
V	87	71	148	233	284	287	432	615
Y	5	4	15	17	22	23	28	38

Table 5: Whole-rock geochemistry of selected samples. DL36 and DL37: Type 1 - Picritic pillow lavas; 25 and 47: Type 2 - Olivine-phyric flows; 26 and PL20: Type 3 - Aphyric flows; 143 and 145: Type 4 - Aphyric flows from Lower Pillow Lavas; * Total iron determined as Fe_2O3; - = not detected; nd = not determined.

The compositional types can be distinguished on most of these diagrams, primarily because of differences in their titanium contents.

Not surprisingly, plots of the HFS elements (particularly Zr, V, and Y vs. Ti), provide the most marked discrimination. The picritic samples (type 1) invariably plot in a very restricted field and contain the lowest observed values of all the incompatible elements. Samples from the Lower Pillow Lavas in the Margi area are plotted for comparison (type 4). The Lower Pillow Lavas are clearly enriched in these elements.

Rubidium and strontium contents are highly variable within all samples analyzed, supporting the conclusion that these elements were easily mobilized during low temperature alteration. Copper and, to a much lesser extent, zinc probably behaved similarly as both are mobile in aqueous solution (Rose et al., 1979). However samples that appear the least altered petrographically contain the highest copper contents (approximately 60 ppm). Such evidence suggests that during low temperature alteration, zinc was less mobile, whereas copper was readily leached from much of the extrusive sequence. Notably, the massive sulphide deposits found within the extrusive sequence are relatively rich in copper and poor in zinc.

Chromium and nickel can be considered compatible elements in these rocks, being preferentially incorporated into spinel and olivine, respectively. The high concentrations of Cr and Ni that occur in the picritic rocks reflect the abundance of these phases. The Lower Pillow Lavas (type 4) and some massive aphyric flows from the Upper Pillow Lava sequence in the Margi area are clearly distinguished by significantly lower amounts of both Cr and Ni.

Compositional types 2 and 3 have higher V/Ti and Y/Ti than the Lower Pillow Lavas. Such differences cannot be explained readily by fractional crystallization processes and, with differences in phase relations and major element compositions, support the argument that the Upper and Lower Pillow Lavas in the Margi area were derived from two distinct parental magmas. Thus, in summary, four compositional types can be distinguished on trace element diagrams. These include three Upper Pillow Lava compositions and a Lower Pillow Lava composition. The HFSE are the most useful for delineating these types, and ratios of pairs of these elements suggest the existence of two distinct magmatic suites.

Glass and 'fresh' lava compositions

Even when it is possible to distinguish geochemical groups using the major and trace element contents of whole rocks, the limits of such an approach must be remembered:

(a) Although this study attempts to 'look through' the affects of alteration by the use of 'immobile' elements, it is unlikely that the concentration of any element remains

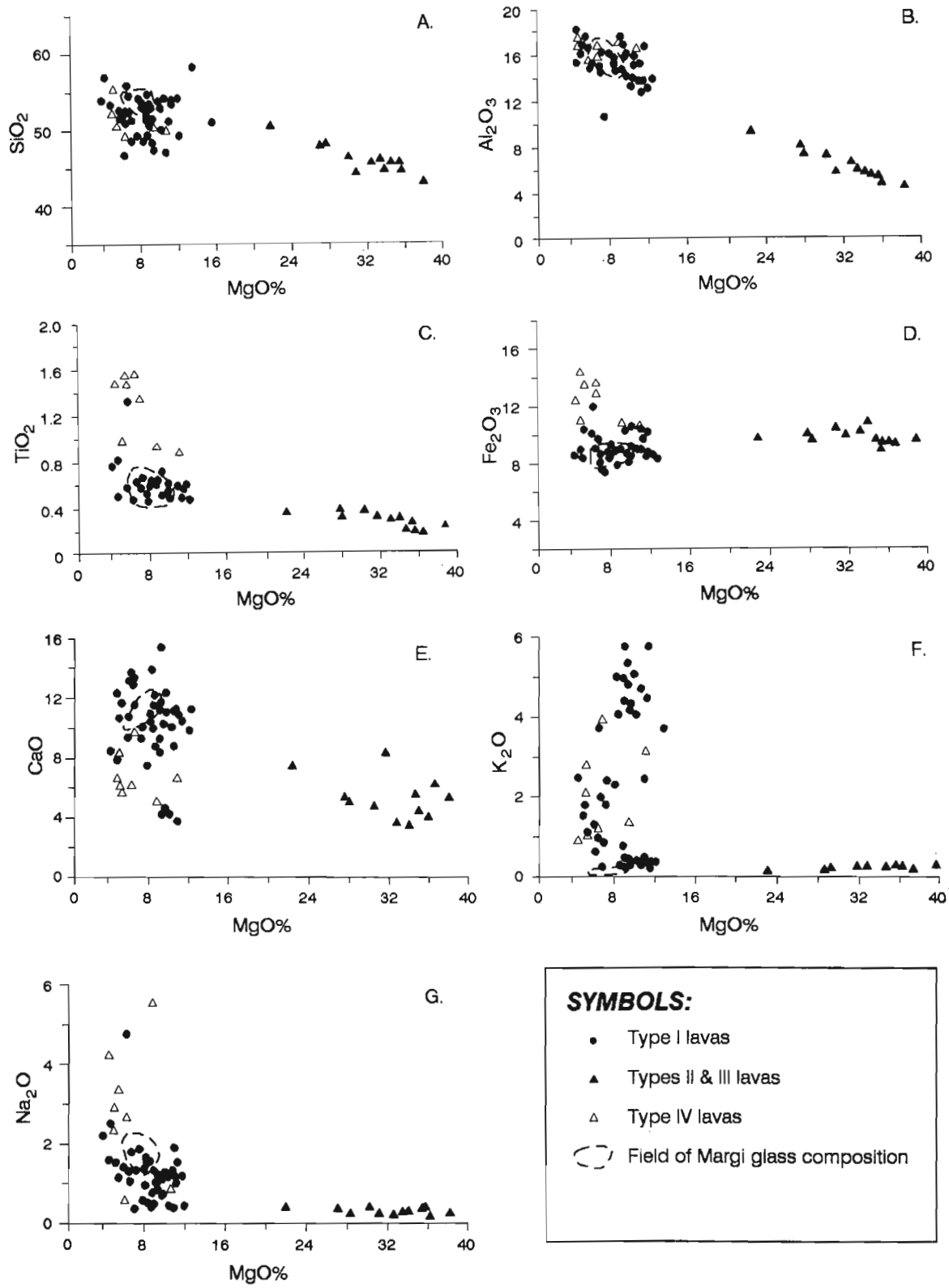

Figure 7: Variation diagrams of whole-rock major element oxide concentration including the field of Margi glasses. • = type 1 lavas; △ = type 2 and type 3 lavas; △ = type 4 lavas.

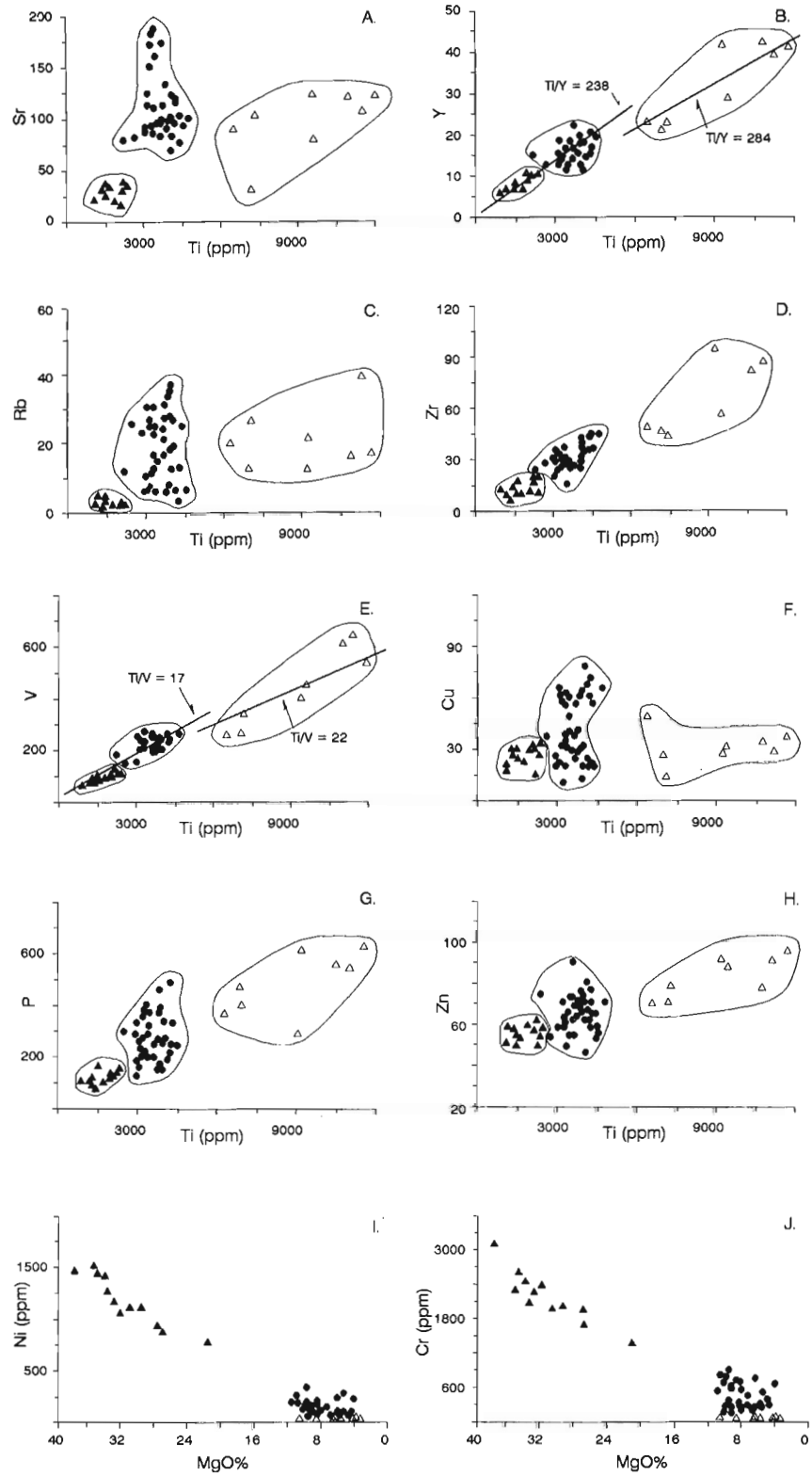

Figure 8: Variation diagrams of whole-rock trace element concentrations. Symbols as Figure 7.

Sample #	5	32	46	61	127
SiO_2 %	53.99	54.31	54.12	54.54	54.26
Al_2O_3	15.03	15.70	16.04	16.09	14.18
TiO_2	0.50	0.49	0.51	0.55	0.48
FeO*	8.03	8.12	8.04	8.22	7.48
MgO	6.99	6.69	6.26	6.00	8.49
CaO	11.27	11.03	11.09	10.91	11.29
Na_2O	1.80	1.81	1.88	1.84	1.70
K_2O	0.17	0.18	0.18	0.18	0.19
P_2O_5	0.07	0.08	0.06	0.08	0.04
Total	97.85	98.31	98.18	98.41	98.11

Table 6: Representative glass analyses. * = total iron as FeO.

completely unaffected, for even if it itself is not mobilized, the addition or removal of other elements indirectly affects the net concentration of those remaining.

(b) The samples analyzed vary markedly in degree and style of alteration, and this undoubtedly increases the scatter of whole-rock compositions as the intensity and even direction of an element's mobility changes with slight changes in alteration conditions.

(c) Finally, there are chemical variations due to post-extrusion processes such as crystal settling and flow differentiation. All contribute to the overall variability of whole-rock compositions and make it more difficult to define the primary chemical characteristics due to subsurface processes of magma generation and evolution.

These problems can, in part, be avoided by examining the geochemistry of glass and 'unaltered' aphyric to microphyric lavas, which can be argued to represent liquid compositions (Table 6). In the present study the selection of the freshest lavas was based upon petrographic examination, but it should be noted that even the freshest contain abundant smectite.

Major element compositions of glass, analyzed by electron microprobe, and fresh lava compositions are plotted on Figure 9 and compared to the two major compositional fields defined by Robinson et al. (1983) for the Troodos extrusives as a whole. Robinson et al. (op cit) used the terms 'arc tholeiite' suite for glasses with relatively low-Mg, high-Ti, and high-Fe, and 'depleted' suite for glasses with high-Mg, low-Ti, and low-Fe. Langdon (1982) compared the latter to komatiites. In Figure 9, continuous trends from the most Mg-rich pillow to the Mg-poor glass occur, with the notable exception of the K_2O-MgO plot. Anomalously high K_2O contents are explained by the presence of potassium-rich smectites.

PETROGENESIS

The analyzed glasses from the Margi area are all from the Upper Pillow Lavas and are clearly part of the high-Mg, depleted suite. However, analyses of associated fresh lavas show that the evolutionary path included compositions much more primitive than those sampled by the glasses. Figure 9 suggests that the separation of the samples into smaller geochemical groups is not feasible. The glass analyses alone, however, show that a division can be based on TiO_2 and Na_2O contents that correspond to distinct stratigraphic levels in the extrusive pile (Figure 10). The higher-TiO_2 and higher-Na_2O analyses belong to rocks of the lower stratigraphic sequence of the Upper Pillow Lavas, whereas the lower-TiO_2 and lower-Na_2O analyses belong dominantly to the upper sequence and, locally, to the upper part of the lower sequence.

Similar stratigraphic discrimination occurs on diagrams using the HFS elements (Figure 10). The most incompatible element-depleted rocks appear to come from the highest part of the stratigraphic section. Ratios between pairs of incompatible trace elements differ between the lower and upper sequences of the Upper Pillow Lavas, with the most marked difference occurring in Ti/V ratios (Figure 11). This suggests the presence of two somewhat different parental magma compositions, although this conclusion is based on a restricted amount of data. Taylor (1990) noted the same feature and concluded that each volcanic unit within the section corresponded to a discrete batch of liquid that could not be related to other units by high-level crystal fractionation. The general up-sequence depletion in the HFS elements implies that these liquids represent either successively higher degrees of partial melting, fusion of heterogeneously depleted mantle, or possibly a progressive remelting of a discrete source. This supports the model developed elsewhere (Malpas and Langdon, 1984) which suggests that an open-system magma chamber, periodically injected with new magma, supplied the extrusive sequence. These magmas, magnesian quartz tholeiites, differ fundamentally in their extreme depletion of HFS elements from the tholeiitic picrites. The latter have been proposed as the primary magmas for high-Al_2O_3 oceanic olivine tholeiites (O'Hara, 1968) which are derived by about 30% partial melting of mantle lherzolite. Such magnesian quartz tholeiites, derived by a second stage or advanced melting process (i.e. heterogeneous mantle), can be treated as primary liquids from which the distinctive magma series identified in the Margi area can be produced by low pressure fractionation. Langdon (1982) and Bailey (1984) have shown that these primary magmas were derived by very small amounts of mantle partial melting (5%) and that the less primitive rocks of the Upper Pillow Lavas, the olivine and aphyric basalts, resulted from fractionation of up to 24–32% olivine from the parental magmas. This early high temperature precipitation of olivine led to its accumulation at the bottom of high level magma chambers. The crystal/liquid mush formed in this manner is represented by the 'ultramafic' pillow lavas of the Margi area, which, since they appear toward the top of the volcanic succession, represent advanced tapping of individual magma chambers (Malpas and Langdon, 1984). Post-extrusion settling of olivine crystals also occurred in the thick massive

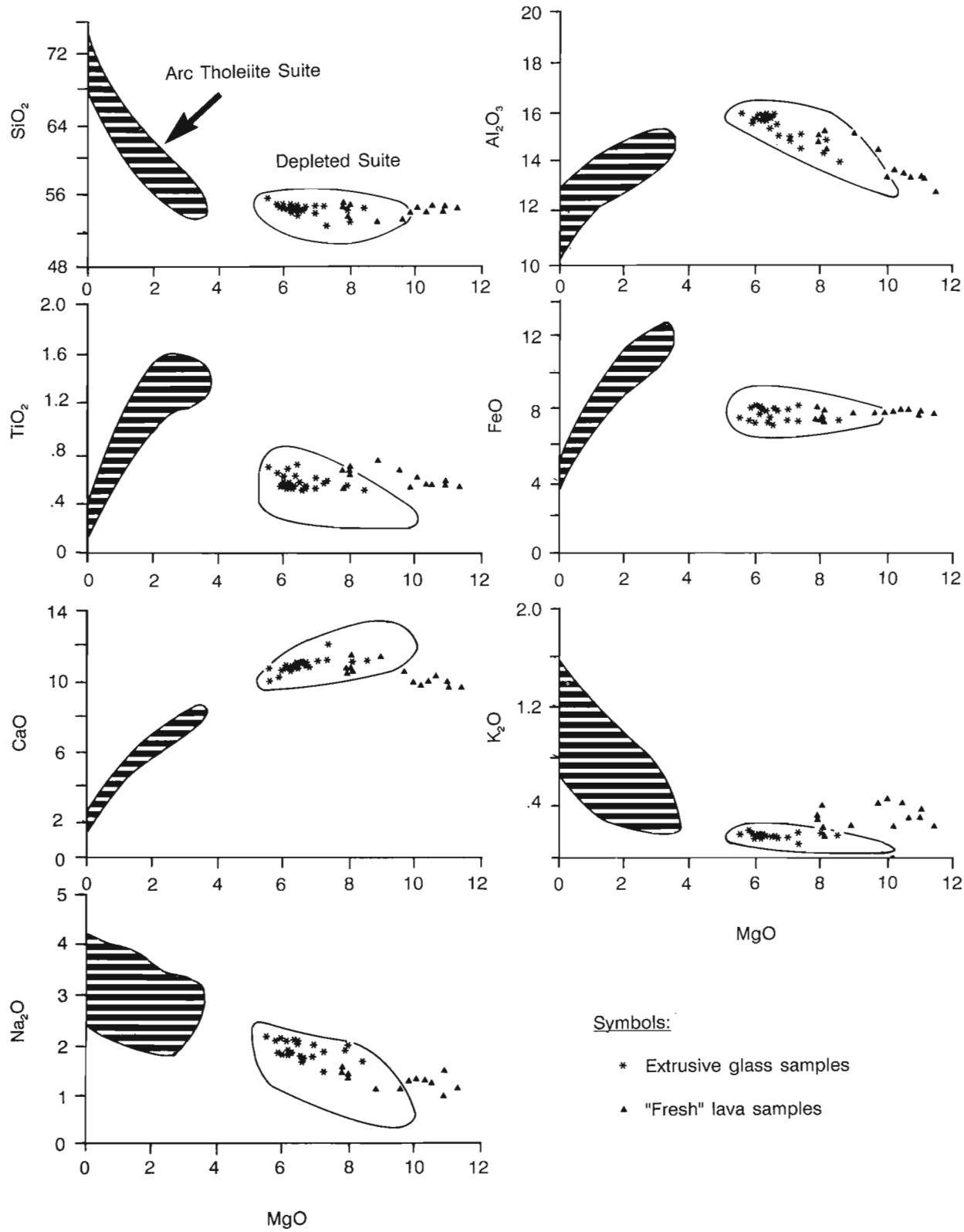

Figure 9: Variation diagrams of glass and 'fresh' lava major element oxide concentrations. * = Extrusive glass samples; △ = Fresh lava samples.

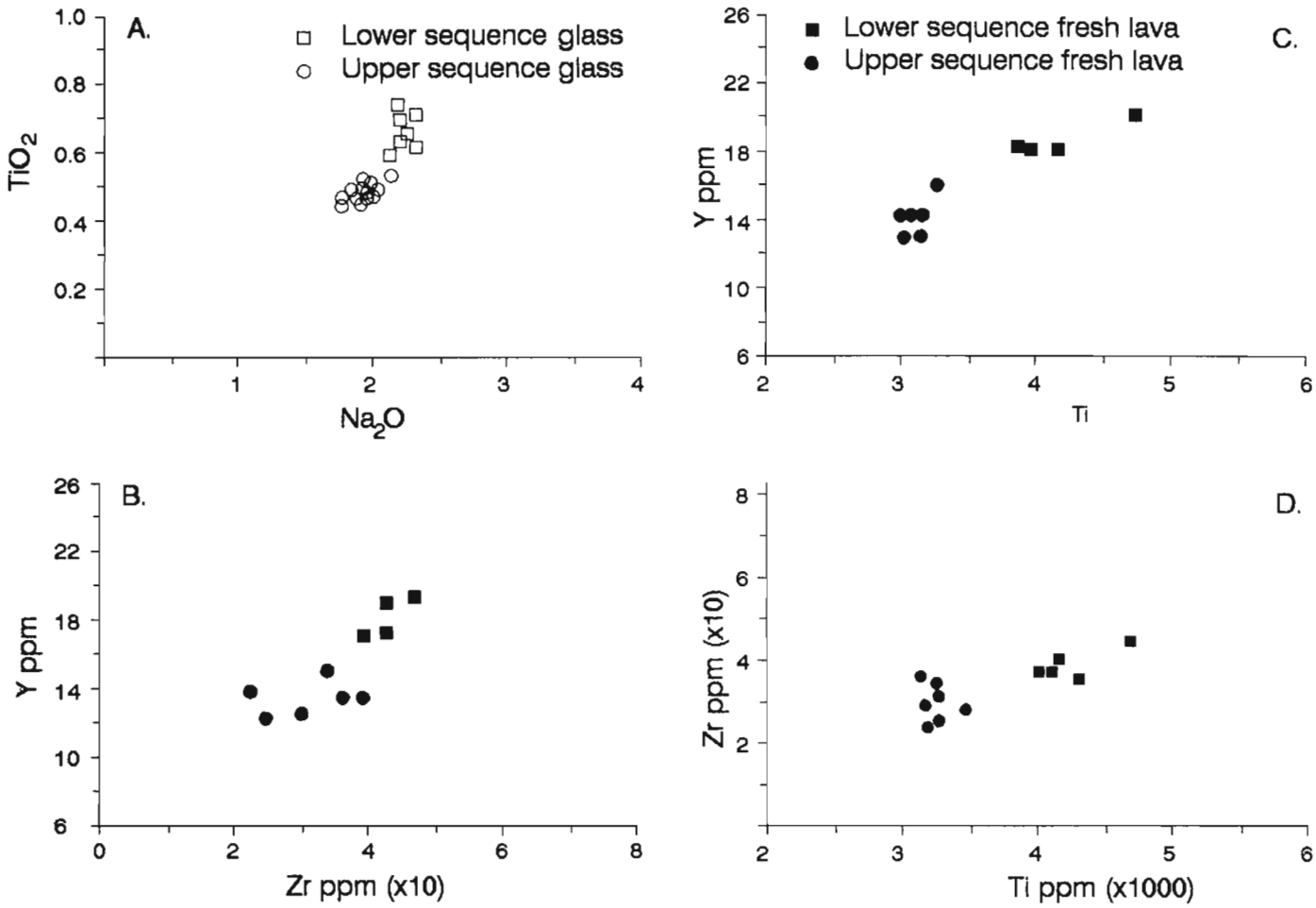

Figure 10: Variation of HFS elements with stratigraphic height in the Upper Pillow Lavas. □ = Lower sequence glass; o = Upper sequence glass dominantly; □ = Lower sequence lava; • = Upper sequence lava dominantly.

flows and gave rise to their zoned nature with olivine-rich bases. Indeed the zonation of these flows produced after extrusion likely mimics a similar zonation in some shallow level magma chambers.

SUMMARY

Petrographic phase relations, together with major and trace element chemistry, suggest the division of the extrusive sequence in the Margi area into two major suites. Only here do these two suites correspond to the classic division of 'Lower' and 'Upper' Pillow Lavas (Gass, 1958). The classic Lower Pillow Lavas are distinguished from overlying rocks by the absence of olivine and the presence of plagioclase microphenocrysts. Rocks of this suite are relatively enriched in Fe, Ti, and the incompatible trace elements, and have been likened to an 'arc-tholeiite' suite (Robinson et al., 1983).

The Upper Pillow Lavas are divisible into two stratigraphic sequences, a lower and an upper sequence. Both are distinguished from the Lower Pillow Lavas by the presence of olivine and from each other by the relative abundance of olivine phenocrysts. Extrusive rocks in both sequences are strongly depleted in incompatible elements and are relatively rich in MgO. This is characteristic of the 'depleted' suite defined by Robinson et al. (1983). The upper sequence is generally even more depleted than the lower, except for a series of glassy flows at the boundary between the two, which are geochemically part of the upper sequence while being more like the lower sequence petrographically. These relationships are depicted in Figure 12.

The ultramafic lavas from the Margi area of Cyprus owe their character to the presence of up to 65 modal percent olivine. The majority of the rocks were formed by post-extrusive gravitational settling of olivine phenocrysts in thick flows. Those that formed picritic pillow lavas had clearly undergone crystal accumulation in shallow magma chambers (Malpas and Langdon, 1984) and were extruded as a crystal mush during advanced tapping of these chambers. The abundance, size, composition, and deformation of the large olivine phenocrysts in these lavas is consistent with their intratelluric

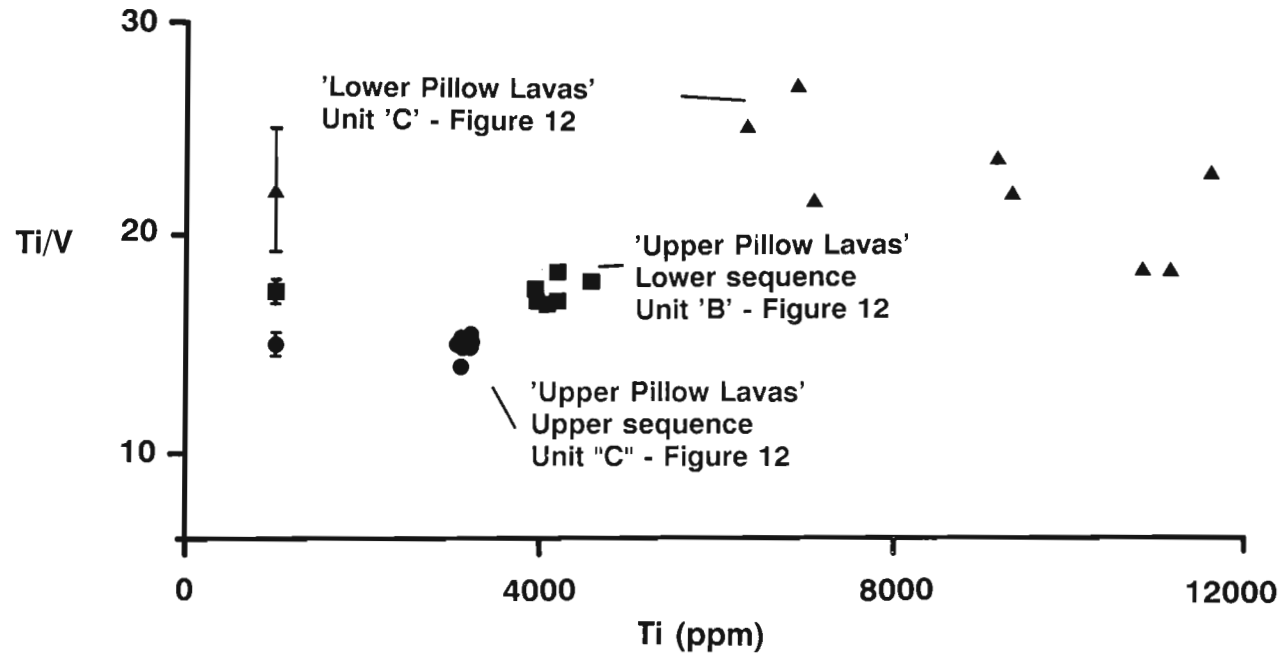

Figure 11: Variation in Ti/V ratio with stratigraphic height. Bars on left of diagram represent mean Ti/V ratios (± 1 S.D) of the sample populations.

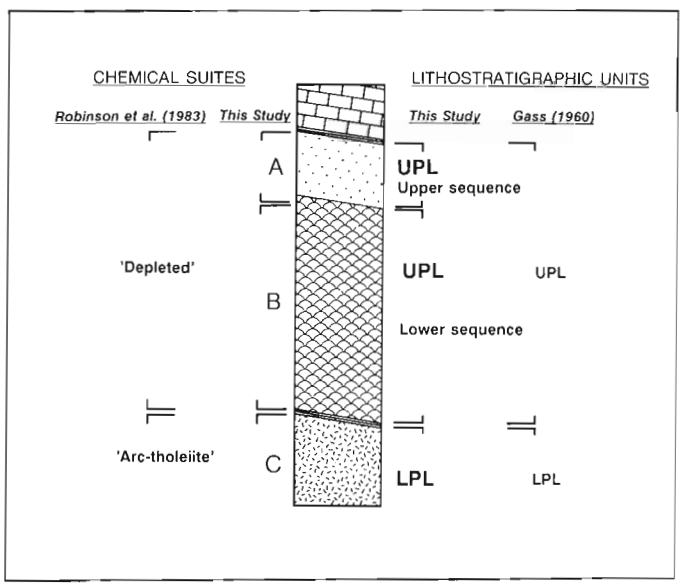

Figure 12: Correlation of lithostratigraphic units and chemical suites.

crystallization in a high temperature environment at a magma chamber floor.

ACKNOWLEDGEMENTS

This work forms part of the MSc theses of the first two authors under the supervision of P.T. Robinson and J. Malpas, respectively. These theses were completed in 1984 (Bailey at Dalhousie University) and 1982 (Langdon at Memorial University). Their work and the supplementary work by the supervisors was supported by NSERC Canada.

REFERENCES

Bailey, D.G.
1984: Stratigraphy and geochemistry of the Troodos ophiolite extrusive sequence in the Margi area, Cyprus; (MSc Thesis), Dalhousie University, Halifax, 215 p.

Cameron, W.E.
1985: Petrology and origin of primitive lavas from the Troodos ophiolite, Cyprus; Contributions to Mineralogy and Petrology, v. 89, p. 239–255.

Cameron, W.E. and Nisbet, E.G.
1982: Phanerozoic analogues of komatiitic basalts; *in* Arndt, N.T. and Nisbet, E.G., Komatiites, George Allen and Unwin, London, p. 29–50.

Cameron, W.E., Nisbet, E.G., and Dietrich, V.J.
1980: Petrographic dissimilarities between ophiolitic and ocean-floor basalts; *in* Panayiotou, A., Ophiolites: proceedings of the International Ophiolite Symposium, Cyprus, 1979, Cyprus Geological Survey Department, Nicosia, p. 182–192.

Coish, R.A. and Taylor, L.A.
1979: The effects of cooling rate on texture and pyroxene chemistry in DSDP Leg 34 basalt: a microprobe study; Earth and Planetary Science Letters, v. 42, p. 389–398.

Gass, I.G.
1958: Ultrabasic pillow lavas from Cyprus; Geological Magazine, v. 95, p. 241–251.

Koehlstedt, D.L., Goetze, C., and Durham, W.B.
1976: Experimental deformation of single crystal olivine with application to flow in the mantle; *in* Strens, R.G.J., The physics and chemistry of minerals and rocks, John Wiley and Sons, London, p. 35–50.

Langdon, G.S.
1982: The petrology, geochemistry and petrogenesis of the Upper Pillow Lavas, Troodos ophiolite complex, Cyprus; (MSc Thesis), Memorial University, St. John's, Newfoundland, 168 p.

Lofgren, G., Donaldsen, C.H., Williams, R.J., Mullins, O., and Usselman, T.M.
1974: Experimentally reproduced textures and mineral chemistry of Apollo 15 quartz normative basalts: 5th Lunar Conference Supplement #5; Geochimica et Cosmochimica Acta, v. 1, p. 549–567.

Malpas, J., and Langdon, G.
1984: Petrology of the Upper Pillow Lava suite, Troodos ophiolite, Cyprus; *in* Gass, I.G., Lippard, S.J., and Shelton, A.W., Ophiolites and Oceanic Lithosphere, Geological Society of London, Special Publication 14, p. 155–167.

O'Hara, M.J.
1968: Are ocean floor basalts primary magma?; Nature, v. 220, p. 683-686.

Poirier, J.P. and Nicolas, A.
1975: Deformation-induced recrystallization due to progressive misorientation of subgrains, with special reference to mantle peridotites; Journal of Geology, v. 83, p. 707–720.

Rautenschlein, M., Jenner, G.A., Hertogen, J., Hofmann, A.W., Kerrich, R., Schmincke, H.–U., and White, W.M.
1985: Isotopic and trace element composition of volcanic glasses from the Akaki Canyon, Cyprus: implications for the origin of the Troodos ophiolite; Earth and Planetary Science Letters, v. 75, p. 369–383.

Robinson, P.T., Melson, W.G., O'Hearn, T., and Schmincke, H.–U.
1983: Volcanic glass compositions of the Troodos ophiolite, Cyprus; Geology, v. 11, p. 400–404.

Rose, A.W., Hawkes, H.E., and Webb, J.S.
1979: Geochemistry in mineral exploration, 2nd edition, Academic Press, London, 657 p.

Schmincke, H.-U., Rautenschlein, M., Robinson, P.T., and Mehegan, J.M.
1983: Troodos extrusive series of Cyprus: a comparison with oceanic crust; Geology, v. 11, p. 405–409.

Searle, D.L. and Vokes, F.M.
1969: Layered ultrabasic lavas from Cyprus; Geological Magazine, v. 106, p. 515–530.

Taylor, R.N.
1990: Geochemical stratigraphy of the Troodos extrusive sequence: temporal developments of a spreading centre magma chamber; Xenophontos, C. and Malpas, J., Field Excursion Guidebook. Troodos 87: Ophiolites and Oceanic Lithosphere, Cyprus Geological Survey Department, Nicosia, p. 173–183.

A Possible Primary Melt Composition for the Ultramafic Lavas of the Margi Area, Troodos Ophiolite, Cyprus

A.V. SOBOLEV[1], L.V. DMITRIEV[1], O.P. TSAMERYAN[1],
N.N. KONONKOVA[1], AND P.T. ROBINSON[2]

[1]Vernadsky Institute of Geochemistry, U.S.S.R. Academy of Sciences, Kosigina 19, Moscow W–334, U.S.S.R.
[2]Center for Marine Geology, Dalhousie University, Halifax, Nova Scotia, B3H 3J5, Canada

Sobolev, A.V., Dmitriev, L.V., Tsameryan, O.P., Kononkova, N.N., and Robinson, P.T., 1991: A possible primary melt composition for the ultramafic lavas of the Margi area, Troodos ophiolite, Cyprus; in Cyprus Crustal Study Project: Initial Report, Holes CY-1 and 1A, eds. Gibson, I.L., Malpas, J., Robinson, P.T., and Xenophontos, C.; Geological Survey of Canada, Paper 90–20, p. 203–218, 1991.

Abstract

A primary melt composition for ultramafic lavas of the Margi area of the Troodos ophiolite has been estimated from the petrography and mineralogy of the flows and a study of primary melt inclusions trapped in olivine and clinopyroxene crystals. This melt is essentially a water-bearing komatiite with about 21 wt.% MgO and 1.2 wt.% H_2O. Fractionation of this melt over a temperature range between 1420°C and 1090°C produced a series of depleted basalts, basaltic andesites, and picrites. This water-bearing komatiite melt represents a previously unrecognized type of ultramafic magma presumably formed by hydrous melting of depleted mantle material. The most probable environment of formation for such a melt is in the upper mantle, above a subduction zone.

Résumé

D'après l'étude pétrographique et minéralogique des coulées de laves ultramafiques et celle des inclusions de fusions primaires retenues dans les crystaux d'olivine et de clinopyrexène, il a été possible d'estimer une composition des laves ultramafiques de l'ophiolite de Troodos dans la région de Margi résulte d'une fusion primaire. Cette fusion est surtout composée d'une komatiite porteuse d'eau avec environ 21% de tm de MgO et 1,2% d'eau H_2O. Le fractionnement de cette fusion à une température variant entre 1420°C et 1090°C a produit des séries de basaltes appauvris, des andésites basaltiques et des picrites. Cette fusion de komatiite porteuse d'eau représente un type du magma ultramafique nonidentifié auparavant et qui aurait été probablement formé par la fusion aquatique du matériel mantellique appauvri. Le milieu le plus propice pour la formation d'une telle fusion serait le manteau supérieur au-dessus d'une zone de subduction.

INTRODUCTION

Knowledge of the conditions under which ultramafic melts originate and evolve is of the utmost importance in understanding the petrology and geochemistry of the mantle. Generation of ultramafic melts in the mantle requires very high temperatures and/or high volatile pressures (Sobolev, 1976). Most ultramafic lavas investigated to date appear to be picrites formed by settling and accumulation of olivine during crystallization of normal basaltic magma. Precambrian komatiites with spinifex textures are the most convincing examples of ultramafic liquids (Arndt and Nisbet, 1982). The only ultramafic melts of Phanerozoic age identified thus far are meimechites from Siberia (Sobolev and Slutsky, 1984) and komatiites from Gorgona Island (Aitken and Echeverria, 1984). Cameron and Nisbet (1982), suggested that some of the ultramafic lavas of Troodos (Gass, 1958) might be similar to komatiites.

The general geology of Troodos has been well described (e.g. see Gass, 1980). The massif is late Cretacious in age and consists, from the base upward, of tectonized harzburgite, layered intrusive rocks such as dunite, wehrlite, pyroxenite, and gabbro, homogeneous gabbro, sheeted dykes and extrusive rocks. Three distinct lava suites have been recognized in the extrusive sequence (Robinson et al., 1983; Schmincke et al., 1983; Mehegan, 1988): a relatively enriched sequence of andesites, dacites and rhyodacites that correspond approximately to the former Lower Pillow Lavas, a more depleted, basalt-basaltic andesite suite which corresponds approximately with the former Upper Pillow Lavas, and a highly depleted basaltic suite associated with the Arakapas Fault Zone (McCulloch and Cameron, 1983; Cameron, 1985). Numerous authors have suggested that Troodos formed in a Cretacious subduction zone environment because of the abundance of intermediate and silicic rocks, the presence of boninites, and the isotopic character of the lavas (Miyashiro, 1973; Pearce, 1975; McCulloch and Cameron, 1983; Robinson et al., 1983). An alternate model, put forward by Duncan and Green (1980), suggests that the Troodos lavas formed by second-stage melting at a mid-ocean ridge. Both models call for derivation from residual mantle, either by hydrous melting above a subduction zone or anhydrous melting beneath a mid-ocean ridge.

The ultramafic lavas of the Margi area of Troodos occur as pillows, massive flows and sills (Gass, 1958; Searle and Vokes, 1969; Malpas and Langdon, 1984; Bailey, 1984; Mehegan, 1988). Olivine phenocrysts commonly comprise as much as 60 modal percent and form subhedral crystals up to 20 mm across. Searle and Vokes (1969) suggested that the olivine had crystallized *in situ* from ultramafic liquids, whereas Gass (1958) and Cameron and Nisbet (1982) suggested that much of the olivine is xenocrystic. More recent studies of these rocks have shown that they owe their ultramafic compositions to accumulation of olivine, either after eruption on to the seafloor, or in shallow level magma chambers before eruption (Malpas and Langdon, 1984; Bailey, 1984).

Little information is available on the primary melts from which these lavas formed or the conditions under which they evolved. In this article we attempt to determine quantitatively, by a study of the phenocryst phases and particularly their melt inclusions, the composition and conditions of crystallization of the primary magma from which these ultramafic lavas were derived. Some of the results of this work were published previously by Sobolev and Naumov (1985) and Sobolev et al. (1986).

PETROGRAPHY

The volcanic rocks of Troodos ophiolite range in composition from ultramafic to silicic (Figure 1). Two samples of ultramafic lavas (Table 1), both from the Margi area on the north flank of Troodos, were selected for detailed study. Sample CY-1 is a coarsely porphyritic picrite, containing about 60 modal percent of olivine. The olivine crystals are subhedral to euhedral and up to 20 mm in diameter. They are set in a poorly crystallized, quenched groundmass containing some fresh glass. Small crystals of chrome spinel occur as inclusions in the olivine phenocrysts and as microphenocrysts in the groundmass. Some of the glass is weakly palagonitized and the olivine is locally altered along cracks. Sample CY-2 is a somewhat less phyric rock, containing two distinct phenocryst assemblages which are distinguished on the basis of size. The first assemblage contains about 40 modal percent phenocrysts, chiefly olivine. The olivine occurs in subhedral crystals from 1–5 mm across, which are commonly rimmed by clinopyroxene. A few grains of pale green clinopyroxene and chromite are associated with the olivine. The second assemblage consists of microphenocrysts of pale-green clinopyroxene and plagioclase that are about 0.5–1 mm across. The very fine-grained groundmass (0.05–0.2 mm) consists of brown clinopyroxene, bronzite, plagioclase, titanomagnetite

Sample	CY-1	CY-2
SiO_2	43.60	45.70
TiO_2	0.17	0.32
Al_2O_3	5.30	7.75
Fe_2O_3	0.56	2.21
FeO	8.05	7.10
MnO	0.10	0.12
MgO	35.28	26.28
CaO	3.61	6.02
Na_2O	0.37	0.55
K_2O	0.17	0.06
P_2O_5	0.05	n.d.
CO_2	0.16	n.d.
H_2O	2.79	3.96
Total	100.16	100.07

Table 1: Compositions of investigated ultramafic lavas of the Margi area. Wet chemical analyses. n.d. = not determined.

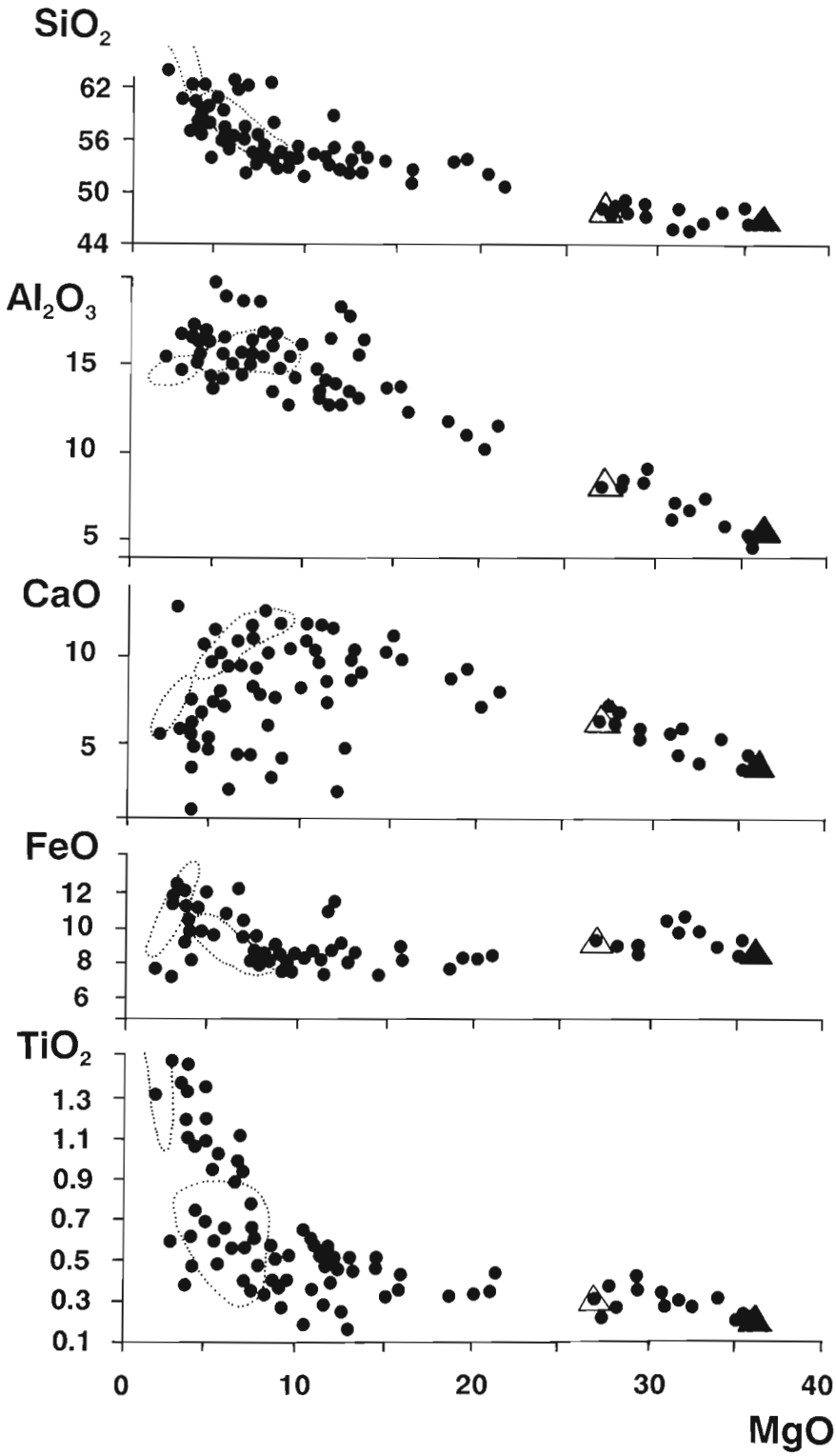

Figure 1: Chemical compositions of volcanic rocks and glasses from the Troodos ophiolite: • = whole-rock lava and dyke compositions (Pantazis, 1980); ▲ = sample CY-1, this study; △ = sample CY-2, this study. Dotted lines enclose fields of volcanic glass compositions (Robinson et al., 1983).

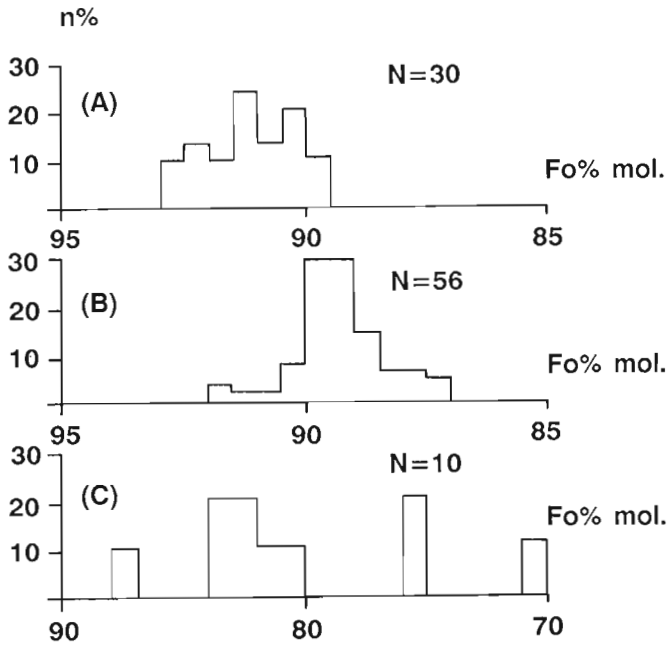

Figure 2: Histograms showing the forsterite content of olivines in the ultramafic lavas of the Margi area, Troodos: (A) olivine phenocrysts, sample CY-1; (B) olivine phenocrysts, sample CY-2; (C) olivine microlites, sample CY-1.

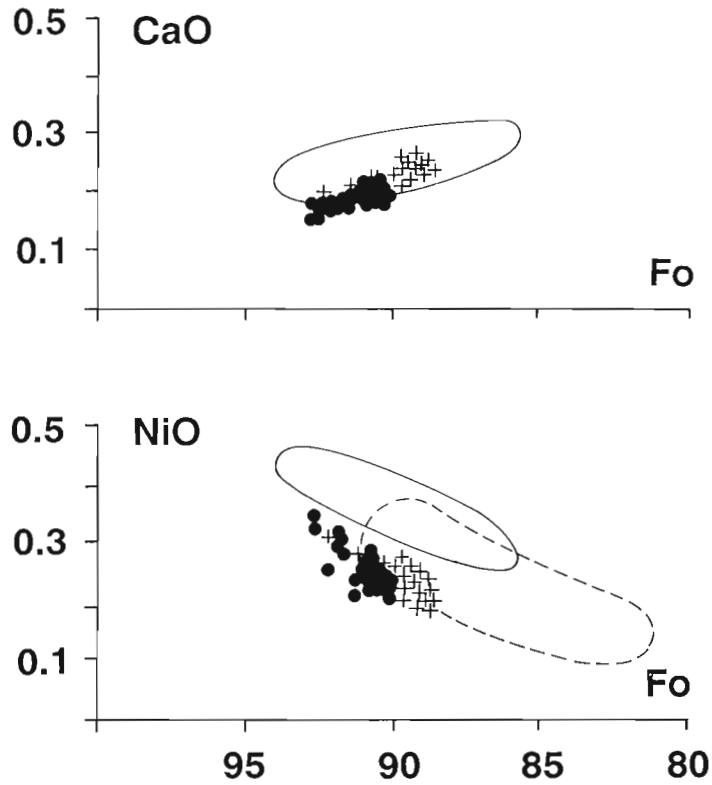

Figure 3: Compositions of olivine phenocrysts from ultramafic lavas of the Margi area, Troodos. • = sample CY-1; + = sample CY-2. Solid line encloses compositional field of olivine from komatiites (Cameron and Nisbet, 1982). Dashed line encloses compositional field of olivine from MORB (Schilling, in press).

and small amounts of interstitial glass. Some of the olivine and the glass is slightly altered.

MINERALOGY

Mineral and glass compositions were determined with a Camebax Microbeam electron microprobe operating at a voltage of 15 kv and a beam current of 50×10^{-9} amps. A beam diameter of 2 μm was used for mineral analyses, whereas a diameter of 5–20 μm was used for glass analyses. Standards used included high magnesian olivine CH-1, pure diopside BD, orthoclase 195/1, glass VG-2 and F-apatite (Lavrentiev et al., 1974; Jarosewich et al., 1979).

Olivine phenocrysts range in composition from Fo_{87} to Fo_{93} (Figure 2, Table 2) and are distinctly more magnesian than olivines in mid-ocean ridge basalts. Despite the wide compositional range of olivine phenocrysts in a given sample, individual grains are unzoned, a phenomenon previously described for Siberian meimechites (Sobolev and Slutsky, 1984). These relationships are believed to reflect crystal-liquid disequilibrium resulting from uprise and mixing of magma. Significant differences in olivine composition exist between the two samples studied (Figure 2), and these probably reflect different degrees of fractionation of the parental magma. Except for having slightly lower Ni contents, these olivines compare very closely to those of komatiites (Cameron and Nisbet, 1982; Sobolev and Slutsky, 1984) (Figure 3).

Groundmass olivine from sample CY-1 consists of skeletal microlites. These crystals are somewhat zoned and range in composition from Fo_{88} to Fo_{70} (Table 3; Figure 2).

Chrome spinel occurs both as small euhedral phenocrysts and as inclusions in olivine and clinopyroxene phenocrysts. These opaque grains are intermediate in composition between chrome spinels from mid-ocean ridge basalts and from boninites (Table 2; Figure 4). They resemble chrome spinels from Precambrian komatiites and from the ultramafic layered series of the Troodos ophiolite. Significant differences in Cr and Mg were noted for chrome spinels from different samples. Chrome spinel inclusions in clinopyroxene have lower Cr and Mg contents than those in olivine.

Clinopyroxene occurs in the groundmass of all samples and as phenocrysts in sample CY-2. All of the analyzed phenocrysts are chrome diopside (Table 2). In sample CY-2, the groundmass grains are Al-augite, somewhat enriched in Ti, whereas in sample CY-1 they are high-alumina, subcalcic

	1	2	3	4	5	6	7	8	9	10
Sample	CY-1	CY-1	CY-2	CY-1	CY-1	CY-2	CY-2	CY-2	CY-2	CY-2
Mineral	Ol	Ol	Ol	Sp	Sp	Sp	Cpx	Cpx	Cpx	Pl
SiO_2	41.03	41.12	40.59	0.05	n.d.	0.04	53.55	53.74	52.31	45.12
TiO_2	n.d.	n.d.	n.d.	0.21	0.36	1.05	0.16	0.18	0.26	0.03
Al_2O_3	0.05	0.04	0.04	10.73	14.95	17.02	2.19	2.15	2.69	35.91
Fe_2O_3*	n.d.	n.d.	n.d.	5.96	6.75	6.35	n.d.	n.d.	n.d.	n.d.
FeO	6.90	8.80	10.36	11.94	14.44	16.14	2.51	3.61	4.58	0.48
MnO	0.13	0.19	0.20	0.30	0.26	0.26	0.04	0.10	0.13	n.d.
MgO	50.79	49.73	48.25	13.97	13.07	12.49	18.68	18.39	17.84	0.12
CaO	0.20	0.21	0.24	0.00	n.d.	n.d.	21.87	21.38	20.93	18.64
Na_2O	n.d.	n.d.	n.d.	n.d.	n.d.	n.d.	0.13	0.19	0.16	1.02
Cr_2O_3	0.09	0.03	n.d.	56.22	50.31	45.06	1.02	0.88	0.69	n.d.
NiO	0.34	0.23	0.25	0.10	n.d.	n.d.	n.d.	n.d.	n.d.	n.d.
Total	99.53	100.16	99.93	99.48	100.14	98.41	100.15	100.62	99.59	101.33
Mg#	92.92	91.00	89.20	67.60	61.70	57.80	93.00	90.10	87.40	91.0**

Table 2: Representative analyses of phenocrysts from Cyprus ultramafic lavas. All are phenocrysts except numbers 9 and 10 which are microphenocrysts of the second generation (see text). Ol = olivine; Sp = spinel; Cpx = clinopyroxene, Pl = plagioclase; Mg# = $Mg/Mg+Fe^{+2}$; * Fe_2O_3 is calculated from stoichiometry of spinel; ** An content of plagioclase.

	1	2	3	4	5	6	7	8
Sample	CY-1	CY-1	CY-1	CY-2	CY-2	CY-2	CY-2	CY-2
Mineral	Ol	Cpx	Gl	Cpx	Opx	Opx	Pl	Mt
SiO_2	39.60	47.70	62.44	53.21	55.55	51.69	47.53	0.11
TiO_2	n.d.	0.74	0.43	0.36	0.16	0.28	0.03	19.60
Al_2O_3	0.27	9.40	18.50	2.16	0.91	1.86	33.78	1.98
FeO^T	n.d.	n.d.	6.75	6.35	n.d.	n.d.	n.d.	26.16*
FeO	18.40	8.80	3.00	7.22	11.35	17.32	0.45	48.98
MnO	0.23	0.14	0.06	0.21	n.d.	0.27	n.d.	0.55
MgO	40.90	12.70	3.88	17.47	29.25	26.10	0.20	0.98
CaO	0.31	19.30	5.21	19.34	2.30	2.35	17.02	n.d.
Na_2O	n.d.	0.18	0.41	0.20	0.01	0.05	1.72	n.d.
K_2O	n.d.	0.00	0.67	n.d.	n.d.	n.d.	0.03	n.d.
Cr_2O_3	0.08	0.13	0.00	0.07	n.d.	0.05	n.d.	0.02
NiO	0.05	0.00	0.00	n.d.	n.d.	n.d.	n.d.	n.d.
Total	99.84	99.09	94.60	100.24	99.53	99.97	100.75	99.33**

Table 3: Representative microprobe analyses of groundmass minerals from lavas of the Margi area. (1) average of 10 analyses; (2) average of 35 analyses; (3) average of 10 analyses; * calculated from spinel stoichiometry; ** including 0.95% V_2O_5; Ol = olivine; Cpx = clinopyroxene; Gl = glass; Opx = orthopyroxene; Pl = plagioclase; Mt = magnetite.

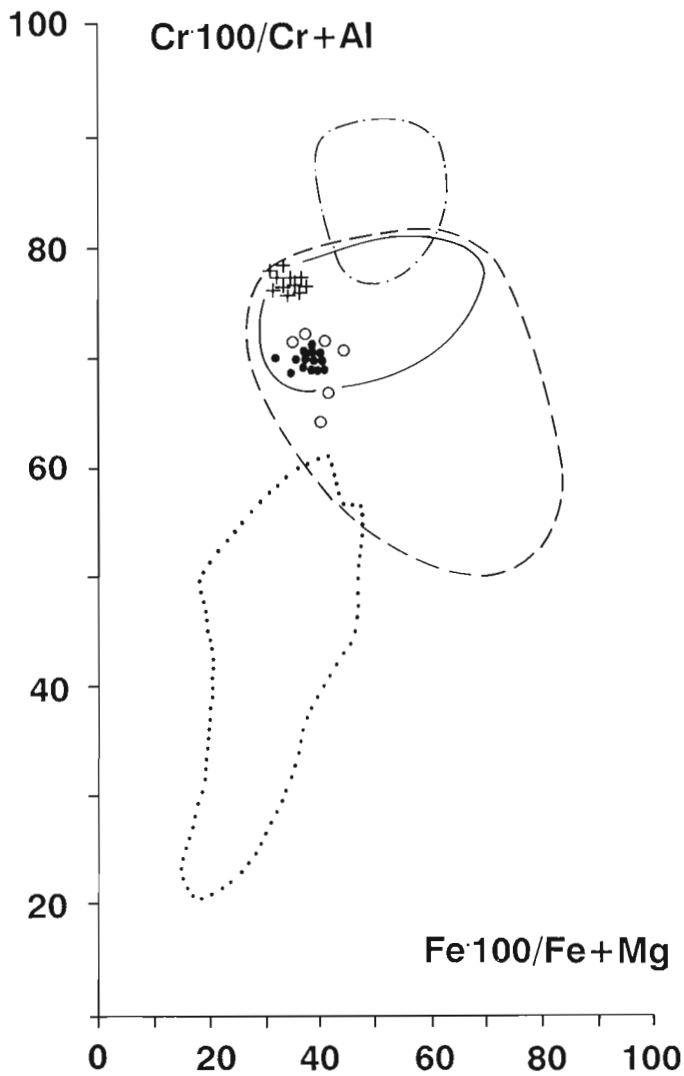

Figure 4: Compositions of spinels from ultramafic lavas of the Margi area, Troodos. + = spinel inclusions in olivine, sample CY-1; • = spinel inclusions in olivine, sample CY-2; o = spinel inclusions in clinopyroxene, sample CY-2. Dashed line encloses compositional field of spinel from Troodos peridotites (Dick and Bullen, 1984); solid line encloses compositional field of spinel from komatiites (Cameron and Nisbet, 1982); dot-dash line encloses compositional field of spinel from boninites (Cameron et al., 1980); dotted line encloses compositional field of spinel from mid-ocean ridge basalts (Dick and Bullen, 1984).

augite. The subcalcic augite occurs together with iron-rich olivine and glass, an assemblage suggesting disequilibrium crystallization of the residual liquid during quenching.

Plagioclase occurs as microphenocrysts and as a groundmass phase in sample CY-2 (Table 2). A few crystals are also present as inclusion in clinopyroxene phenocrysts. The crystals are chiefly bytownite, zoned from about An_{91} in the core to An_{80} in the rims.

Titanomagnetite occurs in the groundmass of sample CY-2 along with plagioclase, augite and bronzite (Table 3).

Orthopyroxene (bronzite) forms elongate prisms, up to 0.5 mm long, in the groundmass of sample CY-2. The mineral is relatively uniform in composition but has somewhat variable iron contents. One bronzite phenocryst with a reaction rim of clinopyroxene was noted in sample CY-2.

Glass fills interstices between skeletal crystals of high-alumina clinopyroxene and iron-rich olivine in the groundmass of sample CY-1. This residual glass is dacitic in composition (Table 3).

MAGMATIC INCLUSIONS

Several types of inclusions — melt, fluid, or crystal — may be trapped in minerals during crystallization. From a study of such inclusions it is possible to determine what phases were present in the magmatic system and the temperatures and pressures at which crystallization occurred.

Methods

The techniques used here are described in detail by Basarova et al. (1979), Sobolev et al. (1983), Roedder (1984), Sobolev and Slutsky (1984), and Clocchiatti and Massare (1985), and thus are only briefly reviewed.

Small amounts of melt become trapped and isolated within a host mineral due to variable rates of crystal growth along different crystallographic axes. Once trapped within a crystal, such inclusions are isolated from the remaining melt and thus record the melt composition and the P-T conditions at the time of trapping. Primary melt inclusions are normally easy to distinguish from secondary inclusions, which occur along fractures in the host crystal.

Natural magmatic systems are polyphase, usually consisting of melt, fluid and crystals (Figure 5). Single-phase inclusions are designated 'normal' inclusions, whereas those containing two or more phases at the time of formation are termed 'combined' or 'polyphase.' However, with decreasing temperature, most single-phase inclusions become polyphase as a result of crystallization or separation of a fluid phase (see Figure 6). The most reliable way to determine the initial character of an inclusion is by heating under a microscope (Figures 6 and 7), although normal and polyphase inclusions can usually be distinguished by optical means alone.

Melt homogenization by heating normally provides reliable information on the melt composition and on the temperature

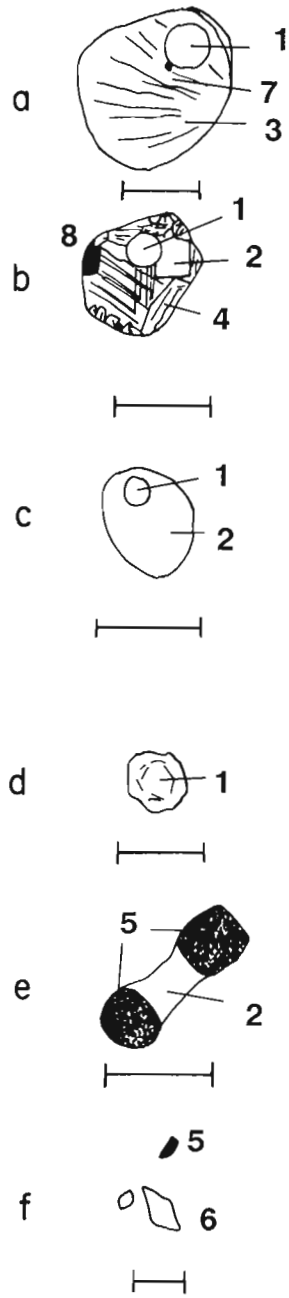

Figure 5: Varieties of primary magmatic inclusions in minerals from the ultramafic lavas of the Margi area: (a) partially crystallized inclusion in an olivine phenocryst, sample CY-1; (b) partially crystallized inclusion in clinopyroxene phenocryst, sample CY-2; (c) glassy inclusion in olivine phenocryst, sample CY-1; (d) fluid inclusion in olivine phenocryst, sample CY-2; (e) polyphase inclusion in olivine phenocryst, sample CY-1; (f) crystalline inclusion in groundmass clinopyroxene grain, sample CY-2. 1 = fluid phase; 2 = glass; 3 = clinopyroxene; 4 = amphibole; 5 = spinel; 6 = plagioclase; 7 = sulphide; 8 = titanomagnetite; scale bar = 50 μm.

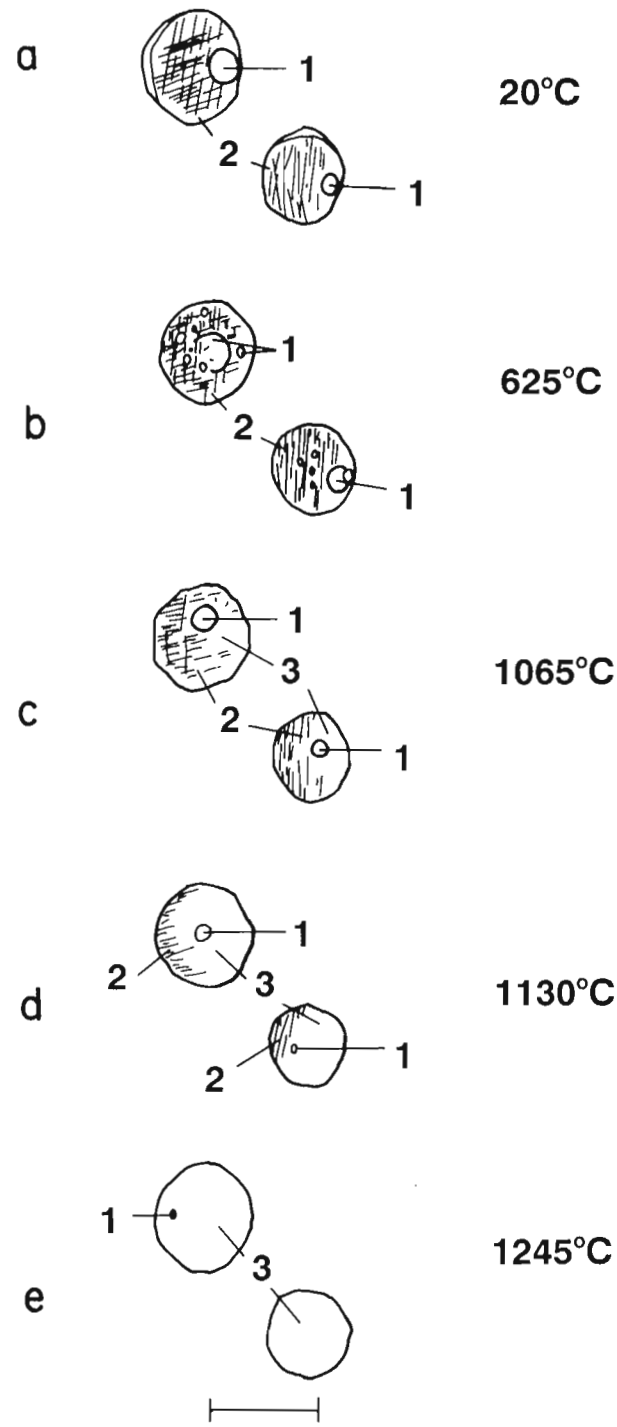

Figure 6: Phase transformations in primary magmatic inclusions in an olivine phenocryst during heating, sample CY-2. 1 = fluid phase; 2 = clinopyroxene; 3 = melt. Note the cores of the inclusions consist of glass (a, b) and melt (c, d, and e). Scale bar = 50 μm.

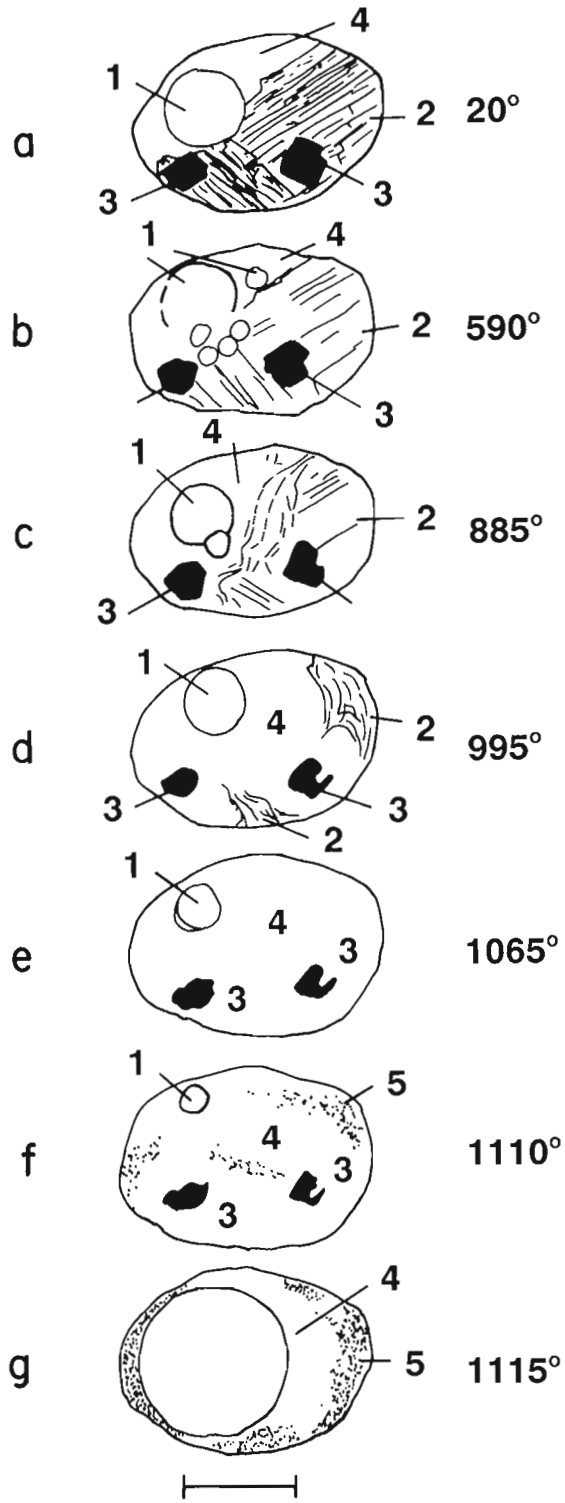

Figure 7: Phase transformations in a primary magmatic inclusion in a clinopyroxene phenocryst, sample CY-2. 1 = fluid phase; 2 = amphibole; 3 = spinel; 4 = glass in (a) and (b) and melt in (d) through (g); 5 = magnetite. Scale bar = 50 μm.

of crystallization of various phases. An example of an inclusion in olivine, heated stepwise to its temperature of homogenization (1245°C) is shown in Figure 6. From such an experiment, the cooling history of the inclusion can be deduced by observing the changes under a microscope as the temperature is allowed to drop. In this case, a very small degree of cooling led to precipitation of olivine on the walls of the inclusion, with a resulting decrease in pressure because the inclusion has a fixed volume. A similar effect also results from the different coefficients of thermal expansion of the melt and host crystal. Such a decrease in pressure of a melt saturated with volatiles leads immediately to the appearance of a fluid phase (Figure 6e). As the temperature continues to drop there is progressive crystallization of the melt, a further drop in the pressure inside the inclusion, and expansion of the fluid phase (Figure 6e to 6a).

The heating stage is designed so that the sample can be quenched at any stage in the experiment, thus fixing the phases in equilibrium at that temperature. These phases can then be analyzed with an electron microprobe.

Potential problems with this technique involve exchange between the inclusion and the host crystal, leakage from the inclusion, kinetics of crystal growth (and dissolution), and changes in pressure and oxidation state within the inclusion. In most cases, these problems can be overcome and usable data obtained. The temperature and compositional data are considered valid if they can be correlated with independent petrological data such as glass compositions, mineral geothermometry, correlations between temperature of crystallization, and composition of the host mineral, etc. Our work on basalts and ultramafic rocks suggests that temperatures can be measured to ±20°C and major element compositions to ±5% relative (Sobolev, 1983).

Inclusions in minerals from ultramafic lavas of Cyprus

Microscopic examination of the Troodos lavas has revealed the presence of four distinct types of inclusions (Figure 5):

1. Normal, partially crystallized inclusions in olivine and clinopyroxene crystals which range from about 20–200 μm in diameter (Figures 5a and 5b). The inclusions in olivine consist of dacitic glass, high-alumina clinopyroxene similar in composition to groundmass clinopyroxene and a fluid phase (Table 4). A few also contain minute opaque minerals, perhaps a sulphide. Inclusions in clinopyroxene are similar and consist of dacitic glass, amphibole, opaques (titanomagnetite?) and a fluid phase (Table 4).

2. Inclusions up to 50 μm across in olivine phenocrysts of sample CY-1 which consist of glass and a fluid phase (Figure 5c).

Sample	CY-1		CY-2	
Phase	Cpx	Gl	Amph	Gl
SiO_2	45.70	63.73	40.19	66.50
TiO_2	0.85	0.27	0.90	0.06
Al_2O_3	11.93	19.55	19.73	18.30
FeO	8.71	1.45	14.54	0.70
MgO	9.65	0.17	7.69	0.05
CaO	22.85	7.83	11.34	6.01
Na_2O	n.d.	2.58	1.64	3.30
K_2O	n.d.	0.33	0.10	0.49
Total	99.69	95.91	96.13	95.41

Table 4: Representative analyses of phases in the melt inclusions in phenocrysts of ultramafic lavas. Cpx = clinopyroxene; Gl = glass; Amph = amphibole. Inclusions from Sample CY-1 are in olivine, those from CY-2 are in clinopyroxene.

3. Low density fluid inclusions up to 100 μm across which have a negative crystal shape corresponding to that of the host mineral (Figure 5d).

4. Small crystalline inclusions such as chromite in olivine and clinopyroxene, olivine in clinopyroxene, or plagioclase in clinopyroxene microphenocrysts (Figure 5f). Inclusions of titanomagnetite are also common in clinopyroxene, plagioclase and orthopyroxene groundmass crystals of sample CY-2. A number of polyphase inclusions such as chromite + melt, melt + fluid, etc. are also present (Figure 5e).

Heating Experiments

Primary melt inclusions from the Troodos lavas were homogenized in a specially cleaned helium atmosphere, using a high temperature heating stage developed at the Vernadsky Institute (Sobolev et al., 1980). The extremely low thermal inertia of the heater permits quenching of the sample in the working environment simply by switching off the power. After homogenization and quenching, the samples were analyzed with an electron microprobe (Table 5). The most magnesian melt composition has about 20 wt.% MgO (Table 5) and is taken as the probable primary magma from which the picritic lavas formed.

Disassociation of water during heating may lead to hydrogen diffusion from inclusions, resulting in erroneously high homogenization temperatures (Roedder, 1984; Sobolev et al., 1983). This effect is most pronounced for inclusions produced from hydrous ultramafic and basaltic magmas such as those of the Troodos ophiolite. Thus, the duration of heating at temperatures greater than 1000°C was limited to 15 minutes.

Heating of an inclusion in olivine produces the following phase transformation (Figures 6a to 6e):

600°C Small bubbles appear in the glass, indicating that the glass is becoming soft.

730°C Melting begins and numerous small bubbles coalesce to form a single large bubble.

950°C The glass is completely melted and clinopyroxene begins to melt.

1120–1150°C The clinopyroxene is completely melted.

1200–1420°C The inclusion is completely homogenized.

A similar sequence occurs for heating of an inclusion in clinopyroxene (Figures 7a–7j):

500–600°C The glass begins to soften.

650–700°C Melting occurs along the boundary between amphibole and glass.

1000–1020°C The amphibole is completely melted, as is most of the ore mineral.

1090–1160°C The inclusion is completely homogenized.

Precise measurements of increases in fluid phase volume after explosion of the inclusions during heating show that the fluid pressures during crystallization of the host minerals were in excess of $0.2–0.3 \times 10^5$ kPa.

An indication of the precision of the temperature measurements is shown in Figure 8, in which the temperature of homogenization of the inclusions is plotted against the melt compositions. The melt compositions change in a regular fashion with temperature and the composition of the host mineral. Crystallization took place over a temperature range between 1420–1090°C and the melt composition changed from ultramafic to andesitic. These data are compatible with fractional crystallization of the primary magma.

Melt Compositions

The melt compositions determined from inclusions correspond closely with the bulk rock and glass compositions of the Upper Pillow Lavas of Troodos (Table 5; Figure 9). In a few samples, the iron content of the melt inclusions is lower than bulk rock and glass compositions. This is believed to be due to the crystallization of magnetite in the inclusions during heating (Figure 7f). The formation of magnetite probably reflects self-oxidation of the melt due to decomposition of H_2O and diffusion of H_2 through the host mineral (Sobolev, 1984).

In Figure 10 the homogenization temperatures of the inclusions are plotted against equilibrium crystallization temperatures calculated from melt and host mineral compositions, using the data of Ford et al. (1983), and Nielsen and Drake (1970). For dry magmas, such as those of mid-ocean ridge and ocean island basalts, the two temperatures are essentially the same. However, for hydrous melts such as those of Troodos, the calculated temperatures are always higher than measured homogenization temperatures.

	1	2	3(2)	4	5(2)	6	7	8	9	10(2)
T(hom)	1420	1415	1370	1305	1240	1215	1155	1115	1110	1090
SiO_2	49.96	49.76	50.81	52.13	53.03	53.09	53.62	55.42	56.93	58.14
TiO_2	0.34	0.33	0.33	0.49	0.54	0.57	0.52	0.44	1.02	0.90
Al_2O_3	10.28	9.96	11.04	13.32	13.22	14.13	15.08	15.19	14.04	15.11
FeO*	6.95	8.75	7.84	5.50	5.77	6.38	6.27	6.30	9.13	6.60
MnO	0.12	0.16	0.11	0.11	0.12	0.10	0.13	0.10	0.20	0.16
MgO	21.12	20.43	18.34	14.54	11.56	10.61	7.56	6.44	5.61	5.00
CaO	8.79	8.63	8.36	10.12	11.14	11.68	11.69	10.61	10.20	9.74
Na_2O	0.92	1.02	1.22	1.72	1.94	1.68	2.05	1.90	2.42	2.29
K_2O	0.10	0.12	0.13	0.13	0.18	0.16	0.17	0.21	0.20	0.31
P_2O_5	0.02	0.03	0.02	0.05	0.07	0.05	0.05	0.03	0.07	0.08
Total	98.60	99.19	98.20	98.11	97.57	98.45	97.14	96.64	99.82	98.41
Mg No.**	0.93	0.92	0.92	0.90	0.89	0.89	0.90	0.88	0.81	0.82

Table 5: Representative microprobe analyses of experimentally homogenized melt inclusions and host minerals from ultramafic lavas of the Margi area. Samples 1–6: host mineral is olivine (samples 1–3 are CY-1), (samples 4–6 are CY-2); samples 7–10: host mineral is clinopyroxene (sample CY-2). * Total iron. ** Magnesium number of host mineral. T(hom) = homogenization temperature (°C).

Water Content

Using the method of Naumov (1979), we attempted to determine quantitatively the composition and percent of fluid in the primary melt from which the Troodos lavas were derived. A very flat and thin melt inclusion in the most magnesian olivine crystal (Fo_{93}) was quenched after heating for one hour at 950°C (Figure 11). The quenched inclusion consists of alumina-rich clinopyroxene (30% by volume), dacitic glass (50% by volume), and a fluid phase (20% by volume). A clearly defined phase boundary is visible at the edge of the fluid cavity. This phase boundary disappears at a temperature of 321°C, thus indicating that the fluid is nearly pure water. A very low salinity is indicated by a freezing point of −0.6°C. Using P-T-V data of Vukalovich (1967), a pressure of about 0.36×10^5 kPa was calculated for the quenching temperature (950°C). A water content of 2.3 wt.% (Table 6) was estimated for the residual glass in the inclusion, using the methods of Burnham (1983) and Nicolls (1980), (Table 6). The partial water pressure estimated from the data of Burnham (1983) was close to 0.3–0.4 kPa.

Sample	1	2	3	4	5	6	7
SiO_2	45.84	64.85	0.00	55.85	40.31	49.89	49.86
TiO_2	0.85	0.28	0.00	0.54	0.00	0.33	0.33
Al_2O_3	11.97	19.93	0.00	16.20	0.00	9.97	10.12
FeO	8.74	1.48	0.00	4.76	12.80	7.85	7.85
MgO	9.68	0.17	0.00	4.48	46.89	20.78	20.78
CaO	22.92	7.98	0.00	14.70	0.00	9.05	8.71
Na_2O	0.00	2.63	0.00	1.42	0.00	0.87	0.97
K_2O	0.00	0.34	0.00	0.18	0.00	0.11	0.11
H_2O	0.00	2.34	100.00	1.87	0.00	1.15	n.d.
Total	100.00	100.00	100.00	100.20	100.00	100.00	98.90
ρ	3.24	2.32	0.07	–	–	–	–

Table 6: Estimate of H_2O content in primary komatiitic melt of the ultramafic lavas of the Margi area. (1), (2) compositions of clinopyroxene and glass, respectively, in inclusion (Figure 11) in olivine (Fo_{92}), recalculated to 100%; (3) composition of fluid phase in same inclusion; (4) calculated total composition of inclusion using estimated composition of clinopyroxene (30% volume), glass (50% volume) and fluid (20% volume); (5) olivine composition (SiO_2, FeO, MgO) calculated from primary melt composition of Troodos ultramafic lavas; (6) calculated primary composition of the inclusion before crystallization of olivine (analysis 5) on the walls of the cavity; (7) primary melt for Cyprus ultramafic magmas (average from analyses 1 and 2, Table 5); ρ calculated densities (g/cm^3).

SUMMARY AND DISCUSSION

The data presented in this paper suggest that the most magnesium olivine in the lavas of the Margi area (Fo_{93}) crystallized from a new type of komatiitic melt with about 21 wt.% MgO and 1.2 wt% H_2O. Fractionation of this melt over a temperature interval between about 1420–1090°C produced the range of compositions observed in the Upper Pillow Lavas of the Margi area. Thus, this melt is considered to represent the primary magma from which these lavas were derived. It differs from Precambrian komatiites (Green et al., 1975) and Siberian meimechites (Sobolev and Slutsky, 1984) primarily in its hydrous nature. Such a magma could be produced by melting of depleted mantle material under the influence of a water-bearing fluid or melt. Thus, our data support the interpretation that the Upper Pillow Lavas of Troodos were formed in a supra-subduction zone environment, as suggested by the glass compositions (Robinson et al., 1983; Rautenschlein et al., 1985) and the whole-rock, isotopic, and REE compositions (McCulloch and Cameron, 1983).

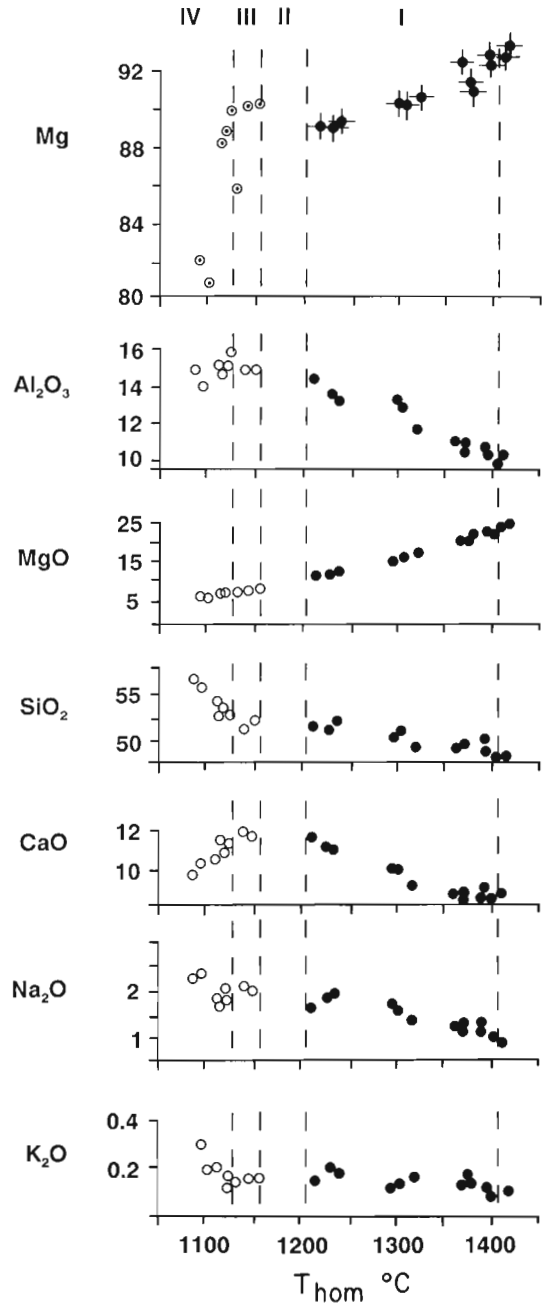

Figure 8: Correlation between homogenization temperatures T(hom) and compositions of melt inclusions in olivine (•) and clinopyroxene (o). Also shown is correlation between T(hom) and Mg number (Mg = 100 Mg/Mg+Fe) of the host mineral for olivine (o) and clinopyroxene (o). Fields I–IV show the liquidus phase assemblages present at different temperatures. I = olivine + Cr-spinel; II = clinopyroxene ± plagioclase; III = clinopyroxene + plagioclase; IV = clinopyroxene + plagioclase + orthopyroxene + titanomagnetite.

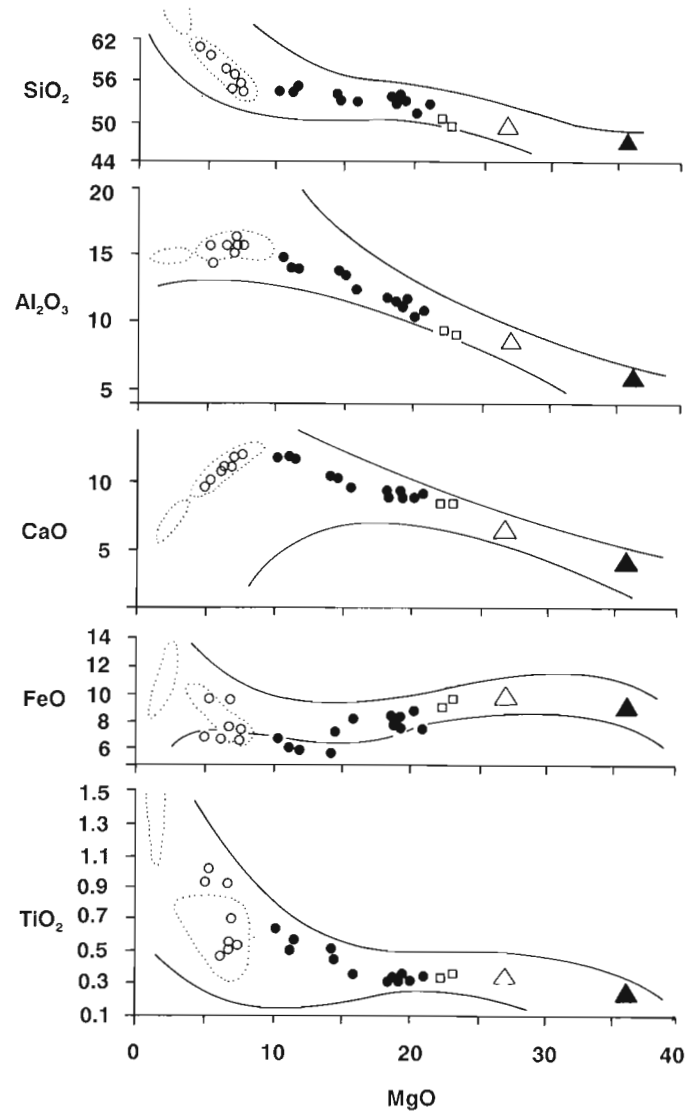

Figure 9: Compositional variations of homogenized melt inclusions in phenocrysts of ultramafic lavas of the Margi area, Troodos. Solid lines show whole-rock compositional range of Troodos lavas and dykes (Pantazis, 1980; Searle and Vokes, 1969); dotted lines enclose fields of volcanic glass compositions of Troodos (Robinson et al., 1983). o = homogenized melt inclusions in clinopyroxene; • = homogenized melt inclusions in olivine; □ = mean compositions of Troodos ultramafic lavas (Searle and Vokes, 1969); ▲ = composition of sample CY-1; △ = composition of sample CY-2.

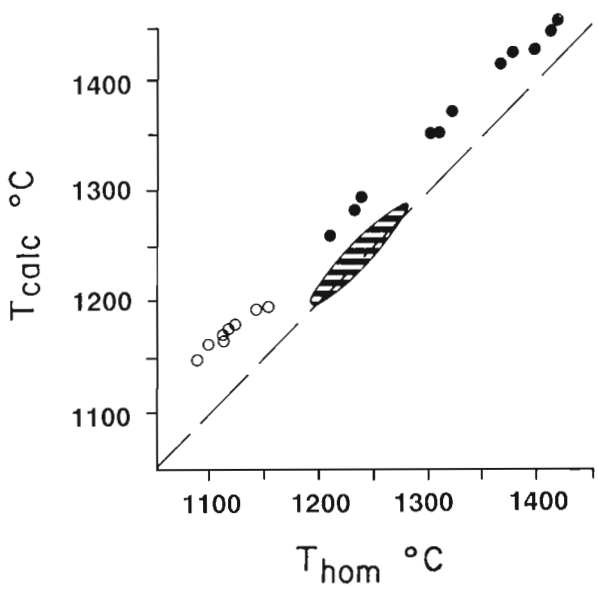

Figure 10: Correlation between homogenization temperatures of melt inclusions T(hom) and calculated temperatures of equilibrium between melt and host mineral T(calc). o = homogenized melt inclusions in clinopyroxene; • = homogenized melt inclusions in olivine. Ruled area encloses temperature data from mid-ocean ridge tholeiites and ocean island basalts.

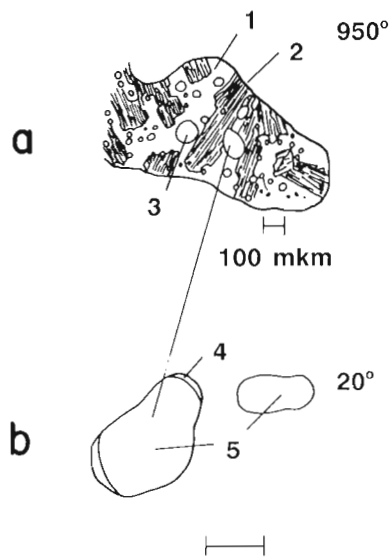

Figure 11: A flat magmatic inclusion in an olivine phenocryst, sample CY-1: a = general view at T = 950°C; b = detailed view of the same inclusion at room temperature after quenching. 1 = melt; 2 = clinopyroxene; 3 = fluid; 4 = H_2O liquid; 5 = H_2O vapor; scale bar = 100 µm.

REFERENCES

Aitken, B.G. and Echeverria, L.M.
1984: Petrology and geochemistry of komatiites and tholeiites from Gorgona Island, Colombia; Contributions to Mineralogy and Petrology, v. 86, p. 94–105.

Arndt, N.T. and Nisbet, E.G.
1982: What is a komatiite?; *in* Arndt, N.T. and Nisbet, E.G., Komatiites, George Allen and Unwin, London, p. 19–27.

Bailey, D.G.
1984: Stratigraphy and geochemistry of the Troodos ophiolite extrusive sequence in the Margi area, Cyprus; (MSc Thesis), Dalhousie University, Halifax, 215 p.

Basarova, T.Y., Bakumenko, O.L., Kostuk, V.P., Panina, L.I., Sobolev, V.S., and Chepuzov, A.I.
1979: Magmatic crystallization from the data on the melt inclusion studies; *in* Sobolev, V.S., Novosibirsk, Transactions of the Institute of Geology and Geophysics, Akademy Nauk Publication, v. 264, 232 p. (in Russian).

Burnham, C.W.
1975: Water and magmas; a mixing model; Geochimica et Cosmochimica Acta, v. 39, p. 1077–1084.

Cameron, W.E.
1985: Petrology and origin of primitive lavas from the Troodos ophiolite, Cyprus; Contributions to Mineralogy and Petrology, v. 89, p. 239–255.

Cameron, W.E. and Nisbet, E.G.
1982: Phanerozoic analogues of komatiitic basalts; *in* Arndt, N.T. and Nisbet, E.G., Komatiites, George Allen and Unwin, London, p. 29–50.

Cameron, W.E., Nisbet, E.G., and Dietrich, V.J.
1980: Petrographic dissimilarities between ophiolitic and ocean-floor basalts; *in* Panayiotou, A., Ophiolites: proceedings of the International Ophiolite Symposium, Cyprus, 1979, Cyprus Geological Survey Department, Nicosia, p. 182–192.

Clocchiatti, R. and Massare, D.
1985: Experimental crystal growth in glass inclusions: the possibilities and limits of the method; Contributions to Mineralogy and Petrology, v. 89, p. 193–204.

Dick, H.J.B. and Bullen, T.
1984: Chromian spinel as a petrogenetic indicator in abyssal and alpine-type peridotites and spatially associated lavas; Contributions to Mineralogy and Petrology, v. 86, p. 54–76.

Duncan, R.A. and Green, D.H.
1980: Role of multistage melting in the formation of oceanic crust; Geology, v. 8, p. 22–26.

Duncan, R.A. and Green, D.H.
1987: The genesis of refractory melts in the formation of oceanic crust; Contributions to Mineralogy and Petrology, v. 96, p. 326–342.

Ford, C.E., Russell, D.G., Craven, J.A., and Fisk, M.R.
1983: Olivine-liquid equilibria: temperature, pressure and composition dependence of the crystal/liquid cation partition coefficients for Mg, Fe^{+2}, Ca and Mn; Journal of Petrology, v. 24, p. 256–265.

Gass, I.G.
1958: Ultrabasic pillow lavas from Cyprus; Geological Magazine, v. 95, p. 241–251.

Gass, I.G.
1980: The Troodos massif: its role in the unravelling of the ophiolite problem and its significance in the understanding of constructive plate margin processes; *in* Panayiotou, A., Ophiolites: proceedings of the International Ophiolite Symposium, Cyprus, 1979, Cyprus Geological Survey Department, Nicosia, p. 23–35.

Green, D.H., Nichols, I.A., Viljoen, M., and Viljoen, R.
1975: Experimental demonstration of the existence of peridotitic liquids in earliest Archean magmatism; Geology, v. 3, p. 11–15.

Jarosewich, E., Nelen, J.A., and Norberg, J.A.
1979: Electron microprobe reference samples for mineral analyses; Smithsonian Contributions to Earth Sciences, v. 22, p. 68-72.

Lavrentiev, Y.G., and Pospelova, L.N., Sobolev, N.V., and Malikov, Y.I.
1974: Electron-probe X-Ray spectral analysis of rock-forming minerals; Industrial Laboratory (A translation of Zavodskaya Laboratoriya), v. 40, p. 811–814 (English), p. 657–660 (Russian).

Malpas, J. and Langdon, G.
1984: Petrology of the Upper Pillow Lava suite, Troodos ophiolite, Cyprus; *in* Gass, I.G., Lippard, S.J., and Shelton, A.W., Ophiolites and Oceanic Lithosphere, Geological Society of London, Special Publication 14, p. 155–167.

McCulloch, M.T. and Cameron, W.E.
1983: Nd-Sr isotopic study of primitive lavas from the Troodos ophiolite, Cyprus: evidence for a subduction-related setting; Geology, v. 11, p. 727–731.

Mehegan, J.M.
1988: Temporal, spatial, and chemical evolution of the Troodos ophiolite lavas, Cyprus: supra-subduction zone volcanism in the Tethys Sea; (PhD Thesis), Dalhousie University, Halifax, 700 p.

Miyashiro, A.
1973: The Troodos ophiolitic complex was probably formed in an island arc; Earth and Planetary Science Letters, v. 19, p. 218–224.

Naumov, V.B.
1979: Determination of concentration and pressure of volatiles in magmas from inclusions in minerals; Geochemistry International, v. 16, p. 33–40.

Nicholls, J.
1980: A simple thermodynamic model for estimating the solubility of H_2O in magmas; Contributions to Mineralogy and Petrology, v. 74, p. 211.

Nielsen, R.L. and Drake, M.J.
1979: Pyroxene-melt equilibria; Geochimica et Cosmochimica Acta, v. 43, p. 1259–1272.

Pantazis, T.M.
1980: Application of a non-linear mapping algorithm in petrographic classification on ophiolites; *in* Panayiotou, A., Ophiolites: proceedings of the International Ophiolite Symposium, Cyprus, 1979, Cyprus Geological Survey Department, Nicosia, p. 205–214.

Pearce, J.A.
1975: Basalt geochemistry used to investigate past tectonic environments on Cyprus; Tectonophysics, v. 25, p. 41–67.

Rautenschlein, M., Jenner, G.A., Hertogen, J., Hofman, A.W., Kerrich, R., Schmincke, H.-U., and White, W.M.
1985: Isotopic and trace element composition of volcanic glasses from the Akaki Canyon, Cyprus: implications for the origin of the Troodos ophiolite; Earth and Planetary Science Letters, v. 75, p. 369–383.

Robinson, P.T., Melson, W.G., O'Hearn, T., and Schmincke, H.-U.
1983: Volcanic glass compositions of the Troodos ophiolite, Cyprus; Geology, v. 11, p. 400–404.

Roedder, E.
1984: Fluid inclusions; Reviews in Mineralogy, v. 12, Mineralogical Society of America, Washington, 644 p.

Schilling, J.-G.
1989: Geochemical and isotopic variations along the Mid-Atlantic Ridge axis from 79°N to 0°N.; The Geology of North America: The Western North Atlantic Region, Geological Society of America, ??, v. M, p. 137–156.

Searle, D.L. and Vokes, F.M.
1969: Layered ultrabasic lavas from Cyprus; Geological Magazine, v. 106, p. 515–530.

Sobolev, V.S.
1976: The origin of magmas and magmatic rocks; *in* Sobolev, V.S., The problems of petrology of the earth's crust and upper mantle, Novosibirsk, p. 112–147 (in Russian).

Sobolev, A.V.
1983: Petrology and geochemistry of ultramafic magmas on the example of meimechites from the northern Siberian platform; (PhD Thesis), Vernadsky Institute of Geochemistry, Moscow, 250 p. (in Russian).

Sobolev, A.V.
1984: Theoretical and experimental investigation of the leakage from hermetic melt inclusions in Geochemistry of magmatic rocks; Abstracts, Moscow (in Russian).

Sobolev, A.V., Clocchiatti, R., and Dhamelincourt, P.
1983: Les variations de temperature et de la composition du magma et l'estimation de la pression partielle d'eau pendant la cristallisation de l'olivine dans les oceanites due Piton de La Fournais (Reunion); Comptes Rendus de L'Academie des Sciences, v. 296, p. 275–280.

Sobolev, A.V., Dmitriev, L.V., Barsukov, V.L., Nevsorov, V.N., and Slutsky, A.B.
1980: The formation conditions of high magnesium olivines from the monomineral fraction of Luna-24 regolith; Proceedings of the 11th Lunar and Planetary Science Conference, p. 105–116.

Sobolev, A.V. and Naumov, V.B.
1985: First direct proof of the presence of water in ultramafic melts and their estimated water content; Transactions of the USSR Academy of Sciences, Earth Science sections, v. 280, p. 102–105, translated from Russian from Doklay Akademii Nauk SSSR, 1985, v. 280, p. 458–461, by Scripta Technica, Inc., 1986.

Sobolev, A.V. and Slutsky, A.B.
1984: The composition and crystallization conditions of Siberian meimechites initial melt in connection with the general problem of ultramafic magmas; Geologia e Geophisica, v. 12, p. 97–109 (in Russian).

Sobolev, A.V., Tsameryan, O.P., Dmitriev, L.V., and Kononkova, N.N.

1986: Water-bearing komatiite as a new type of komatiite melt and origin of ultramafic lavas of the Troodos Mountains, Cyprus; Transactions of the USSR Academy of Sciences, Earth Science sections, v. 286, p. 160–163, translated from Russian from Doklay Akademii Nauk SSSR, 1986, v. 286, p. 422–425, by Scripta Technica, Inc., 1987.

Vukalovich, M.P.

1967: The thermophysical properties of water and water vapor; Moscow, Mashinostrosnie edition, 160 p., (in Russian).

The Physical Properties of Basalts from CCSP Drillholes CY-1 and CY-1A, Akaki Canyon, Cyprus

G.C. SMITH AND F.J. VINE

School of Environmental Sciences, University of East Anglia, Norwich, U.K.

Smith, G.C. and Vine, F.J., 1991: The physical properties of basalts from CCSP Drillholes CY-1 and CY-1A, Akaki Canyon, Cyprus; in Cyprus Crustal Study Project: Initial Report, Holes CY-1 and 1A, eds. Gibson, I.L., Malpas, J., Robinson, P.T., and Xenophontos, C.; Geological Survey of Canada, Paper 90–20, p. 219–234, 1991.

Abstract

Drillholes CY-1 and CY-1A provide a section of approximately 1,200 m into the Troodos ophiolite from the sediment/lava interface. On the basis of the physical properties measured, the section can be divided into three units with a transition zone between the upper and middle units from 165 m to 260 m, and a sharp fault-bounded contact between the middle and lower units at 750 m. These three units correlate with zones of low temperature sea floor weathering, zeolite facies, and greenschist facies metamorphism. The zone between the upper and middle units is characterized by an increase in porosity, conductivity, NRM intensity and susceptibility; a velocity inversion and a reduction in the rate of change of many of the physical properties with depth. The faulted contact between the middle and lower units is characterized by a marked reduction in NRM intensity. Qualitatively, variations in physical properties and lithology with depth are comparable to those observed from geophysical logging of DSDP Drillhole 504B. However, a comparison of laboratory measurements on samples from CY-1 and CY-1A with similar measurements on DSDP samples shows the Troodos rocks to have anomalously low velocities and densities, anomalously high porosity and conductivity and high NRM intensity and susceptibility. The upper 1 km of the Troodos ophiolite thus provides a poor analogue of the upper 1 km of the oceanic crust sampled by the DSDP in terms of the absolute values of various physical properties.

Résumé

Les trous de forage CY-1 et CY-1A présentent une coupe d'environ 1200 m dans l'ophiolite de Troodos à l'interface sédimentaire et coulées de laves. A la lumière des propriétés physiques observées, cette coupe peut être subdivisée en trois unités dont une zone de transition entre les unités supérieures et celle du milieu, de 165 à 260 m, et un contact en faille abrupt entre les unités du milieu et celles inférieure, à 750 m. Ces trois unités sont corrélées aux zones de dégradation à basse température du plancher océanique, au faciés à zéolite, et à un métamorphisme vers le facies schiste vert. La zone située entre les unités supérieures et celles du milieu est caractérisée par une augmentation de la porosité, de la conductivité, de l'intensité et de la susceptibilité en MNR; une inversion de la vitesse et une réduction du taux de changement de plusieurs des propriétés physiques avec une augmentation de la profondeur. Le contact en faille situé entre les unités du milieu et celles inférieure est caractérisé par une forte réduction de l'intensité en MNR. Qualitativement les changements des propriétés physiques et de la lithologie avec la profondeur sont comparables à celles observées dans la description géophysique du trou de forage 504B de DSDP. Une comparaison des échantillons provenant du CY-1 et du CY-1A mesurés en laboratoire et ayant les mêmes mesures que les échantillons du DSDP révèle cependant que les roches de Troodos comportent des anomalies par leur densité et leur vitesse faibles, leur hautes porosité et conductivité et leur hautes intensité et susceptibilité en MNR. En termes de valeur absolue des propriétés physiques, le kilomètre supérieur de l'ophiolite de Troodos présente ainsi une pauvre analogie avec le kilomètre supérieur de la croûte océanique prise en échantillon par le DSDP.

INTRODUCTION

This paper summarizes and discusses measurements of the physical properties of samples from the Cyprus Crustal Study Project (CCSP) Drillholes CY-1 and CY-1A into the Troodos ophiolite.

Drillhole CY-1, situated in Akaki Canyon, on the northern flank of the Troodos Massif, extends 474.88 m into the extrusive section of the ophiolite from the sediment-lava interface through a sequence of basaltic pillow lavas and massive flows intruded by several dykes. Drillhole CY-1A extends to a depth of 701.19 m at a site further up Akaki Canyon, at an estimated stratigraphic level in the section of 500 m, i.e. the top is approximately equivalent to the base of CY-1.

The drillhole penetrates pillow lavas and massive flows and an increasing proportion of dykes down the section, terminating in the 'Basal Group' of the published geological maps, the transition between the extrusive section and the sheeted dyke complex. Significant amounts of pyrite occur sporadically in veins below 250 m. Between 215 and 250 m, drilling problems were encountered in CY-1A, as the drill string penetrated a fault zone, possibly a listric fault (Varga and Moores, 1985) although at this point the northern flank of the Troodos is relatively unrotated. Thus by stacking CY-1 on CY-1A with a gap of approximately 25 m, the two drillholes should provide, by analogy, a reference section of approximately 1,200 m through oceanic seismic layers 2A and 2B and possibly into layer 2C (Houtz and Ewing, 1976).

The properties measured were compressional (P) and shear (S) wave velocities (V_p and V_s), saturated bulk density (ρ_s) and grain density (ρ_g), porosity (ϕ), electrical conductivity (σ), intensity (J_{NRM}) and inclination (I_{NRM}) of the remanent magnetization, and magnetic susceptibility (χ). In addition the following parameters were derived from the above observations: Poisson's ratio, Archie's exponent (m) and the Koenigsberger ratio (Q_n).

Laboratory data on the physical properties of rocks are essential to the interpretation of surface and downhole geophysical measurements. The Deep Sea Drilling Project (DSDP) has sampled layers 2A and 2B extensively but has only recently sampled layer 2C (Anderson et al. 1982) in Drillhole 504B. This drillhole provided samples from a 1075.5 m section through the extrusive layer into the sheeted dyke complex. In this paper we discuss the physical properties of rocks from CY-1 and CY-1A according to lithology and depth in the section, and make a preliminary comparison with values measured on DSDP samples, in particular from 504B.

Experimental Procedure

Samples were taken at approximately 5 m intervals down CY-1 and 10 m intervals down the CY-1A drill core, providing 142 samples for physical property measurements. The measured samples were minicores of 25.4 mm diameter and 10 to 30 mm length.

NRM intensities and inclinations were measured on a Digico Spinner Magnetometer. The measurement of intensity is accurate to better than ±5%. The susceptibilities of the cores were measured on a commercial susceptibility bridge, also accurate to better than ±5%.

A subset of 119 samples of known length and diameter were dried at 80°C under vacuum, weighed, saturated with seawater under vacuum and reweighed. Dry and saturated bulk densities, grain density and effective (interconnected) porosity were then calculated. Dry and saturated bulk densities are estimated to be accurate to $\pm 10\,kg\,m^{-3}$.

The grain or matrix density is calculated by subtracting the mass and volume of the pore fluid and recomputing the density. Accurate porosity results are difficult to obtain. Firstly, it is difficult to ensure that rocks are completely dried before saturation. Secondly, a potentially greater source of error is the fact that it is difficult to ensure that the rocks are fully saturated. We estimate that the measured porosities are accurate to within −10% of the true porosity. Because the porosity is underestimated the calculated grain density will also be low. The maximum resulting error in the value of grain density will be up to $-160\,kg\,m^{-3}$, based on a maximum error of 10% in the porosity for the most porous sample, but will typically be considerably less than this.

A further subset of 47 samples representing the range of textural and mineralogical variations, densities and porosities occurring was selected for seismic velocity and electrical conductivity measurements. The compressional and shear wave velocities and electrical conductivities were determined at a range of pressures up to 0.1 GPa at 20°C with the pore space vented to the atmosphere, allowing water to drain from microcracks as the confining pressure was increased. Seismic velocities were measured by a pulse transmission technique (Birch, 1960). Conductivities were determined from the conductance of the sample at 1582 Hz measured on a Wayne-Kerr conductivity bridge.

The sample was clamped between two steel transducer holders, which act as electrodes for the conductivity measurements, and isolated from the confining pressure medium, in this case oil ('Plexol'), by a PTFE ('Teflon') sleeve.

P and S-wave velocities are estimated to be accurate to $\pm 0.04\,km\,s^{-1}$ from a consideration of the errors incurred in measuring sample dimensions and, more critically, in 'picking' the onset of the P or S-wave. Electrical conductivities are estimated to be accurate to ±5%.

RESULTS

The results of the physical property measurements are summarized in Table 1 for the three lithological classes identified in the drillholes: pillow lavas, massive flows and dykes. The lithological data are based on CCSP core descriptions (Horne and Robinson, 1984, 1986), the Lithologic Unit Summary (Robinson and Gibson, 1990), and visual inspection of the samples.

Property	n	Mean	SE	SD	Geom. Mean
Pillow Lavas					
Comp. vel. (0.05 GPa)(km s^{-1})	16	3.47	0.12	0.49	
Shear vel. (0.05 GPa)(km s^{-1})	16	1.83	0.08	0.30	
Poisson's ratio	16	0.308	0.008	0.032	
Bulk density (kg m^{-3})	55	2,264	17	125	
Grain density (kg m^{-3})	55	2,558	23	171	
Porosity (% vol.)	55	18.87	0.78	5.79	18.06
Elect. cond. (0.05 GPa)(mS m^{-1})	18	83.5	10.6	45.0	72.1
Archie's exp.	18	2.40	0.10	0.41	
NRM intensity (A m^{-1})	61	10.87	1.18	9.20	7.74
Inclination of NRM* (degrees)	61	25.9	1.6	12.7	
Susceptibility (10^{-3} S.I. Units)	61	24.95	2.89	22.6	18.56
Koenigsberger ratio	61	16.63	1.61	12.60	11.70
Massive Flows					
Comp. vel. (0.05 GPa)(km s^{-1})	13	3.55	0.18	0.66	
Shear vel. (0.05 GPa)(km s^{-1})	13	1.96	0.11	0.38	
Poisson's ratio	13	0.281	0.006	0.021	
Bulk density (kg m^{-3})	27	2,297	24	123	
Grain density (kg m^{-3})	27	2,594	28	145	
Porosity (% vol.)	27	18.74	1.29	6.72	17.62
Elect. cond. (0.05 GPa)(mS m^{-1})	14	118.2	20.6	77.1	92.2
Archie's exp.	14	2.26	0.09	0.34	
NRM intensity (A m^{-1})	44	10.90	1.78	11.82	4.69
Inclination of NRM* (degrees)	43	23.2	2.0	12.9	
Susceptibility (10^{-3} S.I. Units)	44	27.07	3.55	23.52	18.67
Koenigsberger ratio	44	13.40	2.03	13.44	6.68
Dykes					
Comp. vel.(0.05 GPa)(km s^{-1})	15	4.82	0.15	0.58	
Shear vel.(0.05 GPa)(km s^{-1})	15	2.62	0.09	0.35	
Poisson's ratio	15	0.289	0.004	0.017	
Bulk density (kg m^{-3})	37	2,580	19	114	
Grain density (kg m^{-3})	37	2,772	15	89	
Porosity (% vol.)	37	10.99	0.81	4.90	9.74
Elect. cond. (0.05 GPa)(mS m^{-1})	14	15.53	5.20	19.46	8.41
Archie's exp.	14	2.61	0.08	0.29	
NRM intensity (A m^{-1})	37	1.99	0.46	2.81	1.01
Inclination of NRM* (degrees)	37	32.5	2.5	15.5	
Susceptibility (10^{-3} S.I. Units)	37	52.82	5.16	31.37	35.06
Koenigsberger ratio	37	1.41	0.38	2.29	0.80

Table 1: Physical Properties of Basalts from CCSP Drillholes CY-1/1A. * The values given are for the modulus of the inclination.

Density and Porosity

Figures 1, 2 and 3 show histograms of bulk and grain density and porosity for 119 samples by lithology. The bulk densities of 55 pillow lava samples range from 2,041 kg m^{-3} to 2,594 kg m^{-3} with a mean and standard deviation of individual values of 2,264 ± 125 kg m^{-3}. Part of the variation in bulk density is due to the very high porosity which ranges from 7.5% to 39.0% with a geometric mean of 18.1%. The grain density ranges from 2,205 kg m^{-3} to 2,917 kg m^{-3} with a mean of 2,558 ± 171 kg m^{-3}.

The bulk densities of 27 samples from the massive flows range from 2,002 kg m^{-3} to 2,697 kg m^{-3} with a mean of 2,297 ± 123 kg m^{-3}. The grain densities range from 2,357 kg m^{-3} to 2,935 kg m^{-3} with a mean of

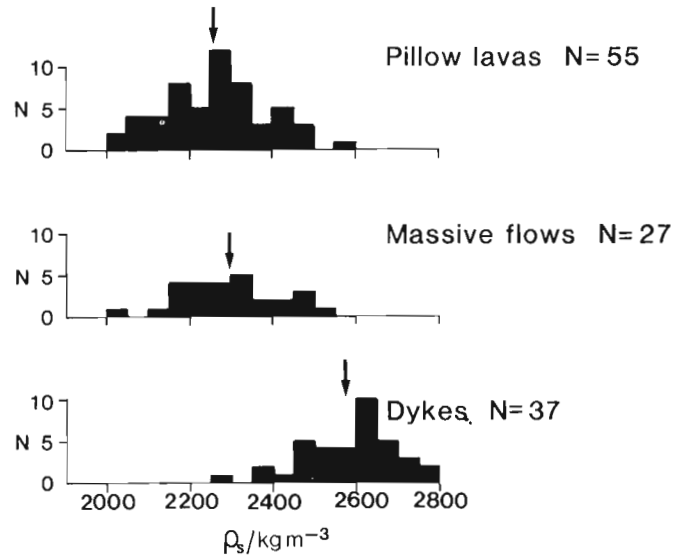

Figure 1: Histograms of saturated bulk density for each major lithology. N is the number of samples. Mean values are arrowed.

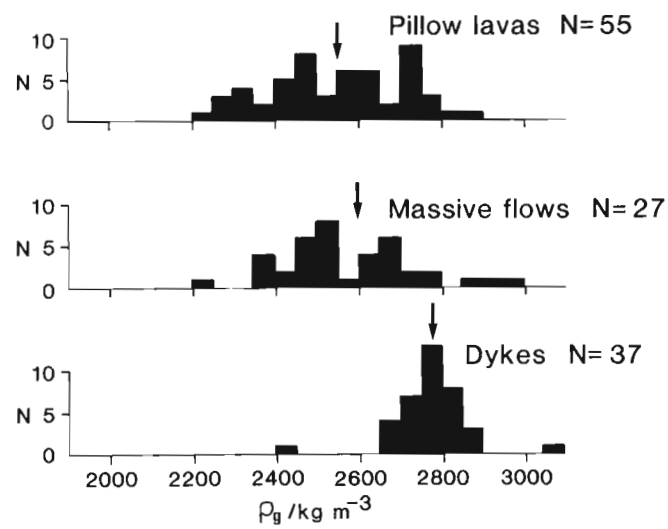

Figure 2: Histograms of grain density for each major lithology. N is the number of samples. Mean values are arrowed.

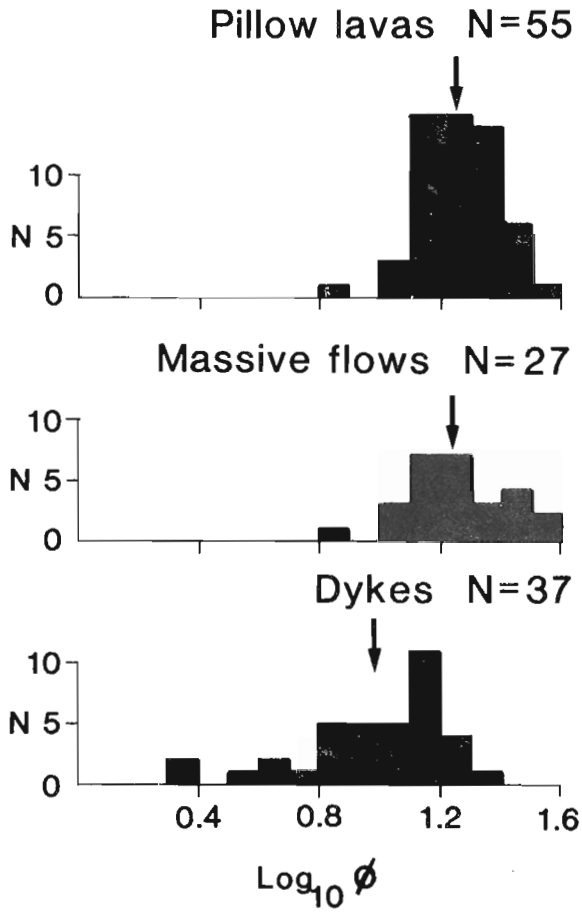

Figure 3: Histograms of $\log_{10}$ (percent porosity) for each major lithology. N is the number of samples. Mean values are arrowed.

$2{,}594 \pm 145\,kg\,m^{-3}$, and porosities range from 7.0% to 33.8% with a geometric mean of 17.6%.

The massive flows have slightly higher mean bulk and grain density than the pillow lavas, but a similar mean porosity. The dykes are of significantly higher bulk and grain density than either the pillow lavas or the massive flows, and have a lower although still notably high porosity. The bulk densities of 37 samples from dykes range from $2{,}278\,kg\,m^{-3}$ to $2{,}772\,kg\,m^{-3}$ with a mean of $2{,}580 \pm 114\,kg\,m^{-3}$, grain densities from $2{,}443\,kg\,m^{-3}$ to $3{,}056\,kg\,m^{-3}$ with a mean of $2{,}772 \pm 89\,kg\,m^{-3}$ and porosities from 2.15% to 23.6% with a geometric mean of 9.74%.

The wide range of grain densities observed reflects wide variations in the degree and style of alteration. In particular, in the upper 200 m of CY-1, averaging shows a low bulk density of $2{,}225\,kg\,m^{-3}$ associated with low grain density thought to result from low temperature submarine weathering, whereas averaging of densities for samples from CY-1 below 260 m gives a mean value of $2{,}360\,kg\,m^{-3}$. Between 200 m and 260 m densities increase with depth. The porosities between 85 m and 215 m are relatively low due to the infilling of fractures and vesicles with clays, zeolites and carbonate.

The bulk density and porosity depth profiles (Figures 4 and 5) show the increase in density below 200 m and a decrease in porosity below 340 m reflecting the transition from predominantly sea floor weathered pillowed lavas at the top of CY-1 to zeolite facies pillows and flows, and to greenschist facies dykes in the lower 100 m of CY-1A. In particular at 250 m in CY-1A (i.e. 750 m depth in the section) the increase in the proportion of dykes is marked by an increase in density and decrease in porosity. Between 375 m and 575 m in CY-1A (875 m and 1075 m depth in the section) lower densities and higher porosities are typically associated with massive flows.

Compressional and Shear Wave Velocities

Compressional (P) and shear (S) wave velocities and Poisson's ratios are given in Table 2 at a confining pressure of 0.05 GPa which is considered to be representative of *in situ* pressures in the oceanic crust. There is a reasonable correlation between the velocities and densities for the samples. The variability in seismic velocities can be explained firstly by variations in mineralogy and thus in grain density, and secondly by variations in porosity.

The P and S wave velocities in the 16 pillow lava samples range from $2.74\,km\,s^{-1}$ to $4.31\,km\,s^{-1}$ and from $1.29\,km\,s^{-1}$ to $2.36\,km\,s^{-1}$ respectively with mean values of $3.47 \pm 0.49\,km\,s^{-1}$ and $1.83 \pm 0.30\,km\,s^{-1}$. The mean Poisson's ratio is 0.308 ± 0.032. Velocities in the 13 massive flow samples range from $2.72\,km\,s^{-1}$ to $4.83\,km\,s^{-1}$ for P-waves and $1.47\,km\,s^{-1}$ to $2.66\,km\,s^{-1}$ for S-waves with mean values of $3.55 \pm 0.66\,km\,s^{-1}$ and $1.96 \pm 0.38\,km\,s^{-1}$ respectively. The mean Poisson's ratio is 0.281 ± 0.021. The mean velocities in the massive flows are slightly higher and the Poisson's ratio slightly lower than in the pillow lavas. However, velocities vary widely so that the two lithological classes are statistically indistinguishable on the basis of their elastic properties. The velocities in the dykes, conversely, are significantly higher than in either the pillow lavas or the massive flows. P and S-wave velocities from 15 samples range from $3.20\,km\,s^{-1}$ to $5.59\,km\,s^{-1}$ and $1.68\,km\,s^{-1}$ to $3.03\,km\,s^{-1}$ respectively with mean values of $4.82 \pm 0.58\,km\,s^{-1}$ and $2.62 \pm 0.35\,km\,s^{-1}$. The mean Poisson's ratio is 0.289 ± 0.017. The higher velocities reflect the higher grain densities and lower porosities of the dykes.

Seismic velocities in general increase down the section (Figure 6) with a P-wave velocity gradient ranging from as much as $4.0\,km\,s^{-1}\,km^{-1}$ in the top 165 m to $1.0\,km\,s^{-1}\,km^{-1}$ in the dykes, reflecting the decrease in porosity, increase in grain density and changes in lithologies with depth. Superimposed on the general trend there are higher velocities between 70 m and 165 m in CY-1 which correlate with the lower porosities in this part of the section, giving a velocity inversion at 165 m. An increase in velocities at about 250 m in CY-1A correlates with the increase in dyke density, although lower velocities are associated with massive flows between 375 and 575 m.

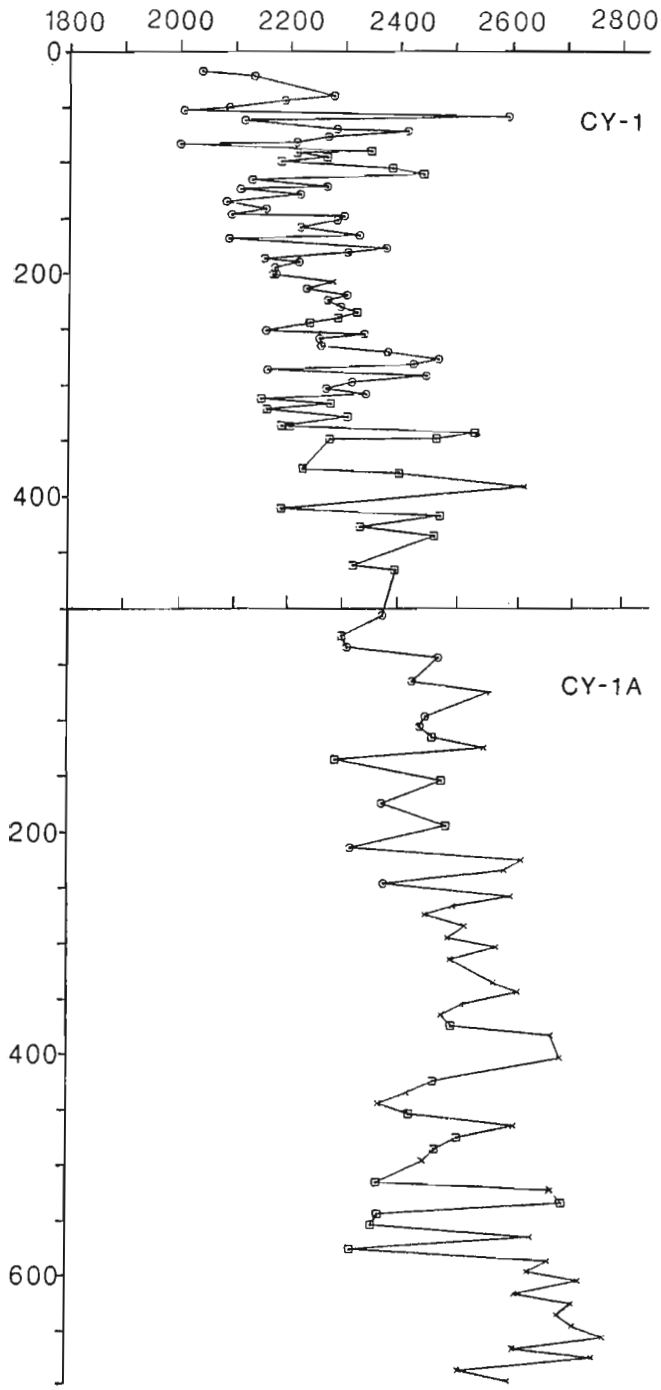

Figure 4: Saturated bulk densities ($kg.m^{-3}$) vs. depth (m) for CY-1 and CY-1A. Samples are coded according to lithology as follows: Circles = pillow lavas, squares = massive flows, X = dykes and + = intrusive (sill).

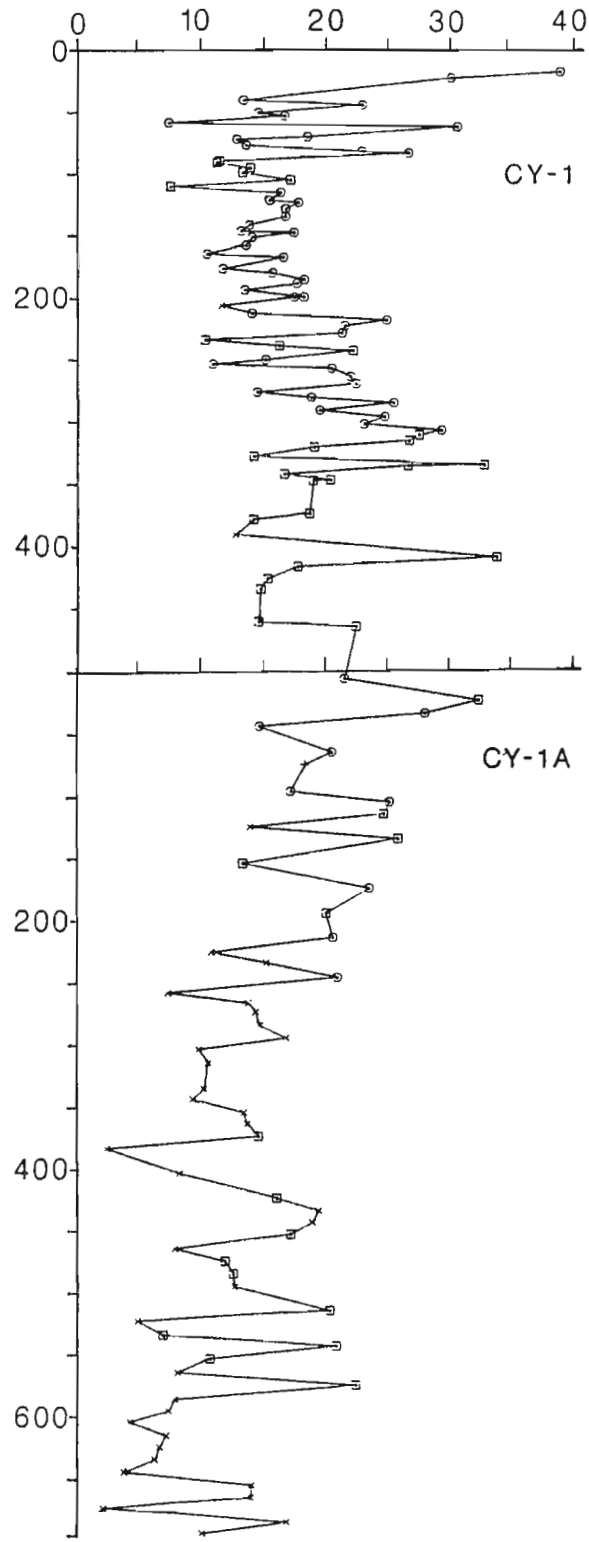

Figure 5: Porosity (%) vs. depth (m) for CY-1 and CY-1A. Symbols as for Figure 4.

Lithology	Depth (m)	Sat. Bulk Density ($kg\,m^{-3}$)	P-Wave Velocity ($km\,s^{-1}$)	S-Wave Velocity ($km\,s^{-1}$)	Poisson's ratio
CY-1					
P. Lava	22.41	2,135	2.74	1.29	0.358
P. Lava	50.35	2,090	2.82	1.51	0.299
P. Lava	71.82	2,414	3.68	1.78	0.347
M. Flow	89.60	2,347	3.20	1.79	0.272
M. Flow	110.28	2,443	3.71	2.09	0.268
P. Lava	115.10	2,131	3.38	1.87	0.279
P. Lava	121.32	2,267	3.54	1.92	0.292
P. Lava	141.18	2,156	3.23	1.78	0.282
P. Lava	151.25	2,285	3.39	1.93	0.260
P. Lava	164.92	2,326	4.10	2.16	0.308
P. Lava	167.57	2,089	2.93	1.55	0.306
P. Lava	185.64	2,154	3.10	1.45	0.360
Dyke	206.53	2,278	3.20	1.68	0.310
P. Lava	257.48	2,254	3.16	1.51	0.352
P. Lava	276.35	2,470	3.32	1.84	0.278
M. Flow	311.55	2,149	3.38	1.67	0.339
M. Flow	315.99	2,275	2.82	1.53	0.291
M. Flow	328.15	2,306	2.72	1.47	0.316
M. Flow	347.62	2,467	3.10	1.74	0.270
M. Flow	378.90	2,400	3.37	1.89	0.271
Dyke	390.89	2,623	4.37	2.28	0.313
M. Flow	426.68	2,329	3.14	1.79	0.259
M. Flow	461.30	2,317	3.14	1.72	0.286
CY-1A					
P. Lava	44.24	2,474	4.25	2.36	0.277
P. Lava	96.84	2,452	4.31	2.24	0.315
Dyke	125.15	2,557	4.65	2.55	0.285
P. Lava	174.85	2,374	3.82	1.99	0.314
Dyke	225.66	2,623	4.87	2.52	0.317
P. Lava	246.62	2,377	3.80	2.08	0.286
Dyke	258.08	2,604	4.79	2.58	0.296
Dyke	274.54	2,453	4.41	2.40	0.290
Dyke	304.03	2,579	4.97	2.77	0.275
Dyke	344.25	2,618	4.82	2.59	0.297
M. Flow	375.02	2,501	4.36	2.39	0.285
Dyke	404.09	2,694	5.35	3.00	0.271
M. Flow	454.11	2,426	4.34	2.44	0.269
M. Flow	485.95	2,472	4.83	2.66	0.282
Dyke	522.84	2,678	5.59	2.97	0.303
M. Flow	544.05	2,370	4.07	2.33	0.256
Dyke	596.55	2,673	5.19	2.90	0.273
Dyke	604.24	2,727	5.38	3.03	0.268
Dyke	635.01	2,690	5.34	2.89	0.293
Dyke	665.68	2,611	4.65	2.52	0.292
Dyke	694.75	2,602	4.76	2.68	0.268

Table 2: Seismic Velocities and Poisson's ratios at 0.05 GPa. P. Lava = Pillow Lava; M. Flow = Massive Flow.

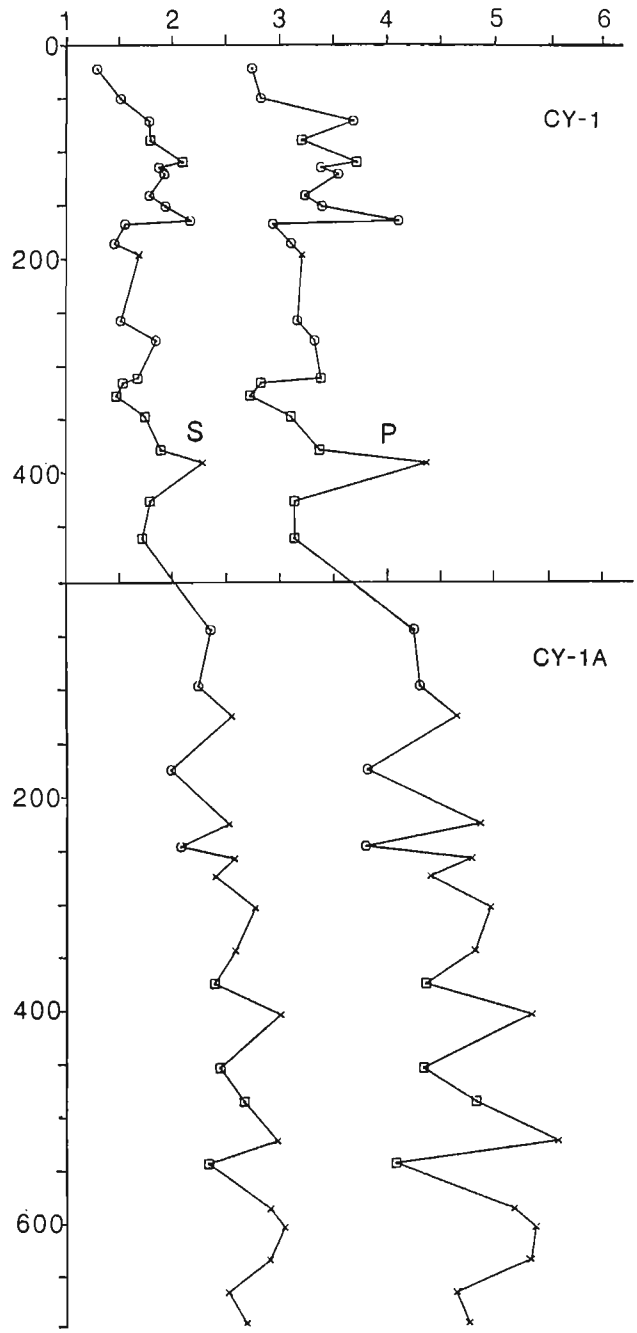

Figure 6: Seismic velocities ($km.s^{-1}$) vs. depth (m) for CY-1 and CY-1A. Symbols as for Figure 4.

Velocities measured under simulated crustal conditions in the laboratory will be systematically higher than *in situ* velocities measured by logging or surface geophysical experiments due to the effect of macroscopic fractures and voids which are not represented in the sample set. Smith and Vine (1987b) describe a substantial discrepancy of as much as $1.0\,km\,s^{-1}$ between P-wave velocities determined from a downhole seismic experiment at CCSP Drillhole CY-2A and laboratory measurements on samples from the drillhole itself through a sequence of massive flows and basaltic intrusives. However, the laboratory velocities measured on samples from CY-1 and CY-1A are low compared to the typical layer 2A, 2B, and 2C velocities of $3.64\,km\,s^{-1}$, $5.19\,km\,s^{-1}$ and $6.09\,km\,s^{-1}$ (Houtz and Ewing, 1976). Further, although the oceanic layer 2A-2B interface is typically defined by high amplitude reflections implying a strong velocity and density contrast, there are no

discontinuities in velocities and densities with depth in the Cyprus section which give a reflection coefficient of sufficient magnitude to correspond to the 2A-2B interface implying that the 2A-2B interface *in situ* reflects a decrease in the amount of macroscopic fractures, rather than change in the velocities or densities of the rocks themselves on a sub-macroscopic level. The crustal section represented in Drillholes CY-1 and CY-1A provides a poor seismic analogue of oceanic seismic layers 2A and 2B having anomalously low velocities especially when cracks are taken into account, and on the basis of the absolute the basis of the absolute velocities measured here does not penetrate layer 2C.

Electrical Conductivity

Observed electrical conductivities, porosities and calculated values of Archie's exponent 'm' are given in Table 3. Conductivities are given at a confining pressure of 0.05 GPa.

The samples are saturated with seawater since it now seems clear that the oceanic crust is saturated with seawater to depths of several kilometres and most probably to the base of the crust (Drury, 1979). The electrical conductivity of laboratory samples depends upon a combination of conduction through pore-fluids, clay mineral conduction and mineral semi-conduction. Where pore-fluid conduction is dominant, the relationship between conductivity and porosity is given by Archie's law (Archie, 1942) which states that:

$$\sigma = a\sigma_f \phi_v^m$$

where σ_f is the conductivity of the pore-fluid (here seawater; $\sigma_f = 4.54\,\mathrm{S\,m^{-1}}$), ϕ_v is the interconnected porosity expressed as a fraction of the rock's volume, and 'a' and 'm' are constants. 'a' is a dimensionless constant typically close to and often taken as 1, and the exponent 'm' has been shown from analogue simulation of porosity using resistor arrays (Shankland and Waff, 1974) to be equal to 1 if the porosity is in the form of narrow ('low aspect-ratio') cracks, and 2 if in the form of rounded voids. However previous measurements on fresh and mineralized lavas (Smith and Vine, 1987a) have shown that in practice the value of 'm' may be as high as 3 where pore-fluid conduction is through randomly connected rounded vesicles. A good correlation between 'm' and porosity was noted. Assuming an Archie relationship between electrical conductivity and porosity, 'm' can be calculated and may give an insight into the nature of the porosity.

The conductivities of the 18 pillow lava samples range from 20.5 mS m^{-1} to 179.0 mS m^{-1} with a geometric mean of 72.1 mS m^{-1}. The mean value of 'm' derived from Archie's law assuming 'a' = 1 and a pore-fluid conductivity of 4.54 S m^{-1} is 2.40 ± 0.41 suggesting that conduction in rounded voids is dominant over conduction through narrow cracks.

The conductivity of the 14 massive flow samples ranges from 22.6 to 278.3 mS m^{-1} with a geometric mean conductivity of 92.2 mS m^{-1}, comparable to the pillow lavas. The Archie's exponent 'm' also has a similar mean value of 2.26 ± 0.34. There is a positive correlation between Archie's exponent and porosity for the pillow lavas and massive flows suggesting that rounded voids constitute a higher proportion of the total porosity in the more porous samples. In CY-1A the conductivity of the pillow lavas and massive flows generally decreases down the section with a decrease in porosity (Figures 5 and 7). Low conductivities are also measured in

Lithology	Depth (m)	Electrical Cond. (mS m^{-1})	Porosity (%)	Archie's Exponent 'm'
CY-1				
P. Lava	22.41	134.0	30.1	2.94
P. Lava	50.35	99.1	14.6	1.99
P. Lava	53.10	179.1	16.8	1.81
P. Lava	71.82	49.7	12.9	2.21
P. Lava	76.70	66.5	13.7	2.12
M. Flow	98.90	76.0	13.4	2.03
P. Lava	121.32	63.5	15.6	2.30
P. Lava	141.18	66.4	13.9	2.15
P. Lava	151.25	57.0	14.1	2.24
P. Lava	164.92	48.3	10.5	2.02
P. Lava	185.64	115.8	18.3	2.16
Dyke	206.53	70.0	11.7	1.94
P. Lava	223.09	100.0	21.6	2.49
M. Flow	239.01	144.5	16.3	1.90
P. Lava	257.48	114.7	20.5	2.32
P. Lava	276.35	93.0	14.5	2.02
P. Lava	307.68	166.2	29.3	2.70
M. Flow	311.55	221.0	27.5	2.34
M. Flow	315.99	221.3	26.7	2.29
M. Flow	335.85	278.3	32.8	2.51
M. Flow	347.62	110.2	20.4	2.34
M. Flow	378.90	87.0	11.2	1.81
M. Flow	426.68	119.5	15.4	1.94
M. Flow	434.98	105.8	14.8	1.97
M. Flow	461.30	118.0	14.6	1.90
CY-1A				
P. Lava	44.24	20.5	14.7	2.82
P. Lava	96.84	34.2	17.3	2.78
Dyke	125.15	8.74	14.0	3.12
P. Lava	174.85	34.6	23.6	3.37
Dyke	225.66	12.5	10.9	2.66
P. Lava	246.62	61.5	21.0	2.76
Dyke	258.08	4.35	7.4	2.67
Dyke	274.54	19.4	14.4	2.82
Dyke	304.03	7.00	9.9	2.80
Dyke	344.25	8.09	9.4	2.68
M. Flow	375.02	22.6	14.7	2.76
Dyke	404.09	8.07	8.4	2.55
M. Flow	454.11	29.7	17.3	2.87
M. Flow	485.95	22.8	12.7	2.56
Dyke	522.84	1.62	5.0	2.65
M. Flow	544.05	97.0	20.9	2.46
Dyke	596.55	4.85	7.9	2.67
Dyke	604.24	1.36	4.3	2.58
Dyke	635.01	2.63	6.3	2.70
Dyke	665.68	44.2	13.9	2.35
Dyke	694.75	24.5	10.1	2.27

Table 3: Electrical Conductivity at 0.05 GPa. P. Lava = Pillow Lava; M. Flow = Massive Flow.

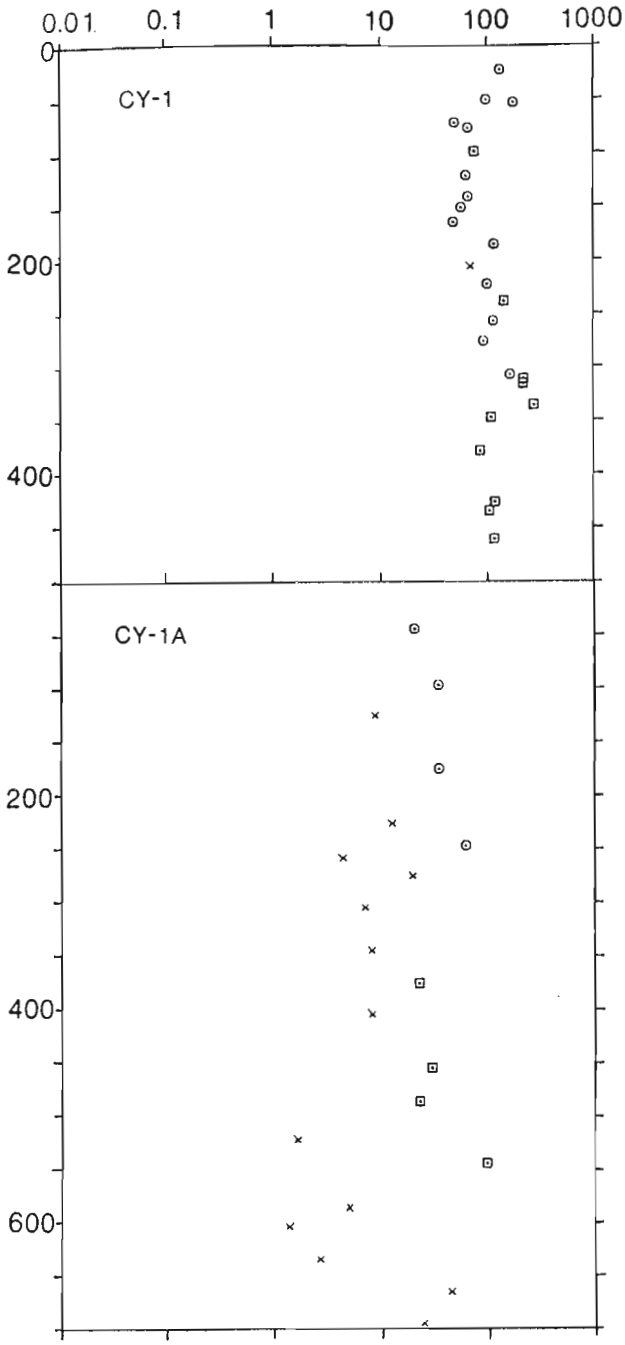

Figure 7: Electrical conductivity ($mS.m^{-1}$) vs. depth (m) for CY-1 and CY-1A. Symbols as for Figure 4.

samples from 70 m to 165 m in CY-1 within the low porosity zone.

Conductivities in the dykes range from 1.36 $mS\,m^{-1}$ to 70.0 $mS\,m^{-1}$ with a geometric mean of 14 samples of 8.41 $mS\,m^{-1}$, an order of magnitude lower than the pillow lavas and massive flows. The mean value of Archie's exponent is 2.61 ± 0.29 implying that despite the lower porosity, conduction is primarily through rounded voids, as it is in the pillows and flows. The high value of m suggests that the rounded voids are relatively poorly interconnected. The conductivity falls at 750 m with a decrease in porosity from the extrusives above to the dykes below. There is a gradual decrease in conductivity with depth as the deeper dykes have lower porosity.

In situ conductivities will be greater than the values determined from these laboratory measurements due to additional conduction in macroscopic pores and fractures not represented in the laboratory sample set. Discrepancies between laboratory and, for example, logging data can give an indication of the extent of large scale fracturing in the crust if the conductivity of the pore fluid is known.

Lithology	N	J_{NRM} (Am^{-1}) Arith.	Geom.	$\chi(10^{-3})$,S.I. Arith.	Geom.	Q_n Arith.	Geom.
Pillow Lava	61	10.87	7.74	24.95	18.56	16.63	11.70
Massive Flow	44	10.90	4.69	27.07	18.67	13.40	6.68
Intrusive Dyke	37	1.99	1.01	52.82	35.60	1.41	0.80

Table 4: Mean Values of Magnetic Properties.

Magnetic Properties

Figure 8 shows histograms of the magnetic properties. NRM intensity, susceptibility, and Koenigsberger ratios are log-normally distributed and it is usual practice therefore to give the geometric mean as a representative value of the sample set. However, in considering the potential of a unit as a source layer for marine anomalies it is the arithmetic mean which is applicable (Harrison, 1976). Therefore in Table 4 we have summarized both mean values of NRM, susceptibility and Koenigsberger ratio.

The magnetic properties of the pillow lavas and the massive flows are comparable. The mean NRM intensity is high, (typically approximately 10 $A\,m^{-1}$) and the susceptibility relatively low (approximately 25×10^{-3} S.I. units) so that the Koenigsberger ratio is of the order of 10.

The dykes have comparable susceptibilities to the immediately overlying pillow lavas and massive flows, but much lower NRM intensities of around 1 $A\,m^{-1}$ giving a Koenigsberger ratio of the order of 1, an order of magnitude lower than the extrusives.

However, of greater significance than a comparison of the average magnetic properties of the various lithological classes is a consideration of variations in the magnetic properties with depth (Figures 9–12).

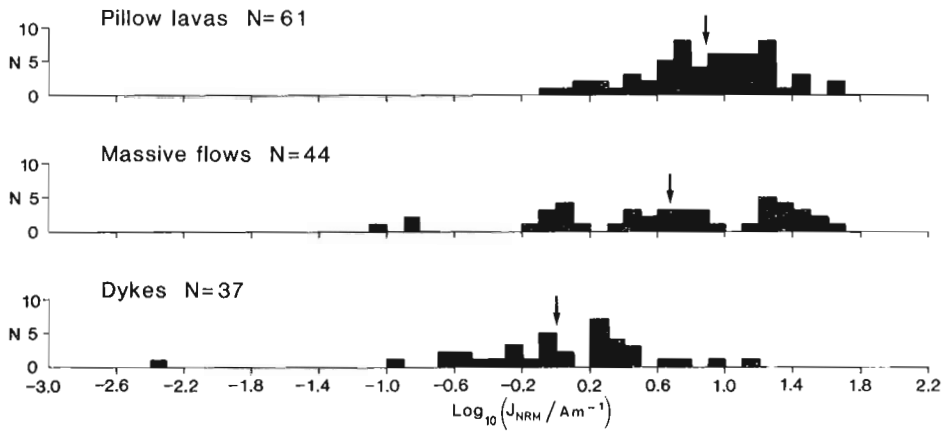

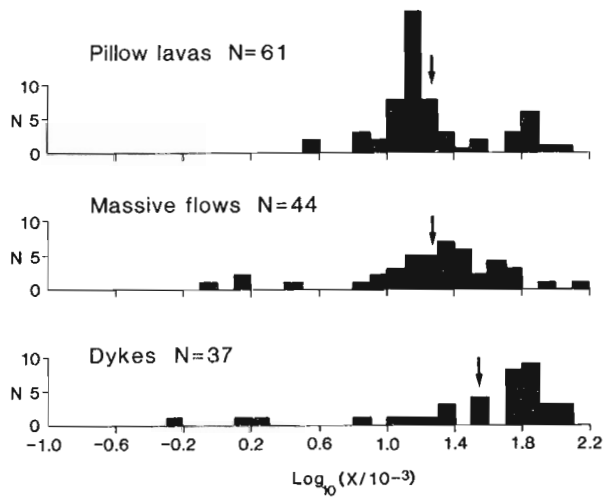

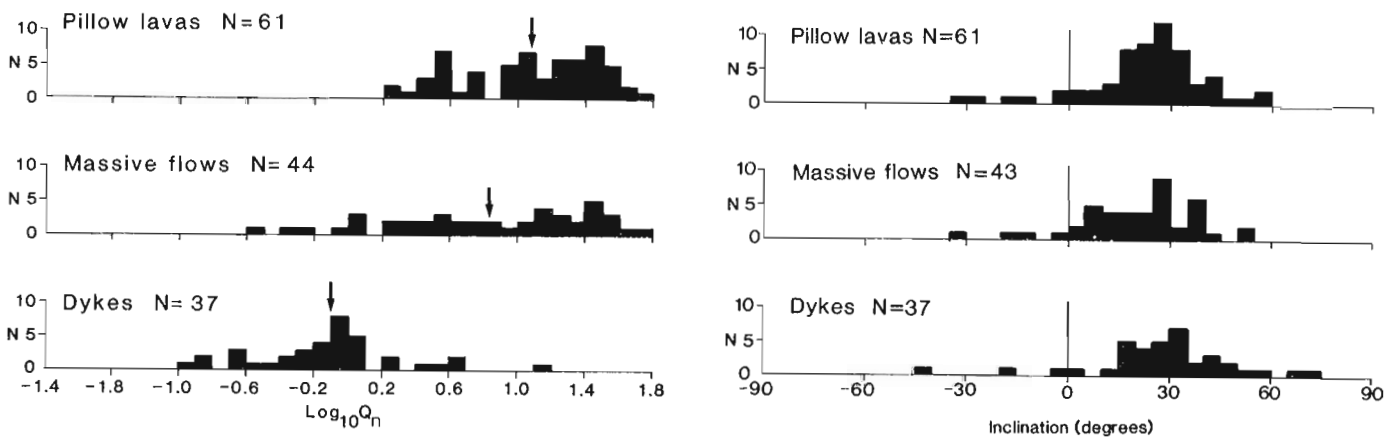

Figure 8: Histograms of $\log_{10}$ (NRM intensity), $\log_{10}$ (magnetic susceptibility), $\log_{10}$ (Koenigsberger ratio) and NRM inclination. N is the number of samples. Geometric mean values are arrowed.

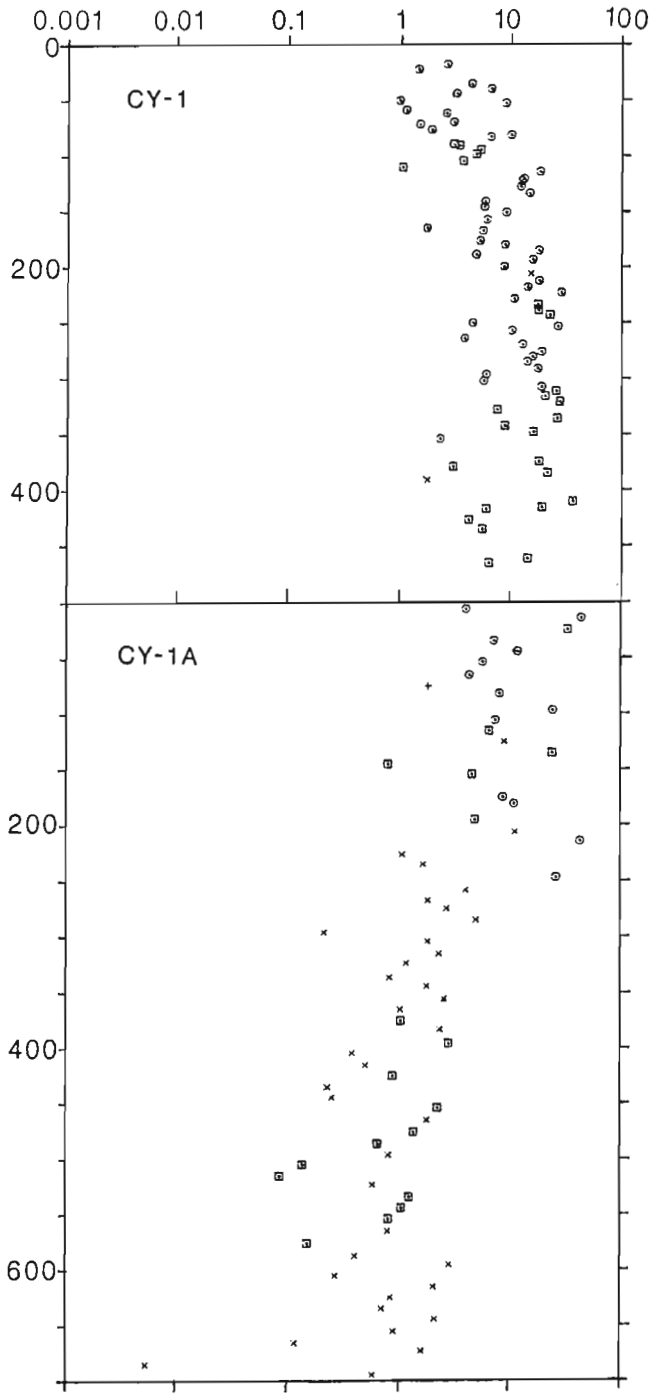

Figure 9: NRM intensity ($A.m^{-1}$) vs. depth (m) for CY-1 and CY-1A. Symbols as for Figure 4.

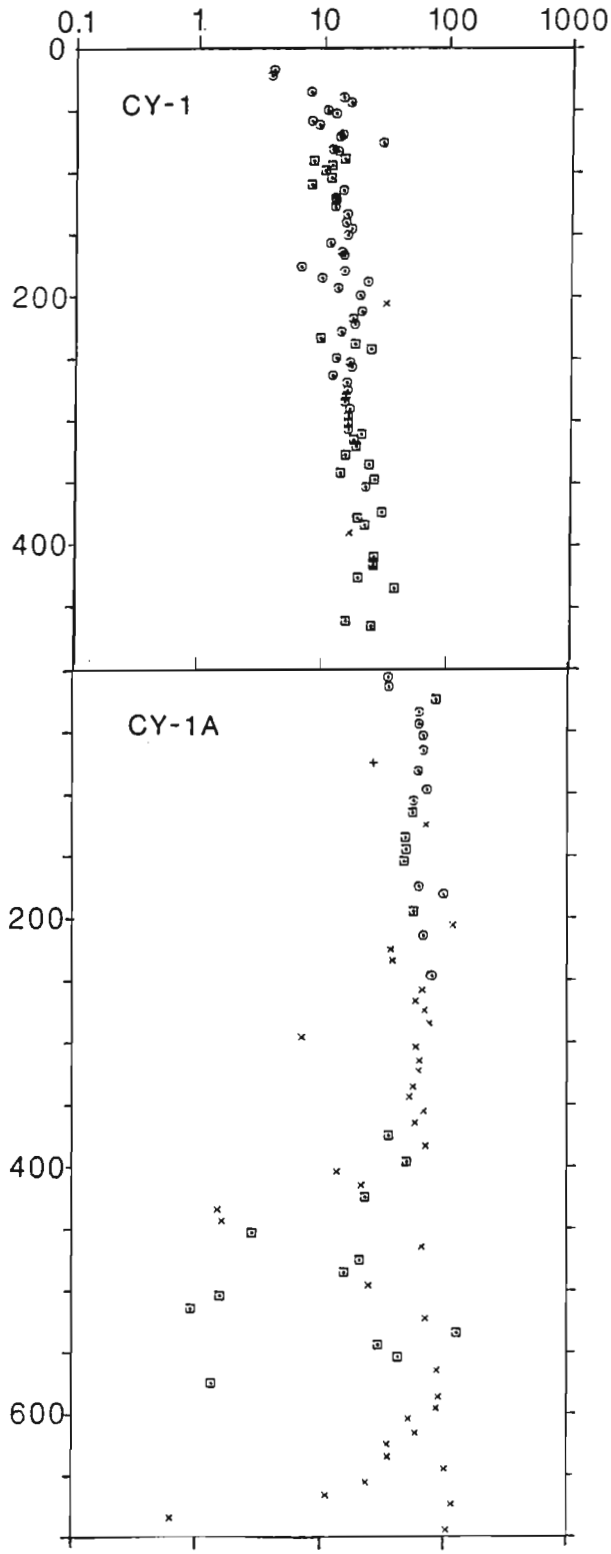

Figure 10: Magnetic susceptibility (10^{-3} S.I. Units) vs. depth (m) for CY-1 and CY-1A. Symbols as for Figure 4.

On this basis the section represented in CY-1 and CY-1A may be divided into three distinct units; an upper unit above 180 m in CY-1 which consists predominantly of pillow lavas with several massive flows, a middle unit of massive flows, pillow lavas and occasional dykes, and a lower unit below the fault at 250 m in CY-1A (750 m in the section) consisting of dykes with some massive flows between 375 and 575 m. NRM intensities within the upper unit are, with one exception less than 15 A m^{-1}, typically 5 A m^{-1}, susceptibilities are mostly between 6 and 15 × 10^{-3} S.I. and Koenigsberger ratios variable but typically about 10. The middle unit has NRM intensities of up to 45 A m^{-1}, typically 10–15 A m^{-1}, but with some lower intensities in dykes towards the base of the unit in CY-1A. There is a distinct increase in susceptibility with depth through this unit from 10–20 × 10^{-3} S.I. units in the upper part of the unit to 25–120 × 10^{-3} S.I. at the base. The range and amplitude of Koenigsberger ratios decreases with depth from 5–50 at the top of the unit to 1–20 towards the base. The lower unit has a considerably lower NRM intensity, 1.0 A m^{-1}, than the upper two units and susceptibilities typically between 10 and 100 × 10^{-3} S.I. but which may be as low as 1 × 10^{-3} S.I. possibly due to hydrothermal alteration associated with pyrite veins. The general trend is of increasing susceptibility with depth.

It is notable that the massive flows occurring in the lower unit have comparable magnetic properties to the dykes, whereas the dykes occurring in the middle unit have comparable magnetic properties to the higher extrusives. This suggests that the boundary between the middle and lower units is metamorphic in character and not merely a function of lithology. The upper unit down to 180 m reflects the effects of low temperature seafloor weathering or halmyrolysis. The contact between the middle and lower units can be typified by the marked change in the range of values of the Koenigsberger ratio which is exactly analogous to that observed by Beske-Diehl and Banerjee (1980) at the zeolite-greenschist facies boundary, which they assumed to be at a depth of 1.5 km in the Troodos ophiolite. It was noted that this boundary fluctuates near the depth where the pillow lavas between dykes become scarce. This occurs at approximately 250 m depth in CY-1A, or 750 m in the section, at the faulted middle-lower unit boundary. Thus the upper, middle and lower magnetic units defined here appear to correspond to intervals of halmyrolysis, zeolite and greenschist facies metamorphism respectively.

Criteria for an adequate marine anomaly source layer have been suggested by a number of authors (Johnson and Pariso, 1985; Levi et al. 1978). Among those relevant to the properties discussed here are; that the NRM intensity should be greater than 5 A m^{-1}, (or greater than 0.1 A m^{-1}, according to Levi et al.), the Koenigsberger ratio should be greater than 1, and that there should be coherent directions of magnetization within the crustal section. The pillow lavas, massive flows and dykes above the zeolite-greenschist facies boundary, with NRM intensities in excess of 5 A m^{-1} are thus, potentially,

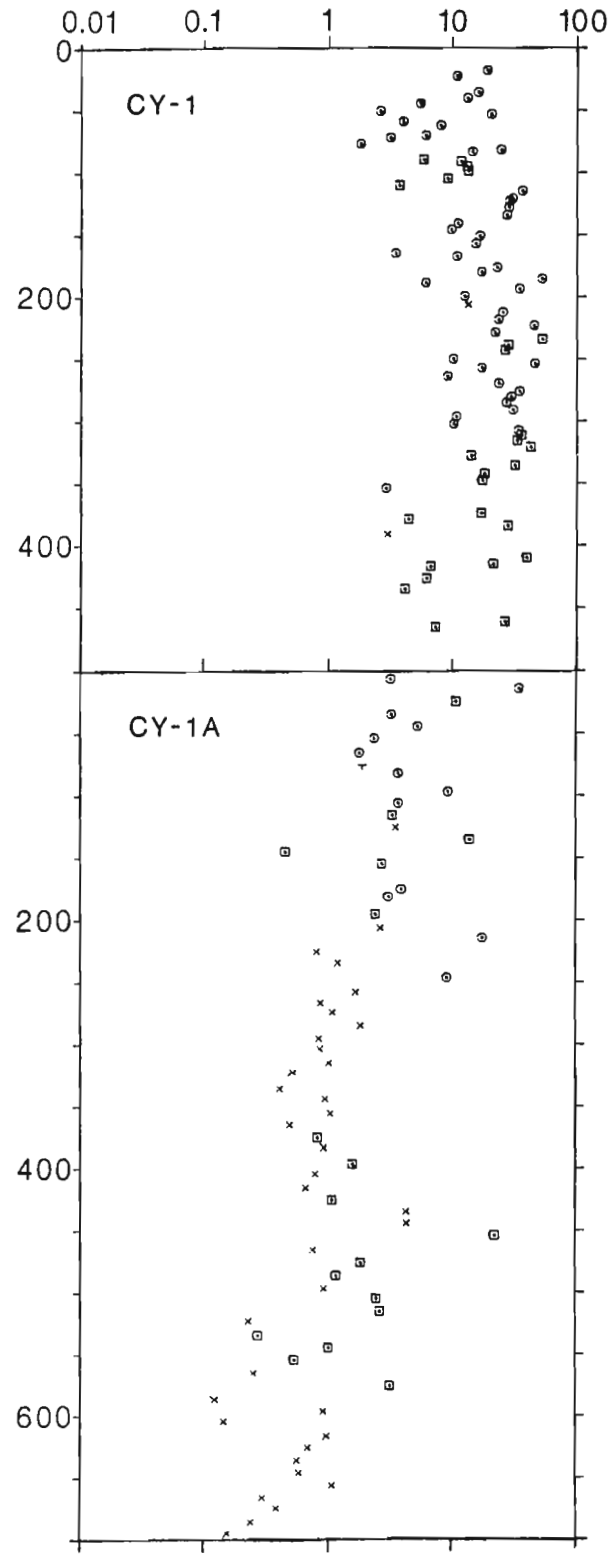

Figure 11: Koenigsberger ratio (Qn) vs. depth (m) for CY-1 and CY-1A. Symbols as for Figure 4.

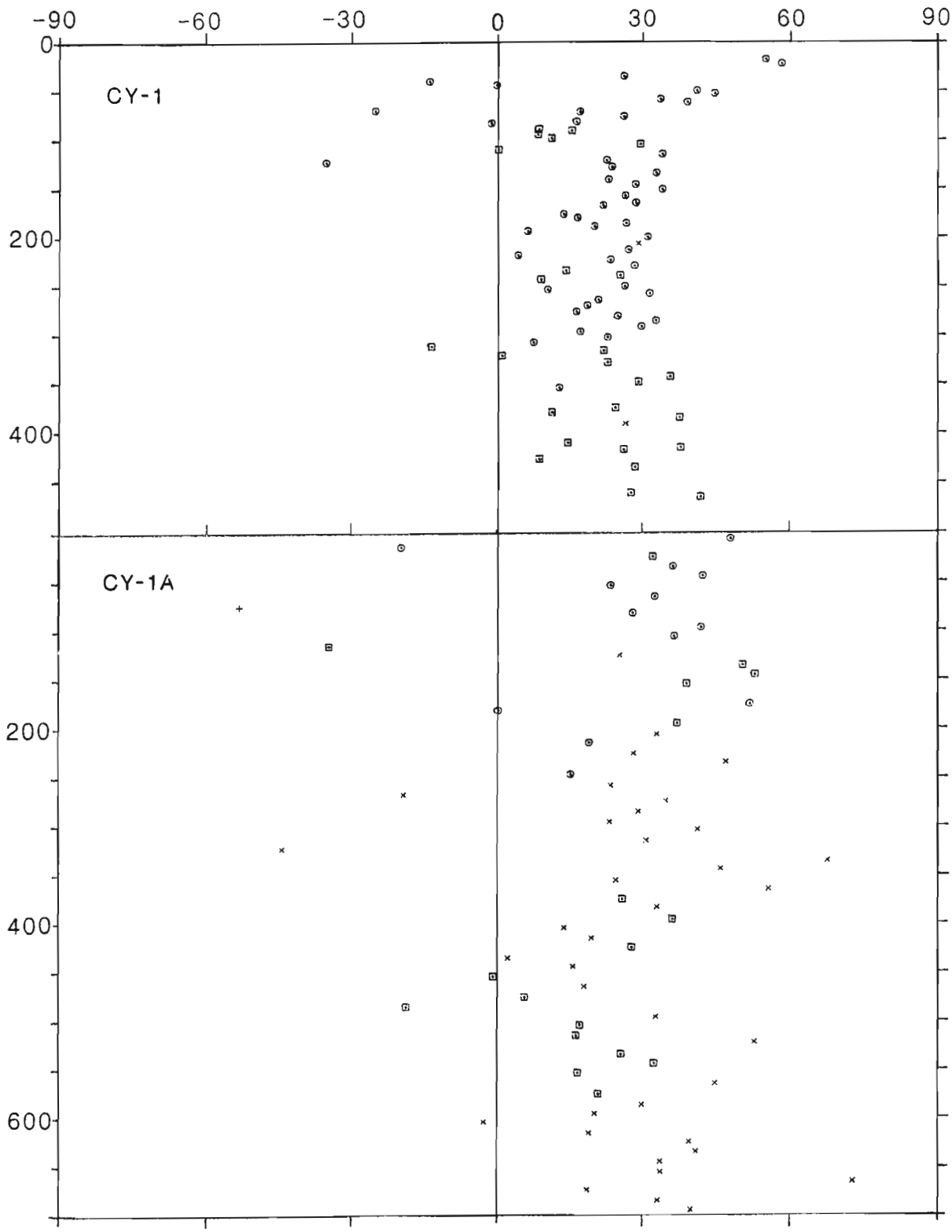

Figure 12: NRM inclinations (degrees) vs. depth (m) for CY-1 and CY-1A. Symbols as for Figure 4.

the most important source layer. The layer thickness of 750 m is consistent with the commonly estimated thicknesses of the oceanic source layer of 500 to 1000 m (Schouten and Denham, 1979; Banerjee, 1984). Although the NRM intensities observed in the Cyprus section in the dykes and flows below the zeolite-greenschist facies boundary are much lower, of the order of $1\,A\,m^{-1}$, this will, if it extends to an appreciable depth, make a significant secondary contribution to the total observed magnetic anomaly (Kidd, 1977). Evidence from CCSP Drillhole CY-4 through the diabase and gabbro suggests that this is the case (Smith and Vine, 1989c). The value of the Koenigsberger ratio is largely an irrelevance. Variations in the induced component of magnetization of the layers of a horizontally layered, i.e. 'one-dimensional,' model have no bearing on the shape of the anomaly. Only lateral magnetization contrasts can produce anomalies.

In this study we have not tested the third condition of directional coherence of the NRM. However, previous work (Vine, Poster and Gass, 1973) suggests that this condition is satisfied in all of the three lithologic units defined here. The dykes however have somewhat higher inclinations than the extrusives (see Table 1), implying that they have acquired a viscous remanent component of magnetisation. Demagnetisation of dykes has shown that they have a tendency to acquire a secondary magnetisation in the direction of the current field on Cyprus (Allerton and Vine, 1987).

DISCUSSION

The 1,200 m section recovered from CCSP Drillholes CY-1 and CY-1A allows the detailed study of the variation in physical parameters through the Troodos section and thus by analogy through the oceanic crust. DSDP Drillhole 504B which penetrated 1075.5 m of oceanic basement south of the Costa Rica Drift (Anderson et al., 1982) has provided a geological section comparable to that obtained from Drillholes CY-1 and CY-1A, allowing the analogy between the upper 1 km of the Troodos ophiolite and the upper kilometre of oceanic crust to be tested.

On the basis of the laboratory measurements three units can be recognised in the Troodos section with a gradational contact between the upper and middle units from 165 m to 260 m and a sharp fault bounded contact between the middle and lower units at 750 m. The contact between the upper and middle units is rather subtle, reflecting the effects of varying degrees of seafloor weathering, or halmyrolysis, on the geological and physical properties of the rocks. Different physical properties are affected to different degrees by halmyrolysis. Further, the degree of halmyrolysis decreases with depth to 260 m (Hall et al. 1987). Thus the contact between the upper and middle units may be drawn at depths ranging from 165 m to 260 m depending on the property from which the contact is defined. For example the base of the upper unit may be drawn at 165 m on the basis of a velocity inversion and an increase in conductivity; at 180 m by an increase in NRM intensity and susceptibility, by an increase in porosity at 215 m or by an increase in density between 200 m and 260 m. It is therefore best to define the depth interval from 165 m to 260 m as a transition zone between an upper unit of seafloor weathered basalts above 165 m and the middle unit of zeolite facies basalts below 260 m. The upper unit is then characterised by relatively steep gradients in physical properties; an increase in seismic velocities, NRM intensity and susceptibility, and a decrease in porosity and electrical conductivity with depth.

The middle unit which extends to 750 m, consists of massive flows and pillow lavas with occasional intrusives. It is characterised by moderate gradients in physical properties: an increase in density, seismic velocities and magnetic susceptibility, a decrease in porosity and electrical conductivity and little change in NRM intensity with depth. The contact between the middle and lower units is defined by sharp contrasts in geological and geophysical parameters. The density and velocities show a slight increase and the porosity, conductivity and NRM intensity a slight decrease. Most diagnostic is the contrast in Koenigserger ratios above and below 750 m. Above, values are almost exclusively greater than 1.0, typically 10.0, below values are almost exclusively less than 10.0, typically 1.0. The lower unit consists predominantly of dykes, with some massive flows between 875 m and 1075 m. Density, velocities and susceptibility continue to increase and porosity and conductivity to decrease with depth. Lower densities and velocities and higher porosities and conductivities are determined for the massive flows in the lower unit. There is, however, little contrast in NRM intensity.

A comparison of the lithological and geophysical data suggests that the upper, middle and lower units correspond to the zones of halmyrolysis, zeolite facies, and greenschist facies metamorphism respectively.

Like the Troodos section, the section from 504B may be divided into three main units. Geophysical logging (Salisbury et al., 1985; Von Herzen et al., 1985; Newmark et al., 1985) shows that within the upper 100 m of pillow basalts and breccias, density and velocities are low but increase rapidly with depth. This is interpreted (Newmark et al., 1985) to be sesmic layer 2A. The next 550 m is composed of pillow basalts, flows and breccias and is characterised by moderate velocity, density and conductivity gradients. This is interpreted to be seismic layer 2B. Evidence of halmyrolysis is seen to a depth of 300 m, well below the 2A–2B 'contact,' with infilling of veins with zeolites noted towards the base of the zone. Higher in the section, many veins and vesicles are open and saturated. Below layer 2B is a transition zone extending over 200 m with a decrease in the proportion of pillows and an increase in dyke density to layer 2C, the sheeted dykes at 780 m. The first evidence of greenschist facies metamorphism occurs at approximately 650 m and is marked by an increase in the gradients of density, velocities, porosity and conductivity. Below 900 m there is little increase in velocity or density, or decrease in porosity or conductivity.

Physical Property	CCSP CY-1 and CY-1A Pillow Lavas	Massive Flows	Dykes	DSDP Leg 37 Basalts	DSDP Leg 46 Basalts	DSDP Leg 49 Basalts	DSDP Leg 51–53 Basalts	DSDP Site 504B Leg 69–70 Basalts	Leg 69–70 Basalts	Leg 83 Basalts	Various DSDP Basalts	49 DSDP Drillholes (10–321)	DSDP Legs 2–14, 26, 34 and 37
Vp+ ($km\,s^{-1}$)	3.47 ±0.49 (16)	3.55 ±0.66 (13)	4.82 ±0.58 (15)	5.94 ±0.34 (79)	6.04 ±0.21 (25)	5.22 ±0.63 (11)	5.48[a] ±0.48 (189)	6.07x ±0.36 (29)	5.75[a] ±0.3 (115)	6.21x ±0.32 (32)	-	-	-
Vs+ ($km\,s^{-1}$)	1.83 ±0.30 (16)	1.96 ±0.38 (13)	2.62 ±0.35 (15)	3.27 ±0.15 (37)	3.19 ±0.71 (25)	-	3.10[a] ±0.21 (65)	3.26x ±0.21 (29)	-	3.33x ±0.18 (32)	-	-	-
P.r+	0.308 ±0.30 (16)	0.281 ±0.021 (13)	0.289 ±0.017 (15)	0.295 ±0.011 (37)	0.306 ±0.018 (25)	-	0.28[a] ±0.01 (65)	0.30x ±0.02 (29)	-	0.30x ±0.02 (32)	-	-	-
ρs ($kg\,m^{-3}$)	2264 ±125 (55)	2297 ±123 (27)	2580 ±114 (37)	2795 ±82 (101)	2800 ±50 (25)	2760 ±160 (11)	2785 ±128 (185)	2860 ±90 (29)	2900 ±60 (115)	2910 ±60 (32)	-	-	-
ρg ($kg\,m^{-3}$)	2558 ±171 (55)	2594 ±145 (27)	2772 ±89 (37)	2949 ±45 (85)	-	-	2914 ±42 (104)	-	3000 ±30 (115)	- -	-	-	2800 ±10 (137)
ϕ (%)	18.9 ±5.8 (55)	18.7 ±6.7 (27)	11.0 ±4.9 (37)	7.81 ±4.15 (85)	3.6 ±2.3 (25)	-	8.4 ±5.5 (104)	2.5 ±3.1 (29)	5.0 ±2.2 (115)	1.3 ±1.9 (32)	-	-	7.04 ±4.33 (137)
σ^{+*} ($mS\,m^{-1}$)	72.1 (18)	92.2 (14)	8.41 (14)	4.55[a] (87)	4.78[a] (20)	19.2 (10)	8.33[a] (48)	- - -	21.6[a] (56)		-	-	5.26 (153)
								Leg 69–70 Pillow Lavas	Leg 69–70 Massive Flows	Leg 83 Dykes			
^{J}NRM ($A\,m^{-1}$)	10.87 ±9.20 (61)	10.90 ±11.82 (44)	1.99 ±2.81 (37)	3.66 ±2.26 (127)	1.72 ±1.39 (110)	5.0 (216)	9.31 (271)	10.2 ±6.9 (40)	4.7 ±3.9 (90)	0.89 ±0.49 (4)	4.14 (294)	2.07 (391)	-
χ 10^{-3} S.I.	24.9 ±22.6 (61)	27.1 ±23.5 (44)	52.8 ±35.6 (37)	4.56 ±4.11 (124)	2.08 ±2.84 (48)	12.9 (43)	18.9 (311)	18.2 ±8.2 (40)	30.3 ±13.6 (90)	13.2 ±0.8 (4)	-	-	-
Q_n	16.6 ±12.6 (61)	13.4 ±13.4 (44)	1.41 ±0.80 (37)	35 ±26 (124)	38 ±32 (48)	21.5 (43)	21.6 (263)	28.1 ±27.4 (40)	7.4 ±9.0 (90)	3.6 ±0.8 (4)	-	-	-
Reference	(1)	(1)	(1)	(2,3)	(4,5)	(6,7)	(8,9)	(10,13)	(11,12, 13)	(14,15)	(16)	(17)	(18)

Table 5: Mean values of the physical properties measured for CY-1 and 1A samples compared with those obtained on basalt samples recovered by the DSDP.

A qualitative comparison of the depth trends in physical properties deduced from laboratory measurements on CY-1 and CY-1A samples and from logging of 504B, shows comparable variations and correlation with geology, pointing to an analogy between the upper, middle and lower units of the Troodos section and oceanic seismic layers 2A, 2B and 2C. However, a true comparison of the physical properties of rocks from the Troodos drillholes with rocks from 504B must be between values determined by similar techniques. Laboratory measurements on samples from 504B give considerably higher velocities and densities, and lower porosity and conductivity than measurements on Troodos samples, as shown in Table 5. Thus although the sections are similar in many respects, velocities and densities through the Troodos section are anomalously low, and porosities and conductivities anomalously high. Further, although the Troodos pillow lavas have a similar NRM intensity to pillow lavas from 504B, the Troodos massive flows and dykes have anomalously high NRM intensity and the dykes much higher susceptibility.

Table 5 also shows mean values of physical properties of basalts from DSDP legs 37, 46, 49 and 51–53, and several compilations of measurements on various DSDP basalts. A comparison of these values with measurements on the Troodos lavas, flows and dykes reinforces the interpretation of the upper 1 km of the Troodos ophiolite as being anomalously porous, having anomalously low velocities and densities, high conductivity, and high NRM intensity and magnetic susceptibility. Although high NRM intensities comparable to those measured from the Troodos have been observed for basalts from some DSDP drillholes, these are typically from young crust close to the ridge crest. Basalts from older crust have much lower NRM intensities than determined from the Troodos extrusives. The upper 1 km of the Troodos therefore appears to provide a poor analogue of the upper 1 km of mature oceanic crust in terms of the absolute values of all the physical properties.

ACKNOWLEDGEMENTS

This research was supported by the U.K. Natural Environment Research Council, grant number GR3/4473.

REFERENCES

Allerton, S. and Vine, F.J.
1987: Spreading structure of the Troodos ophiolite, Cyprus: some palaeomagnetic constraints; Geology, v. 15, p. 593–597.

Anderson, R.N., Honnorez, J., Becker, K., Adamson, A.C., Alt, J.C., Emmermann, R., Kempton, P.D., Kinoshita, H., Laverne, C., Mottl, M.J., and Newmark, R.L.
1982: DSDP Hole 504B, the first reference section over 1 km through layer 2 of the oceanic crust; Nature, v. 300, p. 589–594.

Archie, G.E.
1942: The electrical resistivity log as an aid in determining some reservoir characteristics; American Institute of Mining, Metallurgical, and Petroleum Engineers, Transactions, v. 146, p. 54–62.

Banerjee, S.K
1984: The magnetic layer of the ocean crust — How thick is it?; Tectonophysics, v. 105, p. 15–27.

Beske-Diehl, S. and Banerjee, S.K.
1980: Metamorphism in the Troodos ophiolite: implications for marine magnetic anomalies; Nature, v. 285, p. 563–564.

Birch, F.
1960: The velocity of compressional waves in rocks to 10 kilobars, Part 1; Journal of Geophysical Research, v. 65, p. 1083–1102.

Drury, M.J.
1979: Electrical resistivity models of the oceanic crust based on laboratory measurements on basalts and gabbros; Geophysical Journal of the Royal Astronomical Society, v. 56, p. 241–253.

Hall, J.M., Walls, C., Williamson, M., and Wang, B-X.
1987: Depth trends in magnetic properties in an area of prolonged cold seawater drawdown in uppermost Troodos-type oceanic crust; Canadian Journal of Earth Sciences, v. 24, p. 941–952.

Harrison, C.G.A.
1976: Magnetization of the oceanic crust; Geophysical Journal of the Royal Astronomical Society, v. 47, p. 257–283.

Horne, L.V.B. and Robinson, P.T.
1984: Cyprus Crustal Study Project: CY-1 Core Descriptions; Dalhousie University, Halifax.

Horne, L.V.B. and Robinson, P.T.
1986: Cyprus Crustal Study Project, Hole CY-1A: Edited core descriptions; Dalhousie University, Halifax, 700 p.

Houtz, R. and Ewing, J.
1976: Upper crustal structure as a function of plate age; Journal of Geophysical Research, v. 81, no. 14, p. 2490–2498.

Johnson, H.P. and Pariso, J.E.
1985: Implications for a magnetic model of the ocean crust: new Troodos ophiolite data; EOS Transactions, American Geophysical Union, v. 66, p. 1128.

Kidd, R.G.W.
1977: The nature and shape of the sources of marine magnetic anomalies; Earth and Planetary Science Letters, v. 33, p. 310–320.

Levi, S., Banerjee, S.K., Beske-Diehl, S., and Moskowitz, B.
1978: Limitations of ophiolite complexes as models for the magnetic layer of the oceanic lithosphere; Geophysical Research Letters, v. 5, p. 473–476.

Newmark, R.L., Anderson, R.N., Moos, D., and Zoback, M.D.
1985: Sonic and ultrasonic logging of Hole 504B and its implications for the structure, porosity and stress regime of the upper 1 km of the oceanic crust; *in* Anderson, R.M., Honnorez, J., Becker, K., et al. 1985: Initial Reports of the Deep Sea Drilling Project, v. 83, U.S. Government Printing Office, Washington, p. 479–510.

Robinson, P.T., Gibson, I.L., and Horne, L.V.-B.
1991: Cyprus Crustal Study Project Hole CY-1: lithologic unit summaries; *in* Gibson, I.L., Malpas, J., Robinson, P.T., and Xenophontos, C., Cyprus Crustal Study Project: Initial Report, Holes CY-1 and 1A, Geological Survey of Canada, Paper 90–20.

Salisbury, M.H., Christensen, N.I., Becker, K., and Moos, D.
1985: The velocity structure of layer 2 at Deep Sea Drilling Project Site 504 from logging and laboratory experiments; *in* Anderson, R.N., Honnorez, J., Becker K., et al., Initial Reports of the Deep Sea Drilling Project, v. 83, U.S. Government Printing Office, Washington, p. 529–539.

Schouten, H. and Denham, C.R.
1979: Modelling the oceanic magnetic source layer; *in* Talwani, M., Harrison, C., and Hayes, D., Deep drilling results in the Atlantic Ocean: ocean crust, American Geophysical Union Monograph, p. 151–159.

Shankland, T.J. and Waff, H.S.
1974: Conductivity in fluid bearing rocks; Journal of Geophysical Research, v. 70, p. 4863–4868.

Smith, G.C. and Vine, F.J.
1987a: Electrical conductivity of basalts from CCSP Drill Holes CY-2 and CY-2a at Agrokipia Mines, Cyprus; *in* Robinson, P.T., Gibson, I.L., and Panayiotou, A., Cyprus Crustal Study: Project Initial Report, Holes CY-2 and 2a, Geological Survey of Canada, Paper 85–29, p. 339–346.

Smith, G.C. and Vine, F.J.
1987b: Seismic velocities in basalts from CCSP Drill Holes CY-2 and CY-2a at Agrokipia Mines, Cyprus; *in* Robinson, P.T., Gibson, I.L., and Panayiotou, A., Cyprus Crustal Study Project: Initial Report, Holes CY-2 and 2a, Geological Survey of Canada, Paper 85–29, p. 295–306.

Smith, G.C. and Vine, F.J.
1989c: The physical properties of diabases, gabbros and ultramafic rocks from C.C.S.P. drill hole CY-4 at Palekori, Cyprus; *in* Gibson, I.L., Malpas, J., Robinson, P.T., and Xenophontos, C., Crustal Study Project: Initial Report, Hole CY-4, Geological Survey of Canada, Paper 85–89, p. 295–314.

Varga, R.J. and Moores, E.M.
1985: Spreading structure of the Troodos ophiolite, Cyprus; Geology, v. 13, p. 846–850.

Vine, F.J., Poster, C.K., and Gass, I.G.
1973: Aeromagnetic survey of the Troodos Igneous Massif, Cyprus; Nature, Physical Science, v. 244, p. 34–38.

Von Herzen, R.P., Francis, T.J.G., and Becker, K.
1985: In situ large scale electrical resistivity of ocean crust, Hole 504B; *in* Anderson, R.N., Honnorez, J., Becker, K., et al., Initial Reports of the Deep Sea Drilling Project, v. 83, U.S. Government Printing Office, Washington, p. 237–244.

Magnetic Properties, Oxide Petrography, and Alteration: Cyprus Crustal Study Project Drillholes CY-1 and CY-1A

J.M. HALL[1], B.E. FISHER[1], C.C. WALLS[1], T. WARD[1],
S.L. HALL[1], H.P. JOHNSON[2], AND J. PARISO[2]

[1]Department of Geology, Dalhousie University, Halifax, Nova Scotia, B3H 3J5, Canada
[2]Department of Oceanography, University of Washington, Seattle, Washington, 98195, U.S.A.

Hall, J.M., Fisher, B.E., Walls, C.C., Ward, T., Hall, S.L., Johnson, H.P., and Pariso, J., 1991: Magnetic properties, oxide petrography, and alteration: Cyprus Crustal Study Project Drillholes CY-1 and CY-1A; in Cyprus Crustal Study Project: Initial Report, Holes CY-1 and 1A, eds. Gibson, I.L., Malpas, J., Robinson, P.T., and Xenophontos, C.; Geological Survey of Canada, Paper 90–20, p. 235–256, 1991.

Abstract

Rock magnetic and oxide petrographic data are presented for the 1.04 km section from the sediment-volcanic interface downward in the Troodos ophiolite, Cyprus. Natural remanence intensity, J_O, initial susceptibility, k, and saturation magnetization, J_S, show increase, and mean demagnetization field, MDF, decrease with depth over the upper 0.45–0.6 km of the section. Below this depth J_O drops to uniformly low values, J_S and k are scattered, and MDF shows possible increase with depth. Decrease in low temperature oxidation, followed by increase in hydrothermal alteration, controls properties in the uppermost ~0.55 km of the section. A zone of minimum alteration between 0.26 and 0.41 km corresponds closely to the interval of strongest J_O. Below 0.55 km strong hydrothermal alteration followed by the extensive formation of secondary magnetite, SM, controls magnetic properties. SM formation becomes important when dyke density exceeds ~30% of the section. SM consists of nearly pure, stoichiometric magnetite from which much of the impurities and physical breaks have been expelled or annealed. The formation of multidomain SM leads to low J_O and relatively high k and J_S.

Résumé

Les données pétrographiques des oxydes et propriétés magnétiques des roches sont présentées pour une coupe de 1.04 Km à partir de l'interface sédimentaire-volcanique verse le bas, dans les ophiolites de Troodos, Chypre. L'intensité de la rémanence naturelle, J_O, la susceptibilité initiale, k, et l'aimantation par saturation, J_S, augmentent, et le champ de démagnétisation moyen, MDF, décroit en profondeur dans la partie supérieure de la coupe, entre 0.45 et 0.6 Km. Sous ce niveau, la rémanence naturelle (J_O) diminue aux valeurs uniformes de peu d'élevation, celles de J_O et k sont dispersées, et MDF s'accroît possiblement avec une augmentation de profondeur. Une baisse d'oxydation à basse température, suivie d'un accroîssement de l'altération hydrothermale, contrôlent les propriétés dans la partie supérieure à l'ordre de 0.55 Km de la coupe. Une zone d'altération minimum entre 0.26 et 0.41 Km correspond beaucoup à un intervalle de hautes valeurs de J_O. Sous 0.55 Km, une forte altération hydrothermale suivie d'une formation abondante de magnétite secondaire, SM, contrôlent les propriétés magnétiques. La formation SM devient importante lorsque le densité de dikes dépasse 30% d'une section de coupe. Cette formation est consistuée de magnetite stœchiométrique oú la plupart des impurités et les fractures ont été évacuées ou recuites. La formation de SM à domaines multiple conduit à une basse valeur de J_O et à des valeurs de k et J_O relativement hautes. dépasse 30% d'une section de la coupe. La SM consiste de magnétite stoechiométrique presque pure, de laquelle toutes impureté et fractures one été évacuées ou recuites. La formation de SM à domaines multiples conduit à une basse valeur de J_O et à des valeurs de k et J_O relativement hautes.

INTRODUCTION

The Cyprus Crustal Study Project (CCSP) is a multidisciplinary international re-examination of the Troodos, Cyprus, ophiolite having two major objectives: to determine features of oceanic crust that are not readily accessible in the present oceans and to determine the origin of ophiolites. The project used research drilling as a major tool. This report describes initial results from the magnetic and oxide petrographic examination of material from CCSP drillholes CY-1 and CY-1A.

The Troodos ophiolite (Coleman, 1977; Gass, 1980) is an uplifted segment of Tethyan crust produced in a spreading environment. The Troodos ophiolite is notable in apparently having experienced little alteration and tectonic disruption other than that acquired as it in situ oceanic crust. The ophiolite sequence consists of a pseudo-stratigraphic succession in which an Extrusive Series, consisting of pillowed and sheeted submarine extrusives, overlies a transition to a dyke complex, termed the Basal Group. An underlying zone consisting largely of thin, parallel, subvertical basic dykes, the Sheeted Complex, is succeeded at depth by an unnamed transition to the Plutonic Complex, consisting of high level gabbros with minor plagiogranites and lower level ultramafics.

CCSP drillholes CY-1 and CY-1A, with depths of 475 m and 701 m respectively, and recoveries in excess of 90%, were designed to provide a continuous section through the Extrusive Series and into the transition to the Sheeted Complex, the Basal Group, of the ophiolite. The top of Hole CY-1 is located at within a few metres of the sediment-volcanic interface within the valley of the Akaki-Maroulena stream system (Figure 1). Hole CY-1A is located in the same valley about 1-1/2 km upstream (south) of CY-1. The location of CY-1A was chosen such that it would provide overlap with and extension of the lower part of the section sampled in Hole CY-1. Exact survey of the relative location of the two holes, and measurement of the northwards dips of sediments and sheet flows in their vicinities, has allowed expressions relating hole and true stratigraphic depths to be derived: (i.e.) for Hole CY-1

$$\text{True depth (m)} = \text{Hole depth} \times \cos 20°$$

and for Hole CY-1A

$$\text{True depth (m)} = 373 + \text{Hole depth} \times \cos 15°$$

Where the figure of 373 m is the estimate of the equivalent true depth in the CY-1 section of the top of the CY-1A section.

In this report, samples are referred to in terms of their hole depths, this being the unambiguous means of recovering their locations in the drill cores. However, the sample property lists of Tables 1 and 2 contain both hole and true depths, while the depth profiles of Figures 2–7 are plotted on the basis of true depths.

The upper part of the Extrusive Series in the vicinity of Hole CY-1 is included in the Upper Pillow Lavas (UPL) mapping unit. This consists of frequently red stained, dominantly pillowed units. Clays, iron-hydroxides and carbonates are widespread in this unit. This suite of secondary minerals, together with evidence for a ~25 my delay in sediment sealing of the surface of the extrusives (Hall et al., 1987), indicates that the UPL is a low temperature alteration facies of varying thickness at the top of the Extrusive Series. The macroscopic indicators of intense low temperature alteration are not seen below 260 m depth in Hole CY-1 (0.24 km true depth).

Below this depth low temperature alteration is subdued, the pillows, massive flows, and very occasional dykes being generally gray or dark brown coloured. Such extrusives are included in the Lower Pillow Lavas (LPL) mapping unit, which comprise the lower part of the CY-1 and the upper part of the CY-1A section. At 0.7 km crustal depth there is macroscopic evidence for a fairly rapid increase in alteration to subgreenschist conditions, followed at between ~0.5 to 0.7 km crustal depth by a rapid increase in dyke density from a few percent to about 40% of the section. This density is maintained to the bottom of the CY-1A section at close to 1 km crustal depth. Both dykes and screens of pillowed and massive flows in this zone of higher dyke density have experienced hydrothermal (non-directed) metamorphism of subgreenschist or greenschist grades.

The CY-1/CY-1A profile provides a comparison section for the DSDP Hole 504B — 1.04 km section through uppermost oceanic crust in the Costa Rica Rift area (Anderson et al., 1982). Preliminary comparison of these two sections will be made after the presentation of the CY-1/CY-1A results. At this point it will be useful to note that the 504B section consists of 0.57 km of dominantly extrusives overlying a 0.2 km transition to a possible sheeted complex. Currently it is proposed that sheeted dyke (100% dyke density) conditions occur below 0.8 km. However, in view of the low core recovery rate (averaging 21%) this conclusion is partly based on the interpretation of geophysical and televiewer logging results which may not be very effective at resolving dykes and massive flows. The extrusive interval in Hole 504B has only experienced low temperature alteration, but from 0.89 km depth hydrothermal alteration rises rapidly to sub-greenschist or greenschist conditions, which extend to the base of the section.

SAMPLING AND MEASUREMENTS

Sampling from the drill cores was carried out at the Kokkinoiya core laboratory in Cyprus. Almost all samples are derived from minicores drilled transversely to the main core, with an average of one minicore taken from each 1.5 m core section. Tables 1 and 2 list the samples from Holes CY-1 and CY-1A, respectively. For Hole CY-1 samples are related to units and lithologies as given in Gibson and Robinson, 1983. In the absence of a detailed core description volume for Hole CY-1A, unit and lithological assignments are based on the working core description sheets. For the 192 CY-1 samples, which were obtained in 1982, several properties are

Hole Depth	Crustal Depth	Unit	Lith	Lab	J_O $\times 10^{-4}$	K $\times 10^{-4}$	MDF	J_S	T_C	Oxide classification or Comments
16.36	15.37	2.1	P brc	H.P.	23.3	10.1	139			
17.77	16.70	2.3	P brc	H.P.	19.6	6.8	106			
19.46	18.29	@	P brc	H.P.	72.1	6.1	250			
20.92	19.66	3.3	P	H.P.	79.1	89.0	141			
22.16	20.82	3.8	P	H.P.	54.3	5.5	141			
23.37	21.96	3.12	P	H.P.	94.7	1.3	103			
28.83	27.09	5.3	P	J.H.	33.0	3.4	144	0.67	500	C1 H1 L2? P:S=+1.0
30.31	28.48	5.6	P	J.H.	53.0	6.0	88	0.45	480	C1 H1 L2 P:S=+1.0
32.00	30.07	5.9	P	J.H.	3.1	1.1	249		weak	no oxides
44.34	41.67	8.2	P	H.P.	28.6	9.5	182			
47.55	44.68	8.5	P	H.P.	31.4	8.3	125			
50.33	47.30	9.3	P	H.P.	7.6	6.5	157			
50.96	47.89	9.4	P	H.P.	11.6	9.2	168			
51.60	48.49	9.5	P	J.H.	15.0	7.5	142		585	sm int incr in J and incr at dn=250
53.52	50.29	10.5	P	J.H.	51.0	9.7	116	0.49	490	C1 H1 L2 P:S=+1.0
54.90	51.59	10.7	P	J.H.	93.0	8.8	105	0.48	505	C1 H1 L2 P:S=+1.0
55.95	52.58	11.1	P	J.H.				0.63	540	C1 H1 L2 P:S=+1.0
57.38	53.92	11.4	P	J.H	59.0	10.0	117	0.22	51	C1 H1 L2 P:S=+1.0
58.75	55.21	11.6	P	J.H.	43.0	3.5	136	0.28	540	C1 H1 L2 P:S=+1.0
67.60	63.52	?	bas	H.P.	14.0	6.8	222			core lost from box
69.00	64.84	13.1	P	H.P.	46.4	10.1	165			
69.95	65.73	13.1	P?	H.P.	21.2	8.5	178			
71.75	67.42	14.2	P	H.P.	15.3	8.6	175			
72.55	68.18	14.3	P	H.P.	95.7	9.7	140			
74.14	69.67	14.6	P	H.P.	7.3	15.3	156			
75.35	70.81	15.3	P	J.H.	25.0	10.0	117	0.60	475	C1 H1 L1 P:S=+1.0
76.66	72.04	15.6	P	J.H.	13.0	17.0	132	1.01	540	C1 H1 L2 P:S=+1.0
78.06	73.35	15.8	F/brF	J.H.	100.0	7.8	121			C1 H1 L2 P:S=+1.0
80.66	75.80	16.4	P brc	J.H.	270.0	10.0	119	0.72	515	C1 H1 L2 P:S=+1.0
81.95	77.01	16.9	MF/D	J.H.	130.0	7.8	118	0.59	500	C1 H1 L2 P:S=+1.0
90.90	85.42	18.3	MF	H.P.	78.0	7.5	162			
92.74	87.15	@	MF	H.P.	7.9	6.9	128			
94.28	88.60	@	MF	H.P.	27.9	9.6	173			
94.91	89.19	@	MF	J.H.	54.0	10.0	121		weak	
96.65	90.82	20.2	MF	J.H.	86.0	9.9	112		weak	C1 H1 L1 P:S=+1.0
98.85	92.89	21.1	MF	J.H.	60.0	6.7	96	0.81	455	C1 H1 L3 P:S=+1.0
100.28	94.23	@	MF	J.H.	50.0	8.7	111	0.91	476	C1 H1(3) L3 Sr0.(6?) P:S= +1.0 to +0.95
101.85	95.71	@	MF	J.H.	85.0	7.1	121	0.67	505	C1 H1 L1-3 P:S=+1.0
103.45	97.21	@	MF	J.H.	44.0	9.7	89	0.96	540	C1 H1 L1 P:S=+1.0
110.90	104.21	@	MF	H.P.	21.2	6.3	147			
112.32	105.55	23.1	F	H.P.	119.0	18.1	145			
115.12	108.18	23.2	P	H.P.	107.0	12.9	140			
117.05	109.99	24.2	bas	H.P.	106.0	9.0	154			
118.44	111.30	24.3	P	H.P.	70.2	9.7	167			
119.82	112.60	24.6	MF	H.P.	59.6	9.6	155			
121.22	113.91	25.1	P	H.P.	57.5	13.8	150			
121.75	114.41	25.2	v brc	J.H.	52.0	4.6	91	0.48	455	C1 H1 L1 P:S=+1.0
123.22	115.79	25.3	P	J.H.	115.0	8.4	149	0.39	495	C1 H1 L2 P:S=+1.0
124.50	116.99	25.7	P	J.H.	149.0	10.0	117	0.53	475	C1 H1 L2 P:S=+1.0
126.14	118.53	25.1	P	J.H.	93.0	9.0	138	0.27	510	C1 H1 L1 P:S=+1.0

Table 1: Magnetic and oxide petrographic properties for samples from Holes CY-1.

Hole Depth	Crustal Depth	Unit	Lith	Lab	J_O $\times 10^{-4}$	K $\times 10^{-4}$	MDF	J_S	T_C	Oxide classification or Comments
128.10	120.38	26.2	P	J.H.	149.0	10.0	133	0.45	495	C1 H1 L2 P:S=+1.0
129.55	121.74	26.4	P	J.H.	227.0	12.0	125	0.42	460	C1 H1 L2 P:S=+1.0
131.05	123.15	26.5	P	J.H.	90.0	12.0	103	0.49	480	C1 H1 L1-2 P:S=+1.0
132.46	124.47	26.6	P	J.H.	173.0	9.2	98	0.57	470	C1 H1 L1-2 P:S=+1.0
139.84	131.41	28.5	P	H.P.	58.3	9.1	132			
141.27	132.75	28.8	bas	H.P.	86.2	9.8	136			
142.65	134.05	28.14	P	H.P.	76.7	11.2	119			
144.00	135.32	28.18	bas	H.P.	51.6	7.0	158			
144.42	135.71	@	bas	H.P.	55.0	5.6	120			
146.30	137.48	29.4	P	H.P.	16.1	9.1	114			
147.46	138.57	29.6	P	H.P.	67.1	10.7	129			
149.85	140.81	30.4	P	J.H.	125.0	13.0	84	0.51	485	C1 H1 L1-2 P:S=+1.0
151.20	142.08	30.9	P	J.H.	136.0	7.2	119	0.55	305	C1 H1 L1-2 P:S=+1.0
151.25	142.13	@	P	H.P.	150.0	10.7	112			
151.60	142.46	30.10	P/F	J.H.				0.49	484	C1 H1 L1-2 P:S=+1.0
152.57	143.37	@	P/F	J.H.	23.0	8.7	180	0.55	520	C1 H1 L1 P:S=+1.0
154.25	144.95	30.13	P	J.H.	85.0	10.0	100	0.39	475	C1 H1 L1-2 P:S=+1.0
155.94	146.54	30.14	P/F	J.H.	135.0	11.0	99	0.19	470	C1 H1 L1-2 P:S=+1.0
157.34	147.85	31.2	P	J.H.	197.0	8.1	114	0.52	500	C1 H1 L1-2 P:S=+1.0
157.61	148.11	@	P	J.H.	56.0	6.4	123	0.43	460	C1 H1 L1-2 P:S=+1.0
159.18	149.58	31.5	P	J.H.	89.0	9.4	110	0.45	485	C1 H1 L1 P:S=+1.0
160.75	151.06	32.2	P	J.H.	114.0	7.6	109	0.44	495	C1 H1 L1 P:S=+1.0
162.42	152.63	32.5	P	J.H.	101.0	8.7	121	0.41	475	C1 H1 L1-2 P:S=+1.0
163.84	153.96	@	P	J.H.	67.0	8.8	119	0.43	480	C1 H1 L1-2 P:S=+1.0
164.85	154.91	32.6	P	J.H.	46.0	9.8	121	0.41	440	C1 H1 L1-2 P:S=+1.0
172.44	162.04	34.2	P	H.P.	154.0	11.9	92			
173.36	162.91	34.3	P	H.P.	137.0	10.9	99			
174.85	164.31	34.5	P	H.P.	145.0	14.1	94			
176.68	166.03	34.6	P	H.P.	148.0	11.8	107			
177.78	167.06	35.3	bas	H.P.	98.6	10.8	137			
178.80	168.02	35.7	P	J.H.	151.0	9.1	118	0.52	485	C1 H1 L1 P:S=+1.0
179.04	168.24	35.8	P	H.P.	84.5	6.0	131			
180.22	169.35	35.12	P	H.P.	73.4	13.5	124			
181.65	170.70	35.14	bas	H.P.	74.0	13.3	129			
183.15	172.11	36.1	P	J.H.	58.0	8.3	92	0.28	430	C1 H1 L1-2 P:S=+1.0
184.75	173.61	36.6	P	J.H.	198.0	9.2	91	0.51	505	C1 H1 L2 P:S=+1.0
185.62	174.43	36.11	P	J.H.	178.0	7.6	72	0.42	495	C1 H1 L2 P:S=+1.0 **
187.75	176.43	36.13	P	J.H.	136.0	14.0	87	0.58	495	C1 H1 L1-2 P:S=+1.0
188.85	177.46	37.3	P	J.H.	77.0	13.0	140	0.83	550	C1 H1 L2 P:S=+1.0
190.47	178.99	37.7	P	J.H.	183.0	12.0	67	0.43	505	C1 H1 L2 P:S=+1.0
191.83	180.26	37.11	P	J.H.	138.0	10.0	87	0.47	460	C1 H1 L1-2 P:S=+1.0
193.18	181.53	37.15	P	J.H.	180.0	10.0	95	0.43	470	C1 H1 L2 P:S=+1.0
199.73	187.69	38.8	P	H.P.	132.0	13.6	97			
202.68	190.46	39.8	bas	H.P.	264.0	18.9	110			
204.06	191.76	39.12	bas	H.P.	61.6	11.9	87			
205.58	193.18	40.1	P	J.H.	78.0	13.0	89	0.57	475	C1 H1 L1-2 P:S=+1.0
206.45	194.00	40.3	D	J.H.	44.0	10.0	190	1.09	540	C1 H1 L1 P:S=+1.0
207.56	195.04	40.5	P	J.H.	284.0	11.0	45	0.54	545	C1 H1 L1 P:S=+1.0
209.15	196.54	40.9	P	J.H.	197.0	13.0	70	0.64	355 560	C1 H1 L1 P:S=+1.0

Table 1 (continued)

Hole Depth	Crustal Depth	Unit	Lith	Lab	J_Q $\times 10^{-4}$	K $\times 10^{-4}$	MDF	J_S	T_C	Oxide classification or Comments
210.12	197.45	40.10	P	H.P.	85.5	14.3	93			
211.52	198.77	41.3	P	H.P.	206.0	14.5	104			
212.80	199.97	41.4	P	H.P.	93.3	13.6	123			
214.38	201.45	41.7	bas	H.P.	135.0	14.8	112			
215.81	202.80	42.1	P?	H.P.	103.0	17.8	125			
216.48	203.43	42.2	P	H.P.	120.0	14.8	113			
218.60	205.42	42.5	P	H.P.	139.0	11.4	125			
220.57	207.27	42.9	P	H.P.	156.0	10.1	129			
221.86	208.48	43.2	P	J.H.	115.0	13.0	92	0.86	510	C1 H1 L1 P:S=+1.0
223.11	209.66	43.4	P	J.H.	219.0	14.0	91	0.57	485	C1 H1 L1 P:S=+1.0 *
224.40	210.87	43.7	P	J.H.	277.0	12.0	88	0.51	475	C1 H1 L2 P:S=+1.0
225.09	211.52	43.8	P	J.H.	237.0	10.0	90	0.39	470	C1 H1 L2 P:S=+1.0
226.90	213.22	44.1	P	J.H.	223.0	11.0	97	0.45	465	C1 H1 L1-2 P:S=+1.0
228.15	214.39	@	P	J.H.	151.0	7.6	120	0.39	485	C1 H1 L1-2 P:S=+1.0
229.18	215.36	44.4	P	J.H.	146.0	11.0	103	0.41	475	C1 H1 L1-2 P:S=+1.0
230.12	216.24	44.7	P	J.H.	133.0	8.2	127	0.78	445	C1 H1 L1-2 P:S=+1.0
237.40	223.09	45.1	MF	H.P.	316.0	12.9	119			
239.04	224.63	@	MF	H.P.	116.0	10.9	69			
239.85	225.39	@	MF	H.P.	104.0	16.3	96			
242.01	227.42	47.1	MF	H.P.	48.1	11.6	136			
243.23	228.56	47.2	F	H.P.	202.0	19.8	95			
246.20	231.35	47.3	F/P	H.P.	137.0	10.7	128			
247.31	232.40	48.2	P	J.H.	141.0	8.6	112	0.41	465	C1 H1 L1-2 P:S=+1.0 *
248.48	233.50	48.5	P	J.H.	77.0	8.4	164	0.57	445	C1 H1 L1 P:S=+1.0
250.32	235.23	48.6	P	J.H.	71.0	6.4	95	0.67	425	C1 H1 L1 P:S=+1.0
251.53	236.36	49.3	P	J.H.	99.0	6.4	137	0.40	440	C1 H1 L1-2 P:S=+1.0
252.46	237.24	49.6	P	H.P.	115.0	11.6	147			
253.73	238.43	49.8	P	J.H.	309.0	9.6	105	0.42	465	C1 H1 L1 P:S=+1.0
255.15	239.76	49.1	P	J.H.	105.0	11.0	108	0.57	465	C1 H1 L2 P:S=+1.0 *
261.59	245.82	50.7	MF	H.P.	120.0	13.3	97			
263.21	247.34	51.1	MF	H.P.	84.6	10.6	146			
264.60	248.65	51.3	MF	H.P.	107.0	10.1	146			
265.90	249.87	51.6	MF/P	H.P.	262.0	13.7	145			
267.45	251.32	52.2	MF	H.P.	180.0	12.3	143			
268.60	252.40	52.3	MF	H.P.	143.0	14.6	117			
270.01	253.73	@	MF	H.P.	104.0	11.5	143			
271.50	255.13	52.5	MF	H.P.	221.0	12.5	137			
272.49	256.06	52.5	P(MF)	J.H.	115.0	12.0	99	0.67	325 530	C1 H1 L1 P:S=+1.0
274.15	257.62	53.2	P	J.H.	169.0	12.0	79	0.57	330 540	C1 H1 L1 P:S=+1.0
275.55	258.93	53.4	P	J.H.	84.0	8.8	103	0.48	305 505	C1 H1 L1 P:S=+1.0
276.40	259.73	@	P	J.H.	169.0	11.0	97	0.50	335 555	C1 H1 L1 P:S=+1.0
279.17	262.34	54.2	P	J.H.	135.0	9.8	107	0.49	315 475	C1 H1 L1 P:S=+1.0
280.86	263.92	54.5	P	J.H.	126.0	12.0	93	0.55	335 500	C1 H1 L1 P:S=+1.0
281.88	264.88	54.7	P	J.H.	83.0	12.0	113	0.73	345 520	C1 H1 L1 P:S=+1.0 * and at dn=500
287.52	270.18	55.1	P	J.H.	63.0	9.9	103	0.75	485	C1 H1 L1 P:S=+1.0 int incr in J
288.70	271.29	@	P	H.P.	92.1	12.4	121			
290.15	272.65	56.2	P	H.P.	149.0	12.7	117			
291.25	273.69	56.4	P	H.P.	185.0	12.1	127			

Table 1 (continued)

Hole Depth	Crustal Depth	Unit	Lith	Lab	J_O $\times 10^{-4}$	K $\times 10^{-4}$	MDF	J_S	T_C	Oxide classification or Comments
293.05	275.38	56.6	P	H.P.	141.0	13.0	97			
294.25	276.51	57.3	P	H.P.	128.0	13.5	133			
295.76	277.92	57.6	F/P	H.P.	204.0	15.0	108			
296.78	278.88	@	F/P	H.P.	37.2	8.3	99			
297.95	279.98	@	F/P	H.P.	84.7	13.1	108			
299.52	281.46	57.7	P	J.H.	88.0	12.0	105	0.57	325 520	C1 H1 L1 P:S=+1.0
301.45	283.27	58.3	P	J.H.	63.0	10.0	98	0.46	510	C1 H1 L1 P:S=+1.0
302.57	284.33	@	P	J.H.	124.0	10.0	90	0.56	335 550	C1 H1 L1 P:S=+1.0
303.72	285.41	58.4	P	J.H.	110.0	12.0	89	0.70	330 540	C1 H1-2 L1 P:S=+1.0
304.87	286.49	58.5	P	J.H.	144.0	10.0	103	0.56	330 530	C1 H1 L1 P:S=+1.0
306.26	287.79	59.1	P	J.H.	218.0	13.0	107	0.76	345 520	C1 H1 L1 P:S=+1.0
307.70	289.15	59.3	P	J.H.	183.0	12.0	93	0.67	330 525	C1 H1 L1 P:S=+1.0
308.60	289.99	@	P	J.H.	348.0	12.0	93	0.69	325 510	C1 H1 L1 P:S=+1.0
316.20	297.13	61.1	F	H.P.	79.3	11.6	111			
316.60	297.51	@	F	H.P.	110.0	13.2	96			
318.65	299.44	61.3	MF	H.P.	66.0	17.5	94			
319.11	299.87	@	MF	H.P.	106.0	15.5	91			
321.01	301.65	@	MF	H.P.	226.0	15.5	83			
321.82	302.41	@	MF	H.P.	154.0	16.3	98			
323.15	303.66	@	MF	H.P.	77.2	11.5	93			
324.45	304.89	@	MF	J.H.	415.0	11.0	84	0.82	330 525	C1 H1 L1 P:S=+1.0
325.40	305.78	@	MF	H.P.	193.0	11.6	145			
328.29	308.49	@	MF	J.H.	113.0	13.0	89	0.65	330 545	C1 H1-2 L1-2 P:S=+1.0
339.58	319.10	66.1	MF	H.P.	188.0	19.7	72			
340.81	320.26	66.2	bas	H.P.	102.0	12.4	84			
342.66	321.00	@	bas	H.P.	81.7	10.2	84			
343.85	323.12	@	bas	H.P.	14.7	9.7	85			
345.08	324.27	66.3	MF	H.P.	207.0	25.2	74			
346.60	325.70	67.1	D/F	H.P.	243.0	22.0	88			
347.65	326.69	67.4	intr	H.P.	15.4	12.6	171			
348.39	327.38	67.6	D/F	H.P.	245.0	16.2	95			
353.90	332.56	68.8	P	J.H.	23.0	12.0	92	1.00	320 490	C1 H1 L1 P:S=+1.0 *
374.41	351.83	72.4	F	H.P.	121.0	17.6	86			
375.72	353.06	73.1	D	J.H.	28.0	12.0	86	0.97	305 500	C1 H1 L1 P:S=+1.0
377.52	354.76	73.2	MF	J.H.	406.0	13.0	76	1.07	340 490	C1 H1 L1 P:S=+1.0 *
378.92	356.07	@	MF	J.H.	49.0	11.0	89	0.67	350 495	C1 H1-2 L1-2 P:S=+1.0
380.15	357.23	@	MF	J.H.	511.0	12.0	75	1.03	320 525	C1 H1 L1 P:S=+1.0
381.88	358.85	@	MF	J.H.	72.0	12.0	93	0.87	330 505	C1 H1 L1 P:S=+1.0
383.05	359.95	@	MF	J.H.	167.0	12.0	85	0.85	340 480	C1 H1 L1 P:S=+1.0
384.58	361.39	@	MF	J.H.	146.0	13.0	85	1.47	345 495	C1 H1 L1 P:S=+1.0
385.69	362.43	@	MF	J.H.	86.0	11.0	98	0.95	335 480	C1 H1 L1 P:S=+1.0
410.10	385.37	78.4	MF	J.H.	737.0	17.0	86	1.41	330 530	C1 H1 L1 P:S=+1.0
415.68	390.61	79.3	MF	J.H.	180.0	18.0	90	1.39	335 530	C1 H1 L1 P:S=+1.0
421.60	396.18	80.5	P	H.P.	77.4	15.6	88			
425.70	400.03	81.2	MF	H.P.	206.0	18.5	96			
434.00	407.83	83.2	MF	J.H.	638.0	15.0	87	1.53	330 530	C1 H1-2 L1-2 P:S=+1.0
435.03	408.80	@	MF	J.H.	54.0	19.0	114	1.08	340 540	C1 H1-2 L1-2 P:S=+1.0
465.57	437.50	88.7	intr?	J.H.				0.71	340 548	C1 H1-2 L1 P:S=+1.0

Table 1 (continued)

Hole Depth	Crustal Depth	Unit	Lith	Lab	J_O $\times 10^{-4}$	K $\times 10^{-4}$	MDF	J_S	T_C	Oxide classification or Comments
1.81	374.75	1.01	P	J.H.	89.0	21.0	16	0.91	335 495	C1 H1(6) L1 P:S=+1.0
10.40	383.05	2.09	P	J.H.	52.8	20.8	17	1.23	355 495	C1 H1(6) L1 P:S=+1.0
20.65	392.95	5.01	F	J.H.	316.0	21.2	18	1.19	505	C1 H1 L1 P:S=+1.0
30.00	401.98	6.01	MF	J.H.	31.8	29.5	44	1.61	400 495	C1 H2(1,3)(6)L(1)2-3 P:S=+1.0
40.00	411.64	10.4	F	J.H.	34.7	30.9	20	1.95	445	C1 H1(6) L1 P:S=+1.0
49.50	420.81	12.1	F	J.H.	277.0	35.8	18	1.70	425	no pol-thin
60.08	431.03	15.6	MF	J.H.	264.0	29.7	19	2.02	445	C1 H1-3 L1-3 P:S=+1.0
69.95	440.56	18.1	F	J.H.	758.0	30.7	19	1.83	535	C1 H1 L1 P:S=+1.0
80.67	450.92	20.1	F	J.H.				0.31	565	unoriented, no descr gr size v. small
89.69	459.63	23.3	F	J.H.	28.9	34.3	21	1.90	400 475	unoriented C1 H1(2) L1-3 P:S=+1.0
100.75	470.31	26.4	P	J.H.	37.8	28.1	18	1.38	440	C1 H2-3(4) L2 P:S=+1.0
109.75	479.01	28.4	F/P	J.H.	185.0	26.4	15	1.39	405 500	C1 H1 L1(2) P:S=+1.0
120.00	488.91	30.3	D?	J.H.	100.0	28.7	14	1.11	410	no pol-thin
130.08	498.64	33.1	MF	J.H.	52.9	26.7	16	1.24	420	no pol-thin
140.30	508.52	35.3	MF	J.H.	14.4	20.4	34	0.86	505	C1 H1 L1 P:S=+1.0
150.65	518.51	38.1	MF	J.H.	17.2	30.1	49	1.40	430 505	no pol-thin
160.40	527.93	41.4	bas	J.H.	34.4	33.1	16	1.46	485	H(6) Sr6ah1 P:S=-1.0
170.05	537.25	44.2	P	J.H.	603.0	23.1	42	1.81	530	2 distinct types C1 H1 L1 Sah1? and H4 Sr5-6ah1 H(6) P:S=+0.90?
179.25	546.14	46.4	P	J.H.	103.0	59.2	17	2.24	480	C1 H1-2 L1 P:S=+1.0
189.83	556.36	49.3	P	J.H.	224.0	50.7	15	2.36	535	C1 H1(6) L1 W1 or H(6) Sr6ah3 P:S=?
199.57	565.76	52.1	D?	J.H.	113.0	43.1	34	3.37	560	C1 H3(6) L1 Sr0-3(4-6) P:S=+0.40
210.37	576.20	53.2	D	J.H.	6.7	49.9	27	2.62	465	H(6) Sr6ah1 P:S=-1.0
219.65	585.16	56.2	g brc	J.H.	14.9	0.0	256	0.05	190 600	unoriented unable to classify
230.00	595.16	60.1	unk	J.H.	6.2	24.8	31	1.50	485	C1(2) H2(3-4 L2-4) Sr0-6 P:S-0.40
239.85	604.67	62.3	P	J.H.	29.2	43.3	22	1.91	480	no pol-thin
250.70	615.15	65.1	brc F	J.H.	0.4	2.0	143	0.09	215 625	H(6) no oxides
259.91	624.05	65.2	MF/D	J.H.	19.5	31.7	83	2.39	445 570	C1(2) H3-4 L1 SrO-1 P:S=+0.85
270.23	634.02	69.2	D	J.H.	24.1	31.1	19	1.69	550	C1(2) H3(6) L1 Sr1-4 P:S=-0.50
279.35	642.82	69.2	D	J.H.	22.6	31.9	63	2.19	560	C1(2) H3(4)(6) L!-2 Sr4-6 P:S=-0.40
289.29	652.33	73.1	D?	J.H.	4.6	12.0	21	0.70	550	C1-2 H3-4(5) L2 Sr0-6o0-1 P:S=O.O

Table 2: Magnetic and oxide petrographic properties for samples from Holes CY-1A.

Hole Depth	Crustal Depth	Unit	Lith	Lab	J_O $\times 10^{-4}$	K $\times 10^{-4}$	MDF	J_S	T_C	Oxide classification or Comments
300.05	662.82	75.1	D?	J.H.	12.7	18.0	13	0.28	570	C1 H3^{-4}(5) L1 Sr0-6 or So4 P:S=-0.50 lg decr in J at dn=O incr in J dn=25-100 and 200-250
310.00	672.43	75.1	D?	J.H.	16.3	36.6	21	2.15	570	C1 H3(4)(6) L1 Sr3-6 P:S=-0.80
319.33	681.44	79.4	D	J.H.	15.3	17.3	77	2.00	485	C1(2) H3(4)(6) L1(2) P:S=-0.50
329.90	691.65	81.4	MF	J.H.				1.94	565	unoriented C1-2 H3(6) L1 Sr0-6 P:S=-0.50
339.83	701.24	82.2	D?	J.H.	18.3	32.8	44	1.98	575	C1-2(3) H3-4(6) L1-3 Sr0-6ah1 P:S=-0.20
349.85	710.92	86.1	D	J.H.	22.6	33.8	24	2.08	485 575	C2-3 H2-3(4) L1(2) Sr0-4(5-6)o0-1 P:S=O.O
359.50	720.24	87.3	F/D	J.H.	6.2	0.0	43	1.65	565	C3 H2-3(6) L1 Sr0-6 P:S=-0.65 int incr in J
370.00	730.38	90.2	F?	J.H.	25.3	48.0	82	2.26	570	C1-3 H2-3(6) L1 Sr0-6 P:S=-0.30
380.65	740.67	92.3	D?	J.H.	21.9	39.6	202	1.15	580	C1 H3-4(6) L1 P:S=+1.0 int incr in J
389.82	749.53	94.4	F/P	J.H.	17.3	15.4	195	1.49	580	v poorly oriented C1-2 H3(6) L1 Sr2-6 P:S=-0.70 int incr in J
399.55	758.93	96.1	F?	J.H.	5.0	13.7	146	0.80	575	C1-2 H3(6) L1 Sr(5)6 P:S=-0.90
409.85	768.87	98.2	D	J.H.	10.1	16.4	121	1.27	575	C1-2 H3-4 L1 Sr(2^{-4})5-6ah1 P:S=-0.80
420.38	779.05	101.1	D	J.H.	5.2	9.4	138	0.60	560	C1-2 H(3)4-5(6) L1-2 Sr(0-2)3-6ah3 P:S=-0.30*
430.00	788.34	103.1	F/D	J.H.	4.5	12.5	115	0.57	565	C3 H3(4)(6) L1 Sr(4-5)6 P:S=-0.90
439.71	797.72	104.5	D	J.H.	3.0	10.2	91	0.66	560	C1 H3(6) L1 Sr(4-5)6ah(1) P:S=-0.95
449.50	807.17	106.3	D?	J.H.	9.9	20.9	121	0.90	560	C1 H3(6) L1 Sr(4-5)6 P:S=-0.95
460.05	817.36	109.2	F/P	J.H.	34.1	41.0	98	3.08	565	C1 H3(4)(6) L1 Sr0-6ah2 P:S=-0.20
470.30	827.26	111.1	D	J.H.	4.2	30.8	136	1.31	555	C1-2 H3(4)(6) L1-2 Sr0-6ah1 P:S=+0.40 int incr in J
479.77	836.41	114.1	F?	J.H.	4.5	8.9	429	0.68	570	C1 H3 L1 Sr5-6ah2 P:S=-0.90* at dn=50

Table 2 (continued)

Hole Depth	Crustal Depth	Unit	Lith	Lab	J_O $\times 10^{-4}$	K $\times 10^{-4}$	MDF	J_S	T_C	Oxide classification or Comments
490.45	846.82	116.1	F?	J.H.	2.2	25.1	100	1.35	570	unoriented to core C1(2) H3(6)L1 Sr(5)6ah2 P:S=-0.95*
499.44	855.41	118.1	MF	J.H.	13.9	17.9	132	1.19	575	C2(3) H3(6) L1 Sr(5)6ah4 P:S=-0.95
509.65	865.27	119.3	MF	J.H.	13.6	20.6	283	1.67	555	H(6) Sr6ah2 P:S=-1.O sm incr in J @ dn=25
520.05	875.32	121.2	D	J.H.	21.6	38.9	117	2.70	555	H(4-5)(6) Sr6ah3 P:S=-0.95 int incr in J, lg decr in J at dn=100
529.80	884.73	123.1	MF	J.H.	15.1	24.5	97	1.65	555	H(6) Sr6ah4 P:S=-1.0
539.57	894.17	125.2	brc F	J.H.	1.7	1.4	256	0.31	575	H(6) no.oxides
550.27	904.51	127.2	MF	J.H.	27.8	27.5	224	1.33	555	sm incr in J @ dn=50 H(6) Sr6? P:S=-1.0 (or +1.0)
559.41	913.33	129.3	F?	J.H.	99.0	30.8	135	1.82	470 565	H(6) Sr6ah3 P:S=-1.0
569.80	923.37	130.3	D	J.H.	5.4	25.2	85	1.71	570	H(6) Sr6ah4 P:S=-1.0
580.55	933.75	133.1	D	J.H.	0.4	25.1	175	1.71	565	C2 H3 L1 Sr1-6m1 P:S=O.O int incr in J and at dn=350
590.13	943.01	133.3	D	J.H.	5.7	38.7	89	2.06	565	C2-3 H3-4 L1 Sr(0-3)4-6 P:S=-0.60 int incr in J and at dn=500
599.94	952.48	137.1	D?	J.H.	0.7	22.1	74	0.29	575	int incr in J and at dn=150-200 H(6) Sr6ah! P:S=-1.0
609.84	962.04	139.1	D	J.H.	121.0	54.0	111	3.39	570	Sr6 P:S=-1.0
619.50	971.38	141.2	D?	J.H.	6.3	40.1	88	1.76	560	H(6) Sr6 P:S=-1.0
629.55	981.08	142.1	MF	J.H.	18.3	41.8	190	3.30	580	H(6) Sr6ah3 P:S=-1.0
639.85	991.03	144.2	D	J.H.	11.8	26.3	98	1.71	565	C2-3 H(2)3(6) L1 Sr1-6ah1 P:S=-0.50
649.61	1000.46	144.2	D	J.H.	26.5	41.3	111	2.96	560	C2-3 H3(6) L1-2 Sr2-6ah1 P:S=-0.65
659.77	1010.21	148.1	F?	J.H.	3.1	0.0	116	0.17	575	no mt. H(6) P:S=none all hema. (Sah4?)
670.40	1020.54	151.2	D?	J.H.	8.9	50.7	127	1.64	560	H3-4(6) Sr4-6ah1 P:S=-0.95 incr in J @ dn=25
679.92	1029.73	152.2	F/D	J.H.	6.2	46.0	46	2.59	540	incr in J at dn=350 and 500 H(6) Sr6ah4 P:S=-1.0
689.51	1039.00	155.1	D?	J.H.	1.5	7.9	131	1.62	565	Sr6ah1 P:S=-1.0
700.73	1049.84	156.3	MF	J.H.				1.92	535	unoriented C3 H3(6) L1 Sr5-6ah1 P:S=-0.95

Table 2 (continued)

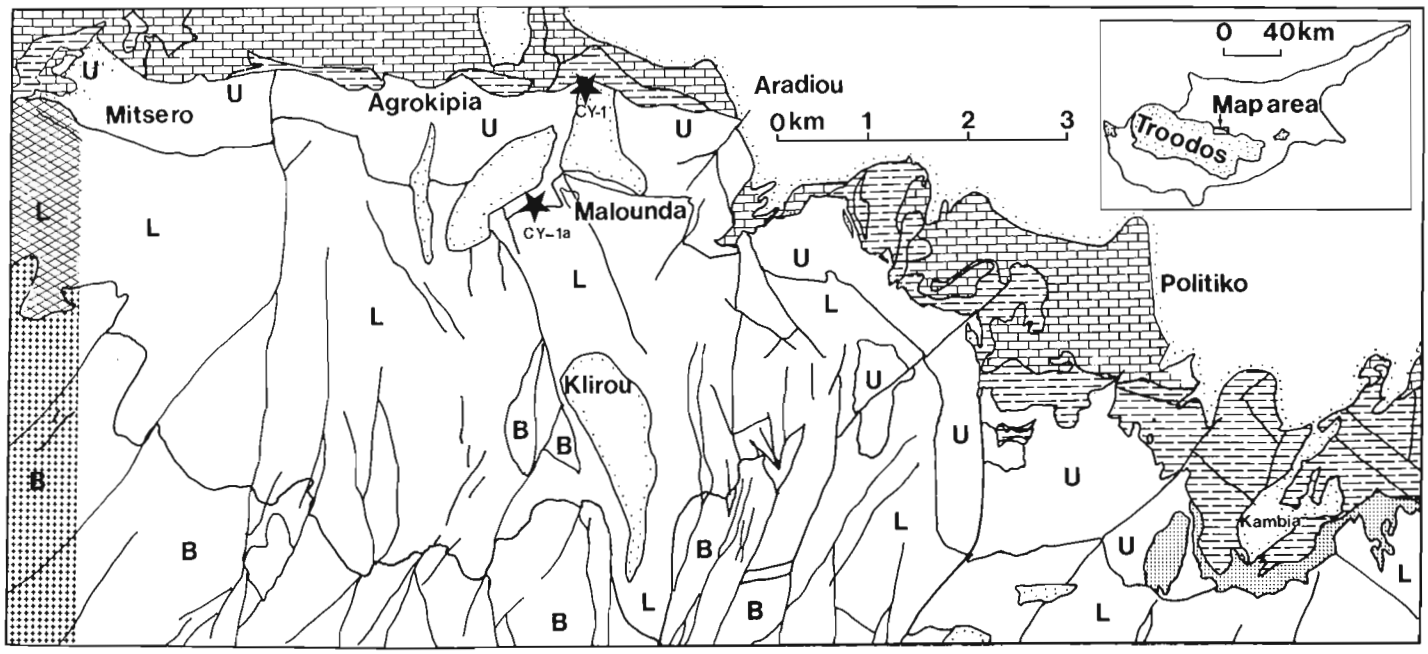

Figure 1: Location map, sites CY-1 and CY-1A. **U** Upper Pillow Lava field mapping unit; **L** Lower Pillow Lava; **B** Basal Group.

available for all samples and the more time consuming measurements on over half the samples. For the CY-1A samples, which were obtained in 1985, a complete suite of measurements is only presently available on 70 samples at 10 m depth spacings. Natural remanence, J_O, and mean demagnetizing field, MDF, measurements were made on both CY-1 and CY-1A samples at Dalhousie University using a Schonstedt DSM-2 magnetometer and GSD-5 alternating field demagnetization unit, and on CY-1 samples at the University of Washington using a cryogenic magnetometer and Schonstedt demagnetization unit. Saturation magnetization, J_S, and Curie temperature measurements were made at Dalhousie University as described in Hall and Ryall (1977). Oxide determinations and measurements were made at Dalhousie University.

MAGNETIC PROPERTIES

(i) Intensity of Natural Remanence, J_O

The distribution with depth of J_O (Figure 2) shows a variety of clearly defined features over different depth intervals. From the surface to 0.56 km depth, values fall within a belt that increases in width with depth.

Low values ($10–20 \times 10^{-4}$ cgs, 1–2 A/m) are present throughout this uppermost zone. The increase in the width of the zone with depth is a consequence of the occurrence of a fraction of increasingly stronger samples: Within the 0–0.1 km interval these stronger samples are typically $\sim 100 \times 10^{-4}$ cgs while below 0.35 km the stronger samples range from 400 to 800×10^{-4} cgs.

A sharp break in this depth trend occurs below 0.56 km. Below this depth all samples are relatively weakly magnetized. With the exception of two samples at $\sim 100 \times 10^{-4}$ cgs, all samples in this lower zone have $J_O \leq 35 \times 10^{-4}$ cgs and many have $J_O \leq 10 \times 10^{-4}$ cgs.

(ii) Mean Demagnetizing Field, MDF

Three zones can be recognized in the depth distribution of this property. From the surface to 0.4 km, MDF (Figure 3) values fall in a belt of 100 oe (10^{-2} Tesla) width, with average values decreasing from 150 oe at the surface to 100 oe at 0.4 km. From 0.4 km to 0.6 km values are without exception low, $\leq$50 oe. From 0.6km to the bottom of the section values are scattered, with a general tendency for minimum values to increase with depth from 20 oe at 0.7 km to 150 oe at 1 km. Irregularly distributed higher values in this third zone range from 200 oe to 400 oe.

(iii) Initial Susceptibility, k

The distribution with depth of k (Figure 4) shows two clear zones. From the surface to 0.6 km values fall within a belt about 16×10^{-4} cgs in width, with average values increasing with exponential trend from $\sim 10 \times 10^{-4}$ cgs at the surface

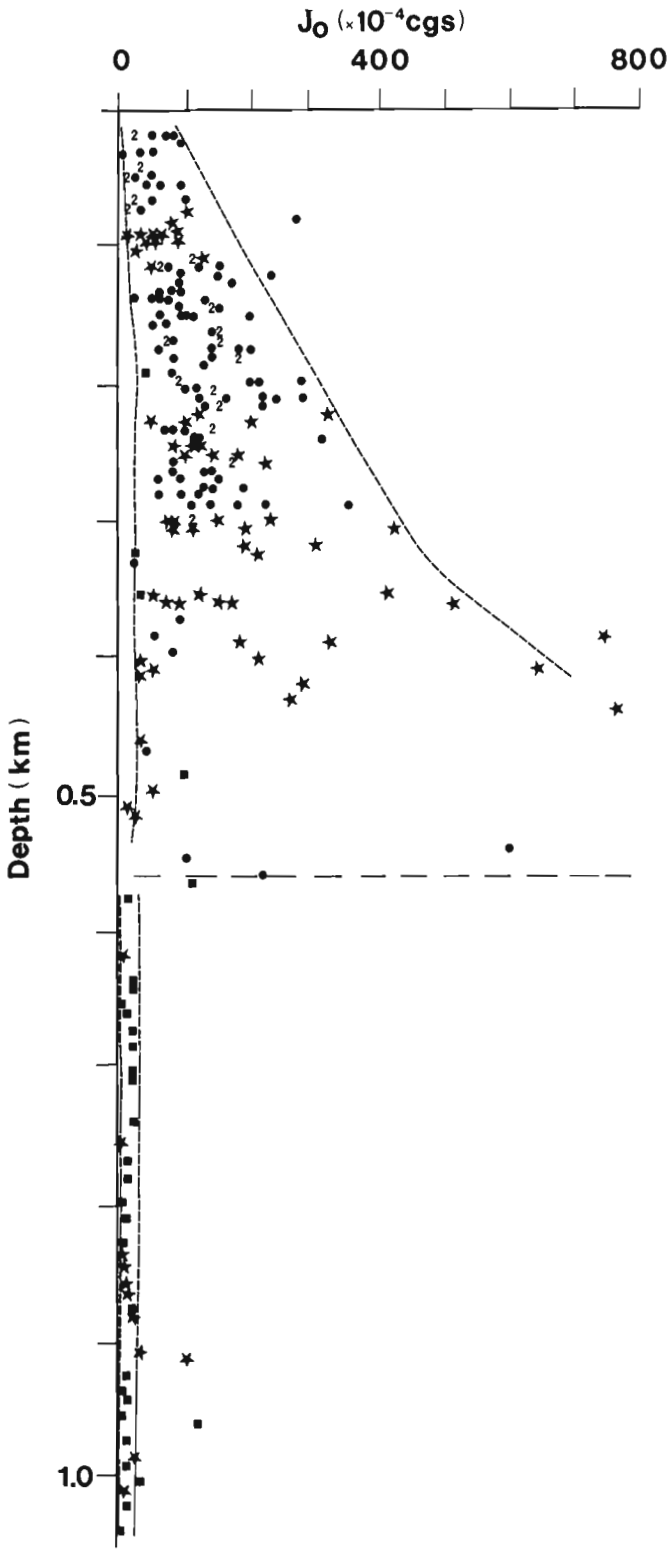

Figure 2: Drillholes CY-1/CY-1A. Distribution with depth of intensity of natural remanence, J_O. In this and successive figures, the following symbols are used for the principal lithologies present: • Sample from pillowed flow; ⋆ sample from massive flow; ■ sample from dyke.

to 40×10^{-4} cgs at 0.6 km. From 0.6 km to the bottom of the section k is broadly scattered between 2×10^{-4} cgs and 48×10^{-4} cgs without any trend with depth.

(iv) Saturation Magnetization, J_S

The distribution with depth of J_S (Figure 5) shows two zones. The boundary between these zones is less clearly defined than for J_O and k. In Figure 5 the boundary is shown tentatively at ~0.44 km. However, if the single low value at this depth is not considered, the boundary would be drawn at between 0.55 km and 0.6 km. The upper zone is characterized by J_S falling within a belt 0.8 cgs in width, with average values increasing with exponential trend from 0.5 cgs at the surface to ~1.5 cgs at 0.44 km (or ~2 cgs at 0.55–0.60 km). The lower zone is characterized by broadly scattered values, ranging from ~0.3 cgs to 3.4 cgs, without any trend with depth.

(v) Curie Temperature T_C

The distribution with depth of T_C (Figure 6) shows four clear zones. From the surface to 0.26 km T_C values lie in belt 100°C in width, with average values decreasing with depth from ~550°C at the surface to ~450°C at 0.26 km. At this latter depth a change in thermomagnetic behaviour occurs: almost all samples in the second zone, from 0.26 to 0.41 km, show two Curie temperatures during the initial heating cycle. The lower of these two T_C values lies between 300°C and 350°C, and the higher usually between 500°C and 550°C. It is possible that the higher T_C for these double T_C samples is an artifact of the heating process. From experience elsewhere, this distribution of T_C values probably indicates that the magnetic phase is rather highly cation deficient titanomagnetite. It is difficult or impossible to prevent these unstable Fe-Ti oxides from phase splitting during heating to 600°C into a magnetite (sensu lato) and possibly a rhombohedral phase. If such phase splitting has generally taken place, then in the natural state the oxides will be characterized by a single, 300–350°C Curie temperature. The third zone extends from 0.41 to 0.63 km. This zone shows somewhat scattered, largely single T_C values in the 375°C to 575°C range, with average values increasing from ~475°C to ~540°C with depth. The fourth zone extends from 0.63 km to the bottom of the section. With a small number of exceptions, T_C is closely confined about ~580°C throughout this zone.

IRON-TITANIUM-OXIDES

Eight properties were measured quantitatively or semi-quantitatively for each of 160 polished surfaces representing all the lithologies present in the section. Sample depths, lithologies, and oxide petrographic properties are listed in Table 1, and are shown as depth profiles in Figures 7 and 8.

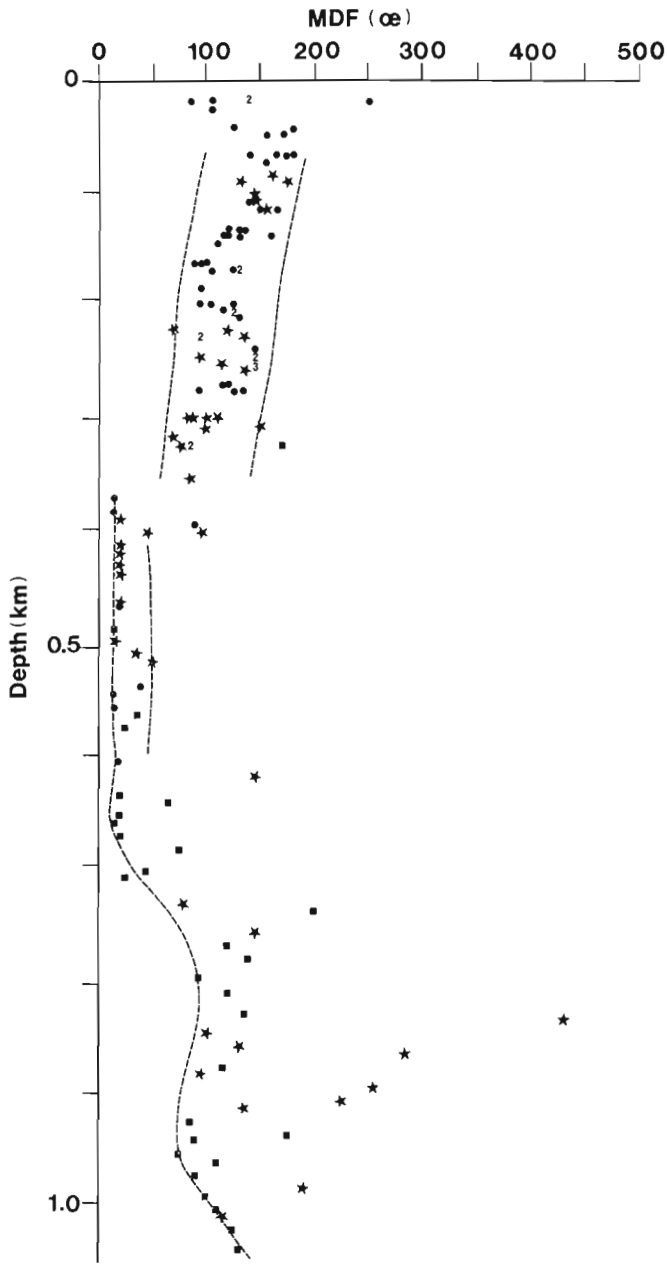

Figure 3: Drillholes CY-1/CY-1A. Distribution with depth of mean demagnetizing field, MDF. Symbols as in Figure 2.

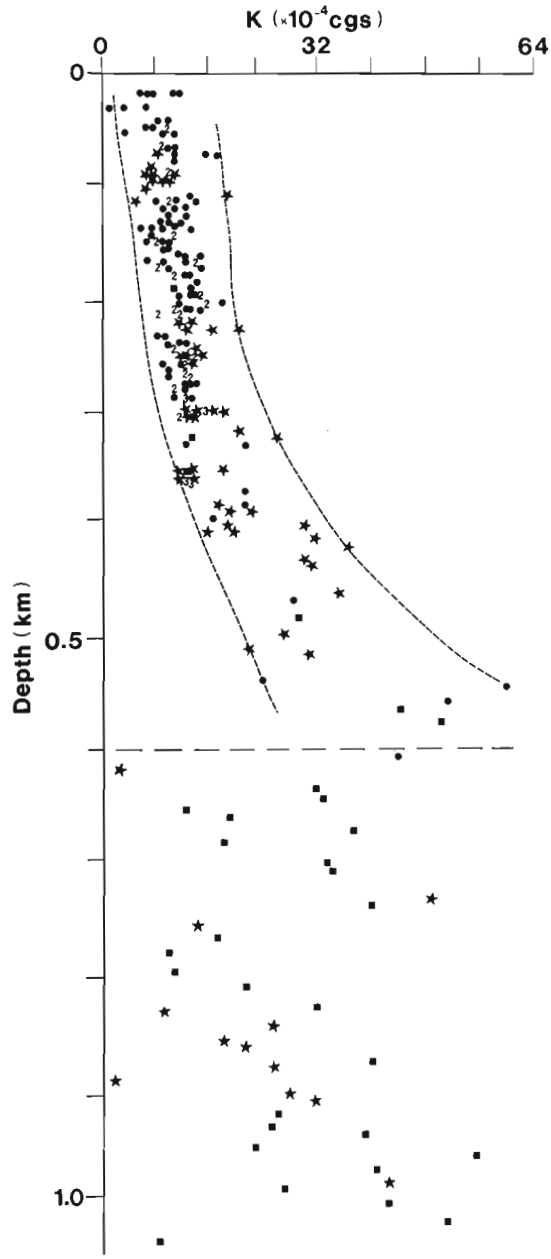

Figure 4: Drillholes CY-1/CY-1A. Distribution with depth of initial susceptibility, k. Symbols as in Figure 2.

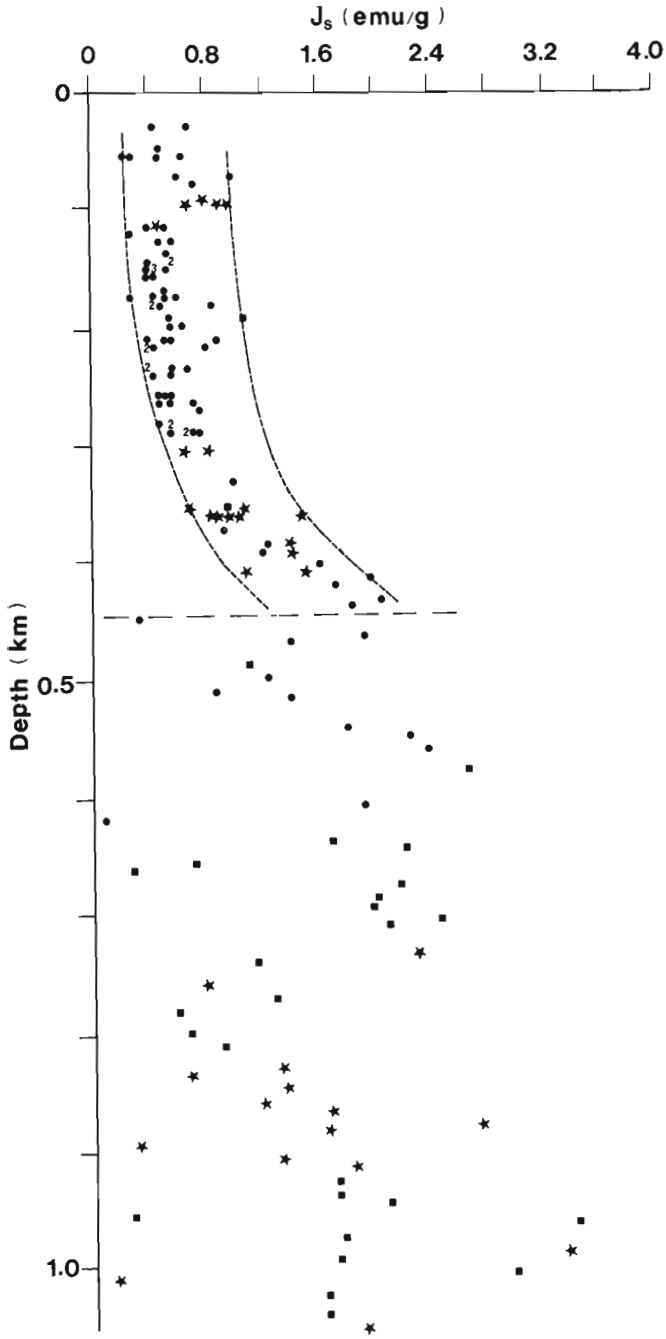

Figure 5: Drillholes CY-1/CY-1A. Distribution with depth of saturation magnetization, J_S. Symbols as in Figure 2.

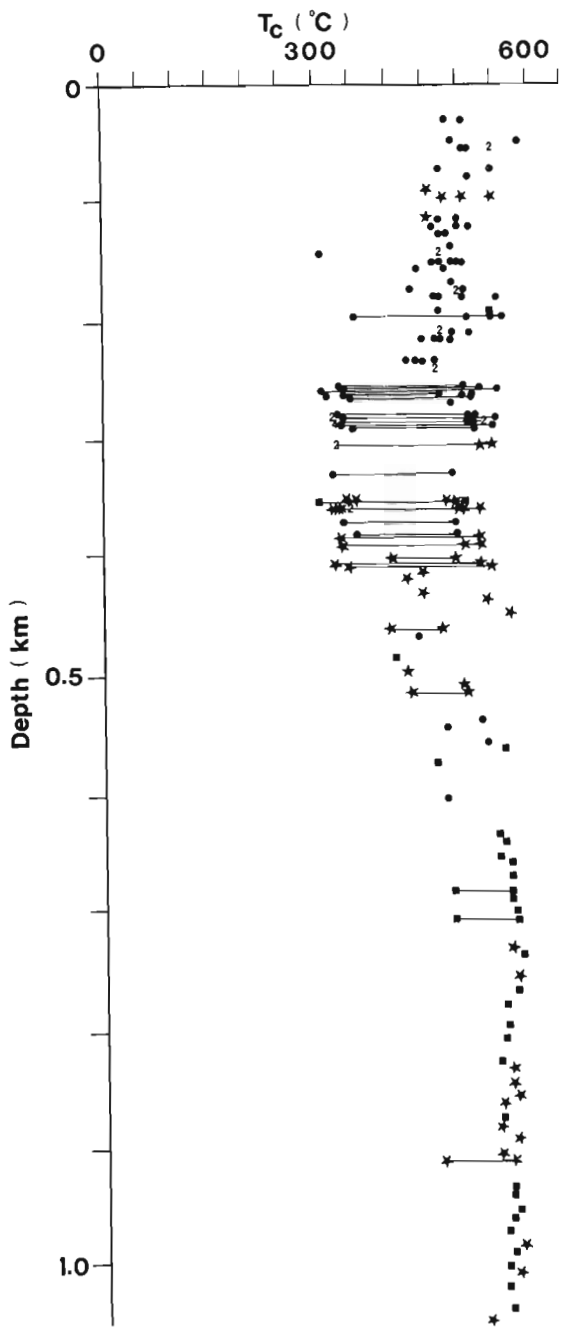

Figure 6: Drillholes CY-1/CY-1A. Distribution with depth of Curie temperature, T_C. Symbols as in Figure 2. Where samples show double Curie temperatures these are joined.

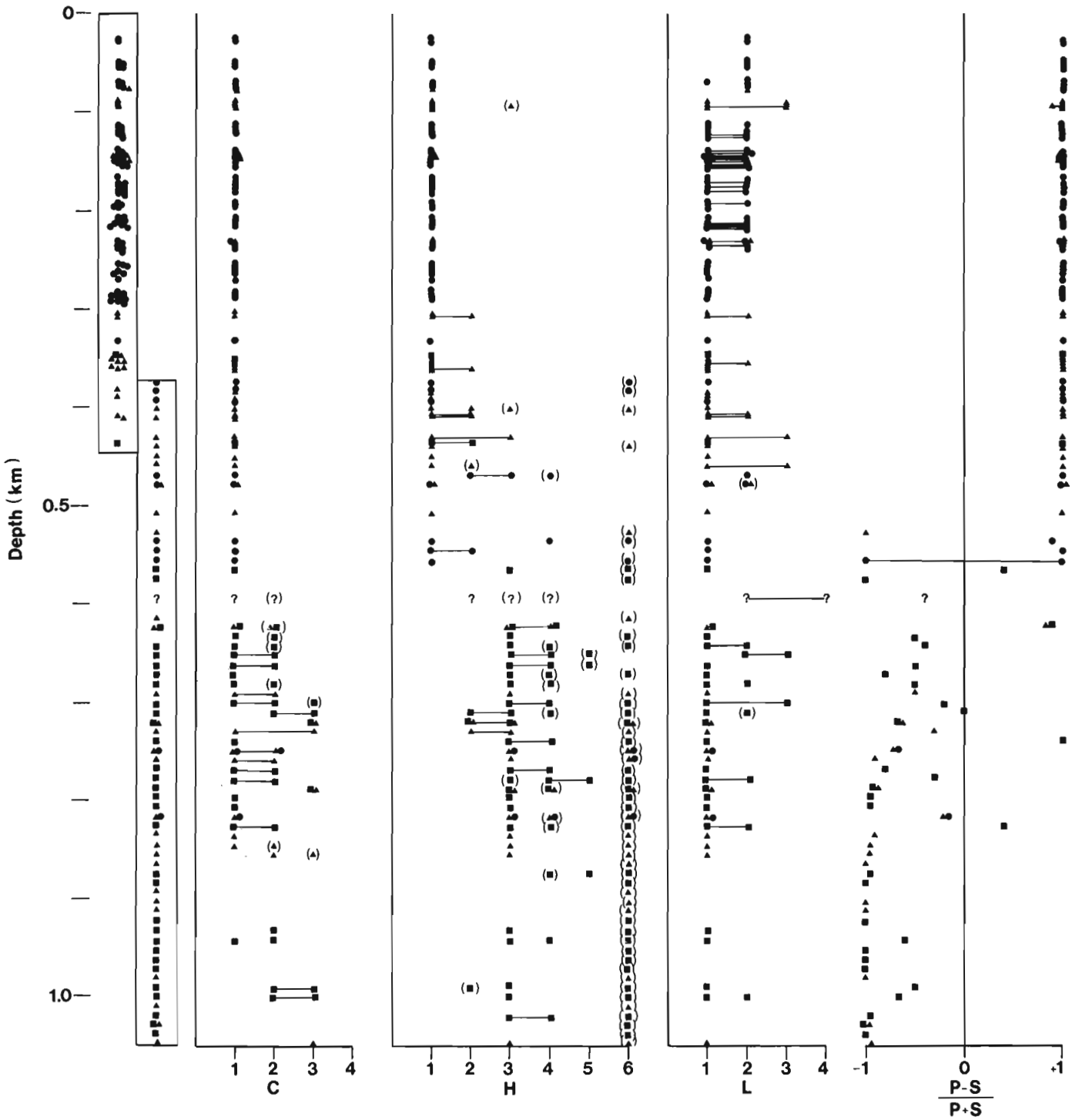

Figure 7: Drillholes CY-1/CY-1A. Distribution with depth of Fe-Ti oxide parameters, I. Explanation of profiles from left to right. Lithological classification of samples: • pillowed flows or pillow breccias; ▲ massive or sheet flows; ■ dykes. Bracketed symbols imply small amount present except in the case for H6 where it implies an uncertain identification. **C** titanomagnetite deuteric oxidation state (as defined in text); **H** titanomagnetite hydrothermal alteration state; **L** titanomagnetite low temperature oxidation; **(P-S)/(P+S)** ratio of secondary to other forms of magnetite.

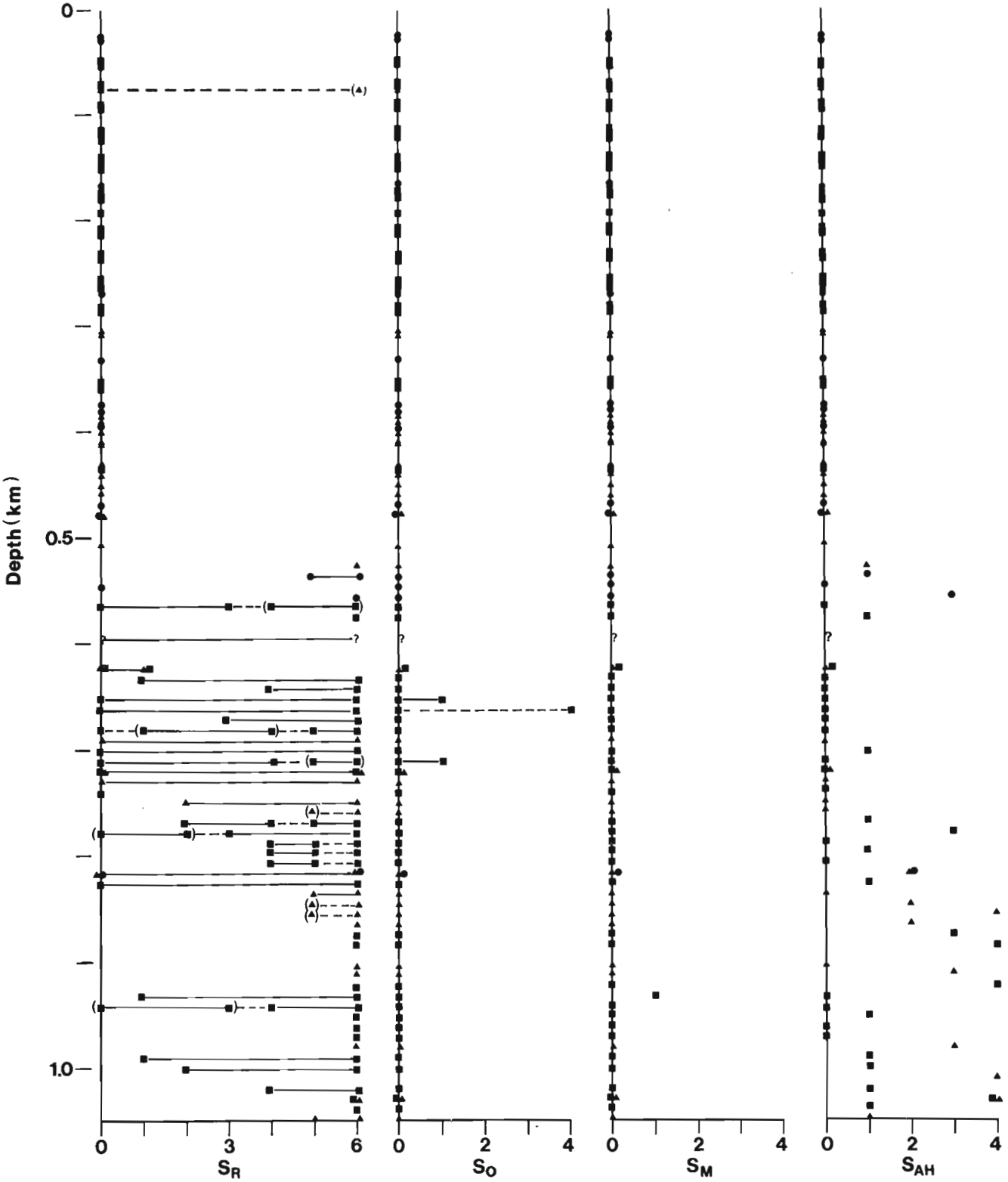

Figure 8: Drillholes CY-1/CY-1A. Distribution with depth of Fe-Ti oxide parameters, II. Explanation of profiles from left to right. Lithological symbols as in Figure 7. S_R titanomagnetite secondary reconstruction (as defined in text); S_O Overgrowths of secondary magnetite on altered primary magnetite; S_M martite development in secondary magnetite; S_{AH} secondary hematite development in secondary magnetite.

All oxide identifications and measurements were made using a Reichert Zeto Pan Pol microscope at a magnification of ×1375.

The properties measured were:

1. titanomagnetite deuteric oxidation state (C)
2. titanomagnetite hydrothermal oxidation state (H)
3. titanomagnetite low temperature oxidation state (L)
4. titanomagnetite secondary reconstruction (S_R)
5. secondary magnetite overgrowths (S_O)
6. martitic alteration in magnetite (S_M)
7. hematitic alteration in magnetite (S_{AH})
8. the relative abundance of primary and secondary magnetite (Ratio R)

The nature of each property measured and the results of each set of measurements are given below.

1. Titanomagnetite Deuteric Oxidation State, C

This is a high temperature form of oxidation, known to occur only during the initial cooling of a rock unit. Several stages of increasing intensity of oxidation are recognized. Before oxidation commences rock units contain uniform grey brown titanomagnetite grains. Oxidation first results in the subsolidus exsolution of ilmenite lamelle. When all the titanium present has been partitioned into ilmenite, oxidation continues with the alteration of the ilmenite lamellae and eventually the residual, near-pure magnetite to phases such as titaniferous hematite, rutile and pseudobrookite. Characteristically, this and other forms of alteration vary rapidly spatially within a rock unit on scales from micrometres (μm) to metres, e.g. Watkins and Haggerty (1968). Another characteristic of many of the samples examined is that the results of several types of alteration are superimposed, so requiring considerable care in identifying a complete paragenetic sequence. The range of alteration stages observed are conveniently classified for within-sample averaging purposes on a 1 (unaltered) to 6 (completely oxidized) scale (Ade-Hall et al., 1971).

Deuteric oxidation state shows rather a well defined increase with depth. From the surface to 0.60 km deuteric oxidation is absent. Between 0.60 and 0.65 km the presence of occasional ilmenite lamellae (C2 state) indicate incipient oxidation. Between 0.65 and 0.70 km occasional lamellae occur in a substantial number of grains. Between 0.70 and 0.85 km some samples have some or all grains with a high density of ilmenite lamellae (C3 state). Below 0.85 km most the small number of samples examined have all magnetite grains with a few or many lamellae. In terms of interval average values, these increase from 1.00 through ~1.1, ~1.5, ~1.8 and ~2.0 through the intervals identified above.

2. Titanomagnetite Hydrothermal Alteration State, H

This category includes a series of hydrothermal alteration states produced through the interaction of titanomagnetite in a range of deuteric alteration states with hot fluids (Ade-Hall et al., 1971). Using results from Iceland (Robinson et al., 1982), where the occurrence of different titanomagnetite alteration states can be correlated with the occurrence of secondary silicate minerals of known stability fields, it is possible to estimate the fluid temperatures needed to produce the different alteration states. As in the case of deuteric oxidation, hydrothermal alteration state often varies from grain to grain within a sample, suggesting that facility of fluid access to a grain, as well as fluid temperature, is important in determining the resulting alteration state. The temperatures equated below with successive alteration states are based on the first occurrence with depth of the state. For a sample characterized by grains showing a range of alteration states, it is suggested that the most altered grains were most likely to have reached or approached equilibrium with the hydrothermal fluid, and thus should be used as a guide to the temperature of the altering fluid.

The first indication of hydrothermal alteration, given in H value of 2 on a 1 to 6 scale, is characterized by either or both small areas of 1 μm anatase granules in titanomagnetite ('granulation'), or the incipient replacement of ilmenite lamellae, produced during deuteric oxidation, by sphene. The fluids responsible for this stage were probably at temperatures of between 50°C and 150°C, with the presence of incipient sphene probably indicating temperatures near the higher end of the interval.

Grains with an H value of 3 are largely or completely granulated or show complete replacement of ilmenite lamellae by sphene. Fluid temperatures of 150–250°C are estimated for this state of alteration.

Grains with an H value of 4 show, in addition to the features characteristic of H = 3, variable erosion of grains. Fluid temperatures of about 260°C are estimated for this state of alteration.

Grains with an H value of 5 or 6 are characterized by the partial or complete, respectively, leaching of iron from grains, leaving translucent pseudomorphs, probably largely consisting of titanium oxides. Fluid temperatures of 290°C and higher are estimated for these states of alteration.

A number of subsequent alteration processes often makes the direct determination of sample hydrothermal alteration state difficult. Thus, reconstruction, or recrystallization, two processes described in detail below, result in the partial or complete loss of the characteristic textures of the different hydrothermal alteration states. However, particularly in the instance of sphene, the characteristic products of hydrothermal alteration are not lost, but are locally redistributed, so allowing an estimate to be made of the hydrothermal alteration component of the history of a sample.

Hydrothermal alteration shows a clear downward increase in intensity. From the surface to 0.3 km this type of alteration is absent. Incipient alteration is seen in the 0.3–0.4 km interval, followed by fairly common alteration of moderate intensity in the 0.4–0.55 km interval. From 0.55 to the bottom of the section, hydrothermal alteration at moderate levels ($3 \leq H \leq 4$) has affected all extrusive and dyke samples. As will be noted from Figure 7, almost all samples below 0.4 km depth are shown as containing possible anatase pseudomorphs after titanomagnetite. Only tentative identification is indicated since, in the absence of electron microprobe analyses, it is possible that these translucent grains are of a phase that is unrelated to the alteration of the Fe-Ti oxides.

3. Titanomagnetite Low Temperature Oxidation State, L

This type of oxidation results from the interaction of water at probably no more than a few tens of degrees centigrade with titanomagnetite. It is particularly well developed in the uppermost part of it in situ oceanic crust where cold seawater saturation or continued drawdown has occurred. A five stage scale of increasing alteration has been recognized by Johnson and Hall (1978).

The profile in Figure 7 suggests that L is rather irregularly distributed with depth. Before this conclusion is accepted consideration must be given to two special circumstances that have made it difficult to determine true values of L over 0–0.26 km and 0.55–1.04 km, respectively.

Most of the samples from the 0–0.26 km interval are from pillowed flows and contain mostly fine grained (≤ 5 μm) altered titanomagnetites. These magnetites are usually gray and are surrounded by red stained silicates. However, curved cracking, recognized elsewhere as evidence for low temperature alteration, is absent from these grains. Since the Johnson and Hall (1978) scale in L depends largely on the presence of these cracks, and the degree in which they widen and become filled with secondary phases, it has not been possible to classify the CY-1 samples using this scale. However, it has been demonstrated that cracking is a grain size related process, and does not occur in grains of ≤ 5 μm. An alternative means of estimating degree of low temperature alteration is through Curie temperature. If the original composition of these CY-1 titanomagnetites was close to that of MORB and many other basalts, where $0.60 \leq x \leq 0.65$ in $(1 - x)Fe_3O_4.Fe_2TiO_4$, then the observed Curie temperatures of 450–550°C imply levels of z, degree of cation deficiency, in excess of 0.95. Such a high level of cation deficiency, which is the fundamental process involved in low temperature oxidation, would be consistent with the gray colouration and evidence for extensive expulsion of iron from the oxides into the surrounding silicates. The appropriate value of L in these circumstances would be 4 or higher (e.g.) Johnson and Hall, 1978, Plate 4, rather than the conservative value of between 1 and 2 shown in Figure 7. If this interpretation is correct, a zone of high L extends from the surface to 0.26 km.

Below 0.26 km primary titanomagnetite is generally brown rather than gray, and adjacent silicates are not red stained. A number of samples contain larger grains which do show curved cracking. This combination of properties is consistent with moderate L values on the Johnson and Hall scale, even where fine grained magnetites fail to show curved cracking.

Below 0.55 km depth, strong hydrothermal alteration and secondary magnetite formation are widespread. Both of these processes are likely to obscure earlier low temperature oxidation. For this reason, the values of L shown for samples below this depth should be considered as minima.

4. Secondary Reconstruction of Magnetite, S_R

This alteration process is apparently a form of thermal metamorphism arising from repeated dyke intrusion. Evidence from Cyprus and elsewhere suggests that it is important where highly hydrothermally altered volcanics contain over 30% of minor intrusions (Hall and Fisher, 1987). The term reconstruction describes the partial or complete pseudomorphing of primary titanomagnetites by nearly pure, stoichiometric secondary magnetite. During this process impurities such as anatase and sphene resulting from hydrothermal alteration tend to be expelled from grains, and curved cracking resulting from low temperature alteration tends to be healed. Various styles of and stages in reconstruction are illustrated in Hall and Fisher, 1987.

In the CY-1/CY-1A sequence reconstruction is absent above 0.53 km, with the exception of the uncertain identification of a minor development, together with some cavity linings, at 0.08 km. The importance of reconstructed magnetite generally increases over the 0.53–0.83 km interval, below which it is the only form of magnetite in most samples. Both dykes and screens of extrusives contain reconstructed magnetites with no apparent preference for development in either lithology.

5. Secondary Magnetite Overgrowths, S_O

This type of secondary magnetite development has the form of clearly defined SM overgrowths that partly mantle altered primary grains. While this type of SM is fairly common elsewhere (e.g. Hall, 1985), in the CY-1/CY-1A profile it only occurs in a small number of samples within the short depth interval between 0.65 and 0.72 km.

6. Ratio, R

This parameter combines the various forms of secondary magnetite and compares the total area of SM with that of altered primary magnetite in a sample. The parameter, ratio, is defined as:

$$R = \frac{\Sigma \text{secondary magnetite} - \Sigma \text{primary magnetite}}{\Sigma \text{secondary magnetite} + \Sigma \text{primary magnetite}}$$

With this definition, R can range from +1.00 (all primary magnetite) to −1.00 (all secondary magnetite).

Since the reconstructed form of secondary magnetite dominates the occurrences of SM, the form of the depth distribution of R closely follows that of S_R: R = +1.00 occurs for all but one sample above 0.53 km. A transition zone characterized by scattered but clearly decreasing average R occurs between 0.53 and 0.83 km. Below 0.83 km, 18 of 22 samples have $R < -0.90$.

7. Martitic Alteration, S_M

The distinctive martitic type of alteration of magnetite consists of lamellae of hematite aligned on octahedral planes in the host magnetite. This type of alteration, which is well developed within the Sheeted Complex of the ophiolite, shows minor development in only one sample, at 0.93 km depth, in the CY-1/CY-1A profile.

8. Secondary Hematite, S_{AH}

Patchy alteration of SM to hematite is a second form of oxidation of SM found in the CY-1/CY-1A profile and elsewhere in the Basal Group and Sheeted Complex of the ophiolite. S_{AH} is a minor feature of SM in the 0.53–0.58 km interval and is present in a sample at 0.7 km depth. It becomes an important feature of S_M below 0.77 km where it is present in most samples, quite frequently at high levels of development.

SUMMARY AND DISCUSSION

A number of the depth distributions described above show property changes at similar depths. Thus, J_O, k and J_S all show gradients, with average values increasing with depth over the upper part of the section. These zones characterized by gradients terminate at between 0.45 and 0.60 km depth. Over this interval MDF and T_C show several segments, each with well defined, but different, depth trends. MDF decreases with depth to 0.45 km, and then shows uniform low values to 0.6 km while T_C decreases with depth to 0.26 km, then shows double Curie temperature behaviour to 0.41 km, below which single T_C increase with depth to 0.63 km.

This uppermost, ~0.5 km, zone, is characterized by the absence of titanomagnetite deuteric oxidation and of hydrothermal alteration above 0.3 km, below which these properties increases to moderate average values by 0.6 km. Low temperature oxidation is probably high to ~0.26 km below which only scattered moderate values occur. Secondary magnetite and secondary hematite are essentially absent in this uppermost, 0.5 km, zone.

Below 0.45–0.60 km, the average values of J_S and k are similar to values for the uppermost zone but the distributions, consisting of broadly scattered values with no depth trends, are quite different from the well confined trends of the uppermost zone. J_O shows a remarkable transition at 0.56 km depth from broadly scattered values ranging up to 800×10^{-4} cgs above this depth to closely confined values with rare exception $\leq 35 \times 10^{-4}$ cgs. Below 0.60 km MDF is scattered with a suggestion of slow, irregular increase with depth. Below 0.63 km T_C is with rare exception confined without depth trend to a narrow band about 580°C. This lower zone is characterized by the increasing deuteric oxidation of titanomagnetite, rather uniform Moderate to high levels of deuteric oxidation and scattered but often low (or indeterminate) values of low temperature oxidation. A striking feature of this lower zone is the importance of secondary magnetite. A transition from dominant primary magnetite to dominant secondary magnetite (SM) occurs at between 0.53 and 0.83 km below which SM is dominant. A further, oxidative stage of alteration of SM is apparent from the rather widespread development of secondary hematite, almost always of the patchy form, particularly below 0.77 km.

The discussion of these results will consider two questions at a preliminary level. Full discussion of these questions will appear elsewhere. These questions are:

- what are the controls on magnetic properties in the section?
- how do the depth distributions of properties compare with those in DSDP Hole 504B?

(a) Controls on magnetic properties in the CY-1/CY-1A section

In order to identify these controls it is useful to consider the combined Curie temperature and oxide data. In the upper zone, in which low temperature oxidation is the principal alteration process, the depth variation of T_C provides a quantitative indication of the intensity of this process. The 0.15 km thick interval between 0.26 and 0.41 km, in which double T_C's occur, is identified as an interval of minimum alteration, with alteration increasing to the surface above this interval, and below it, possibly aided by increasing hydrothermal alteration. It has been widely reported that J_O is related inversely to the degree of low temperature alteration. On the basis of this association, the highest values of J_O would be expected to occur within the zone of minimum low temperature alteration. The data of Figure 2 and Table 1 show that, with one exception, all the values of $J_O \geq 400 \times 10^{-4}$ cgs occur between 0.30 and 0.44 km, closely matching the prediction based on the T_C distribution. The decrease in MDF with depth is also consistent with reports in the literature of the relationship of this property with degree of low temperature oxidation (Ryall, et al., 1977). This result bears on the question of the mechanism of this relationship. It might be expected that the subdivision of grains by curved cracking would increase MDF. However, since such cracking is absent from the small oxide grains in the upper part of the section, some other mechanism must be operative. The initial increases with depth of both J_S and k are also consistent with other reports of the relationship between these properties and degree of low temperature alteration (Ryall et al., 1977). However, the continued increase in these properties where alteration increases again with depth

over the 0.41–0.63 km interval (Figures 6 and 7) appears to require a different explanation. The occurrence of a similar increases with depth in Icelandic rocks has been interpreted in terms of the phase splitting of titanomagnetite during increasing hydrothermal alteration (Hall, 1985, page 99).

The widespread importance of nearly pure and stoichiometric SM at below ~0.53 km appears to provide explanation for the magnetic properties below this depth. The process of the reconstruction of altered primary oxides by SM involves the partial or complete expulsion of impurities such as sphene and anatase from grains, and the healing of physical breaks in grains marking the sites of former lamellae or cracks. Various stages in these processes are illustrated in Hall and Fisher, 1987. These processes will all have the effect of increasing effective grain size, often from the 1–10 μm range to several tens of microns. This increase will probably change the domain state of grains from the pseudo single domain to the multidomain category. In turn, this change may be expected to markedly reduce the ability of grains to retain remanence, which is consistent with the sharp drop in J_O at below 0.51 km while high average levels of k and J_S indicate that magnetite is still relatively abundant. The change from rather well confined depth trends to scattered values of k and J_O with the onset of abundant SM could be the result of spatially variable replacement of highly leached primary magnetites by SM.

(b) Comparison of CY-1/CY-1A and DSDP Hole 504B magnetic property depth distributions

DSDP Hole 504B (Anderson et al., 1982) provides the only continuous section from it in situ oceanic crust that is comparable in depth with the CY-1/CY-1A profile. The 504B section as of July, 1986 extends to close to 1.05 km, essentially identical with the CY-1/CY-1A section. From the basement surface to 0.57 km the 504B section consists almost entirely of extrusives (0.56 km in CY-1/CY-1A) below which a 0.2 km transition interval occurs in which dyke density rises sharply (0.2 km in CY-1/CY-1A). Below .79 km constructional conditions in the two sections are thought to differ. A sheeted dyke complex is thought to occur below this depth in Hole 504B while a very gradual transition to sheeted dyke conditions, extending over 2.3 km, begins in the CY-1/CY-1A section. It is necessary to point out that supposition of sheeted dyke conditions below 0.79 km in Hole 504B is based on 21% core recovery and the results of geophysical logging. A possible alternative interpretation of the Hole 504B data is that this lower part of the sections consists of alternating massive flows and dykes, as is the case in the CY-1/CY-1A section. Alteration in the Hole 504B section is of low temperature type to about 0.89 km, at which depth there is a rapid increase to greenschist conditions.

Extensive compilations of magnetic property data for the Hole 504B profile are reported in various chapters of Anderson, et al. (1985), allowing extensive comparison with the CY-1/CY-1A data (Figure 9). Some oxide data is also available for Hole 504B samples, but this is generally at a much lower density with less complete description than for CY-1/CY-1A, so generally precluding useful comparisons.

The depth distributions of k and J_S in Hole 504B show resemblance in form to CY-1/CY-1A distributions. Thus, k shows regular increase in average value with depth from $\sim 4 \times 10^{-4}$ cgs at that sediment-volcanic interface to $\sim 18 \times 10^{-4}$ cgs at 0.55 km while the increase in the CY-1/CY-1A profile is from $\sim 10 \times 10^{-4}$ cgs to $\sim 40 \times 10^{-4}$ cgs. In Hole 504B J_S increases from 0.6 cgs to 1.5 cgs over this interval while the increase in the CY-1/CY-1A profile is from 0.7 cgs to ~2.0 cgs. Below 0.55 km both properties show scattered values without any recognizable trend with depth.

In contrast with the CY-1/CY-1A profile, J_O in the Hole 504B profile does not show an increase with depth over the uppermost ~0.5 km. Instead, average values are scattered about $\sim 70 \times 10^{-4}$ cgs from the sediment-volcanic interface to 0.4 to 0.5 km, below which values fall to low levels of 10 to 30×10^{-4} over a 0.2 km interval.

The Curie temperature distribution differs from the CY-1/CY-1A at above 0.55 km, below which the distributions are apparently rather similar. From the sediment-volcanic interface to 0.25 km in Hole 504B T_C is closely confined about an average value of ~380°C with no trend with depth. From 0.25 km to 0.55 km T_C is more scattered, but maximum values show an increase with depth from ~380°C at 0.25 km to ~500°C at 0.55 km. Below 0.55 km T_C ranges from 430°C to 590°C, with the majority of values in the 570°C to 590°C interval, and no trend with depth.

It is difficult without detailed oxide data to account for the similarities and differences above 0.55 km between the two profiles. While oxide information is also most desirable below this depth, the magnetic properties show closer resemblance between the two profiles. In this circumstance it is reasonable to suggest that SM formation becomes important at below 0.55 km in the Hole 504B section, and that it would be valuable to examine polished sections to seek its presence.

ACKNOWLEDGEMENTS

We wish to acknowledge Ferenc Stefani, Darlene Van de Rijt, and Norma Keeping for help in preparation of this manuscript. The drilling operations in Cyprus that led to the recovery of the CY-1/CY-1A section were carried out by Bradley Bros. Ltd. of Noranda, Quebec with most effective support from the Cyprus Geological Survey Department. Funding for the drilling operations was provided by IDRC (Canada) grant #3-P-81-1012, Dalhousie University grant #601071, NSERC (UK) grant #GR3/4473, SNF (Denmark) grant #11-11732 Volkswagen Foundation (FRG) grant #I/38 488, and NSF (USA) grant #EAR83-11776.

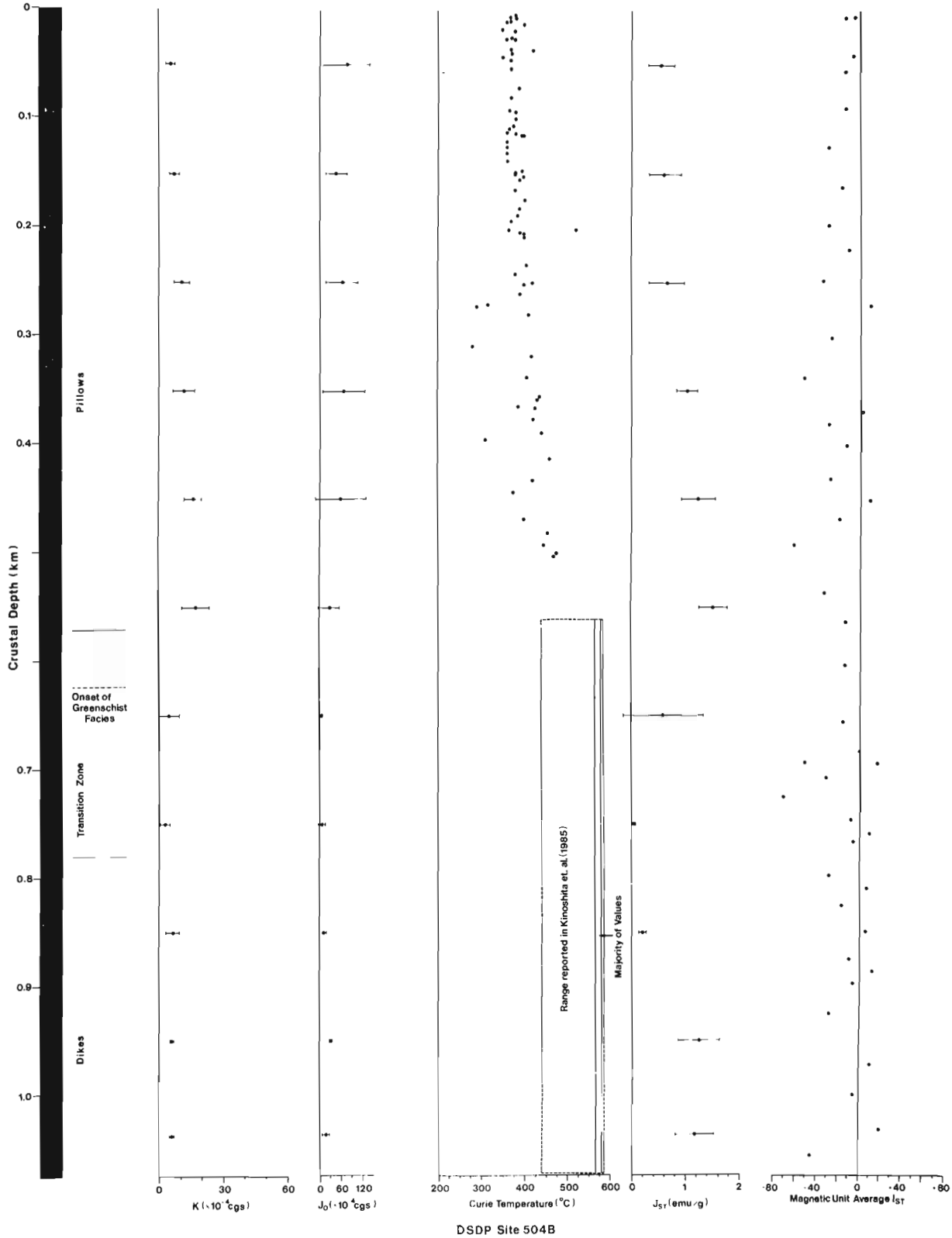

Figure 9: DSDP Hole 504B. Distributions with depth of magnetic properties. Values of k, J_O, and J_S are averages ($\pm$1 standard deviation) for 100 m depth intervals. Values of T_C are for individual samples, where available. Values of I_{ST}, inclination of stable remanance, are cooling unit average values. (Data from various reports in Anderson, et al., 1985.)

REFERENCES

Ade-Hall, J.M., Palmer, H.C., and Hubbard, T.P.
1971: The magnetic and opaque petrological response of basalts to regional hydrothermal alteration; Geophysical Journal of the Royal Astronomical Society, v. 24, p. 137–174.

Anderson, R.N., Honnorez, J., Becker, K., Adamson, A.C., Alt, J.C., Emmermann, R., Kempton, P.D., Kinoshita, H., Laverne, C., Mottl, M.J., and Newmark, R.L.
1982: DSDP Hole 504B, the first reference section over 1 km through layer 2 of the oceanic crust; Nature, v. 300, p. 589–594.

Anderson, R.N., Honnorez, J., Becker, K., et al.
1985: Initial Reports of the Deep Sea Drilling Project, v. 83, U.S. Government Printing Office, Washington, 539 p.

Coleman, R.G.
1977: Ophiolites: ancient oceanic lithosphere?; Springer-Verlag, Berlin, 229 p.

Gass, I.G.
1980: The Troodos massif: its role in the unravelling of the ophiolite problem and its significance in the understanding of constructive plate margin processes; *in* Panayiotou, A., Ophiolites: proceedings of the International Ophiolite Symposium, Cyprus, 1979, Cyprus Geological Survey Department, Nicosia, p. 23–35.

Robinson, P.T., Gibson, I.L., and Horne, L.V.-B.
1991: Cyprus Crustal Study Project Hole CY-1: lithologic unit summaries; *in* Gibson, I.L., Malpas, J., Robinson, P.T., and Xenophontos, C., Cyprus Crustal Study Project: Initial Report, Holes CY-1 and 1A, Geological Survey of Canada, Paper 90–20.

Hall, J.M. and Ryall, P.J.C.
1987: Rock magnetism of basement rocks, Leg 37; *in* Aumento, F., Melson, W.G., et al., Initial Reports of the Deep Sea Drilling Project, v. 37, U.S. Government Printing Office, Washington, p. 489–501.

Hall, J.M.
1985: The Iceland Research Drilling Project crustal section: variation of magnetic properties with depth in Icelandic-type oceanic crust; Canadian Journal of Earth Sciences, v. 22, p. 85–101.

Hall, J.M. and Fisher, B.E.
1987: The characteristics and significance of secondary magnetite in a profile through the dike component of the Troodos, Cyprus, ophiolite; Canadian Journal of Earth Sciences, v. 24, p. 2141–2159.

Hall, J.M., Walls, C., Williamson, M., and Wang, B.-X.
1987: Depth trends in magnetic properties in an area of prolonged cold seawater drawdown in uppermost Troodos-type oceanic crust; Canadian Journal of Earth Sciences, v. 24, p. 941–952.

Johnson, H.P. and Hall, J.M.
1978: A detailed rock magnetic and opaque mineralogical study of the basalts from the Nazca Plate; Geophysical Journal of the Royal Astronomical Society, v. 52, p. 45–64.

Robinson, P.T., Hall, J.M., Christensen, N.I., Gibson, I.L., Fridleifsson, I.B., Schmincke, H.-U., and Schonharting, G.
1982: The Iceland Research Drilling Project: synthesis of results and implications for the nature of Icelandic and oceanic crust; Journal of Geophysical Research, v. 87, p. 6657–6667.

Ryall, P.J.C., Hall, J.M., Clark, J., and Milligan, T.
1977: Magnetization of oceanic crustal layer 2—results and thoughts after DSDP Leg 37; Canadian Journal of Earth Sciences, v. 14, no. 4, pt. 2, p. 684–706.

Watkins, N.D. and Haggerty, S.E.
1968: Oxidation and magnetic polarity in single Icelandic lavas and dikes; Geophysical Journal of the Royal Astronomical Society, v. 15, p. 305–315.

Geology and Geophysics of Boreholes CY-1 and CY-1A of the Cyprus Crustal Study Project: Summary

J. MALPAS[1] AND P.T. ROBINSON[2]

[1]Department of Earth Sciences, Memorial University, St. John's, Newfoundland, A1B 3X5, Canada
[2]Centre for Marine Geology, Dalhousie University, Halifax, Nova Scotia, B3H 3J5, Canada

Malpas, J. and Robinson, P.T., 1991: Geology and geophysics of Boreholes CY-1 and CY-1A of the Cyprus Crustal Study Project: summary; in Cyprus Crustal Study Project: Initial Report, Holes CY-1 and 1A, eds. Gibson, I.L., Malpas, J., Robinson, P.T., and Xenophontos, C.; Geological Survey of Canada, Paper 90–20, p. 257–263, 1991.

Abstract

The CY-1 and 1A boreholes provide together 1185 m of section through the extrusive series of the Troodos ophiolite. The average recovery rate was 94%. Analysis of the recovered samples and the surrounding geology of the Akaki River canyon allows for the division of the extrusive section into approximately ten volcanic units which were developed during a series of volcano-tectonic-hydrothermal cycles. The extrusive rocks are variably altered, depending upon their permeability and local geothermal gradients. Alteration varies from halmyrolysis to incipient greenschist facies metamorphism. The alteration profile clearly affects the physical properties of the rocks. The Troodos volcanics were erupted in a supra-subduction zone environment as demonstrated by their depleted geochemical composition. Comparisons of geochemistry and physical properties of the extrusive section of the Troodos ophiolites and available sections of *in situ* ocean crust are possible. The comparisons suggest that the ophiolite model for the accretion of oceanic lithosphere at present day spreading centres needs further support from deep ocean drilling.

Résumé

Les trous de forage CY-1 et 1A offrent un total de 1185 mètres de coupe à travers les séries extrusives de l'ophiolite de Troodos. Le taux moyen de récupération était de 94%. L'étude des échantillons récupérés et la géologie environnante du canyon du fleuve Akaki permet de diviser la section extrusive en dix unités volcaniques environ, qui ont été formées au cours des séries de cycles volcano-tectonique-hydrothermale. Les roches extrusives sont inégalement altérées selon leur perméabilité et les gradients géothermiques locaux. Les altérations varient de l'halmyrolysis à un métamorphisme naissant vers le faciès schiste vert. Le profil d'altération a une incidence très claire sur les propriétés physiques des roches. L'éruption des roches volcaniques de Troodos s'est effectuée dans le contexte d'une zone de super-subduction, tel que le démontre leur composition géochimique appauvrie. Les comparaisons de la geochimie et le propriétés géochimique de la section extrusive des ophiolites de Troodos ainsi que les coupes disponibles des croûtes océaniques in situ sont possibles, et elles révèlent que le modèle ophiolite de l'accrétion de la lithosphère océanique aux centres d'expansion actuels doit être appuyé par de plus amples preuves provenant de forages océaniques profonds.

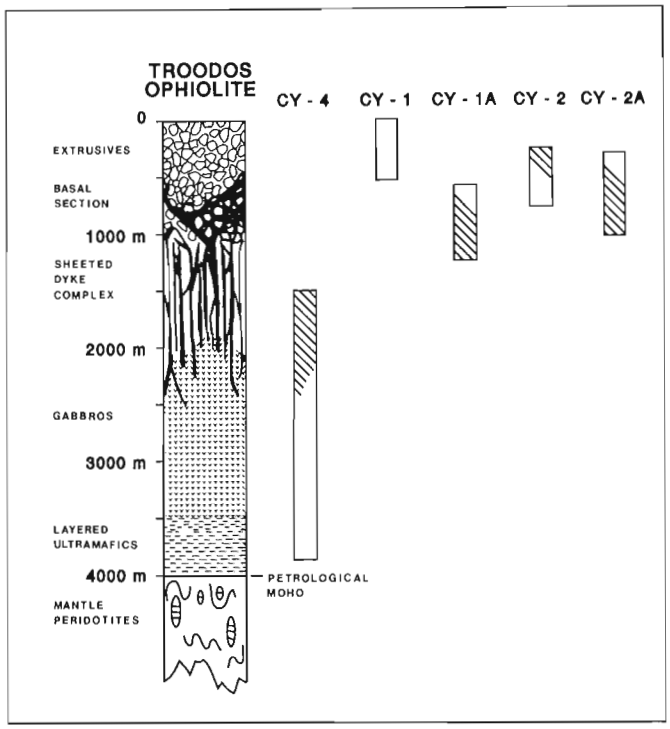

Figure 1: Idealized stratigraphic section of the Troodos ophiolite showing the relative depths of penetration of CCSP Boreholes.

INTRODUCTION

The Cyprus Crustal Study Project was a combined field and research drilling investigation of the Troodos ophiolite. The goal was to develop a three-dimensional picture of the ophiolite in order to understand better its internal geometry, lithology, and structure. From these data, we hoped to gain a better knowledge of the origins of ophiolites, the processes involved in the generation of ocean lithosphere, and the degree to which the ophiolite model can be applied to *in situ* ocean crust. The original plan called for three boreholes into the Troodos massif, one extending from the top of the lavas to the base of the Sheeted Complex, one from the base of the dykes to the base of the gabbros, and one beneath a copper sulphide orebody to sample a hydrothermal upwelling zone (Figure 1). Operational and financial constraints led to a minor modification of this scheme. Holes CY-1 and CY-1A together sampled the extrusive section and the upper part of the Sheeted Complex, whereas hole CY-4 sampled the lower parts of the Sheeted Complex and most of the plutonic section (Gibson et al., 1989). Holes CY-2 and CY-2A penetrated the stockwork zone beneath the Agrokipia orebody (Robinson et al., 1987). Hole CY-3, originally intended to sample the middle portion of the Sheeted Complex, was not drilled.

When the Cyprus Crustal Study Project was initiated, most geologists considered ophiolites to be representative of *in situ* ocean lithosphere formed at mid-ocean ridges although a few petrologists had pointed out significant geochemical differences between some ophiolite lavas and MORB (e.g. Miyashiro, 1973; Pearce, 1975; Cameron et al., 1980; Alabaster et al., 1982). In Troodos, the extrusive sequence had been divided into the Upper Pillow Lavas and Lower Pillow Lavas, but the nature and location of the boundary between the two was equivocal. Some workers considered the distinction to be largely compositional, whereas others suggested that the two were separated by a metamorphic discontinuity. Generally, the volcanic rocks were thought to be highly altered and three subhorizontal metamorphic zones were recognized with zeolite facies rocks overlying those of greenschist facies which, in turn, passed downward into those of amphibolite facies. The rocks were thought to be too highly altered to yield reliable geochemical data on their origin.

Holes CY-1 and 1A were designed to complement field studies of the extrusive sequence and to resolve some of the most important outstanding geological questions. Specific questions to be addressed included: (1) What is the structure of the extrusive section? (2) What is the nature of the lava-dyke transition? (3) What geochemical variations exist in the Troodos lavas? (4) How does alteration of the lavas and dykes vary with depth? and (5) How do the physical and magnetic properties of the lavas and dykes compare with those of *in situ* ocean crust?

Hole CY-1 was spudded at the top of the lava pile in the Akaki River canyon about 1 km north of the village of Malounda. Field mapping in the area revealed the presence of approximately ten lithologic units (Schmincke et al., 1983; Schmincke and Bednarz, 1990), and demonstrated that the lavas had not been pervasively altered but rather contain fresh volcanic glass (Robinson et al., 1983). The entire sequence dips gently to the north and there are few major structures in the area.

We had hoped to penetrate the entire lava sequence in a single hole but poor hole conditions required termination of Hole CY-1 at a depth of 485 m. This hole penetrated the upper part of the extrusive section with a recovery of 92% and included the previously defined boundary between the Upper and Lower Pillow Lavas. Later, Hole CY-1A was spudded about 1 km farther south so as to provide about 50 m of stratigraphic overlap with the base of Hole CY-1 (Figure 2). This hole penetrated 700 m with approximately 96% recovery and sampled the lower part of the extrusive section and the upper part of the dyke complex. Thus, a complete lava stratigraphy was sampled. Data obtained from study of the core material, as well as from exposed sections, have provided answers to most of the questions posed. Here, the results will be discussed under four headings: (1) physical volcanology of the ocean crust, (2) geochemistry of the extrusive rocks, (3) patterns and processes of alteration in the extrusive section, and (4) physical properties of ocean crust.

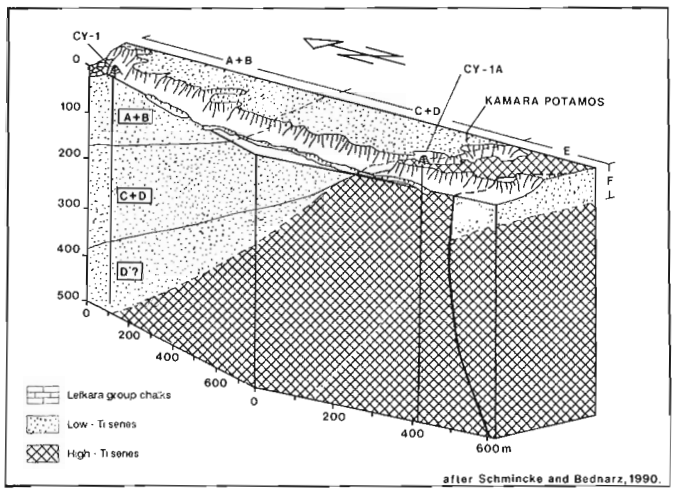

Figure 2: Schematic representation of the geology of the Akaki River canyon in the vicinity of the CY-1 and 1A boreholes.

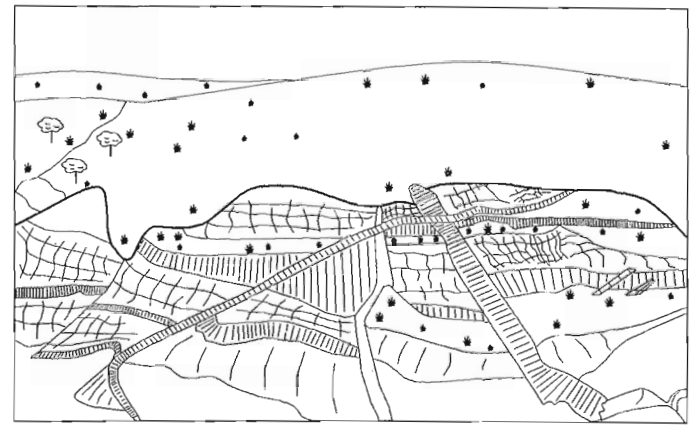

Figure 3: Field sketch of the east bank of the Akaki River canyon in the vicinity of Malounda village showing the thickening of sheet flow lavas adjacent to synvolcanic normal faults. (After Schmincke and Bednarz, 1990).

PHYSICAL VOLCANOLOGY OF THE OCEAN CRUST

Examination of the physical volcanological characteristics of the extrusive rocks of the Troodos ophiolite allows for several comparisons to be made between the Troodos magmas and tholeiitic MORB. Firstly, a higher volatile content of the Troodos lavas compared to MORB is indicated by their generally much higher vesicularity (Schmincke et al., 1983). It might be argued that the high vesicularity was related to extrusion at shallow depths although this not likely since water depths have been estimated at 2000 m from the nature of the overlying sediments (Robertson, pers. comm. in Schmincke and Bednarz, 1990). The high glass content of many of the Troodos volcanic rocks is probably due to the exsolution of volatiles and the concommittant sudden rise of the solidus of the cooling lava. Secondly, the Troodos lavas include a greater proportion of differentiated rock types relative to mid-ocean ridge spreading centres. It is difficult to assess the effect of increased silica on the eruptive viscosity of the lavas, since this was likely offset by the higher volatile contents which would tend to make the lavas less viscous. However, the fact that significant amounts of more differentiated rocks were erupted suggests magma fractionation in small chambers, with infrequent introduction of new magma batches.

The total thickness of extrusive rocks in the Akaki canyon is some 1200 m, but this may be an underestimate due to the unknown offset on a number of faults which cut the section. The thicknesses of the volcanic units identified by Schmincke et al. (1983), vary between 50 and 400 m, the units being defined on the basis of similar physical characteristics and lithologic type. Boundaries are drawn where there are abrupt changes in these features. However, different lithologic types may grade into each other within any one unit, suggesting a gradual change in eruptive conditions.

Schmincke and Bednarz (1990) consider that the volcanic units were erupted relatively quickly. Clearly, the time intervals between the emplacement of individual units must have been relatively short because there is very little sediment deposited in intervolcanic periods. The volcanic rocks, including alternating pillowed flows and sheet flow sequences, appear to have been erupted within a faulted terrain; indeed many faults were clearly active during eruption. These occur as synvolcanic symmetrical growth faults, with displacements of a few metres. Sheet flows thicken against the scarps of down-dropped blocks (Figure 3). The continuation of extensional faulting after eruption of lava resulted in open fissures which increased the permeability of the crust. Circulation of seawater and hydrothermal solutions through the fractures pervasively altered and cemented breccia and rubble and the lavas lining the conduits. Subsequently, new eruptions sealed off much of this circulation and completed one cycle in the volcano-tectonic-hydrothermal sequence. (Schmincke and Bednarz, 1990). Several of these cycles, not always fully developed, overlie one another in the Akaki River section.

GEOCHEMISTRY OF THE EXTRUSIVE ROCKS

One of the prime objectives of the Cyprus Crustal Study Project was to determine the magmatic evolution of the Troodos ophiolite. Lava geochemistry is one of the best guides to magmatic evolution, but the extrusive rocks of Troodos were considered too altered or metamorphosed to provide reliable compositional data. During field studies prior to drilling, fresh volcanic glass was discovered throughout the extrusive sequence, indicating an absence of pervasive metamorphism (Figure 4). On the basis of glass compositions, two distinct lava suites were recognized on the northern flank of Troodos (Robinson et al., 1983; Schmincke, et al., 1983). An early

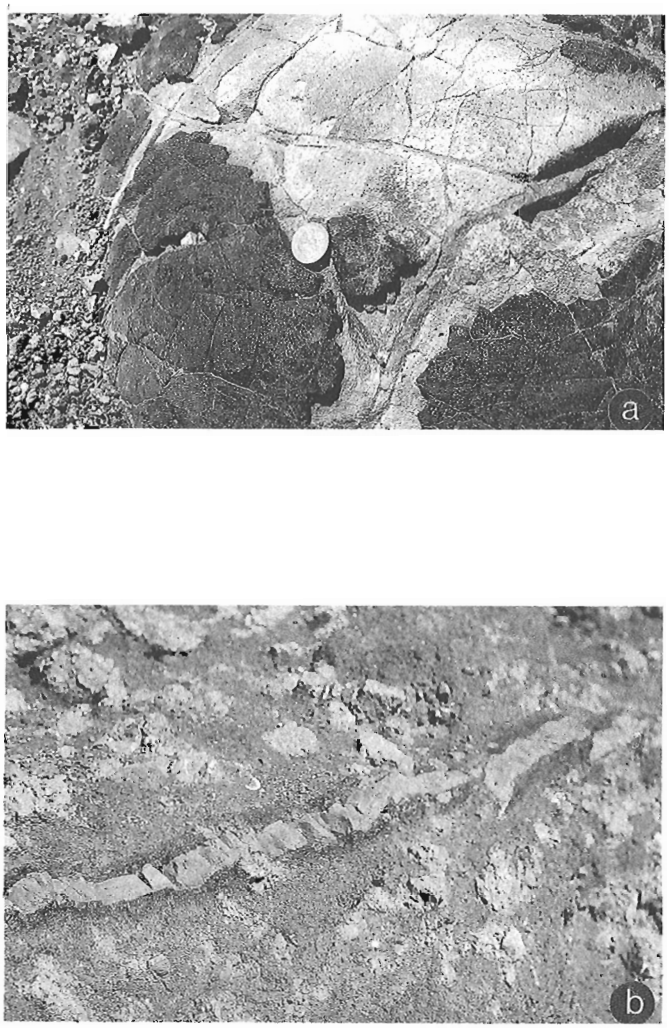

Figure 4: (a) Glassy selvage preserved on aphyric pillow lava; (b) Glassy chilled margin preserved on dyke cutting palagonitized hyaloclastites.

suite of arc-tholeiites, ranging from basalt to rhyodacite, underlies and interfingers with a sequence of depleted lavas, ranging from picrites to andesitic basalts. (A third sequence of even more highly depleted lavas was later recognized on the southern flank of Troodos by Mehegan, 1988).

In the Margi area, these two major suites correspond to the Upper and Lower Pillow Lavas as defined by Bear (1960), but elsewhere their stratigraphic relationships are less clear due to poor field exposures, structural complexity and incomplete sampling. Holes CY-1 and 1A provide a nearly continuous section through the lavas, allowing the high resolution sampling required to determine the precise relationship between the different lava suites. The geochemical data set for Holes CY-1 and 1A includes major element data from volcanic glasses (Mehegan, 1988) and major and minor element data from bulk rocks samples (this volume). This data set was evaluated with cluster analysis, which resulted in the identification of two major magma groups (Mehegan and Robinson, this volume). These major magma groups (A and B) can be further subdivided into five subgroups (A1, A2, B1, B2 and B3) on the basis of trace element chemistry, each representing an important magma type. Subgroup A2 is distinguished from A1 primarily on the basis of lower Zr and TiO_2 contents whereas, subgroups B1, B2, and B3 differ chiefly in their Cr and Ni contents.

All of the analyzed lavas in Hole CY-1 belong to group B and there is a regular repetition of subgroups B1 and B2 downhole (Mehegan and Robinson, this volume). Lavas of subgroup B2 are most abundant near the top of the section where they are intercalated with thin layers of picrite belonging to subgroup B3.

In Hole CY-1A, the lava stratigraphy is partly obscured by three major dyke swarms, but most of the section consists of Group A lavas. Both subgroups A1 and A2 are present and these alternate downhole. Lavas of subgroup A2 are most abundant in the upper part of the hole, whereas those of subgroup A2 dominate below about 185 m (Mehegan and Robinson, this volume). Group B lavas occur in two intervals; 0–15 m and 115–165 m. The uppermost group B lavas are olivine-phyric rocks, with high-Cr contents characteristic of subgroup B3. Between 115 and 165 m, aphyric lavas of subgroups B1 and B2 alternate with each other. A thin layer of A2 lava is intercalated with the group B lavas in this interval.

Group A and B lavas cannot be linked by any simple fractionation scheme and are believed to represent separate parental melts (Tarney and Marsh, this volume; Mehegan, 1988). Major element variations within these groups can be modelled by limited crystal fractionation, but trace element data suggest the presence of several small, discrete subgroups. Thus, the available data suggest that the rocks were fed from a number of small, unique magma supply systems rather than by a single continuously evolving chamber. This is particularly obvious from the lava stratigraphy in the Margi area to the east of the Akaki canyon. Here, lavas of Group B affinity include picritic pillows and massive flows, with concentrations of olivine phenocrysts that have clearly been controlled by gravitational settling, either within the flows themselves or within high level magma chambers prior to eruption. The geochemical stratigraphy described by Bailey et al. (this volume) clearly supports the model of small, independent magma chambers feeding the volcanic rocks.

All of the Troodos lavas have a clear supra-subduction zone signature characterized by very low contents of high field-strength elements. Thus they are believed to have formed by hydrous partial melting of depleted upper mantle material. Once formed, the magmas of Groups A and B followed generally separate evolutionary paths and maintained their distinct compositional identities. Although most Group A lavas are found in the lower parts of the extrusive sequence and most Group B lavas in the upper parts, the two interfinger at various stratigraphic levels. The available data suggest that both lava types were erupted during spreading and were in

part consanguineous, i.e. the Upper Pillow Lavas are not a post-spreading, off-axis sequence.

PATTERNS AND PROCESSES OF ALTERATION IN THE EXTRUSIVE SECTION

Early workers in Troodos were impressed by the abundance of secondary minerals and the obvious colour variations in the lavas, and concluded that all the extrusives were highly altered. Smewing (1975) and Gass and Smewing (1973) redefined the Upper Pillow Lava/Lower Pillow Lava boundary as a metamorphic facies change. The Upper Pillow Lavas were believed to be affected by zeolite facies metamorphism, whereas the Lower Pillow Lavas and much of the Sheeted Complex were thought to have undergone pervasive greenschist facies alteration. Gass and Smewing (op cit) thus interpreted the Lower Pillow Lavas and underlying dykes as an 'axis sequence,' whereas the Upper Pillow Lavas were thought to have formed 'off-axis.'

The discovery of fresh volcanic glass throughout the extrusive section indicates that the lavas have not been pervasively metamorphosed and that the processes of alteration were more complex than originally believed. Gillis (1987) and Gillis and Robinson (1988) concluded that permeability was the principal factor controlling alteration in the lavas and that temperature gradients, bulk rock composition, and lithologic nature of the units were of secondary importance. They recognized five alteration zones in the extrusive sequence which vary widely in lateral extent and thickness. At the top of the sequence is a zone of oxidation alteration called the Seafloor Weathering Zone, in which the rocks are stained red, yellow and brown. This zone reflects downward percolation of seawater and is thickest where the lavas have been exposed the longest on the seafloor. Where the lavas were sealed quickly by the deposition of synvolcanic umbers, the seafloor weathering zone is thin or missing, and fresh volcanic glass occurs at the top of the sequence (e.g. in the Margi area). In other areas, this zone may be several hundred metres thick. Below the Seafloor Weathering Zone is a sequence of darker coloured lavas in which vesicles, fractures, and interpillow spaces are filled with mixtures of clay minerals, zeolite, and minor carbonate. In this Low Temperature Zone, alteration is highly variable and is believed to reflect the penetration of cold seawater into the crust during early hydrothermal circulation. The Low Temperature Zone is underlain by a Transition Zone, characterized by higher temperature zeolite such as laumontite and higher percentages of interlayered clay minerals. This in turn passes downward into the Upper Dyke Zone, in which higher temperatures are indicated by assemblage of chlorite, epidote, sphene, and albite. The Upper Dyke Zone is believed to represent hydrothermal alteration at temperatures of 200–400°C. The Transition Zone is interpreted as a boundary between relatively hot hydrothermal fluids at depth and relatively cold seawater above.

Most of these zones are represented in the drill core from Holes CY-1 and 1A. The Seafloor Weathering Zone is present in the upper parts of Hole CY-1. The exact thickness of this zone is equivocal. Gillis and Robinson (this volume) place the lower boundary at 275 m but Bednarz et al. (this volume) suggest that a transition zone exists between 240.0 and 336.9 metres, in which the effect of low temperature hydrothermal alteration has been overprinted by cold-seawater alteration associated with seafloor weathering. This Seafloor Weathering Zone is characterized by secondary assemblages including smectite, Fe-hydroxides, calcite, and adularia with minor amounts of zeolite (Gillis and Robinson, this volume; Bednarz et al., this volume; Kurnosov et al., this volume). The most pronounced chemical changes in this zone are K_2O enrichment and Na_2O depletion, reflecting replacement of the plagioclase by adularia. CaO is variable, commonly showing depletion in individual samples but enrichment over larger intervals, reflecting an abundance of calcite veins and interpillow limestones. $Fe^{3+}/(Fe^{3+} + Fe^{2+})$ ratios average about 0.7–0.9, reflecting the oxidizing effects of seawater (Bednarz et al., this volume). Temperatures in this zone were probably close to ambient seawater and water/rock ratios were very high (>100). The underlying Low Temperature Zone extends to a crustal depth of about 700 m (about 270 m in CY-1A). It is characterized by an abundance of zeolite, particularly analcime, smectite, and celadonite. Plagioclase is mostly fresh, although some albitization occurs below about 175 m in Hole CY-1A. Most volcanic glass has been altered to smectite or celadonite but fresh glass is abundant locally. The main chemical effects of alteration in this zone are enrichment in Na_2O and MgO, reflecting the presence of albite and smectite, respectively. K_2O is locally enriched where celadonite is abundant (Bednarz et al., this volume). Temperatures were probably less than approximately 170°C and water/rock ratios were relatively high (>20), but not as high as in the overlying Seafloor Weathering Zone (Bednarz et al., this volume; Gillis and Robinson, this volume).

Most of the lower part of Hole CY-1A has been affected by higher temperature hydrothermal alteration of the Upper Dyke Zone. Mineral assemblages are dominated by chlorite, epidote, sphene, and albite. Significant enrichment in Na_2O, and depletion in K_2O and CaO, reflect the pervasive albitization. Temperatures are estimated to have been <350°C and water/rock ratios on the order of 15 or less (Bednarz et al., this volume). In this zone, the section is cut by a series of dyke swarms which are believed to have raised the temperature and caused a local stepped geothermal gradient (Gillis and Robinson, this volume).

Although there are some difference in the style and nature of alteration between the Troodos lava and those of *in situ* ocean crust, similar alteration zones can be recognized in both (Gillis and Robinson, 1988). Thus, we believe that the data from the Troodos ophiolite can shed considerable light on present-day active hydrothermal systems in the ocean crust.

PHYSICAL PROPERTIES OF THE OCEAN CRUST

Holes CY-1 and CY-1A together provide a reference section of approximately 1200 m through equivalents of ocean seismic layers 2A and 2B, and possibly 2C (Houtz and Ewing, 1976). Lithological types identified in the core include pillow lavas, massive flows, and dykes. A number of physical properties were measured on core samples and compared directly to those from Hole 504B of the Deep Sea Drilling Project, the only hole in *in situ* ocean crust that compares in depth with the CY-1/1A profile. These properties are: compressional and shear wave velocities (Vp and Vs), saturated bulk density (s) and grain density (g), porosity (ϕ), electrical conductivity (σ), intensity (J_{NRM}) and inclination (I_{NRM}) of remanent magnetization, and magnetic susceptibility (χ). Poisson's ratio, Archie's exponent (m) and Koenigsberger ratio (Qn) were subsequently derived.

On the basis of laboratory measurements, three units have been recognized within the core, with a gradational contact between the upper and middle units at 165–260 m depending upon the physical property measured, and a sharp, faulted contact between the middle and lower units at 750 m. The gradational contact between the upper and middle units is of particular interest. It is thought to reflect the extent of halmyrolysis, or seafloor weathering of the samples. Halmyrolysis decreases with depth to 260 m, below which seafloor weathering gives way to zeolite facies alteration. Since weathering affects different physical properties of the rocks to different degrees, the contact between upper and lower units cannot be defined in a simple fashion. Essentially, however, the upper unit is characterized by relatively steep gradients in physical properties; an increase in seismic velocities, NRM intensity and susceptibility, and a decrease in porosity and electrical conductivity with depth. The middle unit is characterized by moderate gradients in physical properties; increasing density, seismic velocities, and magnetic susceptibility, decreasing porosity and electrical conductivity, and little change in NRM intensity with depth. The lower unit, which consists predominantly of dykes, also shows significant differences in physical parameters. The sharp, faulted contact with the overlying unit is marked by a slight increase in density and velocities, accompanied by slight decreases in porosity, conductivity, and NRM intensity. Density, velocities, and susceptibility continue to increase and porosity and conductivity to decrease with depth. Smith and Vine (this volume) equate the three units with lithological zones displaying halmyrolysis, zeolite facies, and greenschist facies metamorphism, respectively. However, the model of a simple horizontal metamorphic stratigraphy is not entirely applicable to the Troodos crust, as explained above. By comparison with physical property measurements made on *in situ* ocean crust from DSDP Hole 504B, there is a possible analogy between the upper, middle and lower units of the Troodos section and ocean seismic layers 2A, 2B, and 2C. The analogy is not very satisfactory, however, since velocities and densities in the Troodos crust are anomalously low, and porosities and conductivities anomalously high. Indeed, the upper 1 km of the Troodos crust provides only a poor comparison with *mature* ocean crust in terms of the absolute values of its various physical characteristics.

CONCLUSIONS

The Cyprus Crustal Study Project of the International Crustal Research Drilling Group has provided an opportunity to reinvestigate a range of problems associated with the Troodos ophiolite. It appears clear now that the ophiolite was produced in a supra-subduction zone environment at a consuming plate margin by crustal extension above the down-going lithosphere slab. Ocean crust was produced by processes in multiple magma chambers which, for the most part, developed independently of one another and which contained magmas derived by partial melting of mantle sources with different degrees of depletion. These magma chambers erupted volcanic rocks above a sheeted dyke complex at a series of spreading axes now recognized on the basis of dyke domains. The ocean crust represented by the Troodos ophiolite was altered extensively at the level of the sheeted dykes, but to a lesser extent and only locally in the extrusive complex.

Troodos has long been regarded as a classic example of the ophiolite assemblage. The fact that it originated in a supra-subduction environment begs the question of its correlation with ocean crust formed at present day mid-ocean ridges. Physical property measurements do not support a close analogy with mature ocean crust. However, in terms of the processes of crustal accretion, despite geochemical and physical property differences, the ophiolite model is still the best available, especially where spreading rates are low. Conclusive proof is obviously required by deeper drilling of *in situ* ocean crust.

REFERENCES

Alabaster, A., Pearce, J.A., and Malpas, J.
1982: The volcanic stratigraphy and petrogenesis of the Oman ophiolite complex; Contributions to Mineralogy and Petrology, v. 81, p. 168–183.

Bear, L.M.
1960: The geology and mineral resources of the Akaki-Lythrodondha area; Cyprus Geological Survey Department Memoir, v. 3, 222 p.

Cameron, W.E., Nisbet, E.G., and Dietrich, V.J.
1980: Petrographic dissimilarities between ophiolitic and ocean-floor basalts; *in* Panayiotou, A., Ophiolites: proceedings of the International Ophiolite Symposium, Cyprus, 1979, Cyprus Geological Survey Department, Nicosia, p. 182–192.

Gass, I.G. and Smewing, J.D.
1973: Intrusion, extrusion, and metamorphism at constructive

margins: evidence from the Troodos Massif, Cyprus; Nature, v. 242, p. 26–29.

Gibson, I.L., Malpas, J., Robinson, P.T., and Xenophontos, C., eds.

1989: Cyprus Crustal Study Project: Initial Report, Hole CY-4, Geological Survey of Canada, Paper 88–9, 393 p.

Gillis, K.M.

1987: Multistage alteration of the extrusive sequence, Troodos ophiolite, Cyprus; (PhD Thesis), Dalhousie University, Halifax, 387 p.

Gillis, K.M. and Robinson, P.T.

1988: Distribution of alteration zones in the upper oceanic crust; Geology, v. 16, p. 262–266.

Houtz, R. and Ewing, J.

1976: Upper crustal structure as a function of plate age; Journal of Geophysical Research, v. 81, no. 14, p. 2490–2498.

Mehegan, J.M.

1988: Temporal, spatial, and chemical evolution of the Troodos ophiolite lavas, Cyprus: supra-subduction zone volcanism in the Tethys Sea; (PhD Thesis), Dalhousie University, Halifax, 700 p.

Miyashiro, A.

1973: The Troodos ophiolitic complex was probably formed in an island arc; Earth and Planetary Science Letters, v. 19, p. 218–224.

Pearce, J.A.

1975: Basalt geochemistry used to investigate past tectonic environments on Cyprus; Tectonophysics, v. 25, p. 41–67.

Robinson, P.T., Gibson, I., and Panayiotou, A., eds.

1987: Cyprus Crustal Study Project: Initial Report, Holes CY-2 and CY-2A; Geological Survey of Canada, Paper 85–29, 381 p.

Robinson, P.T., Melson, W.G., O'Hearn, T., and Schmincke, H.–U.

1983: Volcanic glass compositions of the Troodos ophiolite, Cyprus; Geology, v. 11, p. 400–404.

Schmincke, H.-U. and Bednarz, U.

1990: Pillow, sheet flow and breccia flow volcanoes and volcano-tectonic-hydrothermal cycles in the Extrusive Series of the northeastern Troodos ophiolite (Cyprus); *in* Malpas, J., Moores, E.M., Panayiotou, A., and Xenophontos, C., Ophiolites — Oceanic Crustal Analogues. Proceedings of the Symposium 'TROODOS 1987,' Cyprus Geological Survey Department, Nicosia, p. 185–206.

Schmincke, H.-U., Rautenschlein, M., Robinson, P.T., and Mehegan, J.M.

1983: Troodos extrusive series of Cyprus: a comparison with oceanic crust; Geology, v. 11, p. 405–409.

Smewing, J.

1975: Metamorphism of the Troodos Massif, Cyprus; (PhD Thesis,) Milton Keynes, Open University, England, 132 p.

Major Element and Trace Element Analytical Data: Cyprus Crustal Study Project Holes CY-1 and CY-1A

Major element and trace element analytical data: Cyprus Crustal Study Project Holes CY-1 and CY-1A; in Cyprus Crustal Study Project: Initial Report, Holes CY-1 and 1A, eds. Gibson, I.L., Malpas, J., Robinson, P.T., and Xenophontos, C.; Geological Survey of Canada, Paper 90–20, p. 263–283, 1991.

Abstract

Major element data (SiO_2, Al_2O_3, Fe_2O_3, FeO, MgO, CaO, Na_2O, K_2O, H_2O+, TiO_2, P_2O_5, MnO, CO_2) is presented for 281 samples from Hole CY-1 and 187 samples from Hole CY-1A. Data are arranged according to sample depth, and, in addition to the analytical data, the responsible laboratory is also indicated. Comparable information, usually for splits from the same samples, is provided for the trace elements (Rb, Sr, Ba, Zr, Cr, Ni, Co, V, Th, U, Y, Pb, Cu, Zn, Ga, La, Ce), the data tables listing results for 174 samples from CY-1 and 186 samples from CY-1A. The Laboratories are: Ruhr-Universität Bochum, Federal Republic of Germany (BOCHUM); The Open University, U.K. (OU); Memorial University of Newfoundland, Canada (MUN); Geological Survey of Canada, Ottawa (GSC).

Résumé

Les données sur les éléments majeurs (SiO_2, Al_2O_3, Fe_2O_3, FeO, MgO, CaO, Na_2O, K_2O, H_2O+, TiO_2, P_2O_5, MnO, CO_2) sont présentées pour 281 échantillons du forage CY-1 et pour 187 échantillons du forage CY-1A. Les données sont arrangées selon la profondeur échantillonée, et en plus de la donnée analytique, le laboratoire responsable est aussi indiqué. De l'information comparable, habituellement pour des parties des mêmes échantillons, est fournie pour les éléments traces (Rb, Sr, Ba, Zr, Cr, Ni, Co, V, Th, U, Y, Pb, Cu, Zn, Ga, La, Ce), les tables de données énumérant les résultats de 174 échantillons de CY-1 et 186 échantillons de CY-1A. Les laboratoires sont: Ruhr-Universität Bochum, Allemagne de l'Ouest (BOCHUM); The Open University, R.-U. (OU); Université Memorial, Canada (MUN); Commission géologique du Canada, Ottawa (GSC).

Depth(m)	SiO_2	Al_2O_3	Fe_2O_3	FeO†	MgO	CaO	Na_2O	K_2O	H_2O+	TiO_2	P_2O_5	MnO	CO_2	Lab
						CY1 Major Element Data								
19.70	48.80	16.56	7.99	0.92	4.54	6.99	1.39	4.72	4.77	0.51	0.04	0.09	2.39	BOCHUM
19.70	47.42	16.39	.	8.00	4.64	6.93	1.59	4.68	.	0.52	0.03	0.08	.	OU
19.70	47.10	16.20	.	7.57	4.50	6.56	1.49	4.58	.	0.48	0.02	0.09	.	MUN
23.20	45.90	14.60	8.15	1.03	3.73	7.32	0.60	7.55	4.68	0.57	0.08	0.06	5.03	BOCHUM
23.20	45.50	14.60	9.00	0.20	3.62	7.52	0.00	7.62	4.40	0.57	0.10	0.06	6.40	GSC
23.30	44.90	13.70	.	7.87	3.94	7.00	0.59	7.32	.	0.52	0.13	0.06	.	MUN
32.30	47.50	17.20	.	8.48	7.07	3.28	1.42	4.18	.	0.58	0.03	0.08	.	MUN
32.30	49.50	18.03	8.77	1.01	7.03	3.51	1.39	4.24	6.25	0.69	0.04	0.08	0.24	BOCHUM
32.30	47.70	17.60	8.60	1.00	6.78	3.64	1.30	4.24	6.90	0.68	0.05	0.09	0.40	GSC
32.30	48.53	17.75	.	8.75	6.87	3.48	1.12	4.25	.	0.70	0.00	0.08	.	OU
40.40	45.40	16.37	6.98	2.21	8.69	6.22	1.45	2.87	6.18	0.73	0.08	0.15	2.19	BOCHUM
40.40	45.33	16.50	.	8.60	8.94	6.26	1.74	0.28	0.07	0.74	0.06	0.14	.	OU
40.40	44.10	15.90	.	8.23	8.76	5.88	1.54	2.80	.	0.70	0.06	0.13	.	MUN
44.50	44.10	16.20	.	7.49	6.75	5.72	1.24	4.35	.	0.69	0.08	0.11	.	MUN
44.50	46.30	16.75	8.12	0.98	6.61	6.22	1.23	4.51	5.83	0.77	0.11	0.12	2.82	BOCHUM
44.50	45.71	16.56	.	8.31	6.53	6.32	1.33	4.56	.	0.78	0.12	0.11	.	OU
44.50	44.70	16.50	7.50	1.50	6.59	6.39	1.10	4.59	6.20	0.76	0.13	0.12	3.30	GSC
47.30	25.70	8.10	.	6.34	3.98	26.68	0.56	2.76	.	0.27	0.08	0.14	.	MUN
47.30	26.80	7.92	6.79	0.62	3.97	25.81	0.51	2.81	3.08	0.29	0.13	0.14	20.16	BOCHUM
51.70	31.80	9.75	6.22	0.90	5.34	21.10	0.66	2.95	3.88	0.35	0.06	0.11	16.12	BOCHUM
51.70	29.80	9.94	.	6.22	5.38	21.78	0.76	2.92	.	0.34	0.04	0.12	.	MUN
54.70	46.80	14.04	8.74	0.87	6.76	7.07	0.73	5.95	5.03	0.51	0.05	0.11	3.51	BOCHUM
54.70	44.90	13.80	8.50	1.00	6.68	7.30	0.50	6.10	5.20	0.51	0.06	0.11	4.20	GSC
54.70	45.50	13.40	.	8.36	6.83	6.62	0.77	5.80	.	0.48	0.03	0.08	.	MUN
57.00	50.20	15.24	7.85	1.15	7.49	4.08	0.96	6.00	5.65	0.58	0.02	0.10	1.13	BOCHUM
57.00	49.32	15.12	.	8.25	7.55	4.17	0.90	0.60	0.05	0.57	0.04	0.10	.	OU
57.00	48.00	14.60	.	7.57	7.57	3.89	1.06	5.78	.	0.58	0.00	0.10	.	MUN
58.70	32.70	7.85	5.76	1.99	12.62	18.95	0.73	0.61	5.03	0.26	0.04	0.17	12.71	BOCHUM
58.70	30.20	7.30	5.80	1.90	11.60	19.70	0.60	0.67	5.80	0.27	0.04	0.17	15.60	GSC
58.70	29.60	7.15	.	6.81	12.45	19.05	0.74	0.60	.	0.23	0.00	0.16	.	MUN
69.10	44.00	14.00	.	7.65	6.69	8.70	1.28	3.45	.	0.50	0.07	0.09	.	MUN
69.10	46.00	15.55	7.48	1.46	6.49	9.34	1.22	3.65	4.81	0.58	0.07	0.10	3.87	BOCHUM
69.10	44.00	15.70	7.30	1.40	6.48	9.37	1.50	3.69	5.10	0.58	0.06	0.11	4.40	GSC
71.50	45.95	15.22	.	8.51	9.50	10.00	1.50	1.19	.	0.57	0.08	0.13	.	OU
71.50	43.90	14.60	.	7.94	9.48	9.12	1.73	1.15	.	0.51	0.03	0.12	.	MUN
71.50	45.70	15.09	5.63	3.10	9.40	9.62	1.62	1.21	4.56	0.55	0.05	0.13	2.38	BOCHUM
74.10	44.70	15.40	.	7.74	6.30	7.80	1.47	3.54	.	0.55	0.03	0.11	.	MUN
74.10	46.90	16.16	7.89	1.10	6.50	8.36	1.40	3.52	3.44	0.61	0.06	0.12	3.03	BOCHUM
77.40	42.90	14.30	6.70	1.70	7.08	10.00	1.10	3.04	5.20	0.59	0.07	0.13	3.40	GSC
77.40	44.00	15.13	6.81	1.72	7.28	9.87	1.33	2.95	5.14	0.58	0.05	0.12	4.64	BOCHUM
77.40	43.48	15.32	.	7.90	7.53	9.98	1.87	2.95	.	0.59	0.04	0.12	.	OU

† FeO is total iron where Fe_2O_3 is not reported.

Depth(m)	SiO_2	Al_2O_3	Fe_2O_3	FeO †	MgO	CaO	Na_2O	K_2O	H_2O+	TiO_2	P_2O_5	MnO	CO_2	Lab
	CY1 Major Element Data (continued)													
77.40	42.00	14.80	.	7.49	7.28	9.40	1.39	2.92	.	0.57	0.04	0.11	.	MUN
82.10	47.70	15.82	8.77	0.54	6.56	5.40	1.07	5.57	5.77	0.58	0.03	0.11	2.54	BOCHUM
88.50	42.60	14.50	7.20	1.10	5.49	11.30	0.60	4.96	4.00	0.58	0.14	0.10	7.10	GSC
88.50	43.90	14.66	7.72	0.75	5.60	10.82	0.98	4.88	4.31	0.57	0.13	0.10	6.18	BOCHUM
88.50	42.87	14.47	0.84	0.01	5.61	1.08	1.20	4.78	.	0.57	0.12	0.09	.	OU
90.60	39.80	13.68	5.77	1.95	5.35	16.63	1.55	2.29	2.84	0.52	0.07	0.11	8.67	BOCHUM
90.60	39.70	13.50	.	7.01	5.60	16.58	1.64	2.18	.	0.49	0.04	0.11	.	MUN
90.60	38.80	13.60	5.80	1.90	5.36	17.60	1.30	2.41	2.50	0.53	0.10	0.11	10.80	GSC
92.50	44.11	14.55	.	7.65	8.04	12.19	1.92	1.56	.	0.54	0.11	0.13	.	OU
92.50	45.10	14.80	6.09	2.24	8.16	12.17	1.72	1.58	3.62	0.56	0.07	0.14	3.87	BOCHUM
92.50	43.60	14.60	5.50	2.60	7.94	12.50	1.30	1.61	3.60	0.56	0.08	0.13	4.80	GSC
92.50	44.00	14.40	.	7.28	8.19	11.83	1.86	1.50	.	0.50	0.03	0.13	.	MUN
94.10	45.20	16.10	6.70	2.20	7.69	9.38	1.90	2.45	4.50	0.60	0.08	0.13	3.30	GSC
94.10	47.10	15.44	7.39	2.06	8.20	9.19	1.57	2.39	4.52	0.61	0.07	0.13	2.05	BOCHUM
94.10	45.54	15.38	.	8.45	8.03	9.15	1.37	2.28	.	0.60	0.10	0.12	.	OU
94.10	45.10	15.00	.	8.02	8.14	8.75	1.60	2.20	.	0.57	0.02	0.12	.	MUN
95.60	36.30	5.22	5.60	1.67	18.95	14.50	0.62	0.14	6.55	0.20	0.03	0.19	9.99	BOCHUM
95.60	35.00	5.10	5.20	1.90	18.30	15.10	0.30	0.17	6.80	0.20	0.04	0.19	11.60	GSC
95.60	34.60	5.12	.	6.16	19.10	14.22	0.63	0.15	.	0.18	0.04	0.18	.	MUN
96.10	41.80	14.23	6.12	1.87	5.73	14.81	1.51	2.81	3.19	0.56	0.10	0.13	7.39	BOCHUM
96.10	41.00	14.00	6.10	1.70	5.77	15.30	1.20	2.92	2.80	0.56	0.11	0.13	9.00	GSC
96.90	41.90	13.69	3.97	3.34	5.46	13.71	1.11	3.83	3.75	0.51	0.08	0.10	7.64	BOCHUM
96.90	40.70	13.40	6.40	1.10	5.21	14.20	0.80	3.94	3.60	0.51	0.10	0.11	9.30	GSC
99.50	43.14	15.79	.	8.24	7.31	11.40	1.53	1.85	.	0.58	0.09	0.14	.	OU
99.50	43.40	15.80	6.80	2.20	6.99	12.00	1.10	1.98	4.00	0.59	0.10	0.14	4.50	GSC
99.50	44.40	15.95	7.47	1.75	7.39	11.53	1.57	1.93	4.21	0.60	0.09	0.14	3.76	BOCHUM
101.80	38.80	14.60	.	7.67	4.37	16.60	1.60	2.70	.	0.44	0.07	0.10	.	MUN
101.80	38.10	14.40	6.60	1.60	4.20	17.70	1.30	2.77	2.20	0.56	0.11	0.12	10.90	GSC
101.80	39.50	14.57	7.41	1.28	4.30	17.17	1.50	2.70	2.44	0.57	0.10	0.12	9.07	BOCHUM
105.60	40.50	14.60	6.20	2.00	6.47	14.60	1.80	2.17	3.60	0.55	0.07	0.12	7.90	GSC
105.60	40.50	13.94	6.61	1.66	6.52	13.78	1.50	2.04	5.72	0.54	0.07	0.13	6.68	BOCHUM
105.60	40.04	14.00	.	7.21	6.70	13.69	1.60	2.05	.	0.50	0.04	0.12	.	MUN
109.30	42.10	13.90	6.70	1.90	6.78	13.00	1.10	2.58	3.90	0.55	0.06	0.12	6.30	GSC
109.30	41.90	13.90	.	7.37	6.95	11.93	1.50	2.44	.	0.53	0.03	0.11	.	MUN
109.30	42.90	14.37	7.03	1.83	7.12	12.67	1.44	2.52	4.44	0.56	0.07	0.12	5.47	BOCHUM
109.30	42.77	14.23	.	7.96	7.07	12.56	1.37	2.45	.	0.56	0.10	0.11	.	OU
110.70	39.40	12.10	.	6.90	8.13	5.86	1.61	1.19	.	0.45	0.02	0.11	.	MUN
110.70	40.40	12.06	5.83	2.04	8.16	16.28	1.55	1.20	3.08	0.46	0.05	0.11	8.24	BOCHUM
110.70	39.50	12.00	5.70	2.20	8.04	17.00	1.10	1.26	3.40	0.47	0.06	0.11	9.20	GSC
113.50	45.10	15.08	6.71	1.86	5.58	12.18	1.81	2.97	2.76	0.58	0.08	0.11	4.66	BOCHUM

† FeO is total iron where Fe_2O_3 is not reported.

Depth(m)	SiO_2	Al_2O_3	Fe_2O_3	FeO †	MgO	CaO	Na_2O	K_2O	H_2O+	TiO_2	P_2O_5	MnO	CO_2	Lab
	CY1 Major Element Data (continued)													
120.80	43.80	14.30	7.10	1.20	6.03	11.40	1.00	4.24	4.10	0.56	0.08	0.11	6.60	GSC
120.80	43.50	14.10	.	7.19	6.14	10.70	1.25	4.06	.	0.52	0.01	0.11	.	MUN
120.80	44.50	14.31	7.37	0.94	6.08	11.07	1.15	4.13	4.24	0.55	0.06	0.11	5.21	BOCHUM
126.00	45.26	16.18	.	7.83	7.91	8.15	1.65	3.06	.	0.64	0.08	0.16	.	OU
126.20	44.30	15.60	.	7.26	7.74	7.62	1.70	2.98	.	0.65	0.07	0.16	.	MUN
126.20	46.10	16.10	6.87	1.58	7.76	8.04	1.68	3.05	5.29	0.63	0.07	0.16	3.08	BOCHUM
132.10	45.32	15.87	.	8.09	8.69	7.00	1.28	3.37	.	0.65	0.10	0.12	.	OU
132.10	44.50	14.20	.	7.49	8.65	6.65	1.39	3.17	.	0.54	0.06	0.12	.	MUN
132.10	45.60	15.79	5.79	2.69	8.67	6.97	1.37	3.31	5.59	0.64	0.08	0.13	2.75	BOCHUM
135.50	46.16	15.45	.	7.85	7.13	6.78	1.12	4.69	.	0.63	0.07	0.11	.	OU
135.50	45.10	15.20	.	7.51	7.28	6.39	1.34	4.59	.	0.54	0.03	0.10	.	MUN
135.50	46.90	15.71	6.29	2.12	7.24	6.77	1.21	4.67	5.17	0.63	0.05	0.12	3.29	BOCHUM
135.50	45.40	15.50	6.10	2.10	7.17	6.97	0.90	4.69	5.80	0.63	0.07	0.12	4.10	GSC
140.80	47.50	14.68	6.32	1.42	8.03	7.92	1.20	4.42	4.35	0.54	0.06	0.12	2.92	BOCHUM
140.80	46.60	14.50	.	6.88	8.07	7.48	1.26	4.39	.	0.51	0.04	0.08	.	MUN
148.20	48.00	16.33	7.84	0.99	7.86	6.95	1.54	4.25	4.50	0.51	0.09	0.10	1.75	BOCHUM
148.20	46.10	15.80	.	7.69	7.87	6.58	1.62	4.24	.	0.45	0.06	0.10	.	MUN
148.20	46.60	15.80	7.60	1.00	7.54	7.03	1.20	4.27	4.70	0.50	0.09	0.09	2.70	GSC
151.20	46.30	15.15	.	7.79	8.98	8.66	1.73	2.08	.	0.48	0.00	0.12	.	OU
152.20	47.90	15.49	5.76	2.72	9.21	8.67	1.54	2.14	4.64	0.49	0.02	0.12	2.19	BOCHUM
152.20	45.90	15.00	5.50	2.70	8.69	8.85	1.20	2.15	5.40	0.48	0.03	0.12	2.80	GSC
152.20	45.40	14.70	.	7.10	8.99	8.16	1.52	2.04	.	0.44	0.02	0.12	.	MUN
165.10	46.00	14.30	.	6.60	10.24	8.57	1.53	2.41	.	0.54	0.04	0.11	.	MUN
165.10	47.24	14.56	.	7.33	10.17	9.11	1.58	2.49	.	0.56	0.05	0.11	.	OU
165.10	47.30	14.78	5.84	1.98	10.09	9.09	1.42	2.51	4.09	0.56	0.05	0.11	1.96	BOCHUM
169.30	44.00	14.20	.	6.50	8.36	5.83	1.27	4.58	.	0.54	0.02	0.07	.	MUN
169.30	46.40	14.63	7.53	0.22	8.83	6.21	1.21	4.74	5.39	0.54	0.06	0.07	3.55	BOCHUM
173.50	44.10	14.00	.	6.53	4.08	11.46	1.31	4.79	.	0.49	0.02	0.07	.	MUN
173.50	44.80	14.42	7.23	0.38	4.12	11.69	1.19	4.89	3.94	0.53	0.06	0.08	6.76	BOCHUM
173.50	43.80	14.20	7.10	0.40	4.11	12.10	1.00	4.96	3.90	0.53	0.07	0.08	8.10	GSC
180.40	46.60	14.37	6.78	0.83	7.46	9.91	1.54	3.22	3.98	0.53	0.07	0.09	3.87	BOCHUM
180.40	45.10	14.10	.	6.48	7.40	9.64	1.66	3.08	.	0.48	0.01	0.09	.	MUN
183.60	47.00	13.97	6.46	1.26	6.25	11.20	1.54	3.58	3.18	0.52	0.07	0.08	4.70	BOCHUM
183.60	45.70	13.70	.	6.69	6.24	10.80	1.60	3.48	.	0.49	0.02	0.08	.	MUN
185.00	43.70	14.10	.	7.09	5.96	11.47	1.68	3.83	.	0.55	0.07	0.08	.	OU
185.10	44.50	13.40	.	6.74	5.95	11.10	1.45	3.78	.	0.44	0.07	0.08	.	MUN
185.10	44.80	14.15	7.18	0.61	5.82	11.50	1.37	3.87	3.97	0.54	0.08	0.09	5.71	BOCHUM
185.10	43.30	13.80	7.00	0.70	5.65	11.80	0.90	3.93	4.20	0.54	0.09	0.08	6.80	GSC
188.30	48.80	15.10	5.60	2.00	8.92	9.17	1.30	2.65	3.50	0.48	0.06	0.12	1.60	GSC
188.30	49.80	15.34	5.83	1.92	9.18	8.90	1.70	2.57	3.31	0.47	0.05	0.11	0.11	BOCHUM

† FeO is total iron where Fe_2O_3 is not reported.

Depth(m)	SiO_2	Al_2O_3	Fe_2O_3	FeO †	MgO	CaO	Na_2O	K_2O	H_2O+	TiO_2	P_2O_5	MnO	CO_2	Lab
	CY1 Major Element Data (continued)													
188.30	48.50	15.10	.	6.99	9.31	8.41	1.93	2.59	.	0.42	0.03	0.10	.	MUN
188.30	48.99	15.44	.	7.22	9.39	8.92	2.04	2.53	.	0.47	0.05	0.10	.	OU
194.10	48.40	16.48	8.53	0.60	9.90	2.64	1.11	5.07	6.35	0.66	0.04	0.09	0.83	BOCHUM
194.10	46.30	15.80	.	7.91	9.90	2.40	1.18	4.97	.	0.59	0.03	0.08	.	MUN
197.70	46.45	15.10	.	7.89	9.21	5.23	1.30	4.67	.	0.61	0.02	0.12	.	OU
197.70	45.60	14.90	5.40	2.80	8.65	5.21	1.00	4.71	6.50	0.59	0.09	0.13	3.80	GSC
197.70	47.20	15.12	6.38	2.09	9.12	5.19	1.25	4.68	5.88	0.59	0.06	0.12	2.62	BOCHUM
197.70	45.50	14.60	.	7.51	8.99	4.92	1.32	4.60	.	0.58	0.03	0.11	.	MUN
200.70	47.60	14.96	5.20	2.62	8.94	8.65	2.09	2.06	3.68	0.58	0.05	0.10	3.04	BOCHUM
200.70	44.60	14.30	.	6.70	8.87	8.03	2.20	1.95	.	0.55	0.11	0.09	.	MUN
200.70	46.83	14.86	.	7.42	8.89	8.66	2.42	2.00	.	0.59	0.07	0.09	.	OU
203.50	48.10	15.50	.	6.59	9.36	7.87	2.20	1.55	.	0.49	0.06	0.09	.	MUN
203.50	48.66	16.37	.	7.20	9.58	8.50	2.38	1.55	.	0.59	0.05	0.09	.	OU
203.50	49.00	16.36	4.76	2.91	9.48	8.44	2.23	1.60	3.37	0.59	0.07	0.09	1.47	BOCHUM
208.90	44.62	14.42	.	7.59	9.18	9.15	2.20	2.35	.	0.59	0.05	0.14	.	OU
208.90	45.60	14.58	4.83	3.21	9.21	9.17	1.85	2.42	4.08	0.58	0.06	0.15	3.95	BOCHUM
208.90	43.50	14.80	4.60	3.10	8.86	9.39	2.20	2.49	5.20	0.58	0.05	0.15	4.90	GSC
214.40	45.86	15.17	.	8.00	8.94	5.57	1.26	4.82	.	0.61	0.10	0.14	.	OU
218.00	48.10	16.90	6.10	2.70	8.52	4.48	1.40	3.76	6.00	0.70	0.08	0.12	1.20	GSC
218.00	49.24	16.35	.	8.50	8.57	4.43	1.54	3.79	.	0.72	0.06	0.11	.	OU
223.10	48.00	15.20	6.00	2.80	8.09	3.90	1.10	4.82	6.40	0.67	0.06	0.10	2.10	GSC
223.10	49.30	16.00	7.07	2.62	8.34	3.90	1.41	4.85	5.26	0.68	0.06	0.10	1.37	BOCHUM
223.10	49.07	15.50	.	8.12	8.49	6.72	2.38	2.07	.	0.72	0.08	0.08	.	OU
233.90	43.40	13.80	.	7.60	8.05	9.23	2.02	2.94	.	0.55	0.20	0.16	.	MUN
233.90	41.40	14.40	5.50	3.00	7.85	9.88	1.60	3.16	5.00	0.68	0.09	0.18	6.20	GSC
233.90	42.26	14.79	.	7.98	7.97	9.48	1.93	2.99	.	0.68	0.12	0.17	.	OU
237.50	48.20	15.90	5.10	3.30	8.16	6.86	2.60	2.17	4.30	0.71	0.09	0.09	2.00	GSC
237.50	47.70	15.20	.	7.74	8.57	6.28	2.59	2.11	.	0.67	0.05	0.08	.	MUN
240.00	48.87	15.77	.	7.85	7.89	7.94	2.76	1.71	.	0.75	0.09	0.08	.	OU
240.00	49.00	16.00	7.90	2.98	7.78	8.07	2.63	1.73	2.61	0.76	0.08	0.08	1.41	BOCHUM
240.00	48.10	15.70	4.90	3.30	7.67	8.12	2.90	1.82	3.10	0.75	0.08	0.09	2.30	GSC
240.00	48.30	15.50	.	7.67	7.90	7.58	2.84	1.79	.	0.70	0.05	0.08	.	MUN
244.50	47.50	16.30	4.70	3.50	10.60	3.48	2.80	2.44	7.60	0.69	0.09	0.12	0.20	GSC
244.50	45.90	15.10	.	7.48	10.55	3.22	2.40	2.26	.	0.68	0.04	0.10	.	MUN
246.70	47.61	15.41	.	7.70	9.15	6.92	1.96	3.28	.	0.73	0.08	0.14	.	OU
246.70	44.60	14.80	.	6.94	8.99	6.40	1.99	3.15	.	0.68	0.05	0.13	.	MUN
246.70	46.30	15.00	5.10	2.80	8.82	6.93	1.80	3.29	5.50	0.71	0.10	0.14	3.00	GSC
246.70	47.60	15.60	5.20	2.93	9.06	6.93	1.97	3.28	4.57	0.71	0.08	0.14	2.18	BOCHUM
254.00	47.60	15.40	5.13	2.72	8.57	7.66	1.90	3.44	4.25	0.71	0.10	0.13	2.87	BOCHUM
254.00	46.99	15.08	.	7.34	8.43	7.61	1.88	3.42	.	0.70	0.10	0.13	.	OU

† FeO is total iron where Fe_2O_3 is not reported.

Depth(m)	SiO_2	Al_2O_3	Fe_2O_3	FeO †	MgO	CaO	Na_2O	K_2O	H_2O+	TiO_2	P_2O_5	MnO	CO_2	Lab
	CY1 Major Element Data (continued)													
259.20	45.50	13.20	.	7.69	10.73	5.13	2.50	1.20	.	0.58	0.04	0.11	.	MUN
259.20	48.87	14.02	.	9.02	11.18	5.83	2.56	1.19	.	0.63	0.11	0.12	.	OU
261.20	47.93	15.46	.	7.24	9.33	6.09	2.53	2.99	.	0.71	0.05	0.15	.	OU
261.20	46.30	15.00	.	6.66	9.17	5.58	2.39	2.88	.	0.66	0.02	0.14	.	MUN
261.20	46.30	15.80	4.90	2.60	8.84	6.07	2.70	3.07	5.40	0.70	0.08	0.16	2.40	GSC
266.30	48.58	15.53	.	8.54	8.71	5.44	2.53	2.92	.	0.80	0.11	0.14	.	OU
266.30	49.00	15.70	6.27	2.91	8.65	5.53	2.41	2.93	4.44	0.79	0.10	0.14	1.64	BOCHUM
266.30	45.50	14.80	.	7.72	8.32	4.99	2.56	2.71	.	0.75	0.07	0.13	.	MUN
268.80	46.30	15.00	.	7.39	7.99	6.22	2.35	2.81	.	0.68	0.05	0.13	.	MUN
268.80	47.60	15.44	.	7.95	8.02	6.70	2.46	2.91	.	0.76	0.10	0.14	.	OU
273.40	47.90	14.90	4.40	3.70	9.51	8.74	2.40	0.72	4.30	0.46	0.06	0.08	1.90	GSC
273.40	49.74	15.30	.	7.91	9.84	8.76	2.73	0.62	.	0.47	0.04	0.08	.	OU
273.40	49.70	15.50	5.13	3.13	9.82	8.70	2.64	0.68	2.48	0.47	0.05	0.08	1.66	BOCHUM
273.40	47.80	13.90	.	7.13	9.58	8.03	2.56	0.64	.	0.39	0.02	0.07	.	MUN
279.70	44.60	13.90	.	7.53	8.97	8.45	2.48	2.10	.	0.65	0.07	0.10	.	MUN
279.70	46.50	14.40	5.66	2.85	9.06	9.19	2.36	2.11	3.77	0.69	0.09	0.10	3.69	BOCHUM
279.70	44.60	14.10	5.50	2.80	8.78	9.09	2.00	2.14	4.80	0.68	0.10	0.10	4.40	GSC
279.70	45.76	14.02	.	7.92	8.79	9.02	2.19	2.03	.	0.68	0.11	0.10	.	OU
281.90	47.38	15.12	.	7.89	8.76	8.65	2.40	2.53	.	0.73	0.12	0.13	.	OU
281.90	45.60	14.60	.	7.33	8.62	7.67	2.35	2.54	.	0.67	0.05	0.11	.	MUN
283.50	42.20	13.20	.	7.28	9.31	9.04	2.41	1.61	.	0.61	0.06	0.10	.	MUN
283.50	44.74	14.05	.	7.83	9.70	9.75	2.47	1.66	.	0.66	0.14	0.11	.	OU
283.50	42.70	13.60	5.10	2.90	9.28	9.77	2.10	1.72	5.50	0.65	0.10	0.12	5.40	GSC
287.20	43.30	13.30	5.01	2.85	8.84	10.10	2.33	2.75	4.49	0.63	0.09	0.14	5.54	BOCHUM
287.20	41.60	12.70	.	6.81	8.76	9.01	2.39	2.63	.	0.60	0.03	0.14	.	MUN
289.20	41.20	12.60	.	6.74	8.96	10.74	2.26	1.47	.	0.54	0.05	0.14	.	MUN
289.20	44.06	13.29	.	7.51	9.35	11.50	2.84	1.49	.	0.62	0.11	0.14	.	OU
292.80	45.60	15.00	4.60	3.20	9.89	6.36	2.30	2.15	6.30	0.62	0.08	0.15	2.30	GSC
292.80	47.61	15.14	.	7.61	10.22	6.39	2.31	2.11	.	0.64	0.08	0.14	.	OU
292.80	45.40	14.50	.	6.79	9.97	5.59	2.54	2.06	.	0.62	0.02	0.13	.	MUN
297.70	46.64	14.90	.	7.47	10.03	7.23	2.64	2.01	.	0.61	0.08	0.13	.	OU
297.70	45.50	14.80	4.70	3.00	9.80	7.30	2.40	2.06	6.20	0.60	0.08	0.15	3.10	GSC
297.70	47.10	15.10	5.00	3.18	10.10	7.26	2.52	2.05	4.27	0.61	0.07	0.14	2.48	BOCHUM
297.70	44.00	14.20	.	6.78	9.91	6.63	2.64	1.89	.	0.57	0.01	0.13	.	MUN
301.50	46.70	14.30	.	7.14	9.38	6.16	2.51	2.49	.	0.57	0.04	0.11	.	MUN
301.50	48.58	15.06	.	7.83	9.42	6.70	2.44	2.61	.	0.59	0.08	0.12	0.00	OU
304.50	47.00	14.90	.	6.96	9.21	9.24	2.44	0.46	.	0.56	0.04	0.09	.	MUN
304.50	48.83	15.87	.	7.70	9.54	10.08	2.67	0.39	.	0.63	0.07	0.09	.	OU
304.50	47.10	15.50	4.50	3.30	8.92	10.00	2.00	0.49	4.60	0.62	0.06	0.10	2.00	GSC
309.00	47.11	15.40	.	8.23	8.22	8.52	2.58	1.47	.	0.66	0.11	0.09	.	OU

† FeO is total iron where Fe_2O_3 is not reported.

Depth(m)	SiO_2	Al_2O_3	Fe_2O_3	FeO †	MgO	CaO	Na_2O	K_2O	H_2O+	TiO_2	P_2O_5	MnO	CO_2	Lab
	CY1 Major Element Data (continued)													
309.05	47.30	15.40	5.55	3.13	8.21	8.42	2.60	1.48	3.61	0.65	0.08	0.10	2.77	BOCHUM
318.10	50.00	15.41	.	8.19	10.32	6.97	2.62	0.70	.	0.58	0.07	0.06	.	OU
318.10	49.50	15.60	5.40	2.70	8.95	6.91	2.70	0.95	5.20	0.56	0.07	0.06	0.30	GSC
321.40	47.10	15.30	5.10	3.10	7.74	10.10	2.20	0.99	4.30	0.55	0.06	0.07	2.60	GSC
321.40	46.90	14.80	.	7.55	7.83	9.38	2.71	0.96	.	0.54	0.04	0.06	.	MUN
321.40	48.83	15.55	.	8.01	8.08	10.06	2.76	0.90	.	0.58	0.09	0.07	.	OU
321.40	48.50	15.50	6.24	3.25	8.02	10.00	2.52	0.94	2.45	0.56	0.06	0.07	1.74	BOCHUM
328.60	50.84	16.16	.	7.98	8.84	8.89	2.65	1.16	.	0.58	0.11	0.08	.	OU
328.60	48.60	15.20	.	7.17	8.68	8.28	2.57	1.16	.	0.60	0.03	0.08	.	MUN
333.50	50.40	16.10	6.23	3.37	8.90	6.38	2.88	1.06	3.08	0.66	0.07	0.09	0.54	BOCHUM
333.50	49.92	15.72	.	9.02	8.67	6.31	2.89	1.03	.	0.65	0.08	0.09	.	OU
336.90	51.10	16.90	4.68	3.58	7.89	9.88	2.40	0.34	2.20	0.53	0.05	0.08	0.18	BOCHUM
336.90	51.15	16.86	.	7.92	7.93	9.84	2.72	0.28	.	0.53	0.08	0.08	.	OU
336.90	49.90	16.50	4.70	3.50	7.62	9.99	2.00	0.37	3.70	0.53	0.07	0.08	0.20	GSC
337.90	48.10	15.20	.	8.04	8.21	7.18	2.85	0.19	.	0.60	0.01	0.08	.	MUN
337.90	50.69	16.07	.	8.82	8.28	7.76	3.07	0.12	.	0.67	0.05	0.08	.	OU
337.90	49.70	16.10	5.20	3.70	8.17	7.72	3.00	0.22	4.10	0.66	0.08	0.08	0.20	GSC
342.20	52.70	16.30	4.19	3.49	6.50	10.30	2.50	0.81	1.60	0.65	0.07	0.09	0.26	BOCHUM
342.40	52.30	15.60	.	6.95	6.56	9.86	2.71	0.83	.	0.60	0.03	0.09	.	MUN
342.40	52.73	16.10	.	7.48	6.55	10.35	2.77	0.75	.	0.66	0.10	0.09	.	OU
348.00	54.85	13.48	.	10.35	7.50	4.12	2.76	0.80	.	0.57	0.06	0.15	.	OU
348.80	54.20	13.30	7.49	3.44	7.39	3.97	2.57	0.84	5.50	0.56	0.02	0.15	0.21	BOCHUM
354.20	48.80	16.40	5.50	3.80	8.59	7.21	3.50	0.37	4.60	0.64	0.09	0.10	0.30	GSC
354.20	50.83	16.11	.	9.17	9.23	7.31	3.39	0.21	.	0.66	0.11	0.10	.	OU
354.20	47.80	14.20	.	8.23	8.84	6.69	0.29	0.04	.	0.49	.	0.09	.	MUN
361.30	50.40	15.80	6.52	3.19	9.60	6.42	2.92	0.36	2.89	0.65	0.06	0.11	0.25	BOCHUM
361.30	49.00	15.70	5.70	3.70	9.20	6.45	2.60	0.37	6.10	0.65	0.07	0.11	0.30	GSC
361.30	49.96	15.51	.	9.01	9.45	6.40	3.12	0.29	.	0.66	0.07	0.11	.	OU
361.30	47.50	14.70	.	8.36	9.21	5.73	2.87	0.32	.	0.59	0.04	0.10	.	MUN
367.10	50.75	15.77	.	8.38	9.11	7.23	2.79	0.45	.	0.65	0.10	0.11	.	OU
375.10	53.50	15.70	3.40	5.00	7.26	9.21	2.20	0.31	2.40	0.61	0.08	0.10	0.50	GSC
375.10	52.93	15.21	.	8.18	7.33	8.89	2.27	0.19	.	0.61	0.10	0.09	.	OU
375.10	52.40	15.10	.	8.01	7.36	8.56	2.47	0.30	.	0.59	0.04	0.09	.	MUN
375.80	50.97	13.84	.	7.49	10.24	9.97	2.31	0.12	.	0.49	0.09	0.17	.	OU
375.80	48.60	13.40	.	6.70	10.30	9.37	2.19	0.20	.	0.42	0.02	0.17	.	MUN
375.80	50.60	13.80	5.01	3.64	10.40	9.98	2.21	0.19	2.16	0.48	0.05	0.17	1.38	BOCHUM
377.50	53.10	15.00	.	6.88	7.46	9.32	2.48	0.10	.	0.54	0.02	0.13	.	MUN
377.50	52.43	15.38	.	7.32	7.35	9.67	2.45	0.02	.	0.60	0.06	0.13	.	OU
377.50	52.40	15.50	3.40	4.10	7.44	10.00	2.30	0.15	2.50	0.60	0.08	0.14	1.60	GSC
381.30	50.10	16.40	4.20	4.60	7.29	10.30	2.20	0.18	4.00	0.63	0.08	0.13	0.20	GSC

† FeO is total iron where Fe_2O_3 is not reported.

Depth(m)	SiO_2	Al_2O_3	Fe_2O_3	FeO †	MgO	CaO	Na_2O	K_2O	H_2O+	TiO_2	P_2O_5	MnO	CO_2	Lab
	CY1 Major Element Data (continued)													
381.30	50.58	15.96	.	8.57	7.38	10.15	2.51	0.05	.	0.64	0.08	0.12	.	OU
381.30	48.60	15.60	.	8.07	7.46	9.56	2.35	0.13	.	0.62	0.03	0.12	.	MUN
386.60	52.60	13.90	.	8.92	6.17	7.96	2.50	0.86	.	0.53	0.04	0.10	.	MUN
386.60	54.70	14.60	7.58	2.62	6.24	8.55	2.42	0.93	2.01	0.58	0.06	0.11	0.09	BOCHUM
386.60	53.56	14.49	.	9.30	6.12	8.46	2.30	0.86	.	0.58	0.06	0.10	.	OU
386.60	53.60	14.60	7.10	2.70	6.07	8.66	2.10	0.97	3.20	0.58	0.08	0.11	0.10	GSC
390.70	50.60	12.90	3.48	3.87	12.60	9.87	1.76	0.14	2.54	0.40	0.04	0.20	1.40	BOCHUM
390.70	50.55	12.89	.	7.04	12.34	9.87	1.82	0.07	.	0.40	0.05	0.20	.	OU
390.70	49.20	12.30	.	6.43	12.57	9.15	1.83	0.15	.	0.37	0.00	0.19	.	MUN
397.50	48.70	15.60	4.70	4.10	9.47	6.43	2.40	0.52	5.10	0.64	0.09	0.11	1.40	GSC
397.50	50.24	15.75	.	8.66	9.82	6.50	3.10	0.44	.	0.66	0.08	0.10	.	OU
402.20	47.90	15.50	.	7.37	9.25	5.49	3.03	0.54	.	0.62	0.04	0.10	.	MUN
402.20	51.20	16.50	5.45	3.19	9.67	6.05	3.04	0.58	3.17	0.68	0.06	0.10	0.36	BOCHUM
402.20	51.08	16.10	.	8.24	9.49	6.09	3.10	0.52	.	0.68	0.06	0.10	.	OU
410.20	47.30	16.20	.	6.90	5.34	11.83	3.10	0.86	.	0.62	0.04	0.11	.	MUN
410.20	47.23	16.21	.	7.10	5.25	12.44	3.05	0.78	.	0.68	0.11	0.11	.	OU
413.20	49.24	16.77	.	8.19	6.11	8.74	3.22	0.81	.	0.78	0.10	0.08	.	OU
413.20	48.20	16.40	.	7.82	6.06	8.26	3.16	0.91	.	0.69	0.08	0.08	.	MUN
413.20	49.30	17.30	5.10	3.30	6.19	8.85	3.20	0.94	4.70	0.77	0.11	0.09	0.20	GSC
416.85	54.80	14.70	6.82	2.98	5.52	8.19	2.38	1.10	1.99	0.66	0.07	0.10	0.10	BOCHUM
416.85	53.00	14.20	.	8.55	5.55	7.70	2.46	1.08	.	0.65	0.05	0.10	.	MUN
426.30	52.90	14.10	.	8.09	6.14	8.06	2.65	0.61	.	0.56	0.03	0.11	.	MUN
426.30	53.92	14.47	.	8.82	6.26	8.63	2.87	0.57	.	0.63	0.08	0.11	.	OU
429.45	50.57	16.22	.	7.74	8.96	9.30	2.53	0.09	.	0.67	0.11	0.09	.	OU
429.45	49.70	16.20	3.90	3.90	8.66	9.32	2.10	0.20	5.10	0.66	0.05	0.11	0.20	GSC
429.45	48.00	15.10	.	6.97	8.85	8.61	2.46	0.16	.	0.66	0.03	0.09	.	MUN
434.60	49.60	15.70	2.90	3.80	7.33	11.70	1.90	0.15	2.80	0.68	0.08	0.14	2.50	GSC
434.60	50.50	16.00	3.89	3.31	7.75	11.50	2.44	0.12	1.38	0.68	0.06	0.13	2.26	BOCHUM
434.60	48.90	15.40	.	6.16	7.57	10.90	2.58	0.14	.	0.62	0.01	0.12	.	MUN
434.66	50.28	16.06	.	6.65	7.63	11.53	2.65	0.05	.	0.69	0.10	0.12	.	OU
440.00	49.76	14.65	.	8.96	8.13	9.80	2.45	0.84	.	0.56	0.08	0.11	.	OU
445.00	50.19	15.15	.	7.93	10.48	8.43	2.82	0.13	.	0.62	0.12	0.10	.	OU
445.90	48.00	14.00	.	7.23	10.26	7.85	2.53	0.21	.	0.59	0.03	0.09	.	MUN
445.90	50.70	15.20	4.89	3.52	10.50	8.42	2.63	0.20	2.85	0.62	0.07	0.10	0.32	BOCHUM
445.90	47.30	14.60	4.10	3.60	9.80	8.16	2.70	0.27	9.10	0.59	0.07	0.11	0.30	GSC
450.45	50.60	14.90	5.45	3.32	10.40	8.39	2.60	0.24	2.78	0.61	0.07	0.11	0.44	BOCHUM
455.90	50.00	15.00	7.54	2.32	10.80	8.39	2.48	0.19	2.62	0.62	0.08	0.12	0.36	BOCHUM
465.65	51.60	16.00	7.41	2.40	7.03	8.50	2.75	0.52	2.50	0.68	0.07	0.12	0.16	BOCHUM
468.00	51.42	15.98	.	7.71	8.92	7.92	3.03	0.25	.	0.70	0.07	0.10	.	OU
468.42	51.30	16.20	5.31	2.81	9.03	7.90	2.75	0.31	2.88	0.70	0.06	0.10	0.37	BOCHUM

† FeO is total iron where Fe_2O_3 is not reported.

Depth(m)	SiO_2	Al_2O_3	Fe_2O_3	FeO†	MgO	CaO	Na_2O	K_2O	H_2O+	TiO_2	P_2O_5	MnO	LOI	CO_2	S	Total	Lab
	CY1A Major Element Data																
5.20	47.4	14.2	.	8.28	11.94	5.58	2.39	1.72	.	0.68	0.06	0.16	8.08	.	.	100.49	MUN
10.50	48.2	15.14	5.86	2.74	10.56	4.44	5.68	1.00	5.80	0.73	0.06	0.19	.	0.59	0.03	101.02	BOCHUM
10.50	46.1	14.4	.	8.21	10.65	4.22	5.60	1.01	.	0.68	0.10	0.17	8.76	.	.	99.90	MUN
17.10	48.4	15.5	.	11.09	7.49	7.58	2.77	0.31	.	0.88	0.08	0.16	5.93	.	.	100.19	MUN
19.30	48.4	15.8	.	11.16	7.30	7.90	2.80	0.09	.	0.88	0.08	0.17	5.42	.	.	100.00	MUN
27.70	55.3	14.89	7.40	4.34	4.40	6.87	2.97	0.49	1.42	1.24	0.09	0.22	.	0.13	0.03	99.79	BOCHUM
27.70	55.7	14.5	.	12.05	4.41	6.66	3.01	0.50	.	1.12	0.09	0.21	2.57	.	.	100.82	MUN
30.30	50.6	15.0	.	13.41	4.48	7.34	2.65	0.70	.	1.20	0.08	0.22	4.48	.	.	100.16	MUN
40.80	51.0	15.50	10.96	2.84	5.58	6.25	3.18	0.60	2.36	1.48	0.11	0.24	.	0.16	0.04	100.30	BOCHUM
40.80	48.9	15.6	.	13.69	5.39	5.92	3.07	0.59	.	1.32	0.15	0.22	6.05	.	.	100.90	MUN
43.80	54.7	15.88	5.76	4.20	4.24	8.59	2.68	0.16	2.30	0.79	0.07	0.18	.	0.04	0.04	99.63	BOCHUM
43.80	54.6	15.3	.	10.31	4.31	8.40	2.71	0.16	.	0.80	0.07	0.17	2.86	.	.	99.69	MUN
48.90	52.6	15.0	.	11.84	4.94	6.72	3.28	0.53	.	1.20	0.10	0.17	3.01	.	.	99.39	MUN
53.40	49.1	15.2	.	12.35	6.34	6.86	3.00	0.41	.	1.20	0.07	0.19	4.79	.	.	99.51	MUN
62.10	54.6	15.49	7.34	3.95	4.52	6.85	3.25	0.64	1.67	1.30	0.10	0.28	.	0.13	0.03	100.15	BOCHUM
62.10	54.1	15.0	.	11.49	4.47	6.52	3.23	0.65	.	1.32	0.08	0.25	2.56	.	.	99.67	MUN
65.60	56.2	14.7	.	11.19	3.95	5.68	3.47	0.76	.	1.28	0.12	0.25	2.55	.	.	100.15	MUN
68.40	49.4	15.0	.	10.68	7.40	8.66	2.52	0.07	.	0.80	0.06	0.17	4.63	.	.	99.39	MUN
69.25	54.3	15.38	6.34	1.90	8.16	9.77	2.26	0.13	1.49	0.47	0.04	0.12	.	0.19	0.03	100.58	BOCHUM
69.25	53.2	14.6	.	8.17	8.23	9.36	2.20	0.13	.	0.48	0.07	0.11	3.69	.	.	100.24	MUN
73.00	52.7	14.5	.	8.28	7.93	10.66	2.26	0.08	.	0.64	0.07	0.14	3.11	.	.	100.37	MUN
89.50	48.7	16.2	.	11.84	6.80	7.28	3.09	0.34	.	1.08	0.09	0.18	4.46	.	.	100.06	MUN
97.00	56.2	14.1	.	11.13	4.90	6.74	3.10	0.29	.	0.88	0.09	0.15	2.79	.	.	100.37	MUN
97.00	56.4	14.59	6.43	4.13	4.80	6.88	3.11	0.28	1.37	0.96	0.08	0.16	.	0.09	0.03	99.31	BOCHUM
101.10	48.7	15.7	.	10.78	7.15	7.36	3.00	0.62	.	0.88	0.08	0.17	5.17	.	.	99.61	MUN
106.40	49.0	16.0	.	10.54	6.85	8.08	2.96	0.48	.	0.80	0.07	0.18	4.24	.	.	99.20	MUN
111.90	49.0	15.6	.	10.11	7.48	7.52	2.96	0.34	.	0.84	0.08	0.19	5.35	.	.	99.47	MUN
111.90	50.3	16.65	6.71	3.47	7.48	7.93	3.06	0.34	2.20	0.92	0.09	0.21	.	0.23	0.03	99.62	BOCHUM
115.30	49.2	16.0	.	9.56	7.98	7.14	3.25	0.34	.	0.80	0.06	0.18	5.20	.	.	99.71	MUN
118.00	50.6	13.5	.	9.17	10.60	8.66	2.28	0.17	.	0.52	0.05	0.15	4.80	.	.	100.50	MUN
119.20	55.1	14.5	.	9.32	5.89	7.14	3.16	0.32	.	0.80	0.06	0.21	4.09	.	.	100.59	MUN
119.20	55.6	15.37	6.23	3.00	6.03	7.35	3.17	0.31	1.87	0.80	0.07	0.23	.	0.74	0.03	100.80	BOCHUM
122.30	49.2	15.6	.	11.06	7.27	7.58	3.05	0.45	.	0.80	0.06	0.21	4.85	.	.	100.13	MUN
125.80	50.2	15.7	.	10.35	7.36	6.34	3.22	1.44	.	0.84	0.07	0.19	4.51	.	.	100.22	MUN
129.10	55.1	15.49	5.40	3.24	5.91	6.92	3.62	0.83	1.67	0.79	0.08	0.22	.	0.19	0.03	99.49	BOCHUM
129.10	55.4	14.8	.	8.86	5.84	6.72	3.64	0.87	.	0.80	0.08	0.20	3.08	.	.	100.29	MUN
136.10	50.1	15.9	.	8.79	8.03	6.44	3.47	1.49	.	0.72	0.06	0.18	5.01	.	.	100.19	MUN
138.20	55.4	14.0	.	7.24	5.45	8.28	3.24	0.84	.	0.64	0.04	0.18	4.75	.	.	100.06	MUN

† FeO is total iron where Fe_2O_3 is not reported.

Depth(m)	SiO_2	Al_2O_3	Fe_2O_3	FeO†	MgO	CaO	Na_2O	K_2O	H_2O+	TiO_2	P_2O_5	MnO	LOI	CO_2	S	Total	Lab
	CY1A Major Element Data (continued)																
142.00	54.1	15.87	5.13	2.93	6.39	7.07	3.37	1.43	2.10	0.69	0.07	0.20	.	0.58	0.03	99.96	BOCHUM
142.00	52.4	15.4	.	8.08	6.28	6.84	3.47	1.47	.	0.68	0.07	0.18	3.94	.	.	98.81	MUN
147.40	51.9	15.4	.	8.33	7.03	6.62	3.34	1.61	.	0.68	0.06	0.20	5.09	.	.	100.26	MUN
151.10	51.4	15.4	.	8.05	7.61	5.36	3.11	2.07	.	0.72	0.06	0.20	6.29	.	.	100.27	MUN
154.60	52.6	16.69	6.05	2.95	8.12	5.61	3.69	0.51	3.38	0.79	0.07	0.12	.	0.24	0.03	100.85	BOCHUM
154.60	51.9	15.6	.	8.86	7.88	5.32	3.53	0.52	.	0.76	0.05	0.11	5.44	.	.	99.97	MUN
156.90	50.3	15.1	.	8.26	8.67	8.72	2.40	0.19	.	0.56	0.04	0.16	5.01	.	.	99.41	MUN
167.80	51.1	15.1	.	9.39	7.35	4.84	4.00	0.57	.	0.84	0.06	0.21	5.50	.	.	98.96	MUN
175.60	50.9	16.39	6.99	2.92	8.29	4.72	4.42	0.52	2.71	0.90	0.08	0.21	.	0.40	0.03	99.48	BOCHUM
175.60	49.0	15.4	.	9.88	8.03	4.52	4.34	0.53	.	0.80	0.05	0.18	6.37	.	.	99.10	MUN
185.70	50.3	16.36	7.46	4.13	8.19	3.92	4.20	0.92	3.57	1.12	0.10	0.28	.	0.23	0.03	100.81	BOCHUM
185.70	48.8	15.6	.	11.61	7.84	3.68	4.07	0.93	.	1.00	0.08	0.24	5.77	.	.	99.62	MUN
193.55	50.0	15.1	.	10.07	8.20	4.40	4.81	0.62	.	0.76	0.07	0.15	5.56	.	.	99.74	MUN
202.60	57.3	14.15	6.21	4.04	5.09	2.42	4.73	1.78	2.35	1.13	0.11	0.23	.	0.48	0.04	100.06	BOCHUM
202.60	56.6	13.7	.	10.27	5.04	2.30	4.64	1.81	.	0.92	0.09	0.21	4.11	.	.	99.69	MUN
205.80	52.3	13.9	.	12.45	6.42	3.38	4.20	0.11	.	1.00	0.09	0.30	5.24	.	.	99.39	MUN
212.00	50.1	14.6	.	12.86	6.87	3.02	4.86	0.56	.	1.08	0.09	0.28	5.58	.	.	99.90	MUN
224.40	53.7	14.5	.	8.45	7.66	7.56	3.24	0.30	.	0.60	0.07	0.19	3.98	.	.	100.25	MUN
224.40	53.5	15.00	4.62	3.70	7.74	7.82	3.20	0.29	2.16	0.65	0.06	0.22	.	0.25	0.03	99.24	BOCHUM
228.50	51.9	14.1	.	8.45	8.71	8.06	3.36	0.19	.	0.44	0.03	0.14	4.70	.	.	100.08	MUN
231.70	50.1	14.5	.	9.21	8.88	9.08	2.84	0.10	.	0.48	0.27	0.13	4.75	.	.	100.34	MUN
237.60	49.6	14.9	.	9.21	8.62	8.86	2.35	0.09	.	0.52	0.04	0.17	5.67	.	.	100.03	MUN
237.60	50.7	15.86	5.99	3.29	8.95	9.22	2.45	0.08	2.29	0.57	0.05	0.19	.	0.71	0.04	100.39	BOCHUM
259.00	54.5	14.4	.	12.39	5.53	2.68	4.26	0.12	.	1.16	0.12	0.19	3.85	.	.	99.56	MUN
259.00	54.9	14.88	4.76	6.99	5.64	2.80	4.75	0.12	3.72	1.32	0.09	0.21	.	0.33	0.03	100.54	BOCHUM
267.90	53.4	13.9	.	13.80	5.80	2.60	2.85	1.33	.	0.96	0.11	0.35	4.40	.	.	99.50	MUN
271.20	59.1	13.0	.	10.95	4.15	3.08	2.63	0.95	.	0.96	0.07	0.32	3.18	.	.	98.39	MUN
271.20	58.5	13.53	3.79	7.30	4.23	3.13	2.73	0.93	3.28	1.01	0.09	0.35	.	0.46	0.67	100.00	BOCHUM
276.80	56.1	12.8	.	10.48	4.33	4.88	3.48	0.64	.	0.88	0.08	0.33	4.88	.	.	98.88	MUN
282.00	52.4	15.2	.	8.46	8.61	5.96	3.22	0.48	.	0.52	0.03	0.14	4.05	.	.	99.07	MUN
288.55	52.2	14.5	.	9.05	9.24	6.56	2.99	0.59	.	0.52	0.01	0.15	5.09	.	.	100.90	MUN
288.55	52.0	15.25	3.14	5.67	9.58	6.83	3.08	0.58	3.41	0.48	0.04	0.17	.	0.27	0.03	100.53	BOCHUM
290.90	53.3	13.7	.	14.22	5.89	2.16	2.98	0.73	.	1.00	0.06	0.30	4.35	.	.	98.69	MUN
298.10	58.0	13.8	.	11.34	4.34	3.08	3.35	1.06	.	1.00	0.08	0.26	0.23	.	.	99.54	MUN
303.55	57.0	14.92	3.87	6.90	4.92	2.30	5.03	0.16	3.56	1.13	0.10	0.22	.	0.38	0.05	100.54	BOCHUM
303.55	57.3	14.4	.	11.30	4.86	2.20	4.80	0.16	.	1.08	0.09	0.20	3.30	.	.	99.69	MUN
310.40	57.4	14.41	3.43	6.88	5.43	2.43	4.08	0.48	3.80	1.07	0.10	0.24	.	0.09	0.08	99.92	BOCHUM
310.40	59.0	13.9	.	10.80	5.35	2.30	3.98	0.49	.	1.04	0.08	0.22	3.35	.	.	100.51	MUN

† FeO is total iron where Fe_2O_3 is not reported.

Depth(m)	SiO_2	Al_2O_3	Fe_2O_3	FeO†	MgO	CaO	Na_2O	K_2O	H_2O+	TiO_2	P_2O_5	MnO	LOI	CO_2	S	Total	Lab
	CY1A Major Element Data (continued)																
315.10	58.8	14.4	.	11.30	4.85	1.86	4.38	0.29	.	1.04	0.08	0.24	3.12	.	.	100.36	MUN
318.80	57.4	12.3	.	10.92	5.68	2.56	2.65	0.44	.	1.00	0.09	0.28	4.98	.	.	98.30	MUN
318.80	57.3	13.02	4.08	7.22	5.79	2.64	2.71	0.43	4.83	0.97	0.09	0.31	.	0.19	0.69	100.27	BOCHUM
322.70	50.0	16.32	3.40	7.71	8.16	3.90	4.17	0.91	4.08	1.11	0.10	0.27	.	0.13	0.03	100.29	BOCHUM
322.90	57.4	13.5	.	12.17	5.03	2.04	3.19	0.48	.	1.08	0.08	0.31	3.74	.	.	99.02	MUN
341.20	54.9	14.7	.	10.97	5.90	4.22	3.69	0.68	.	1.04	0.10	0.21	3.55	.	.	99.96	MUN
341.20	54.8	14.86	3.77	6.54	5.91	4.33	3.64	0.65	3.88	1.05	0.09	0.23	.	0.08	0.04	99.87	BOCHUM
347.70	53.7	14.8	.	10.97	7.41	2.74	3.61	0.39	.	0.96	0.07	0.34	4.36	.	.	99.35	MUN
347.70	53.8	15.40	3.02	7.49	7.55	2.84	3.76	0.38	4.92	1.01	0.08	0.37	.	0.05	0.14	100.81	BOCHUM
357.45	54.2	14.53	4.19	6.98	5.64	3.64	4.13	0.07	4.17	1.36	0.12	0.24	.	0.10	0.07	99.44	BOCHUM
357.45	55.8	14.2	.	11.83	5.53	3.56	4.11	0.06	.	1.36	0.11	0.23	3.74	.	.	100.53	MUN
364.25	56.5	14.4	.	11.54	4.47	3.12	4.90	0.02	.	1.36	0.10	0.21	3.14	.	.	99.76	MUN
364.25	56.1	14.90	4.26	6.76	4.64	3.29	4.97	0.02	3.76	1.34	0.12	0.23	.	0.14	0.04	100.57	BOCHUM
371.65	52.7	14.50	4.08	7.47	5.98	4.46	3.05	0.84	5.35	1.32	0.10	0.32	.	0.25	0.07	100.49	BOCHUM
371.65	52.6	14.2	.	12.54	5.90	4.40	2.99	0.87	.	1.28	0.10	0.29	4.05	.	.	99.22	MUN
377.30	52.9	14.8	.	11.54	7.25	2.14	4.28	0.06	.	1.24	0.10	0.22	4.35	.	.	98.88	MUN
380.80	52.8	14.7	.	11.72	7.21	2.60	4.43	0.14	.	1.20	0.07	0.19	4.43	.	.	99.49	MUN
384.70	52.8	14.9	.	12.08	7.17	1.62	4.59	0.03	.	1.12	0.17	0.26	4.17	.	.	98.91	MUN
384.70	53.0	15.01	7.08	4.34	7.35	1.52	4.54	0.03	4.71	1.11	0.09	0.27	.	0.10	0.04	99.19	BOCHUM
387.10	52.6	13.3	.	11.77	6.44	4.44	1.60	1.26	.	1.28	0.11	0.26	6.03	.	.	99.09	MUN
390.20	62.0	13.8	.	9.56	3.25	1.76	5.18	0.07	.	1.20	0.21	0.27	2.53	.	.	99.83	MUN
396.15	63.2	13.66	2.69	5.48	2.98	2.44	5.06	0.03	2.62	0.95	0.21	0.22	.	0.20	0.05	99.79	BOCHUM
396.15	64.5	13.1	.	8.46	3.04	2.38	5.08	0.03	.	1.04	0.22	0.21	2.27	.	.	100.33	MUN
404.60	50.9	14.6	.	8.30	8.54	6.76	2.62	0.47	.	0.48	0.06	0.13	6.68	.	.	99.54	MUN
408.90	64.8	12.3	.	7.99	2.31	3.16	4.77	0.11	.	0.76	0.16	0.16	2.32	.	.	98.84	MUN
410.40	54.0	14.9	.	11.32	6.25	2.50	3.60	0.50	.	1.00	0.10	0.25	4.55	.	.	98.97	MUN
410.40	53.9	15.17	3.16	7.38	6.33	2.62	3.70	0.49	4.55	1.06	0.09	0.27	.	0.13	0.08	98.93	BOCHUM
416.55	55.1	14.5	.	11.12	5.96	3.42	4.13	0.50	.	1.00	0.08	0.27	3.41	.	.	99.49	MUN
420.60	52.6	15.0	.	11.84	6.80	2.94	4.41	0.20	.	1.04	0.10	0.22	4.08	.	.	100.23	MUN
422.45	60.4	13.8	.	9.64	3.46	2.12	4.87	0.06	.	1.08	0.23	0.35	2.76	.	.	98.77	MUN
422.45	60.0	14.21	3.20	6.50	3.53	2.10	4.95	0.06	3.21	1.21	0.16	0.37	.	0.04	0.30	99.84	BOCHUM
424.90	60.2	14.6	.	9.90	3.77	2.12	5.22	0.04	.	1.12	0.19	0.31	2.74	.	.	100.21	MUN
428.25	54.3	14.4	.	12.61	5.98	2.76	3.86	0.24	.	1.20	0.08	0.22	3.63	.	.	99.28	MUN
431.15	58.3	15.08	3.06	6.74	3.50	2.84	5.32	0.04	3.07	1.26	0.14	0.32	.	1.25	0.06	100.98	BOCHUM
431.15	58.0	14.7	.	10.17	3.44	2.76	5.14	0.05	.	1.20	0.13	0.30	2.59	.	.	98.48	MUN
437.00	51.0	14.7	.	10.82	8.15	3.64	3.66	0.60	.	0.88	0.09	0.19	4.63	.	.	98.36	MUN
439.40	56.3	13.8	.	11.12	4.64	3.44	4.14	0.03	.	1.24	0.12	0.24	3.26	.	.	98.33	MUN
441.00	52.0	15.42	3.33	6.94	8.35	3.81	4.33	0.37	4.37	0.93	0.08	0.19	.	0.52	0.05	100.69	BOCHUM

† FeO is total iron where Fe_2O_3 is not reported.

Depth(m)	SiO_2	Al_2O_3	Fe_2O_3	FeO†	MgO	CaO	Na_2O	K_2O	H_2O+	TiO_2	P_2O_5	MnO	LOI	CO_2	S	Total	Lab
	CY1A Major Element Data (continued)																
441.00	51.0	14.8	.	10.76	8.16	3.56	4.38	0.38	.	0.92	0.08	0.18	4.60	.	.	98.82	MUN
442.00	50.9	15.7	.	10.95	8.19	2.72	4.77	0.12	.	0.96	0.13	0.19	4.70	.	.	99.33	MUN
447.25	53.9	15.1	.	11.06	6.50	3.60	4.75	0.20	.	1.04	0.06	0.18	3.55	.	.	99.94	MUN
449.30	55.1	14.70	3.10	7.08	6.69	2.36	4.66	0.05	4.02	1.04	0.09	0.18	.	0.13	0.03	99.23	BOCHUM
449.30	55.5	14.5	.	10.80	6.64	2.26	4.66	0.05	.	1.00	0.10	0.16	3.76	.	.	99.34	MUN
451.65	51.7	15.1	.	11.48	6.42	4.16	4.21	0.48	.	1.04	0.09	0.20	3.85	.	.	98.73	MUN
457.30	59.3	13.6	.	10.35	3.22	2.46	4.97	0.07	.	0.96	0.16	0.21	2.79	.	.	98.09	MUN
459.50	58.4	14.53	3.56	7.07	3.82	2.24	5.17	0.11	3.18	1.27	0.14	0.24	.	0.35	0.12	100.20	BOCHUM
459.50	59.3	14.2	.	10.95	3.79	2.24	5.09	0.10	.	1.24	0.13	0.23	2.79	.	.	100.06	MUN
460.75	57.4	14.6	.	11.81	4.19	3.16	4.71	0.02	.	1.24	0.11	0.23	2.85	.	.	100.32	MUN
462.10	53.8	13.7	.	14.14	4.99	2.48	3.78	0.03	.	1.20	0.11	0.28	3.61	.	.	98.12	MUN
464.55	58.3	14.68	2.85	7.14	3.23	3.45	4.96	0.06	3.02	1.31	0.13	0.17	.	0.86	0.04	100.20	BOCHUM
464.55	57.8	14.6	.	10.82	3.21	3.38	4.97	0.06	.	1.24	0.12	0.17	3.25	.	.	99.42	MUN
470.10	52.4	15.4	.	11.75	5.82	4.04	4.96	0.32	.	1.08	0.08	0.18	3.40	.	.	99.43	MUN
472.70	49.1	15.7	.	10.11	7.35	5.28	4.99	0.22	.	0.76	0.04	0.17	5.14	.	.	98.86	MUN
475.60	60.8	12.2	.	10.99	4.72	4.84	2.34	0.03	.	1.20	0.10	0.19	3.45	.	.	100.86	MUN
475.60	59.4	12.43	3.40	6.96	4.72	5.00	2.37	0.03	3.70	1.21	0.12	0.20	.	0.45	0.04	100.03	BOCHUM
483.60	51.2	15.7	.	12.00	7.14	2.78	4.94	0.14	.	0.84	0.16	0.22	5.37	.	.	100.49	MUN
486.20	62.2	14.0	.	9.07	2.40	3.38	4.86	0.02	.	1.08	0.15	0.16	2.09	.	.	99.41	MUN
493.60	47.5	14.97	3.60	6.63	5.10	9.85	2.93	0.23	3.94	0.71	0.06	0.21	.	4.26	0.04	100.03	BOCHUM
493.60	48.0	14.8	.	11.04	5.10	9.48	2.99	0.24	.	0.72	0.05	0.20	7.62	.	.	100.24	MUN
497.80	50.0	14.77	2.14	6.37	11.08	4.63	3.06	0.51	5.64	0.34	0.03	0.23	.	2.37	0.03	101.20	BOCHUM
497.80	48.2	14.0	.	8.04	11.70	7.16	2.18	0.86	.	0.28	0.00	0.19	7.81	.	.	100.42	MUN
501.00	58.9	14.1	.	9.98	3.25	3.36	5.03	0.05	.	0.88	0.09	0.23	3.44	.	.	99.31	MUN
507.00	49.4	14.3	.	8.50	8.11	6.82	3.60	0.20	.	0.48	0.02	0.20	8.47	.	.	99.10	MUN
508.80	59.9	14.63	4.41	4.77	3.02	2.68	5.33	0.02	2.72	1.18	0.15	0.23	.	0.13	0.18	99.35	BOCHUM
509.30	61.5	14.3	.	9.49	3.09	1.56	5.60	0.01	.	1.08	0.14	0.20	2.47	.	.	99.44	MUN
512.00	61.2	14.8	.	10.55	3.26	1.90	5.26	0.01	.	1.12	0.14	0.20	2.29	.	.	100.73	MUN
516.80	57.9	13.77	4.89	6.43	4.93	1.57	4.32	0.01	3.99	1.22	0.11	0.31	.	0.31	0.52	100.28	BOCHUM
517.65	58.2	14.4	.	11.67	4.64	1.48	4.88	0.01	.	1.24	0.10	0.30	2.88	.	.	99.80	MUN
521.10	51.3	14.4	.	11.26	5.82	5.38	4.27	0.06	.	1.04	0.07	0.33	5.92	.	.	99.85	MUN
523.90	54.0	14.7	.	11.75	5.39	3.48	4.03	0.18	.	0.96	0.08	0.36	4.63	.	.	99.56	MUN
527.25	58.4	14.3	.	10.72	3.36	3.42	5.06	0.06	.	1.32	0.14	0.27	3.10	.	.	100.15	MUN
528.80	55.1	14.53	5.65	6.52	5.16	2.28	4.57	0.01	4.07	1.37	0.10	0.34	.	0.41	0.07	100.18	BOCHUM
530.05	53.8	13.2	.	12.40	5.94	4.28	3.34	0.01	.	1.32	0.10	0.33	4.14	.	.	98.86	MUN
532.80	54.3	14.5	.	12.67	5.06	3.60	4.06	0.01	.	1.24	0.08	0.30	3.23	.	.	99.05	MUN
535.60	49.4	14.5	.	11.26	6.40	5.58	4.00	0.13	.	1.00	0.06	0.29	7.14	.	.	99.76	MUN
536.80	55.3	13.25	5.80	7.85	6.17	1.19	3.55	0.01	4.43	1.19	0.10	0.37	.	0.19	0.43	99.83	BOCHUM

† FeO is total iron where Fe_2O_3 is not reported.

Depth(m)	SiO_2	Al_2O_3	Fe_2O_3	FeO†	MgO	CaO	Na_2O	K_2O	H_2O+	TiO_2	P_2O_5	MnO	LOI	CO_2	S	Total	Lab
	CY1A Major Element Data (continued)																
538.25	53.5	14.5	.	11.84	5.57	3.68	3.83	0.01	.	1.24	0.13	0.50	3.54	.	.	98.34	MUN
542.10	61.4	13.6	.	9.20	2.59	3.06	5.39	0.01	.	1.00	0.28	0.35	2.18	.	.	99.06	MUN
548.80	56.6	15.61	4.01	6.71	3.80	2.25	5.55	0.02	3.29	1.19	0.21	0.36	.	0.01	0.84	100.45	BOCHUM
550.10	61.9	14.1	.	10.00	2.84	1.80	5.67	0.01	.	1.12	0.23	0.26	1.86	.	.	99.79	MUN
552.90	63.8	14.0	.	9.31	2.68	1.68	5.75	0.01	.	1.08	0.21	0.24	1.68	.	.	100.44	MUN
559.80	55.9	14.3	.	12.47	5.90	3.24	3.43	0.01	.	1.16	0.09	0.39	3.27	.	.	100.16	MUN
560.80	53.5	13.08	5.57	7.64	6.59	2.38	2.86	0.01	4.94	1.16	0.09	0.41	.	0.49	1.11	99.83	BOCHUM
561.65	52.1	14.8	.	11.48	6.55	4.04	4.27	0.12	.	1.08	0.15	0.29	5.28	.	.	100.16	MUN
563.60	50.6	15.8	.	10.12	7.53	3.40	5.23	0.08	.	0.96	0.12	0.21	4.70	.	.	98.75	MUN
568.55	54.7	14.5	.	11.72	4.91	4.92	3.20	0.00	.	1.28	0.12	0.24	3.15	.	.	98.74	MUN
579.75	51.3	15.2	.	14.90	7.37	1.08	3.68	0.01	.	0.96	0.07	0.38	4.64	.	.	99.59	MUN
580.80	47.2	16.66	5.20	10.43	7.41	1.91	3.74	0.05	5.71	1.01	0.09	0.42	.	0.34	0.49	100.66	BOCHUM
589.10	54.3	14.3	.	14.16	5.82	1.88	3.82	0.07	.	0.92	0.07	0.32	3.68	.	.	99.34	MUN
596.40	61.0	13.7	.	10.16	3.45	2.28	4.72	0.09	.	1.13	0.14	0.20	2.68	.	.	99.55	MUN
600.80	52.9	14.65	7.18	7.55	5.90	1.71	3.89	0.12	4.51	0.99	0.08	0.32	.	0.35	1.26	101.41	BOCHUM
601.60	54.5	14.2	.	14.45	5.89	1.38	3.58	0.11	.	0.88	0.10	0.28	4.00	.	.	99.37	MUN
607.05	55.4	15.1	.	12.28	5.65	3.10	4.35	0.01	.	1.00	0.14	0.28	3.32	.	.	100.63	MUN
609.70	54.5	14.5	.	13.18	5.79	1.90	4.70	0.01	.	1.24	0.09	0.26	3.22	.	.	99.39	MUN
616.10	53.0	14.94	3.97	6.75	5.81	3.16	4.74	0.02	3.77	1.02	0.09	0.27	.	0.84	0.26	98.64	BOCHUM
616.10	54.5	14.6	.	11.13	5.80	3.00	4.73	0.01	.	0.88	0.08	0.26	3.77	.	.	98.76	MUN
620.10	56.1	14.7	.	12.00	6.45	1.46	4.53	0.01	.	0.88	0.06	0.26	3.71	.	.	100.16	MUN
624.00	63.1	12.8	.	10.09	2.70	2.62	5.00	0.01	.	1.00	0.17	0.15	2.24	.	.	99.88	MUN
629.40	63.8	13.1	.	9.60	2.80	1.78	5.48	0.02	.	1.04	0.17	0.17	1.69	.	.	99.65	MUN
629.40	62.5	13.64	3.59	5.73	2.82	2.01	5.39	0.01	2.22	1.12	0.18	0.18	.	0.06	0.08	99.53	BOCHUM
631.90	63.0	12.8	.	8.07	2.37	2.86	5.48	0.03	.	1.00	0.16	0.15	2.41	.	.	98.33	MUN
636.40	52.3	15.9	.	10.95	8.25	2.08	4.12	0.49	.	0.80	0.07	0.30	4.76	.	.	100.02	MUN
636.40	51.8	16.37	3.14	7.28	8.59	2.30	4.26	0.49	4.91	0.90	0.08	0.32	.	0.29	0.06	100.79	BOCHUM
641.70	52.2	15.2	.	10.95	7.87	2.36	4.31	0.24	.	0.80	0.08	0.30	4.49	.	.	98.80	MUN
641.70	51.6	15.52	3.70	6.65	8.01	2.58	4.29	0.23	4.50	0.91	0.08	0.32	.	0.26	0.09	98.74	BOCHUM
649.05	53.8	14.6	.	11.66	6.15	3.48	4.39	0.23	.	0.86	0.09	0.28	3.39	.	.	98.93	MUN
652.80	60.6	13.34	4.66	5.22	3.19	1.98	5.12	0.01	2.29	1.17	0.16	0.18	.	0.63	0.51	99.15	BOCHUM
652.80	62.1	13.2	.	9.60	3.15	1.74	5.33	0.01	.	1.00	0.15	0.17	2.13	.	.	98.58	MUN
666.40	53.7	14.87	4.67	6.47	6.44	3.46	4.00	0.54	3.60	1.12	0.09	0.33	.	0.15	0.02	99.46	BOCHUM
666.40	54.5	14.4	.	11.66	6.22	3.18	4.06	0.56	.	1.00	0.10	0.31	3.28	.	.	99.27	MUN

† FeO is total iron where Fe_2O_3 is not reported.

Depth(m)	Rb	Sr	Ba	Zr	Cr	Ni	Co	V	Th	U	Y	Pb	Cu	Zn	Ga	La	Ce	Lab
	CY1 Trace Element Data																	
19.70	49	116	110	24	286	90	.	271	0	0	18	1	61	80	11	12	12	MUN
19.70	47	110	68	34	343	99	25	259	.	.	18	.	122	126	.	.	.	BOCHUM
23.20	55	125	97	40	419	118	27	377	.	.	22	.	95	104	.	.	.	BOCHUM
23.35	55	124	133	30	334	103	.	365	.	8	24	6	264	119	18	15	10	MUN
32.30	54	93	36	47	492	144	26	180	.	.	13	.	68	79	.	.	.	BOCHUM
32.30	52	94	66	41	438	131	.	200	0	2	13	3	68	69	11	3	8	MUN
40.40	33	104	10	51	233	124	21	257	.	.	22	.	78	92	.	.	.	BOCHUM
40.40	32	105	46	45	142	106	.	271	1	0	23	1	70	76	10	8	16	MUN
44.50	46	116	24	52	194	80	16	239	.	.	25	.	90	103	.	.	.	BOCHUM
44.50	42	115	71	48	123	71	.	250	0	0	25	0	78	84	13	7	10	MUN
47.30	26	106	86	22	622	216	.	150	4	.	14	5	40	59	4	14	9	MUN
47.30	32	107	10	26	1201	238	5	180	.	.	17	.	42	73	.	.	.	BOCHUM
51.70	28	114	67	24	378	198	.	150	3	1	16	2	57	51	4	8	13	MUN
51.75	34	111	10	31	734	223	5	163	.	.	15	.	98	85	.	.	.	BOCHUM
54.70	54	92	10	36	713	106	5	205	.	.	18	.	72	82	.	.	.	BOCHUM
54.70	54	94	64	27	456	90	.	208	0	2	17	0	66	64	9	8	15	MUN
57.00	54	93	37	39	399	85	14	225	.	.	12	.	85	90	.	.	.	BOCHUM
57.00	49	93	73	32	264	68	.	236	1	0	10	0	71	78	18	2	12	MUN
58.70	11	75	10	28	1280	656	40	136	.	.	11	.	63	66	.	.	.	BOCHUM
58.70	9	71	34	17	672	635	.	113	0	0	10	0	57	53	8	14	6	MUN
69.10	41	93	10	43	376	94	14	191	.	.	19	.	90	89	.	.	.	BOCHUM
69.10	39	96	50	36	208	85	.	190	0	3	15	0	80	80	10	5	8	MUN
71.50	21	81	10	37	285	104	31	221	.	.	18	.	136	73	.	.	.	BOCHUM
71.50	17	82	50	32	141	91	.	230	.	0	22	2	100	66	9	10	10	MUN
74.10	45	90	24	43	135	69	10	199	.	.	17	.	90	82	.	.	.	BOCHUM
74.10	38	86	39	34	53	57	.	184	.	0	17	0	78	69	15	7	13	MUN
77.40	40	89	10	40	130	72	17	180	.	.	17	.	211	86	.	.	.	BOCHUM
77.40	30	87	64	33	42	56	.	187	.	.	16	1	120	72	12	11	14	MUN
82.10	53	96	19	38	107	65	9	171	.	.	16	.	81	81	.	.	.	BOCHUM
82.10	50	96	74	31	61	46	.	176	0	5	14	0	74	71	14	12	7	MUN
88.50	43	118	16	39	116	62	12	193	.	.	22	.	95	72	.	.	.	BOCHUM
88.50	39	120	87	32	73	51	.	177	0	3	22	5	81	58	12	11	9	MUN
90.60	30	108	10	36	256	76	11	245	.	.	18	.	71	60	.	.	.	BOCHUM
90.60	25	114	72	.	148	64	.	223	.	7	30	0	69	49	9	10	10	MUN
92.50	25	85	10	38	319	95	25	225	.	.	19	.	96	91	.	.	.	BOCHUM
92.50	16	88	60	30	177	82	.	230	1	1	19	4	77	69	11	15	7	MUN
94.10	29	85	10	39	366	111	31	232	.	.	17	.	71	91	.	.	.	BOCHUM
94.10	27	89	54	34	200	98	.	226	0	.	17	0	63	77	16	13	7	MUN
95.60	14	48	10	22	1728	1060	51	88	.	.	8	.	54	51	.	.	.	BOCHUM
95.60	4	49	11	11	968	1038	.	71	0	2	2	4	40	37	5	11	7	MUN
96.10	28	106	23	39	165	94	17	248	.	.	17	.	78	63	.	.	.	BOCHUM
96.10	26	107	74	34	82	80	.	221	4	7	19	3	65	49	11	6	5	MUN
96.90	37	87	10	36	111	71	10	226	.	.	20	.	169	132	.	.	.	BOCHUM
96.90	33	93	47	28	59	55	.	209	0	0	22	0	68	49	12	13	10	MUN

Depth(m)	Rb	Sr	Ba	Zr	Cr	Ni	Co	V	Th	U	Y	Pb	Cu	Zn	Ga	La	Ce	Lab
	CY1 Trace Element Data (continued)																	
99.50	28	88	10	39	324	98	30	226	.	.	17	.	95	88	.	.	.	BOCHUM
99.50	24	94	72	34	187	88	.	233	.	2	19	0	78	71	16	9	11	MUN
101.80	35	108	28	38	298	86	5	247	.	.	18	.	77	73	.	.	.	BOCHUM
101.80	28	118	79	31	152	72	.	230	5	3	19	5	65	57	13	16	12	MUN
105.60	28	89	10	37	273	74	20	212	.	.	17	.	68	69	.	.	.	BOCHUM
105.60	20	97	64	31	148	65	.	205	0	0	20	0	66	59	11	16	9	MUN
109.30	33	90	10	35	425	99	12	196	.	.	17	.	66	73	.	.	.	BOCHUM
109.30	25	94	69	32	186	85	.	200	0	2	16	0	63	60	13	11	9	MUN
110.70	27	87	10	34	601	233	27	209	.	.	15	.	52	65	.	.	.	BOCHUM
110.70	18	89	56	28	339	229	.	196	0	1	15	0	53	53	12	7	12	MUN
113.50	37	107	16	39	245	90	18	245	.	.	17	.	48	54	.	.	.	BOCHUM
113.50	27	116	111	32	140	75	.	244	0	2	21	1	41	41	12	12	8	MUN
120.80	40	90	70	38	258	80	13	182	.	.	19	.	75	69	.	.	.	BOCHUM
120.80	36	93	117	32	159	72	.	189	0	0	19	0	71	61	14	10	8	MUN
126.20	35	101	42	2	133	60	7	194	.	.	16	.	84	71	.	.	.	BOCHUM
126.20	28	104	80	37	81	50	.	201	0	0	18	2	79	67	13	10	9	MUN
132.10	37	73	10	44	92	55	26	221	.	.	20	.	81	81	.	.	.	BOCHUM
132.10	29	75	47	36	45	47	.	219	1	1	22	1	75	72	14	5	6	MUN
135.50	46	85	10	45	88	56	12	239	.	.	17	.	82	84	.	.	.	BOCHUM
135.50	39	87	73	36	59	43	.	190	1	0	16	0	71	68	13	14	15	MUN
140.80	40	72	15	38	277	67	11	185	.	.	18	.	46	67	.	.	.	BOCHUM
140.80	35	75	63	29	156	56	.	193	0	2	20	0	57	55	10	4	6	MUN
148.20	38	59	25	34	266	74	17	238	.	.	19	.	46	67	.	.	.	BOCHUM
148.20	36	60	68	27	226	59	.	253	7	3	19	0	48	60	13	3	3	MUN
152.20	28	70	10	34	285	85	24	226	.	.	14	.	46	76	.	.	.	BOCHUM
152.20	23	71	67	21	190	78	.	.	0	0	11	0	51	67	12	12	7	MUN
165.10	29	87	56	32	300	103	37	217	.	.	13	.	91	73	.	.	.	BOCHUM
165.10	18	79	59	29	175	75	.	217	0	4	18	0	66	61	10	7	6	MUN
169.30	44	58	10	39	128	61	11	161	.	.	18	.	61	70	.	.	.	BOCHUM
169.30	40	58	72	31	97	57	.	161	2	1	17	1	49	56	12	9	10	MUN
173.50	45	77	22	37	119	62	5	115	.	.	18	.	74	65	.	.	.	BOCHUM
173.50	35	75	71	30	74	49	.	115	0	1	18	0	69	59	9	13	7	MUN
180.40	36	63	10	36	278	73	5	119	.	.	18	.	48	74	.	.	.	BOCHUM
180.40	31	63	51	31	214	59	.	131	0	0	19	0	48	57	14	13	12	MUN
183.60	31	63	39	28	193	55	.	188	0	0	14	0	53	49	14	8	10	MUN
183.60	38	65	10	36	272	66	5	188	.	.	18	.	52	60	.	.	.	BOCHUM
185.10	36	68	57	32	174	51	.	168	0	4	18	0	64	49	11	10	10	MUN
185.10	44	68	10	38	217	60	6	147	.	.	20	.	64	63	.	.	.	BOCHUM
188.30	28	60	10	34	271	60	12	214	.	.	15	.	44	70	.	.	.	BOCHUM
194.10	41	64	15	42	138	59	28	239	.	.	16	.	65	75	.	.	.	BOCHUM
194.10	34	65	83	35	106	44	.	257	0	.	17	2	63	68	12	7	8	MUN
197.70	36	81	10	41	193	69	11	216	.	.	19	.	51	79	.	.	.	BOCHUM
197.70	27	76	40	31	156	55	.	244	1	0	20	0	49	64	11	1	8	MUN
200.70	13	78	42	30	197	94	.	275	0	3	16	2	85	60	10	10	14	MUN

Depth(m)	Rb	Sr	Ba	Zr	Cr	Ni	Co	V	Th	U	Y	Pb	Cu	Zn	Ga	La	Ce	Lab
	CY1 Trace Element Data (continued)																	
200.70	22	78	10	41	262	109	20	245	.	.	17	.	80	71	.	.	.	BOCHUM
203.50	9	101	59	34	110	46	.	260	0	0	15	0	27	65	15	7	6	MUN
203.50	17	99	10	40	166	55	18	259	.	.	18	.	23	77	.	.	.	BOCHUM
208.90	13	78	40	34	160	103	.	252	1	0	20	3	68	62	13	11	13	MUN
208.90	23	76	10	37	273	109	17	230	.	.	17	.	64	74	.	.	.	BOCHUM
214.40	30	88	54	33	103	42	.	247	0	2	16	2	50	63	11	15	11	MUN
218.00	28	77	58	38	80	43	.	313	1	1	22	0	61	75	16	10	15	MUN
223.10	48	79	44	40	120	65	35	209	.	.	16	.	151	93	.	.	.	BOCHUM
223.10	34	67	58	35	89	42	.	236	2	0	22	.	58	71	13	4	10	MUN
233.90	46	73	46	38	55	29	.	252	0	0	22	.	40	57	11	7	7	MUN
237.50	18	78	44	40	59	28	.	266	2	2	19	1	52	65	14	6	12	MUN
240.00	39	98	33	45	65	46	35	243	.	.	16	.	958	155	.	.	.	BOCHUM
240.00	26	89	44	45	45	29	.	270	0	2	23	0	3	.	15	5	9	MUN
244.50	12	74	49	38	123	36	.	283	0	0	15	0	112	67	13	4	14	MUN
246.70	18	78	45	44	121	50	.	241	0	.	20	0	46	70	12	7	12	MUN
246.70	28	91	21	47	182	72	37	210	.	.	17	.	81	84	.	.	.	BOCHUM
254.00	22	68	42	40	130	42	.	222	1	3	22	0	46	59	9	9	15	MUN
254.00	36	77	29	45	185	60	28	205	.	.	18	.	48	69	.	.	.	BOCHUM
259.20	13	59	36	37	86	39	.	179	0	0	23	2	119	57	13	8	12	MUN
261.20	20	80	66	44	128	42	.	248	0	0	17	0	45	62	12	6	9	MUN
266.30	33	87	36	52	81	48	30	193	.	.	22	.	58	85	.	.	.	BOCHUM
266.30	19	70	46	45	56	31	.	220	2	1	27	6	46	65	13	6	10	MUN
268.80	18	81	58	45	76	37	.	244	0	1	23	0	46	65	11	10	7	MUN
273.40	21	96	17	34	265	94	35	227	.	.	34	.	145	71	.	.	.	BOCHUM
273.41	10	82	36	32	221	57	.	253	1	1	13	0	109	55	14	4	7	MUN
279.70	32	82	18	44	238	71	30	202	.	.	16	.	91	84	.	.	.	BOCHUM
279.70	15	70	37	41	169	44	.	216	.	1	17	0	40	62	7	9	13	MUN
281.90	15	85	46	39	150	43	.	245	0	0	22	0	43	68	11	8	13	MUN
283.50	14	69	33	39	190	42	.	216	5	0	22	3	37	59	10	11	12	MUN
287.20	38	80	27	41	228	66	27	161	.	.	16	.	43	64	.	.	.	BOCHUM
287.20	24	70	56	36	196	42	.	188	1	1	20	2	44	45	12	8	11	MUN
289.20	12	76	19	39	292	141	.	198	0	4	18	0	39	57	12	10	4	MUN
292.80	13	78	39	35	119	38	.	245	0	2	19	0	51	61	12	10	7	MUN
297.70	14	80	23	34	147	38	.	230	3	0	177	3	53	58	13	3	9	MUN
297.70	25	93	21	37	204	66	33	209	.	.	16	.	357	84	.	.	.	BOCHUM
301.50	19	63	39	35	214	39	.	215	0	0	17	0	38	55	11	12	15	MUN
304.50	5	75	17	33	159	48	.	239	0	2	18	1	113	61	13	7	7	MUN
309.05	12	70	41	31	50	30	.	255	0	.	23	0	38	69	10	11	10	MUN
309.05	25	84	10	36	68	49	30	219	.	.	20	.	129	89	.	.	.	BOCHUM
316.80	4	63	27	30	198	53	.	259	0	0	16	0	95	65	11	7	11	MUN
318.10	10	65	29	27	193	50	.	231	0	0	14	0	50	65	11	2	8	MUN
321.40	16	77	31	28	130	40	.	241	0	2	17	0	47	58	12	6	11	MUN
321.40	27	86	12	33	206	66	28	225	.	.	15	.	155	73	.	.	.	BOCHUM
328.60	26	73	65	31	171	49	.	251	0	0	15	.	34	64	14	7	9	MUN

Depth(m)	Rb	Sr	Ba	Zr	Cr	Ni	Co	V	Th	U	Y	Pb	Cu	Zn	Ga	La	Ce	Lab
	CY1 Trace Element Data (continued)																	
333.50	24	88	24	41	87	54	37	231	.	.	22	.	84	95	.	.	.	BOCHUM
333.50	8	76	50	34	70	35	.	282	0	0	23	0	44	76	13	10	10	MUN
336.90	7	68	45	27	158	41	.	265	0	1	19	0	52	58	12	10	10	MUN
336.90	20	77	19	31	199	57	35	249	.	.	14	.	56	81	.	.	.	BOCHUM
337.90	3	83	38	35	84	35	.	280	0	2	22	3	78	79	16	15	8	MUN
342.20	34	98	15	38	145	54	24	214	.	.	15	.	32	68	.	.	.	BOCHUM
342.40	21	90	42	36	93	36	.	222	3	1	18	0	36	57	12	10	11	MUN
347.10	.	81	46	34	106	38	.	267	0	1	17	1	84	55	11	5	11	MUN
348.80	33	53	14	36	95	44	25	183	.	.	18	.	149	75	.	.	.	BOCHUM
348.80	15	44	74	31	72	21	.	216	0	0	21	0	80	51	9	11	4	MUN
354.20	5	79	45	35	65	30	.	263	0	0	18	0	59	75	14	9	6	MUN
361.30	3	75	37	33	38	24	.	265	3	0	19	.	62	77	10	11	7	MUN
361.30	17	89	26	40	58	41	31	228	.	.	15	.	116	114	.	.	.	BOCHUM
367.10	7	76	34	35	54	26	.	264	.	1	27	0	47	78	11	11	8	MUN
375.10	5	82	41	33	59	28	.	247	3	6	21	5	53	60	10	9	13	MUN
375.80	14	98	10	30	482	242	35	207	.	.	14	.	1268	291	.	.	.	BOCHUM
375.80	3	84	33	32	264	196	.	225	0	.	19	0	76	53	8	6	5	MUN
377.50	3	85	27	34	48	30	.	252	5	2	19	5	52	59	17	2	14	MUN
381.30	3	89	28	33	50	32	.	270	.	.	23	0	62	71	16	7	11	MUN
386.60	40	85	23	36	88	45	28	194	.	.	13	.	51	86	.	.	.	BOCHUM
386.60	25	78	44	34	40	27	.	213	3	8	15	0	19	59	12	5	12	MUN
390.70	13	76	10	24	880	340	50	197	.	.	11	.	385	70	.	.	.	BOCHUM
390.70	4	65	10	24	430	298	.	205	0	0	137	0	90	54	9	.	0	MUN
397.50	2	76	23	35	99	39	.	283	0	0	247	1	57	75	11	8	15	MUN
402.20	18	91	17	40	107	55	30	229	.	.	22	.	72	97	.	.	.	BOCHUM
402.20	5	77	33	36	90	33	.	274	.	2	25	4	56	79	14	8	8	MUN
410.20	15	90	34	36	86	36	.	255	0	0	23	0	15	61	12	6	9	MUN
413.20	20	96	25	41	31	18	.	274	2	3	26	4	30	74	15	10	11	MUN
416.85	37	84	25	40	58	37	26	205	.	.	16	.	47	91	.	.	.	BOCHUM
416.85	28	74	39	35	36	19	.	224	1	3	20	1	15	70	12	7	6	MUN
426.30	12	77	44	35	90	31	.	203	2	0	18	0	22	58	14	11	8	MUN
429.45	4	85	42	35	93	38	.	280	4	6	23	7	84	72	14	9	4	MUN
434.60	2	84	47	36	140	48	.	269	0	0	19	0	56	64	12	5	12	MUN
434.60	13	97	10	40	203	72	31	239	.	.	18	.	71	97	.	.	.	BOCHUM
440.00	23	77	26	32	207	56	.	201	0	3	16	0	21	62	12	4	10	MUN
445.90	1	66	21	29	164	51	.	227	0	0	23	0	55	67	9	11	8	MUN
445.90	16	80	10	35	279	78	33	219	.	.	20	.	55	87	.	.	.	BOCHUM
450.45	17	80	14	34	273	80	35	227	.	.	16	.	403	94	.	.	.	BOCHUM
450.45	5	70	53	30	202	50	.	252	2	6	19	5	52	68	15	6	11	MUN
455.90	17	80	10	35	280	84	35	225	.	.	23	.	207	96	.	.	.	BOCHUM
465.65	23	93	45	40	120	46	33	201	.	.	17	.	131	92	.	.	.	BOCHUM
468.42	16	101	25	40	164	53	31	211	.	.	16	.	83	87	.	.	.	BOCHUM

Depth(m)	Ti	Rb	Sr	Ba	Zr	Cr	Ni	Co	V	Th	U	Y	Pb	Cu	Zn	Ga	Lab
	CY1A Trace Element Data																
5.20	0.78	13	78	0	37	295	114	.	259	0	0	20	11	47	.	10	MUN
10.50	.	14	88	21	47	345	147	37	219	.	.	18	.	64	71	.	BOCHUM
10.50	0.85	11	83	9	40	248	113	.	277	0	0	25	3	49	.	9	MUN
17.10	1.06	7	83	0	45	19	13	.	412	0	0	29	9	77	.	13	MUN
19.30	1.13	2	89	0	50	13	12	.	434	0	0	27	4	84	.	15	MUN
27.70	.	16	83	41	56	4	17	30	406	.	.	24	.	23	102	.	BOCHUM
27.70	1.29	11	84	25	54	0	0	.	443	0	0	33	0	14	.	10	MUN
30.30	1.37	15	87	18	54	0	0	.	447	0	0	33	6	49	.	16	MUN
40.80	.	19	88	41	65	10	16	35	399	.	.	32	.	53	120	.	BOCHUM
40.80	1.64	12	87	15	63	0	0	.	447	0	0	39	10	32	.	13	MUN
43.80	.	7	103	13	52	15	25	35	302	.	.	21	.	162	93	.	BOCHUM
43.80	0.83	3	104	23	48	3	4	.	334	0	0	25	0	110	.	12	MUN
48.90	1.25	13	96	25	52	9	4	.	444	0	0	34	0	12	.	17	MUN
53.40	1.42	9	96	0	55	9	5	.	492	0	3	29	3	43	.	16	MUN
62.10	.	16	93	39	60	10	19	30	437	.	.	25	.	42	113	.	BOCHUM
62.10	1.43	17	96	26	57	5	2	.	496	0	0	31	10	29	.	13	MUN
65.60	1.48	23	101	18	69	0	0	.	323	0	0	36	1	9	.	17	MUN
68.40	0.96	4	88	1	44	24	16	.	375	0	0	29	1	67	.	12	MUN
69.25	.	7	72	14	34	236	66	32	229	.	.	15	.	90	71	.	BOCHUM
69.25	0.51	0	68	10	27	197	41	.	256	0	6	21	5	64	.	7	MUN
73.00	0.67	2	81	0	38	180	41	.	258	0	6	25	10	45	.	10	MUN
89.50	1.28	8	95	7	51	6	9	.	441	0	0	29	17	47	.	13	MUN
97.00	.	10	86	25	52	14	24	34	319	.	.	27	.	20	76	.	BOCHUM
97.00	1.03	9	82	5	47	7	2	.	377	0	0	32	1	8	.	15	MUN
101.10	1.07	12	101	1	50	21	17	.	378	0	0	28	6	52	.	13	MUN
106.40	1.09	13	101	0	49	21	14	.	383	0	0	27	0	62	.	13	MUN
111.90	.	11	113	19	58	23	39	38	271	.	.	23	.	81	84	.	BOCHUM
111.90	1.02	7	111	8	54	11	16	.	334	0	0	28	19	51	.	15	MUN
115.30	0.91	7	114	9	50	16	23	.	285	0	3	27	7	43	.	14	MUN
118.00	0.51	4	64	17	25	239	51	.	253	0	0	18	3	63	.	9	MUN
119.20	.	12	77	0	45	34	34	35	294	.	.	22	.	31	77	.	BOCHUM
119.20	0.82	8	75	14	39	24	13	.	340	0	0	26	0	17	.	13	MUN
122.30	0.94	5	78	20	40	27	13	.	376	0	1	26	5	83	.	10	MUN
125.80	0.96	16	88	31	47	13	20	.	339	0	0	27	4	63	.	14	MUN
129.10	.	18	91	34	50	28	40	30	258	.	.	19	.	12	82	.	BOCHUM
129.10	0.87	16	91	11	44	17	18	.	304	2	0	26	0	6	.	14	MUN
136.10	0.81	13	89	21	46	48	31	.	283	0	0	26	0	48	.	14	MUN
138.20	0.70	17	97	16	45	22	24	.	242	0	0	20	0	4	.	10	MUN
142.00	.	29	98	14	50	39	50	27	210	.	.	18	.	23	65	.	BOCHUM
142.00	0.74	26	97	17	45	20	24	.	243	7	0	26	19	9	.	11	MUN
147.40	0.74	24	97	28	44	29	27	.	246	0	0	20	10	7	.	14	MUN
151.10	0.79	23	86	34	44	14	23	.	269	0	0	22	1	29	.	13	MUN
154.60	.	9	106	41	53	40	39	31	237	.	.	22	.	52	68	.	BOCHUM
154.60	0.88	2	101	15	47	29	19	.	301	0	0	27	0	25	.	12	MUN
156.90	0.63	3	75	10	30	173	48	.	292	0	0	21	1	54	.	11	MUN
167.80	1.00	10	87	0	51	21	13	.	344	0	0	25	13	56	.	15	MUN
175.60	.	11	95	25	58	28	38	29	270	.	.	22	.	59	82	.	BOCHUM

Depth(m)	Ti	Rb	Sr	Ba	Zr	Cr	Ni	Co	V	Th	U	Y	Pb	Cu	Zn	Ga	Lab
	CY1A Trace Element Data (continued)																
175.60	1.02	6	92	11	52	15	15	.	347	0	0	27	0	39	.	15	MUN
185.70	.	17	90	70	65	15	28	39	333	.	.	27	.	73	92	.	BOCHUM
185.70	1.32	13	88	33	57	7	8	.	428	0	0	32	0	45	.	16	MUN
202.60	.	22	63	87	65	12	22	25	358	.	.	26	.	47	115	.	BOCHUM
202.60	1.34	21	61	74	62	7	3	.	470	0	0	32	6	30	.	12	MUN
205.80	1.40	2	73	9	51	5	0	.	542	8	0	29	25	31	.	12	MUN
212.00	1.53	5	72	32	55	3	2	.	595	0	0	33	9	36	.	18	MUN
224.40	.	8	87	24	41	158	47	24	235	.	.	18	.	34	78	.	BOCHUM
224.40	0.67	8	94	18	37	135	25	.	281	0	0	21	11	23	.	11	MUN
228.50	0.53	4	80	22	34	262	55	.	231	0	0	20	6	16	.	11	MUN
231.70	0.54	3	57	1	22	119	43	.	278	0	0	20	0	24	.	12	MUN
237.60	.	5	60	0	31	139	64	34	258	.	.	15	.	141	101	.	BOCHUM
237.60	0.61	3	58	0	24	106	38	.	307	0	0	18	4	58	.	10	MUN
259.00	.	5	102	48	60	11	13	32	306	.	.	29	.	30	113	.	BOCHUM
259.00	1.51	2	100	10	55	3	0	.	399	1	0	36	9	14	.	14	MUN
267.90	1.30	9	77	69	56	7	2	.	425	0	0	33	11	93	.	13	MUN
271.20	.	9	72	60	62	10	14	29	250	.	.	29	.	91	144	.	BOCHUM
271.20	1.12	5	71	52	57	0	0	.	316	0	0	35	0	46	.	12	MUN
276.80	1.15	6	91	43	59	0	0	.	317	0	0	36	5	52	.	12	MUN
282.00	0.53	7	99	57	29	55	26	.	289	0	0	19	0	61	.	10	MUN
288.50	0.50	4	79	28	24	191	39	.	280	0	0	19	4	57	.	9	MUN
288.55	.	9	80	32	31	253	62	36	245	.	.	12	.	101	149	.	BOCHUM
290.90	1.25	5	72	46	56	4	1	.	445	0	0	34	0	83	.	10	MUN
293.55	0.96	4	97	48	44	25	30	.	352	3	0	28	3	65	.	14	MUN
298.10	1.21	7	87	31	61	0	0	.	346	0	0	36	3	28	.	11	MUN
303.55	.	4	103	44	65	13	17	32	285	.	.	30	.	59	140	.	BOCHUM
303.55	1.35	2	102	0	62	0	0	.	395	1	9	36	15	34	.	11	MUN
310.40	.	7	89	38	65	19	15	25	235	.	.	31	.	30	114	.	BOCHUM
310.40	1.25	4	87	16	61	0	0	.	307	0	1	38	13	16	.	11	MUN
315.10	1.33	9	95	0	64	0	0	.	368	0	0	38	2	34	.	14	MUN
318.80	.	4	57	20	60	14	14	27	237	.	.	28	.	117	146	.	BOCHUM
318.80	1.12	6	61	13	59	0	0	.	314	0	0	34	8	70	.	11	MUN
322.70	.	16	92	55	65	10	25	31	318	.	.	28	.	71	93	.	BOCHUM
322.70	1.23	0	77	42	63	0	0	.	343	0	0	40	0	168	.	14	MUN
341.20	.	9	101	46	60	4	21	27	341	.	.	25	.	34	112	.	BOCHUM
341.20	1.15	4	96	24	56	0	0	.	422	0	0	32	0	19	.	14	MUN
347.70	.	7	83	59	60	10	22	33	302	.	.	26	.	89	188	.	BOCHUM
347.70	1.15	0	82	30	53	2	3	.	394	0	0	32	7	46	.	12	MUN
357.45		6	28	64	85	12	12	28	349	.	.	34	.	40	130		BOCHUM
357.45	1.65	0	27	0	78	0	0	.	457	0	0	39	3	18	.	13	MUN
364.25	.	6	24	43	87	10	14	26	292	.	.	36	.	37	127	.	BOCHUM
364.25	1.55	2	23	0	83	0	0	.	370	0	0	42	0	13	.	15	MUN
371.65	.	7	31	41	78	12	17	32	386	.	.	29	.	46	146	.	BOCHUM
371.65	1.57	5	33	18	74	3	0	.	506	0	0	35	13	14	.	12	MUN
377.30	1.42	0	82	0	64	2	0	.	445	0	0	37	3	27	.	11	MUN
380.80	1.40	2	85	20	62	0	2	.	463	0	0	35	8	33	.	14	MUN
384.70	.	3	40	25	64	13	21	38	305	.	.	27	.	47	173	.	BOCHUM

Depth(m)	Ti	Rb	Sr	Ba	Zr	Cr	Ni	Co	V	Th	U	Y	Pb	Cu	Zn	Ga	Lab
	CY1A Trace Element Data (continued)																
384.70	1.40	1	41	1	64	3	0	.	447	0	0	33	0	21	.	13	MUN
387.10	1.56	7	31	50	72	7	0	.	512	0	0	33	1	5	.	11	MUN
390.20	1.28	3	64	0	115	0	0	.	42	0	0	53	10	4	.	16	MUN
396.15	.	4	52	18	117	5	10	11	39	.	.	47	.	1	96	.	BOCHUM
396.15	1.06	2	52	0	116	0	0	.	38	0	0	56	9	0	.	13	MUN
404.60	0.50	3	67	43	30	144	31	.	259	1	0	17	9	55	.	11	MUN
408.90	0.84	2	69	0	113	0	0	.	39	4	0	52	11	13	.	12	MUN
410.40	.	7	84	57	65	14	20	36	319	.	.	28	.	88	155	.	BOCHUM
410.40	1.12	4	84	24	61	1	1	.	375	9	0	30	3	51	.	13	MUN
416.55	1.05	4	109	16	56	0	0	.	364	11	0	27	17	49	.	11	MUN
420.60	1.34	3	91	7	61	6	3	.	416	10	0	34	8	38	.	15	MUN
422.45	.	3	67	33	110	5	10	13	46	.	.	43	.	74	194	.	BOCHUM
422.45	1.27	2	66	0	106	0	0	.	57	6	0	49	4	43	.	11	MUN
424.90	1.40	1	42	0	96	0	0	.	155	8	0	46	13	21	.	14	MUN
428.25	1.38	0	82	9	53	3	0	.	498	0	0	33	13	41	.	14	MUN
431.15	.	2	57	36	101	2	11	13	142	.	.	40	.	33	122	.	BOCHUM
431.15	1.41	0	55	0	91	0	0	.	164	22	0	50	13	17	.	15	MUN
437.00	1.06	4	86	29	50	21	15	.	393	0	0	29	0	37	.	13	MUN
439.40	1.46	3	68	2	79	0	0	.	379	9	4	40	5	15	.	16	MUN
441.00	.	5	100	21	52	25	35	37	296	.	.	22	.	52	102	.	BOCHUM
441.00	1.02	2	103	14	46	16	14	.	379	10	5	31	13	31	.	12	MUN
442.00	1.14	3	80	0	49	18	13	.	401	12	3	29	12	37	.	11	MUN
447.25	1.18	2	102	8	55	9	7	.	390	13	0	31	13	39	.	15	MUN
449.30	.	6	70	33	62	16	27	30	293	.	.	25	.	44	110	.	BOCHUM
449.30	1.19	3	71	0	53	6	6	.	392	14	0	33	8	24	.	13	MUN
451.65	1.02	2	99	20	59	3	6	.	373	12	0	33	17	35	.	15	MUN
457.30	1.14	2	34	0	86	0	0	.	211	9	0	46	25	45	.	13	MUN
459.50	.	4	27	34	82	7	11	18	173	.	.	34	.	46	90	.	BOCHUM
459.50	1.44	3	30	0	74	0	0	.	230	2	0	44	13	15	.	13	MUN
460.75	1.54	3	58	8	71	0	0	.	378	0	1	39	17	21	.	12	MUN
462.10	1.47	0	37	0	59	9	0	.	488	0	0	31	7	66	.	11	MUN
464.55	.	5	94	51	88	5	9	15	65	.	.	38	.	7	108	.	BOCHUM
464.55	1.43	1	99	2	87	0	0	.	76	6	0	45	19	5	.	14	MUN
470.10	1.22	2	105	34	56	10	6	.	424	8	0	30	11	41	.	12	MUN
472.70	0.82	3	83	9	42	35	25	.	299	15	0	25	20	50	.	14	MUN
475.60	.	3	75	26	86	7	9	16	112	.	.	36	.	27	74	.	BOCHUM
475.60	1.28	2	74	12	80	0	0	.	133	20	1	43	32	10	.	16	MUN
483.60	1.05	5	61	0	42	13	17	.	400	16	0	28	21	72	.	12	MUN
486.20	1.13	2	55	0	101	0	0	.	70	15	0	47	11	43	.	15	MUN
493.60	.	4	101	0	47	10	25	33	286	.	.	22	.	96	85	.	BOCHUM
493.60	0.75	2	101	7	40	0	2	.	333	8	0	25	14	57	.	11	MUN
497.80	.	9	64	0	16	118	58	38	218	.	.	10	.	183	79	.	BOCHUM
497.90	0.28	6	70	37	8	295	67	.	260	10	0	13	18	57	.	9	MUN
501.00	1.62	3	75	0	80	0	0	.	115	11	0	36	16	21	.	14	MUN
507.00	0.47	3	90	3	25	253	49	.	281	0	0	18	14	62	.	8	MUN
508.80	.	3	64	31	100	8	11	6	82	.	.	41	.	84	86	.	BOCHUM
509.30	1.30	2	34	0	104	0	0	.	50	10	0	52	15	75	.	16	MUN

Depth(m)	Ti	Rb	Sr	Ba	Zr	Cr	Ni	Co	V	Th	U	Y	Pb	Cu	Zn	Ga	Lab
									CY1A Trace Element Data (continued)								
512.00	1.30	3	33	0	94	0	0	.	72	16	0	45	2	25	.	11	MUN
516.80	.	4	54	40	64	8	11	22	177	.	.	30	.	27	152	.	BOCHUM
517.65	1.52	1	20	0	68	0	0	.	231	11	0	36	9	23	.	11	MUN
521.10	1.12	4	79	0	54	9	2	.	408	8	0	32	6	27	.	8	MUN
523.90	1.17	1	80	7	55	1	4	.	385	8	0	33	4	19	.	11	MUN
527.25	1.51	2	77	0	81	0	0	.	142	1	0	38	4	4	.	12	MUN
528.80	.	4	22	41	70	3	15	21	335	.	.	28	.	10	241	.	BOCHUM
530.05	1.59	0	60	6	67	12	0	.	531	5	2	40	13	49	.	14	MUN
532.80	1.63	3	63	0	64	12	0	.	608	19	0	35	13	46	.	11	MUN
535.60	1.22	4	76	0	58	12	11	.	392	7	0	33	4	20	.	13	MUN
536.80	.	9	17	33	64	14	17	35	346	.	.	22	.	285	264	.	BOCHUM
538.25	1.48	1	51	2	61	13	3	.	519	10	1	36	29	6	.	13	MUN
542.10	1.11	1	56	0	100	0	0	.	34	16	0	54	8	17	.	13	MUN
548.80	.	10	45	34	108	6	12	11	53	.	.	46	.	626	187	.	BOCHUM
550.10	1.23	2	47	0	101	0	0	.	44	0	0	50	9	116	.	13	MUN
552.90	1.19	3	44	0	97	0	0	.	43	5	5	47	15	36	.	13	MUN
559.80	1.45	3	49	9	56	9	0	.	571	12	9	32	14	37	.	11	MUN
560.80	.	4	27	33	57	9	18	30	365	.	.	26	.	171	196	.	BOCHUM
561.65	1.19	2	83	13	60	16	9	.	372	0	0	36	7	30	.	13	MUN
563.60	1.00	1	80	5	51	18	13	.	351	7	0	28	5	51	.	8	MUN
568.55	1.50	0	70	0	62	2	0	.	435	0	0	36	0	14	.	15	MUN
579.75	1.07	2	14	0	57	0	2	.	381	4	0	29	0	013	.	11	MUN
580.80	.	12	61	16	61	8	25	14	308	.	.	25	.	1345	159	.	BOCHUM
589.10	1.02	2	63	13	48	0	4	.	419	0	0	27	9	198	.	13	MUN
595.40	1.19	4	73	8	85	0	0	.	174	3	8	41	11	91	.	13	MUN
600.80	.	8	58	30	56	2	21	28	309	.	.	23	.	609	136	.	BOCHUM
601.60	1.00	1	54	19	51	4	3	.	396	4	0	28	5	438	.	12	MUN
607.05	1.08	1	42	0	55	3	2	.	427	5	0	31	16	31	.	14	MUN
609.70	1.52	4	23	10	66	5	0	.	493	11	0	32	0	93	.	13	MUN
616.10	.	4	39	15	62	11	21	27	287	.	.	25	.	181	147	.	BOCHUM
616.10	1.11	3	37	0	56	0	2	.	367	16	0	31	16	101	.	11	MUN
620.10	1.06	1	30	0	41	10	14	.	368	9	7	25	15	154	.	11	MUN
624.00	1.10	0	39	0	91	0	0	.	67	3	0	42	12	227	.	11	MUN
629.40	.	2	39	15	99	2	13	7	57	.	.	46	.	69	74	.	BOCHUM
629.40	1.23	3	42	0	94	0	0	.	68	0	0	42	9	42	.	12	MUN
631.90	1.16	4	47	0	90	0	0	.	83	0	5	45	7	120	.	8	MUN
636.40	.	7	77	18	58	28	36	23	214	.	.	23	.	76	136	.	BOCHUM
636.40	0.93	2	80	15	53	14	18	.	281	3	0	30	5	43	.	13	MUN
641.70	.	7	74	20	60	23	34	25	240	.	.	22	.	54	137	.	BOCHUM
641.70	0.95	2	74	7	53	10	15	.	306	4	0	29	7	28	.	13	MUN
649.05	1.12	4	87	13	61	1	3	.	360	0	0	35	6	40	.	14	MUN
652.80	.	4	31	41	88	8	5	13	139	.	.	35	.	375	61	.	BOCHUM
652.80	1.28	3	36	0	88	0	0	.	177	9	2	45	21	178	.	14	MUN
666.40	.	8	100	31	68	12	24	25	308	.	.	30	.	147	102	.	BOCHUM
666.40	1.14	2	102	30	61	0	5	.	370	0	0	36	0	82	.	14	MUN